DEFORMATION OF SAND IN PLANE STRAIN AND AXISYMMETRIC COMPRESSION

a thesis presented by
Colin Thornton
for the degree of
Doctor of Philosophy

Department of Civil Engineering
University of Aston in Birmingham

October 1974

The research work described in this thesis was carried out in the Department of Civil Engineering at the University of Aston in Birmingham during the five-year period from October 1969. Until December 1971, the author held a Science Research Council research studentship, and for the remaining period has been employed by the University as a lecturer in civil engineering.

SUMMARY

Small scale laboratory experiments, in which the specimen is considered to represent an element of soil in the soil mass, are essential to the evolution of fundamental theories of mechanical behaviour. In this thesis, plane strain and axisymmetric compression tests, performed on a fine sand, are reported and the results are compared with various theoretical predictions.

A new apparatus is described in which cuboidal samples can be tested in either axisymmetric compression or plane strain. The plane strain condition is simulated either by rigid side platens, in the conventional manner, or by flexible side platens which also measure the intermediate principal stress. Close control of the initial porosity of the specimens is achieved by a vibratory method of sample preparation.

The strength of sand is higher in plane strain than in axisymmetric compression, and the strains required to mobilize peak strength are much smaller. The difference between plane strain and axisymmetric compression behaviour is attributed to the restrictions on particle movement enforced by the plane strain condition; this results in an increase in the frictional component of shear strength. The stress conditions at failure in plane strain, including the intermediate principal stress, are accurately predicted by a theory based on the stress-dilatancy interpretation of Mohr's circles.

Detailed observations of rupture modes are presented and measured rupture plane inclinations are predicted by the stress-dilatancy theory.

Although good correlation with the stress-dilatancy theory is obtained during virgin loading, in both axisymmetric compression and plane strain, the stress-dilatancy rule is only obeyed during reloading if the specimen has been unloaded to approximate ambient stress conditions.

The shape of the stress-strain curves during pre-peak deformation, in both plane strain and axisymmetric compression, is accurately described by a combined parabolic-hyperbolic specification.

ACKNOWLEDGEMENTS

I would like to thank my tutor, Mr. D. H. Bennett, for his help and enthusiastic encouragement throughout the research period. My thanks are also due to Dr. A. P. S. Selvadurai, for many stimulating and helpful discussions during the preparation of this thesis.

Thanks also go to Mr. W. C. Parsons and his team of technicians, especially to Mr. M. Lyons for his valuable assistance during the experimental work.

Appreciation is expressed to Miss H. Russell who typed the manuscript, to Miss P. Sage who traced many of the diagrams, and to Dr. S. Dyson who kindly gave permission to reproduce the photographs of his apparatus from his thesis.

Finally, and most of all, I would like to thank my wife Margaret for her understanding, support, and constant encouragement, particularly during the preparation of the thesis.

CONTENTS

CHAPTER ONE

1. INTRODUCTION.

1.1. Object and scope of the investigation.

For a rigorous analysis and comprehension of geotechnical engineering problems, both large scale and small scale laboratory investigations are necessary. Ideally, the problem is to formulate theories of soil behaviour from small scale elemental tests, which can then be accommodated in mathematical solutions of boundary value problems; these in turn can be scrutinised by large scale model tests, applied to real field problems, and verified by post-constructional field observations.

The rigorous analysis of real field problems would appear to be intractable due to the inherent inhomogeneity of natural soil deposits, the complex stress states developed in the soil mass due to the interaction of soil and structure, and the complications arising from constructional processes. Consequently, in attempting to predict field performance, the engineer must consider the results of any analysis in the light of his experience, intuition, and engineering judgement.

The assessment of contemporary analytical techniques and the development of engineering judgement can be greatly enhanced by information obtained from model tests on artificially prepared beds of uniform sand or remoulded clay. However, even with such idealised testing conditions, the exact solution of boundary value problems is formidable due to the lack of a general, physically sound, mathematical relationship between stress and strain.

Small scale laboratory experiments, in which the specimen of soil is considered to represent an element of soil in the soil mass, are essential to the evolution of any mathematical theory of mechanical

behaviour. Generally, geotechnical problems are of a three dimensional nature and the stress conditions applied to an element of soil in the ground are such that the three principal stresses are all different. It is, therefore, necessary to develop apparatuses capable of applying such complex stress states to small homogeneous specimens of soil in the laboratory, and much recent research has been directed to this particular problem. The results of these investigations have, however, tended to emphasize the complexity of the problem rather than indicate a tractable solution.

Two dimensional problems, on the other hand, are far more amenable to rigorous examination, both experimentally and theoretically. Thus, the plane strain condition, in which no movement occurs in the direction of the intermediate principal stress, is of particular importance in the development of soil mechanics theories. It is for this reason that the present research program was initiated, and it is anticipated that it will form part of a more extensive, detailed investigation into the plane strain behaviour of soils.

Whilst some axisymmetric compression tests were performed in the course of the research program, this thesis is primarily concerned with the deformation of sand in plane strain and a new plane strain apparatus was developed for this purpose. Details of the apparatus design and sample preparation procedures adopted will be provided in Chapter 2. Particular attention will be given to the need to prepare homogeneous specimens of sand at pre-selected initial porosities and a vibratory method of controlling the initial porosity of saturated sand specimens will be described.

The results of triaxial compression tests and plane strain tests, performed on a fine sand in the course of the research program, will be presented and discussed in Chapters 3 and 4. These two chapters constitute a phenomenological study of the shearing behaviour of sand

and include the results of tests in which cycles of unloading and reloading were performed. Both strength and deformation characteristics will be considered and detailed observations of the formation of rupture planes will be presented.

Having presented the experimental data obtained from the testing program, the second part of the thesis will be devoted to theoretical considerations.

In Chapter 5, a number of particulate mechanics theories will be reviewed, a critical appraisal of theories pertaining to regular packings will be presented, and the experimental results presented in previous chapters will be re-analysed in terms of the stress-dilatancy theory.

In the absence of a general, physically sound, theoretical stress-strain relationship, boundary value problems can be analysed using sophisticated numerical techniques, e.g. the finite element method. Such analyses can take into account the non-linear stress-strain response of soil, but require details of the complete stress-strain behaviour obtained from elemental tests. This is most economically achieved by fitting mathematical functions to the observed behaviour. The ability of simple parabolic and hyperbolic functions to represent triaxial compression and plane strain stress-strain curves will be assessed in Chapter 6.

Since a knowledge of the intermediate principal stress is necessary to a complete understanding of the plane strain behaviour of soils, attempts were made to measure the intermediate principal stress during plane strain tests conducted in the course of the research program. In Chapter 7, the experimental results will be compared with theoretical predictions based on the stress-dilatancy interpretation of Mohr's circles of stress and strain.

Finally, in Chapter 8, a few concluding remarks will be added to complete the presentation.

1.2. Details of the sand tested.

The sand used in all the tests reported in this thesis was a fine sand, passing No. 100 and retained on No. 300 B.S. sieves, and consisted predominantly of sub-rounded quartz particles. The specific gravity of the particles was determined according to BS 1377 and the average value obtained, from four tests, was 2.649.

The maximum porosity was found to be 48.96% (mean of ten tests) using the air-dry 'rapid tilt' method recommended by Kolbuszewski (1948). The minimum porosity was taken as 37.98%, which was the minimum value achieved by the vibratory method of sample placement described in Chapter 2.

There was not sufficient sand available to avoid having to re-use the sand, once tested. Consequently, the batch of sand was washed, dried, and re-sieved periodically, and any excess fines were removed. The amount of fines collected over the complete testing program only amounted to about 2%, by weight, of the total batch, thus indicating that this should have had an insignificant effect on the test results.

1.3. Terminology used.

The majority of the terms used in this thesis are common to much current soil mechanics research and as such are widely accepted and unambiguous. Certain terms, however, may convey different meanings to different investigators. Particular attention will be given to clarifying the meaning of any possibly ambiguous terms and definitions of symbols used will be provided at relevant points in the text.

All the experiments were conducted under fully drained conditions and the effective and total stresses were, therefore, assumed to be equal. Consequently, in order to simplify the presentation, stresses have been denoted by the symbol σ, except where any ambiguity is possible, in which case the conventional symbol σ' has been used for effective stress.

Natural strains are used throughout, and are expressed as percentages, compression being taken as positive.

During the test program a number of triaxial compression specimens were consolidated under the pressure applied to the surrounding cell water, without any additional vertical load being applied via the plunger. In the text, this is referred to as ambient consolidation; other workers have used the terms isotropic, or spherical, consolidation to describe this process.

CHAPTER TWO

2. APPARATUS DESIGN AND SAMPLE PREPARATION TECHNIQUE.

2.1. General design considerations.

In order to obtain consistent test results from which deformational behaviour can be fully understood, either empirically or theoretically, it is essential that the measurement of stress and strain is as accurate as possible. It is also vital to ensure that the loads or deformations applied to a specimen are those that are intended and that the measured quantities are solely due to material behaviour and not partly the result of 'apparatus interference'.

It has long been realised that, whereas the strength of soil specimens could be obtained relatively accurately, the stress-strain characteristics remained ambiguous due to the non-uniformity of the specimen deformation and the inadequacy of mensural precision. Consequently much recent development has concentrated on the rectification of these deficiencies.

Implicit in the use of boundary measurements of stress (or load) and strain to evaluate triaxial test data is the assumption that the soil sample is initially homogeneous and deforms uniformly throughout the test. It is therefore desirable to conceive of an apparatus which will achieve such a condition. Although recently developed analytical methods, such as finite element analysis, do not require such restrictions, Perloff and Pombo (1969), Girijavallabhan (1970), these more sophisticated analytical techniques, at present, invoke assumptions which have not been shown to apply to soils.

The most conspicuous indication of non-uniform conditions in the conventional triaxial apparatus is the commonly observed 'barrelling' of initially cylindrical samples when tested. These non-uniformities are due

to end restraint caused by friction between the rigid platens and the sample.

An extensive series of investigations into possible techniques to overcome specimen end restraint was carried out at Manchester University and was reported by Rowe and Barden (1964). The most successful method was found by interposing lubricated rubber membranes between the specimen and the end platens.

By using this 'free' end technique, virtually complete elimination of any 'barrelling' of the sample was achieved. A comparison with tests performed using 'fixed' ends showed that tests with frictionless end conditions produced lower peak strengths and much flatter stress-strain curves at peak. A comparison was also made between tests conducted on samples of height to diameter ratios of 1:1 and 2:1 which resulted in the adoption of 4" high by 4" diameter samples, with 'free' ends, since the results were more uniform and the taller specimens tended to be unstable. It was also found that the short specimens produced multiple failure surfaces which did not occur until very large strains were reached.

The strength of soil when tested in the triaxial apparatus varies with the height to diameter ratio of the specimen. However there exists a range of specimen proportions over which the strength is insensitive to the ratio of height to diameter. If the ends of the specimen are not lubricated then the strength increases with decrease in the height to diameter ratio if the ratio is less than 2:1. Consequently the ratio of height to diameter normally used for triaxial testing is either 2:1 or 2.5:1.

Bishop and Green (1965) found that, by using a sandwich of two membranes with silicone grease between, the strength of 1:1 samples with frictionless ends could be reduced further, to agree with the strength as given by 2:1 samples with fixed ends; and that further increase in the number of membranes used had no significant effect on strength.

Further evidence to support the use of lubricated platens was provided by Kirkpatrick and Belshaw (1968), and Kirkpatrick and Younger (1970). Triaxial compression tests on dry sand using both 'free' and 'fixed' end platens were performed in which radiographic techniques were used to investigate the variation of strain within the samples. Kirkpatrick and Belshaw (1968) demonstrated that lubricated platens produce relatively homogeneous strain conditions within the sample and that equality of radial and tangential strain exists; whereas the use of rough platens caused the radial and tangential strains to be widely divergent over large regions of the sample and non-uniform strain conditions to occur throughout the sample. That the rough platens produced 'rigid' zones at the ends of the specimen, as suggested by earlier investigators, was clearly demonstrated. Kirkpatrick and Younger (1970), using non-tilting platens, showed that similar improvements in the homogeneity of axial strain could be achieved using lubricated platens.

The measurement of the change in the dimensions of the specimen may be achieved by either direct or indirect techniques. Axial strain is usually calculated from the axial displacement of the piston, measured relative to the top of the cell by means of a dial gauge. The volumetric strain is determined from the volume of pore-fluid traversing the specimen boundary at the drainage connections, and for tests on saturated sand samples this can be measured simply by connecting direct to a burette, the size depending on the accuracy required. Lateral strains are more difficult to measure and are usually indirectly obtained from the knowledge of the volumetric and axial strains.

Deformation can also be measured using dynamic techniques which normally involve the use of linear variable differential transformer transducers (L.V.D.T.'s) and the replacement of dial gauges by such instruments is an obvious development. Radial and internal measurements pose greater problems. Embedded transducers have been tried, Truesdale and Rusin (1963), and Januskevicius and Vey (1965), but problems of calibration

and interference of the instrument on sample behaviour have not yet been resolved. Greater success has been achieved in the measurement of lateral boundary strain using 'strain belts', Amirsoleymani (1966) and Holubec (1966). However, dynamic techniques suffer either from sealing problems or the necessity to use a fluid other than water in the cell in order to prevent possible electrical breakdowns. Even if such problems are overcome, the instruments necessarily impart a finite force on the sample ans also tend to be inconvenient in size, necessitating the use of larger than normal confining cells.

Some investigators have used optical methods for determining the change in sample dimensions: e.g. Escario and Uriel (1961), Roscoe, Schofield and Thurairajah (1963), and Lee and Morgan (1966). The advantage of optical methods is that the complete sample profile can be determined. Dudley (1971) used both optical tooling and photogrammetry to determine the change in profile during the triaxial test. That photogrammetry allows a record of the sample shape to be obtained by one simple brief action makes it more attractive than other optical techniques. However, such information is also obtainable using radiographic methods which of course provide much more, in the form of internal strain patterns, and would appear to provide the greatest potential in the furtherance of research into the deformational behaviour of soil.

2.2. Selective review of plane strain apparatuses.

Comprehensive reviews of previous laboratory investigations, covering conventional triaxial, plane strain and multi-axial compression apparatuses, direct and simple shear devices, and hollow-cylinder and torsion tests, have been provided by Green (1969) and Dyson (1970), and the reader is directed to these references for information not provided herein. The review provided in this section will be restricted to apparatuses that have had a direct influence on the design of the apparatus used in this research program.

According to continuum mechanics theory, the plane strain condition is said to exist when no movement, either boundary or internal strain, occurs in one of the directions of principal stress. An apparently simple method of applying such conditions to soil samples is to use cuboidal specimens constrained in one direction by rigid side platens rigidly connected together.

However, when developing such an apparatus, it is necessary to determine the extent to which the test results are due to interference of the apparatus rather than true soil behaviour. Consequently it is useful to determine the extent to which platens are essential and the conditions under which they may be omitted.

Kummeneje (1957), reported by Bjerrum and Kummeneje (1961), performed tests on specimens of dry sand, 120mm high, 40mm wide, the length being made long enough (300mm and 600mm) that the friction between the axial platens and the sample was sufficient to induce a condition that approximated to plane strain. Measurements of sample length, before and after the tests, indicated that the quasi-plane strain condition was satisfied.

Cornforth (1961), using the Imperial College plane strain apparatus, carried out a few tests with the side platens removed, and concluded that peak strengths corresponding to the plane strain condition could be achieved, provided that the specimen was made sufficiently long. Deformational characteristics were slightly affected by the omission of the end platens although the paucity of results precluded any definite conclusions being made.

Lee (1970), from only three tests, concluded that the use of side platens was essential, since the results showed that, whilst the plane strain tests exhibited greater strengths than triaxial compression tests, a significant difference in strength was recorded depending on whether or not the side platens were used. This difference would appear to be due to the inadequate amount of axial platen friction developed in the tests with

no side platens, the size of the specimens being 1.1" by 2.8" in cross-section and 2.4" high.

Marachi et al (1969) reported a series of tests to investigate the effects of varying the dimensions of cuboidal specimens tested with and without the side platens in position. The test results demonstrated that, when the side platens were used to maintain the plane strain condition, variation in the cross-sectional dimensions had no significant effect on the strength-porosity relationship. However, when tested without the side platens the strength varied from a value near the triaxial compression strength, for specimens of square cross-section, to a value slightly less than the plane strain strength, for specimens of long rectangular cross-section.

They also conducted a series of tests to investigate the amount of intermediate principal strain which could be permitted before the strength exhibited differed significantly from that obtained in a 'true' plane strain test. Variation of the intermediate principal strain was obtained by inserting rubber washers between the side platens and the clamping nuts of the tie bars, the amount of strain permitted being dependent on the thickness and number of washers used. It was found that provided the ratio of intermediate to major principal strain at failure was less than 0.25 no significant deviation from the plane strain strength value was obtained.

Marachi's results must however be treated with caution since there was no provision of any form of lubrication between the axial platens and the specimen. In fact the variation in strength obtained for the triaxial compression specimens was as much a function of the shear stresses developed along the axial platen/specimen interfaces as of the sample dimensions.

It is concluded that the use of side platens is essential for the investigation of plane strain behaviour, especially for the determination of deformation characteristics, since lubricated axial platens are necessary

to achieve uniform deformation, thus precluding the use of long specimen lengths to induce higher strengths caused by platen friction.

The usual form of plane strain apparatus is typified by that developed at Imperial College, London, and used by Wood (1958) to perform tests on a compacted moraine. The specimen was 4" high, 2" wide, and 16" long, enclosed in a specially manufactured membrane. The specimen was loaded via two pistons passing through the top of a specially designed cell and bearing onto a rigid top platen at the quarter-length points, rotating bushes being used to reduce piston friction. The cell pressure and the axial load were applied in an identical manner to the conventional triaxial apparatus. An ingenious method was used to maintain the plane strain condition and simultaneously determine the intermediate principal stress during a test. The strain control device, referred to as the 'end clamp', consisted of two rigid aluminium platens in contact with the ends of the specimen, and connected by four symmetrically positioned tie rods. Silicone grease was smeared onto the contact faces of the platens to reduce end friction. In order to determine the intermediate principal stress, a rigid disc was attached to one of the end platens. The remote face of the disc was attached to the rubber diaphragm of a pressure cell which was connected to a null indicator system. During a test the mercury thread null indicator was balanced to maintain a constant volume of de-aired water in the pressure cell and thereby prevent any longitudinal displacement of the specimen. By noting the pressure required to balance the null indicator, the deviator stress applied to the ends of the specimen could be deduced, although uncertainties existed as to the correct effective working area of the diaphragm. The apparatus was also used to investigate the plane strain behaviour of sand, Cornforth (1961), and clay, Wade (1963). Cornforth's test results clearly indicated that the specimen deformation was highly non-uniform due to friction along the axial platen/sample interfaces, which would also produce errors in the determination of the

intermediate principal stress, since a certain amount of longitudinal deformation would be prevented by friction alone, without the aid of the end clamp.

A similar type of plane strain apparatus was developed at Manchester University, Wightman (1967), although no provision was made to measure the intermediate principal stress. The specimen size was 4" by 4" by 8" long and polished stainless steel side platens formed an integral part of the pedestal which was screwed into the cell base. Deflection of the side platens was prevented by two tie rods near the top. The bottom axial platen sat inside the cuboidal sample sheath and was screwed down onto an O-ring set in the pedestal. The sample sheath was sealed at the top between two plates which were bolted together to form the top axial platen, the procedure being facilitated by the use of a specially designed clamping frame. Lubricated membranes were used on both axial and side platens in order to minimise non-uniform deformation. Axial deformation was measured inside the cell using dial gauges mounted on rods screwed into the cell base, and an internal proving ring was used to measure the axial load.

This apparatus was modified by Ismael (1969). The cuboidal sample sheath was dispensed with and a standard 6" dia. triaxial membrane was used, which was drawn into a rectangular section by applying a vacuum to the former. The membrane was sealed by O-rings in the normal manner on 6" dia, discs attached to the 6" by 4" rectangular top and bottom platens, the transition from rectangular to circular sections being smoothed out by an epoxy based plastic filler material. This modification greatly simplified the preparation of samples. From a series of tests on samples of various heights, which exhibited similar stress-strain behaviour, a sample of dimensions 4" by 4" by 6" long was adopted. The plane strain condition was maintained by polished rigid side platens, separate from the pedestal, and supported against the specimen by four tie rods. A load cell, inside the cell, was used to determine the axial load.

In a later development, a further load cell was incorporated to determine the intermediate principal stress, Tong (1970).

Plane strain tests can also be performed in certain multi-axial apparatuses and such devices may well afford a greater degree of control in the intermediate principal stress direction; although the construction and operation of multi-axial apparatuses are far more complex than plane strain devices.

Green (1969) developed an apparatus which was referred to as an independent stress control (ISC) cell although the sample was deformed in two directions by strain controlled boundaries using two pairs of non-tilting, rigid, lubricated platens. The apparatus was contained within a large triaxial cell and the cell pressure provided the stresses in the third direction. The axial load was measured internally by an encapsulated transducerised proving ring, and a loading frame (the ISC belt) controlled the deformation in one of the two lateral directions. The ISC belt incorporated a hydraulic ram at one end and an encapsulated transducerised proving ring at the other end. The belt was suspended on four fine brass wires so that the line of action of the belt remained coaxial with the specimen during a test. The deformation in the ISC belt direction was measured directly between the belt platens using a pair of encapsulated dial gauges.

The cross-section of the axial platens varied from square at the active face, through a transition, to circular so that the cylindrical sample sheath could be easily sealed by O-rings. Platen interference at the edges was minimised by varying both the size of the lateral platens and the sample dimensions to provide adequate initial gaps between the vertical and lateral platens. Due to the presence of the ISC belt platens it was not possible to enlarge the axial platens in that direction. Consequently small errors would result in the deduced values of stress and strain.

At the commencement of the research program described in this thesis it was intended that the author would use an apparatus developed by Dyson (1970), and first reported by Bennett(1969). However, the author had serious reservations about the performance of Dyson's apparatus and, after carrying out a series of tests to evaluate its limitations, elected to develop a new plane strain apparatus.

The new apparatus, which is described in the following sections, incorporates features of previous apparatuses used at Manchester University and Imperial College, London; plus certain details of the apparatus designed by Dyson. It is therefore relevant to review Dyson's apparatus but, rather than contain the review in this chapter, the apparatus together with results and assessment of the evaluation program are presented as a separate entity in Appendix A.

2.3. Apparatus design.

2.3.1. General details.

In order to avoid errors in the determination of axial deviator load, due to friction between the plunger and the cell bushing, it was decided to measure the load inside the cell using a load cell. The triaxial cell used by Dyson was too small to accommodate the load cell and so a larger cell was necessary. However, instead of using the manufacturer's cell base a new base was designed to fit the cell and to accommodate the various fittings required, including those related to Dyson's apparatus. Four studs were fitted into the underside of the base so that by the use of two stainless steel square bars, which passed under the pedestal of the loading machine, the cell could be firmly clamped to the machine.

The axial load cell was of the instrumented plunger type and since the plunger diameter did not correspond to the diameter of the cell bushing it was necessary to insert a bushing which would ensure the verticality of the plunger and also prevent excessive leakage of the cell water.

Due to the design of the axial load cell there was insufficient space to use dial gauges bearing on the top axial platen. Therefore an external dial gauge had to be used, but errors due to cell expansion were eliminated by providing a pedestal fixed to the cell base. The method adopted was similar to that used by Green (1969). One of the tie rods which bolted the cell to the base was omitted and was replaced by a brass rod which extended above the top of the cell to support the pedestal for the dial gauge. Since no proving ring was used the dial gauge was fixed to the cross-beam of the loading frame.

The change in volume of the specimen was determined using two 10ml burettes, graduated to 0.02ml. The two 10ml burettes together with a 50ml burette, which was used only for sample preparation, were interconnected so that each could be switched into the drainage system in turn, and the water level in the burettes not in use could be adjusted without interfering with the volume change readings.

De-aired water was used to fill the cell and the water was pressurised by means of a mercury pot control system of the type described by Bishop and Henkel (1957). Normally cell pressure is recorded on a Bourdon gauge. However, Bourdon gauge dials are often inaccurate due to entrapped air, and must be calibrated. Moreover, the divisions on the scale are relatively large and interpolation is often necessary to determine the pressure readings. If the deviator stresses are considered the effects of errors in cell pressure readings are small but, when test results are expressed in terms of stress ratios, then very small errors in cell pressure values have a significant effect on the results. It was therefore considered desirable to insert a pressure transducer into the supply system to record the cell pressure. For this purpose a transducer block was used similar to the type used by Dyson (1970). The transducer block consisted of a rigid, cylindrical, brass block into which a pressure transducer was permanently fixed. Two water supply taps and a de-airing screw were interconnected with the transducer through small

diameter holes in the block, and the whole assembly was attached to a Klinger tap at the side of the cell base.

Dyson used an oscillograph to record the outputs from his electronic measuring devices, but this method had certain limitations. In order to obtain the required accuracy it was necessary to use galvanometers which gave a full scale deflection of more than two paper-trace widths. Therefore it was necessary to reset the galvanometers during a test. Consequently any drift in the datum setting could not be accounted for. Interpretation of the paper trace output was rather tedious. In the tests reported in this thesis all load cell and pressure transducer outputs were recorded on a digital voltmeter which was incorporated into a datalogger. Details of the calibration of such instruments are given in Appendix B.

2.3.2. Sample sheath and axial platens.

When preparing cuboidal test specimens a cylindrical sample sheath may be used which is pulled into the required shape by evacuating the space between the sheath and the rectangular specimen former; alternatively a preformed sample sheath may be used which fits the initial specimen dimensions. If a cylindrical sheath is used which is slightly oversized then wrinkles will occur. Reades (1972) found that the manufacturer's specification did not meet the required tolerances to prevent this. Tong (1970) reported that the commercially manufactured preformed sheaths used in the original plane strain apparatus at Manchester University were prone to leaks at the corners.

Early plane strain apparatuses employed preformed sheaths, Cornforth (1961) and Wightman (1967), which were sealed, top and bottom, between flanges and this necessitated rather elaborate setting-up procedures. Green (1969) simplified the method of sealing cuboidal specimens by varying the cross-section of the axial platens from rectangular to circular so that a simple O-ring seal could be used.

Dyson (1970) evolved a simple process of manufacturing preformed latex rubber sheaths. This involved dipping a perspex former into a tank of pre-vulcanised, ammonia-stabilised latex, and, after an elapsed time, which depended on the thickness of the sheath required, the former was slowly withdrawn. Upon drying the thin latex film coating the former took up the same shape as the former. The latex was then peeled off the former and tested for leaks. Complete details of the manufacturing process are given by Dyson (1970), Appendix A.

Since the membranes used by Dyson were found to be reliable the same method was adopted in the present research program to manufacture preformed specimen sheaths.

Because of the simplicity of the sealing method involved, and for other reasons dealt with in section 2.4, the axial platens used in the present apparatus were based on Green's design, although the drainage details are of the type used by Dyson for his top stress-cell.

It is not possible to use the same axial platens for both triaxial compression tests and plane strain tests on identical sized specimens, and also ensure that the sample does not expand beyond the edges of the platens during the test. Therefore, for convenience, one size of platen was used and the sample dimensions were altered to suit the type of test.

All specimens were approximately 60mm high but the lateral dimensions varied. For triaxial compression tests the specimen size was approximately 60mm by 53mm by 51mm which allowed for a lateral expansion of about 10% before the sample overlapped the edges of the platens(the platen dimensions being 58mm by 65mm). Plane strain test specimens had dimensions of 60mm by 59mm by 51mm which allowed an overlap in the restrained direction and permitted about 25% lateral strain to be accommodated on the platens, in the other direction. Two formers were therefore required. Fig. 2.1. shows the two formers used for the new apparatus, B for plane strain tests and C for triaxial compression tests, together with the former, A, used by Dyson.

Each axial platen was machined from one piece of aluminium alloy. The detailed design of both axial platens is shown in Fig. 2.2. Drainage was required at both ends of the specimen and this was facilitated by filter paper drains connected to rectangular bauxilite porous stones set into peripheral channels in the rectangular section of the platens. The bottom platen was screwed into the cell base against an O-ring set in the bottom of the platen. The top platen was recessed at the top to reduce self-weight.

In order to obtain uniform lateral deformation of the specimen, during a test, a sandwich of two lubricated membranes was interposed between each axial platen face and the specimen.

2.3.3. Side platens.

The conventional method of ensuring zero lateral strain in one direction is to use rigid side platens acting against opposite vertical faces and bolted together to prevent movement. This ensures that no boundary movement can occur although strains may exist internally in that direction.

The plane strain concept also requires that there are no shear stresses on planes normal to the direction of zero movement. In order to prevent shear stresses developing on the side platen/specimen interfaces, a lubricated membrane technique is used similar to that used on the axial platen/specimen interfaces. This will permit a slight boundary movement due to the compression of the membranes and grease. This small amount of movement has to be tolerated unless a much more complicated apparatus is used, in which any lateral movement can be compensated for by inward movement of the side platens. However, it would appear that satisfactory compensation is difficult to achieve due to the varying rate of compression of the lubricated membranes during a test, Reades (1972).

Although some plane strain tests with rigid side platens were carried out in this research program, the majority of the plane strain

tests were performed using flexible side platens.

If the boundaries between the specimen and the side platens are flexible then, of course, a true plane strain condition is not obtained. This fact leads to an anomoly in the terminology used, but, for simplicity, the term plane strain will be retained when considering tests using flexible side platens.

It is worthwhile to differentiate between two possible types of flexible platen. The author would term the first type as being an 'active' platen, and the second a 'passive' platen.

The 'active' type of flexible platen is one in which the stresses acting on the specimen boundary are controlled by some external mechanical device, as in the soil box used by Ko and Scott (1967) and modified by Menzies (1970). The 'flexible bag' therefore applies a uniform stress to the specimen and this results in a non-uniform boundary deformation.

The 'passive' type of flexible platen is one in which the water-filled 'flexible bag' is sealed off and when the specimen attempts to expand against the platen the response is an increase in the pressure in the bag due to the incompressibility of water. An example of this type of flexible side platen was used by Dyson (1970) when conducting plane strain tests.

With the 'passive' type of flexible side platen, if outward movement of the specimen boundary occurs at some point on the face of the water-filled bag then, since the bag remains at constant volume, there must be an equal and opposite amount of movement elsewhere on the boundary. Consequently there is a redistribution of strain at the specimen boundary and the average lateral movement is limited to that due to compression of rubber membranes and grease film.

It must also be remembered that, although a 'passive' platen will not produce a true plane strain condition, the plane strain condition does not necessarily occur on site; it is merely a convenient assumption

which is used to analyse certain field problems. The author considers that the condition obtained using 'passive' flexible side platens, whereby lateral movement may occur in opposite directions at different locations in the soil in such a way that the average lateral strain is zero, may be a better simulation of actual site conditions than the true plane strain condition. It is therefore of interest to compare the results of tests using both simulations, and to fully investigate specimen behaviour when 'passive' flexible side platens are used.

The comparison of flexible and rigid platens is also required since it has not yet been established that specimen behaviour is not influenced by the type of boundary condition employed. The clarification of this point has become important with the increased amount of investigation recently carried out on the design of multi-axial apparatuses, Green (1969), Menzies (1970), Procter and Barden (1971).

2.3.3.1. Rigid side platens.

At an early stage in the investigation a number of plane strain tests were performed, using rigid side platens, in which no provision was made to determine the intermediate principal stress. The rigid side platens were made of aluminium alloy and were bolted in position by means of four $\frac{1}{8}$" dia. stainless steel rods. In order to prevent any lateral force from being transmitted by friction to the cell base each side platen was seated on two ball bearings set in recesses in the bottom of the platen.

2.3.3.2. Flexible side platens.

The flexible side platens used in this research program were developed from the 'side stress-cells' used by Dyson (1970), which are described in Appendix A. Dyson's design and the present design are contrasted in Fig. 2.3. The main differences are the method of sealing and the material used for the rubber bag.

Dyson used latex rubber bags made by the same dipping technique as used for the cuboidal sample sheaths. In order that the average lateral strain in the intermediate principal stress direction remains zero it is vital to ensure that no change in volume of the rubber bag occurs. Because of shrinkage, and distortion with continued use, this was difficult to achieve using latex rubber as the bag material.

In the present design the bags were made of silicone rubber (Silcoset 105), as used by Lewin (1971). This material possesses excellent compressive properties but is weak in tension. It can be formed into any shape by casting in a suitably designed mould, and requires no heat treatment. Shrinkage is negligible and under test conditions it proved to be durable and retained its original shape after continuous use over a period of twelve months.

Initially, the sealing was attempted using the same method as Dyson, that is, the backing plate was secured to the side frame by screws passing through holes in the flange of the rubber bag. However the silicone rubber tended to split around the punched holes in the flange when the assembly was screwed together. As shown in Fig. 2.3, the method finally adopted was to seal against a thick, fully confined flange by bolting the backing plate to the side frame through holes remote from the rubber bag.

Dyson concluded that, in his tests, the plane strain state was not achieved throughout the test due to exposure of the rubber bag during the early part of the shear stage. In order to minimise this shortcoming certain other modifications were made; the thickness of the rubber was increased at the edges and the complete face of the side platen, including the rigid confining rim, was covered by a 2mm thick sheet of soft rubber. Also, in order to ensure that the bag fitted perfectly into the compartment formed by the side frame and the backing plate, the bag was cast insitu.

The method of manufacturing the bag and assembling the side platen is illustrated in Figs. 2.4-2.6. The side frame was placed on a polished square aluminium plate and positioned by four pins passing through the holes used for the tie rods. A measured amount of silicone rubber solution, having been thoroughly de-aired, was poured into the mould and then, using the pins as guides, a perspex former was placed on top. The rubber solution was thereby displaced to fill the void between the upper former and the lower mould. A weight was then placed on the perspex former to provide a slight pressure and the assembly was left overnight to allow the rubber solution to set.

After the rubber had set, with the perspex former still in position, the assembly was turned over and the aluminium plate and pins were removed. A sheet of soft rubber was then glued to the exposed face of the platen. When the adhesive had set the perspex former was removed and replaced by the aluminium backing plate, which was then bolted to the side frame.

To prevent the silicone rubber from adhering to the confining components, the inside of the lower mould and the surface of the plate and the upper former were lightly sprayed with a silicone spray. Also, it was found that removal of the plate and the former was assisted if the complete assembly was placed in an oven at 30°C for a few minutes.

The rubber bag was filled with de-aired water through saron tubing via a connection in the backing plate at the bottom of the bag compartment. Air was removed through a de-airing screw near the top of the compartment. The supply tubes for the side platens were connected to a common duct in the base of the cell and the pressure in the bags was recorded by a pressure transducer set in a transducer block at the side of the cell base.

Calibration tests for the flexible side platens are described in Appendix B.

2.4. Sample preparation technique.

2.4.1. Introduction.

The importance of initial specimen homogeneity and subsequent uniform deformation, in tests employing boundary measurements of stress and strain, was pointed out in Section 2.1. It is also desirable to be able to reproduce initial porosities within close tolerances so that a reliable comparison can be made of the deformational behaviour as other test conditions are varied.

Since the placement of particulate material is effected within a gravitational field the resultant specimen must be anisotropic, the degree of anisotropy depending on the geometrical arrangement of the particles. Porosity, being a scalar property, cannot define the internal geometry of the specimen. Recently attempts have been made to measure the anisotropic structure of sand by radiographic techniques, Arthur and Dunstan (1970). They concluded that all the hitherto methods of measuring structural parameters were incapable of defining the irregular packing of granular material.

It can be seen that the term homogeneity, applied to the state of a granular mass, in no way implies isotropy. For the purpose of this investigation a sample will be deemed to be homogeneous if the distribution of porosity within the specimen is uniform.

The porosity distribution within a specimen can be investigated by impregnating the specimen with a suitable chemical grout and then analysing the distribution of particles over the face of a thin section of the specimen, Windisch and Soulié (1970), Ramamurthy (1971). However, the above techniques were outside the scope of this research program and knowledge of the structural composition of specimens was limited to that obtained from overall porosity measurements.

An indication of porosity uniformity within the sample could be obtained from observations of subsequent deformation during a test. It

has frequently been observed that the base of a triaxial compression specimen expands more than the top. Green (1969) demonstrated that this was not due to gravitational effects, and it would appear that this phenomenon is due to porosity variations along the height of the specimen as a result of the sample preparation technique used.

In order to produce specimens of sand for subsequent testing in a triaxial apparatus it is necessary to form the specimen within a mould the internal dimensions of which are identical to the desired initial specimen dimensions. The sand may be deposited as a continuous rain of particles, either under water or in air; or the sand may be spooned into the mould. If the sand is deposited in air then the specimen may be tested dry; or if a saturated specimen is required then saturation may be obtained by flooding the voids, although it is difficult to ensure full saturation.

The initial overall porosity can be controlled by varying the height of fall and intensity of rain if the sand is deposited in air but if deposition under water is used this is restricted due to the small terminal velocity of the particles.

A saturated sample may be densified by either tamping or vibrating. The most common method of density control consists of building the specimen in layers by spooning the sand into the mould and then tamping each layer. It appears that, with an appreciable amount of experience, consistent overall porosities can be achieved. The method is, however, limited to a range of densities from very dense to medium dense. Loose sand specimens are notoriously difficult to prepare and, to the author's knowledge, no method has yet been found which encourages uniform deformation of such specimens when sheared.

At the start of the research program it was decided that a method of sample preparation was required which gave results at least as consistent as the 'spooning and tamping' method, without the need to develop a similar level of personal skill. In addition, it was thought

to be advantageous to develop a method which did not produce a layered specimen.

The author elected to deposit the sand as a continuous rain, under water, and to use a vibratory method of density control. Before describing the method adopted and assessing the results, it is of interest to review previous vibratory densification methods and the application of such techniques to triaxial sample preparation.

2.4.2. Review of vibratory methods of density control.

It is commonly accepted that vibrations cause a densification of sand, and a number of investigators have studied this effect. The topic has been studied from various aspects including strength reduction, liquefaction, means of obtaining maximum compaction, and control of compaction (i.e. density) in general. Most laboratory experiments have been conducted on laterally confined specimens with loads applied over the full surface area (controlled dynamic stress tests) or on samples placed on a vibrating table (controlled frequency tests).

This review is primarily concerned with density control and one of the most comprehensive investigations into this aspect was implemented by Selig (1963). The investigation was restricted to a single, uniformly graded sand in an air-dry condition; and only one size of container was used since an earlier study by Alyanak (1961) had indicated that the diameter of the mould was not a significant parameter. The vibration unit was an electrodynamic vibration exciter which provided a sinusoidal, unidirectional (vertical) force; the frequency and amplitude being adjustable. In the majority of the tests the sand was poured into the mould before the mould was vibrated. The results showed that, with all other factors constant, density increased with an increase in any one of the four vibration parameters: amplitude, frequency, velocity, and acceleration. The best correlation was achieved by plotting acceleration against frequency thereby obtaining contours of density. It was also

noted that, if any one of the four vibration parameters was increased beyond a certain value, then the density began to decrease thereafter.

These observations, in general, agreed with the work of Alyanak (1961) who, although primarily concerned with maximum density, noted that the porosity decreased, with increasing intensity of vibration, down to a minimum and then started to increase. Alyanak, who used a mechanical vibrator, concluded that there was an optimum value of maximum acceleration, for the particular frequency used, which gave a minimum value of porosity.

Selig (1963) also conducted a series of tests in which the sand was deposited during vibration, and compared the results with the test series in which the sand was deposited before vibration. At low acceleration levels the results of each series was the same but at accelerations greater than 'optimum' the series in which the sand was deposited during vibration gave higher densities. In fact Selig claimed that there was no density decrease at high acceleration levels for tests in which deposition occurred during vibration.

Appreciating that the density of a specimen prepared under constant vibration conditions need not necessarily be uniform, Selig investigated the variation of density within the specimens. When the sand was poured into the mould with a fixed height of fall and no vibration was applied the density was found to increase from the top of the specimen to the base. The density variation in specimens in which the sand was deposited before vibration was found to vary with acceleration level. At low levels of acceleration the density decreased appreciably from the top to the base of the specimen. The variation in density was less at higher acceleration levels. Specimens which were deposited during vibration were found to have a random distribution, giving an appearance of being uniform throughout the specimen.

Prakash and Gupta (1967) performed both vertical vibration tests and horizontal vibration tests. They obtained the same characteristic curves

as previous researchers for tests in which the specimens were vibrated vertically. Horizontally vibrated specimens, however, did not decrease in density at higher acceleration levels. They also found that horizontal vibrations were more effective than vertical vibrations in that they required far less time of vibration to reach the terminal density. Prakash and Gupta also concluded that coarse and well-graded sands are more easily compacted than uniform fine sands; and comparable degrees of compaction can be achieved whether the sand is dry or saturated.

D'Appolonia (1968) conducted controlled acceleration tests and investigated the effect of surcharge on the density obtained. For tests in which no surcharge was applied the density achieved was found to correlate with acceleration. The characteristic density-acceleration curve (Fig. 2.7) obtained agreed with previous investigations. Very little densification occurred until the acceleration reached 1g; most of the densification occurred at about 1g; maximum density was obtained at about 2g; and the density decreased with further increase in acceleration level. D'Appolonia found that specimens vibrated with a constant surcharge pressure acting over the surface of the sand behaved in a similar way to specimens tested without a surcharge pressure. No densification occurred below a critical level of acceleration. This critical acceleration was a function of the static confining stress and the initial density. Above the critical acceleration the density achieved was related to the confining stress, higher densities being associated with lower confining stresses.

Whitman and Ortigosa (1968) found that there were three distinct ranges of acceleration with different densification characteristics. They explained the behaviour by considering the dynamic stresses set up when vibrations are applied to sands. There was relatively little densification for accelerations less than 1g and Whitman and Ortigosa suggested that the densification that did occur was due to acceleration-induced dynamic stresses rather than the accelerations alone. The reasons for the

considerable densification that occurred over the range of acceleration from 1g to 2g were thought to be twofold: first, because of intervals within each cycle of vibration when the particles were more of less free of each other and thus were able to re-orientate into denser packing arrangements; and second, the impacts which followed these 'free-fall' periods produced large dynamic stresses which forced the particles together. They were unable to clarify the reasons for the decrease in density which frequently occurred when the acceleration level was greater than 2g. This decrease in density they termed 'overvibration'. They found that the degree of 'overvibration' was influenced by the test conditions and that with some containers no overvibration occurred. As a result of their research, which also included controlled dynamic stress tests, Whitman and Ortigosa concluded that it is the dynamic stresses associated with acceleration rather than the accelerations themselves that control the amount of densification which occurs during vibration.

From the work reviewed above it would appear that, except for the conclusions of Whitman and Ortigosa, the controlling parameter in the densification of sands is the maximum acceleration level of the vibrations. However, recent work reported by Brumund and Leonards (1972) suggests that it is transmitted energy that governs the densification process. They conducted model tests on dynamically loaded footings using a counter-rotating eccentric-mass type vibrator to apply both the static and dynamic loads. The authors were primarily concerned with settlement and correlations between final settlement and peak acceleration were found to be dependent on the static weight applied. The only unique relationship for the complete test program was that between final settlement and transmitted energy, and the relationship was found to be linear.

Although vibration has been used as a method of controlling the initial density of specimens used in triaxial apparatuses the degree of sophistication of the techniques used is not comparable with the previously reviewed research work. Most researchers have merely knocked the side of

the mould with an object, attempting to correlate the number of blows with the density obtained. The results were far from successful. Other workers have held some form of vibrator against the sides of the mould, with little success in the results obtained, Green (1969), Dyson (1970), Reades (1972).

As far as the author is aware, the most successful application of vibration to triaxial specimen preparation has been achieved at Manchester University, Parikh (1967), Ismael (1969), and Tong (1970). In the main, however, the method was limited to very dense specimens although a high degree of repeatability was obtained. The method was to clamp the cell base to the top of a mechanical vibrator, the design of which was based on Alyanak's apparatus. An extension collar was required and this was held in place by rubber bands. Having filled the specimen mould with distilled water the sand was deposited, either by spooning or by syphoning, and the vibrator motor was switched on using a suitable frequency and amplitude of vibration. Ismael (1969) claimed to have extended the method to cover a range of densities, by using different frequencies. However, the calibration curve of porosity against frequency appears to be untypical, although the labelling of the axes was rather obscure. Also, the alleged calibration curve appears to have been obtained from only four points and no correlation between the calibration curve and results of samples subsequently prepared was included.

2.4.3. Apparatus.

It was pointed out in Section 2.4.1. that triaxial specimens of sand need to be formed in a mould until a confining stress can be applied to support the specimen. The specimen mould consisted of four perspex plates held together by two tie rods and eight screws; the screw fixings were added after it was found that the mould tended to twist if the tie rods alone were used. The bottom inside edges of the mould were recessed

so that the mould sat on the bottom axial platen and could be adequately secured by inserting strips of card into the gaps between the overhanging part of the mould and the sides of the platen. The mould was made taller than the required specimen height thus providing a recessed upstand at the top to allow the sample sheath to be turned back over the mould, remote from the final sand surface.

Previous research workers, who deposited sand under water via a funnel, have found difficulty in preventing disturbance to the specimens near the top. Although disturbance always occurs due to placement of the top platen, additional disturbance can occur as the sample sheath is detached from the funnel, and as it is sprung back around the top platen when the platen has been positioned. It was partly for this reason that the top axial platen shape used by Dyson (1969) was rejected.

In order to minimise the disturbance due to manipulation of the sample sheath an extension collar was provided. The extension collar consisted of a rectangular perspex frame around which was stretched the top portion of one of the sample sheaths used by Dyson (1969). This sheath was sealed by an O-ring to a bung fixed to the end of a funnel. Fig. 2.8. shows diagrammatically how the specimen mould and extension collar were assembled. Strips of rubber were glued to the top rim of the mould and the bottom rim of the collar, and the collar was bolted to the mould as shown. To prevent the two sheath from adhering together a strip of plasticine, which had been wetted, was placed around the top rim of the mould before the collar was placed. This provided an adequate seal between the mould and the collar.

The vibration equipment consisted of a power oscillator and a small electric vibrator which was supported by a stand clamped to the triaxial cell base. The vibrator was rigidly connected to the specimen mould by a T-shaped connecting piece which was bolted to the mould and screwed into the arm of the vibrator. The power oscillator had both amplitude and frequency controls but, in this research program, the amplitude was kept

at the maximum setting and the frequency was varied to achieve the desired initial porosity. Although it was desirable to measure the actual accelerations applied to the mould each time a specimen was prepared, the apparatus required was only available for a very short period of time. Therefore actual measurements of acceleration were limited to a few calibration tests at the start of the research program. Details of these calibration tests and the apparatus used are given in Section 2.4.5.

2.4.4. Sample preparation procedure.

Prior to assembling the apparatus, certain preparations were carried out. A quantity of sand was weighed in a beaker. The sand was then submerged, boiled thoroughly and allowed to cool. The beaker was then filled with de-aired water. The rectangular bauxilite strips were saturated by boiling them in a dish of water. They were then left to cool in the dish.

Four rectangular rubber membranes were cut to a size slightly smaller than the face of the axial platens. The membranes were lightly smeared with silicone grease on one side only. One of the membranes was placed on a rectangular aluminium plate with the greased side face downwards. Trapped air was carefully removed with a straight edge. A second membrane was then placed on top and any trapped air was removed. The remaining two lubricated membranes were similarly placed on a second aluminium plate. The membrane-covered plates were then assembled to form a 'sandwich' with a third aluminium plate interposed between the non-greased sides of the two upper membranes. The plates, in this arrangement, were then loaded to 1000lbf in an Amsler testing machine. In this way any excess grease was removed and it was felt that the thickness of grease film would be consistent throughout the research program.

The lubricated membranes were then transferred to the faces of the axial platens, carefully removing any trapped air present. The axial

platens, with membranes, were then assembled together with the ball bearing which would transfer the deviator load to the plunger; and an initial height reading was taken using a height vernier placed on the cell base.

With both the top and bottom drainage taps open, water was flushed through the drainage system to remove any air present. The taps were then closed. After the datum readings on the pressure transducers had been checked sample preparation could proceed.

Different stages of the subsequent setting up procedure are illustrated in Figs. 2.9-2.12. The bottom drainage tap was opened slightly, to allow water to slowly escape into the peripheral drainage channels in the bottom axial platen, and then closed again. The bauxilite strips were inserted and the specimen sheath was stretched over the platen and sealed with O-rings. Filter paper strips were inserted between the sides of the platen and the sheath. The bottom drainage tap was then opened to allow water to flood the space between the platen and the sheath until the water level was about 5 mm above the face of the platen. The filter paper strips were turned over to form a cross over the lubricated membranes. Any entrapped air was carefully removed from around the platen.

The specimen mould, which had previously been assembled, was then positioned. The top of the specimen sheath was held together whilst the mould was placed around it. Using pieces of card to wedge the mould around the platen the mould was brought down hard to seat onto the platen (Fig. 2.9.).

The specimen sheath was then stretched back over the rim of the mould taking care that the corners were correctly fitted. De-aired water was introduced into the mould to a level just below the rim. Strips of plasticine were placed on the rim. The extension collar was placed on top, and was bolted to the mould to ensure an adequate seal. A funnel

was positioned over the mould and the extension collar sheath was sealed to the bung, which was attached to the funnel, using an O-ring. More de-aired water was then admitted, to a level just above the neck of the funnel.

The vibrator, which was permanently bolted to its stand with the T-shaped connecting piece attached, was then assembled. The vibrator was bolted to one side of the specimen mould, via the connecting piece. Then, carefully checking the alignment of the vibrator, the stand was clamped to the cell base. The vibrator was then wired to the power oscillator. The set-up at this stage of sample preparation is shown in Fig. 2.10.

A platform was placed on the cross-beam of the loading frame to support the beaker of sand. The frequency control on the power oscillator was set at the required position and the oscillator was switched on. The sand was then syphoned into the funnel from whence it settled through the water into the mould.

Since vibrations can be used to segregate different sized particles it was thought that vibrations applied during deposition would tend to offset segregation due to sedimentation. During deposition it was observed that, providing the amplitude control was at its maximum setting, the sand surface inside the mould appeared to remain reasonably horizontal as the height increased.

The vibrations were continued for five minutes after all the sand had transferred to the mould. The vibrator was then switched off.

After the sand had been deposited the excess water in the funnel was syphoned out and the funnel was removed. The extension collar and plasticine were removed after the remaining excess water had been syphoned off. The water level was then just below the upper rim of the specimen mould. The surface of the sand tended to be slightly concave. Therefore the sand surface was levelled and the specimen was then re-vibrated, at the same frequency setting, for a further five minutes.

After this additional vibration the sand surface was found to be flat and horizontal.

Filter paper strips were placed across the top of the mould to form a cross. The top drainage tap was opened and, when water emerged in the peripheral drainage channels, the bauxilite strips were inserted. The top platen was then carefully lowered into the mould as shown in Fig. 2.11. The specimen sheath was carefully turned back to fit around the platen. Water was introduced around the sides of the platen to remove any pockets of air. The specimen sheath was then sealed around the top platen with O-rings. In an attempt to simulate sample/platen interface conditions similar to those at the base of the specimen the vibrator was switched on for about one minute.

Both drainage lines were then opened to a burette, which had previously been lowered, in order to apply a small suction to the specimen. This suction also removed the water surrounding the sides of the platens, as can be seen in Fig. 2.12. When the water level in the burette had become steady the specimen mould was carefully dismantled and the specimen dimensions were measured.

The total height of the specimen and platens, plus the ball bearing, was measured with a height vernier. By subtracting from this measurement the initial height reading the height of the specimen could be calculated. Lateral dimensions were measured using a vernier micrometer gauge. Nine readings, distributed about the sides of the specimen, were taken to determine each average lateral dimension. An allowance was made for the thickness of the specimen sheath. The burette reading was noted before and after the specimen dimensions were measured.

If the subsequent test was to be a triaxial compression test then sample preparation was complete. The triaxial cell was positioned and bolted to the cell base. De-aired water was run into the cell with the air release valve open. When the cell was full the burette was raised,

level with the mid-height of the specimen. When the burette level was steady the reading was noted and the specimen was ready to be consolidated.

When plane strain tests were to be performed the side platens were assembled and bolted to two opposite vertical faces of the specimen, after the specimen dimensions had been determined. The manner in which this was carried out, for the different types of platen used, will be described in Chapter 4. The testing techniques used during both the consolidation and shear stages of the various test series will be covered in the respective chapters.

2.4.5. Calibration of vibration system.

Before discussing the results of the calibration tests it is worthwhile explaining the vibration system used. The system consisted of a small moving coil exciter which was driven by a power oscillator. This type of exciter consists of one or two coils moving in an annular gap with a strong magnetic flux in it. The flux is provided by a permanent magnet system. The moving coils are coupled to a rod which transmits the force from the coil to the object to be vibrated. Therefore, since the coil is in a constant magnetic field, the force exerted is proportional to the supply current only.

The amplitude of current supplied to the exciter was controlled by the amplitude setting on the power oscillator. The frequency control on the power oscillator allowed the frequency of vibrations, applied to the specimen mould, to be varied. The amplitude of vibrations, applied to the specimen mould, was dependent on both the frequency and the amplitude of current provided to the exciter. However, in the tests carried out, only the maximum amplitude setting on the power oscillator was used since lower current amplitudes did not appear to produce sufficient force to overcome significant damping, for the specimen size chosen.

As mentioned in Section 2.4.3 calibration tests were performed at the start of the research program to obtain an indication of the

variation of acceleration and amplitude applied in the subsequent tests. Fig. 2.13 provides a diagrammatic layout of the apparatus used in the calibration tests.

Two tests were performed. The first test was carried out with the specimen mould and funnel filled with water. In the second test 350g of sand had previously been deposited into the mould through water, and the funnel and extension collar had been removed. It was anticipated that the results of the two tests would indicate the range of accelerations and amplitudes which would occur during deposition in subsequent tests.

The procedure used in the calibration tests was that as the frequency was first of all increased to 500 Hz, and then decreased to zero, voltage readings on the a.c. voltmeter were recorded and the waveforms were observed on the oscilloscope. Observation of the resulting waveforms showed that a well defined sine wave could be guaranteed providing that the frequency was higher than about 30 Hz. For this reason subsequent tests were conducted at frequencies higher than this value.

Using the manufacturer's calibration for the accelerometer the accelerations could be determined from the a.c. voltmeter readings. The observed variation of acceleration with frequency for the two tests is shown in Fig. 2.14. Since acceleration is equal to the product of the amplitude of vibration and the square of the frequency the variation of amplitude with frequency could be obtained. This is shown in Fig. 2.15. It can be seen from Figs. 2.14 and 2.15 that, for the system used, although the variation of acceleration with frequency was complex (two zones of resonance occurred), the amplitude decreased at a decreasing rate with increase in frequency.

The repeatability achieved by the porosity control technique will be discussed in Section 2.4.6. However, it is appropriate to examine the porosity-frequency relationship obtained in association with the

results of the calibration tests. Fig. 2.16 shows the results of the porosity control technique for the first series of tests performed. At low frequency levels the porosity decreased as the applied frequency was increased until an 'optimum' frequency was reached which gave a minimum value of porosity obtainable. As the frequency was raised above this level the porosity increased but the rate of increase decreased sharply at about 300 Hz and higher frequencies tended to produce the same porosity. The results are in general agreement with the work of previous investigators.

As can be seen from the graph the porosity obtained at high frequencies is approximately the same as that obtained due to deposition through water without vibration. The porosities obtained at frequencies higher than 300 Hz are probably the result of disturbance caused by placement of the top axial platen and other effects which occurred between deposition and measurement of the specimen.

In all cases the sand was densified from a loose state and it was not possible to loosen the sample by varying the frequency. Presumably this was because the applied force was not sufficient to overcome any locked-in stresses that had developed. Loosening of initially dense specimens may be possible with a larger exciter but the resultant porosity distribution may be highly non-uniform.

In this research program interest was restricted to frequencies greater than 50 Hz and no observations can be made concerning the effects of using lower frequencies. Within the range of frequencies used it is clear from Fig. 2.14 that acceleration does not control the density obtained, for the vibration system used. This conclusion conflicts with the work of a number of previous researchers. However, it is significant that these investigators used a constant amplitude system (mechanical vibrator) as opposed to the constant force system used by the author.

A comparison of Figs. 2.16 and 2.15 shows that both density and

amplitude decrease at a decreasing rate as the frequency is increased (for frequencies greater than 'optimum'). However, results of previous investigators demonstrated that the amplitude was not the controlling parameter. From the limited evidence provided by the author's tests it would appear that: either the density is controlled by a combination of two vibration parameters (possibly amplitude and frequency); or that, in agreement with the conclusion of Brumund and Leonards (1972), the controlling parameter is the transmitted energy. The latter supposition may well warrant further investigation.

2.4.6. Repeatability of porosity control technique.

The results obtained by the porosity control technique are shown in Fig. 2.16-2.20. The electrical exciter had been used in earlier tests (not reported in this thesis) but, although the results of these early tests indicated that control of the initial porosity was possible using vibration, the scatter in the results was unacceptable. The main reason for the scatter was that the exciter was merely positioned against the side of the specimen mould, without being rigidly clamped to it. Consequently excessive damping occurred. As a result of these early tests the exciter was rigidly bolted to the specimen mould for the tests reported in this thesis.

Fig. 2.16 shows the results of the first series of tests carried out with the exciter bolted to the specimen mould. These specimens were subsequently tested in triaxial compression and the average cross-sectional area of the specimens was approximately 3467 mm^2. Although the number of tests in this series do not permit any conclusions to be drawn regarding repeatability of the method, Fig. 2.16 does indicate that, for a given apparatus and vibration system, a calibration curve can be obtained against which the repeatability of the results can be assessed.

All the specimens prepared for plane strain tests had approximately the same cross-sectional area, namely 3048 mm^2. The results of these tests are shown in Fig. 2.17-2.19. Fig. 2.17 shows the results of the porosity control technique for the specimens which were subsequently tested using rigid side platens. With the exception of one specimen the results indicate a remarkable degree of repeatability. It would appear that any porosity desired within the range covered was obtained to $\pm$ 0.2% by applying the frequency of vibration given by the curve shown. A comparison with Fig. 2.16 indicates that the size of the specimen affects the relationship between porosity and frequency. The results of specimens which were subsequently tested using flexible side platens are shown in Fig. 2.18. These specimens were identical to other plane strain specimens prior to the side platens being assembled. However, as can be seen from Fig. 2.18 there is considerably more scatter in these tests than in the previous ones. These results imply that the porosity obtained is only repeatable to within $\pm$ 0.5%.

The results of all the plane strain test specimens are combined in Fig. 2.19. It would appear that the scatter in porosity varies between $\pm$ 0.2% for very dense specimens to $\pm$ 0.5% for medium dense specimens. However, from Fig. 2.17 and 2.18, it would appear that the accuracy of control deteriorated with use. The cause of this deterioration may be due to wearing of screwthreads in the perspex and distortion of the perspex mould with continued use, since inadequate clamping of the various parts of the assembly would cause a loss of transmission of the vibratory force. It is thought that, with a slightly improved mould design (e.g. the use of aluminium instead of perspex), and with more attention given to ensuring rigid connections between the various parts of the assembly, an accuracy of $\pm$ 0.2% in porosity could be obtained.

Fig. 2.20 shows the results of sample preparation for the triaxial tests carried out towards the end of the research program. The average cross-sectional area of these specimens was 2713 mm^2. The results shown a very poor correlation and emphasize the importance of adequate clamping. In order to change the cross-sectional area of the specimens for this series of tests, without manufacturing a new mould, aluminium plates were inserted between the specimen sheath and the mould. However, due to an oversight, these plates were not rigidly connected to the sides of the mould. Consequently the transmission of the vibrations to the specimen was not consistent.

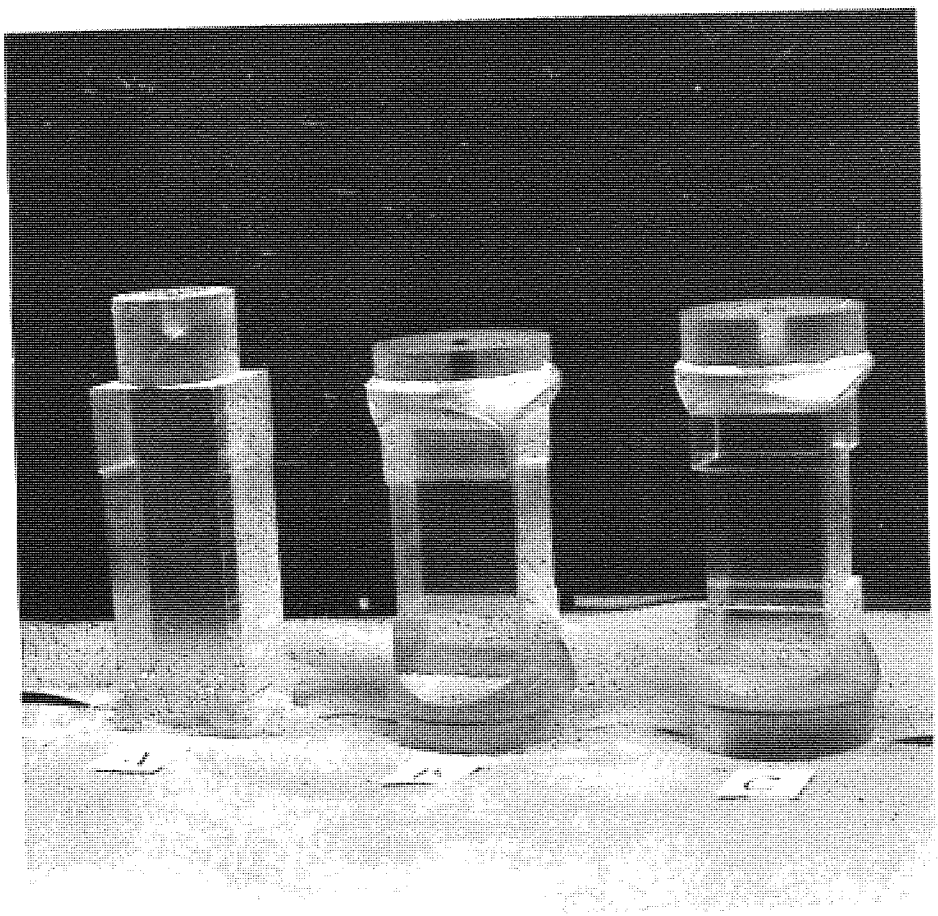

Fig. 2.1

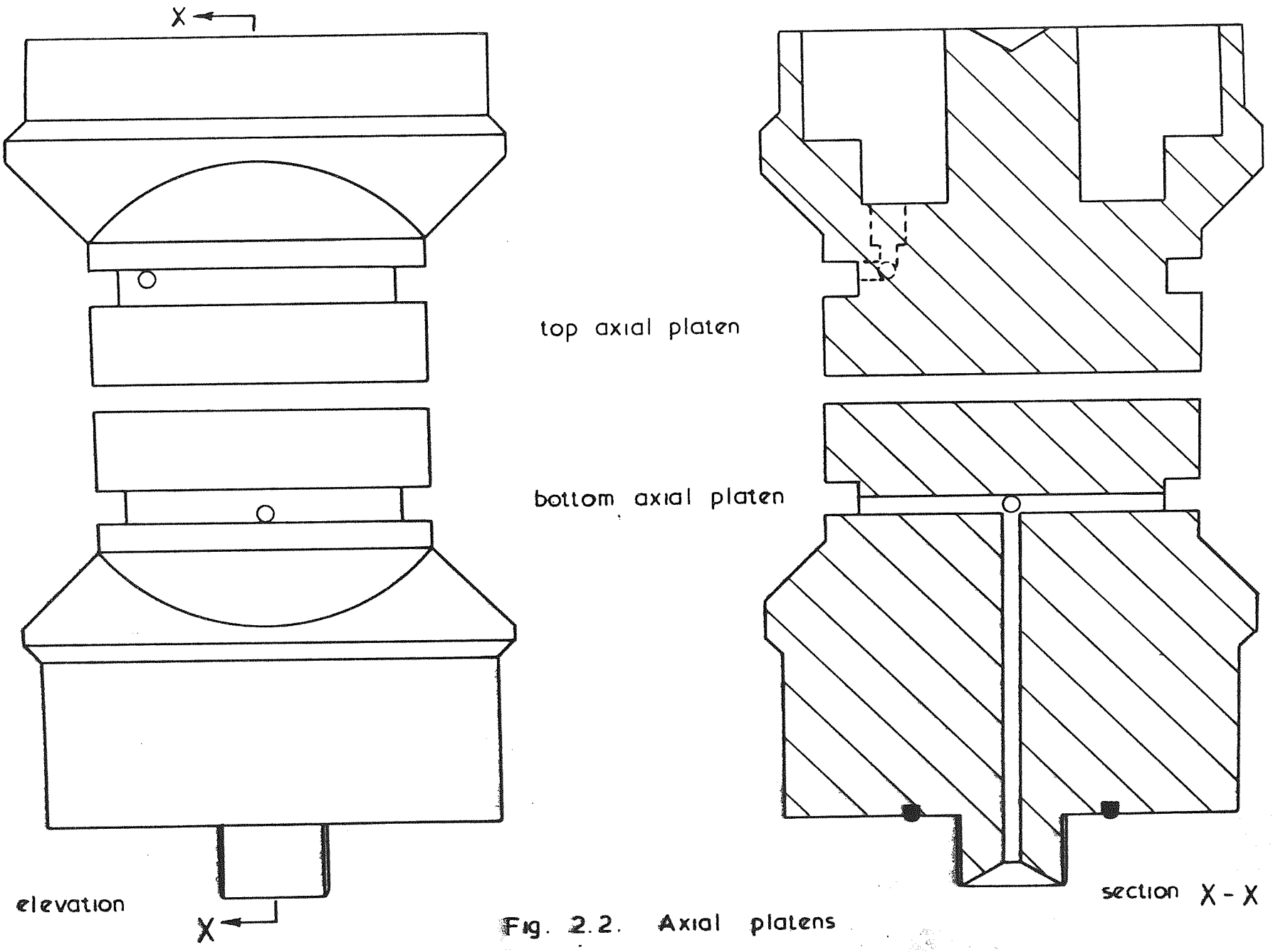

Fig. 2.2. Axial platens

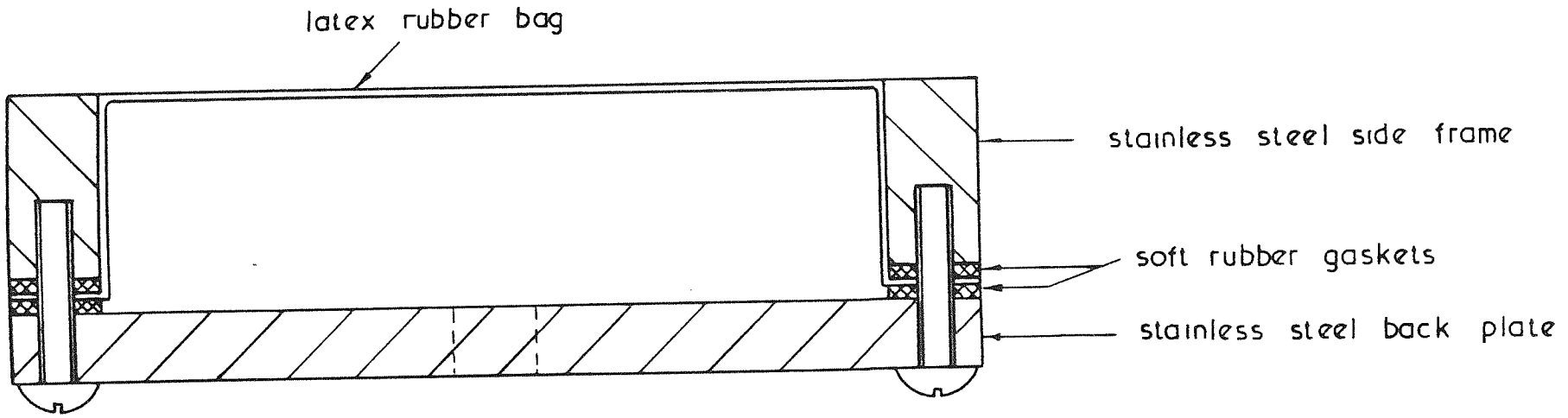
latex rubber bag
stainless steel side frame
soft rubber gaskets
stainless steel back plate
side stress - cell

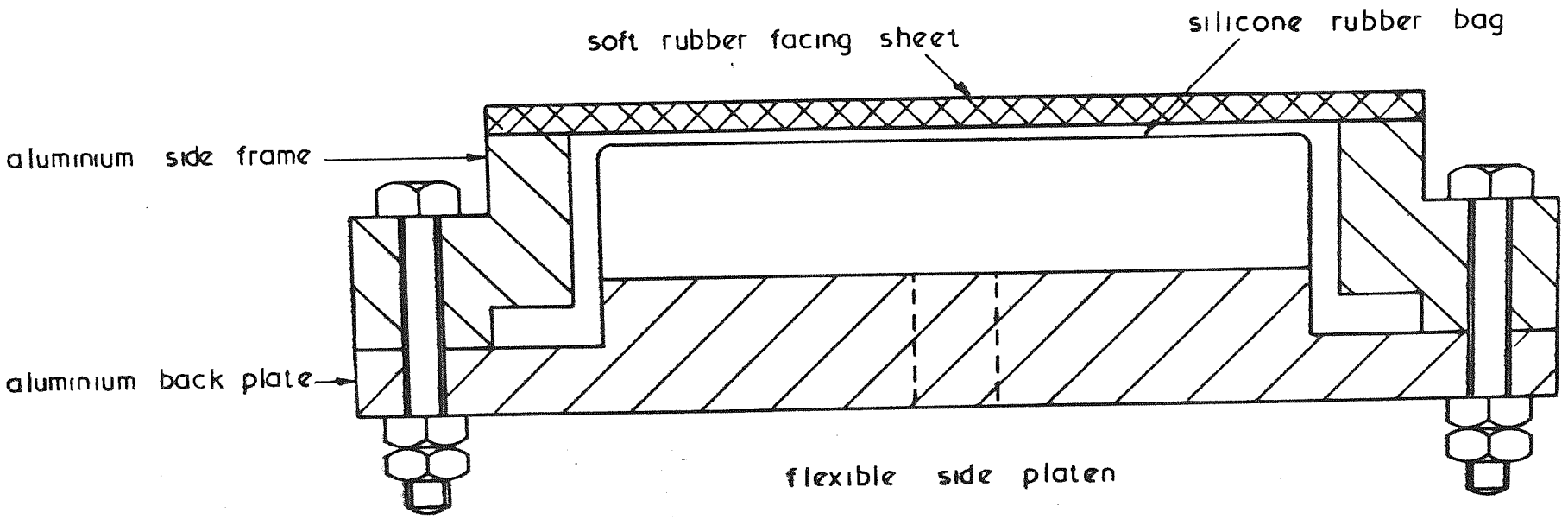
soft rubber facing sheet
silicone rubber bag
aluminium side frame
aluminium back plate
flexible side platen

Fig. 2.3

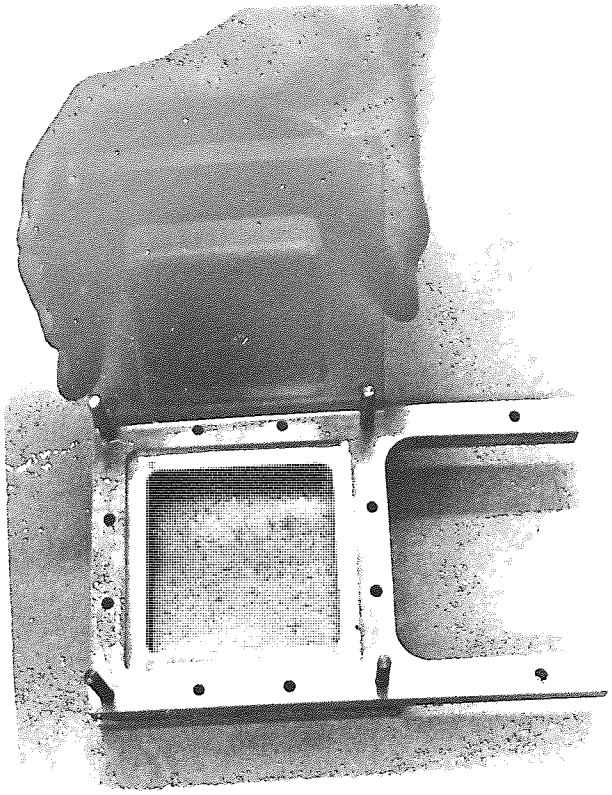

Fig. 2.4

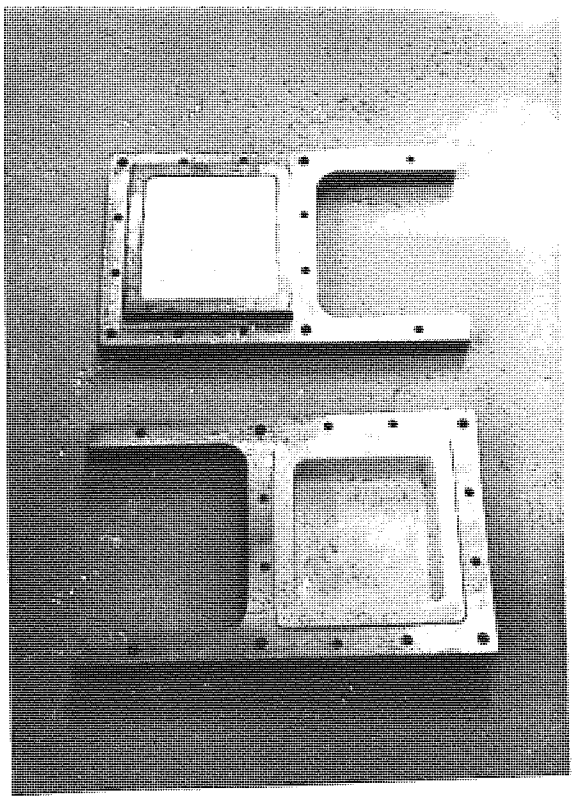

Fig. 2.5

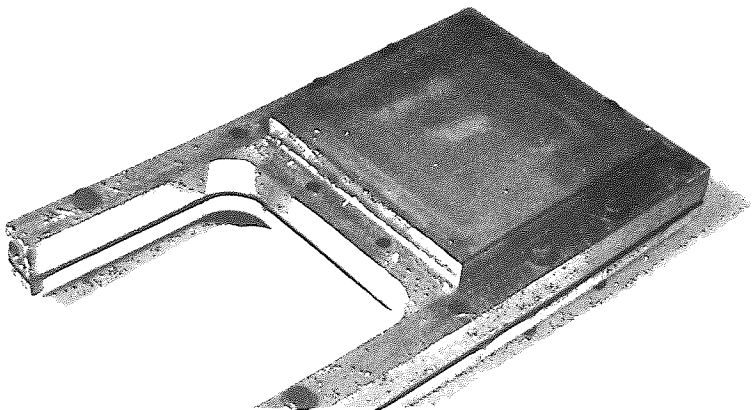

Fig. 2.6

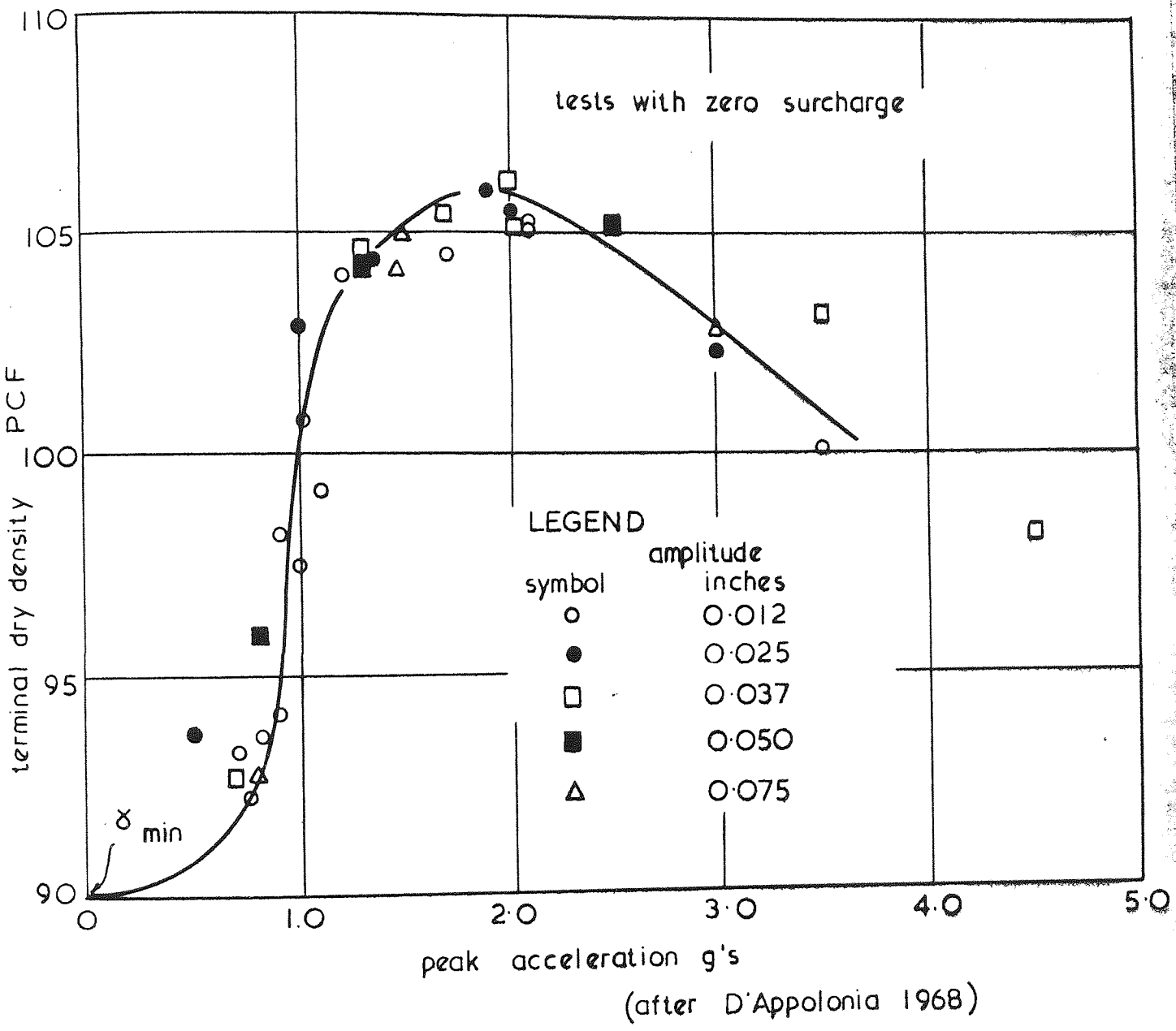

Fig . 2.7. Correlation between terminal density and peak acceleration

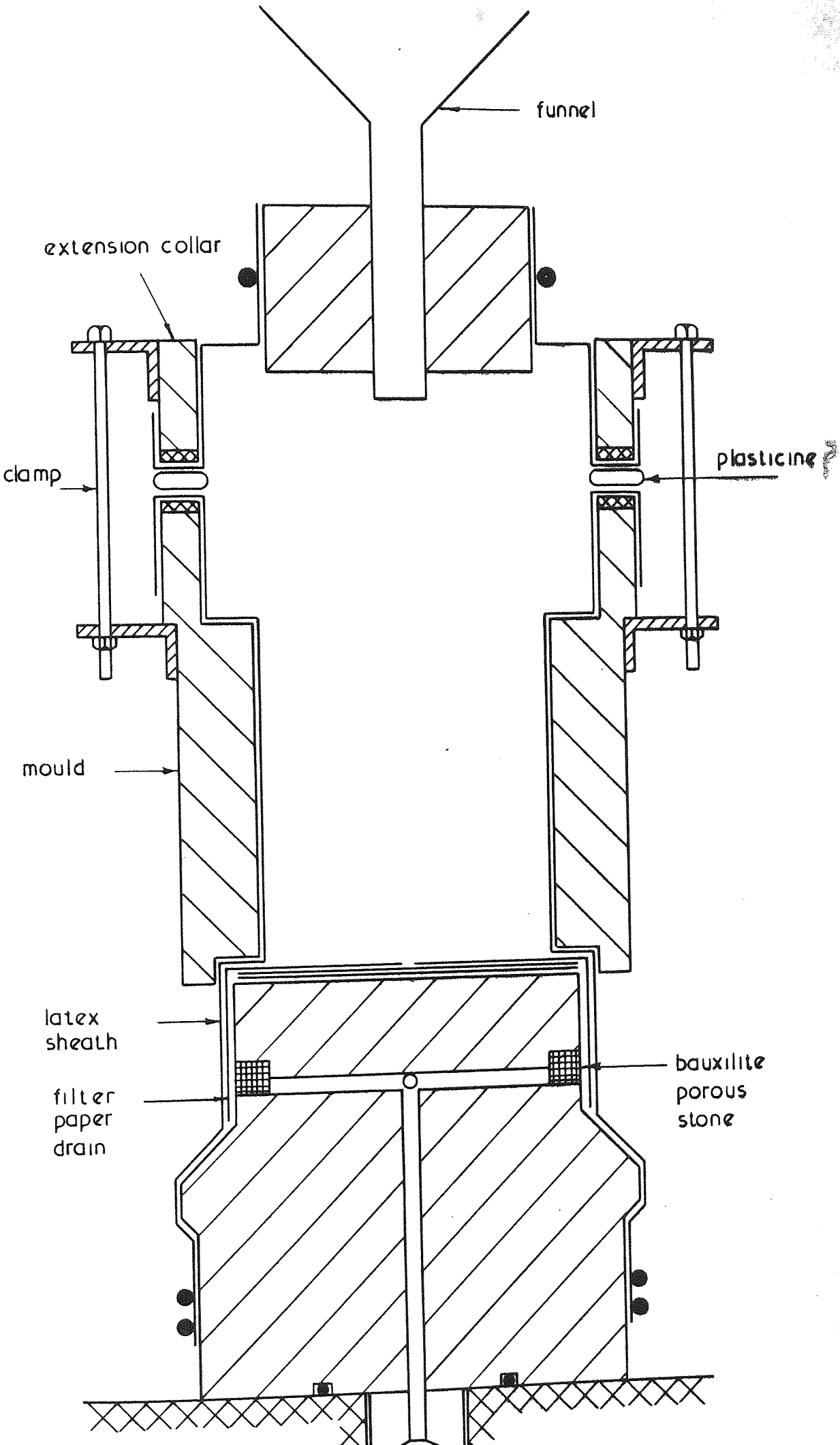
funnel
extension collar
clamp
plasticine
mould
latex sheath
filter paper drain
bauxilite porous stone

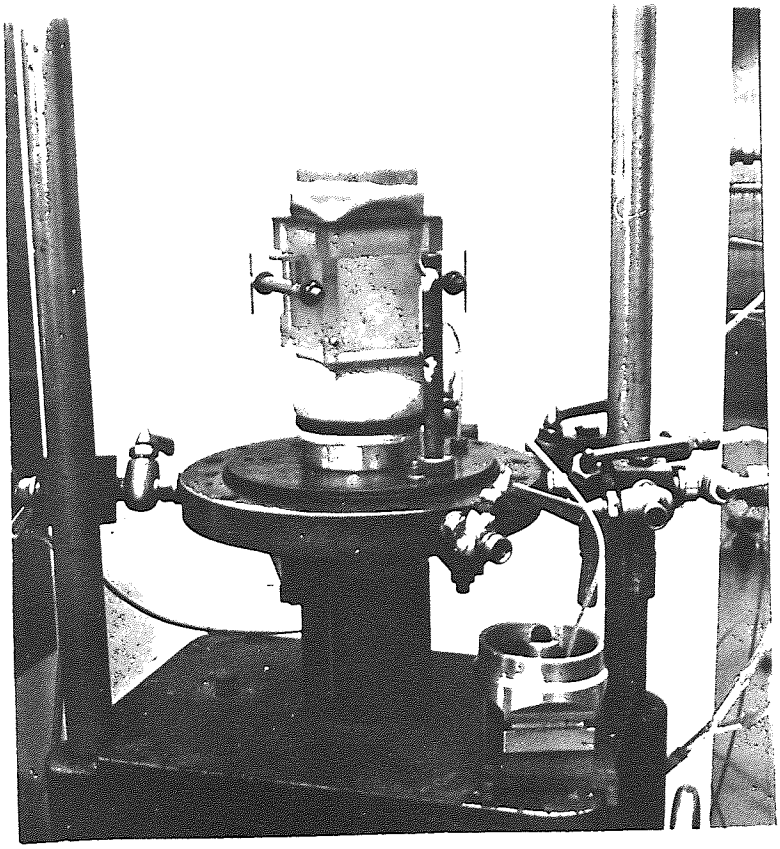

Fig. 2.9

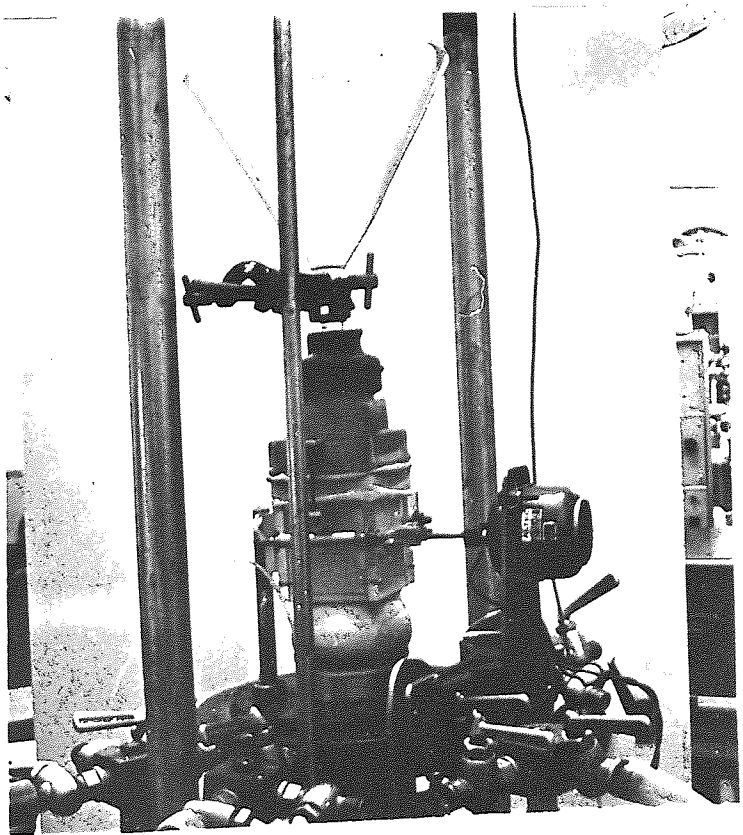

Fig. 2.10

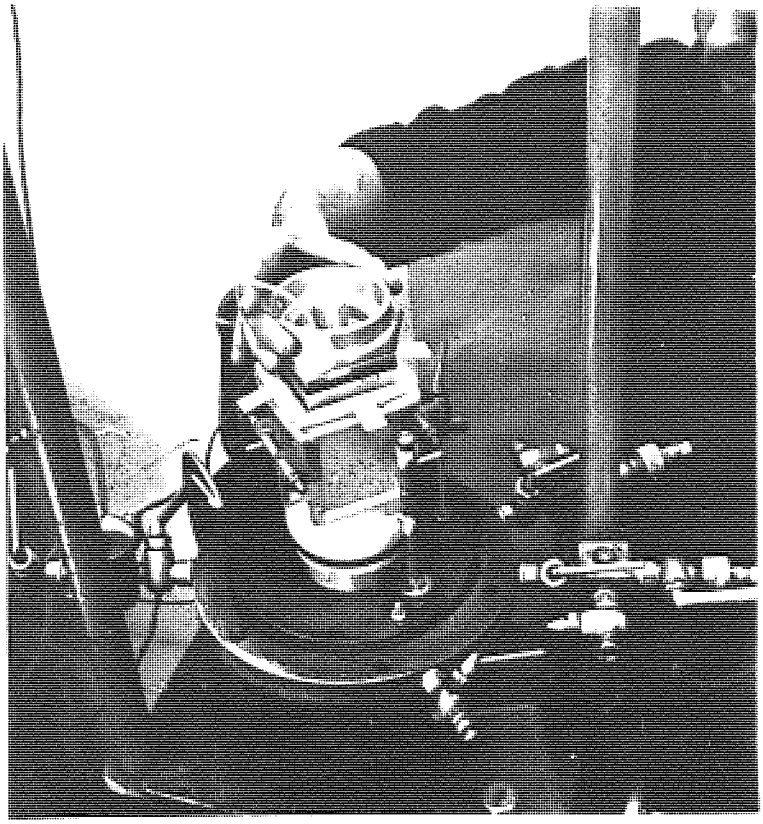

Fig. 2.11

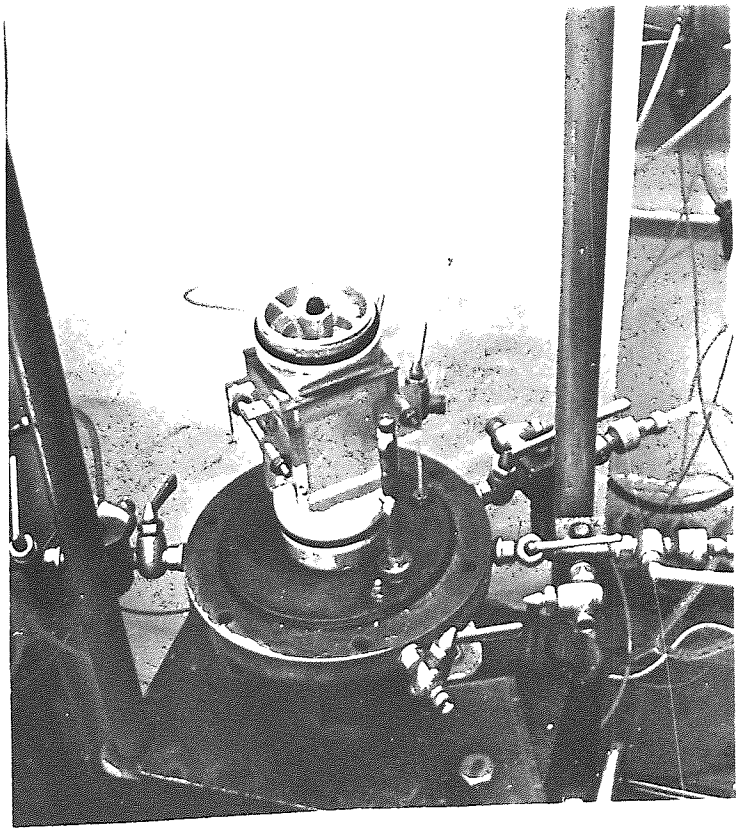

Fig. 2.12

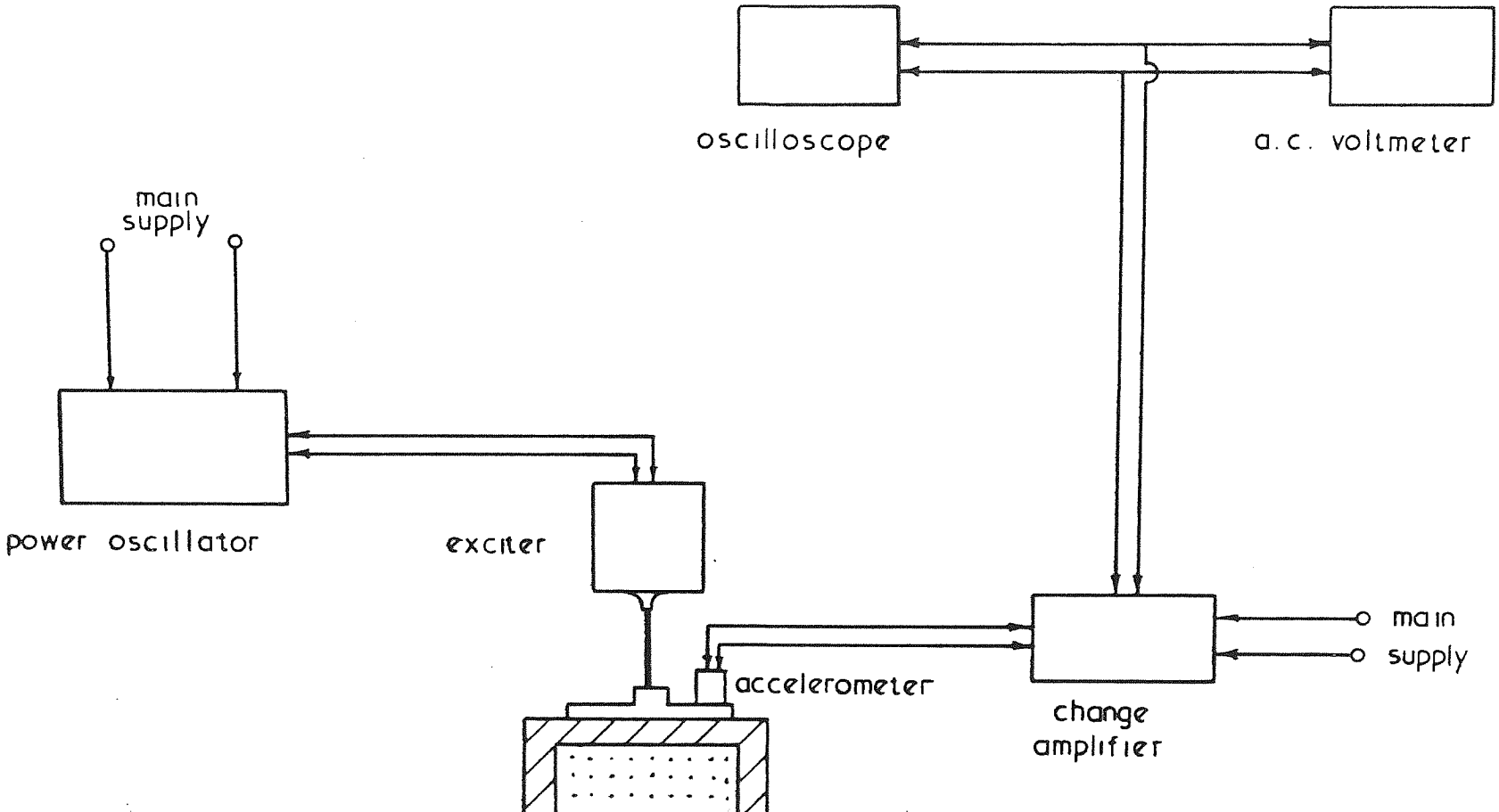

Fig . 2.13 Apparatus layout for calibration of vibration system

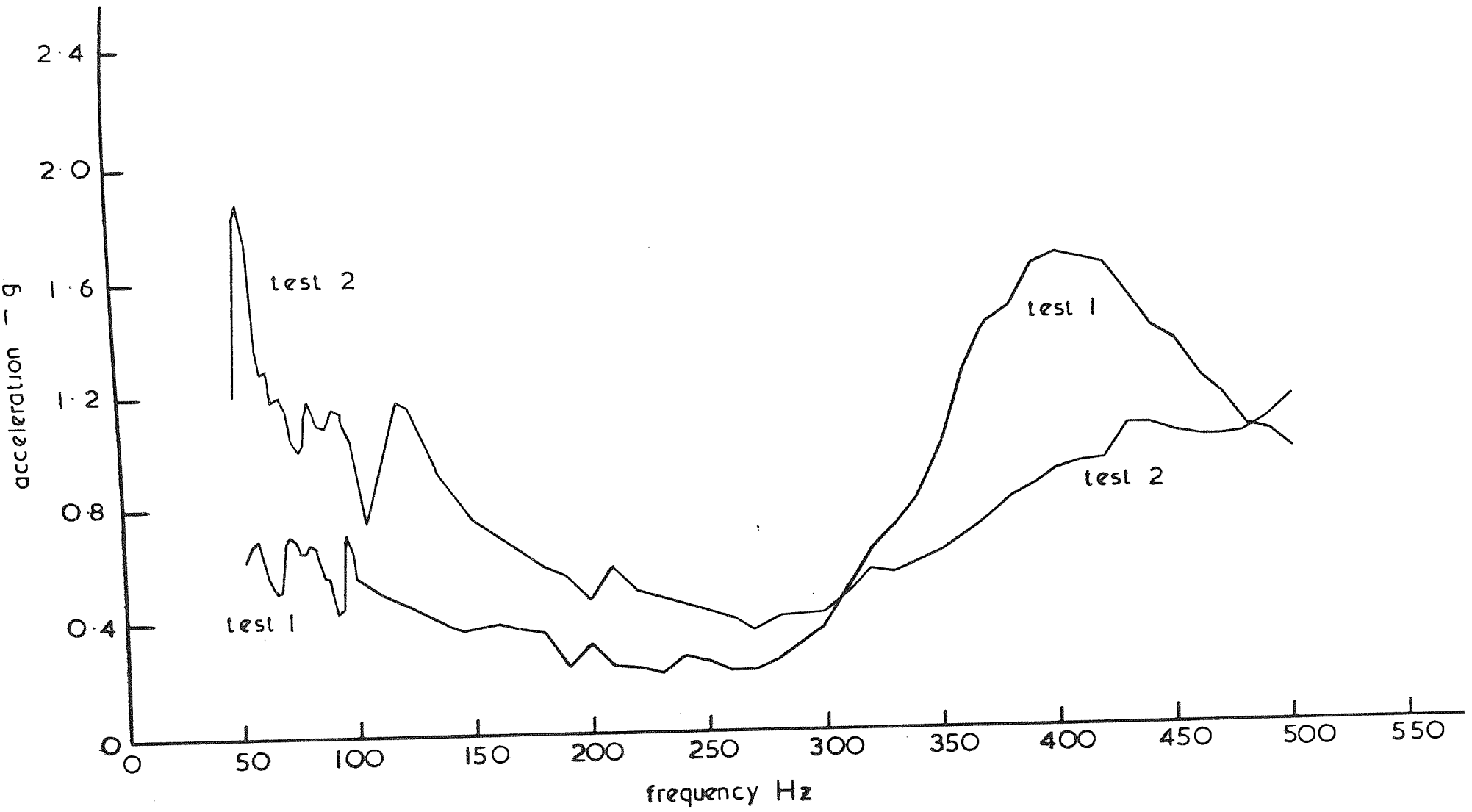
2·4
2·0
1·6
1·2
0·8
0·4
0
acceleration - g
test 2
test 1
test 1
test 2
0
50
100
150
200
250
300
350
400
450
500
550
frequency Hz

Fig. 2.14

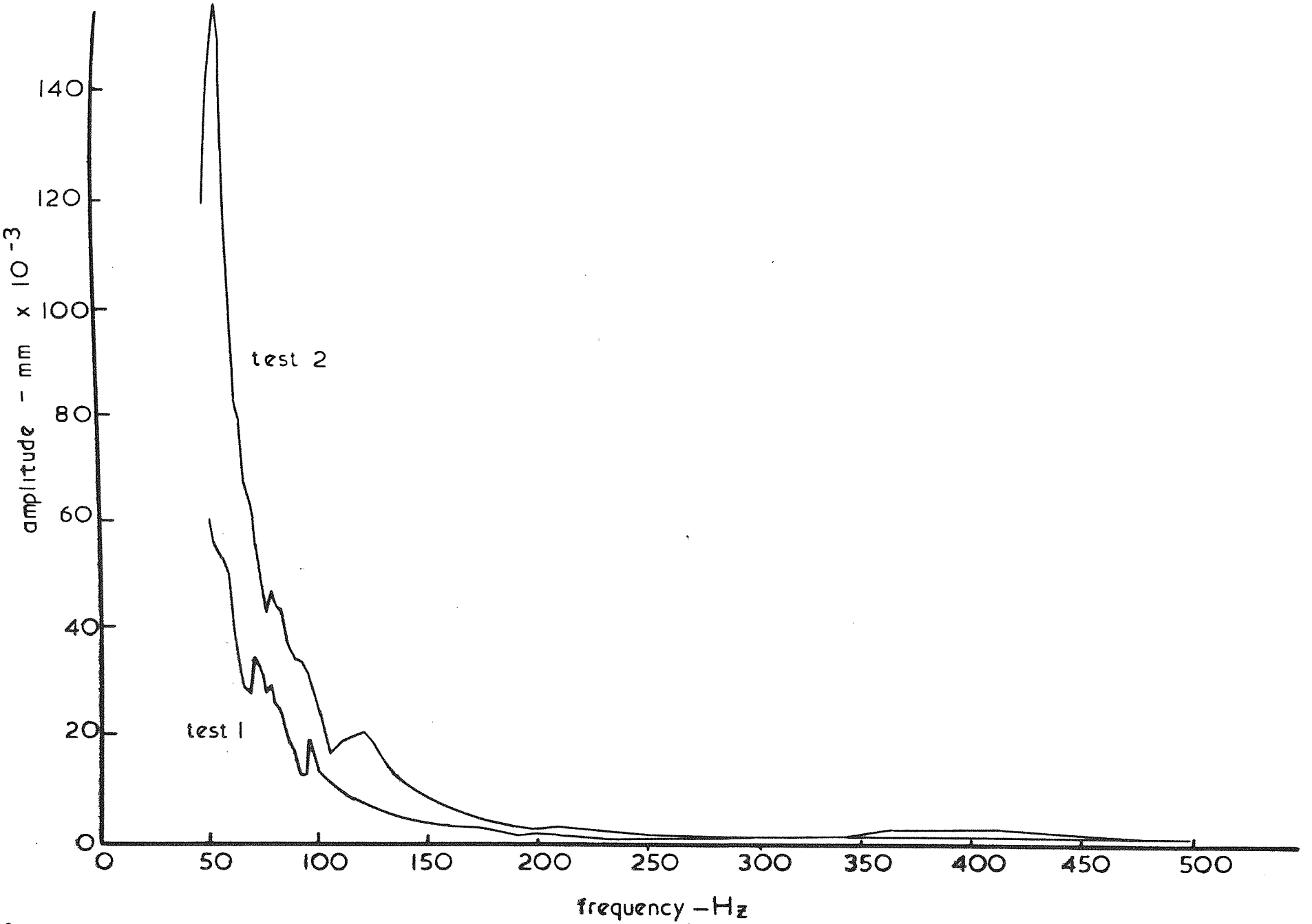
amplitude - mm x 10⁻³
140
120
100
80
60
40
20
0
test 2
test 1
0
50
100
150
200
250
300
350
400
450
500
frequency – Hz

Fig . 2.15

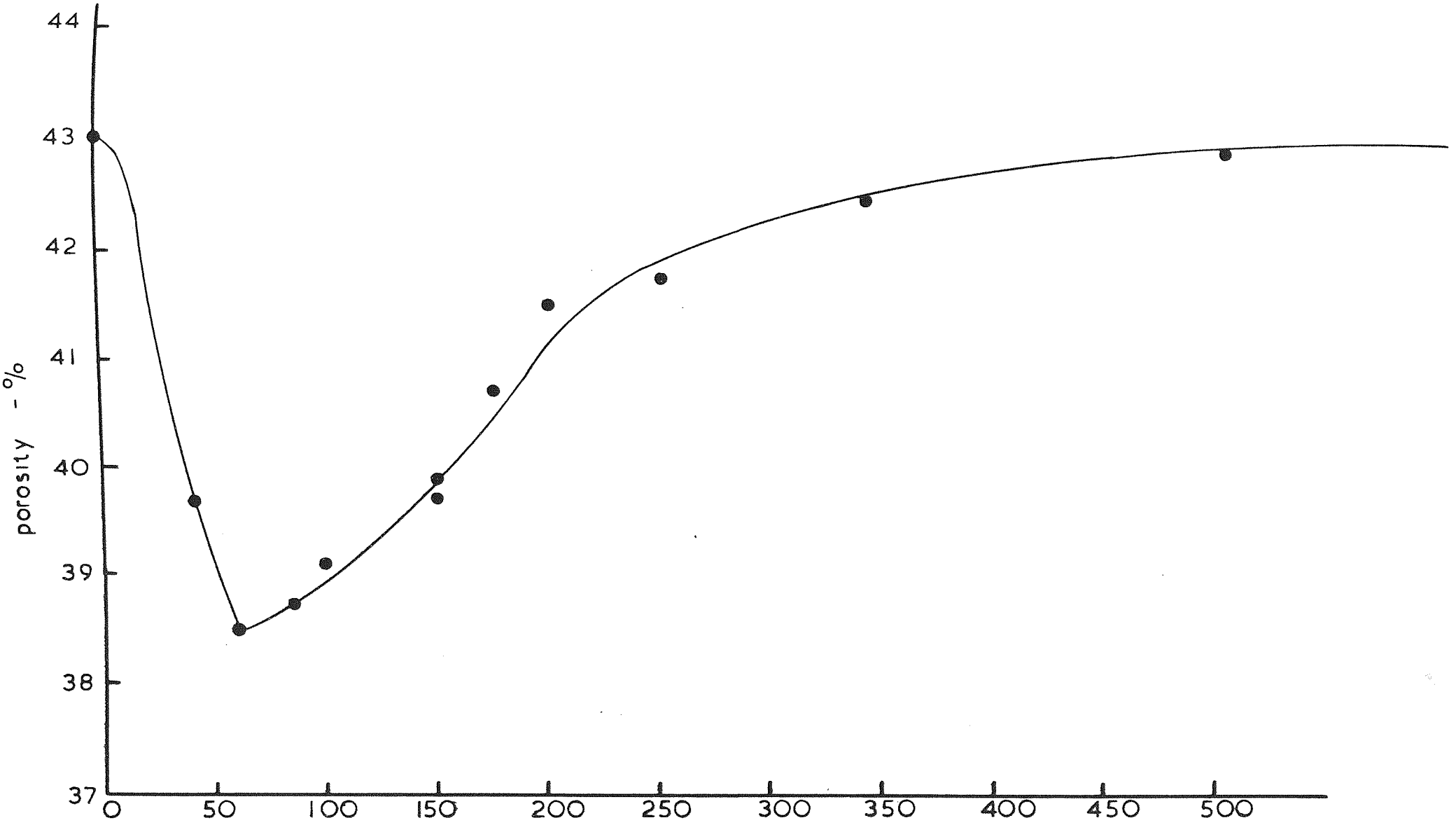
44
43
42
41
40
39
38
37
porosity - %
0
50
100
150
200
250
300
350
400
450
500
frequency Hz

Fig. 2.16

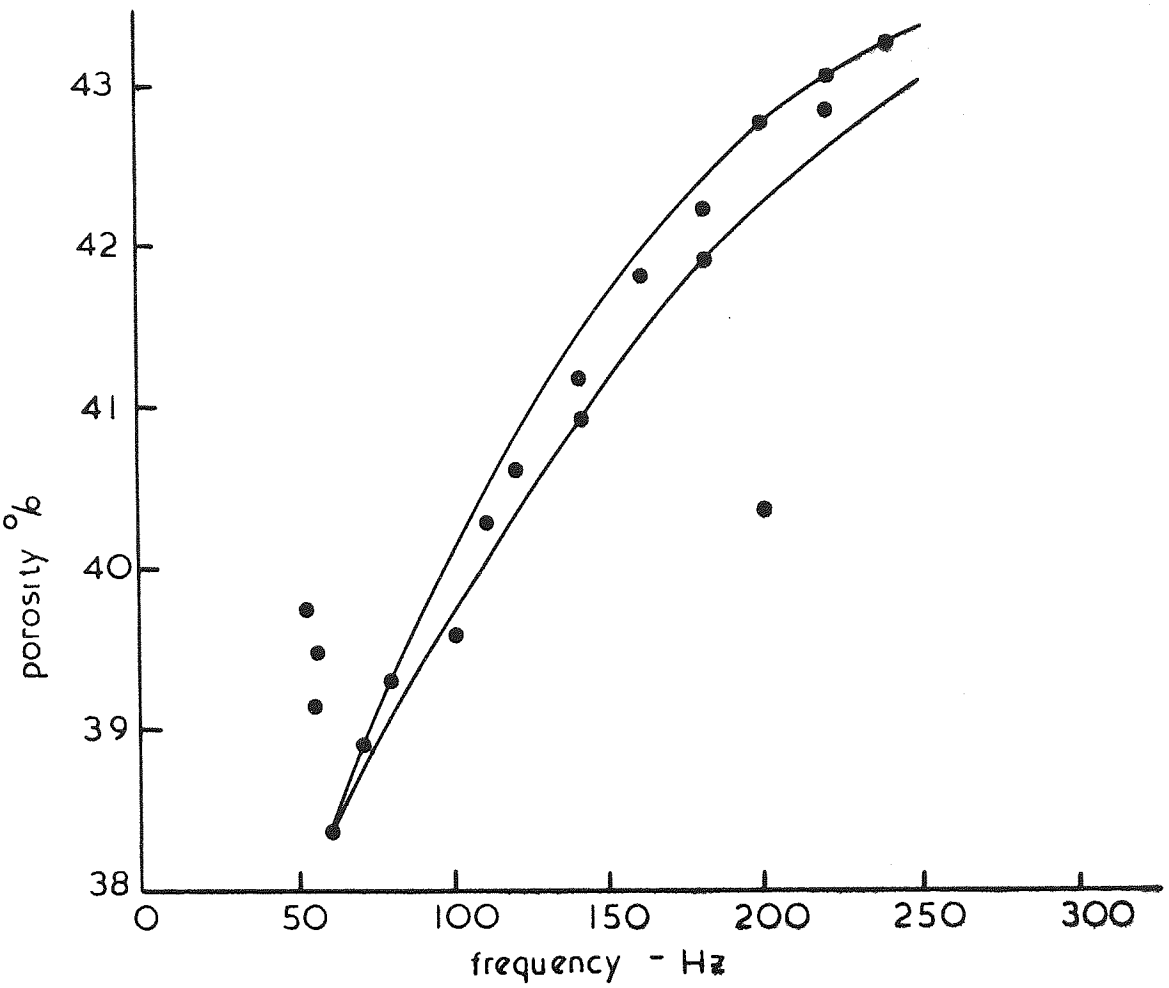
43
42
41
40
39
38
porosity %
0
50
100
150
200
250
300
frequency - Hz

Fig. 2.17

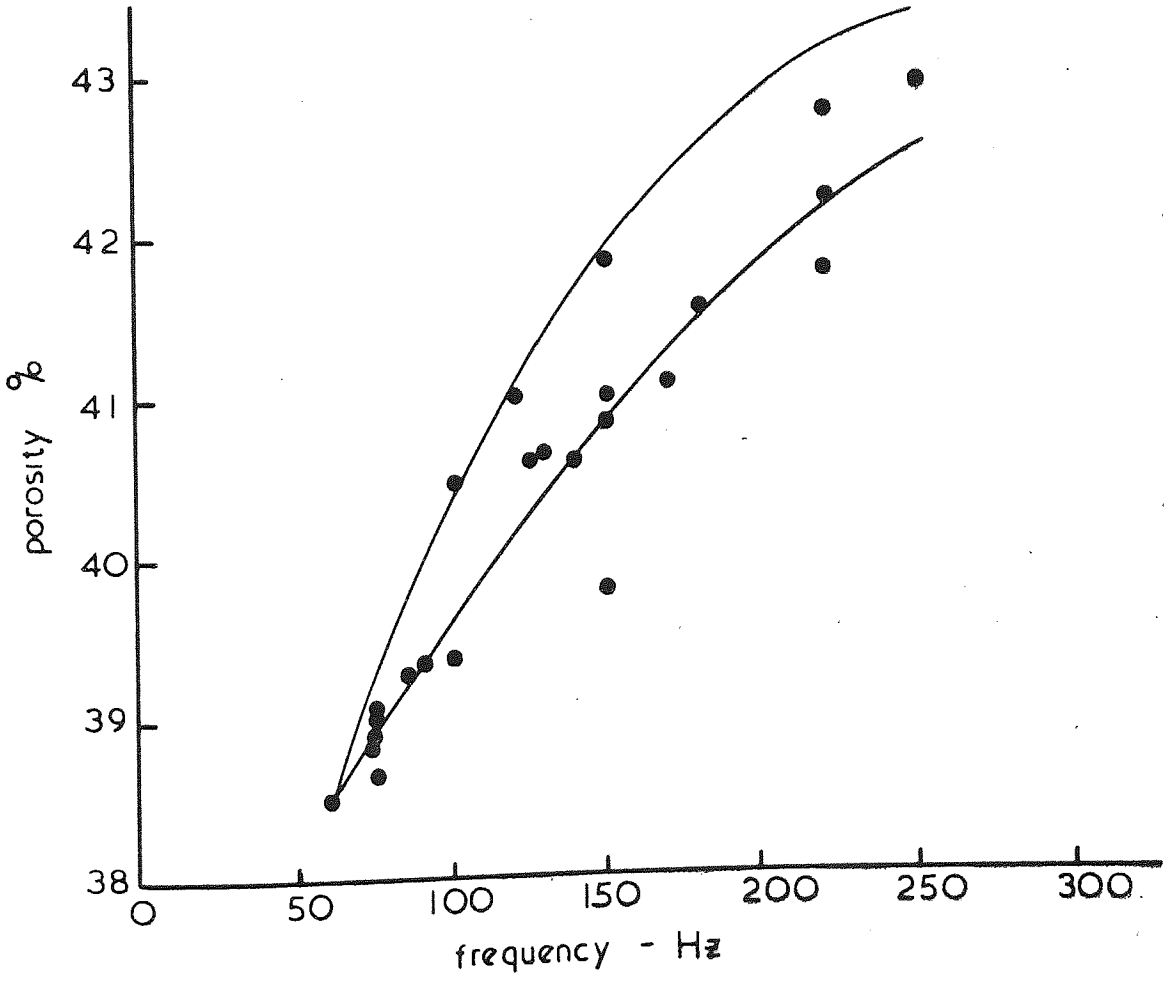
43
42
41
40
39
38
porosity %
0
50
100
150
200
250
300
frequency - Hz

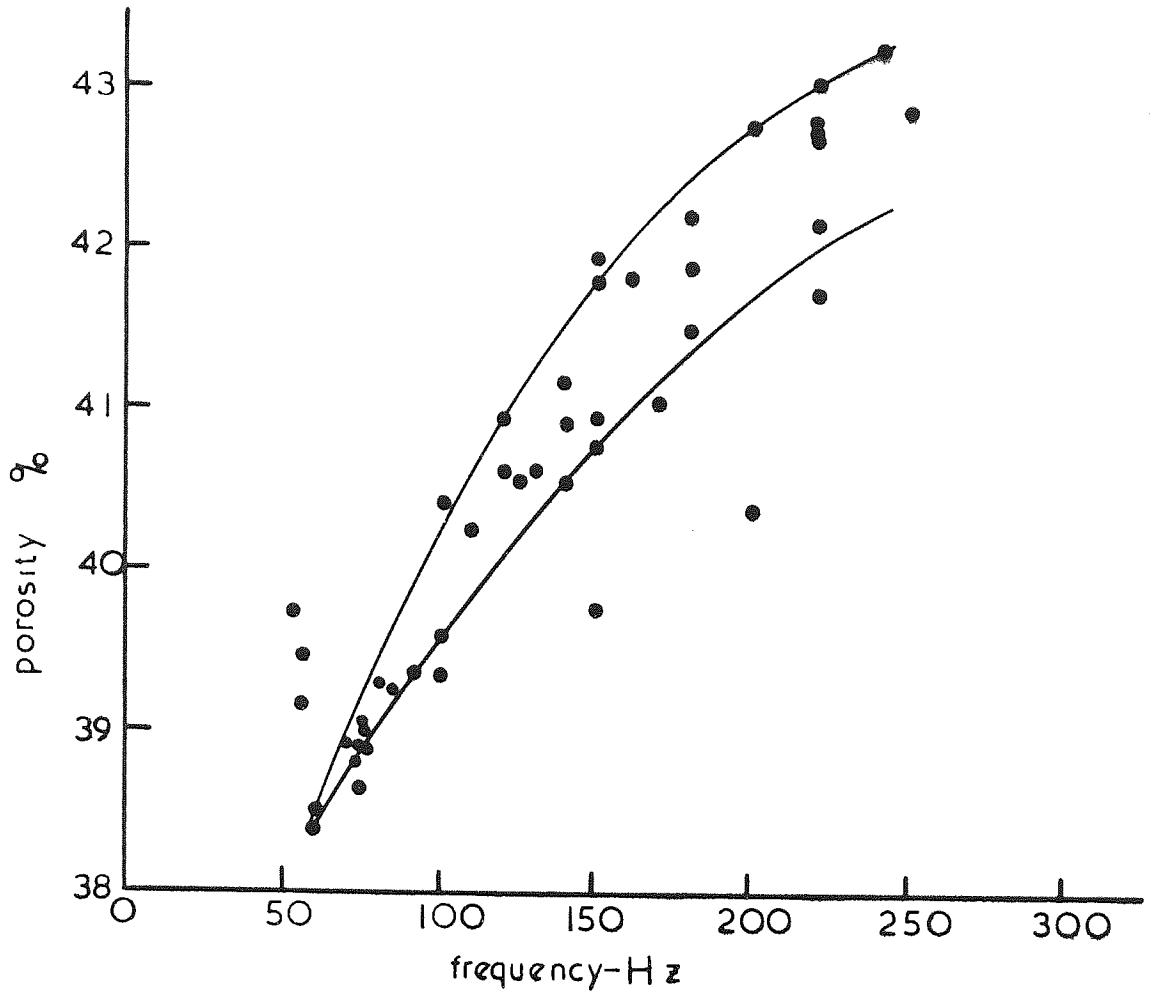
43
42
41
40
39
38
porosity %
0
50
100
150
200
250
300
frequency-Hz

Fig. 2.19

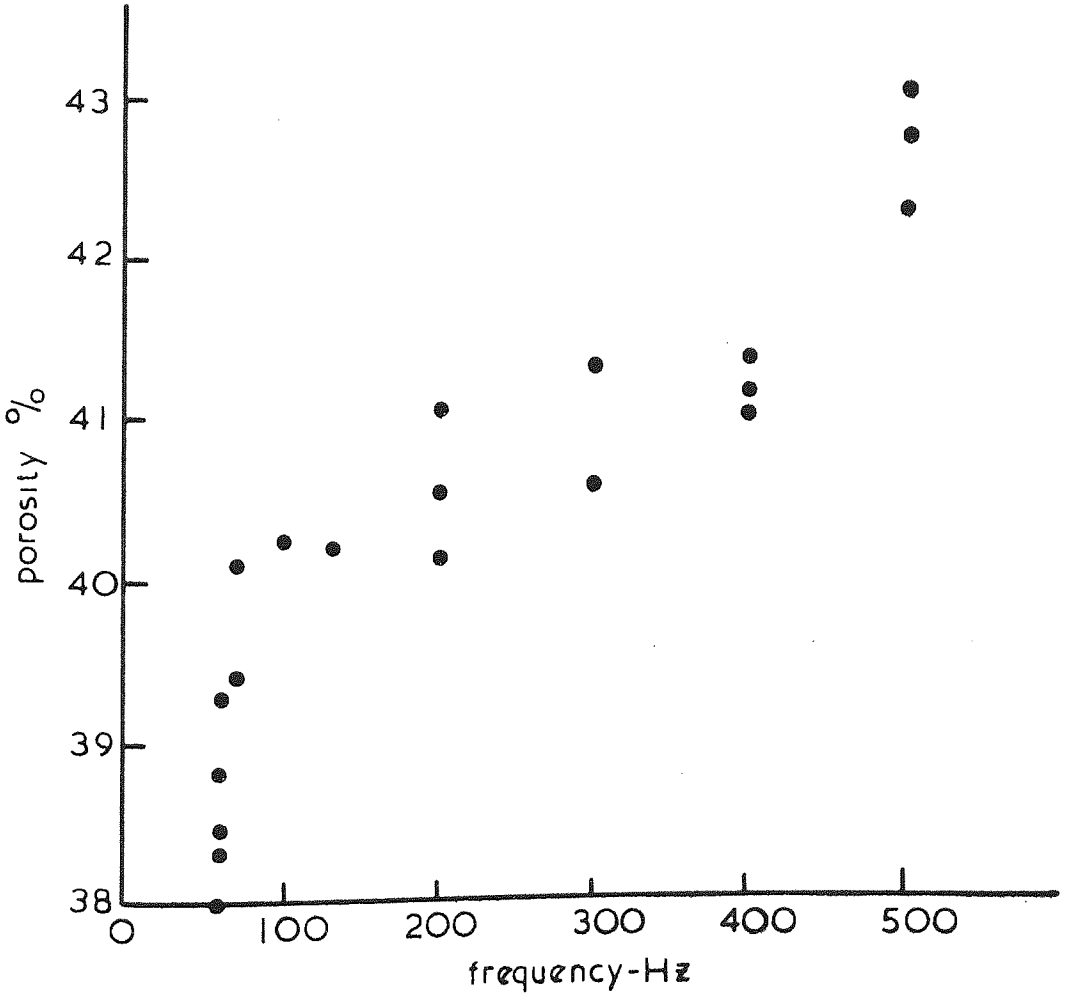
43
42
41
40
39
38
porosity %
0
100
200
300
400
500
frequency-Hz

CHAPTER THREE

3. TRIAXIAL COMPRESSION TESTS.

3.1. Introduction.

Although earlier triaxial compression tests had been performed on rock and concrete, it was not until the early 1930's that the precursor of the modern triaxial compression apparatus was first used to study soil behaviour. The apparatus, or variations of it, quickly became accepted as an important research tool in the newly developing field of soil mechanics, and in the next two decades many variations and improvements in the technique of triaxial testing were developed, notably of Casagrande, Geuze, and Taylor.

Due to its relative simplicity, its versatility, and the degree of controlled deformation that it allowed, the triaxial test became the most widely used apparatus for the testing of soil specimens, both for research and routine purposes. Bishop and Henkel (1957) provided a detailed and extensive documentation of triaxial testing apparatus and techniques which has become a standard text for routine testing and provides the basis of much recent research.

The conventional triaxial compression test is only strictly relevant to the few field conditions in which axisymmetric states of stress exist. Nevertheless, because of the vast amount of documented evidence concerning the triaxial compressive behaviour of soils, the triaxial compression test provides the most reliable standard against which new apparatuses can be assessed, and permits comparisons to be made with tests conducted under non-axisymmetrical states of stress, or strain.

Since the research program reported in this thesis involved the performance of plane strain tests on sand in a new apparatus it was necessary to conduct a number of triaxial compression tests on the same sand. In order to facilitate the use of the same axial platens as used

for the plane strain tests the triaxial compression tests were performed on cuboidal specimens. Recent research has indicated that there is little difference between the stress-strain behaviour due to differences in specimen shape provided that end-lubrication is adequate, Green (1969), Dyson (1970), and Reades (1972).

The results of the triaxial compression tests are reported in this chapter but, before describing the tests and discussing the results, a brief resumé of previous investigations into the triaxial compression behaviour of sand is provided in the following section.

3.2. Experimental behaviour of sand in triaxial compression.

One of the most important factors affecting the strength and deformation of granular materials, is the initial void ratio, or porosity, of the sample. Casagrande (1936) showed that whereas loose sands compress during shear with a gradual increase in the mobilized shearing resistance until a maximum shear strength is reached at very large strains, dense sands expand during shear with a rapid increase in mobilized shearing resistance to a maximum at relatively low strains after which the shearing resistance gradually reduces to that of an initially loose sand. He defined a critical void ratio at which a sand will shear at constant volume and demonstrated that the critical void ratio decreases with increase in confining pressure.

In order to explain the influence of the void ratio on the strength of sand, Taylor (1948) suggested that part of the shear strength was used to provide the energy necessary for the specimen to expand against the confining pressure. He therefore concluded that the shear strength of a sand comprised of two factors, namely, friction and a volume change component.

A detailed analysis of the factors contributing to the strength of granular materials, using the stress-dilatancy theory, has been provided by Rowe (1962), (1964), Rowe et al (1964). It was concluded that there

are three strength components of granular material: strength mobilized by frictional resistance; strength developed by energy required to rearrange and reorient the particles; and strength developed by energy required to cause dilatation of the specimen. It was also proposed that the last component can be subdivided into energy absorbed in friction as the mass dilates and energy required to do external work during the changes in volume that occur. (A comprehensive review of the stress-dilatancy theory is provided in Chapter 5.)

The strength and deformation of sand is also significantly affected by the confining pressure used. Various researchers have shown that the effect of increasing the confining pressure is to reduce the 'brittleness' of the stress-strain curve, increase the strain to failure, decrease the tendency to dilate, and decrease the strength, Hall and Gordon (1963), Hirschfeld and Poulos (1963), Vesic and Barksdale (1963), Bishop et al (1965), Lee and Seed (1967). The strength reduction is associated with crushing and suppression of dilatancy. Consequently it has been observed that at high confining pressures dense sands behave in a similar manner to loose sands.

Ponce and Bell (1971) showed that at very low pressures loose sands dilate and the behaviour is similar to that of dense sands at moderate pressures.

As a result of the above mentioned strength variations the failure envelope is curved, especially for initially dense sands. The curvature is also related to the gradation of the sand, being more marked for sands which are initially of uniform grain size. As the confining pressure is increased crushing occurs and the sand becomes more graded, resulting in less variation in the angle of shearing resistance. Consequently, for any sand, the angle of shearing resistance tends to become constant at confining pressures above a certain limiting value for the particular soil.

Although the effect of grading on the curvature of the failure envelope has been established its effect on the angle of shearing

resistance at a given confining pressure and relative porosity is not clear. Early studies, Bishop (1948) and Chen (1948), showed that at a given porosity uniformily graded sand exhibits a higher strength than well graded sand. However, at their minimum porosities the well graded sand was stronger than the uniform sand. Other studies either did not permit any clear conclusions to be made, Kirkpatrick (1965), or the effect of grading on strength was found to be minimal, Koerner (1970).

The fact that the angle of shearing resistance increases with decrease in the particle size was demonstrated by Kirkpatrick (1965) and Koerner (1970). Chen (1948) and Koerner (1970) showed that angular sands exhibit higher strengths than sands comprising of more rounded particles.

The observed stress-strain characteristics of granular material are generally of a non-linear form. Consequently most researchers have contented themselves with a qualitative description or graphical record of the stress-strain curves obtained. No theoretical stress-strain relationship has, as yet, been obtained which will accurately predict the actual shape of the stress-strain curves for sand. However, a number of investigators have used mathematical functions to fit experimentally observed stress-strain curves.

Kondner (1963), Kondner and Zelasko (1963) proposed a simple hyperbolic form of mathematical relation to describe pre-peak stress-strain curves for soils. Brinch Hansen (1963) proposed two alternative forms, one to account for the possible parabolic shape of the stress-strain curve at small strains, and the other to provide a maximum stress at a finite strain as well as accounting for the parabolic shape at the start of a shear test. The alternative formulae of Brinch Hansen are equivalent to other empirical formulae provided by Brinch Hansen which were themselves modified forms of some theoretical relationships deduced by means of a simple assumption concerning the distribution states of particle contacts on a potential rupture surface, Brinch Hansen (1965).

Desai (1971) employed mathematical spline functions to describe stress-strain curves for various types of soil. One advantage of spline functions is their ability to describe behaviour exhibiting decreasing stress beyond peak. However the mathematical equations involved are extremely cumbersome.

Wroth and Bassett (1965) suggested the use of exponential functions to describe the stress-strain relations for sand. Their proposed formula, although of an empirical nature, was based on the critical state theory developed at Cambridge. When the mathematical curves were compared with experimental results obtained from the simple shear apparatus it was found that although the proposed mathematical formula adequately described the general shape of the stress-strain curves for sand, including the post-peak stage of a test, the mathematical curve at no stage coincided with the experimental curve and overestimated the peak strength by 15%.

It has been demonstrated that the strength of sand in triaxial compression is independent of the stress path provided that the mean principal stress (or cell pressure) at failure is the same, Bishop and Eldin (1953), Cornforth (1961). It would appear that the stress-strain relation for sands is also independent of stress path for cases of increasing principal stress ratio. Karst et al (1965) obtained a nearly unique relationship between the principal effective stress ratio and axial strain, irrespective of the stress path followed. A similar result was obtained by Khayatt (1967).

If, during the shear stage of a triaxial compression test, the axial deformation is reversed and the sample is completely unloaded it is found that only a small proportion of the axial strain is recovered. If the sample is then reloaded it is found that the unload-reload cycle produces an hysteresis effect. This has been observed by a number of experimenters, Bishop and Henkel (1953), Karst et al (1965), Makhlouf and Stewart (1965), Holubec (1966), Khayatt (1967). Other investigators have observed similar

hysteresis effects during dynamic cyclic tests to investigate the effect of vibrations, Seed and Lee (1966), Hardin and Black (1966), and Timmerman and Wu (1969).

The unload-reload behaviour of sand is best illustrated by the results of the research carried out by Makhlouf and Stewart (1965). It was found that the irrecoverable strains continued at a decreasing rate with continuous cycling and that the width of the hysteresis loop also decreased as the number of cycles increased. No attempt was made to determine whether or not the hysteresis and irrecoverable strains could be eliminated by extensive cycling. Even Timmerman and Wu (1969), using an electrical exciter to apply the stress cycles, found that irrecoverable strains may still occur after 200,000 cycles.

Makhlouf and Stewart (1965) considered that the slope of the reloading curve could be used to define the modulus of elasticity of sand which was found to increase with density and confining pressure. They also concluded that, at a given initial density and confining pressure, the modulus of elasticity depended on the range of deviator stress cycled and the magnitudes of either the maximum or minimum stress limits to the cycle. However, an examination of the results given in the paper would appear to indicate that the modulus of elasticity, as defined by the writers, is dependent solely on the deviator stress at the start of reloading, for a sand at a given initial density and confining pressure.

The above review describes research that has been carried out during a period in which triaxial testing techniques have been continuously improved. One of the most significant improvements during this period has been the successful introduction of 'end-lubrication' to promote uniform deformation of test samples. Consequently, of the work described above, one would expect the earlier test data to be less reliable and conclusions should be viewed with caution where uniform specimen deformation is essential to the correct interpretation of the results.

3.3. Test program and testing procedures.

The triaxial compression tests carried out in the course of this research project can be divided into three distinct series, as shown in Table 3.1.

Table 3.1.

TEST SERIES	CONSOLIDATION	SHEAR	NUMBER OF TESTS
1	Ko	monotonic	12
2	ambient	cyclic	8
3	ambient	monotonic	4

3.3.1. First series.

This series of tests (TC 1 - 12) was the first series of tests carried out with the new apparatus described in Chapter 2. The primary object of this test series was to test the efficiency of the lubricated membranes and the performance of the apparatus in general. It was decided to consolidate the specimens under zero lateral strain conditions so as to obtain estimates of Ko against which the consolidation of the plane strain specimens could be compared. The specimen dimensions were the same as those envisaged for the plane strain tests. Consequently the lateral dimension in one direction was greater than the platen dimension. The effect of this on the test results will be discussed in sections 3.5 and 3.6.

The procedure used to prepare a specimen ready for testing was described in section 2.4.4. Having filled the cell and raised the burette level with the mid-height of the specimen, the air release valve was closed. The specimen was then standing under a small all-round pressure of about 10 kN/m^2. Before the consolidation stage was started the pedestal of the loading machine was raised to bring the plunger into contact with the top platen. Contact was made sufficient to change the

load cell output voltage by 0.2 mV which corresponded to a deviator stress of approximately 10 kN/m^2. When the level in the burette was steady the deflection dial gauge was zeroed and the drainage system was switched to a 10 ml burette.

The method used to control the Ko consolidation stage was the burette method proposed by Bishop (1950). After the initial readings on the datalogger and the burette had been taken, the motor drive was connected at a nominal rate of axial deformation of 0.03 mm/min. As the specimen was strained axially, the cell pressure was adjusted, using a screw-control cylinder, to maintain equality between the change in volume of the specimen and the volume swept out by the top platen. Charts prepared beforehand and based on the initial cross-sectional area, as measured, greatly assisted this operation.

As the cell pressure approached 100 kN/m^2 the motor was switched off and the cell pressure was then connected to the pre-set self-compensating mercury control system. The pedestal of the loading machine was then manually adjusted to obtain the required correlation between the axial and volumetric strains. A couple of minutes were allowed to elapse in order to ensure that consolidation was complete and then the specimen was sheared by applying axial deformation at a nominal rate of 0.03 mm/min, the same as that used during Ko consolidation. This rate corresponded to a strain rate of approximately 3% per hour, the choice being dictated by the convenience of taking readings and making any adjustments rather than drainage requirements.

During the first 1% axial strain that occurred readings of the dial gauge, burette, and datalogger were recorded at intervals of 0.05 mm deflection. Thereafter, the intervals were increased to 0.1 mm.

At the conclusion of the test the motor drive was stopped, the clutch disengaged, and the specimen was unloaded by hand until the plunger was well clear of the top platen. The drainage taps at the cell

base were then closed to seal off the specimen. The self-compensating mercury control system was disconnected and the cell pressure was reduced to atmospheric. This method of sustaining the specimen during dismantling was used in order to prevent excessive wrinkling of the sample sheath, Green (1969).

The cell was drained and carefully dismantled. Any photographs or measurements of the specimen were then taken if required. The specimen was removed and the apparatus was cleaned in preparation for the next test.

3.3.2. Second series.

The second series of triaxial compression tests (TC 13 - 20) was conducted after all but a few plane strain tests had been performed. The cross-sectional area of these specimens was smaller than the previous specimens and permitted lateral expansion of the specimens to occur throughout the tests without overlapping of the platens. The purpose of this series of tests was to provide information about the triaxial compression behaviour of sand when subjected to cycles of loading, and to provide a basis for comparison with cyclic loaded plane strain tests. For simplicity, the specimens were consolidated under ambient stress conditions.

Ambient consolidation was carried out by increasing the cell pressure to 100 kN/m^2 in increments and allowing complete consolidation to occur for each increment. When the consolidation stage was complete a deviator stress of about 10 kN/m^2 was applied by manually adjusting the pedestal of the machine. The specimen was then sheared at a rate of 3% axial strain per hour. Cycles of loading, involving either complete or partial removal of deviator stress, were conducted at various stages of the test. During the unload-reload cycles readings were taken at 0.01 mm intervals on the dial gauge. At the termination of the tests the apparatus was dismantled as described in section 3.3.1.

All the tests in this series except TC 20 were sheared at a constant cell pressure of 100 kN/m^2. In order to investigate the effect of stress path on the unload-reload behaviour TC 20 was sheared with the axial stress nominally constant. In order to compare this test with the constant cell pressure tests TC 20 was consolidated to an ambient stress of 550 kN/m^2. When consolidation was complete the motor drive was connected and the specimen was axially compressed at a nominal rate of 3% per hour. As the axial deformation was applied the cell pressure was simultaneously reduced so that the axial load remain constant.

Since lateral deformation of the specimen occurred the axial stress varied slightly during the test but, for convenience, the test will be referred to as a constant axial stress test.

One unload-reload cycle was performed during the test. This required the cell pressure to be increased during unloading and reduced again during reloading. Using the chosen rate of strain, 3% per hour, the cycle of stress required rapid variation of cell pressure and readings were taken as frequently as possible. The procedures at the end of the test were as described previously.

3.3.3. Third series.

Tests TC 21 - 24 were conducted in an attempt to explain discrepancies between the two previous triaxial compression test series. The testing procedure was identical to that of the second series of tests except that the shear stage consisted of a simple monotonic increase in axial strain.

TC 21 - 23 were similar sized specimens to those of the second series but TC 24 initially overlapped the platens in one direction.

3.4. Consolidation.

The consolidation stage of the tests reported in this thesis was treated merely as a preliminary stage to the shear deformation stage which was the primary area under investigation. Consequently ambient consolidation stages have not been analysed and discussion of the zero

lateral strain consolidation stages will be restricted to consideration of the stress measured.

Bishop (1958) proposed two alternative methods of measuring Ko in the triaxial apparatus. The first method (the burette method) was based on the correlation of axial and volumetric strains to ensure zero lateral strain, as described in section 3.3.1. The second method employed an annular lateral strain indicator which was supported by friction between the indicator pads and the specimen sheath at the mid-height of the specimen.

Andrawes (1964) performed tests to check the accuracy and performance of the two methods proposed by Bishop (1958). He rejected the lateral strain indicator on the grounds that it was difficult to assemble satisfactorily, it produced indentations on the specimen surface, the monitored diameter was not necessarily the one on which the average deformation occurred, and the indicator was not sufficiently sensitive to small changes in cell pressure. Andrawes (1964) also concluded that the value of Ko obtained using the burette method was fairly approximate and did not establish with any certainty whether Ko was a constant or not. The approximation of the resulting values of Ko was attributed to the indeterminacy of the errors present in the strain measurements.

Andrawes (1964) advocated an interpolation method of evaluating Ko, rather than direct measurement, in order to avoid the problem of error corrections. Assuming that Ko could be reasonably considered to be constant throughout a test, a stress controlled test could be performed in which the ratio of major to minor principal stress was constant throughout and equal to the reciprocal of Ko. This test would fulfil the zero lateral strain condition. However, since Ko is unknown before a test, it was proposed that two or more constant stress ratio tests were carried out and, after the results had been corrected for the inherent errors, the value of Ko could be interpolated from the results.

Whilst the interpolation method would be attractive if the evaluation of Ko was a major objective of this research, it was not used because of the number of additional tests required. As already described in section 3.3.1. it was decided to use the burette method proposed by Bishop (1950) since it was considered to be adequate for use in the preliminary stage of tests to investigate shear behaviour, Cornforth (1961), Wightman (1967), Wade (1963), Ismael (1969), Tong (1970), and Dyson (1970).

During the Ko consolidation stages of the tests carried out no attempt was made to account for the errors involved in the strain measurements. Nor were any corrections applied to the results except those also applied to the shear stage results, i.e. correction for compressibility of lubricated membranes and load cell. The principal stress ratio varied at the start of the test but became reasonably constant at stress levels higher than about 30 kN/m^2. The mean of the last three readings taken was used to calculate the value of Ko.

The calculated results, with the axial strain corrections applied, indicated that all the specimens contracted laterally. However, if a correction for membrane penetration was applied to the volumetric strains then the calculated lateral strains would be less, possibly zero, or even negative indicating lateral expansion. Since membrane penetration was minimised rather than calibrated (Appendix B) then lateral compression or expansion can only be assessed by comparing the values of Ko obtained with theory and previous work. It has been found that the value of Ko is sensitive to small lateral movements and any outward movement produces incorrectly low values of Ko.

Many investigators have referred to the work of Jaky (1944) who derived the following theoretical expression for Ko:-

$$Ko = (1-\sin\phi)\ \frac{(1 + \frac{2}{3}\sin\phi)}{(1 + \sin\ \phi\ )} \qquad (3.1)$$

He also suggested that for practical purposes the above expression could be simplified to

$$Ko = 1-\sin \phi \qquad (3.2)$$

All subsequent research has tended to support equation 3.2, see for example Wroth (1972).

The results of the Ko consolidation stages of the first series of triaxial compression tests performed are shown in Fig. 3.1. together with equations 3.1. and 3.2. The values of ϕ used to plot the results were the values obtained from the shear stages of the same tests, after adjustments had been made to allow for the overlapping of the platens (see section 3.5.). It would appear that the results tended to agree with the theoretical expression rather than the $(1-\sin \phi)$ approximation, and in fact are slightly less than those indicated by the theoretical line.

The analysis is complicated by the fact that the results of the ambient consolidated triaxial compression tests gave higher values of ϕ, see section 3.5. If these higher values of ϕ are used the results shown in Fig. 3.1 move to the right by about 2°, and nearer to the $(1-\sin \phi)$ approximation. This can best be shown by Fig. 3.2 which gives the experimental values of Ko plotted against initial porosity. Superimposed on this graph are three lines A, B and C. Line A represents the $(1-\sin \phi)$ approximation using the values of ϕ obtained from the Ko consolidation triaxial compression tests. Lines B and C are the theoretical curves using the results of the ambient consolidated triaxial compression tests, line B being the simple approximation and line C the more elaborate expression.

If the experimental results are compared with line A then it would indicate that a rather excessive amount of lateral expansion occurred. Even a comparison of the results with lines B and C would appear to indicate that a small amount of lateral expansion occurred if previous experimental results are accepted.

3.5. Failure characteristics.

Unless stated otherwise, the term failure will be used to denote the point on the stress-strain curve at which the strength is a maximum, as defined by the ratio of major to minor principal stress.

The variation of the maximum principal stress ratio with initial porosity, for the triaxial compression tests performed, is shown in Fig. 3.3. Fig. 3.3a shows the results obtained from the Ko consolidated tests (TC 1 - 13). The variation of maximum stress ratio with porosity can be reasonably approximated by a straight line. The results of the ambient consolidated specimens are shown in Fig. 3.3b, with the mean line obtained from the Ko consolidated tests superimposed. Although the variation of strength with porosity is similar there is an appreciable difference in the maximum values of principal stress ratio obtained, for the two sets of results.

The solid circles in Fig. 3.3b represent the results of the cyclic tests, including TC 20 (n_i = 41.34%) which was sheared with the axial stress constant. This implies that, for a given mean stress at failure, the strength is stress path independent. In an attempt to clarify the reasons for the difference in the strengths obtained the third series of tests were performed. The results of these tests are denoted by open circles. Tests TC 21 - 23 were subjected to a monotonic increase in axial compression to determine if the cyclic loading produced the increase in strength. TC 24 (n_i = 41.9%) was a similar test but the specimen dimensions were such that the specimen overlapped the platens in one direction from the start of the test, as was the case for the Ko consolidated specimens. It is clear from Fig. 3.3b that neither of these reasons were the cause of the strength difference observed.

Since stress path did not appear to affect the results, demonstrated by the agreement of the constant axial stress test with the other tests performed during the same period, the possibility of strength depending on the type of consolidation was ruled out, although no additional Ko

consolidated tests were performed. That strength is independent of the type of consolidation has been demonstrated by Eldin (1951), Cornforth (1961), Tong (1970), and Dyson (1970).

Due to the overlapping of the platens in the Ko consolidated tests (and TC 24) the recorded axial stresses were in error. Therefore the results of these tests were adjusted using the area of the specimen contained on the platens at any one time to calculate the deviator stress. These adjusted results are shown in Fig. 3.3c which also includes the mean strength-porosity lines obtained from Figs. 3.3a and 3.3b.

Although the adjusted results of the oversized specimens may not describe the precise stress conditions in the specimens, only the adjusted values will be referred to hereafter.

Fig. 3.4 shows the variation of the volumetric strain rate with initial porosity. Both the maximum volumetric strain rate and the volumetric strain rate at failure are plotted. In all the triaxial compression tests the volumetric rate of expansion increased to a maximum and then reduced slightly before the maximum principal stress ratio was reached. There was no apparent difference between the results of the different test series and Fig. 3.4 indicates that a reasonably good linear correlation of both the maximum volumetric strain rate and the volumetric strain rate at failure with initial porosity, for the range of porosities tested.

The variation of the major principal strain at failure with initial porosity, for the various triaxial compression tests, is shown in Fig. 3.5. The results of the first series of tests, in which the specimens were consolidated under approximately zero lateral strain conditions, are reasonably consistent. The results of the other triaxial compression tests show an appreciable scatter which is of a random nature, there being no distinction between tests which were subjected to a monotonic increase in axial strain and the cyclic tests. It is clear however that Ko

consolidated specimens exhibited smaller axial strains to failure than did tests subjected to ambient consolidation.

When lubricated membranes are used to ensure uniform specimen deformation the resulting stress-strain curves tend to exhibit less well defined peaks than when 'fixed ends' are used, Rowe and Barden (1964), Bishop and Green (1965). This was true of the tests reported in this chapter. Consequently it is difficult to determine the exact axial strain at which the maximum principal stress ratio was reached. In order to show this, lines have been drawn on Fig. 3.5, for each test, to indicate the range of axial strain over which the principal stress ratio was within 1% of its maximum value. As can be seen from Fig. 3.5, the range tended to be between 2.5% and 4.5% axial strain over the range of porosities tested. Clearly, for practical purposes, precise knowledge of the axial strain to failure is not essential.

Although the strength of cohesionless material may be expressed by the maximum principal stress ratio it is usual in boundary value problems to use the term angle of internal shearing resistance, ϕ , where

$$\phi = \sin^{-1}\left[\frac{\left(\sigma_1/\sigma_3\right)_{max} - 1}{\left(\sigma_1/\sigma_3\right)_{max} + 1}\right] \qquad (3.3)$$

Figs. 3.6 and 3.7 show the angle of internal shearing resistance plotted against initial porosity and volumetric strain rate at failure respectively. Both figures are obscured by the apparent difference in strength between the Ko consolidated tests and the later tests. In order to draw comparisons between triaxial compression and plane strain behaviour, which will be dealt with in Chapter 4, it is necessary to decide which set of results is relevant. However, this will be postponed until after the stress-dilatancy behaviour has been discussed in Chapter 5.

Due to the scatter in the results of both sets of tests shown in

Fig. 3.6. it is not clear whether the strength-porosity relation is linear or slightly non-linear. Therefore, for simplicity, a straight line relationship has been assumed. For similar reasons straight lines have been fitted to the results shown in Fig. 3.7 although the true relationship between ϕ and the volumetric strain rate at failure may be slightly non-linear, and still be compatible with the experimental data.

Bishop (1971) suggested that by plotting strength against the rate of volume change at failure, as in Fig. 3.7, the residual or critical state strength could be obtained by extrapolation to the strength axis. It is interesting to note that, although there was no apparent difference in the volumetric strain rate at failure between the Ko consolidated tests and the ambient consolidated tests, the critical state strengths obtained from the two sets of results differed. The results of the Ko consolidated tests indicate a value of $\phi_{cv} = 35^{o}$ whereas the other test results give $\phi_{cv} = 37^{o}$.

3.6. Mode of rupture.

It has been observed that, when specimens of sand are tested in triaxial compression, multiple slip planes occur at very large strains if short specimens with lubricated ends are used, Rowe and Barden (1964), Bishop and Green (1965). Prior to the introduction of lubricated membranes to encourage uniform specimen deformation it was commonly found that, soon after the maximum principal stress ratio had been passed, a single rupture surface formed and this surface was frequently found to be slightly S-shaped. In this section rupture surface patterns, which were observed in the triaxial compression test series, will be described.

Towards the end of the first triaxial compression test performed, TC 1, rupture surfaces were observed which were rather steeply inclined to the base platen. However, after dismantling the cell these discontinuities were no longer visible. During test TC 2 the specimen was

closely observed in order to determine when and how these discontinuities occurred. Two discontinuities were first sighted at about 9.4% axial strain. They appeared to be caused by the specimen overlapping the base platen. The test was stopped at 10.5% axial strain. The cell was dismantled and the inclination of the rupture surfaces was measured. The rupture surfaces were found to emanate from the bottom edges of the specimen where the specimen overlapped the platen. Both surfaces were approximately plane and were inclined at about 70° and 75° to the horizontal.

During test TC 3 the progressive nature of the discontinuities was observed. As in the previous test, two rupture surfaces were visible. The discontinuities were initiated at the two bottom overlapping edges of the specimen at about 7.9% axial strain. The discontinuities then progressively increased in length until they had reached the mid-height of the specimen at about 12.4% axial strain. With further increase in axial strain, one of the discontinuities continued to lengthen until at 19.3% axial strain, when the test was terminated, it was visible over three-quarters of the height of the specimen. Unfortunately the discontinuities were no longer visible after the cell had been removed but their inclination to the horizontal was about 70°. Test TC 4 was discontinued at about 8% axial strain because of an apparatus defect but no rupture surfaces were observed either during or after the test.

During test TC 5 the progressive nature of the rupture surfaces was again monitored. Two discontinuities were initiated at the bottom overlapping edges of the specimen at about 9.2% axial strain and had progressed to the mid-height of the specimen by about 12.7% axial strain. Then, at 14.5% axial strain, multiple slip planes suddenly appeared, emanating from both the top and bottom specimen/platen interfaces. Unfortunately it was not possible to measure the inclination of the planes as excessive wrinkling of the specimen sheath occurred when the plunger was lifted off the top platen. The multiple slip planes were

observed to be less steeply inclined than the edge initiated discontinuities.

The same pattern was repeated during test TC 6. Once it had been established that the maximum principal stress ratio had been passed no more load and volume change readings were taken but deformation of the specimen was allowed to continue and photographs of the specimen at various stages of the test were taken. Fig. 3.8a shows the specimen at 10% axial strain. The discontinuity emanating from the lower overlapping edge of the specimen can be clearly seen. At about 16% axial strain multiple slip planes suddenly appeared as shown in Fig. 3.8b. It is clear from the photographs that the inclination of the multiple slip planes are much less than that of the edge discontinuity. After the end of the test, when the cell had been dismantled, the inclinations of the various rupture surfaces were measured. It was found that all the multiple slip planes were inclined at approximately 62° to the horizontal, whereas the edge initiated discontinuity was at an inclination of 72°. Test TC 7 behaved in exactly the same way as TC 6 but the specimen was lost on dismantling.

In the remainder of the Ko consolidated tests the tests were terminated before any multiple slip planes formed. With the exception of TC 12, discontinuities were observed emanating from the overlapping edges of the specimens. In tests TC 8 and TC 11 the inclinations of the discontinuities were not measured but measurements of TC 9 and TC 10, after the tests, both gave values of α , the inclination of the rupture surface to the horizontal, to be about 70°.

Test TC 12 was prepared without vibration in order to compare the uniformity of deformation with that obtained using vibrated specimens. No rupture surfaces were observed. The specimen expanded excessively at the base and little expansion was observed at the top. When the cell pressure was removed the specimen collapsed and so no final measurements of the specimen dimensions were possible.

The ambient consolidated tests were carried out on smaller specimens which did not expand beyond the edges of the axial platens. None of these tests exhibited rupture surface formation. Nor were rupture planes visible during TC 24, which was on an oversized specimen, since the test was terminated soon after the maximum principal stress ratio had been reached.

Although no final measurements of the specimen dimensions were taken for the triaxial compression test series it is clear from Figs. 3.8a and 3.8b that the lateral deformation was reasonably uniform even at large strains when multiple slip planes had occurred. It would be expected therefore that the required uniformity of deformation during the pre-peak stage of the test was obtained and that the efficiency of the lubricated membranes was satisfactory. Any non-uniformities within the specimen would appear to be solely due to the edge initiated discontinuities.

As already explained, the edge discontinuities only occurred in specimens which expanded beyond the edges of the platens. The overlapping of the platens increased as the test proceeded causing an increase amount of stress redistribution at the edges of the platens, and thus acted as a stress raiser. Eventually failure occurred locally and a rupture surface was initiated. Continued strain then caused failure to occur in adjacent zones and the discontinuity progressively advanced into the adjacent zones.

According to Mohr-Coulomb theory, the inclination of rupture planes can be predicted from a knowledge of the angle of internal shearing resistance, where the angle of inclination of the rupture plane to the major principal stress direction is given by:

$$\alpha = 45^{\circ} + \frac{\phi}{2} . \qquad (3.4)$$

The theory, however, implies that the rupture surface occurs at failure, i.e. when the principal stress ratio is a maximum. In all the

triaxial compression tests observed the edge discontinuities were not visible until well after the maximum principal stress ratio had been passed. It is possible that the specimen sheath masked the rupture surface initially and that only after additional deformation did the discontinuity become visible through the sheath. In order to observe the discontinuities as early as possible in the tests, a desk lamp was directed at the specimen so as to emphasize the relief on the specimen surfaces. Nevertheless it is still a possibility that the discontinuities were formed at an earlier stage in the test.

However, even if it is assumed that the discontinuities did in fact occur at peak then the measured values of α are not supported by the theoretical values. Using peak stress values one can obtain a maximum possible value of α, given by equation 3.4. From the results of the Ko consolidated tests the maximum possible values of α range between 63.7^{o} and 66.7^{o}. These values are not supported by the observed angles of inclination of the edge discontinuities. Even if the strengths obtained from the ambient consolidated specimens are used the theoretical values are only increased by about 1^{o}, and are still much less than the average inclination of 70^{o} observed in the tests.

It is therefore concluded that the Mohr-Coulomb theory does not correctly predict the inclination of rupture surfaces. Other theories are available which purport to allow predictions of rupture surface inclinations to be made but these theories, at present, appear to be controversial, King and Dickin (1970), (1971), Rowe (1971), Bransby (1971). For convenience, discussion and analysis of these theories will be postponed until Chapter 5 in which the stress-dilatancy theory of Rowe (1962) will be covered in detail.

However, it is possible to make a few observations concerning the inclination of rupture planes without resorting to any mathematical theory. If a discontinuity is initiated at a certain location within a specimen of sand and then progresses through the specimen the possible

directions followed by the discontinuity are limited. It is physically impossible for a discontinuity to pass through a particle and so the inclination of the discontinuity at any location in the specimen is dictated by the spacial arrangement of the particles. From this simple fact two observations emerge. First, since the edge discontinuities and the multiple slip planes occurred at different stages of the test and were at different inclinations, it is clear that packing alone does not control the rupture mechanism. Secondly, the observed inclinations, see Fig. 3.8b, also clearly demonstrate that the orientation of the particles varied throughout a triaxial compression test.

3.7. Deformation characteristics.

With the notable exception of the work carried out at Manchester University to substantiate the stress-dilatancy theory of Rowe (1962), most previous research work on the elemental testing of sands has been directed primarily to consideration of the failure characteristics only. Consideration of deformation characteristics has tended to be limited to general qualitative statements about the shape of the stress-strain curves obtained. All the tests performed in this research program exhibited stress-strain curves which corroborate the work of earlier investigators, with respect to the shape of the curves (see Section 3.2). The results of all the triaxial compression tests, showing principal effective stress ratio and change in volume plotted against axial strain, are given in Appendix C.

The stress-strain curves obtained from the tests in which the axial strain was monotonically increased merely confirm the results of the extensive amount of previous research into the triaxial compression behaviour of sands. There has been, however, less research done in which cycles of unloading and reloading have been applied to specimens of sand. It is worthwhile, therefore, to discuss the cyclic test results in some depth and this will be provided in Section 3.7.1.

In order to analyse deformation problems it has often been found convenient to assume the soil to be linearly elastic. Consequently either the initial tangent or secant modulus has been used to define the stress-strain relationship for the soil. Soils, however, exhibit non-linear stress-strain curves and more sophisticated computer methods of analysis, for example finite element methods, are able to take account of this non-linearity. It is common in these methods to vary the deformation modulus, as the load is increased incrementally, by using the instantaneous values of either the tangent or secant modulus at successive points along the stress-strain curves. It is necessary, therefore, to input into the computer details of the complete stress-strain curve. This can be prohibitive due to the amount of data storage required. Thus, in this context, the use of empirically fitted mathematical functions to describe the stress-strain curves is extremely useful. In this research program, hyperbolic and parabolic curves have been used to provide a concise method of storing the stress-strain data obtained from the tests, however, this will be discussed later in Chapter 6.

3.7.1. Triaxial deformation of sand subject to cyclic loading.

The cyclic test results are given in Appendix C but, unlike the results of the monotonic tests, the lateral strain rather than the volumetric strain has been plotted against the axial strain. Typical examples of the behaviour of specimens subjected to cycles of stress are also given in Fig. 3.9 - 3.12.

It is clear from the results that during virgin loading the strains are predominantly irrecoverable, and that the strains recovered during unloading are not perfectly elastic since the unload-reload cycle produces a small but significant hysteresis effect. The shape of the stress-strain curve subsequent to an unload-reload cycle would appear to be unaffected by the cycle and follows the shape which would have been expected of a monotonic test. This observation is also confirmed by

Fig. 3.13 in which the results of one of the cyclic tests (TC 18, n_i = 39.28%) is compared with a monotonic test (TC 21, n_i = 39.40%). It can also be seen from Fig. 3.13 that the difference in lateral strain for the two tests is solely due to the deformations that occurred during each unload-reload cycle.

Close examination of the results clearly shows that the reload curve is non-linear. It would appear that the curvature is independent of initial porosity, and is unaffected by the maximum previous values of stress ratio or axial strain, until the maximum previous value of axial strain is reached. As already noted, once the maximum previous value of stress ratio has been passed the curve is similar to the anticipated virgin loading curve. The section of the curve between the maximum value of axial strain and the maximum previous value of stress ratio may be regarded as a transition stage and it is interesting to note that this transition stage is similar for all pre-peak cycles.

Fig. 3.9 shows the results of test TC 13 in which one cycle of partial unloading was carried out. It can be seen that the width of the hysteresis loop is significantly affected by the amount of unloading permitted. It would appear that, during unloading, irrecoverable strains only become significant when low stress ratios are reached. No specimen was subjected to complete unloading because of uncertainties due to the flexibility of the load cell (see Appendix B). However, consideration of all the cyclic test results indicates that, for similar values of minimum stress ratio, the width of the hysteresis loop increased with the maximum previous value of both stress ratio and axial strain. Thus the width of the hysteresis loop appears to be governed by the amount of total work done prior to unloading.

During test TC 19 (Fig. 3.11) the specimen was unloaded at peak and the behaviour during this cycle does not appear to be different from the behaviour during pre-peak cycles. During test TC 18 (Fig. 3.10) however, an unload-reload cycle was applied long after the maximum stress ratio had

been reached. The behaviour of the specimen during this post-peak cycle appears to be somewhat different from pre-peak cyclic behaviour. Although the width of the hysteresis loop is much greater than that of the pre-peak cycles this may be expected due to the large axial strain at which unloading was commenced. However, both the unload and reload curves, in comparison with pre-peak cycles, exhibit a far greater curvature. This suggests that the recoverable strains during post-peak cycles may not predominate to the same extent as may be suggested by pre-peak cycles.

Fig. 3.12 shows the results of test TC 20 during which the axial stress remained approximately constant. It was required to compare the results of this test with a constant cell pressure test of similar initial porosity. This comparison is shown in Fig. 3.14 and Fig. 3.15. The consolidation cell pressure for test TC 20 was selected so that the mean stress at failure was similar for the two tests.

From Fig. 3.14 it can be seen that, for a given mean stress at failure, the strength and the virgin loading curve are reasonably independent of stress path. This conclusion was also reached by Karst et al (1965) and Barden and Khayatt (1968). However, although this may be true for tests with a common mean stress at failure, both the strength and the shape of the stress ratio-strain curve are known to be dependent on mean stress.

Roscoe (1970) demonstrated that, for a common mean stress at the end of consolidation, although the strength was only slightly affected the axial strain to failure, and consequently the shape of the stress ratio-strain curve, was greatly affected by the applied stress path. Although the stress ratio-strain curve may be independent of stress path for a given mean stress level at failure, if the stress ratio-strain data is to be applied to an element of soil in the ground (e.g. in a finite element analysis), then it is necessary to anticipate the stress path which will be followed by the element, when loaded, in order to predict

the mean stress at failure for the element and thus select the appropriate deformation curve.

A cursory glance at Fig. 3.14 might suggest that the pre-peak cyclic behaviour is also independent of stress path. However, closer inspection clearly indicates that the reload curve for the constant axial stress test specimen was concave initially rather than convex. Thus the reloading behaviour of sand appears to be stress path dependent, see also Barden and Khayatt (1968).

Fig. 3.15a and Fig. 3.15b show the effect of stress path on volumetric strain and lateral strain respectively. The behaviour of test TC 14 was characteristic of all the cyclic constant cell pressure tests performed and it is interesting to note that, although some volumetric compression may occur initially, all the specimens expanded laterally from the start of the shear stage. This was true of all the tests performed whether cyclic or monotonic, including the plane strain tests reported later. Indeed, it is difficult to conceive a mechanism by which a uniform specimen would compress laterally under application of a deviator stress with the cell pressure constant.

If volumetric strains are considered, Fig. 3.15a, the effect of stress path is considerable. In contrast to the constant cell pressure test specimen, the constant axial stress test specimen expanded from the start and the expansion was at a decreasing rate. Also, during the unload-reload cycle there was a distinct difference in behaviour. The constant cell pressure test specimen underwent volumetric compression throughout the unload-reload cycle until the maximum previous value of axial strain was reached, after which the specimen expanded. When the constant axial stress test specimen was unloaded considerable volumetric compression occurred but the specimen rapidly expanded immediately reloading was commenced. It is noted that during the reloading state of test TC 20 a temporary constant volume condition occurred and this probably explains the 'overshooting' of the stress ratio-axial strain curve in Fig. 3.14.

Fig. 3.15b shows that both specimens immediately expanded laterally when shearing was commenced although the constant cell pressure test specimen expanded at an increasing rate and the constant axial stress test specimen expanded at a decreasing rate. During unloading, both specimens compressed laterally but the lateral compression was much greater for the constant axial stress test specimen. Both specimens expanded laterally immediately reloading was commenced, and in the same manner as at the start of the tests. It is noted that, during an unload-reload cycle, the lateral strain-axial strain curves were only retraced when the mean stress was reducing. Thus it would appear that, except for the constant stress ratio case, Rowe (1971), the only occasions when strains are even approximately elastic are when the mean stress is reducing at stress ratio levels below the maximum previous value of stress ratio.

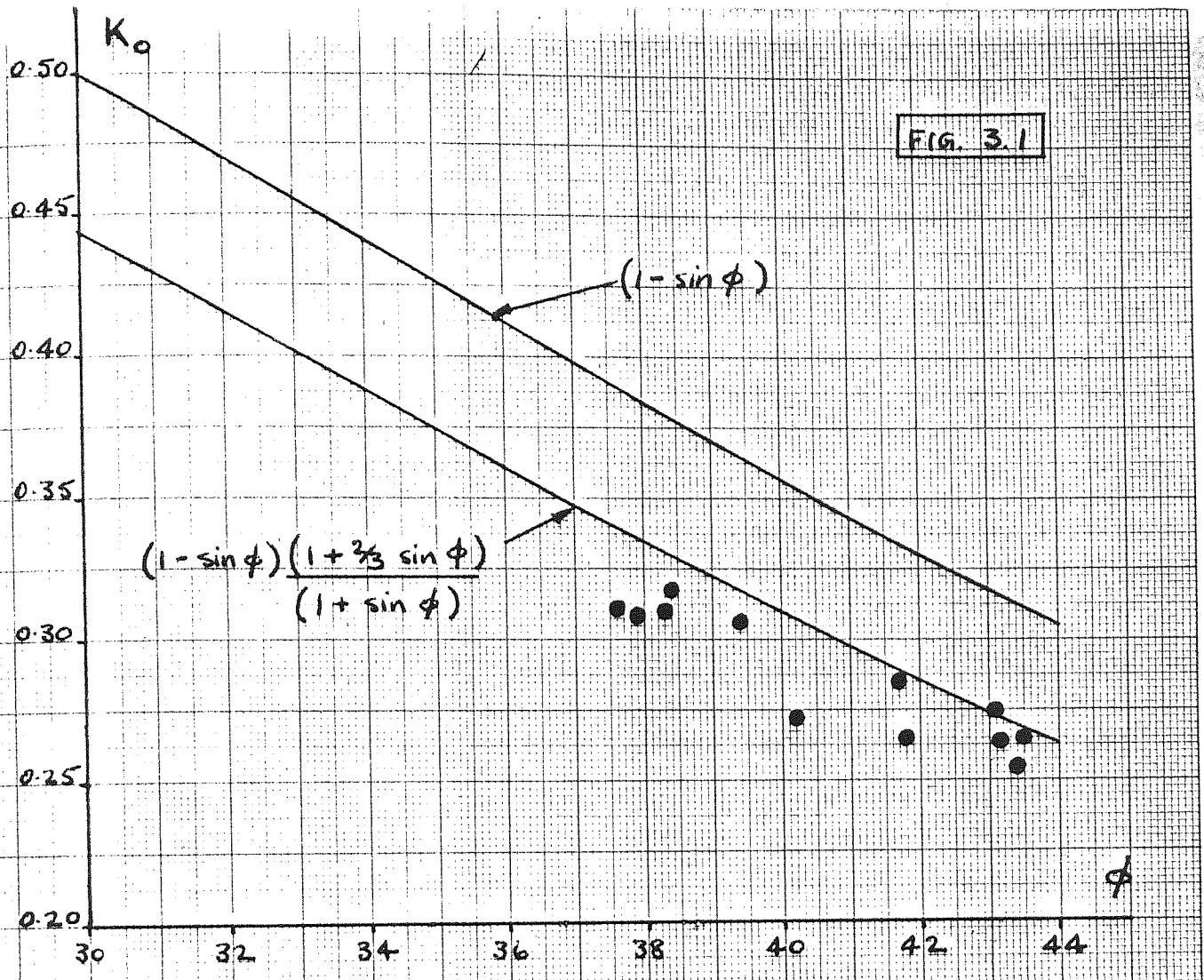
K_o
0·50
0·45
0·40
0·35
0·30
0·25
0·20
30
32
34
36
38
40
42
44
ϕ
$(1-\sin\phi)$
$(1-\sin\phi)\dfrac{(1+\frac{2}{3}\sin\phi)}{(1+\sin\phi)}$

FIG. 3.1

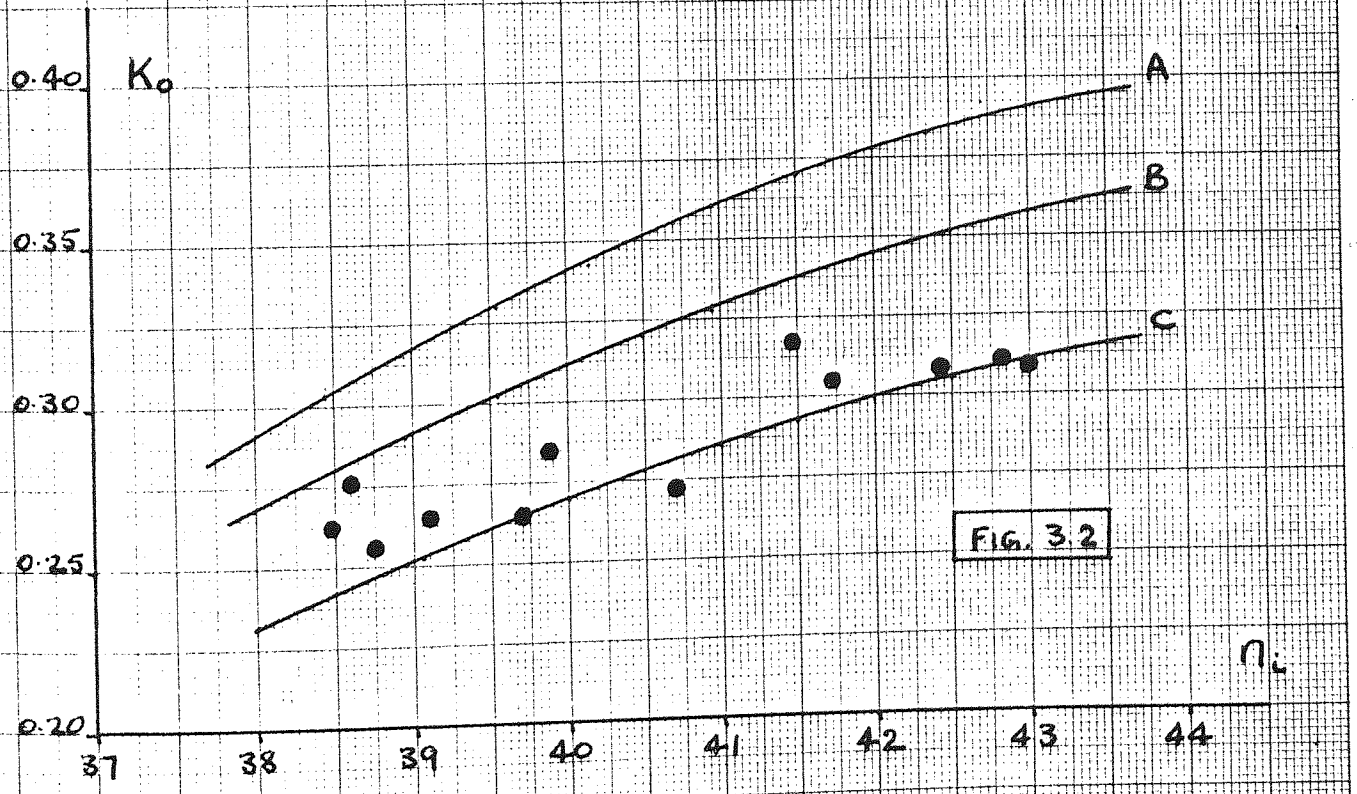
K_o
0·40
0·35
0·30
0·25
0·20
37
38
39
40
41
42
43
44
ϕ
A
B
C

FIG. 3.2

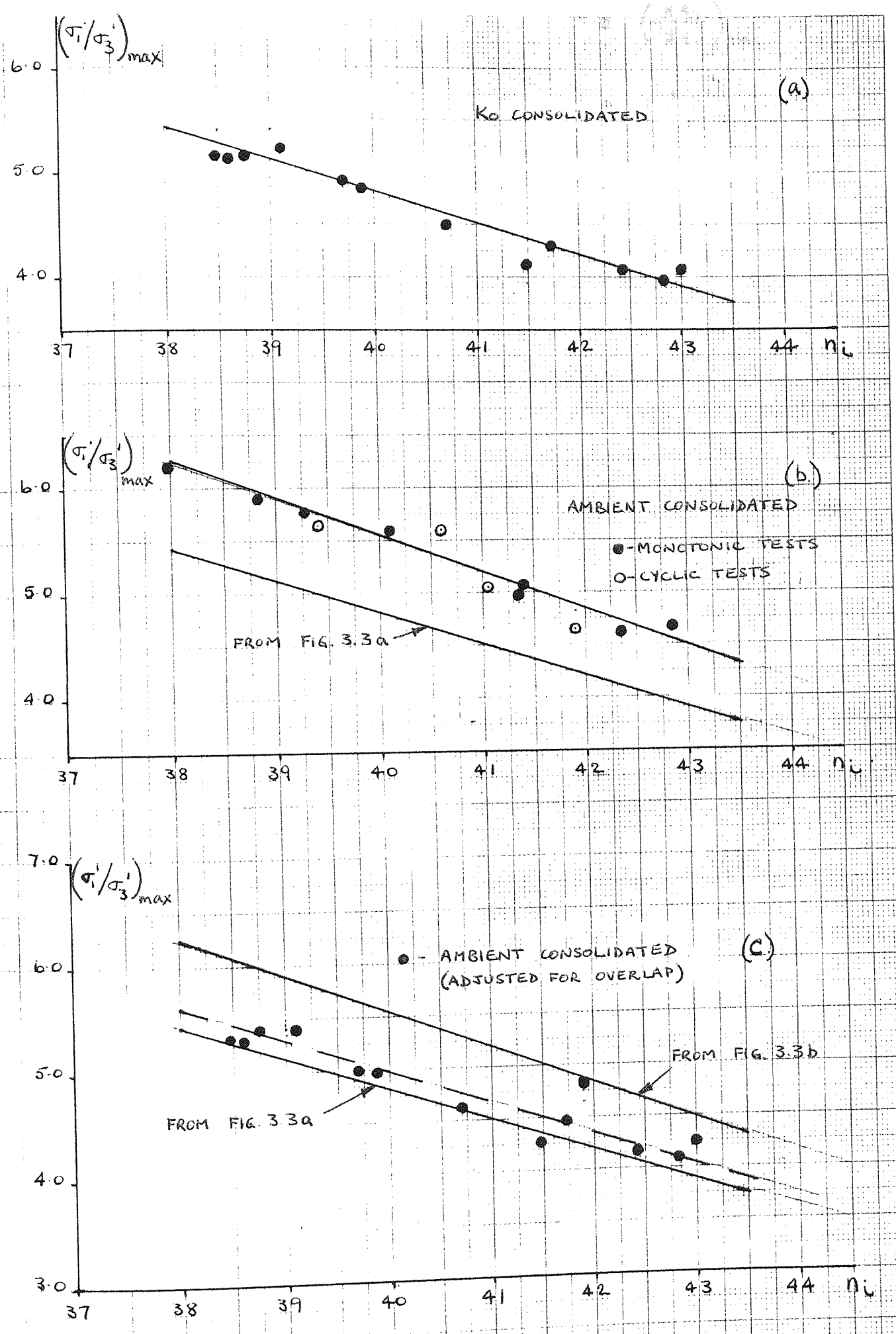
$(\sigma_1'/\sigma_3')_{max}$
6·0
5·0
4·0
(a)
K_o CONSOLIDATED
37
38
39
40
41
42
43
44
n_i
$(\sigma_1'/\sigma_3')_{max}$
6·0
5·0
4·0
(b)
AMBIENT CONSOLIDATED
●-MONOTONIC TESTS
O-CYCLIC TESTS
FROM FIG. 3.3a
37
38
39
40
41
42
43
44
n_i
$(\sigma_1'/\sigma_3')_{max}$
7·0
6·0
5·0
4·0
3·0
(c)
● - AMBIENT CONSOLIDATED
(ADJUSTED FOR OVERLAP)
FROM FIG. 3.3b
FROM FIG. 3.3a
37
38
39
40
41
42
43
44
n_i

FIG. 3.3.

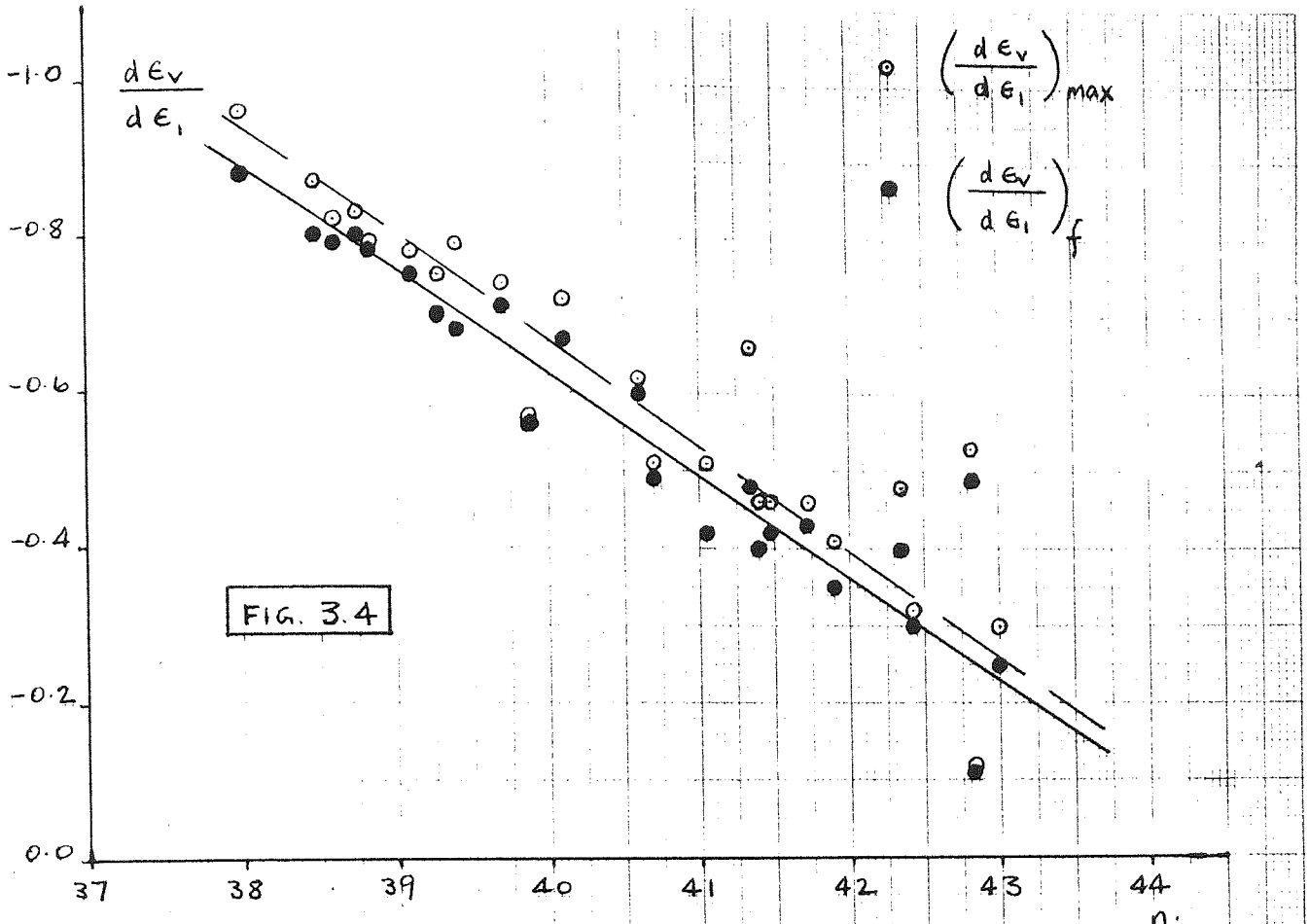
$\frac{d\epsilon_v}{d\epsilon_1}$
$\left(\frac{d\epsilon_v}{d\epsilon_1}\right)_{max}$
$\left(\frac{d\epsilon_v}{d\epsilon_1}\right)_f$
-1·0
-0·8
-0·6
-0·4
-0·2
0·0
37
38
39
40
41
42
43
44
n_i

FIG. 3.4

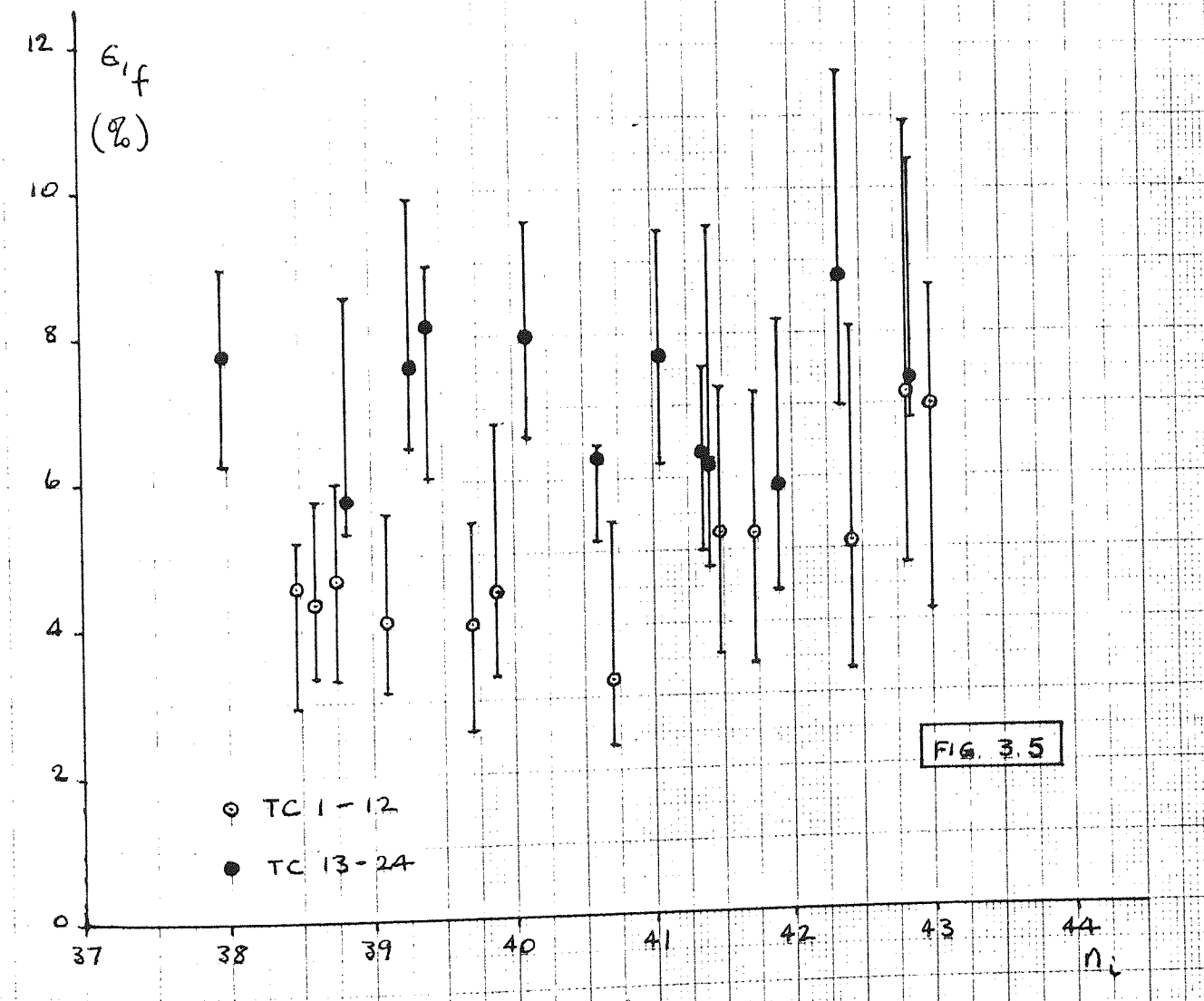
ϵ_{1f}
(%)
12
10
8
6
4
2
0
37
38
39
40
41
42
43
44
n_i
TC 1 - 12
TC 13 - 24

FIG. 3.5

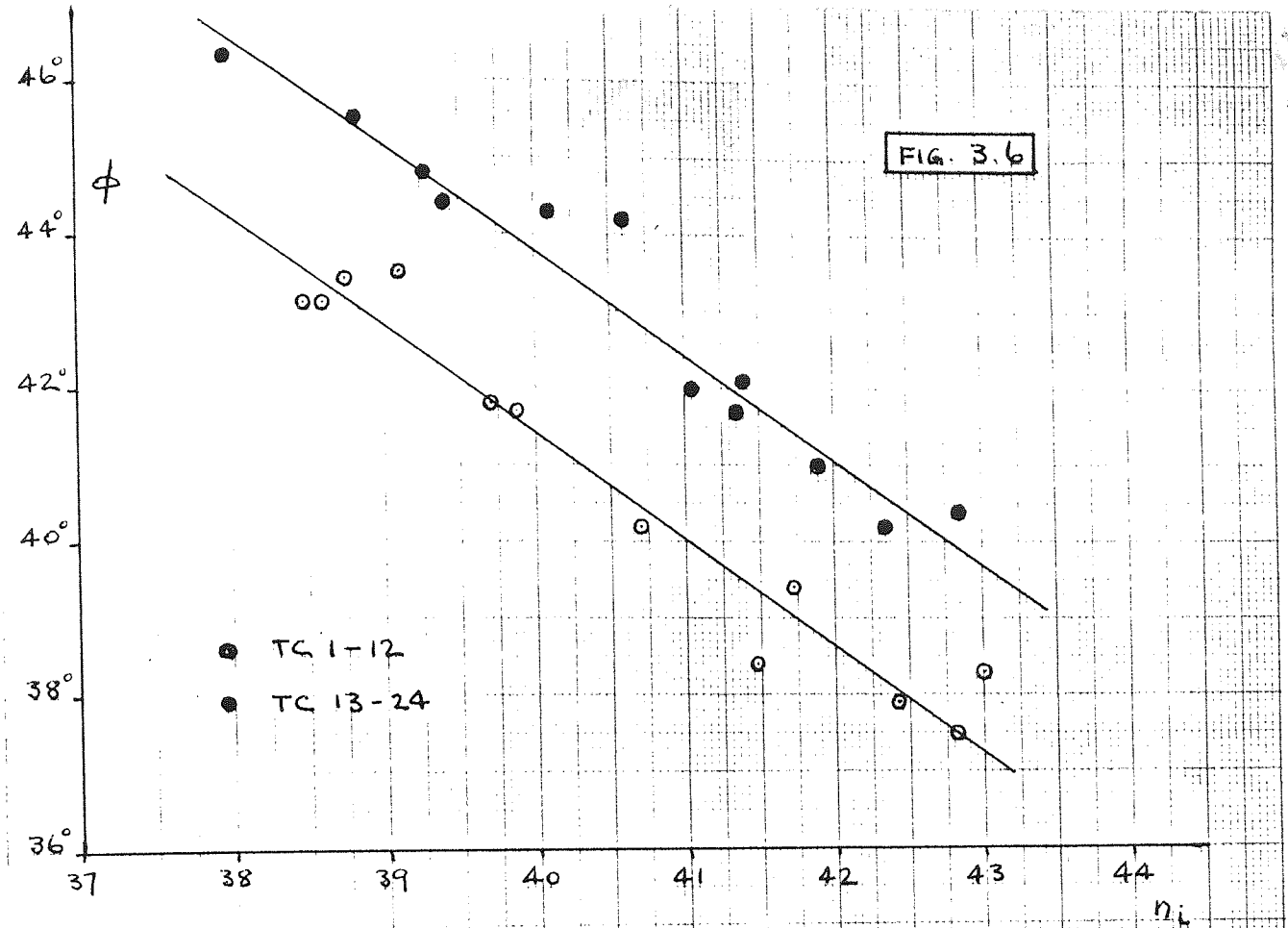
46°
44°
42°
40°
38°
36°
φ
TC 1-12
TC 13-24
37
38
39
40
41
42
43
44
n_i

FIG. 3.6

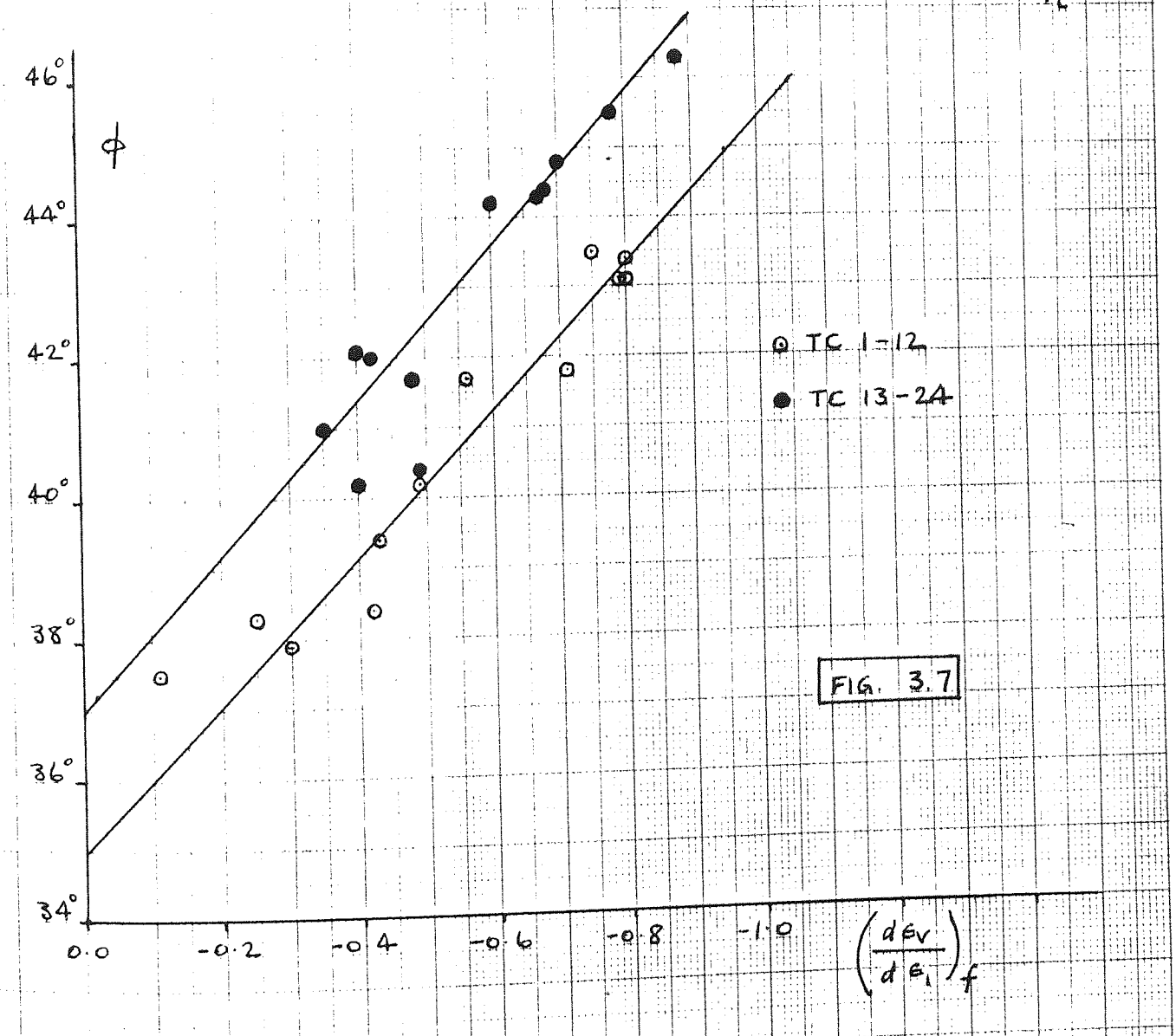
46°
44°
42°
40°
38°
36°
34°
φ
TC 1-12
TC 13-24
0.0
-0.2
-0.4
-0.6
-0.8
-1.0
$\left(\frac{d\epsilon_v}{d\epsilon_1}\right)_f$

FIG. 3.7

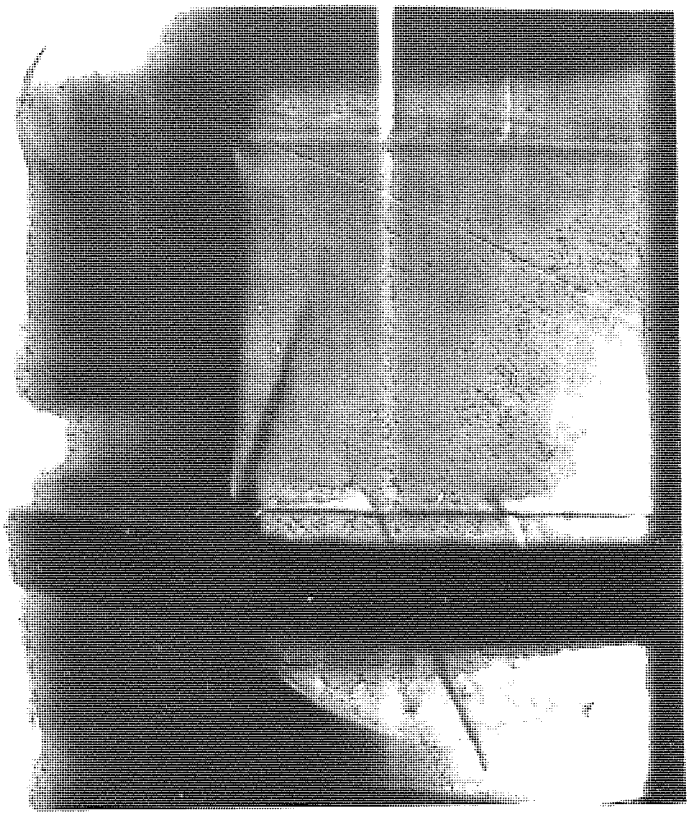

Fig. 3.7a

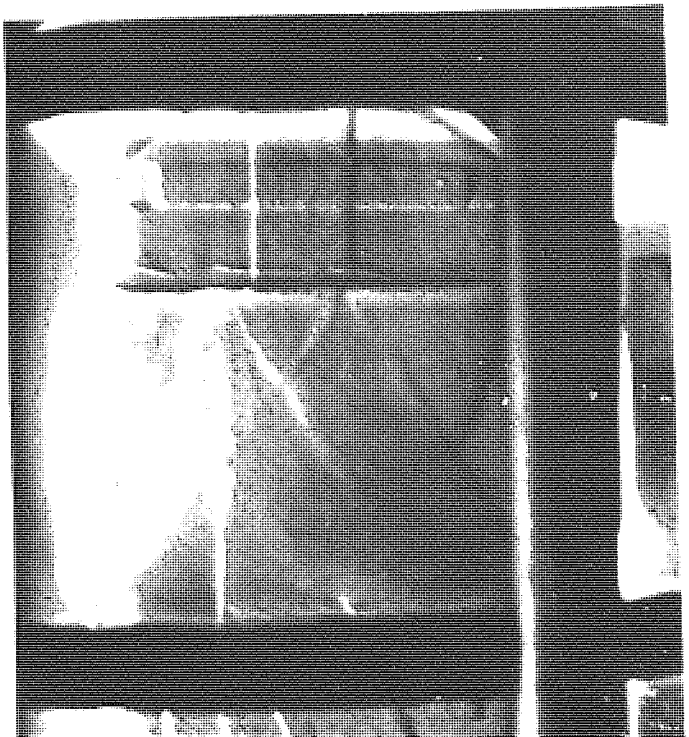

Fig. 3.7b

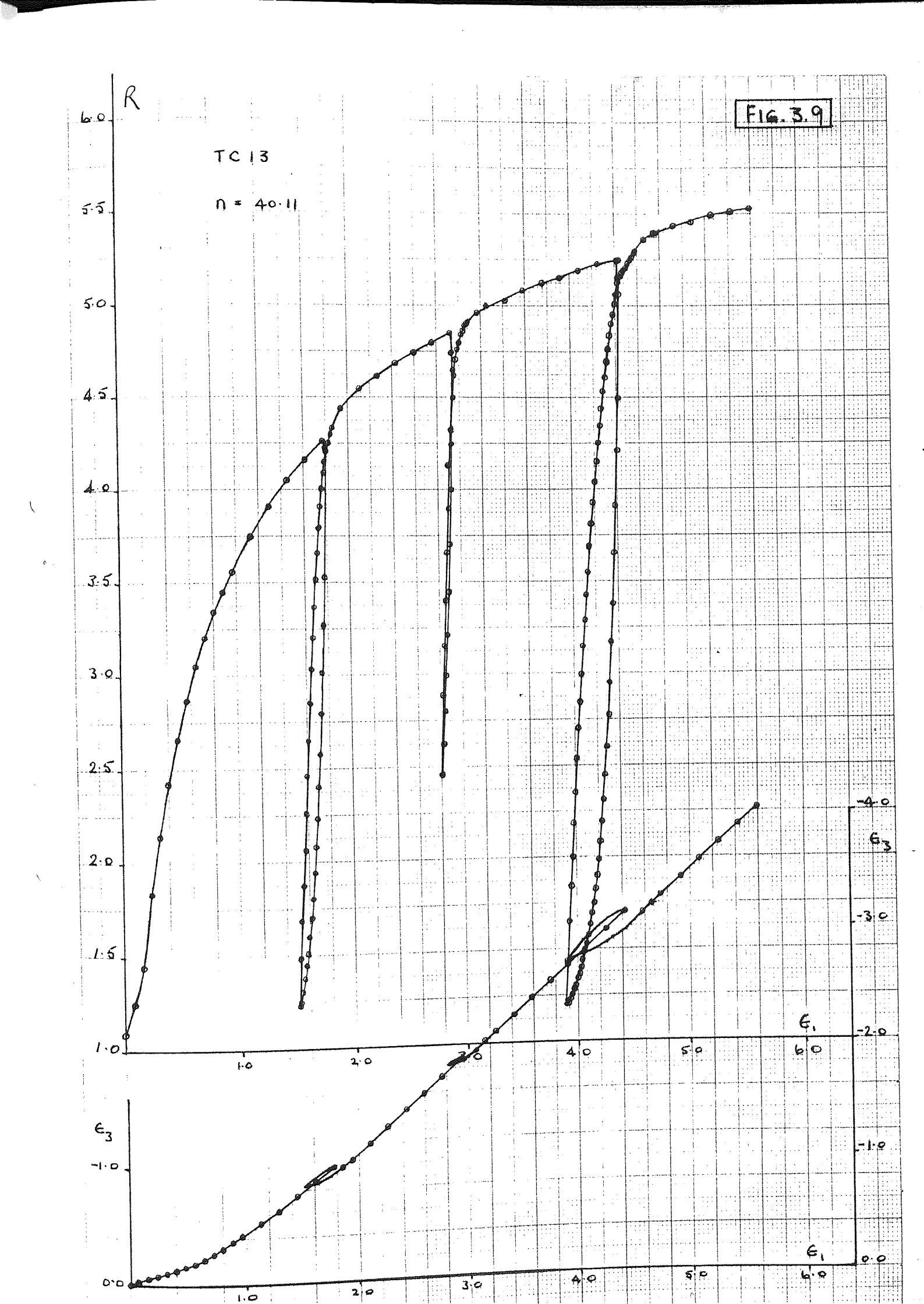
R
FIG. 3.9
TC 13
n = 40·11
6·0
5·5
5·0
4·5
4·0
3·5
3·0
2·5
2·0
1·5
1·0
1·0
2·0
3·0
4·0
5·0
6·0
ϵ_1
ϵ_3
-4·0
-3·0
-2·0
ϵ_3
-1·0
0·0
1·0
2·0
3·0
4·0
5·0
6·0
ϵ_1
-1·0
0·0

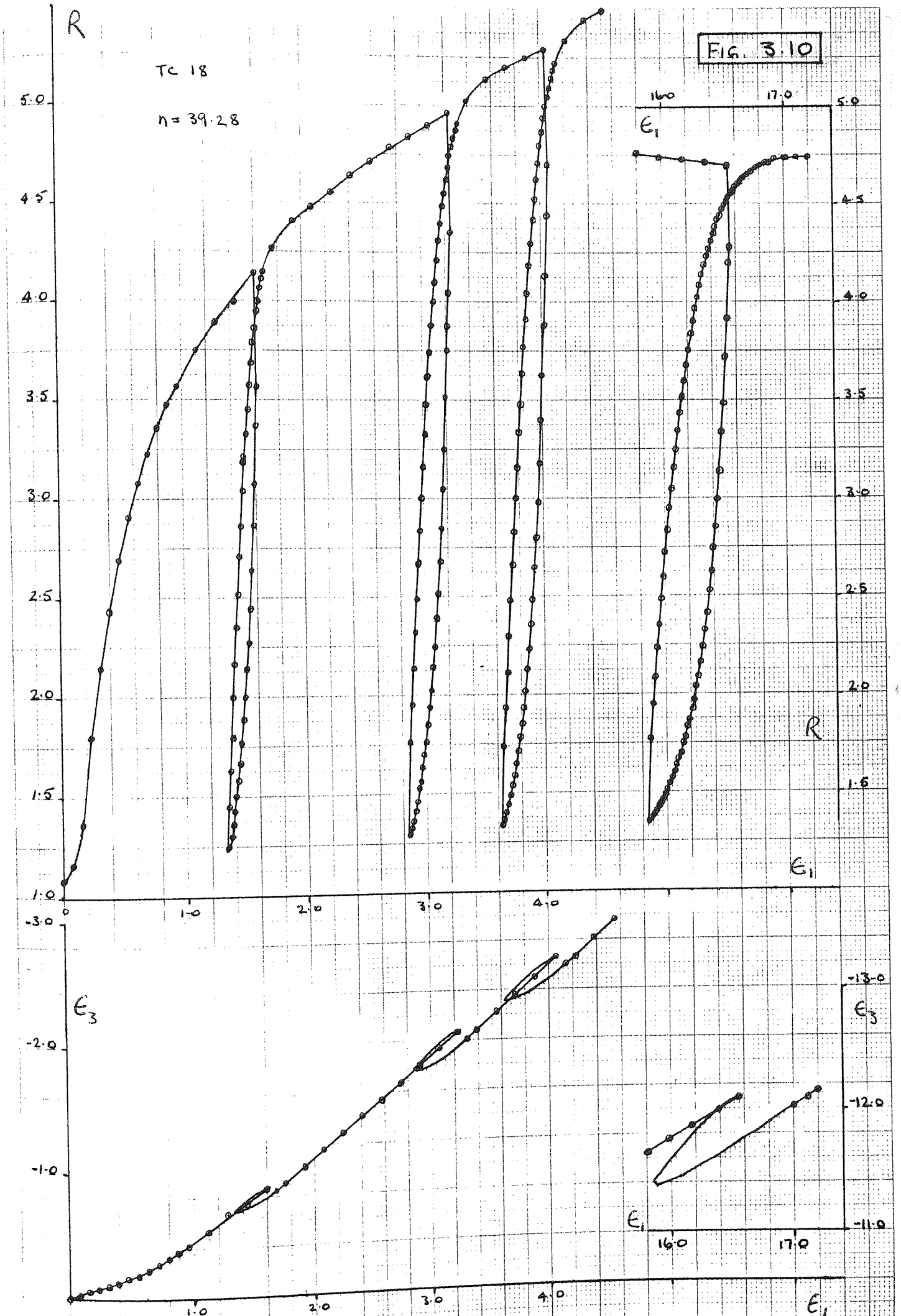
FIG. 3.10
R
Tc 18
n = 39.28
5.0
4.5
4.0
3.5
3.0
2.5
2.0
1.5
1.0
0
1.0
2.0
3.0
4.0
ϵ_1
16.0
17.0
R
ϵ_3
-3.0
-2.0
-1.0
-13.0
-12.0
-11.0

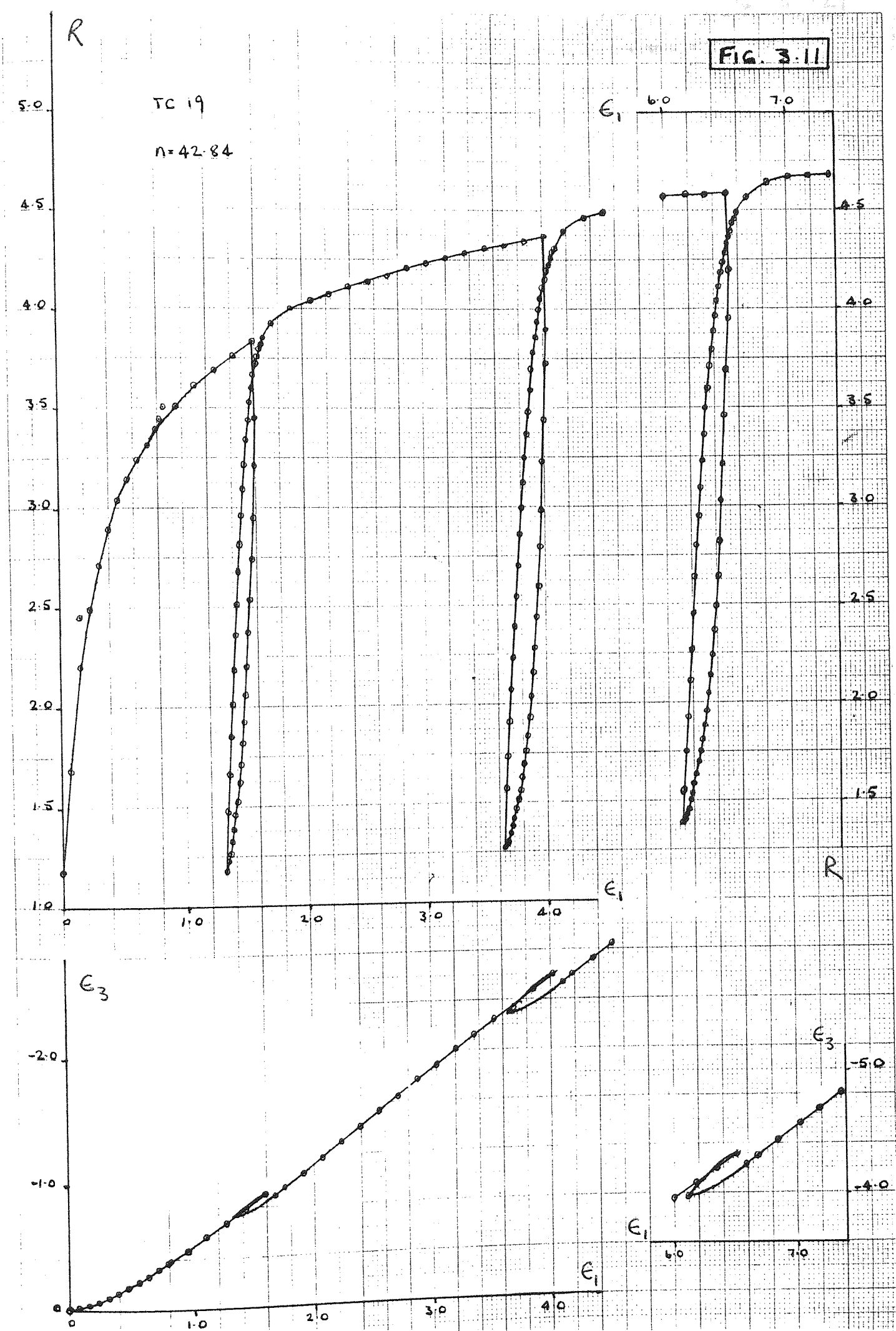
FIG. 3.11
R
TC 19
n = 42·84
5·0
4·5
4·0
3·5
3·0
2·5
2·0
1·5
1·0
0
1·0
2·0
3·0
4·0
ϵ_1
6·0
7·0
ϵ_3
-2·0
-1·0
-5·0
-4·0

FIG. 3.12

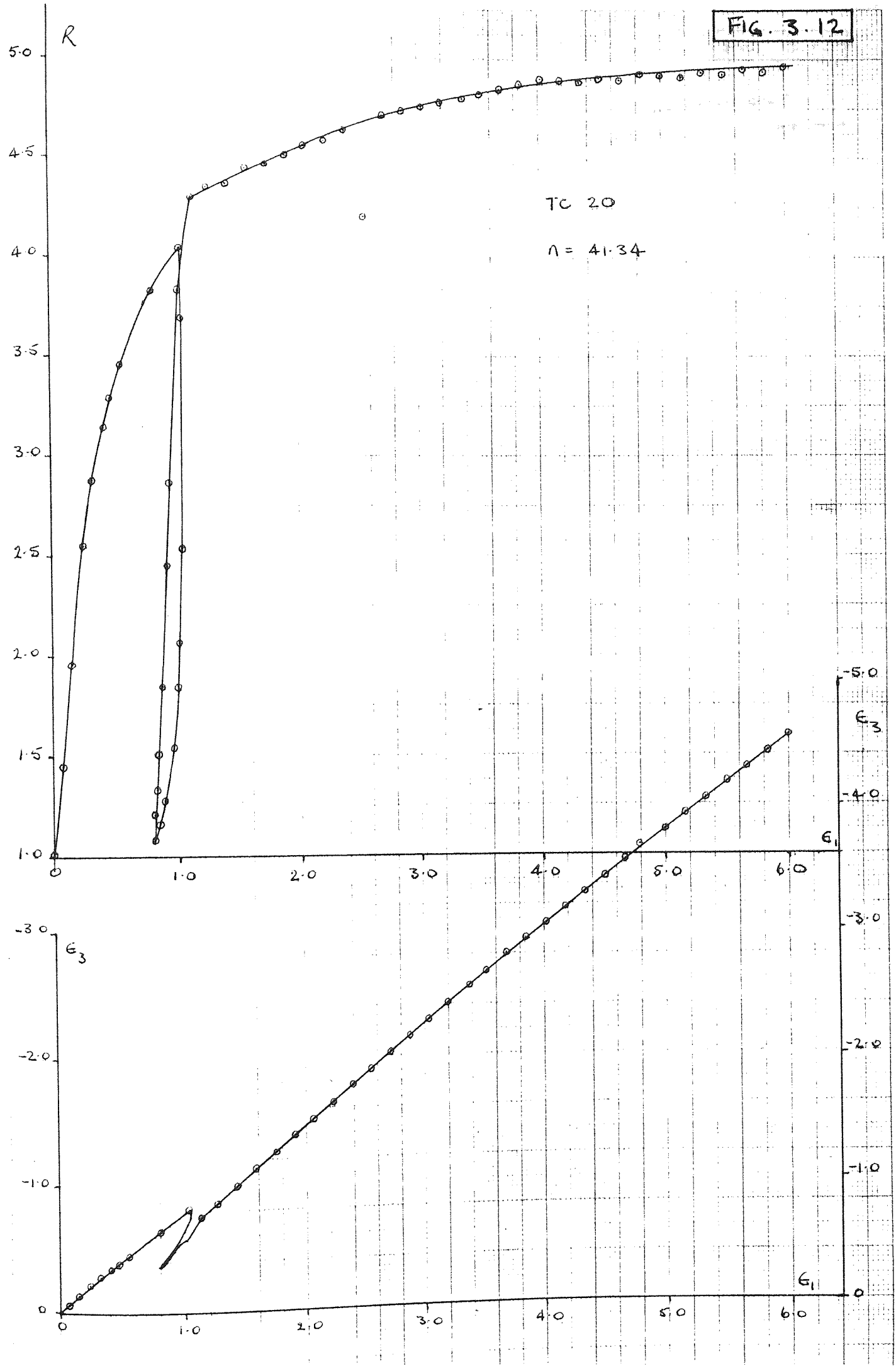
R
5·0
4·5
4·0
3·5
3·0
2·5
2·0
1·5
1·0
0
1·0
2·0
3·0
4·0
5·0
6·0
TC 20
n = 41·34
-5·0
-4·0
-3·0
-2·0
-1·0
0
ϵ_3
ϵ_1

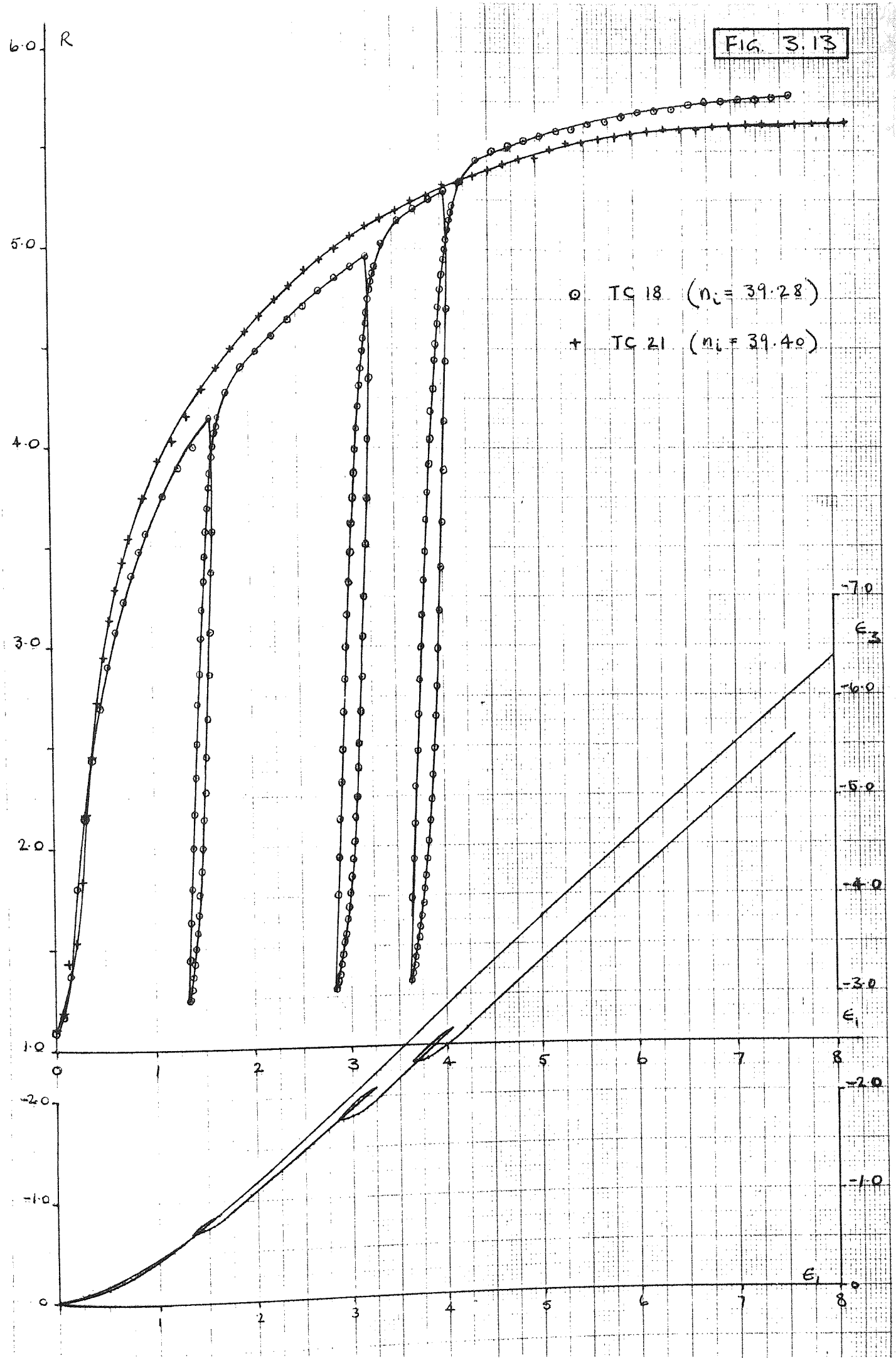
FIG. 3.13
R
6·0
5·0
4·0
3·0
2·0
1·0
o TC 18 (n_i = 39·28)
+ TC 21 (n_i = 39·40)
-7·0
ϵ_3
-6·0
-5·0
-4·0
-3·0
ϵ_1
0
1
2
3
4
5
6
7
8
-2·0
-1·0
0
ϵ_1

FIG. 3.14

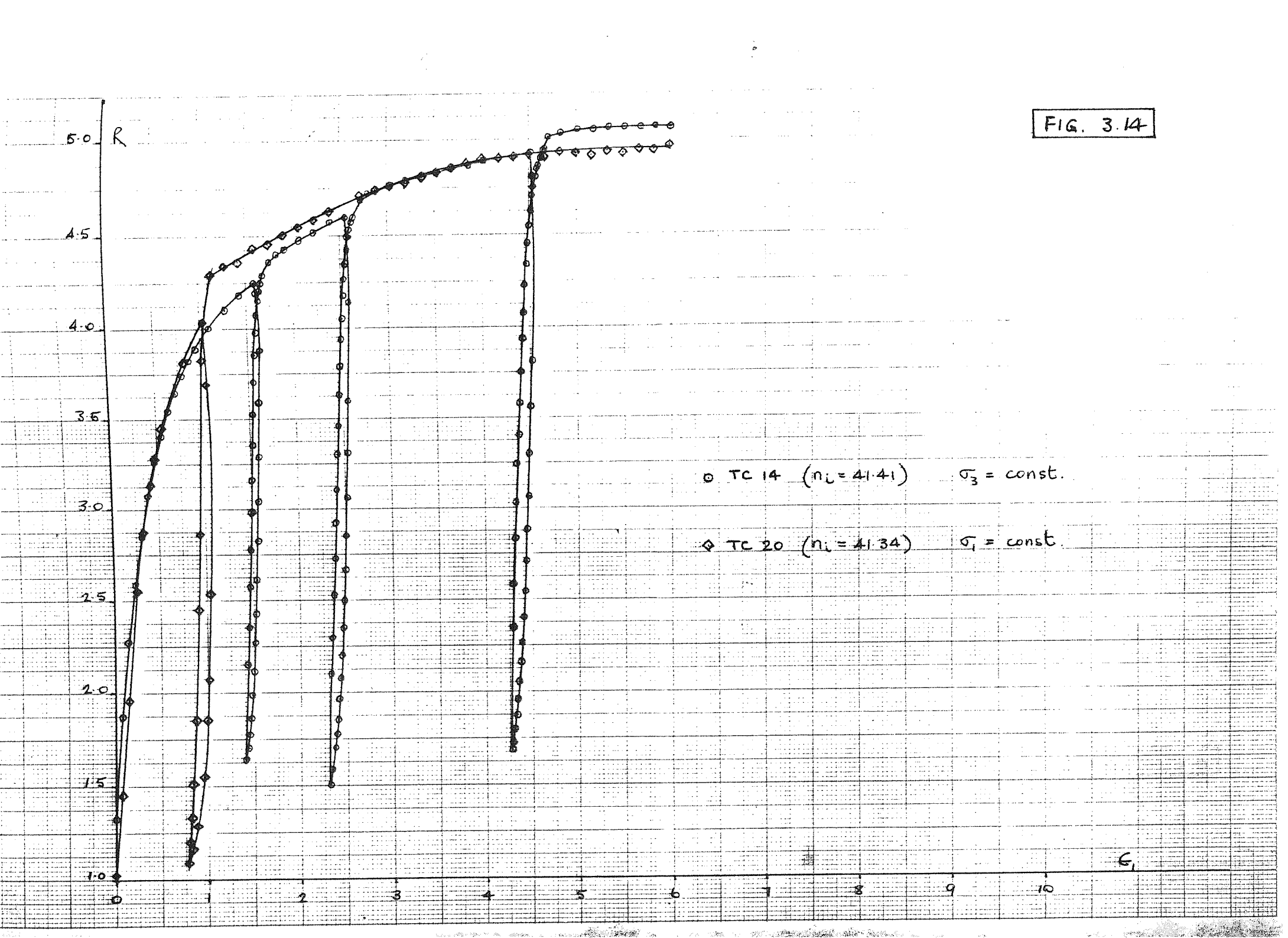
R
5·0
4·5
4·0
3·5
3·0
2·5
2·0
1·5
1·0
0
1
2
3
4
5
6
7
8
9
10
ϵ_1
⊙ TC 14 $(n_i = 41.41)$ σ_3 = const.
◇ TC 20 $(n_i = 41.34)$ σ_1 = const.

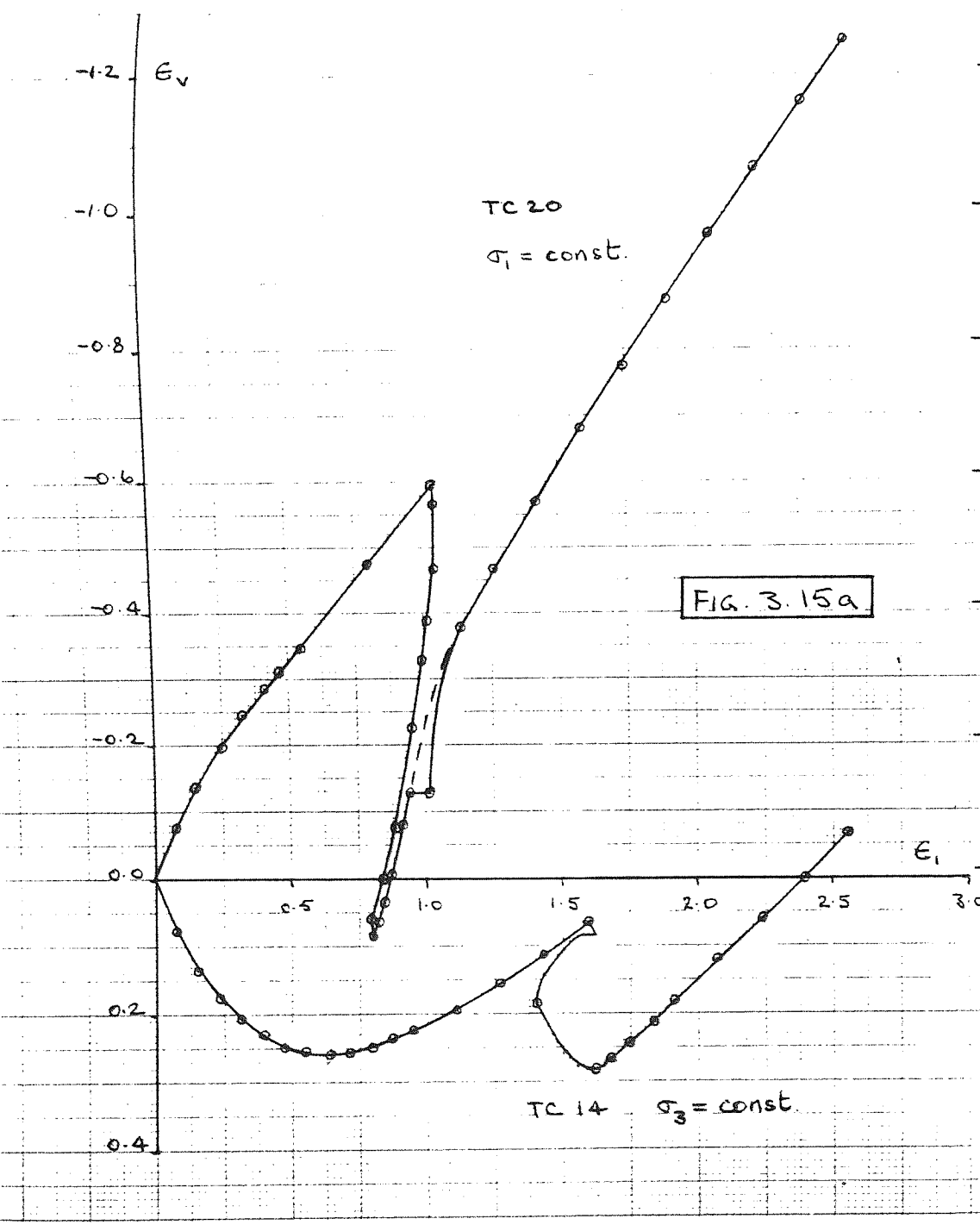

FIG. 3.15a

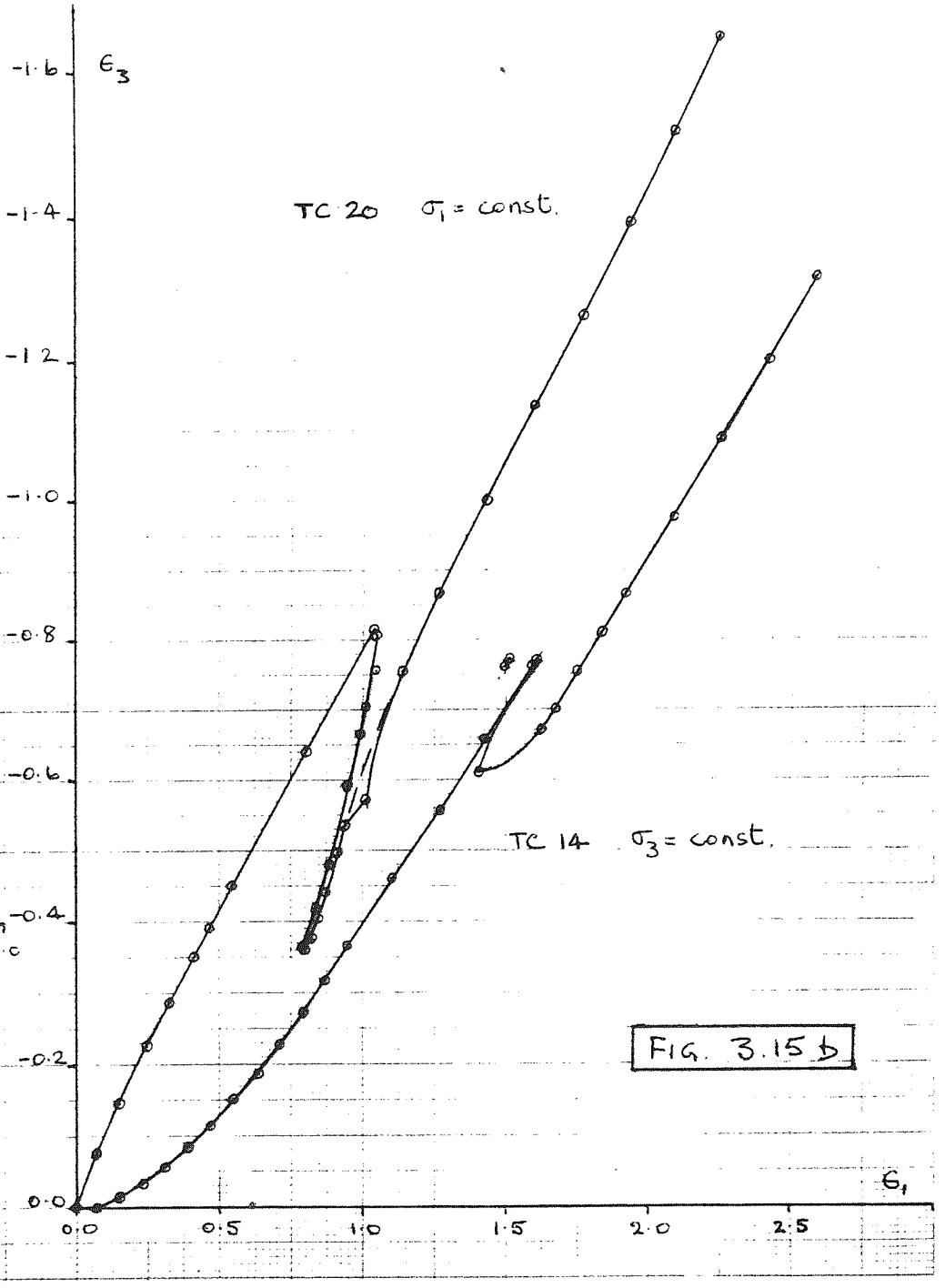

FIG. 3.15b

CHAPTER FOUR

4. PLANE STRAIN TESTS.

4.1. Introduction.

It was pointed out in the previous chapter that the triaxial compressive behaviour of soils is well documented and that the triaxial compression test has become a standard test in most soil mechanics laboratories. As a result of its widespread use, most design methods and analyses have employed soil properties obtained from triaxial compression tests. However, deformation in the field rarely occurs under axisymmetric conditions and many field problems approximate closely to the plane strain state in which no movement occurs in one of the directions of principal stress. Clearly, for these situations, a laboratory plane strain test is more relevant.

The first plane strain tests were carried out in the late 1950's and since then various plane strain devices have been designed but the prime object of most investigations has been to correlate the strengths obtained in plane strain tests with triaxial compression strengths. Although most engineering designs are based on strength parameters the trend towards deformational analyses underlines the need for more research into the plane strain deformation of soils. Noting that less attention has been given to the deformation of soil in plane strain, Reades (1972) suggested that this may be of greater significance than differentiating between slight variations in strength. Bishop (1971), as a result of recent work on the strength of soil under generalised stress conditions, has suggested that the plane strain test has been rather underestimated in soil mechanics. The need for a greater understanding of the behaviour of soil in the plane strain test is therefore apparent.

The main object of the research reported in this thesis was to investigate the behaviour of sand under conditions of plane strain with particular reference to the stress-strain behaviour. The results of the plane strain tests carried out are presented and discussed in this chapter.

4.2. Review of previous work.

All the previous experimental evidence shows that the stress-strain and volume change curves obtained from plane strain tests exhibit the same characteristic shape as those obtained from triaxial compression tests. There are, however, significant differences in the behaviour of granular materials when tested in plane strain and triaxial compression conditions. There is general agreement, from tests using a variety of apparatuses, that the effect of preventing any movement in one orthogonal direction is to increase the strength of the soil and to decrease both the volumetric and axial strains to failure.

Most researchers have been concerned primarily with the effect of initial porosity on the difference in strength between plane strain and triaxial compression specimens. Some researchers, for example Cornforth (1961), Wade (1963), Sultan and Seed (1967), found that the strength difference increased linearly with decreasing porosity whereas others, such as Wightman (1967), Lee (1970), Reades (1972), reported strength differences which remained approximately constant over a major proportion of the porosity range. Reades (1972) pointed out that the more recent research investigations show somewhat greater increases in strength over the looser range of porosities than did earlier work. This may well be a result of improved testing technique. Although the test results of Cornforth (1961) and Wade (1963) suggested that the strength-porosity curves for plane strain and triaxial compression coincide at the very loose end of the porosity range, it has recently been suggested that this may not be so, Rowe (1969) and Green (1971).

It has been shown by Marachi et al (1969), Lee (1970), Ismael (1969), and Tong (1970) that, not only does the mean stress level affect the plane strain behaviour of sand in the same way as in triaxial compression (see section 3.2) but, with increase in stress level the differences in behaviour between plane strain and triaxial compression specimens are reduced. Consequently it is difficult to compare the strength differences obtained by the various researchers. A quantitative correlation between the results of the various investigations is also complicated by the different physical properties of the materials tested. As previously stated, there is agreement that the plane strain strength of granular material is generally higher than the triaxial compression strength but unless the difference can be related to the physical properties of the material tested no definitive conclusions can be drawn. Nevertheless, certain authors have attempted to derive methods of predicting the plane strain strength of soils.

Finn and Mittal (1963) postulated that the triaxial compression strength was a lower bound to the plane strain strength and that the upper bound could be obtained using isotropic elastic theory, assuming that the axial strain to failure was the same as in triaxial compression. Since this assumption and the assumptions of isotropic elasticity are not supported by the experimental behaviour of granular material such a theoretical treatment is of little significance.

Parry (1971a) suggested that a strength criterion for clays at critical state which had previously been proposed (Parry, 1965) could equally apply to sands. The only restriction made by Parry (1971a) was that it was only strictly applicable if strains were completely uniform. Although it was a critical state strength criterion, Parry suggested that, for sands, it may be more valid for peak strengths due to the pronounced localised strains that occur during post-peak behaviour.

The proposed criterion was

$$(\sigma_1 - \sigma_3)_f = \psi \quad (2\, p_e - 3\, p_{cs} + \sigma_{nf}) \qquad (4.1)$$

where ψ = constant for a particular soil

p_e = the 'equivalent stress' (see Schofield and Wroth, 1968)

σ_{nf} = effective stress normal to the plane of maximum stress obliquity

However, since sands are unstable when looser than described by the critical state it is not possible to measure the 'equivalent stress', Consequently it was assumed that $p'_e/p'_{cs} = 2$ for sands. It was also necessary to assume a value of $m = \sigma_2/(\sigma_1 + \sigma_3)$ in plane strain in order to predict the plane strain strength. Parry assumed $m = 0.4$ but, as pointed out by Green (1971b) the measured value of m varies considerably from this value for different soils. Green (1971b) also expressed concern regarding the sensitivity of the predictions to the above assumptions.

Rewriting the expression for plane strain (equation 20C, Parry, 1971a) in terms of angle of shearing resistance gives

$$\sin \phi_{PS} - \frac{\psi}{2} \cos^2 \phi_{PS} = \frac{\psi}{3} (1 + m) \qquad (4.2)$$

$$\text{Thus} \qquad \phi_{PS} = \sin^{-1} \left\{ \frac{-6 \pm [36 + 12\, \psi^2 (5 + 2m)]^{\frac{1}{2}}}{6\, \psi} \right\} \qquad (4.3)$$

Equation 4.3 demonstrates that the predicted plane strain strength increases with m. The measured values of m, for sands, vary between 0.3 and 0.4. The corresponding predicted differences between ϕ_{PS} and ϕ_{TC} for $\phi_{TC} = 40^\circ$ are 1.8° and 3.3° which would appear to be low for sands.

A few experimenters have measured the intermediate principal stress in plane strain tests and these measured values of m have been used to assess the validity of equation 4.3. The results are shown in Table 4.1.

Table 4.1.

Reference		m measured	$\phi_{PS}-\phi_{TC}$ predicted	$\phi_{PC}-\phi_{TC}$ measured
Cornforth (1961)	loose sand	0.40	2.0°	1.8°
	dense sand	0.29	2.0°	3.8°
Wade (1963)	loose sand	0.34	1.8°	1.2°
	dense sand	0.29	1.6°	2.6°
Green (1969)	dense sand	0.35	2.4°	5.3°
Tong (1970)	dense sand	0.30	2.3°	4.5°
Reades (1972)	loose sand	0.37	2.0°	2.5°
	dense sand	0.37	3.0°	5.0°

It can be seen from Table 4.1 that the correlation is only reasonable for tests on loose specimens. It is possible, therefore, that despite the questionable assumptions used to derive equation 4.1 the proposed strength criterion may provide reasonable estimates of the difference between ϕ_{cv} in plane strain and triaxial compression tests. Unfortunately the only measurements of m at or near the critical state are provided by Cornforth's (1961) tests in which the accuracy of the measurements of the intermediate principal stress have been questioned, Green (1969).

Thus, whilst the proposed strength criterion of Parry (1965) may or may not predict the plane strain strength of clays, it is clear that it cannot be extended to predict the peak strength of sand in plane strain, as suggested by Parry (1971a), (1971b).

Rowe (1969) outlined a method by which the range of peak strengths of sands could be predicted for triaxial compression and plane strain conditions. The method was based on the stress-dilatancy theory and predicted that

$$1 \leq \frac{(\sigma_1/\sigma_3)_{PS}}{(\sigma_1/\sigma_3)_{TC}} \leq \frac{\tan^2(45^{\circ} + \phi_{cv}/2)}{\tan^2(45^{\circ} + \phi_{\mu}/2)} \qquad (4.4)$$

For a given sand, the method required a knowledge or measurement of the angle of interparticle friction, ϕ_μ ; the maximum and minimum porosities; and, for an intermediate porosity, an estimate of the rate of dilatation at peak.

Rowe (1969) also demonstrated that the plane strain strength could be predicted from the results of direct shear tests using the following expression:

$$\tan \phi_{DS} = \tan \phi_{PS} \cdot \cos \phi_{cv} \qquad (4.5)$$

Cornforth (1961) conducted both constant cell pressure and constant axial stress tests under plane strain conditions and found no significant difference in strength, for the same cell pressure at failure. Tong (1970) similarly demonstrated that the strength was independent of stress path and also showed that the variations with axial strain of both the ratio of the major to minor principal stress and the ratio of the intermediate to minor principal stress were unaffected by stress path. From Tong's (1970) Fig. 6.55 it would also appear that the strength and strain to failure in plane strain were the same for Ko and ambient consolidated specimens, and that the effect of overconsolidation was small.

Since shear strength can be related to the volumetric strain rate it is interesting to note that similar volumetric strain rates at failure in triaxial compression and plane strain have been observed, Cornforth (1961), Wightman (1967), Ismael (1969), Tong (1970), Dyson (1970) Reades (1972).

The most significant difference, especially with regard to deformational analyses, between plane strain and triaxial compression is the axial strain to failure. Both Cornforth (1961) and Reades (1972) report that the axial strain to failure in triaxial compression was approximately three times greater than in plane strain, for a given initial porosity. The small axial strain required to mobilize the

maximum shear strength in plane strain tests has been confirmed by other previous experimental work.

Finn et al (1967) extended the analysis of Leussink and Wittke (1963) to predict the volume changes that would occur in triaxial compression and plane strain for regular arrays of rigid spheres. The analysis predicted smaller volume expansion in plane strain than in triaxial compression. Although the experimental results agreed with the prediction the initial volumetric compression in plane strein was greater than in triaxial compression and the theoretical analysis ignored any pre-peak deformation. A more appropriate interpretation of the analysis, which is supported by the experimental results, would be that the theory predicts that the rate of volumetric expansion during post-peak behaviour decreases more rapidly in plane strain than in triaxial compression.

Lee (1970) suggested that it was possible to construct theoretical post-peak curves based on the work of Leussink and Wittke (1963) and Finn et al (1967), and to add these to pre-peak curves based on a simple isotropic elastic model. In this way complete theoretical stress-strain-volume change curves could be obtained for plane strain and triaxial compression. The theoretical curves showed that if tested in plane strain then a specimen would be both stiffer and stronger than if tested in triaxial compression, and that the volummetric compression prior to peak would be greater and the post-peak volumetric expansion would be less.

However, the theoretical curves predicted larger axial strains to failure for plane strain conditions and this was not supported by the experimental evidence. Although Lee (1970) offered no reason for this discrepancy it is clearly due to the inadequacy of the theoretical model. The model is incorrect for sands in that it assumes that no slip deformation occurs prior to peak and assumes that the pre-peak deformation is purely elastic resulting in compressive volume changes. As a result the model predicts coincidence of the peak stress ratio with minimum

volume as opposed to the well established fact that peak stress ratio coincides (or nearly coincides in the case of triaxial compression) with the maximum rate of volumetric expansion. Clearly any theoretical model must permit the simultaneous occurrence, during pre-peak deformation, of both elastic and slip deformation.

Measurements of the intermediate principal stress during plane strain tests on sands have been obtained by Cornforth (1961), Wade (1963), Green (1969), Tong (1970), Dyson (1970), and Reades (1972). Cornforth (1961) and Wade (1963) both found that $\sigma_2/(\sigma_1 + \sigma_3)$ only increased slightly during pre-peak deformation and could be adjudged to be approximately constant throughout. Reades (1972) conducted plane strain tests on ambient consolidated specimens and found that the variation of $\sigma_2/(\sigma_1 + \sigma_3)$ was similar to that observed by Cornforth (1961) and Wade (1963) except during the early stages of the tests.

All the experimental evidence shows that the ratio σ_2/σ_3 at failure increases with initial density. However, the variation of $\sigma_2/(\sigma_1 + \sigma_3)$ at failure with initial density is less consistent. According to the results of Cornforth (1961) and Wade (1963), $\sigma_2/(\sigma_1 + \sigma_3)$ at failure, increases with porosity. Dyson (1970) obtained a similar variation when conducting constant cell pressure tests, but found that the ratio was independent of porosity for constant axial stress tests. The apparent difference due to stress path decreased with increase in porosity and tests on loose specimens showed no effect of stress path on the value of $\sigma_2/(\sigma_1 + \sigma_3)$ at failure. Tong (1970) measured the intermediate principal stress during tests on dense sand and found no significant difference due to stress path in the values of $\sigma_2/(\sigma_1 + \sigma_3)$ at failure. Although there was appreciable scatter due to difficulties in controlling the movement of the side platens, Reades (1972) concluded that $\sigma_2/(\sigma_1 + \sigma_3)$ at failure was relatively independent of the initial porosity.

It has been suggested by Green (1969) that the intermediate principal stress as measured by Cornforth (1961) and Wade (1963) is low due to friction between the axial platens and the specimen. This may account for the apparent dependence of $\sigma_2/(\sigma_1 + \sigma_3)$ on porosity. For the reasons given in Appendix A the results of Dyson (1970) are open to question. However, it may be significant that the errors associated with the imperfections of Dyson's apparatus would be greatest during constant cell pressure tests on dense specimens.

Generally, the reported values of $\sigma_2/(\sigma_1 + \sigma_3)$ at failure range between 0.3 and 0.4 and the more recent work would suggest that the value obtained is relatively independent of both porosity and stress path.

Several investigators have attempted to fit empirical expressions to the variation of the intermediate principal stress, both during deformation and at failure in plane strain. As a result of the observation originally made by Wood (1958) that $\sigma_2 \simeq K_o.\sigma_1$ throughout a test, it has been suggested that $\sigma_2/(\sigma_1 + \sigma_3) = 0.5 \cos^2 \phi$, Cornforth (1961), Wade (1963), Bishop (1966). Green (1969) noted that for dense sand the ratios σ_1/σ_2 and σ_2/σ_3 were approximately equal and therefore suggested the relationship $\sigma_2^2 = \sigma_1.\sigma_3$. The only theoretical prediction of the value of the intermediate principal stress at failure in plane strain known to the Author is that provided by Parkin (1965). Parkin's theoretical treatment was confined to dense packings of rigid spheres and predicted that $\sigma_2 = (\sigma_1 + \sigma_3)/3$ at failure in plane strain. Further discussion of the theory advanced by Parkin (1965) will be presented in Chapter 5.

4.3. Test program and testing procedures.

The plane strain tests reported in this chapter include tests using rigid side platens and tests using flexible side platens. Details of the two types of platen were described in Chapter 2.

The main purpose of the series of tests employing rigid side platens

was to enable a comparison to be made between the 'passive bag' method of simulating plane strain conditions and the more conventional rigid platen technique. No provision was made to measure the intermediate principal stress in these tests. Tests conducted with rigid side platens will be denoted by the suffix PSR as opposed to PS which will be used to denote tests employing flexible side platens. The series of plane strain tests performed using flexible side platens included a few tests in which cycles of loading were applied during shear. All the plane strain tests were sheared at a constant cell pressure of 100 kN/m^2.

The sample preparation technique was the same as for the triaxial compression tests and was described in Chapter 2. However, it was necessary to assemble the side platens around the specimen before the confining cell was positioned and this will be dealt with in sections 4.3.1 and 4.3.2.

In order to ensure plane strain deformation throughout the shear stage all the specimens were consolidated under nominally Ko conditions. Generally the testing procedures were similar to those used for the triaxial compression test series but a variety of methods of controlling the consolidation stage were attempted and these will be described in the following sections.

4.3.1. Tests with rigid side platens.

With the specimen standing under a small suction the side platens were assembled prior to the main confining cell being positioned. Difficulty was found in establishing when adequate contact had been made with the sides of the specimen without inducing an unnecessary prestress. It was also necessary to ensure that the side platens were vertical and parallel and this was checked using a vernier caliper. Contact with the sides of the specimen was registered by a change in water level in the 50 ml burette. However, this procedure was complicated due to there

being four tie-rods to be adjusted in turn. A number of early test results were discarded due to subsequent interference between one side platen and the axial platen.

The majority of the tests using rigid side platens were consolidated in the same manner as described in section 3.3.1. Tests PSR 8, 9, and 10, however, were not consolidated in the conventional sense but were initially loaded under constant major principal stress ratio, σ_1/σ_3, conditions before being sheared at a constant cell pressure.

4.3.2. Tests with flexible side platens.

The assembling of the flexible side platens was much more satisfactory. Due to the sensitivity of the pressure transducer any slight contact with the specimen registered a change in the reading on the digital voltmeter. However, in order to ensure that contact was achieved over the full area of the sides of the specimen it was necessary to permit a small initial prestress. A change of 0.10 mV recorded on the digital voltmeter was found to be acceptable, this being equivalent to less than 1 kN/m^2.

No attempt was made to carry out the consolidation stage under conditions of zero lateral strain. Instead, a different technique was tried which is described below.

An increment of cell pressure was applied and the specimen was allowed to consolidate. The pressure recorded by the 'passive bags' was found to be slightly less than the cell pressure, according to the calibration tests. This was presumably due to a small amount of stress being transferred to the rigid flange. The apparent underestimation of stress decreased from about 1.5 kN/m^2, at a cell pressure of 10 kN/m^2, to less than 0.5 kN/m^2 at 100 kN/m^2, as the cell pressure was increased in increments of 10 kN/m^2. This would seem to be a good indication of the accuracy of the 'passive bag' technique of measuring the intermediate

principal stress.

When the specimen had fully consolidated under the increment of cell pressure the deviator stress was manually adjusted to raise the pressure recorded by the 'passive bags' to correspond with the cell pressure. The additional consolidation resulting from the increase in deviator stress occurred almost instantaneously.

The next cell pressure increment was then applied and the procedure was repeated until the deviator stress adjustment had been made after the cell pressure had been raised to 100 kN/m^2. The specimen was then sheared at constant cell pressure.

4.4. Consolidation.

It will be recalled that the stress ratios during consolidation obtained from the Ko-consolidated triaxial compression tests agreed more with Jaky's (1944) original theoretical expression for Ko than with the $(1-\sin \phi)$ approximation. These results are replotted in Fig. 4.1, together with Jaky's theoretical curves based on the triaxial compression strength obtained from the Ko consolidated specimens.

The stress ratios measured during the consolidation stage of the plane strain tests using rigid side platens are also shown in Fig. 4.1, plus three tests which were initially loaded at a constant stress ratio, $\sigma_3/\sigma_1 = (1-\sin \phi)$. It can be seen that, when the same method of controlling the consolidation stage was used, much lower results were obtained in the plane strain tests than in the triaxial compression tests. This confirms that lateral expansion occurred during the consolidation stage of the triaxial compression tests since the presence of the side platens produced higher deviator stresses in the plane strain tests. The lateral restraint provided by the side platens also produced excessive lateral expansion along the unrestrained axis of the specimen. That this did indeed occur was clearly demonstrated by the formation of lips in the sample sheath at the edges of the axial platens.

Tests PSR 8, 9 and 10, which were initially loaded at constant stress ratio, were performed in order to assess the significance of the consolidation stage on the subsequent deformation during shear.

Fig. 4.2 shows the stress ratios (σ_3/σ_1) obtained during the consolidation stage of the tests employing flexible side platens, together with the two theoretical lines of Jaky (1944). As might be expected from the technique described in section 4.3.2 there is considerable scatter in the results.

4.5. Failure characteristics.

In this section the failure characteristics of the plane strain tests performed in the course of this research program will be discussed. The tests can conveniently be divided into two types: tests in which rigid side platens were used to provide lateral constraint, and tests which were conducted using the flexible side platens described in section 2.3.3.2. The two series of plane strain tests will be dealt with separately before comparing the two sets of results. In order to assess the effect of preventing deformation in the direction of one of the orthogonal axes the plane strain test results will also be compared with the results of the triaxial compression tests reported in Chapter 3.

4.5.1. Tests employing rigid side platens.

The failure characteristics obtained from the series of tests employing rigid side platens are shown in Fig. 4.3-4.5. Fig. 4.3a, b, and c, show the effect of initial porosity on the maximum principal effective stress ratio, the axial strain to failure, and the volumetric strain rate at failure, respectively. The results show that both the principal effective stress ratio and the volumetric strain rate at failure decrease with increase in initial porosity. Fig. 4.3c suggests a non-linear variation in the rate of volumetric strain at failure with initial porosity. This may suggest that the variation of the principal

effective stress ratio, Fig. 4.3a, was also non-linear. However, a linear variation of the principal effective stress ratio with initial porosity would fit the experimental results equally well.

From Fig. 4.3b it can be seen that, except for the two loose specimens and allowing for the low initial principal stress ratios in tests PSR 8, 9 and 10, the axial strain to failure was more or less constant. It is remarkable that over an appreciable range of densities a mere 1% axial strain was sufficient to mobilize the maximum shear strength, under the test conditions imposed.

The variation of the angle of internal shearing resistance with initial porosity is shown in Fig. 4.4. Since this is merely an alternative way of expressing the variation of strength with porosity the results shown reflect the results shown in Fig. 4.3a. In Fig. 4.5 the angle of internal shearing resistance is plotted against the volumetric strain rate at failure. It can be seen that there is an appreciable scatter when the results are plotted in this manner, but a straight line intercepting the vertical axis at 38° provides a reasonable fit to the experimental results.

4.5.2. Tests employing flexible side platens.

The results of the plane strain tests conducted using the flexible side platens are shown in Fig. 4.6-4.12. Since the intermediate principal stress was measured during these tests three principal stress ratios can be calculated; σ_1/σ_3, σ_1/σ_2 , and σ_2/σ_3 . The three principal stress ratios at failure are plotted against initial porosity in Fig. 4.6. The results clearly show that, over the range of porosities tested, the ratio σ_1/σ_3 at failure varied linearly with initial porosity. All the measured stress ratios were within $\pm$ 5% of the linear interpretation shown. Fig. 4.6 also shows that the ratio σ_2/σ_3 at failure varied with initial porosity in the same manner as did σ_1/σ_3 . It is worth noting, however, that the intermediate principal stress - axial strain curves

did not exhibit a peak but tended to remain more or less constant during post failure deformation. In many tests the intermediate principal stress continued to increase after the major principal stress had reached a maximum. Thus the principal stress ratios σ_1/σ_2 and σ_2/σ_3 plotted in Fig. 4.6 are not necessarily maximum values but are the values corresponding to the maximum value of σ_1/σ_3. Consequently this may account for the scatter shown in Fig. 4.6 especially for tests on dense specimens. Allowing for experimental scatter, the ratio σ_1/σ_2 was reasonably constant over the porosity range tested the mean value being 2.943. In selecting the straight line representations of the experimental data shown in Fig. 4.6 it was necessary to accound for the inter-relationship between the three principal stress ratios. Consequently the line representing the variation of σ_2/σ_3 with porosity was calculated from the lines fitted to the other two principal stress ratios. It is worth noting that the ratios σ_2/σ_3 and σ_1/σ_2 are approximately equal for the dense specimens. Green (1969) made the same observation but, although he only conducted tests on dense specimens he suggested that the relationship $\sigma_2 = \sqrt{\sigma_1\ \sigma_3}$ may apply to all densities. It is clear from Fig. 4.6 that this is not true but the relation proposed by Green (1969) may usefully define the upper limit to the intermediate principal stress at failure, for a given sand.

Within the limits of experimental measurement, the maximum volumetric strain rate occurred when the principal stress ratio σ_1/σ_3 reached a maximum value. Fig. 4.7 shows the volumetric strain rate at failure plotted against initial porosity and it can be seen that the results are adequately defined by the straight line shown.

The variation of the major principal strain at failure with initial porosity is shown in Fig. 4.8. The results appear to indicate the unusual effect that the axial strain to failure increased with increase in density. However, the axial strain to failure is affected to some

extent by the initial principal stress ratio σ_1/σ_3 at the start of the shear stage. Fig. 4.2 showed that compared with the theoretical values of Ko, the initial principal stress ratios were low for the dense specimens and high for the loose specimens. It would appear from Fig. 4.8 that these differences were reflected in the measured axial strains to failure. Therefore, allowing for the deviations from the zero lateral strain condition during consolidation, the axial strain to failure during the shear stage of the plane strain tests would appear to be constant, for the range of porosities tested.

The angle of shearing resistance is plotted against initial porosity and volumetric strain rate at failure in Fig. 4.9 and Fig. 4.10 respectively. Allowing for experimental scatter both graphs indicate linear relationships.

In Fig. 4.11 the ratio $o_2/(\sigma_1 + \sigma_3)$ at failure is plotted against initial porosity. Due to the experimental scatter obtained from tests on dense specimens it is not clear from the graph as to whether the ratio is dependent on porosity or not. Considering Fig. 4.11 alone it would be reasonable to take the mean value of 0.295 and to consider the ratio to be independent of porosity. However, the ratio $\sigma_2/(\sigma_1 + \sigma_3)$ is related to the three principal stress ratios and can be expressed as

$$\frac{\sigma_2}{\sigma_1 + \sigma_3} = \frac{1}{\sigma_1/\sigma_2 + \sigma_3/\sigma_2} \qquad (4.13)$$

Since it was clear from Fig. 4.6 that the ratio σ_2/σ_3 varied with initial porosity equation 4.13 demonstrates that it is not possible for both σ_1/σ_2 and $\sigma_2/(\sigma_1 + \sigma_3)$ to be independent of porosity.

Consequently it has been assumed that the ratio σ_1/σ_2 is independent of porosity and the straight lines shown in Fig. 4.6 have been used to calculate $o_2/(\sigma_1 + \sigma_3)$. The calculated variation of $\sigma_2/(\sigma_1 + \sigma_3)$ at failure is shown in Fig. 4.11 and can be seen to be small for the range of porosities tested.

The ratio $\sigma_2/(\sigma_1 + \sigma_3)$ is also plotted against the angle of internal shearing resistance in Fig. 4.12. Superimposed on this graph are the two theoretical curves

$$\frac{\sigma_2}{(\sigma_1 + \sigma_3)} = \frac{\cos^2 \phi}{2} \qquad (4.14)$$

and $$\sigma_2 = \sqrt{\sigma_1 \sigma_3} \qquad (4.15)$$

It can be seen that the experimental scatter is exaggerated when the results are plotted in this way but the theoretical curves, nevertheless, provide reasonable limits to the range of results obtained.

4.5.3. Comparison of plane strain test results.

The results of the two series of plane strain tests are combined in Fig. 4.13-4.17. It can be seen from Fig. 4.13 and Fig. 4.14 that, generally, the strengths obtained from tests employing flexible side platens were slightly higher than those obtained from tests with rigid side platens. However, allowing for the scatter in the results, although the maximum difference in ϕ was of the order of 1.5°, there was reasonable agreement at both ends of the porosity range tested.

It would appear that the different test conditions affected the variation of strength with porosity and, in this respect, it is interesting to compare Fig. 4.13 and Fig. 4.14 with Fig. 4.16. Fig. 4.16 shows the variation of the volumetric strain rate at failure with initial porosity for the two plane strain test series. The similarity between the strength variations shown in Fig. 4.13 and Fig. 4.14 with the variation of the rate of volumetric strain at failure, for the two series of tests, is remarkable. In Fig. 4.17 the angle of internal shearing resistance is plotted against the volumetric strain rate at failure. Although there was appreciable scatter in the results of the tests with rigid side platens Fig. 4.17 indicates general agreement between the two series of tests; thus implying that the frictional component of strength was not affected by the different test conditions.

Consequently it is reasonable to suppose that the differences in strength are due to differences in dilatation which resulted from the different boundary conditions used to impose plane strain.

However, the above reasoning does not clarify which of the two series of tests is more representative of the plane strain state. It was demonstrated by Rowe and Barden (1964) and Bishop and Green (1965) that, for triaxial compression tests, more uniform specimen deformation resulted in larger axial strains to failure and stress-strain curves which exhibited less pronounced peaks. As can be seen from Fig. 4.15 the axial strain to failure for the tests with rigid side platens was only half the axial strain to failure for tests using flexible side platens. The tests conducted with rigid side platens also produced more pronounced peaks to the stress-strain curves than did the tests with flexible side platens. (The stress-strain curves for all the tests are provided in Appendix C.) The uniformity of specimen deformation obtained in both series of tests appeared to be good from visual observations. More details of the deformation of the tests with flexible side platens will be provided later in this chapter.

The above observations plus the greater overall consistency of the test results obtained using flexible side platens lead to the conclusion that the flexible side platens produced more reliable plane strain results. It is presumed that the specimens constrained by rigid side platens failed 'prematurely' as a result of the rigid boundaries used to apply the plane strain condition.

4.5.4. Comparison with triaxial compression tests.

The results of the triaxial compression tests were reported in Chapter 3 and it will be recalled that different strength-porosity relationships were obtained from the two series of tests. The results of the two triaxial compression test series are combined in Fig. 4.18 - 4.22 with the results of the plane strain test series in which the

flexible side platens were used.

The strength-porosity relationship for the three series of tests are shown in Fig. 4.18 and Fig. 4.19. For the range of porosities tested, it would appear that the difference in ϕ obtained from the plane strain tests and the triaxial compression tests was approximately constant, whichever triaxial compression test series is considered. However, whereas the plane strain strengths were 3.5^{o} higher than those obtained from the triaxial compression tests which were consolidated under ambient stress conditions; when compared with the Ko-consolidated triaxial compression tests, the angle of internal shearing resistance for the plane strain tests was 6^{o} higher.

The variations with porosity of the axial strain to failure, for the three test series considered, are shown in Fig. 4.20. Since the axial strain to failure is affected by the value of the initial stress ratio at the start of the shear stage, it is only relevant to compare the plane strain test results with the results of the Ko-consolidated triaxial compression tests. It can be seen from Fig. 4.20 that whereas the axial strain to failure increased with increase in porosity for the triaxial compression tests the axial strain to failure in plane strain was constant over the porosity range tested. However, it would be anticipated that the axial strain to failure in plane strain would increase with porosity for specimens with initial porosities higher than those tested.

Fig. 4.20 clearly shows that in order to mobilize the maximum strength smaller strains are required in plane strain than in triaxial compression. It was pointed out in section 3.5 that in the triaxial compression tests the principal stress ratio was within 1% of its maximum value over a wide range of axial strain. In the plane strain tests the range of axial strain over which more than 99% of the peak strength was mobilized was generally less than 0.5%.

In order to assess which of the two triaxial compression test series provides the more representative strengths it is useful to consider Fig. 4.21 and Fig. 4.22. The volumetric strain rate at failure is plotted against initial porosity in Fig. 4.21 and the angle of internal shearing resistance is plotted against the volumetric strain rate at failure in Fig. 4.22. It can be seen from Fig. 4.21 that there was no significant difference between the results of the two triaxial compression test series but that the volumetric strain rate tended to be higher for the plane strain tests except perhaps for the dense specimens.

Fig. 4.22 clearly indicates a significant difference in behaviour between the two triaxial compression test series and implies that the frictional component of strength was different in the two types of test. This would not be expected to be true due to the similarity of the test conditions applied. In Chapter 5 it will be shown, in terms of stress-dilatancy theory, that the difference in the frictional strength component applied throughout the test, not merely at peak. It will also be shown that the plane strain test results and the results of the triaxial compression tests which were consolidated under Ko conditions correlate closely with the work of Parikh (1967), Wightman (1967), Ismael (1969) and Tong (1970), on a similar sand to the one used in this research program. Although special tests were conducted to attempt to resolve the difference in the triaxial compressive strengths observed, as described in Chapter 3, no explanation was found. However, it is considered that the ambient consolidated triaxial compression test results are in error and that the Ko-consolidated triaxial compression tests are more reliable in terms of strength. Evidence to support this statement will be provided in Chapter 5.

According to Bishop (1971), extrapolation of the test results to the strength axis in Fig. 4.22 provides a method of estimating the critical state strength since this corresponds to zero rate of volumetric strain at failure. If Bishop's suggestion is accepted then the results given

in Fig. 4.22 indicate that ϕ_{cv} in plane strain is 3^{o} higher than ϕ_{cv} in triaxial compression.

4.6. Mode of rupture.

The plane strain test series using rigid side platens were generally terminated at axial strains between 1% and 2% beyond the axial strain at failure. In all the tests rupture surfaces were visible after the side platens had been removed. The inclination of the rupture surfaces to the horizontal was measured with a protractor. Various rupture patterns were observed which, along with the patterns observed in the tests employing flexible side platens, will be described in section 4.6.1.

The mode of rupture was also investigated during the series of tests conducted with flexible side platens. Tests PS 1 - PS 8 were stopped at axial strains between 1.5% and 2.5% after peak and rupture planes were evident on removal of the side platens.

Due to the presence of the side platens it was not possible to observe when the rupture planes first appeared. Therefore, in order to assess when rupture planes were initiated, the remainder of the monotonic tests, with the exception of PS 16 and PS 20, were terminated between 0.25% and 0.75% axial strain beyond the axial strain at failure. When the side platens were removed at the end of test PS 20 the rupture planes were clearly visible.

At the end of tests PS 9 - PS 19 the following procedure was adopted. After the side platens had been removed and the measurements of the final specimen dimensions had been taken, the O-rings were removed from around the top axial platen, the sample sheath was turned back, and the top axial platen was carefully removed. Then, with extreme care so as not to disturb the specimen, the sample sheath was cut away from the specimen. The specimen surfaces were then examined in detail for any signs of a rupture plane. If no evidence of a slip

surface was observed then a small brass block was placed on top of the specimen and a slight load was applied by hand to see if a slip plane could be induced.

Rupture planes were visible before the sample sheath was cut away in tests PS 10 and PS 14. This was remarkable since tests PS 10 and PS 14 were terminated at only 0.264% and 0.343% axial strain beyond peak respectively. In test PS 16 there was no evidence of a rupture plane when the side platens were removed but a single plane could be clearly seen when the sample sheath was removed. In tests PS 15, 18, and 19 there was no evidence of slip planes when the sample sheath was removed but slip planes were induced by applying a slight pressure to the top of the specimen. Tests PS 9, 11, 12, 13 and 17 provided no evidence of slip planes even after applying a small load to the unsheathed specimen.

The same procedures were applied to the cyclic tests but, with the exception of test PS 23, slip planes could be seen without removing the sample sheath. Test PS 23 was stopped immediately after peak and provided no evidence of rupture plane formation.

4.6.1. Rupture patterns.

The various rupture patterns observed in both series of plane strain tests are shown in Fig. 4.23. The rupture planes which passed between both axial platens will be termed primary slips. The other rupture planes which outcropped along the vertical sides of the specimens will be termed secondary slips. Secondary slips were always observed to be less steeply inclined than the primary slips and appeared to be initiated at a late stage in the tests, when the primary slips had already formed.

The reason for the presence of the secondary slips is attributed to the low height to width ratio. If a primary slip outcrops along the vertical side of a specimen as observed when testing taller specimens, then, with continued deformation the two parts of the specimen above and below the slip plane will be free to slide over each other. When the

primary slip does not outcrop along the specimen sides then such freedom of movement is not permitted and the fractured specimen is able to support a higher load. The slip plane then acts as a stress raiser, where it is intercepted by the axial platens, and subsequently initiates secondary slip planes if the applied deformation is continued.

In all the tests except PSR 1, PSR 2 and PSR 10 the measured slip plane inclinations at each side of the specimen were identical. There was a difference of 3^{o} in test PSR 1 and a difference of 2^{o} in both test PSR 2 and test PSR 10. All the rupture surfaces observed were found to be both smooth and planar. Two views of one of the slip planes present at the end of test PS 25 are shown in Fig. 4.24 and Fig. 4.25. The well defined nature of the plane was typical of all the slip planes observed in the plane strain tests.

Since the slip planes were found to emanate from a point along the axial platen/specimen interface rather than from the corners of the specimens, this fact, together with the smooth planar nature of the rupture surfaces, clearly indicate very uniform deformation of the specimens prior to rupture. Fig. 4.26 shows the specimen after the sample sheath had been removed at the end of test PS 12. The test was stopped at 0.256% axial strain beyond peak and no slip planes could be seen. That the specimen deformed uniformly is clearly seen from the photograph.

It was noticed that the slip planes invariably emanated from the edge of a filter paper strip. This demonstrates that the slightest imperfection on the specimen boundary is sufficient to initiate slips during post-peak deformation. Consequently it is suggested that when the post-peak behaviour of plane strain specimens is to be investigated considerable attention must be given to the platen/specimen boundaries.

4.6.2. Slip plane inclinations.

King and Dickin (1970) reported plane strain tests on sand, using

frictionless end platens, in which the inclination of the rupture planes were measured. The rupture surfaces were first observed on the uncovered faces of the specimens very soon after peak. Very soon afterwards they could be seen through the perspex side platens. The rupture pattern was that of Mode B in Fig. 4.23 although one slip plane invariably emerged from the top edge of the specimen. King and Dickin (1970) reported tests on two different specimen sizes and found that the height to breadth ratio apparently influenced the inclination of the rupture surfaces, the inclination increasing with increase in height to breadth ratio. Rowe (1971) suggested that this was due to non-uniformity of specimen density or boundary shear.

Further tests were reported by King and Dickin (1971) which confirmed that their test results, both rupture plane inclination and peak stress ratio, were influenced by the height to breadth ratio of the specimens. The measured inclinations of the rupture planes varied from 54.5°, for specimens with the height equal to the breadth, to 64° when the height to breadth ratio was between 3 and 5. In contrast, Rowe (1971) reported slip plane inclinations measured by Tong (1970) who carried out plane strain tests on dense sand with a number of specimen geometries; the measured inclinations only varied between 69° and 72°. Green (1969) observed that rupture planes formed well beyond failure in his plane strain tests. The measured inclinations at the end of the tests were 62° and 68°. Plane strain tests performed by Reades (1972) gave rupture planes inclined at 62.5° and 67° for dense specimens, 67° for medium dense, and 60° for loose specimens.

There would appear to be three alternative methods of predicting the inclination of rupture planes, King and Dickin (1971). The most commom method assumes that the Mohr-Coulomb theory is correct and that rupture planes are formed along planes on which the ratio of shear stress to normal stress is maximum. The theory implies that failure occurs at peak and the inclination of the rupture plane, α , is given

by the equation

$$\alpha = 45 + \frac{\phi_{max}}{2} \tag{4.16}$$

or $$\tan \alpha = \sqrt{R_{max}} \tag{4.17}$$

It is worth noting that there is no reocrd of slip planes having been observed at peak stress ratio although King and Dickin (1970) detected slip planes after only 0.25% post-peak axial strain. Rowe (1962) argued that slip planes were the result of failure rather than the cause, and therefore must necessarily occur after peak stress ratio has been reached. Rowe (1971) suggested that the inclination of the slip plane must be related to the applied stress ratio at the stage of formation of the slip plane.

The stress-dilatancy theory of Rowe (1962) offers an alternative prediction of the slip plane inclination which is given by the following equation

$$\tan \alpha = \sqrt{\frac{\sigma_1}{\sigma_3}\left(1 - \frac{d\varepsilon_v}{d\varepsilon_1}\right)} \tag{4.18}$$

which can be re-expressed as

$$\tan \alpha = \sqrt{R.D} \tag{4.19}$$

where D = dilatancy factor (see Chapter 5)

As a result of passive earth pressure tests on model retaining walls, Roscoe (1970) considered that the Mohr-Coulomb criterion had to be restated. He suggested that a rupture surface would develop in a soil element along a plane which was a direction of zero-extension at the instant when the peak stress ratio was attained on any other plane of the element. Consequently Bransby (1971) suggested that the inclination of the rupture plane to the horizontal in plane strain tests would be given by the equation

$$\alpha = 45 + \nu/2 \tag{4.20}$$

where ν = angle of dilatation, Bent Hansen (1958)

and $\sin \nu = \frac{D-1}{D+1}$

therefore $\tan \alpha = \sqrt{D}$ (4.21)

Since the maximum rates of dilatation normally measured in plane strain tests lie within the limits $1 \leq D \leq 2$, the limiting values of α, according to the zero-extension line hypothesis, are 45° and 55°. The minimum value of α observed in the plane strain tests was 65° which would require a value of $D = 4.6$ in order to comply with equation 4.21. Therefore, although good correlation between rupture plane inclinations and lines of zero-extension have been obtained in passive earth pressure tests, James (1965), Bransby (1968), the zero-extension line theory does not predict the inclination of rupture planes in elemental plane strain tests.

The observed inclinations of the rupture planes in the plane strain tests performed are shown in Fig. 4.27 and Fig. 4.28, for tests employing rigid side platens and flexible side platens respectively. In both figures the observed values of α are plotted against initial porosity together with the two theoretical lines corresponding to equation 4.16 and equation 4.19, assuming that the slips were formed at peak stress ratio. The instantaneous values of α were calculated throughout each test using the stress-dilatancy prediction and the range of α values obtained during post-peak deformation of each test is indicated by a vertical line in Fig. 4.27 and Fig. 4.28.

It was demonstrated in section 3.6 that in triaxial compression tests rupture planes formed well beyond failure and that the edge discontinuities, which formed due to expansion beyond the edges of the axial platens, were far more steeply inclined than the Mohr-Coulomb theory would predict, even if they had been formed at peak. The $45 + (\phi_{max})/2$ line shown in Fig. 4.27 and Fig. 4.28 corresponds, of course, to the maximum possible values of α according to Mohr-Coulomb theory. It is

noted that nearly all the observed inclinations fall above this line. Furthermore, the tests which were terminated between 0.13% and 0.76% post-peak axial strain suggested that, even in the relatively 'brittle' plane strain condition, rupture planes were not formed at peak stress ratio. Although the evidence was not totally conclusive, since PS 10 and PS 14 both exhibited rupture planes at only 0.264% and 0.343% post-peak axial strains, the remaining nine tests which were stopped within 0.76% post-peak axial strain provided no evidence of rupture planes when the sample sheath was removed at the end of the tests. Therefore, it would appear that the inability of the Mohr-Coulomb theory to predict the slip plane inclination extends to the plane strain condition as well as the triaxial compression case.

As can be seen from Fig. 4.27 there appears to be an appreciable amount of scatter in the results of the tests with rigid side platens. The reasons for the scatter are not clear but it is thought that it may be due to the rigid boundaries used to apply the plane strain condition. It is noted that a significant amount of scatter in the measured slip plane inclinations was obtained by Green (1969) and Reades (1972) who also used rigid side platens.

The results of the tests employing flexible side platens, shown in Fig. 4.28, were far more consistent. If the unusual results obtained in tests PS 4 (n_i = 39.27%) and PS 10 (n_i = 39.81%) are ignored then it is clear that the observed slip plane inclinations agree extremely well with the post-peak range of calculated values of α based on the stress-dilatancy theory, assuming that the slip planes formed at some point in the tests after peak stress ratio had been reached. However, it was not possible to isolate the exact point in the test when a slip plane formed by identifying the corresponding calculated value of α with any sudden change in the stress-strain or volume change curves. Nevertheless, it is concluded that the experimental results verify the stress-dilatancy prediction of the rupture plane inclination in elemental tests.

4.7. Deformation characteristics.

Discussion of the plane strain deformation characteristics provided in this section will be limited to the results obtained from the series of tests performed with flexible side platens.

In order to ensure a correct interpretation of the deformational behaviour of test specimens it is necessary to prepare homogeneous specimens which, when tested, will deform uniformly. Although the use of lubricated platens permit a greater degree of expansion to occur at the ends of a specimen the technique does not guarantee that the deformation of the specimen will be uniform. Non-uniform deformation of specimens tested with lubricated platens can occur due to density variations within the specimen and the tendency, as noted by Green (1969), is for specimens to expand more at the base than at the top. However, Kirkpatrick and Younger (1970) noted that, in triaxial compression tests, the predominant expansion at one end of the specimen usually occurred after an axial strain of 6%.

Evidence to suggest that the plane strain specimens tested were homogeneous and deformed uniformly has been provided in the previous section. On completion of most of the plane strain tests the final specimen dimensions were measured. Therefore, by comparing these measurements with the initial specimen dimensions an approximate quantitative assessment of the uniformity of lateral deformation can be obtained. Two parameters to describe the degree of bulging, B, and the tendency to expand into a trapezoidal shape, T, can be obtained from the following expressions.

$$B = \frac{2\,\varepsilon_m}{\varepsilon_t + \varepsilon_b} \qquad (4.22)$$

$$T = \frac{\varepsilon_t}{\varepsilon_b} \qquad (4.23)$$

where ε_t = average lateral strain at the top of the specimen

ε_b = average lateral strain at the base of the specimen

ε_m = average lateral strain at the mid-height of the specimen.

These two parameters are plotted against initial porosity in Fig. 4.29. For comparative purposes the results of plane strain tests performed by Reades (1972) are also included. It is clear from Fig. 4.29 that the degree of bulging that occurred in the tests was negligible. The results also indicate that the tendency for specimens to expand unequally at the ends was largely overcome, except for the very dense specimens. There was a tendency for the very dense specimens to expand more at the top than at the base and it is noted that the same results was observed by Reades (1972), who prepared his specimens by spooning and tamping.

4.7.1. Monotonic tests.

The stress-strain curves obtained from all the plane strain tests are provided in Appendix C. It is evident from these graphs that whereas all the plane strain tests exhibited smooth pre-peak curves the post-peak behaviour was somewhat inconsistent. Although one would expect the major principal stress ratio to decrease rather rapidly to a constant value during post-peak deformation, a number of tests exhibited post-peak curves which showed a marked fluctuation in the major principal stress ratio. Nor were the minor principal stress ratio-axial strain curves consistent during post-peak deformation. In a number of tests the minor principal stress ratio remained approximately constant during post-peak deformation whereas the minor principal stress ratio continuously increased in other tests. However, there appears to be a correlation between the two stress ratios. Tests in which the minor principal stress ratio continuously increased after peak also exhibited fluctuations in the major principal stress ratio during post-peak deformation; specimens

which showed a marked decrease in major principal stress ratio after peak also indicated that the minor principal stress ratio was constant during post-peak deformation. This latter group of tests is considered to exhibit the more representative post-peak behaviour.

Irregular post-peak stress-strain curves were also observed in some of the plane strain tests using rigid side platens (see Appendix C), and Green (1969), using rigid side platens, observed post-peak irregularities in his plane strain tests. The cause of the irregular post-peak stress-strain curves would thus appear to be due to something other than the type of side platen used. Although the experimental evidence is not conclusive, it is thought that the fluctuations in the major principal stress ratio during post-peak deformation were due to the formation of slip planes which intercepted both axial platens along the specimen/platen interfaces, see section 4.6.1.

It was also shown in section 4.6 that slip planes formed at an early stage of post-peak deformation and thus no reliable conclusions can be drawn from the post-peak deformation curves.

Fig. 4.30 shows that the major principal stress ratio and lateral strain plotted against axial strain for two plane strain tests, PS 11 (n_i = 42.80) and PS 14 (n_i = 39.07), and two triaxial compression tests, TC 3 (n_i = 42.83) and TC 9 (n_i = 39.09). The inappropriateness of applying triaxial compression test data to plane strain deformation problems is clearly shown.

The intermediate principal stress is plotted against the sum of the other two principal stresses for two representative plane strain tests, PS 8 and PS 20, in Fig. 4.31. Sketchley (1971) performed plane strain tests on remoulded kaolin and found that the ratio $\sigma_2/(\sigma_1 + \sigma_3)$ remained constant throughout pre-peak deformation. Fig. 4.31, however, clearly shows that this is not the case for sands. After an initial decrease, the ratio $\sigma_2/(\sigma_1 + \sigma_3)$ gradually increased to failure and the variation of σ_2 with $(\sigma_1 + \sigma_3)$ was non-linear throughout.

4.7.2. Cyclic tests.

The results of the five plane strain tests which were subjected to cycles of unloading and reloading are given in Appendix C. Both major and minor principal stress ratio, and the volumetric strain, are plotted against axial strain in these figures. The results of three tests, PS 23, PS 24 and PS 25, are also shown in Figs. 4.32, 4.33 and 4.34, respectively.

It can be seen from the test results that the cyclic behaviour of sand under plane strain conditions was similar to that observed in the cyclic triaxial compression tests, see section 3.7.1. On unloading the specimens, the recoverable strains were small and not perfectly elastic since reloading produced a small amount of hysteresis. The reload curves were slightly non-linear and the anticipated virgin loading curve was regained once the load had increased above the maximum previous value of the major principal stress ratio.

The specimens were usually unloaded until the major principal stress ratio had reached its value at the start of the shear stage and then reloaded. However, when reloading was commenced, the stress conditions were not the same as at the start of virgin loading since the intermediate principal stress was not reduced to its initial value by the unloading process. It would appear from the test results that the different values of σ_2 at the start of reloading did not affect the subsequent reload behaviour.

Fig. 4.32 shows the results of test PS 23 in which a smaller cycle of loading was applied during pre-peak deformation. It is clear that the width of the hysteresis loop was less than that produced by unloading to the initial value of σ_1/σ_3 . Also, close inspection of the data indicates that the reload curve was initially steeper than the other reload curves. That the reload curve and the amount of hysteresis are affected by the degree of unloading is also indicated by a

comparison of the post-peak cycles shown in Fig. 4.33 and Fig. 4.34.

From the test results shown in Appendix C it would appear that the reload curves obtained during pre-peak cycles were independent of porosity and were only dependent on the major principal stress ratio at the start of reloading. This observation was also confirmed by using curve fitting techniques described in Chapter 6.

Since the above conclusion is the same as that made for triaxial compression reload behaviour it is interesting to compare the reload curves obtained for the two different test conditions. However, the cyclic triaxial compression tests were generally unloaded to an approximate ambient stress condition and so no definitive comparison can be made. A careful comparison of the test results indicates that the plane strain reload curves were initially steeper than the reload curves obtained in triaxial compression. This result is not unexpected since it has been shown that, for both triaxial compression and plane strain conditions, the initial tangent modulus increases with the value of the major principal stress ratio at which reloading is commenced.

Generally the plane strain test specimens were unloaded to a major principal stress ratio between 2.75 and 3.5, and this range of initial values did not appear to affect the subsequent reload behaviour of any significant degree. However, during test TC 13, see Fig. 3.9, the triaxial compression specimen was partially unloaded to a major principal stress ratio of 2.47, and the subsequent reload behaviour can be compared with plane strain reload behaviour. In Fig. 4.35, a direct comparison is provided of the reload curve obtained during the partial unload cycle in test TC 13 with the second reload curve obtained in test PS 22 which was reloaded from a major principal stress ratio of 2.68. Fig. 4.35 shows the increase in major principal stress ratio during reloading plotted against the increase in axial strain. Although this is the only direct comparison available from the test results, the agreement is so striking that it is tentatively concluded

that the reload behaviour of sand is not significantly affected by the general test conditions, i.e. plane strain or triaxial compression, but is dependent on the value of the major principal stress ratio from which reloading is commenced.

It can be seen from the test results that the specimens decreased in volume throughout the unload-reload cycle until the maximum previous value of axial strain was reached, after which the specimens expanded. All specimens, however, expanded laterally immediately reloading was commenced. Thus the plane strain behaviour is similar to triaxial compression behaviour in this respect.

The test results show that the intermediate principal stress reduced only slightly during unloading. When reloaded, the slope of the minor principal stress ratio-axial strain curve was less that the slope of the unloading curve. After the maximum previous value of axial strain had been reached the minor principal stress ratio increased to coincide with the anticipated virgin loading curve. Consequently the minor principal stress ratio-axial strain curves did not indicate any hysteresis effect due to the unload-reload cycles and this was more marked when post-peak cycles were performed. To the Author's knowledge there is no published data regarding the behaviour of the intermediate principal stress during cyclic loading under plane strain conditions. Therefore it is of particular interest to analyse this aspect of the tests in more detail.

Fig. 4.36 shows the minor principal stress ratio, the volumetric strain, and the lateral strain, all plotted against the axial strain for one pre-peak cycle of loading performed during test PS 24. The interesting feature of this graph is the similarity between the shape of the minor principal stress ratio curve and the lateral strain curve during the load cycle. As a result of this observation the minor principal stress ratio was also plotted against lateral strain.

A typical pre-peak cycle is illustrated in Fig. 4.37, and Figs. 4.39-4.41 show examples of post-peak cyclic behaviour.

Comparing Fig. 4.37 with Figs. 4.38-4.41, it is clear that the slope of the unloading curve was steeper during post-peak unloading than when unloaded during pre-peak deformation. This was also true when the minor principal stress ratio was plotted against axial strain, as shown in Appendix C, and reaffirms the conclusion made in Chapter 3 that the elastic strains are less significant during post-peak behaviour.

From Fig. 4.37 it can be seen that, when the minor principal stress ratio is plotted against lateral strain for a cycle of loading applied during pre-peak deformation, a small hysteresis effect is observed. However, this may be the result of uncertainties in the strain measurements when the direction of stress change is reversed, see Appendix B. Nevertheless, it would appear that the intermediate principal stress is related to the lateral strain rather than the axial strain. Since the lateral strains induced in a plane strain test are approximately twice the lateral strains induced during triaxial compression, see Fig. 4.30, it seems reasonable to suggest that the intermediate principal stress is related to the lateral strain that would have occurred in the direction of the intermediate principal stress had the specimen not been constrained in that direction.

Figs. 4.38-4.41 show that hysteresis was negligible during post-peak cycles and that the minor principal stress ratio curves were similar to the $\sigma_2/\sigma_3 - \varepsilon_1$ curves once the maximum previous value of axial strain (indicated on the graphs by an arrow) had been reached. It is thought that the minor principal stress ratio-lateral strain curves obtained during post-peak cycles are indicative of an unstable internal structure and probably indicate the presence of slip planes formed prior to the start of the unload-reload cycle.

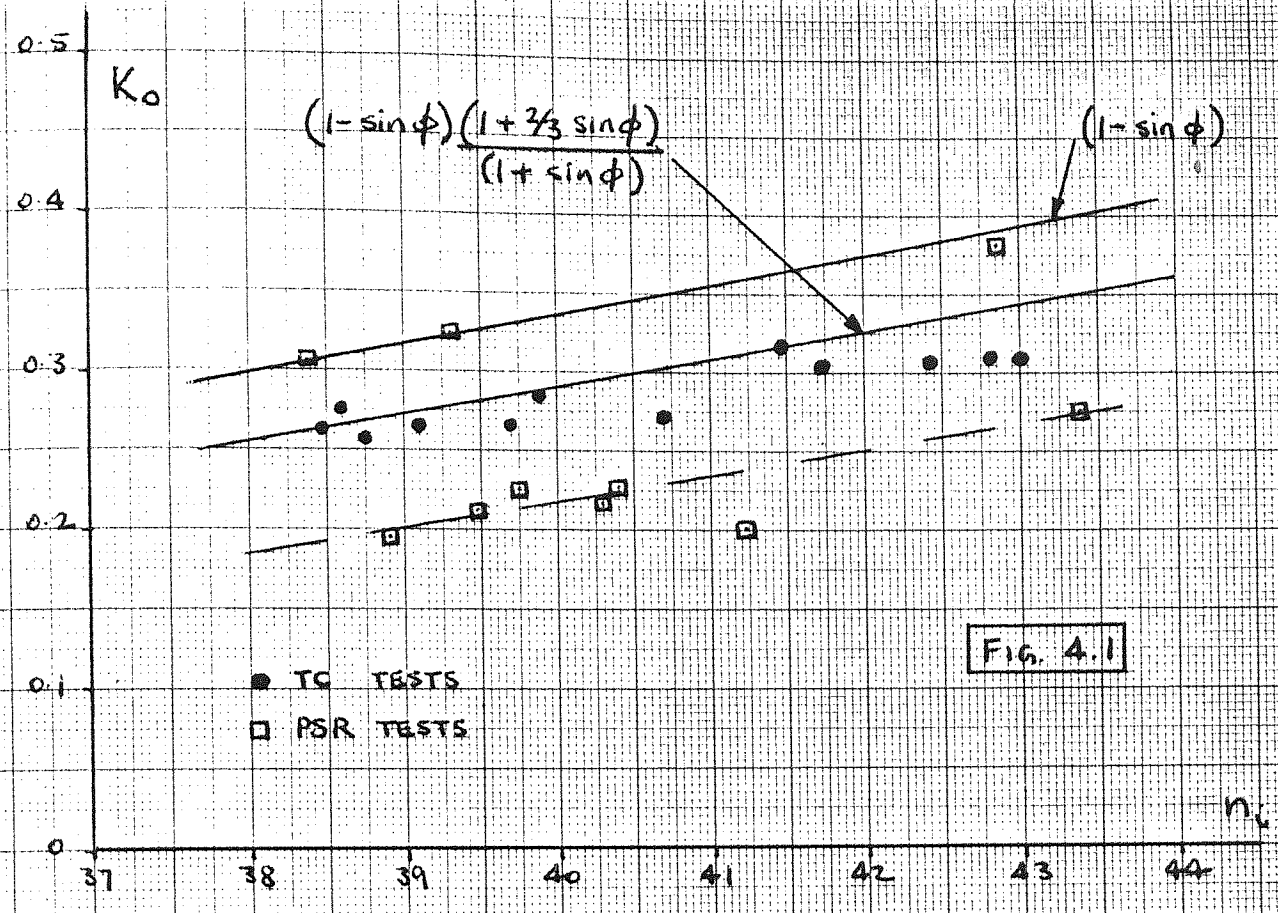
0·5
K_o
$\frac{(1-\sin\phi)(1+\frac{2}{3}\sin\phi)}{(1+\sin\phi)}$
$(1-\sin\phi)$
0·4
0·3
0·2
0·1
TC TESTS
PSR TESTS
0
37
38
39
40
41
42
43
44
η_i

FIG. 4.1

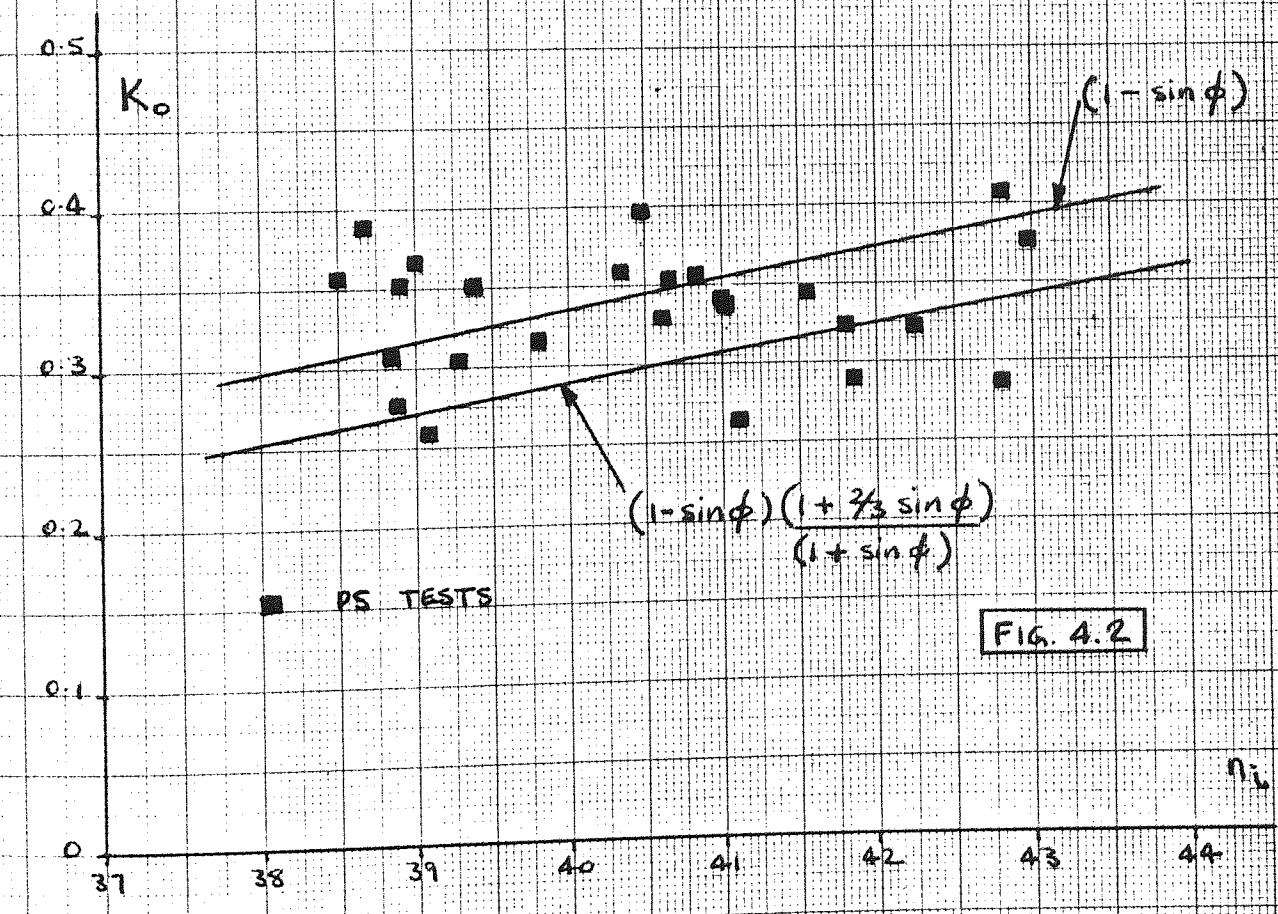
0·5
K_o
$(1-\sin\phi)$
0·4
0·3
$(1-\sin\phi)\frac{(1+\frac{2}{3}\sin\phi)}{(1+\sin\phi)}$
0·2
PS TESTS
0·1
0
37
38
39
40
41
42
43
44
η_i

FIG. 4.2

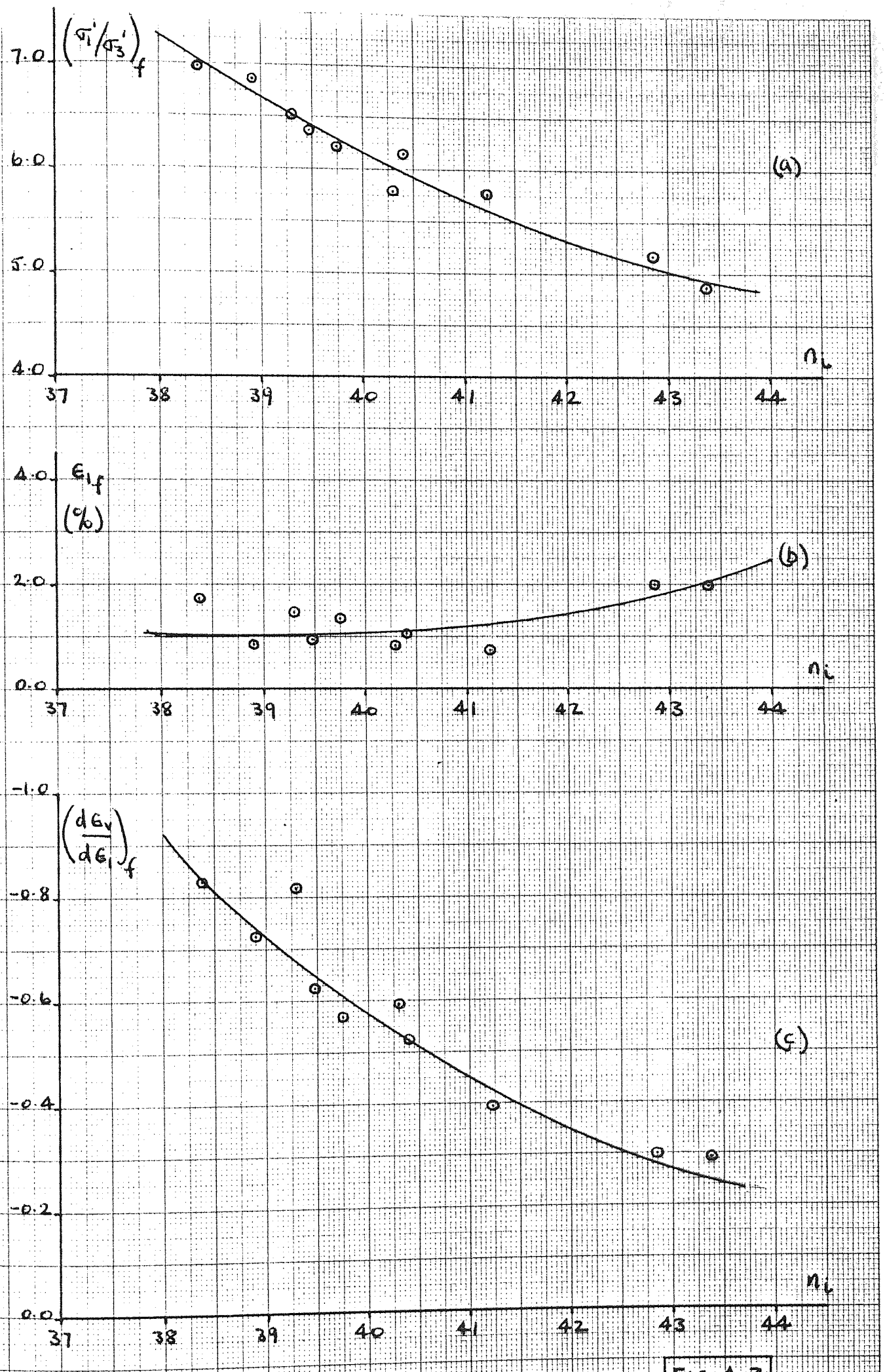

FIG. A.3

PLANE STRAIN TESTS (RIGID SIDE PLATENS)

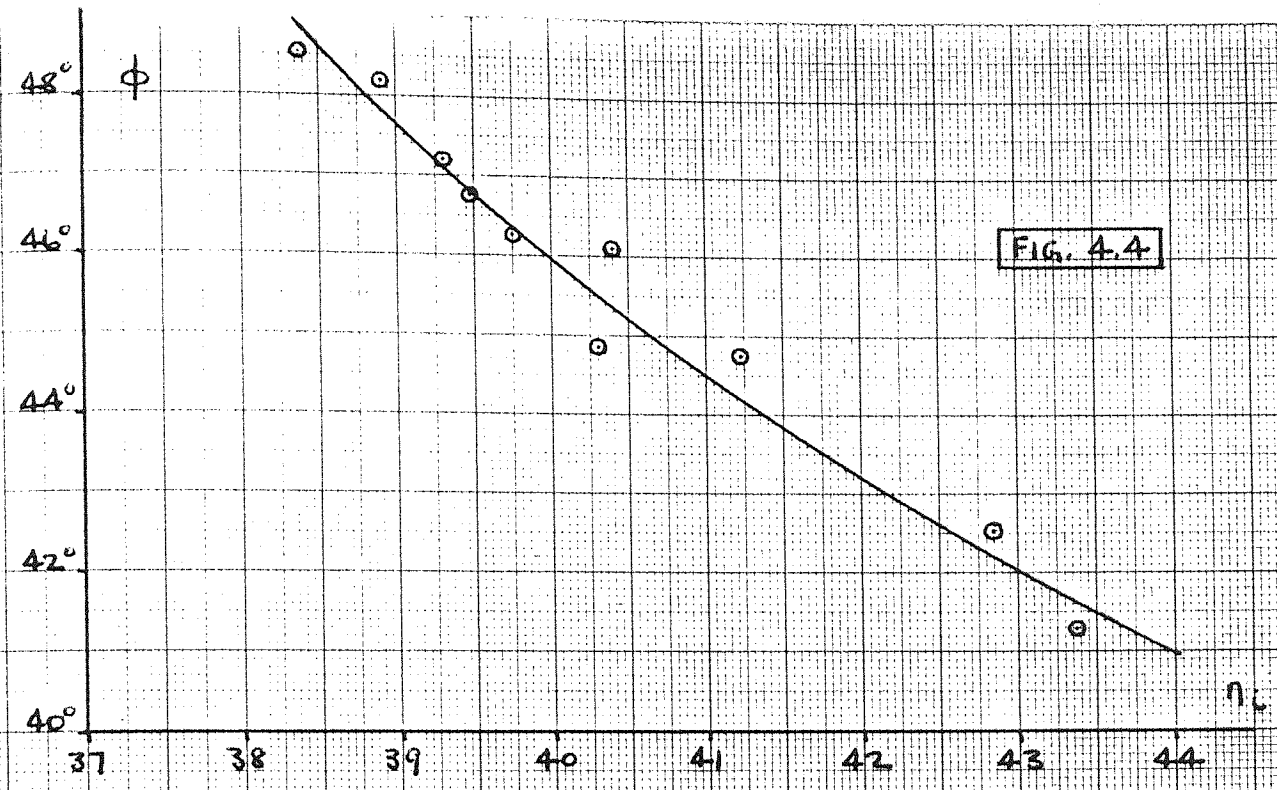

FIG. 4.4

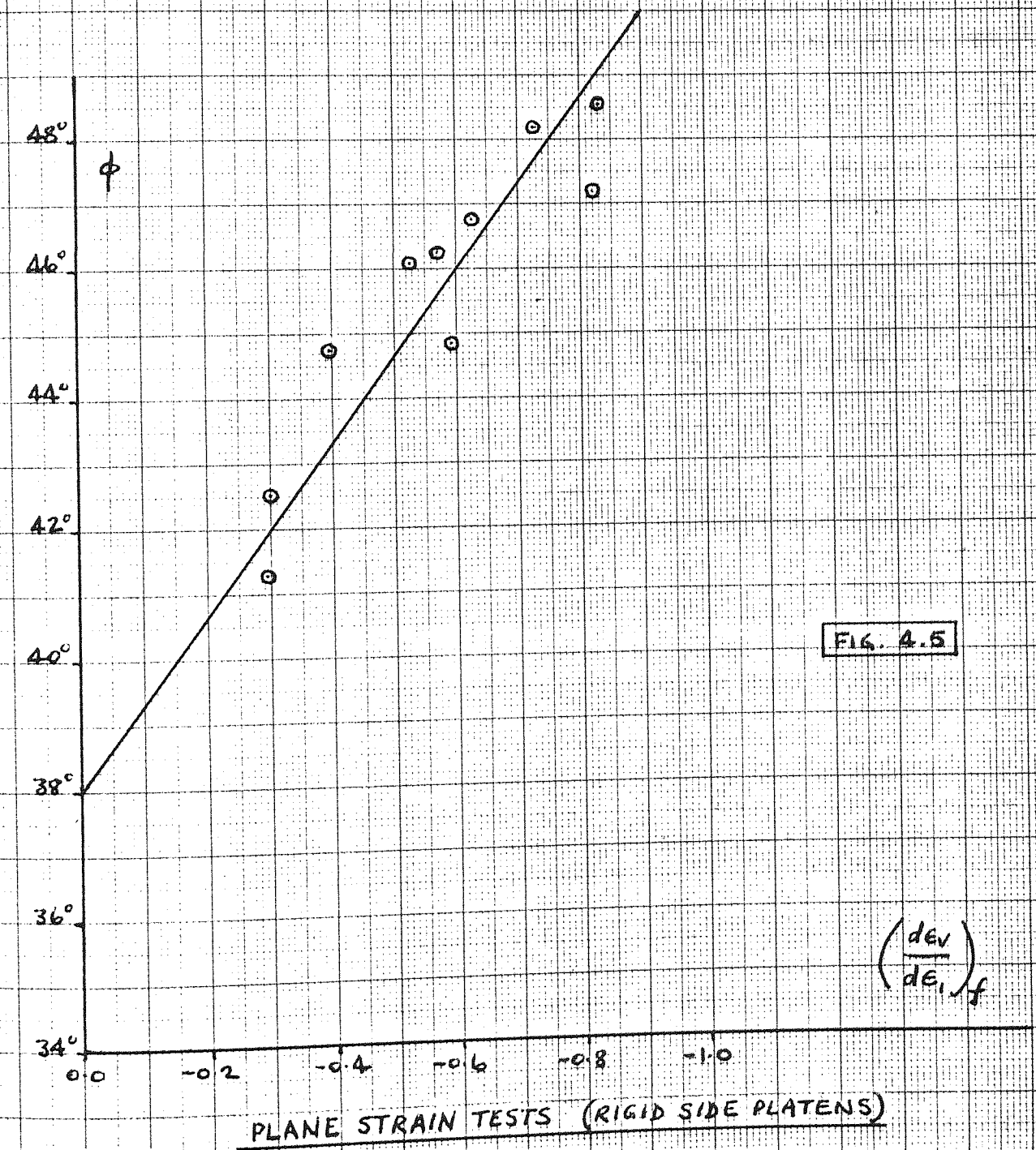

FIG. 4.5

PLANE STRAIN TESTS (RIGID SIDE PLATENS)

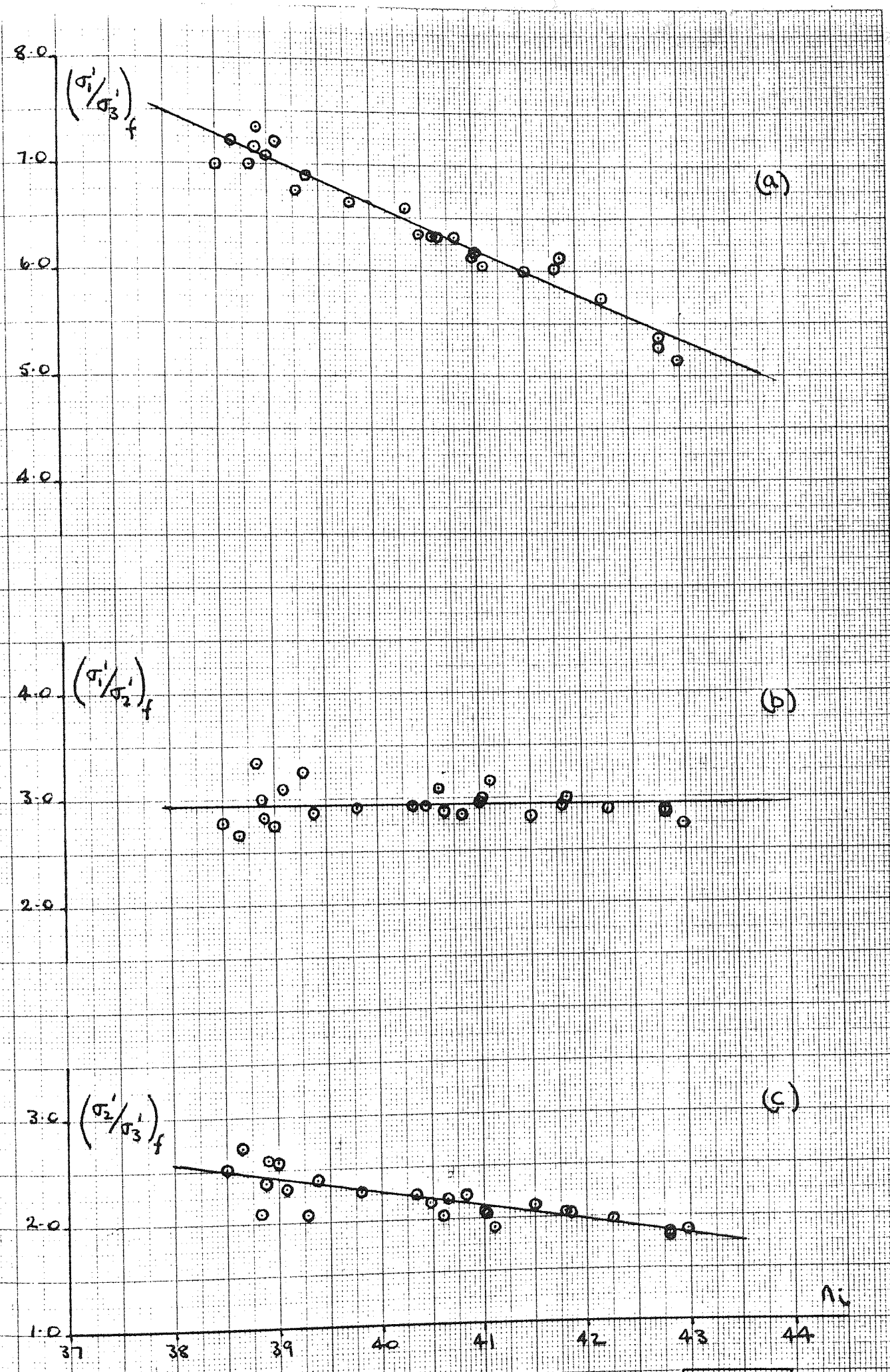

FIG. 4.6

PLANE STRAIN TESTS (FLEXIBLE SIDE PLATENS)

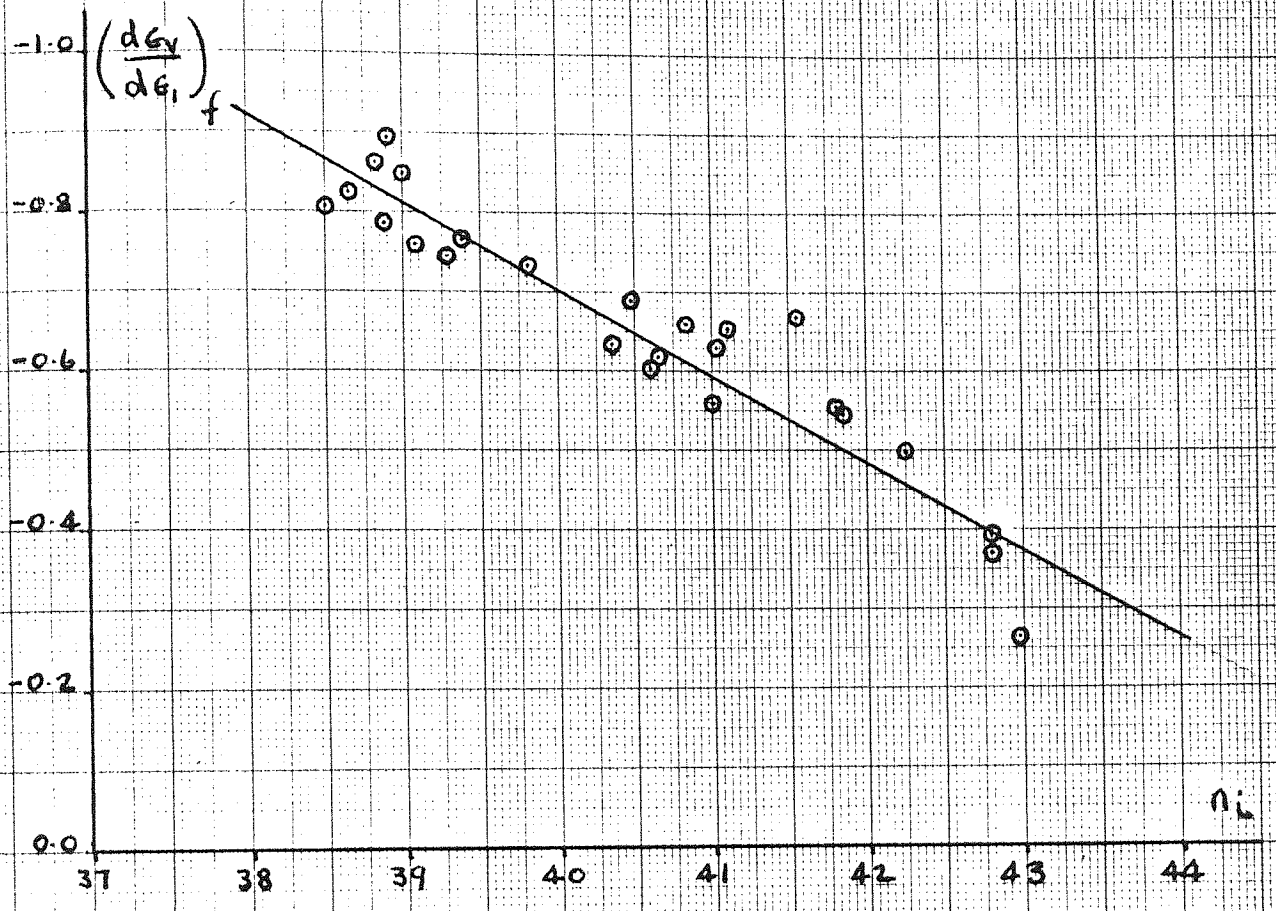

FIG. 4.7

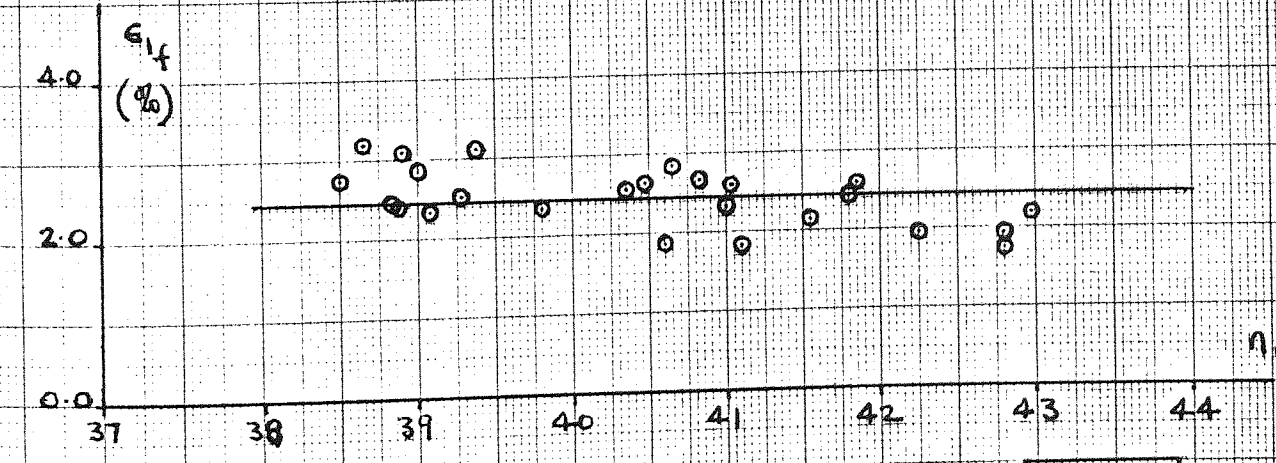

FIG. 4.8

PLANE STRAIN TESTS (FLEXIBLE SIDE PLATENS)

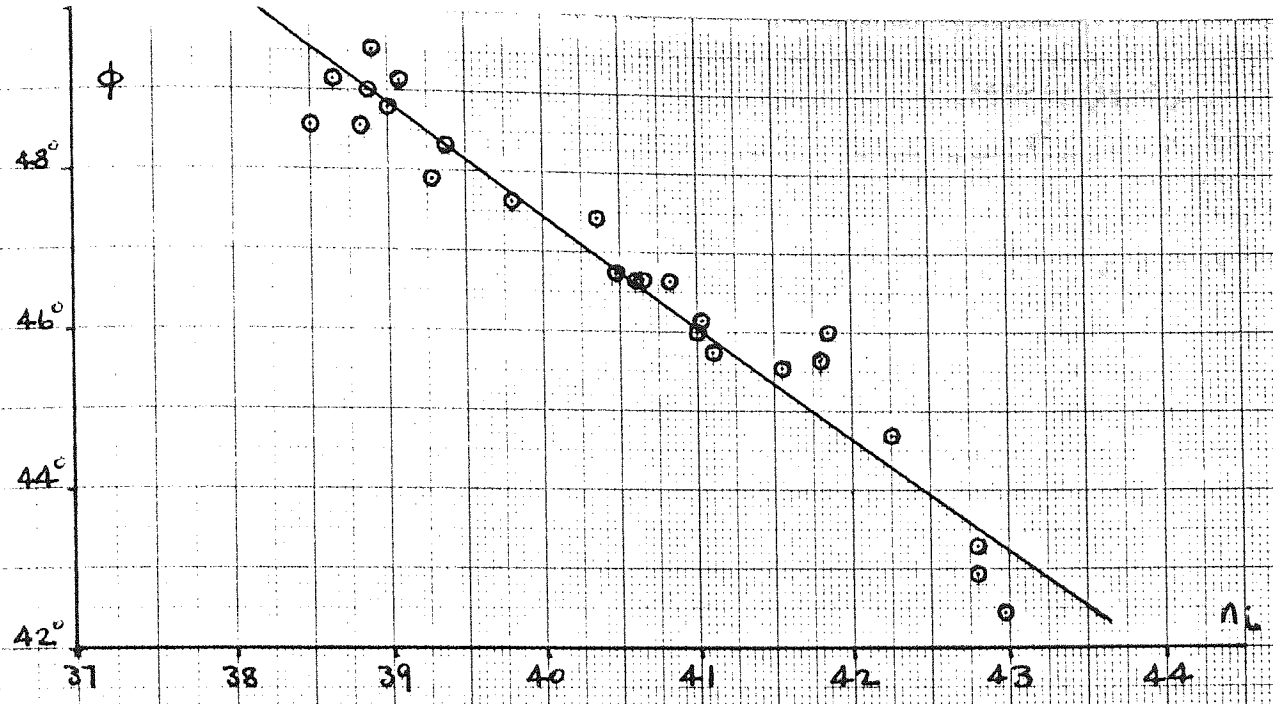

FIG. 4.9

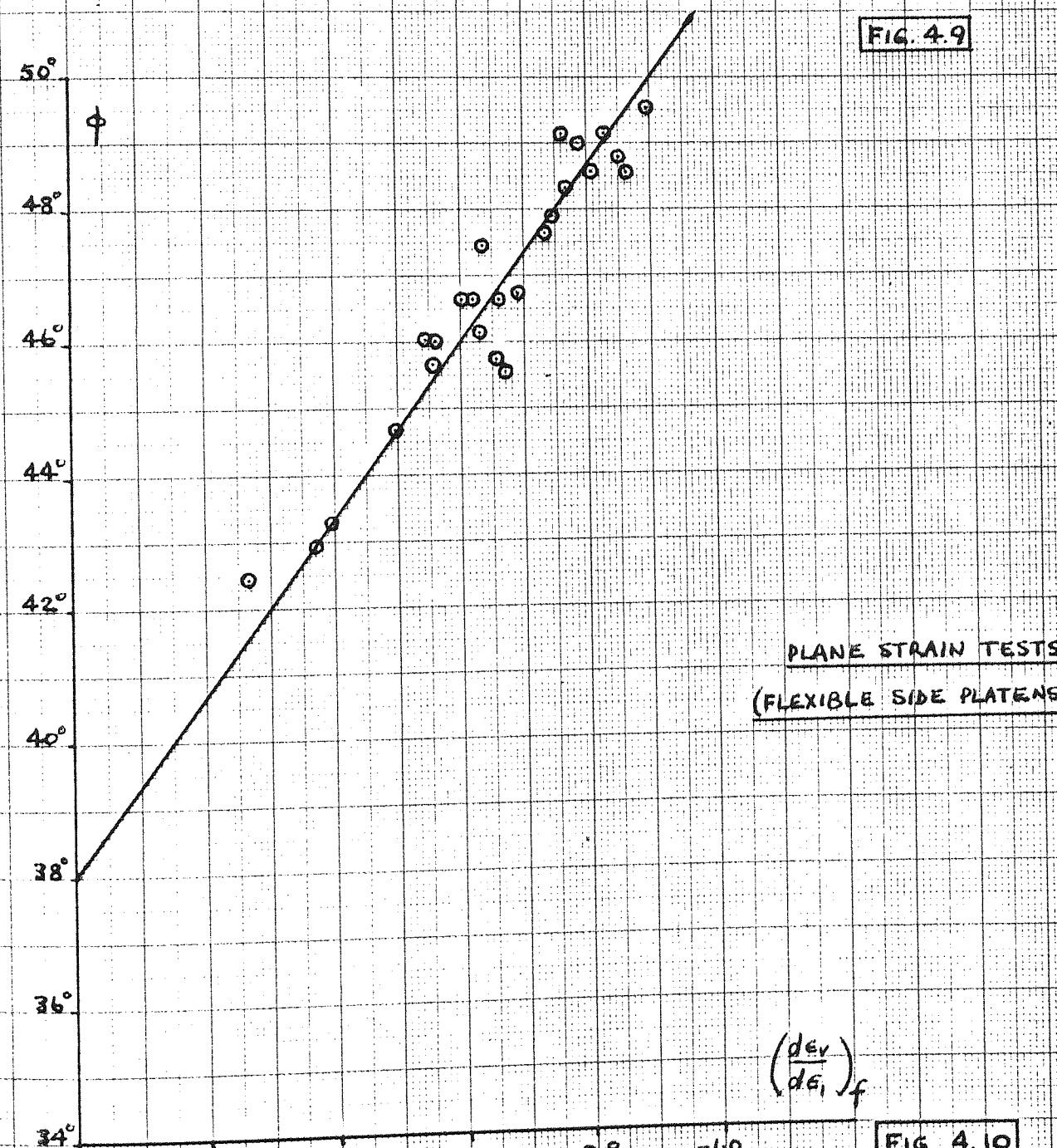

PLANE STRAIN TESTS

(FLEXIBLE SIDE PLATENS)

$\left(\frac{d\epsilon_v}{d\epsilon_1}\right)_f$

FIG. 4.10

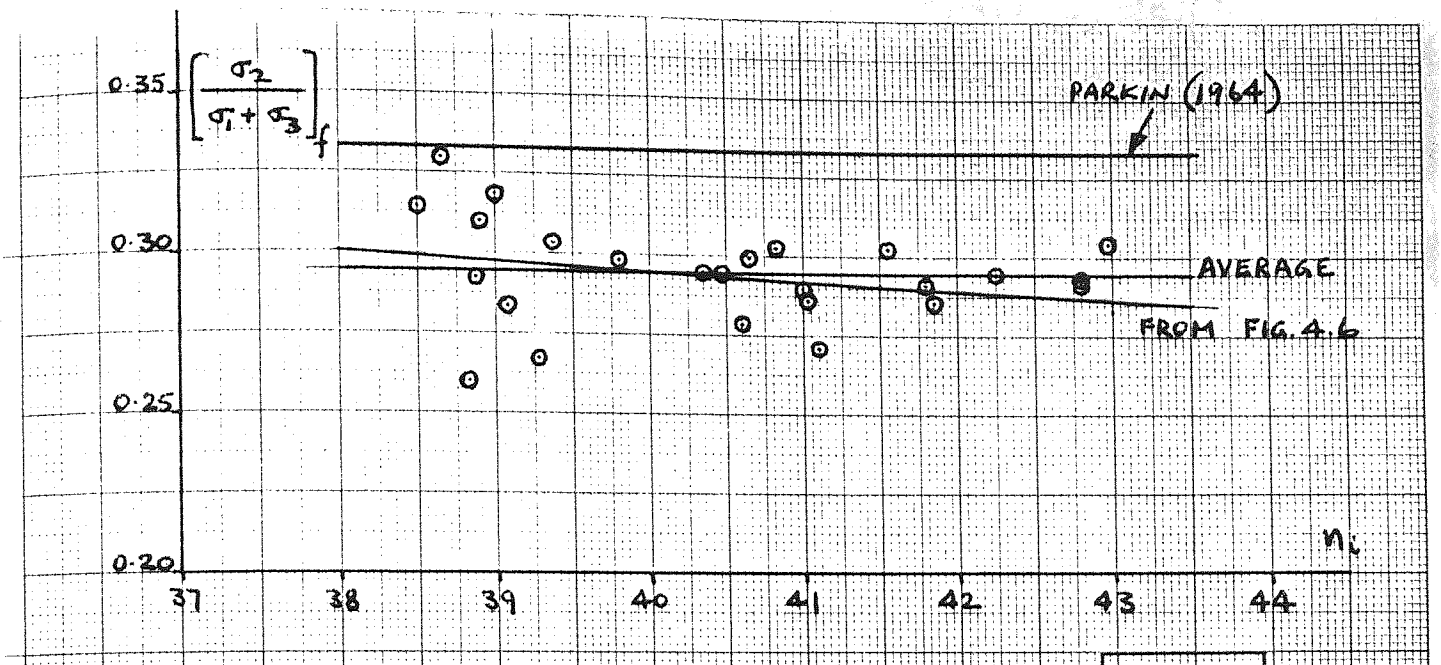

FIG. 4.11

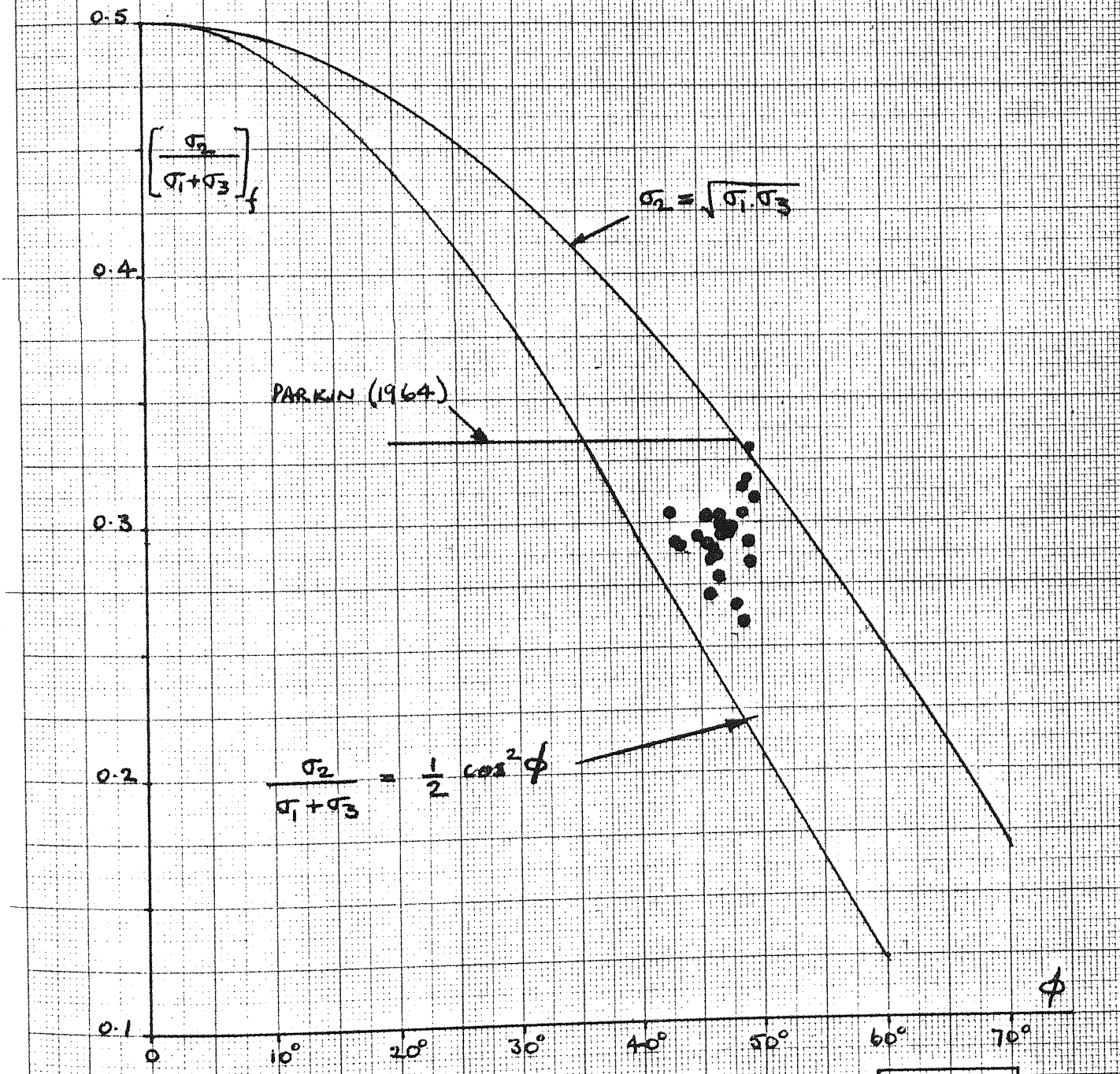

FIG. 4.12

PLANE STRAIN TESTS (FLEXIBLE SIDE PLATENS)

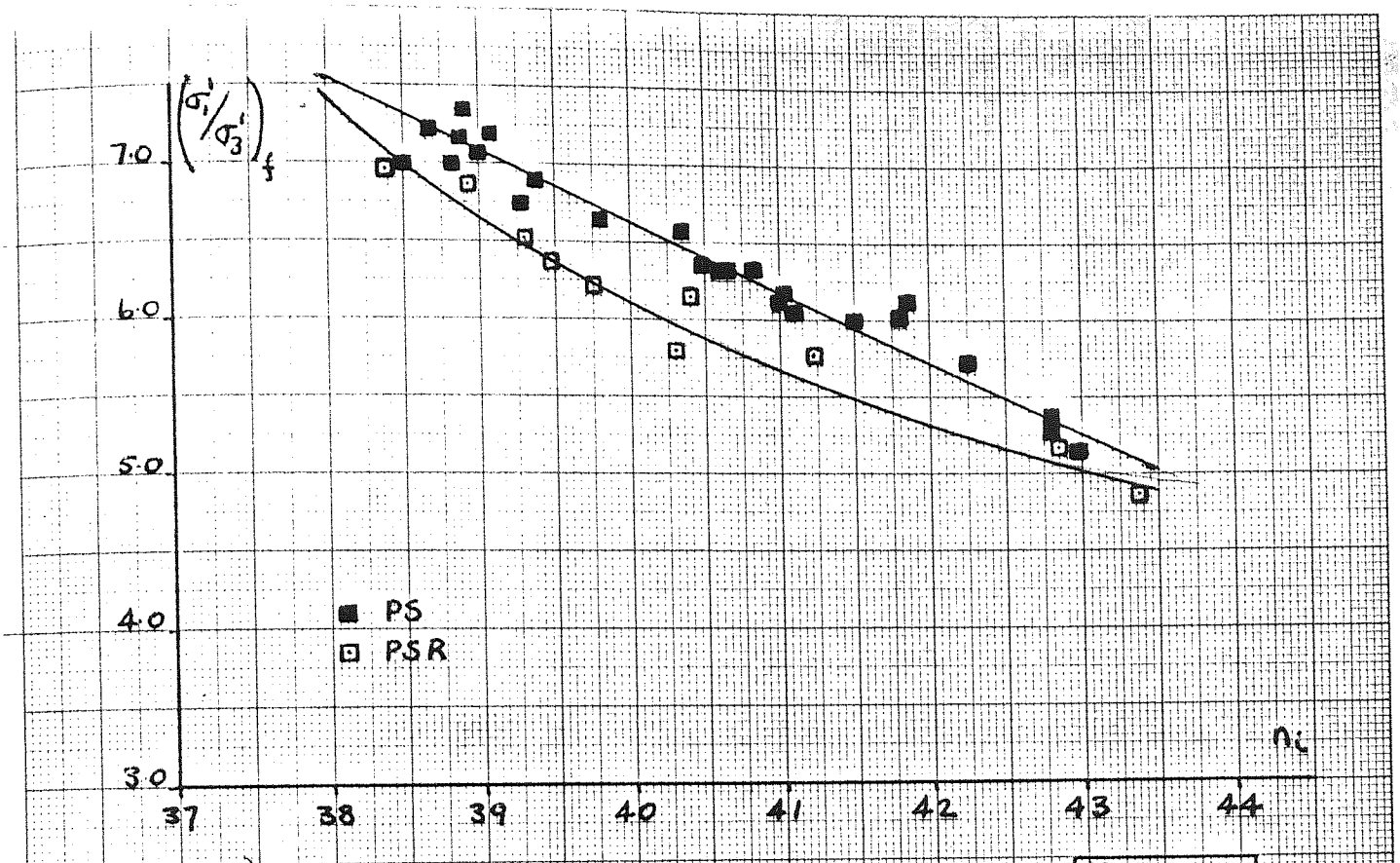

FIG. 4.13

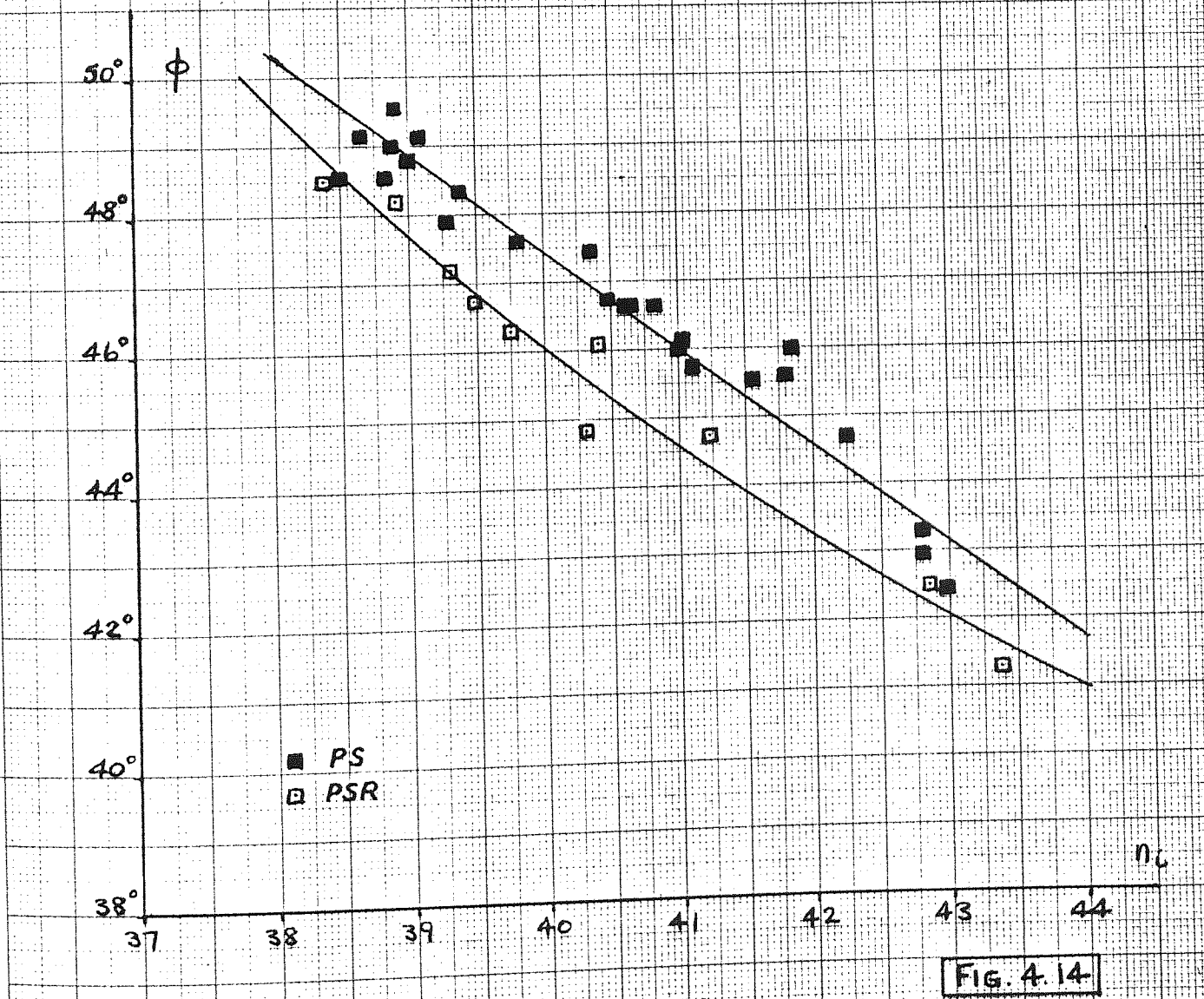

FIG. 4.14

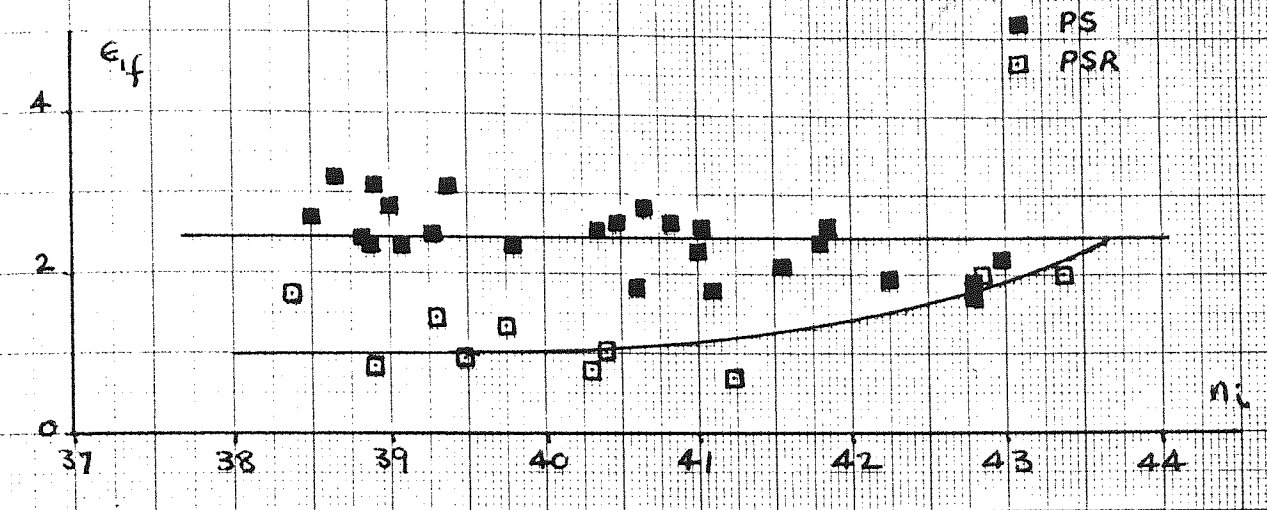

FIG. 4.15

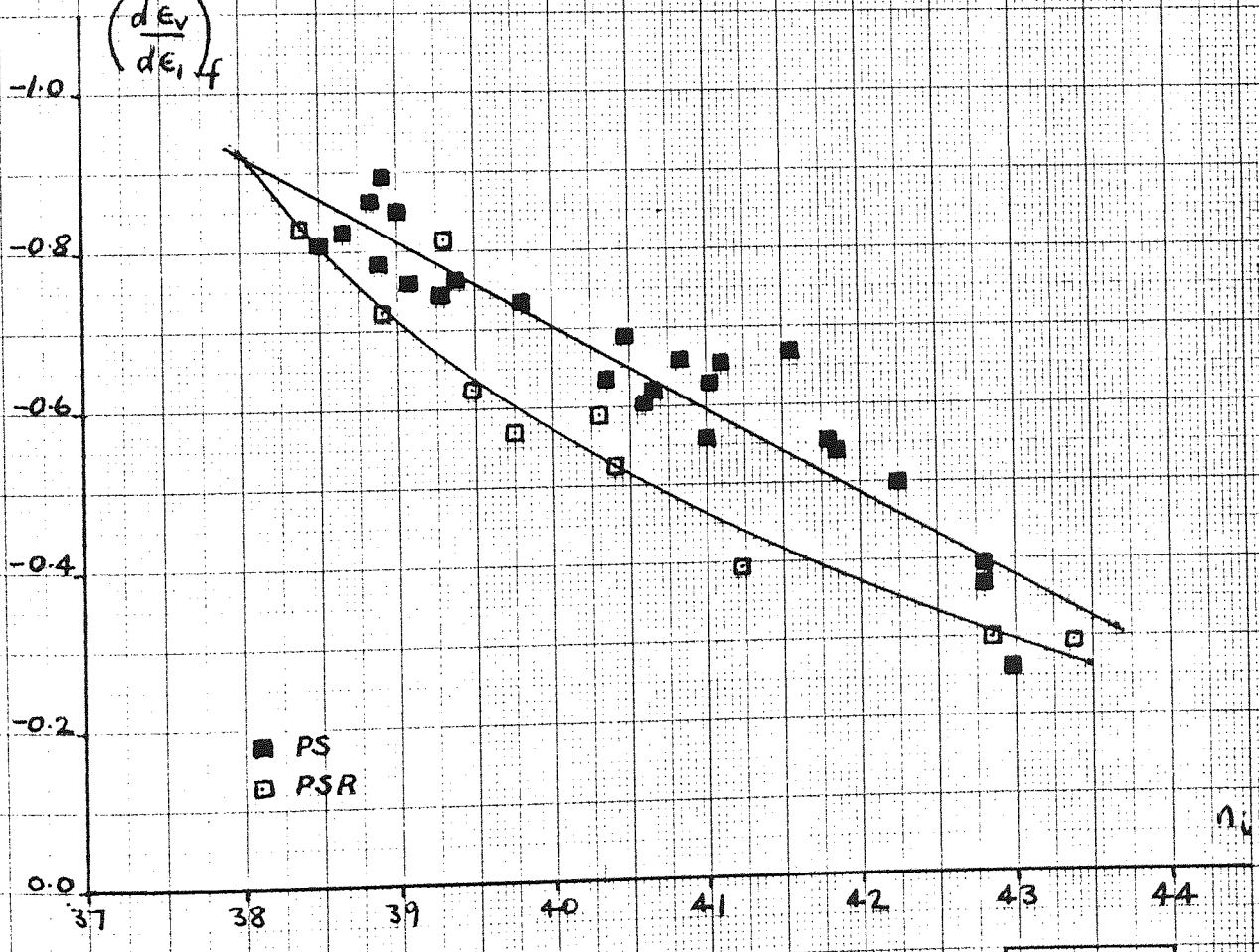

FIG. 4.16

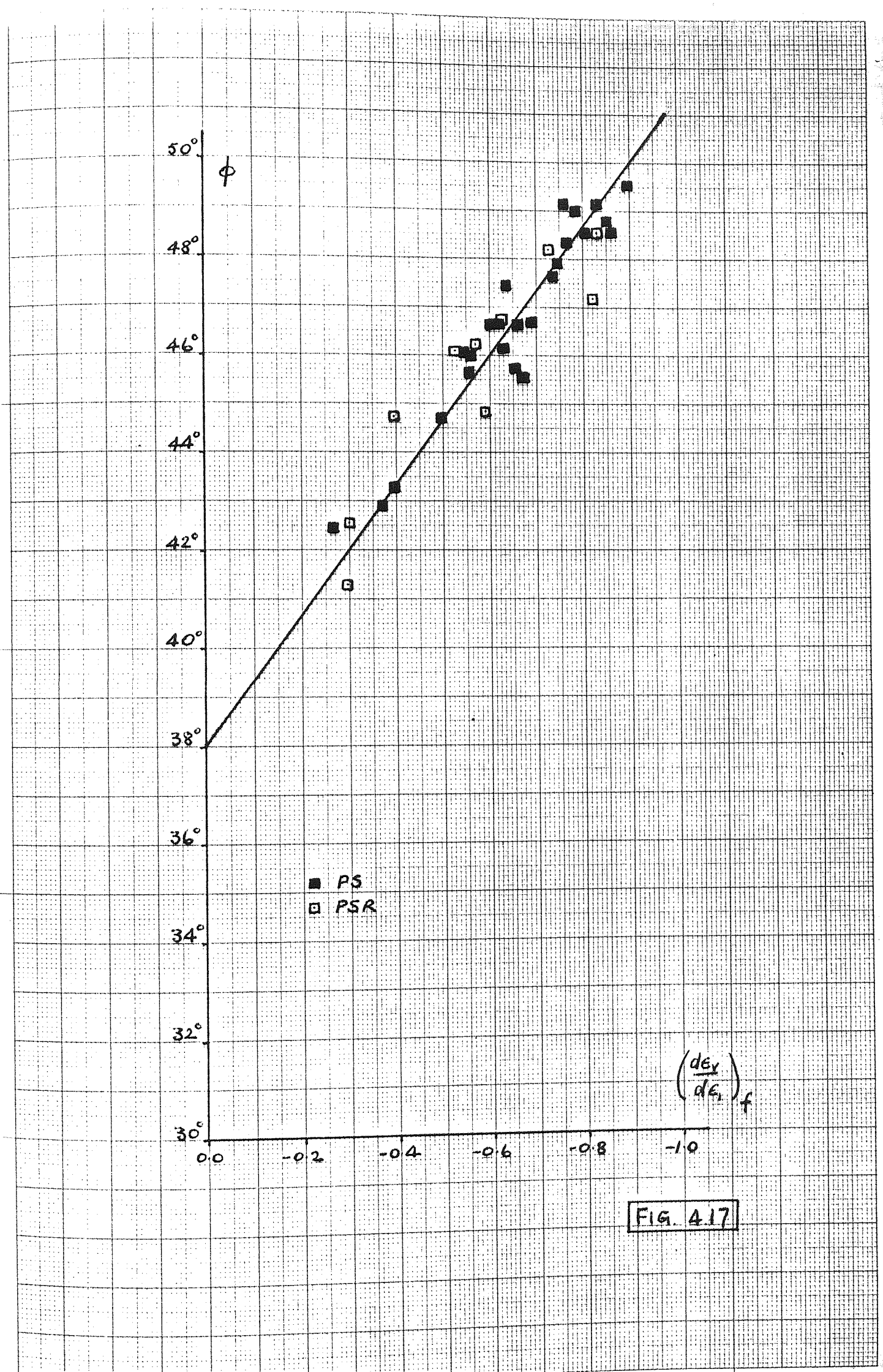
50°
φ
48°
46°
44°
42°
40°
38°
36°
34°
32°
30°
PS
PSR
0.0
-0.2
-0.4
-0.6
-0.8
-1.0
$\left(\frac{d\epsilon_y}{d\epsilon_1}\right)_f$

FIG. 4.17

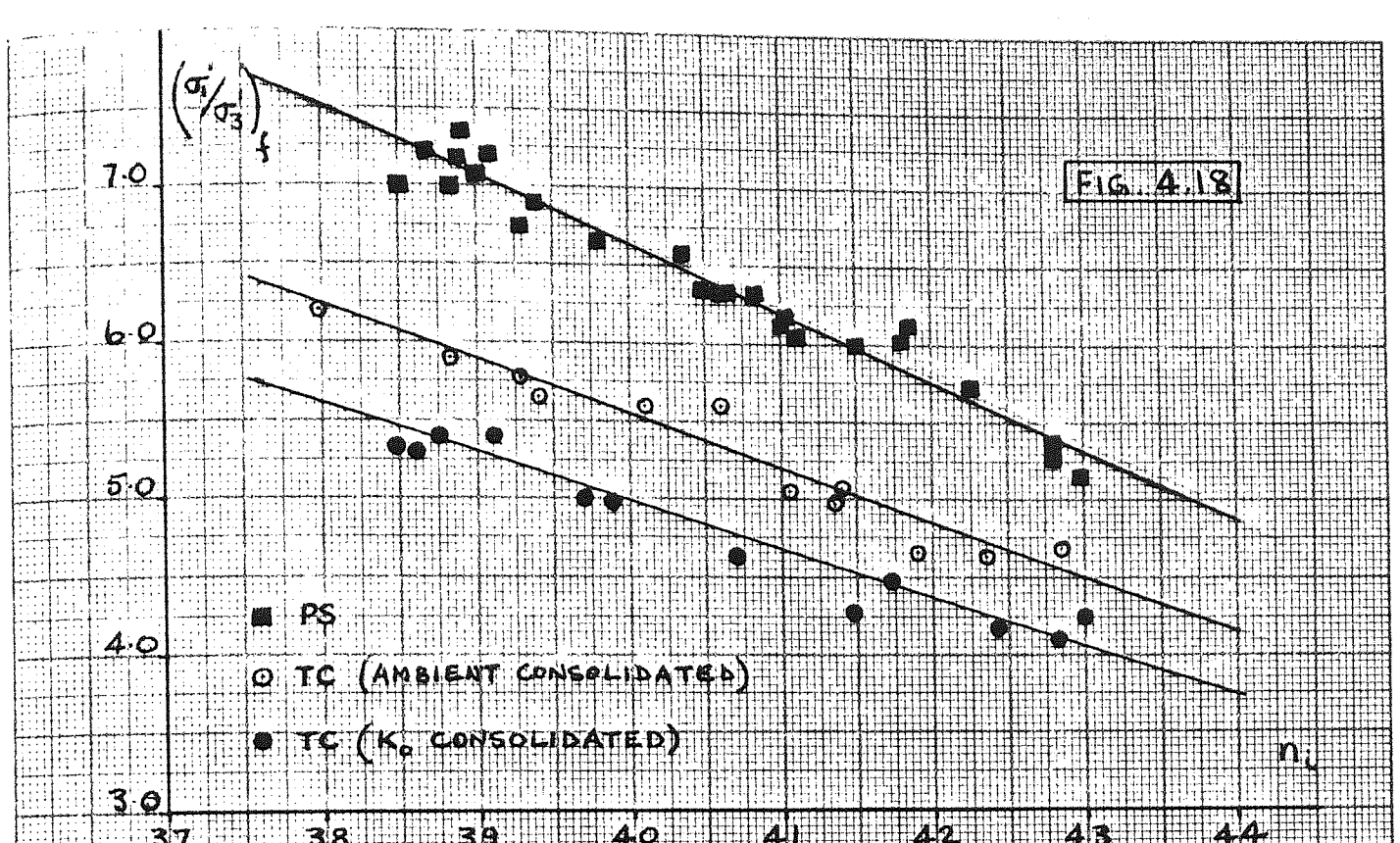

FIG. 4.18

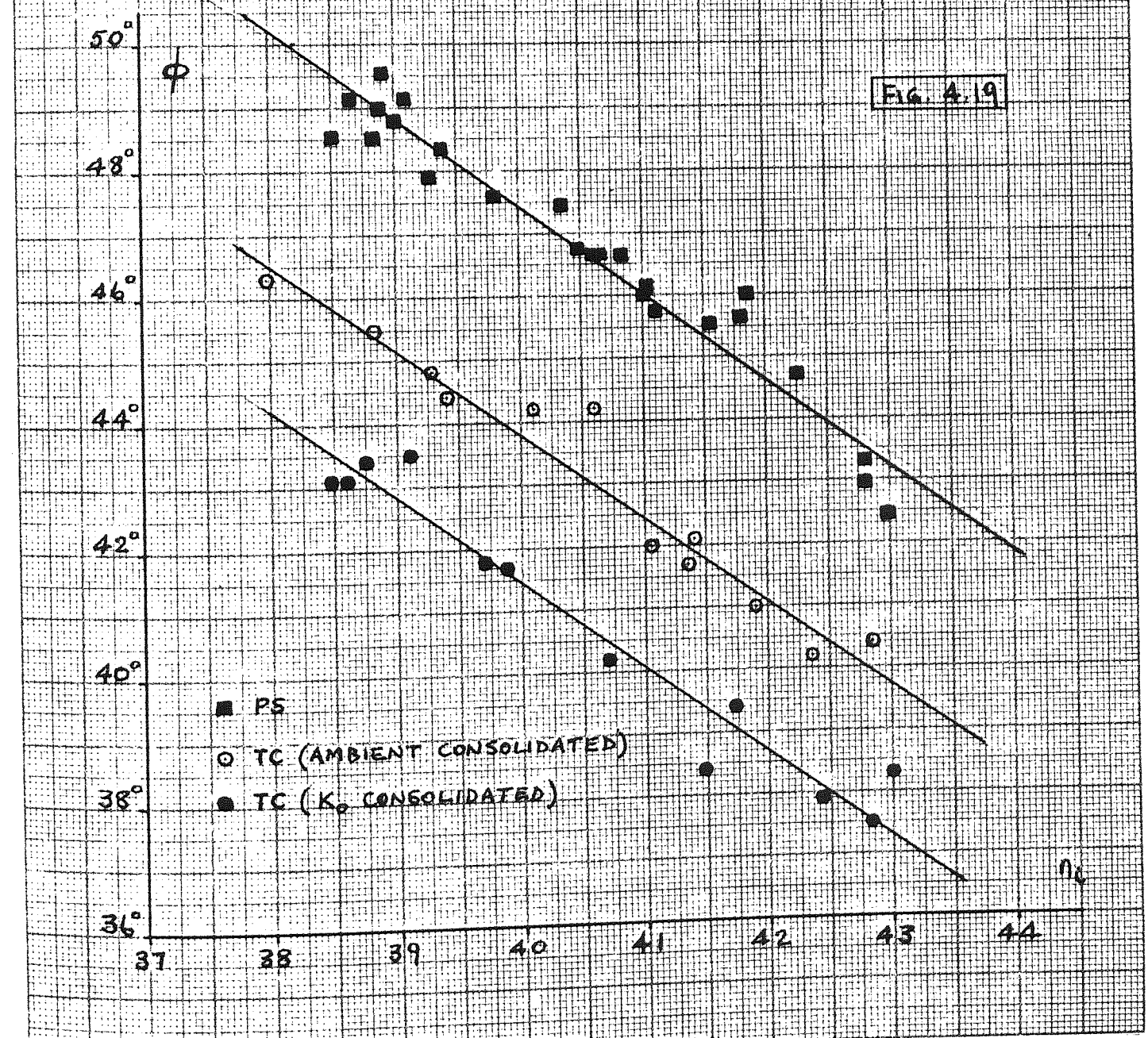

FIG. 4.19

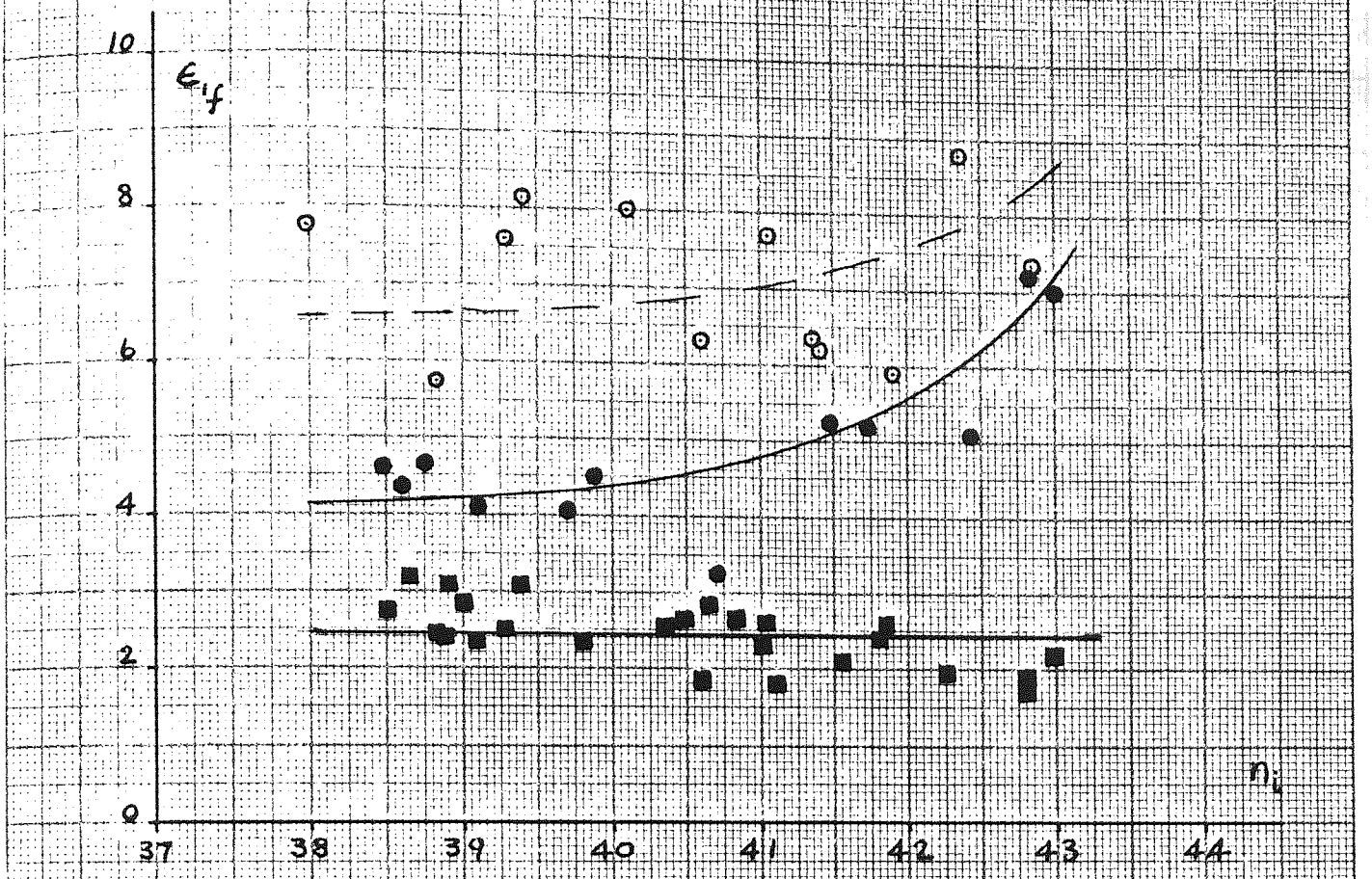

FIG. 4.20

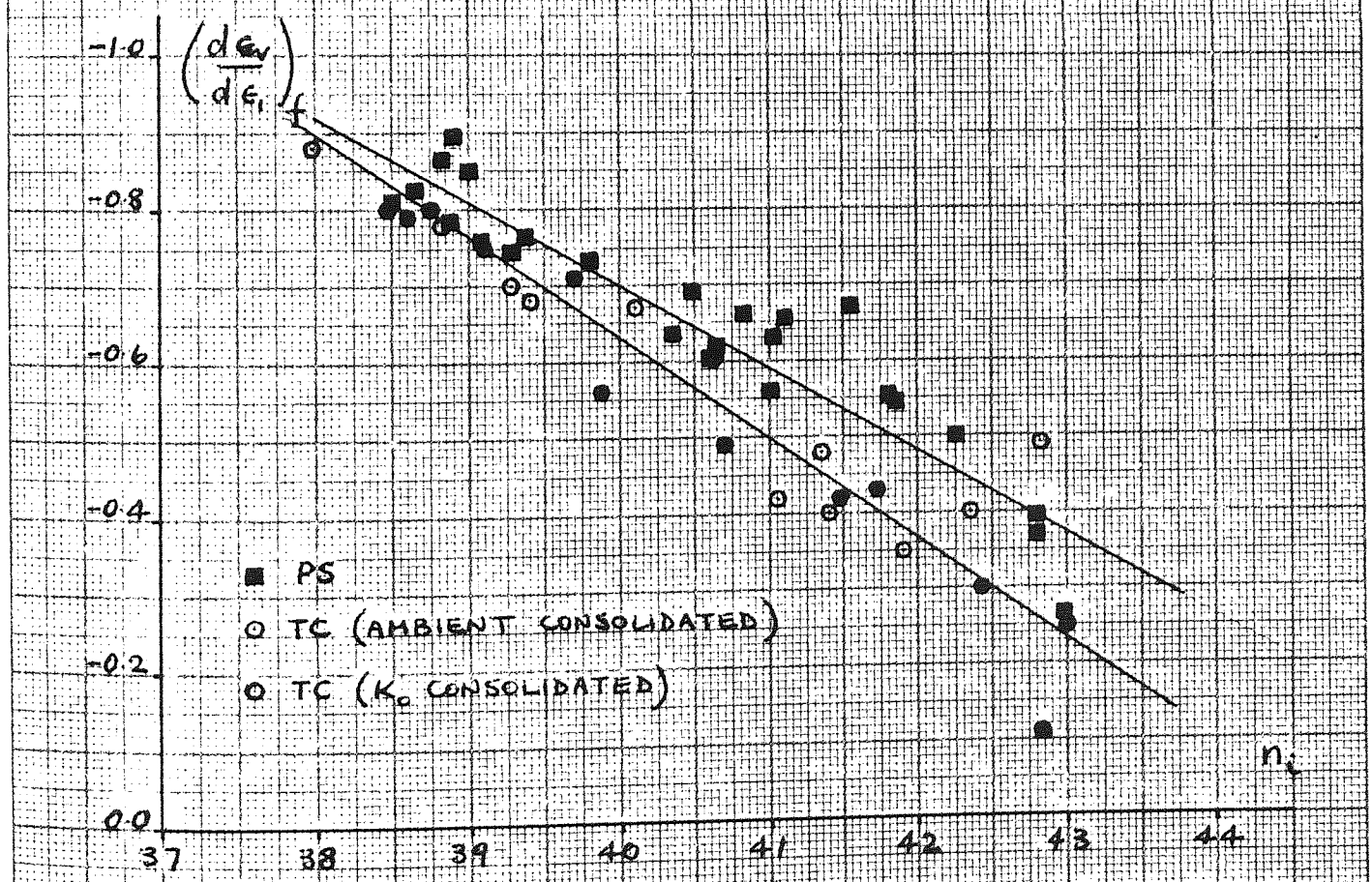

FIG. 4.21

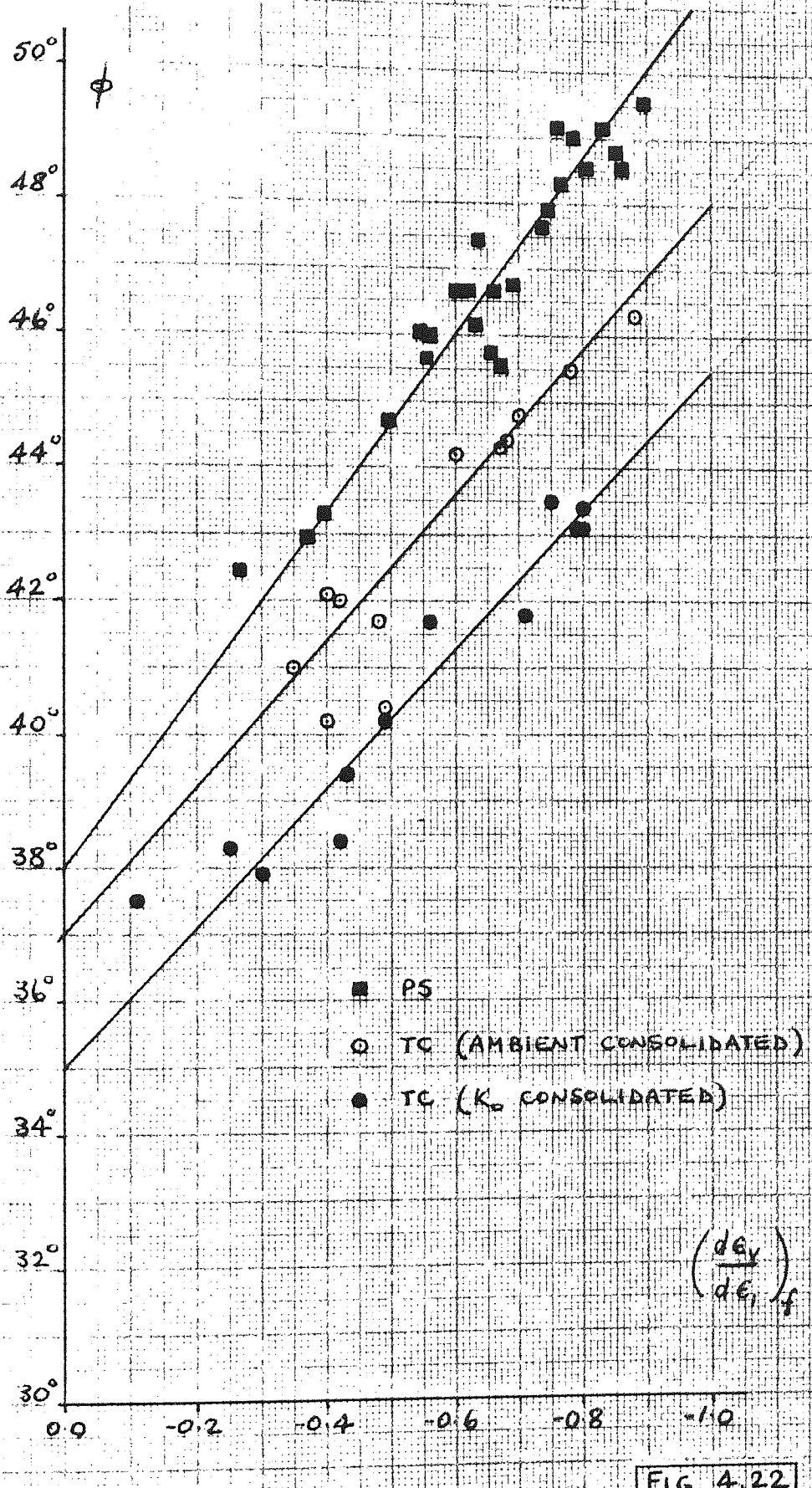
50°
48°
46°
44°
42°
40°
38°
36°
34°
32°
30°
φ
0.0
-0.2
-0.4
-0.6
-0.8
-1.0
PS
TC (AMBIENT CONSOLIDATED)
TC (K₀ CONSOLIDATED)
$\left(\frac{d\epsilon_v}{d\epsilon_1}\right)_f$

FIG. 4.22

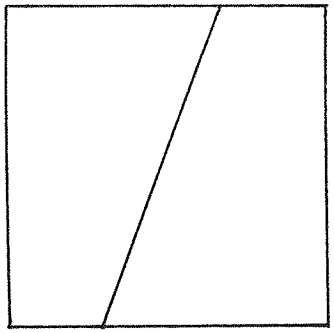

MODE A

PSR 1,2,5,8,9,10.

PS 2,4,6,8,10,14, 15,16,18.

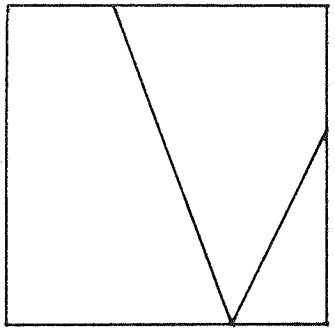

MODE B

PSR 6,7.

PS 5,7,20,21,24, 25.

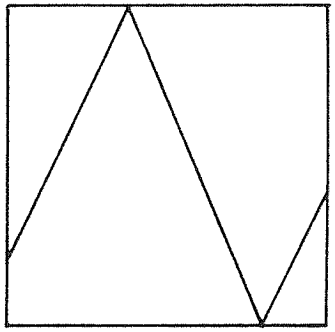

MODE C

PSR 4.

PS 1,3.

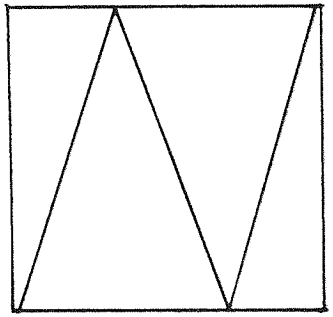

MODE D

PS 19.

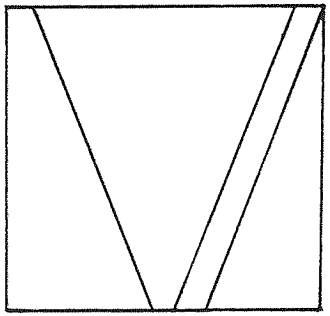

MODE E

PS 22

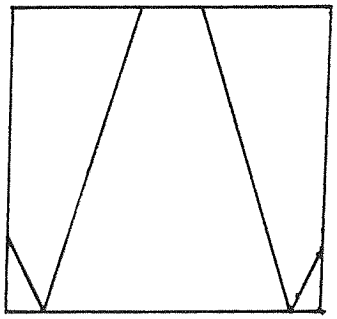

MODE F

PSR 3

Fig. 4.23

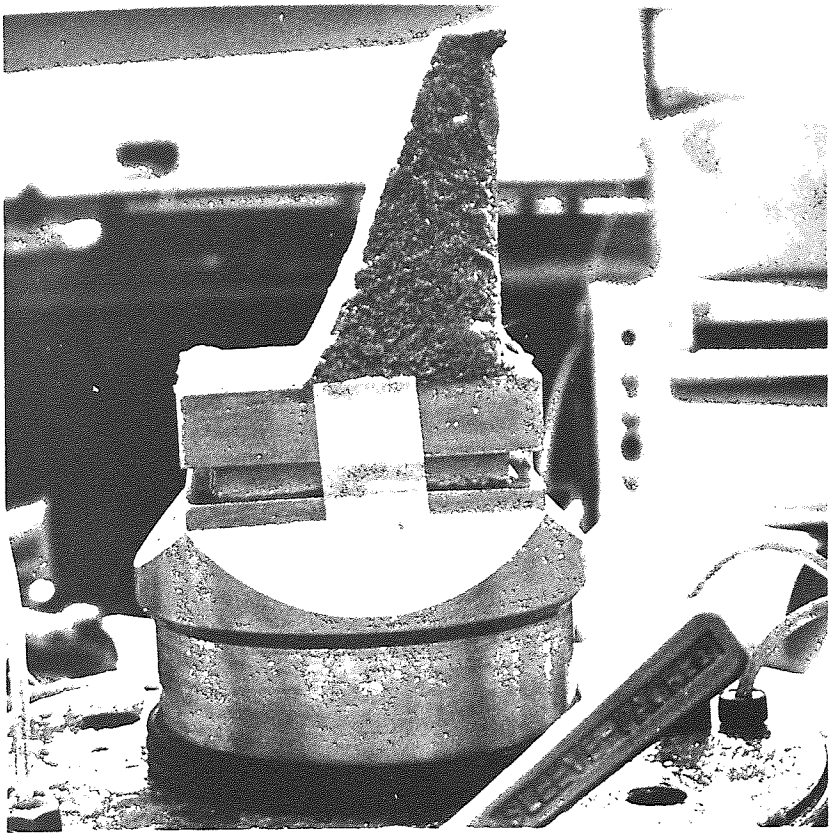

Fig. 4.24

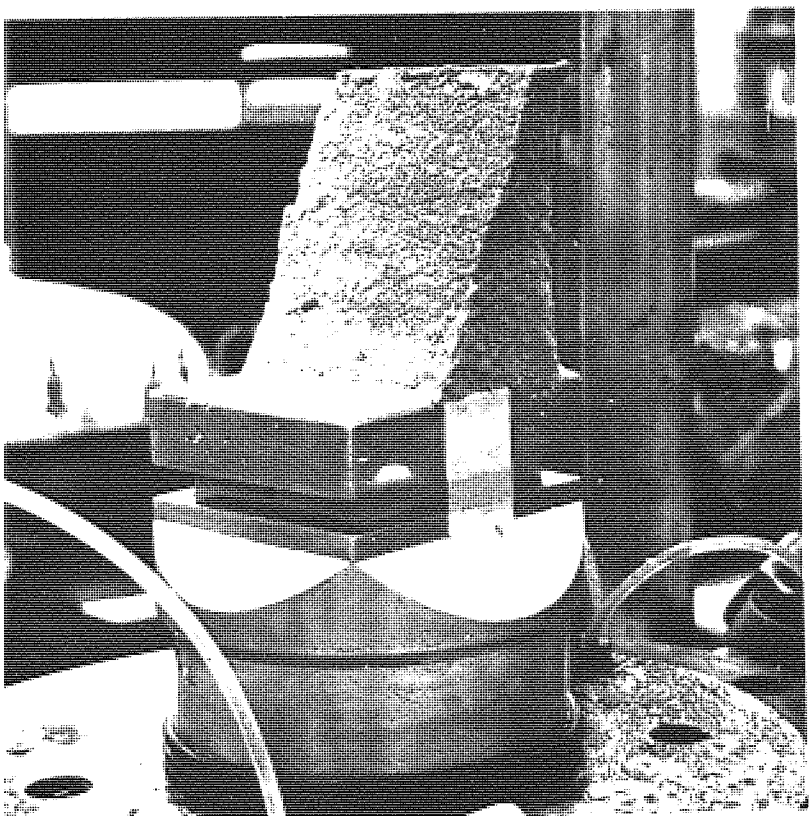

Fig. 4.25

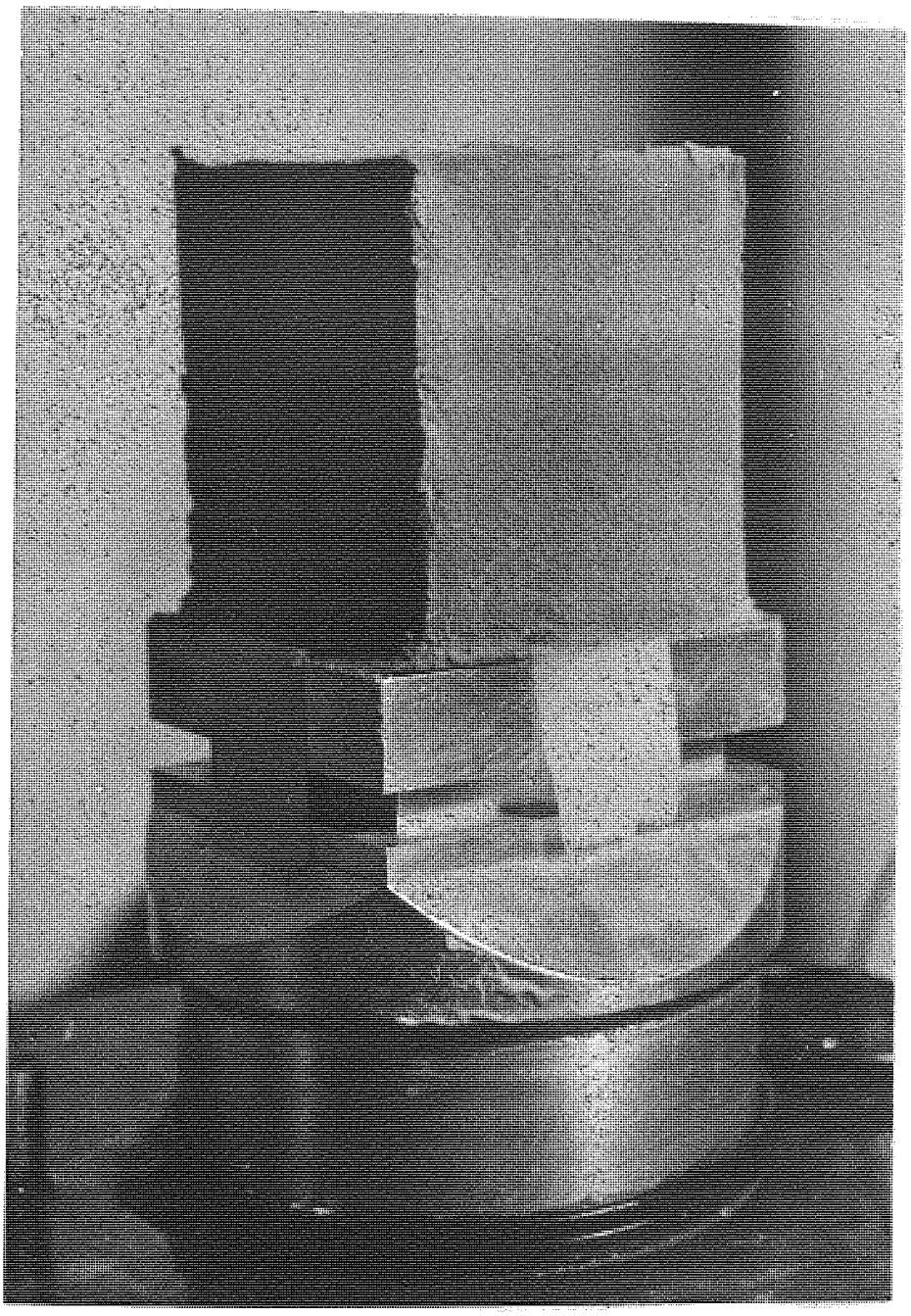

Fig. 4.26

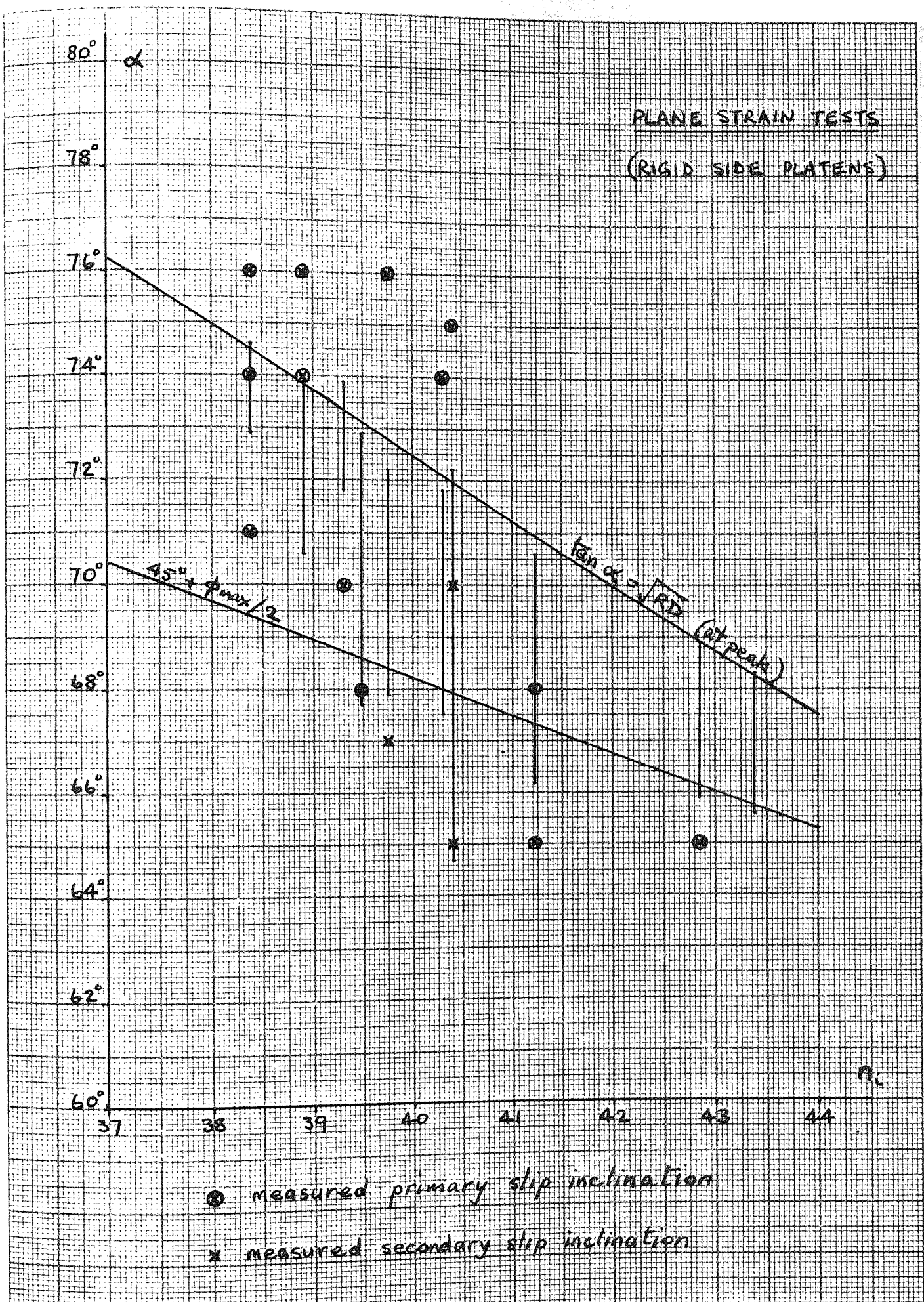
PLANE STRAIN TESTS
(RIGID SIDE PLATENS)
80°
78°
76°
74°
72°
70°
68°
66°
64°
62°
60°
α
37
38
39
40
41
42
43
44
n_L
$45° + \phi_{max}/2$
$\tan \alpha = \sqrt{K_D}$
(at peak)
⊗ measured primary slip inclination
× measured secondary slip inclination

FIG. 4.2

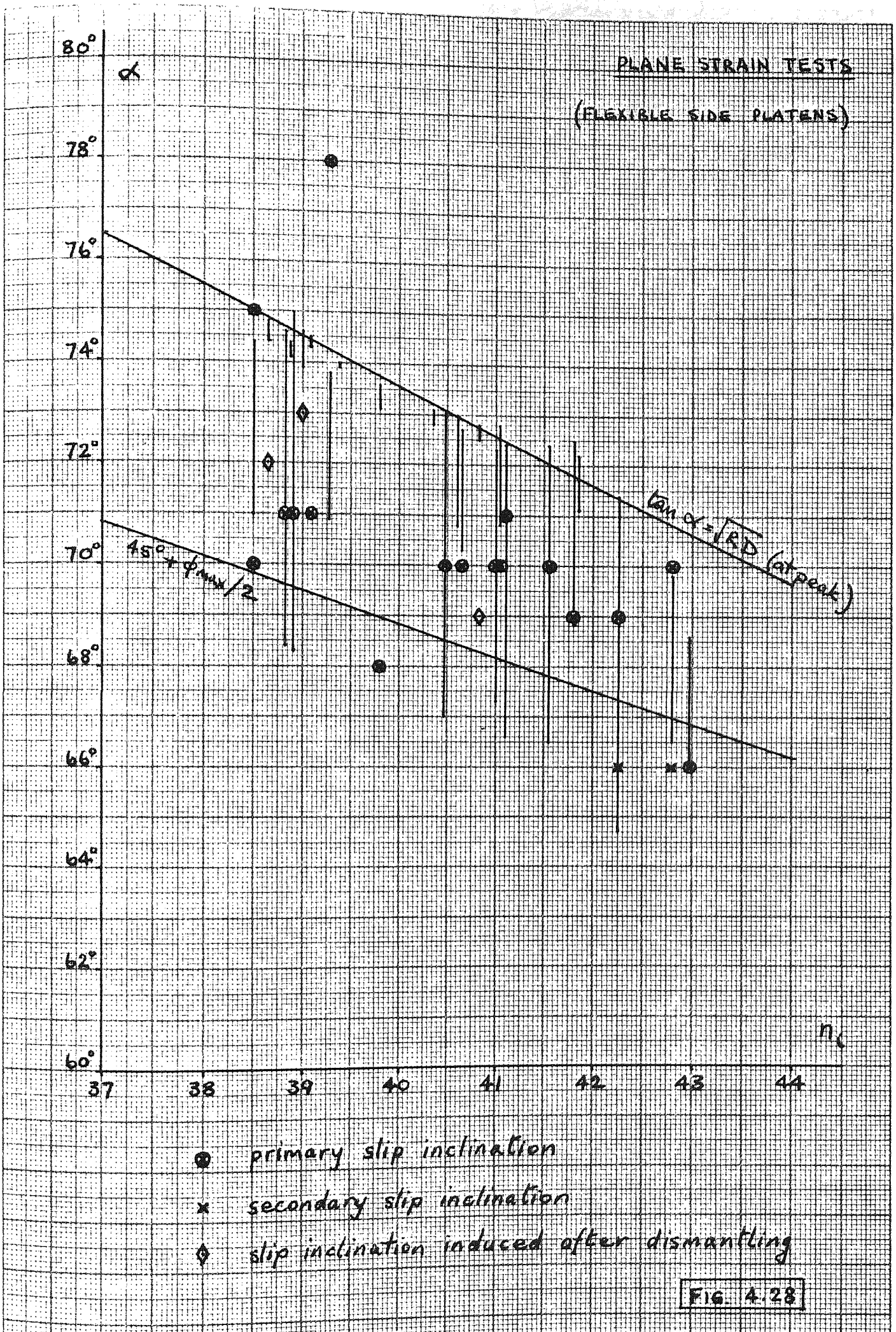
PLANE STRAIN TESTS
(FLEXIBLE SIDE PLATENS)
80°
78°
76°
74°
72°
70°
68°
66°
64°
62°
60°
α
n_ϵ
37
38
39
40
41
42
43
44
$\tan\alpha = \sqrt{K_D}$ (at peak)
$45° + \phi_{max}/2$
primary slip inclination
secondary slip inclination
slip inclination induced after dismantling

FIG. 4.28

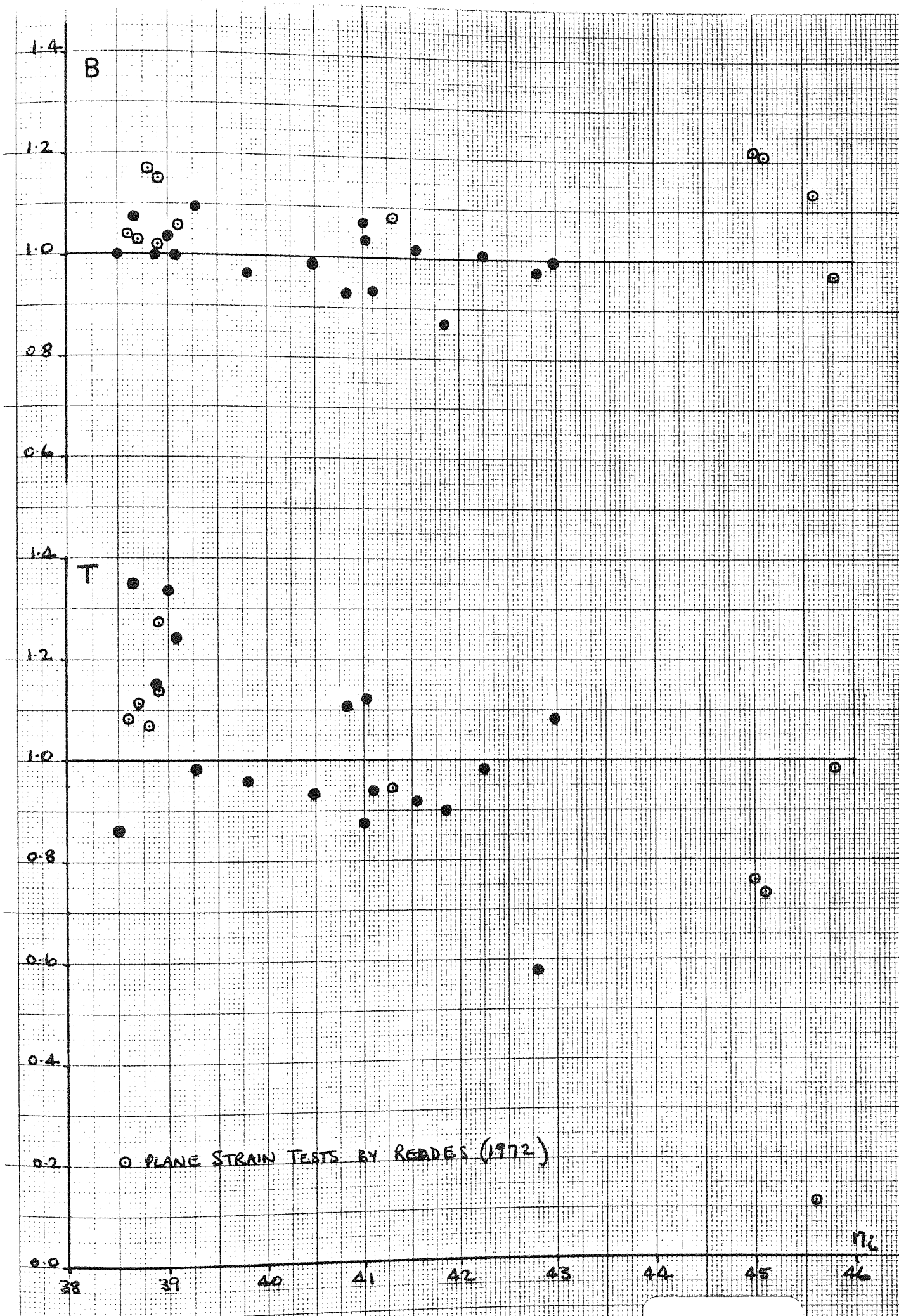
B
T
1·4
1·2
1·0
0·8
0·6
0·4
0·2
0·0
38
39
40
41
42
43
44
45
46
n_i
⊙ PLANE STRAIN TESTS BY READES (1972)

FIG. 4.29

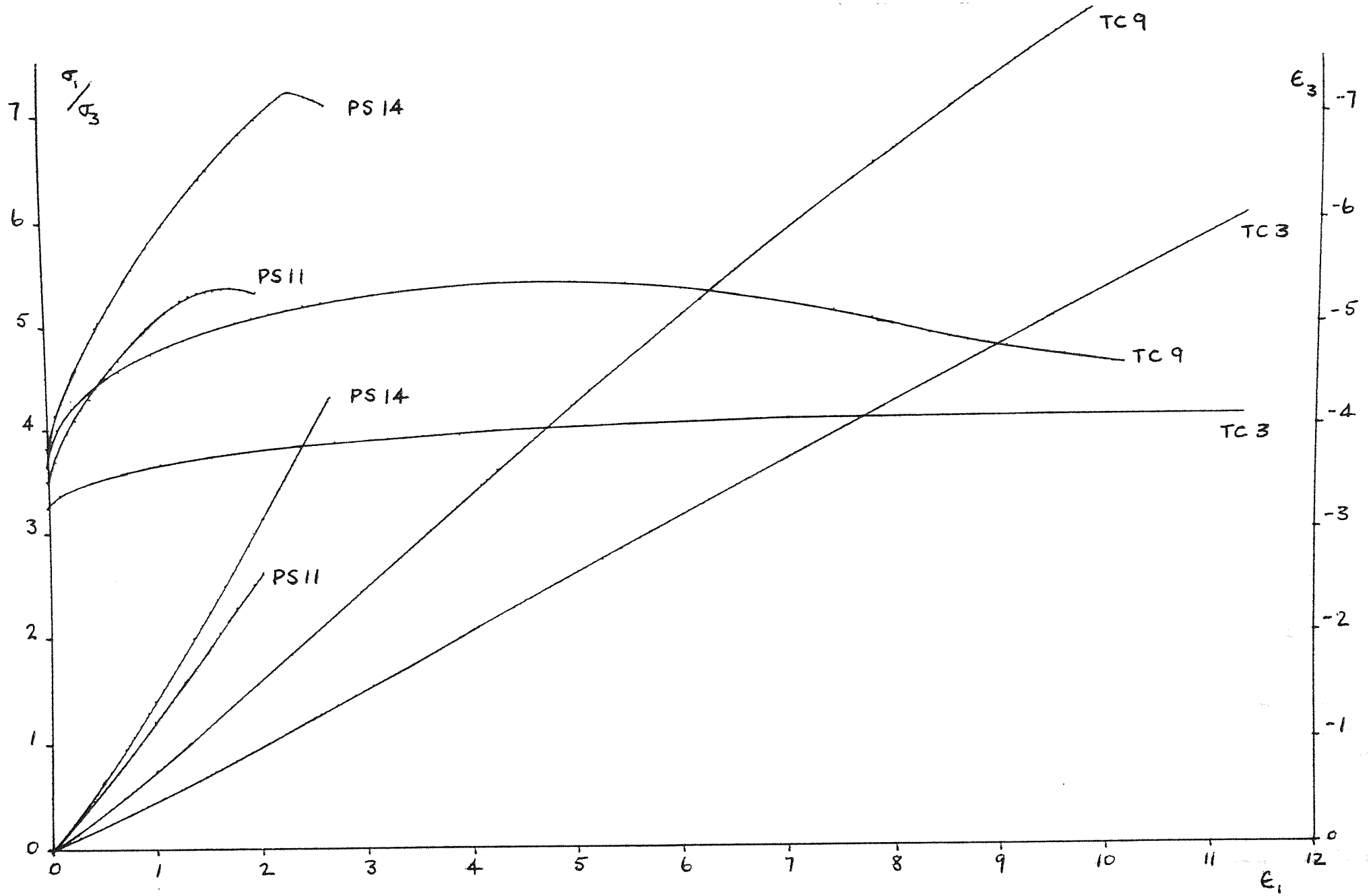
σ_1/σ_3
ϵ_3
ϵ_1
PS 14
PS 11
PS 14
PS 11
TC 9
TC 3
TC 9
TC 3
0
1
2
3
4
5
6
7
8
9
10
11
12
-1
-2
-3
-4
-5
-6
-7

Fig. 4.30

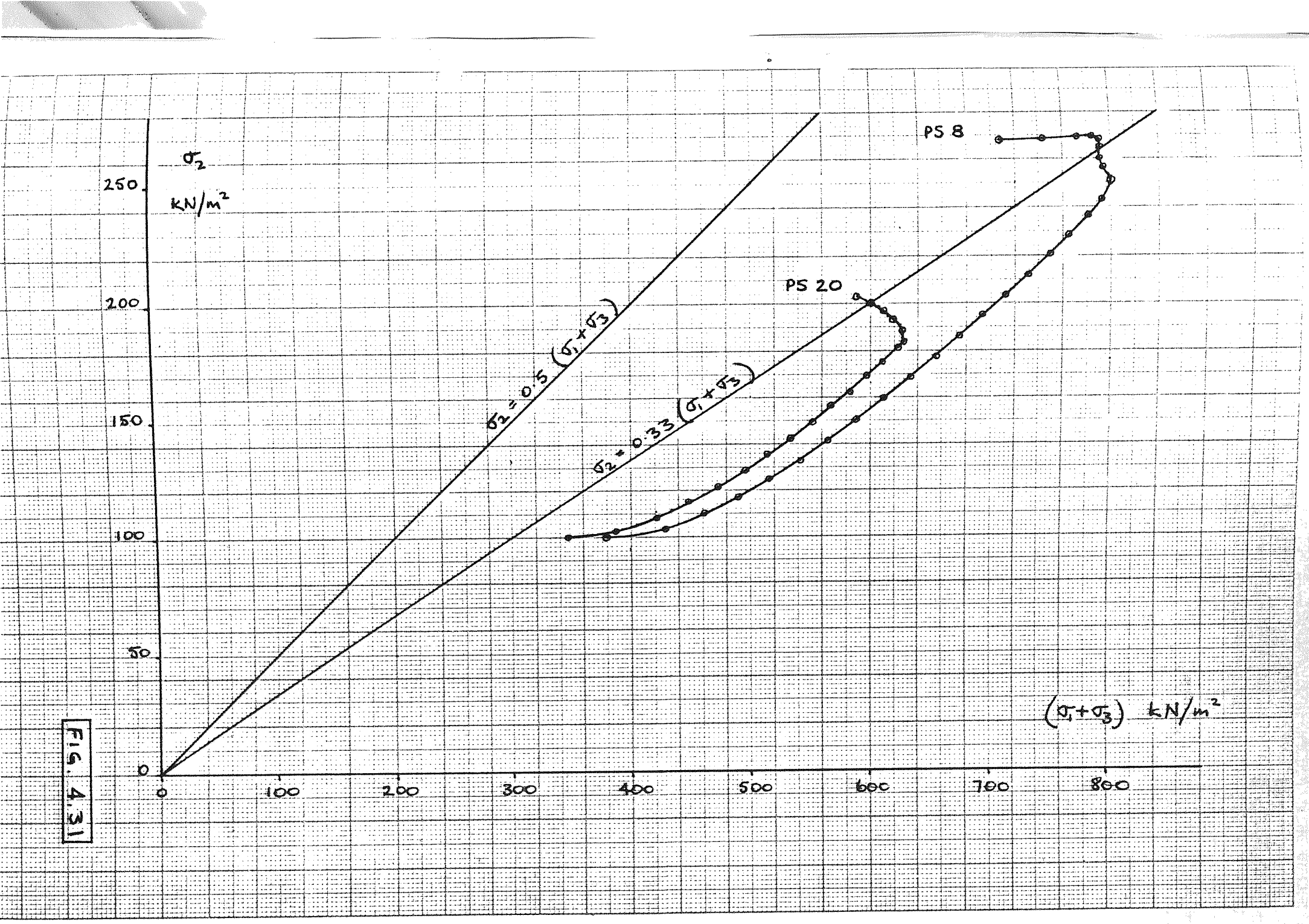
σ_2
kN/m²
250
200
150
100
50
0
0
100
200
300
400
500
600
700
800
PS 8
PS 20
$\sigma_2 = 0.5\,(\sigma_1 + \sigma_3)$
$\sigma_2 = 0.33\,(\sigma_1 + \sigma_3)$
$(\sigma_1 + \sigma_3)$ kN/m²

FIG. 4.31

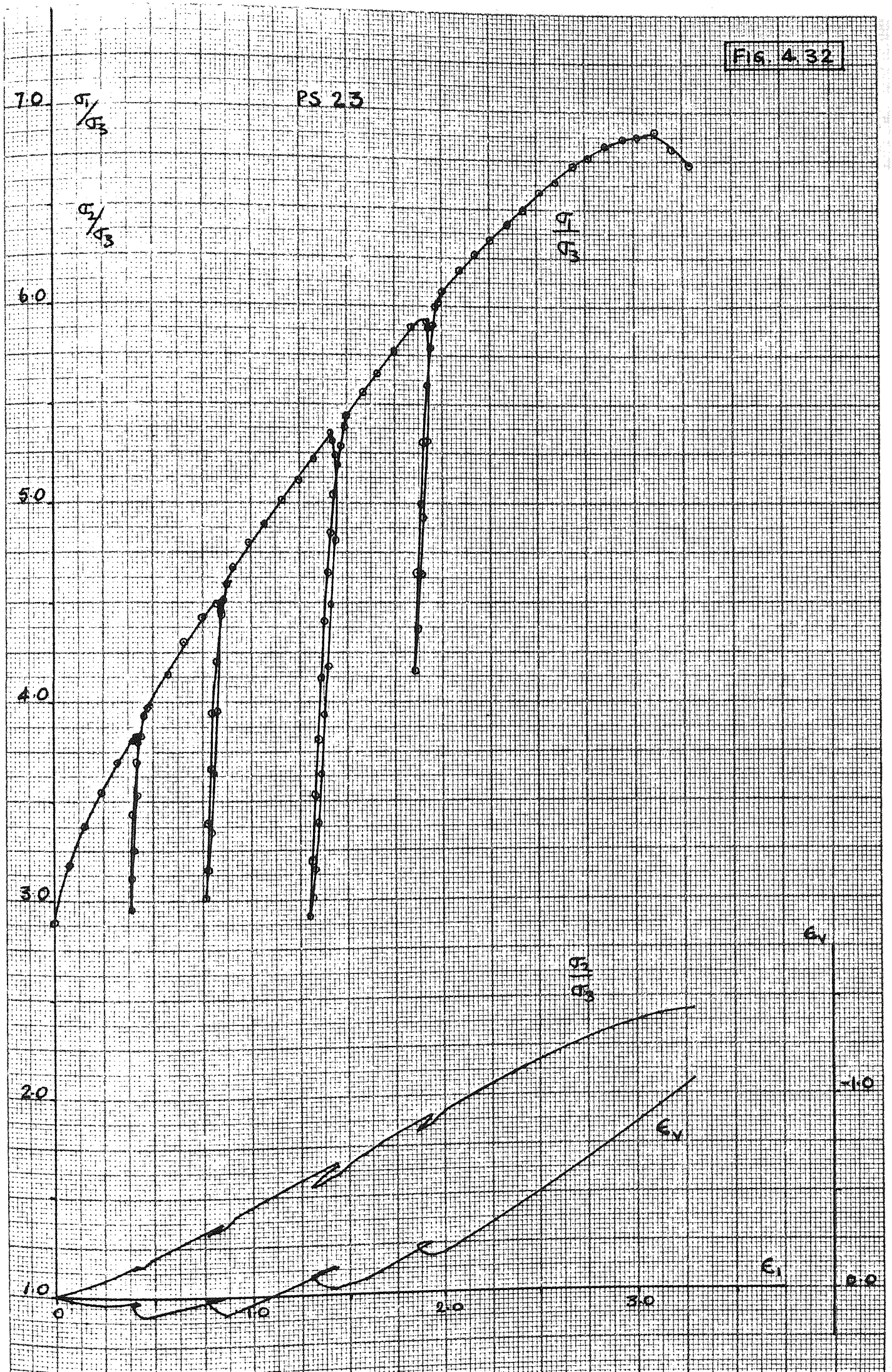
Fig. 4.32
PS 23
7.0
6.0
5.0
4.0
3.0
2.0
1.0
0
1.0
2.0
3.0
σ_1/σ_3
σ_3/σ_3
σ_1/σ_3
ε_v
ε_v
ε_1
-1.0
0.0

PS 24

FIG. 4.33

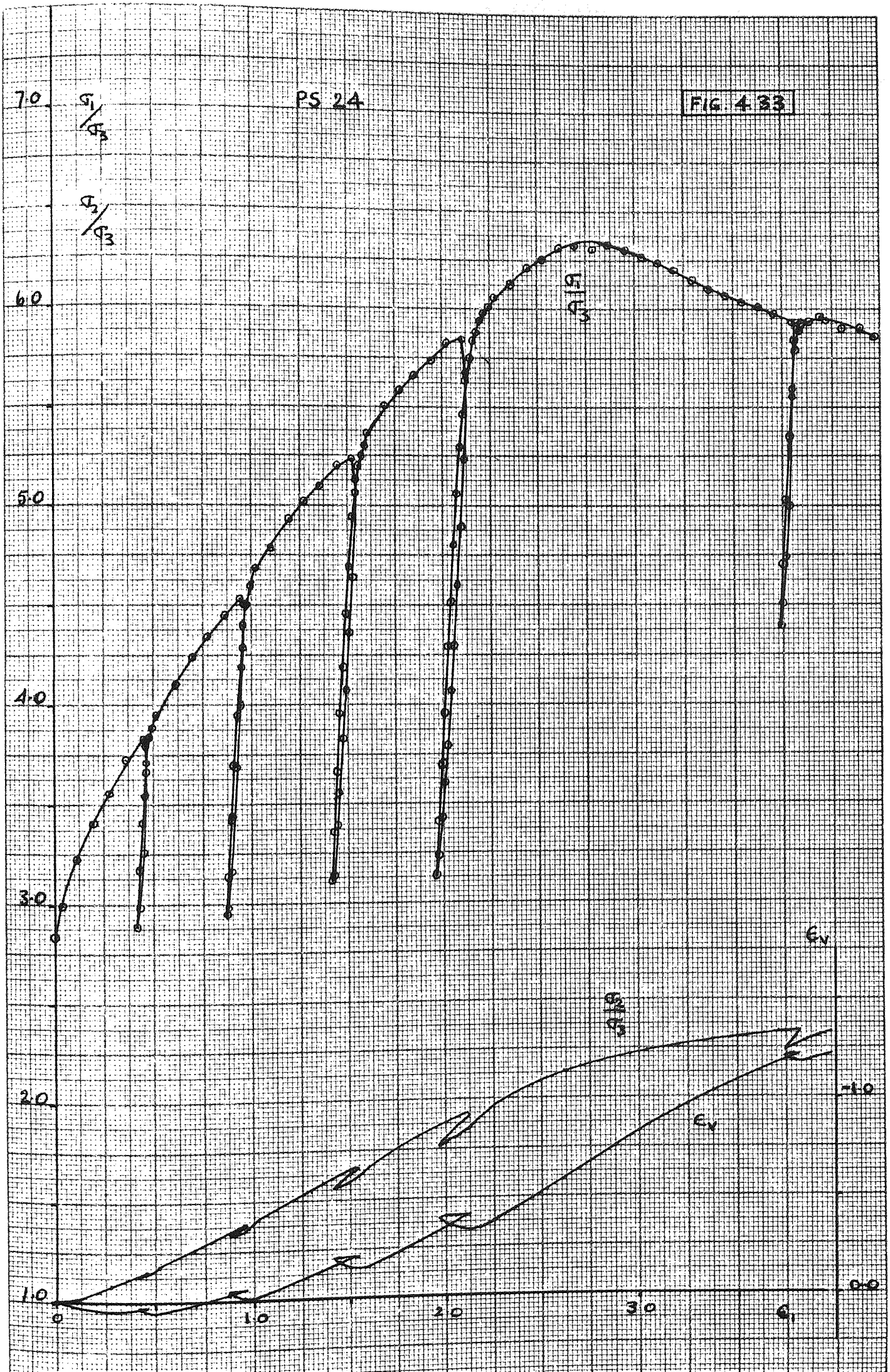

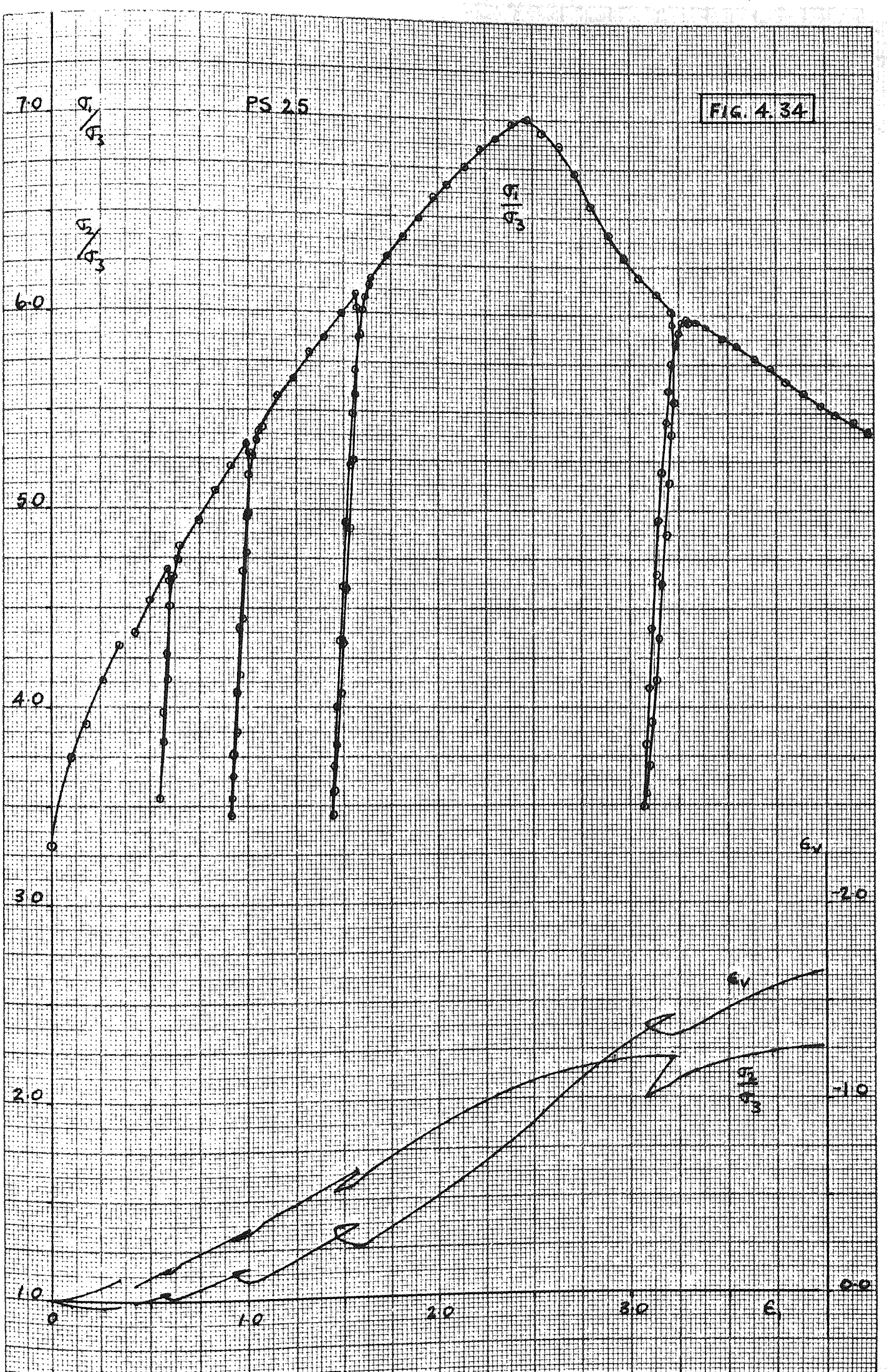
PS 25
FIG. 4.34
σ_1/σ_3
σ_2/σ_3
7.0
6.0
5.0
4.0
3.0
2.0
1.0
0
1.0
2.0
3.0
ϵ_1
ϵ_v
-2.0
-1.0
0.0

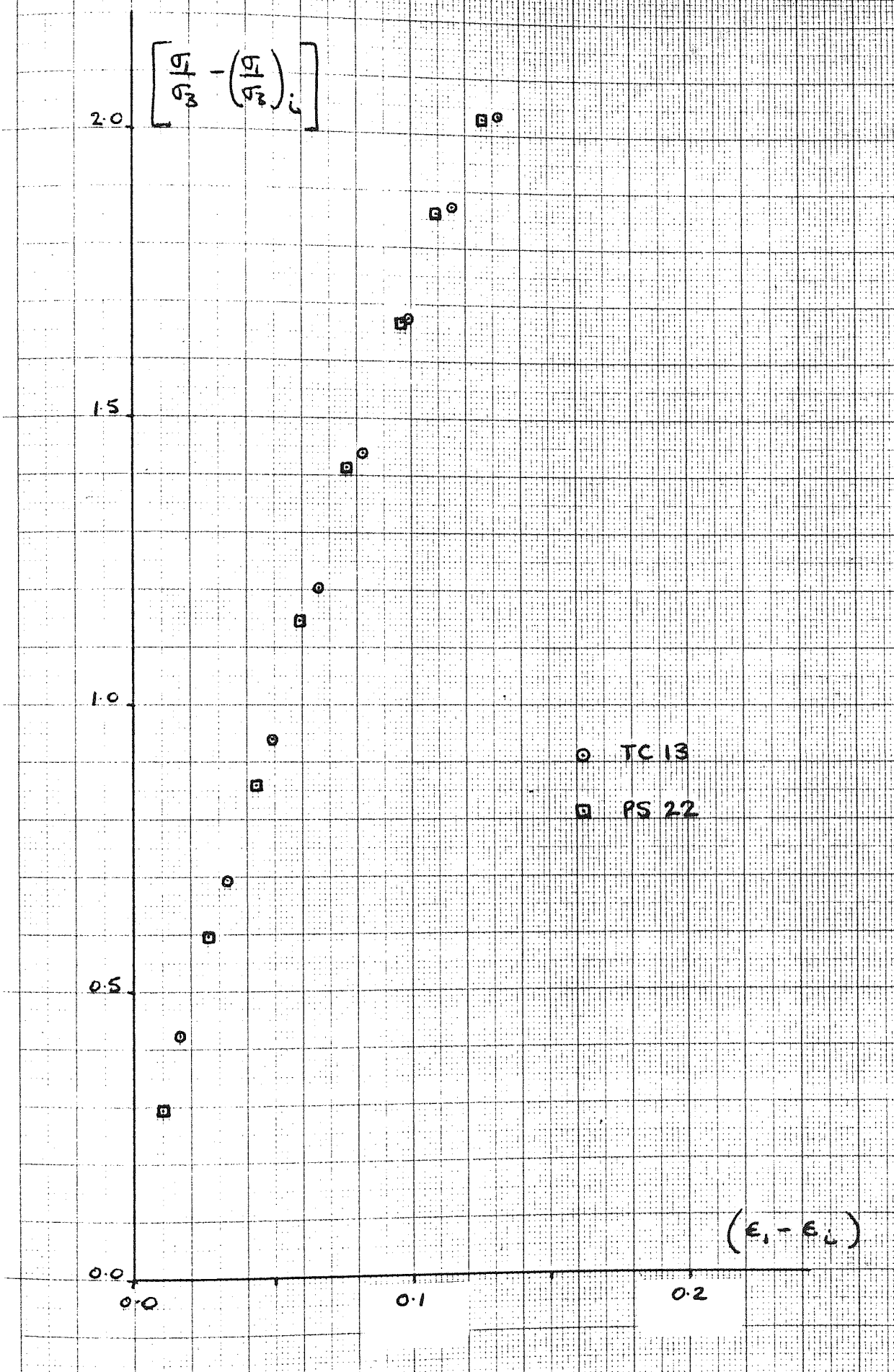
$\left[\frac{\sigma_1}{\sigma_3} - \left(\frac{\sigma_1}{\sigma_3}\right)_i\right]$
2·0
1·5
1·0
0·5
0·0
0·0
0·1
0·2
$(\epsilon_1 - \epsilon_i)$
TC 13
PS 22

FIG. 4.35

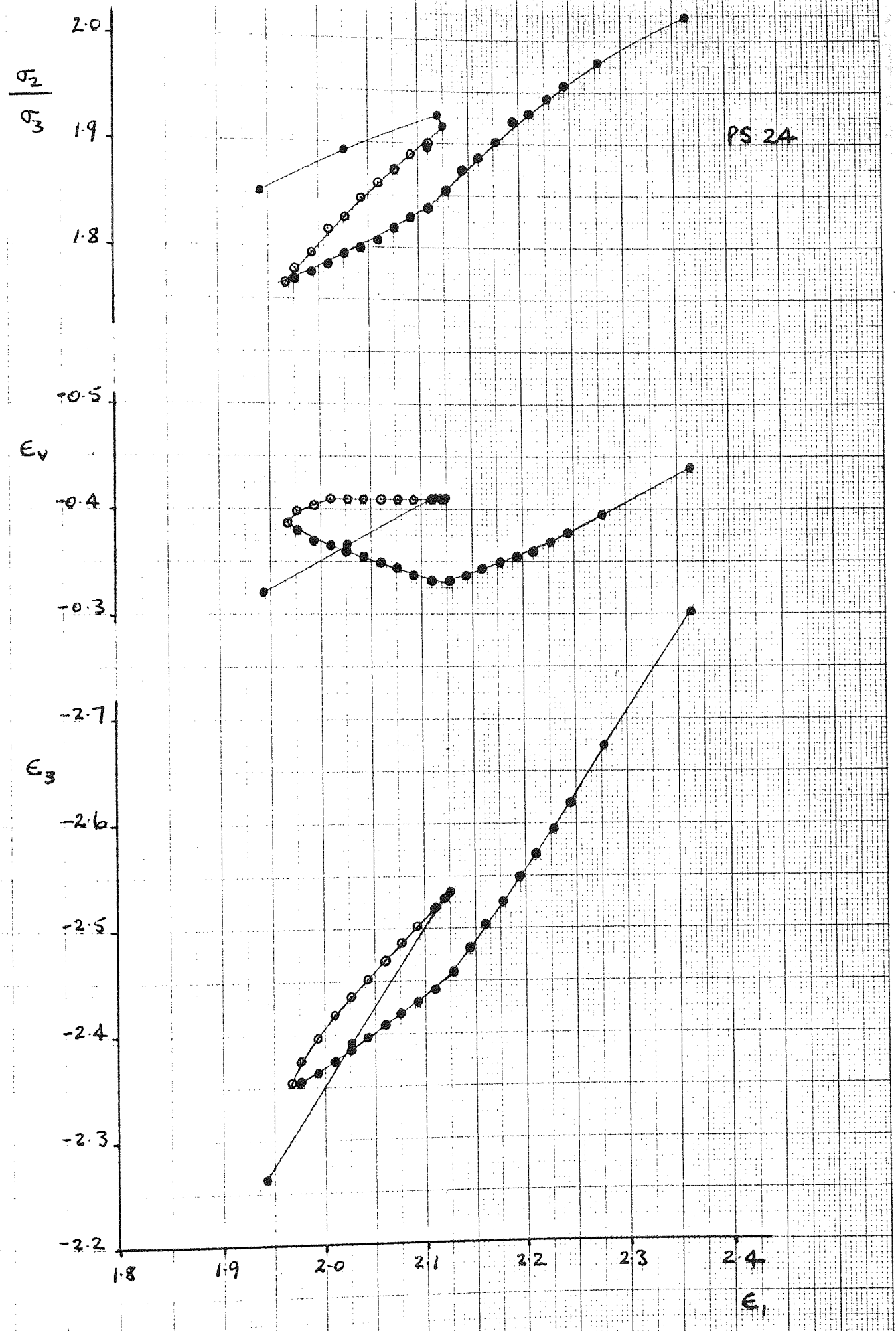
PS 24
$\frac{\sigma_2}{\sigma_3}$
2·0
1·9
1·8
ϵ_v
-0·5
-0·4
-0·3
ϵ_3
-2·7
-2·6
-2·5
-2·4
-2·3
-2·2
1·8
1·9
2·0
2·1
2·2
2·3
2·4
ϵ_1

FIG. 4.36

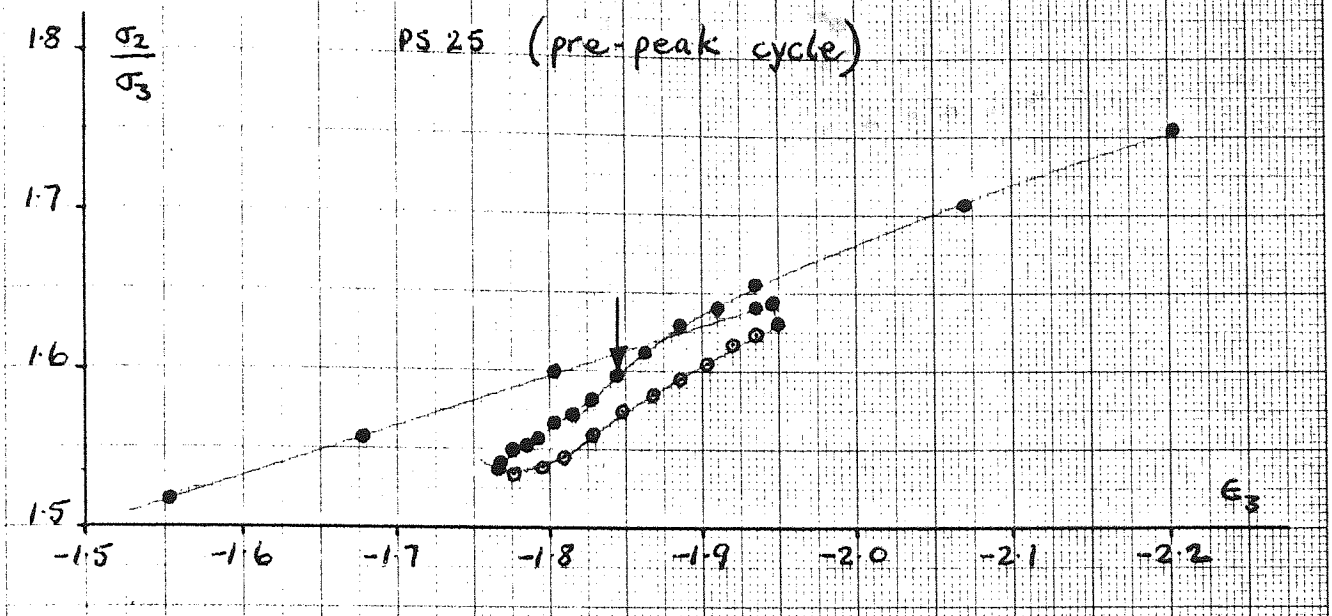

FIG. 4.37

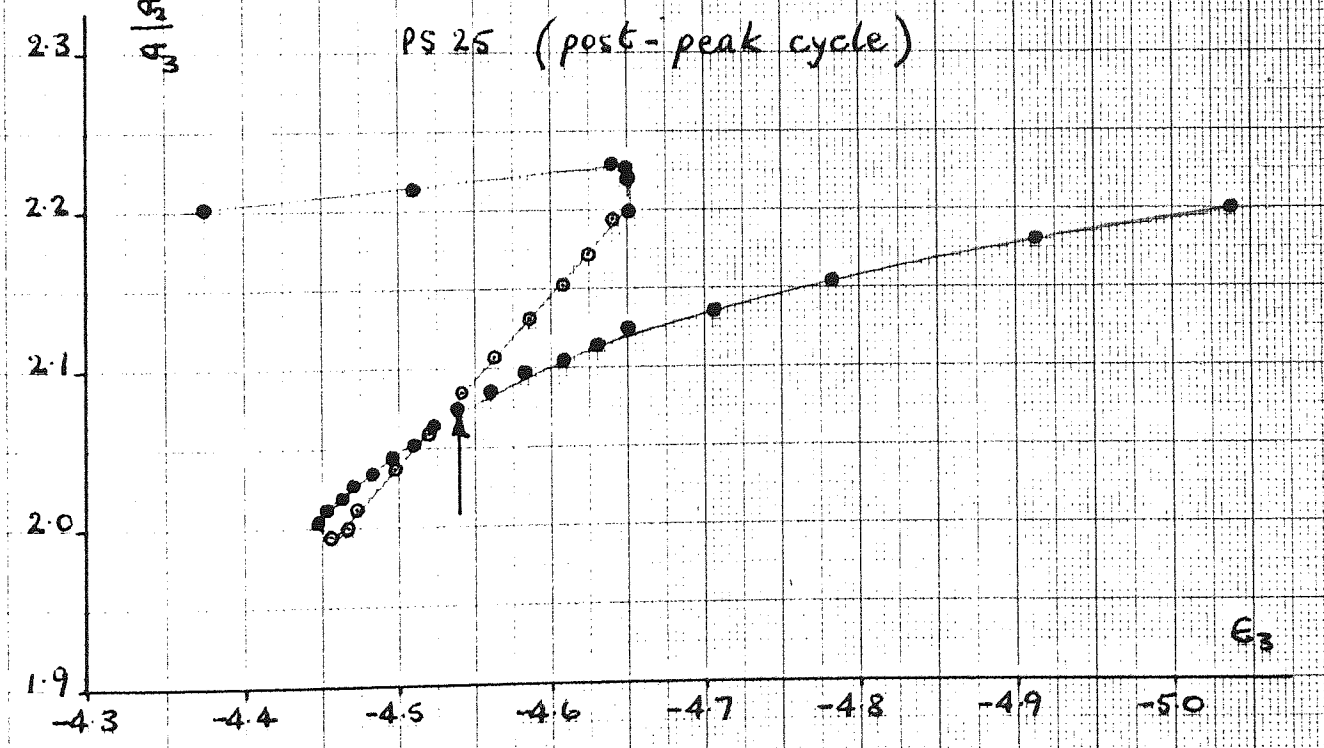

FIG. 4.38

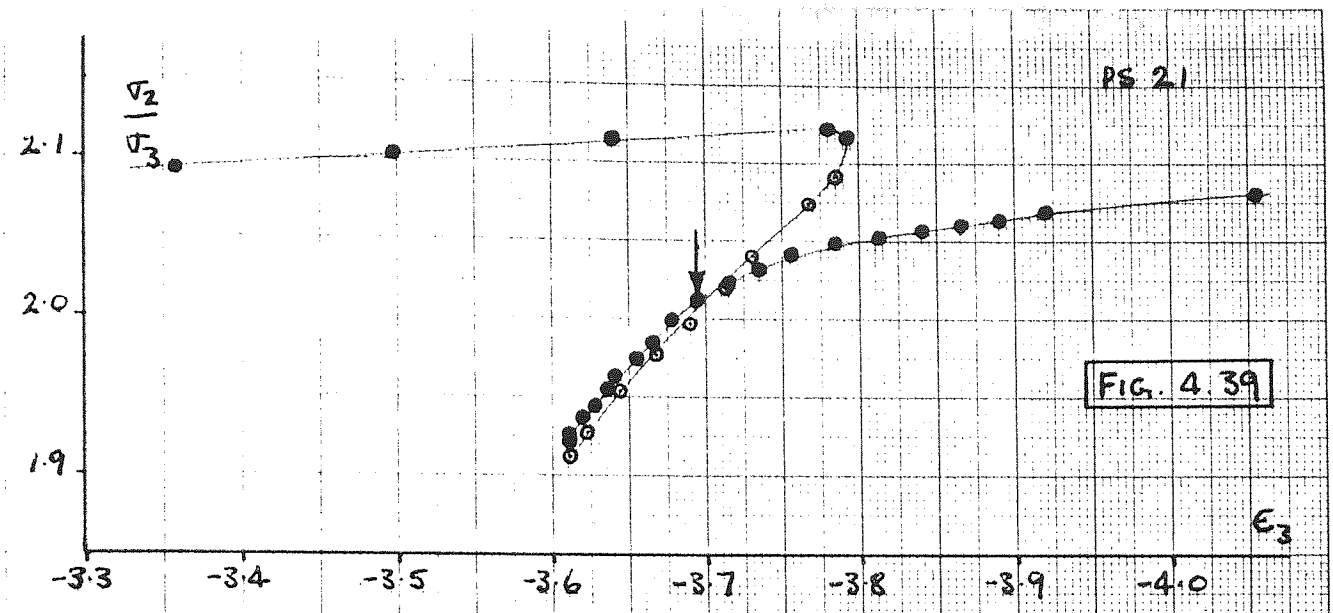

FIG. 4.39

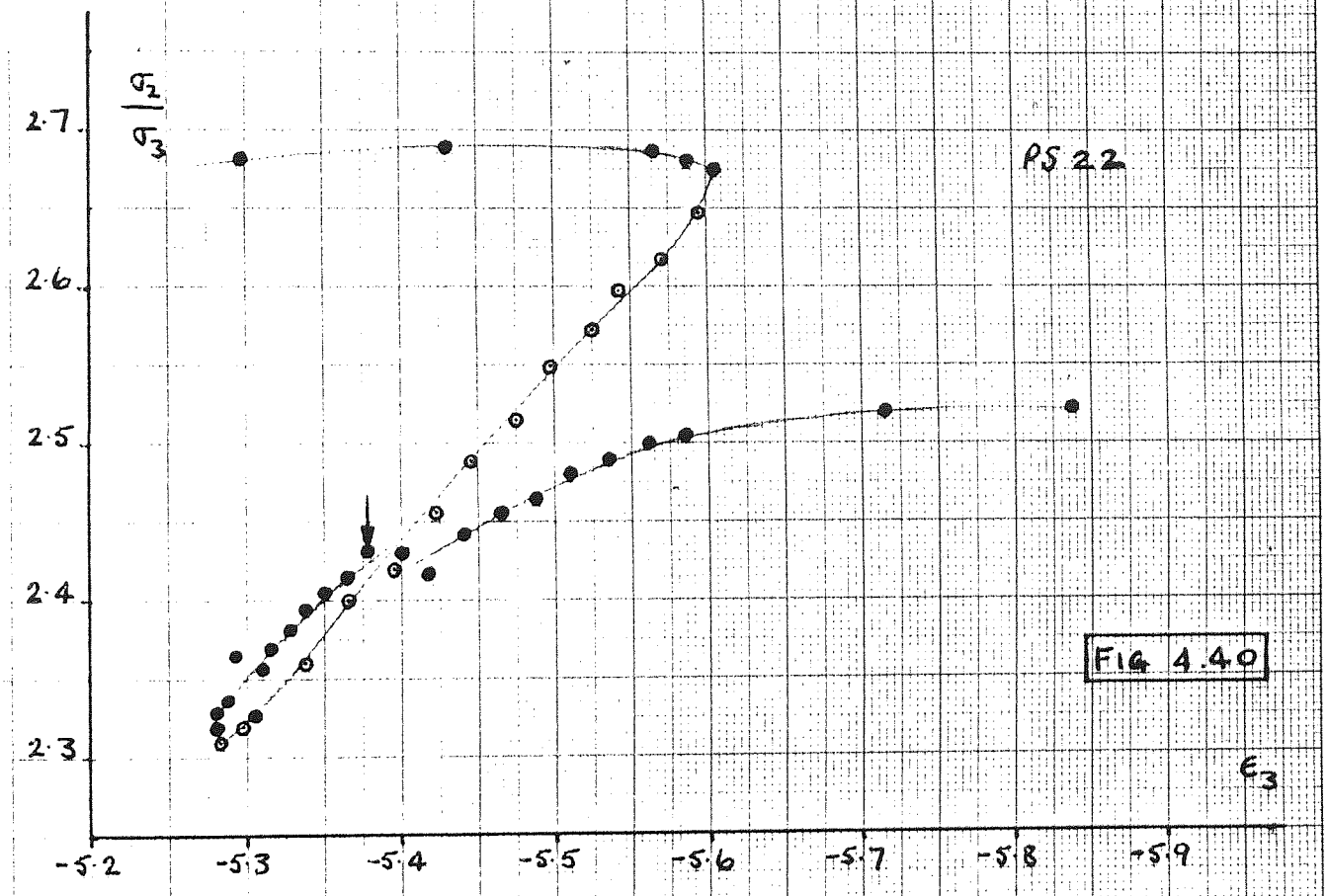

FIG 4.40

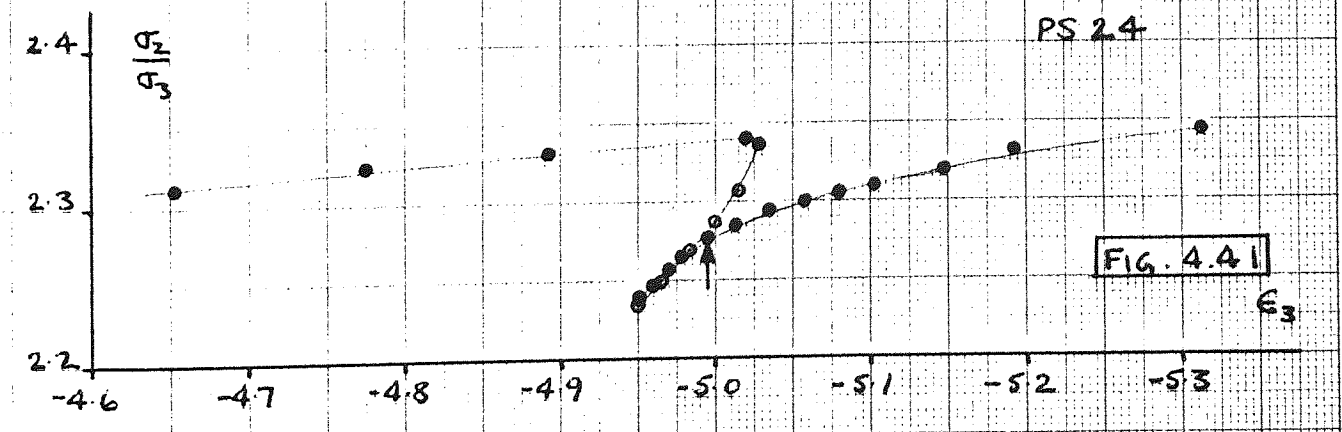

FIG. 4.41

CHAPTER FIVE

5. THEORIES OF PARTICULATE MECHANICS.

5.1. Introduction.

In the two previous chapters the results of triaxial compression and plane strain tests have been presented, and the observed behaviour of the specimens was discussed. Chapter 3 and 4 therefore constitute a phenomenological study of the shearing behaviour of sand. Any relationships thereby obtained are necessarily empirical with the attendent danger that it may not be possible to extend their use to more general conditions such as are encountered in geotechnical problems. Extrapolation to analyse field problems would be more reliable if the observed phenomena were interrelated by a physical theory which provided a meaningful explanation of the parameters involved. Such a physical model would then provide the basis for the assumptions required to develop a mathematical theory which would relate the response of the physical system to applied loadings and thereby provide a mathematical idealization of the mechanical behaviour of the material.

A number of theories have been developed which describe the mechanical behaviour of soil using either the methods of continuum mechanics, in which the discrete nature of the soil is disregarded, or those of particulate mechanics, in which the relationships between individual particles are of primary importance. All materials are composed of discrete molecules which are connected to each other by forces of mutual attraction and repulsion. However, the concept of stress and the requirement that boundary distances are large compared with distances between molecules, in effect, transform a body composed of discrete molecules into a statistical macroscopic equivalent amenable of mathematical analysis, Harr (1966). This statistical macroscopic equivalent

body can then be analysed using theories of continuum mechanics. Since continuum mechanics theory is well advanced it is an attractive proposition to attempt to develop a concept of a continuum that matches the experimentally observed behaviour of soil in elemental deformation tests. The critical state theory developed at Cambridge University is such an approach and has achieved considerable success in modelling the stress-strain behaviour of clays, Roscoe et al (1958), Schofield and Wroth (1968), Roscoe (1970). However, materials which possess negligible interparticle bonds, such as sand, have proved more difficult to relate to continuum mechanics theory. Consequently, in order to develop a theoretical model to describe the behaviour of sand it has been necessary to consider the less well developed theories of particulate mechanics.

In this chapter a number of particulate mechanics theories will be reviewed. Most of the theories are only strictly applicable to regular arrays of spheres. However, the results of the tests reported in previous chapters will be re-analysed in terms of one of these theories, namely the stress-dilatancy theory which, it has been suggested, Rowe (1962), can be extended to describe the shearing behaviour of sand.

5.2. Internal geometry and interparticle contact behaviour.

Any theoretical treatment of the mechanical behaviour of particulate material must be related to the spacial arrangement of the particles and the load-deformation behaviour at the inter-particle contacts. The contact behaviour will be dependent not only on the applied external loadings and the mechanical properties of the particles but also on the geometric relationship between the particles. Since sand consists of a random arrangement of irregular shaped particles of varying sizes an element of sand can only be analysed on a statistical basis. In order to develop a sound statistical approach, an understanding of simpler internal geometries is of benefit. Consequently, a lot of research has

been carried out on regular arrays of equal spheres.

In regular packings of equal spheres each sphere is in contact with a fixed number of neighbouring spheres. Therefore the coordination number (number of spheres in contact with a given sphere) is constant and the porosity is uniform throughout the mass. However, equal spheres can be arranged to form a number of different regular arrays. Graton and Fraser (1935) identified six basic regular arrays which give porosities varying from 25.95% (rhombic) to 47.64% (simple cubic). The respective coordination numbers range from 12 to 6. It was noted that different geometrical arrangements of the particles can give similar porosities and that initially loose packings, when possible, will tend to increase their coordination numbers in order to form a more stable arrangement.

A number of researchers have studied the geometry of random arrays of equal spheres. Smith et al (1929) used acetic acid to determine experimentally the number of contacts in random packings of lead shot. A statistical analysis of their results showed that the standard deviation from the mean coordination number for the mass of particles increased with density. Random packings of cylindrical rods and equal spheres were studied by Biarez (1961) who noted that, as a result of deposition in a gravity field, the structure was anisotropic since there were more points of contact in a horizontal plane than in a vertical plane. It was also shown that the degree of anisotropy was altered by external loadings. The anisotropic nature of random arrays of equal spheres was also recognised by Kallstenius and Bergau (1961) who suggested that the spheres tended to form 'chains'.

A clearer picture of the formation within a random array of equal spheres was provided by Kolbuszewski (1965) who published photographs of a single layer of equal spheres randomly deposited in a narrow container. Both dense and loose assemblies were illustrated. Kolbuszewski (1965) described the structure as consisting of groups of densely packed

particles separated by a network of 'discontinuities'. The 'discontinuities' were termed macropores and it was noted that the network of macropores was less developed in the dense assembly. Alternatively, the mass of spheres could be described as consisting of dense zones in a loose matrix, the dense zones being smaller and more numerous in the assembly with the higher overall porosity.

The macroscopic stress-strain behaviour of a particulate material will depend on the load-deformation characteristics at the inter-particle contacts. Assuming the particles to be sufficiently hard to resist local failure or crushing at the contacts, the type of deformation possible at the contacts will depend on the geometric arrangement of the particles, the applied external loading and the coefficient of interparticle friction.

If the inter-particle forces are normal to the contact surfaces then the contacts will deform according to Hertz's theory (see Timoshenko and Goodier, 1951), resulting in a stress-strain relationship which is elastic but non-linear. However, the inter-particle forces, generally, will deviate from the normal as a result of the internal geometry and the applied shear stresses. The consequent tangential components of the inter-particle forces will be resisted by the surface friction of the particles. If a tangential force is applied in the plane of contact between two particles then slip will start at the perimeter of the contact surface and progress radially inwards, Mindlin and Deresiewicz (1953). This type of deformation is not only non-linear but also inelastic due to energy dissipation. If the obliquity of the inter-particle force is sufficient to overcome friction over the whole of the contact area then rigid body sliding occurs which will be arrested only when new contacts are formed such that the obliquity is suitably reduced.

It is clear that, in general, the overall deformation of a particulate assembly will be composed of deformation due to changes in

the geometry of the packing and deformation of the particles themselves. A comprehensive treatment of regular arrays based on the deformation of the particles themselves, including local slip due to oblique forces, has been provided by Duffy and Mindlin (1957), Deresiewicz (1958), and Thurston and Deresiewicz (1959). Since the behaviour is not truly elastic, due to the effect of the oblique forces, the stress-strain relations had to be derived in incremental form. Furthermore, since the coefficients involved were dependent on the initial stress and stress path, integration of the incremental relationships could only be accomplished for specific loading conditions.

The extension of the above approach to deal with random arrays, in which both the variation in geometry and the distribution of contact forces are much more complex, would appear to be intractable. According to Rowe (1971), it would also appear to be impossible to isolate the parameters involved by experimental means. An alternative approach is to assume the particles to be rigid and thereby ignore the deformation of the particles themselves. Theoretical treatments of regular arrays of rigid spheres will be reviewed in the following section.

5.3. Theories pertaining to regular arrays of rigid spheres.

Theoretical treatments of regular arrays of rigid spheres, generally, have been limited to the determination of the limiting stress conditions required to cause failure although Rowe (1962) and Leussink and Wittke (1963), as a result of their approach, have been able to predict post-failure stress-strain curves. The following review will be restricted to analyses of the two densest packings: the densest quadratic (face centred cubic), and the densest hexagonal (rhombic). Since the original forms of the solutions obtained were not always similar for identical arrays the original equations will be transformed into similar forms for comparison. However, in order to aid identification, the originally derived expressions will also be provided.

5.3.1. Strength of regular arrays:- theoretical solutions.

During their investigations into the elastic behaviour of regular packings, Thurston and Deresiewicz (1959) noted that the applied axial load had a limiting value beyond which the geometrical arrangement of the spheres was altered. The failure process was envisaged as one in which sliding occurred in one direction only, as a result of a series of shearing displacements of individual layers of spheres. From the analysis of a face centred cubic array of equal spheres subjected to an increasing axial stress under axisymmetric compression conditions the following expression was obtained to define the failure condition:

$$\frac{\sigma_1 - \sigma_3}{\sigma_3} = \left[\frac{\sqrt{6} + 8\mu}{\sqrt{6} - 4\mu}\right] \qquad (5.1a)\ *$$

which can be transformed to give

$$\frac{\sigma_1}{\sigma_3} = 2\left[\frac{\sqrt{6} + 2\mu}{\sqrt{6} - 4\mu}\right] \qquad (5.1b)$$

or when expanded

$$\frac{\sigma_1}{\sigma_3} = 2 + 2\sqrt{6}\mu + 8\mu^2 + (\text{higher terms in } \mu) \qquad (5.1c)$$

Rennie (1959) assumed the same failure mechanism as envisaged by Thurston and Deresiewicz (1959) in order to determine the minimum stress ratio required to cause failure of a 'close-packed' array of spheres. The critical stress ratio was obtained by permitting the major and minor principal stresses to rotate relative to the packing and determining the least favourable orientation of the packing relative to the principal stress directions. The following solution was obtained

$$\frac{\sigma_1}{\sigma_3} = \frac{3\sqrt{1 + 4\mu^2/3} + 1 + 4\mu\sqrt{2/3}}{3\sqrt{1 + 4\mu^2/3} - 1 - 4\mu\sqrt{2/3}} \qquad (5.2a)$$

* μ = coefficient of interparticle friction = $\tan \phi_\mu$

Rennie (1959) gives the expanded form* as

$$\frac{\sigma_1}{\sigma_3} = 2 + 2\sqrt{6}\mu + 7\mu^2 - 8\sqrt{6}\mu^3/9 + (\text{higher terms in } \mu) \qquad (5.2b)$$

However, Rennie (1959) noted that a rotation about some other axis might give a smaller critical stress ratio and suggested that the critical stress ratio should be less than that given by equation 5.2. It was also suggested that if the minor and intermediate principal stresses were nearly equal then the validity of equation 5.2 was doubtful. Parkin (1965) demonstrated that equation 5.2 was valid for a restricted range of values of the intermediate principal stress but, within that range, was independent of the magnitude of the intermediate principal stress. He also showed that Rennie's (1959) analysis was valid for

$$\frac{\sigma_1 + \sigma_3}{3} \leqslant \sigma_2 \leqslant \sigma_1$$

Parkin (1965) also extended Rennie's work to cover the remaining range of stress conditions including the axisymmetric compression case. The same technique of rotating the major and minor principal stress directions to find the least favourable orientation was used but, in contrast to Rennie (1959) who only considered one pair of broken contacts at opposite points on a diameter of each sphere, it was necessary to consider two pairs of broken contacts on perpendicular diagonals. Due to the complexity of the derived expression for the critical stress ratio the solution was obtained by computer and was found to be significantly dependent on the magnitude of the intermediate principal stress. However, for the axisymmetric compression case, Parkin (1965) provided the expanded form:

$$\frac{\sigma_1}{\sigma_3} = 2 + 4\mu + (\text{higher terms in } \mu) \qquad (5.3)$$

* The expanded form given by Rennie (1959), equation 5.2b, is incorrect, as will be shown in section 5.3.2.

Both face centred cubic and rhombic packings were studied by Dantu (1961) who investigated the conditions of limiting equilibrium of such arrays under axisymmetric compression conditions. For the face centred cubic arrangement the critical stress ratio was given as

$$\frac{\sigma_1}{\sigma_3} = 2 \left[\frac{1 + \mu}{1 - \mu} \right] \tag{5.4a}$$

which when expanded, gives

$$\frac{\sigma_1}{\sigma_3} = 2 + 4\mu + 4\mu^2 + (\text{higher terms in } \mu) \tag{5.4b}$$

The critical stress ratio for the rhombic array was

$$\frac{\sigma_1}{\sigma_3} = 4 \left[\frac{\sqrt{2} + \mu}{\sqrt{2} - 2\mu} \right] \tag{5.5a}$$

or

$$\frac{\sigma_1}{\sigma_3} = 4 + 6\sqrt{2}\mu + 12\mu^2 + (\text{higher terms in } \mu) \tag{5.5b}$$

As a result of employing an angular definition of the packing geometry, Rowe (1962) was able to derive a general expression for the axisymmetric compression strength of regular arrays. The equation was given as

$$\frac{\sigma_1}{\sigma_3} = \tan \alpha . \tan (\phi_\mu + \beta) \tag{5.6}$$

where β is the inclination of the interparticle slip direction to the minor principal plane and α is 'a geometrical property of the packing'.

For a face centred cubic array $\beta = 45^\circ$ and $\alpha = 63.5^\circ$, thus equation 5.6 can be transformed to give

$$\frac{\sigma_1}{\sigma_3} = 2 \left[\frac{1 + \mu}{1 - \mu} \right] \tag{5.7a}$$

or

$$\frac{\sigma_1}{\sigma_3} = 2 + 4\mu + 4\mu^2 + (\text{higher terms in } \mu) \tag{5.7b}$$

For the rhombic case $\beta = 54.7^{\circ}$, and $\alpha = 70.6^{\circ}$, which gives

$$\frac{\sigma_1}{\sigma_3} = 2\sqrt{2} \left[\frac{\sqrt{2} + \mu}{1 - \sqrt{2}\mu} \right] \qquad (5.8a)$$

or

$$\frac{\sigma_1}{\sigma_3} = 4 + 6\sqrt{2}\mu + 12\mu^2 + (\text{higher terms in } \mu) \qquad (5.8b)$$

Leussink and Wittke (1963) obtained a general solution for axi-symmetric compression conditions which was only dependent on the angle of interparticle friction and the inclination of the interparticle contact planes. The solution was given by

$$\frac{\sigma_1}{\sigma_3} = 2 \tan j_o \cdot \tan (j_o + \rho) \qquad (5.9)$$

where ρ is the angle of interparticle friction and j_o is the angle between the normal lines at the contact points and the minor principal plane.

For the face centred cubic array, $j_o = 45^{\circ}$, and therefore

$$\frac{\sigma_1}{\sigma_3} = 2 \left[\frac{1 + \mu}{1 - \mu} \right] \qquad (5.10a)$$

or

$$\frac{\sigma_1}{\sigma_3} = 2 + 4\mu + 4\mu^2 + (\text{higher terms in } \mu) \qquad (5.10b)$$

For a rhombic array, $j_o = 54.7^{\circ}$, in which case

$$\frac{\sigma_1}{\sigma_3} = 2\sqrt{2} \left[\frac{\sqrt{2} + \mu}{1 - \sqrt{2}\mu} \right] \qquad (5.11a)$$

or

$$\frac{\sigma_1}{\sigma_3} = 4 + 6\sqrt{2}\mu + 12\mu^2 + (\text{higher terms in } \mu) \qquad (5.11b)$$

Leussink and Wittke (1963) also analysed the plane strain case but were unable to obtain a general formula although the solutions were only dependent on the interparticle friction and the inclination of the contact planes. For the face centred cubic packing the critical

stress ratio was given as

$$\frac{\sigma_1}{\sigma_3} = 2 \tan jo \left[\frac{\tan jo + \tan \rho / \sqrt{1 + \sin^2 jo}}{1 - 2 \tan \rho \tan jo / \sqrt{1 + \sin^2 jo}} \right] \qquad (5.12a)$$

substituting for $jo = 45^o$ gives

$$\frac{\sigma_1}{\sigma_3} = 2 \left[\frac{\sqrt{3} + \sqrt{2\mu}}{\sqrt{3} - 2\sqrt{2\mu}} \right] \qquad (5.12b)$$

or, when expanded

$$\frac{\sigma_1}{\sigma_3} = 2 + 2\sqrt{6\mu} + 8\mu^2 + (\text{higher terms in } \mu) \qquad (5.12c)$$

For the rhombic packing the solution was given as

$$\frac{\sigma_1}{\sigma_3} = \frac{2}{3} \tan jo \left[\frac{\tan jo + \tan \rho}{1 - \tan \rho \tan jo} \right]$$

$$+ \frac{4}{3} \tan jo \left[\frac{\tan jo \tan \rho / \sqrt{1 + 3 \sin^2 jo}}{1 - 4 \tan \rho \tan jo / \sqrt{1 + 3 \sin^2 jo}} \right] \qquad (5.13a$$

with $jo = 54.7^o$ the above equation becomes

$$\frac{\sigma_1}{\sigma_3} = \left[\frac{4 + 2\sqrt{2}\,\mu}{3 - 3\sqrt{2}\,\mu} \right] + \left[\frac{8 + 4\mu\sqrt{2/3}}{3 - 4\sqrt{6}\,\mu} \right] \qquad (5.13b)$$

and the expanded form is

$$\frac{\sigma_1}{\sigma_3} = 4 + 2\sqrt{2}\,(1 + 2\sqrt{3})\mu + 36\mu^2 + (\text{higher terms in } \mu) \qquad (5.13c$$

5.3.2. Strength of regular arrays:- critical appraisal.

The above solutions show that the strength of a regular array of equal spheres is not only dependent on the angle of interparticle friction and the type of packing, but also on the directional freedom to collapse.

Under axisymmetric compression failure conditions, sliding occurs at all the points of contact between adjacent layers, resulting in a decrease in the spacing between the layers without changing the basic geometry of the packing. Consequently, the intersphere spacing within a layer increases and, under axisymmetric compression conditions, there is no directional restriction on such outward lateral movement. However, the same failure mechanism is not possible in a plane strain test since no lateral movement is permitted in the direction of the intermediate principal stress. As a result of the two dimensional nature of the allowable movement the original packing geometry must change when the critical stress ratio is reached.

Previous researchers have sometimes distinguished between the 'twinning', or plane sliding, model of Thurston and Deresiewicz (1959) and Rennie (1959), and the 'dilation', or multiple slip, model of Rowe (1962) and Dantu (1961). Trollope and Parkin (1963) suggested that Rennie's work demonstrated that the failure mechanism was one of plane sliding rather than of general dilation as assumed by Rowe (1962). Parikh (1967) compared 'twinning' solutions with solutions based on the dilation mechanism and concluded that the 'twinning' solutions did not yield the most critical stress ratios. Similarly, Rowe (1964a), (1970), and Horne (1965) have also suggested that the 'twinning' assumption is incorrect since the strengths obtained are greater than the solutions based on the dilation mechanism.

The above mentioned comparisons would appear to have been made without due consideration being given to the relevant test conditions. Parkin (1965) demonstrated that Rennie's solution was not applicable to axisymmetric compression conditions, and in fact Rennie suggested this limitation in the original paper, Rennie (1959). It is not surprising, therefore, that Rowe's solution for the strength of a face centred cubic array of spheres yields lower stress ratios.

It has also been implied, Rowe (1970), that Parkin's (1965) theoretical treatment gives less critical stress ratios than the analysis of Rowe (1962), for face centred cubic arrays. It was suggested that 'the difference might lie on the approximate treatment of higher μ terms'. However, since all the solutions dealt with in section 5.3.1 have higher order terms when expanded it is instructive to compare the solutions in detail.

Since some uncertainty has arisen in respect of the relevant test conditions applicable to the various solutions, the comparisons will be made with respect to the equations obtained by Leussink and Wittke (1963) who clearly distinguished between axisymmetric compression and plane strain. It is clear that the solutions obtained by Dantu (1961) and Rowe (1962) agree exactly with Leussink and Wittke's axisymmetric compression solutions for similar packings. If the higher order terms in μ are ignored, the face centred cubic solutions also agree with Parkin's (1965) axisymmetric compression solution to the first order in μ. Therefore, although not actually stated in the original paper, Parkin's assumed failure mechanism would appear to be similar to that assumed by Rowe (1962).

The solution obtained by Thurston and Deresiewicz (1959) exactly agrees with the plane strain solution of Leussink and Wittke (1963) for a face centred cubic packing. It would appear that Thurston and Deresiewicz assumed an incorrect failure mechanism for their axisymmetric compression analysis and thus, inadvertantly, obtained a plane strain solution. Leussink and Wittke's plane strain solution for a face centred cubic array also agrees with the solution of Rennie (1959) to the first order term in μ.

It was indicated in section 5.3.1 that the expanded form given by Rennie (1959) is incorrect. It is useful to obtain the correct expanded form of equation 5.2 before making further comparisons. In

order to expand equation 5.2a it is first of all necessary to expand the term $\sqrt{1 + 4\mu^2/3}$ using the binomial theorem. Limiting the expansion to the fourth order term in μ and substituting in equation 5.2a gives the following expression

$$\frac{\sigma_1}{\sigma_3} = \frac{4 + 4\sqrt{6}\,\mu/3 + 2\mu^2 - 2\mu^4/3}{2 - 4\sqrt{6}\,\mu/3 + 2\mu^2 - 2\mu^4/3} \qquad (5.14)$$

which when expanded gives

$$\frac{\sigma_1}{\sigma_3} = 2 + 2\sqrt{6}\,\mu + 7\mu^2 + 8\sqrt{6}\mu^3/3 + 4\mu^4 + \ldots\ldots \qquad (5.15)$$

The corresponding expanded form of Leussink and Wittke's solution is

$$\frac{\sigma_1}{\sigma_3} = 2 + 2\sqrt{6}\mu + 8\mu^2 + 16\sqrt{6}\mu^3/3 + 64\mu^4/3 + \ldots\ldots \qquad (5.16)$$

It is clear from equations 5.15 and 5.16 that the two solutions only agree to the first order term in μ and that if the higher order terms are considered then Rennie's solution predicts a more critical stress ratio.

Both Rennie (1959) and Parkin (1965) considered their solutions to be valid only to a first order in μ. If all the solutions reviewed in section 5.31 are assumed to be similarly restricted then it is clear that there is no real disagreement between the various investigators. It is also clear that, in a regular array of spheres, the failure mechanism depends on the test conditions: failure will occur by plane sliding in a plane strain test but by multiple slip in an axisymmetric compression test. Consequently, the axisymmetric compression and plane strain solutions for the strength of a close packed array of spheres can be summarised by restating Leussink and Wittke's solutions in the approximate expanded forms given below in Table 5.1.

Table 5.1 STRENGTH OF REGULAR ARRAYS

test conditions	type of packing: face centred cubic	rhombic
axisymmetric compression	$2 + 4\mu$	$4 + 6\sqrt{2}\mu$
plane strain	$2 + 2\sqrt{6}\mu$	$4 + (1 + 2\sqrt{3})2\sqrt{2}\mu$

However, if the 'exact' solutions are considered then the Rennie-Parkin model predicts the most critical stress ratios. Since the validity of this statement is not generally accepted, Rowe (1964a), (1970), Horne (1965), Parikh (1967), two specific cases will be considered.

Using the method outlined in Parkin's (1965) paper the solutions given by the Rennie-Parkin model have been calculated for an angle of interparticle friction, $\phi_\mu = 28^\circ$. The values of the critical stress ratios for axisymmetric compression and plane strain conditions obtained in this way are compared with those given by Leussink and Wittke's face centred cubic solutions (equations 5.10a and 5.12b) in Table 5.2.

Table 5.2 COMPARISON OF 'EXACT' SOLUTIONS

	axisymmetric compression	plane strain
Leussink and Wittke	6.540	21.75
Rennie-Parkin	5.174	7.98

Rowe (1970) provided a rough comparison of predicted axisymmetric compression strengths by comparing the stress-dilatancy predictions with data obtained by scaling from the diagrams published by Parkin (1965), (1967). Rowe made the following observation:

'Nevertheless, there is exact agreement at zero friction followed by a discrepancy increasing with ϕ_μ, and in this connection it is recalled that the Rennie solution was for a 'small amount of friction' and 'to first order in the coefficient of friction' and that the same was noted by Parkin (1965). It would be of interest if Parkin could supply his solution for $\mu = 0.726$ applicable to feldspar.'

Although not strictly applicable to feldspar, Parkin's 'exact' solution for $\mu = 0.726$ has been calculated, and predicts a stress ratio of 6.59 as opposed to 7.7 given by Rowe (1970) using Horne's (1965) solution. Since the above references to the validity of the Rennie-Parkin model should also apply to the stress-dilatancy treatment of regular packings the Rennie-Parkin model is clearly the more rigorous analysis and predicts the more critical stress ratios for axisymmetric compression conditions.

Rowe (1970) also suggested that the stress-dilatancy theory predicted lower plane strain strengths than did the Rennie-Parkin model. However, the analysis provided in Rowe's (1970) reply to Parkin (1970) appears to contain a fundamental error. In order to clarify this point it is necessary to quote directly from the two contributions.

Parkin (1970) states:- 'Further comment relates to equation (8), namely

$$R = \tan \alpha \tan (\phi_\mu + \beta) \quad (= \sigma_1/\sigma_2)$$

which was stated to have been derived by Parkin (1965a) among others. The equation originates from Rowe (1962), where it is stated to apply 'whatever the geometrical arrangement of the solids', with reference to the analysis of ideal packings.

I have not myself made this claim, but agree that an illustrative two-dimensional analysis of mine can, with α suitably defined, be put into the form of equation (8). However, in the general case the anisotropy of the solutions is such that α and β are not independent of ϕ_μ, but involve the angle between the principal axes of stress and strain ψ, which varies with $\tan^3 \phi_\mu$.

I would not venture to define α and β, except for the case of plane strain, whereupon α (identified with the plane of interlock) = $54.7 + \psi$ and $\beta = 54.7 - \psi$. If the following data are extracted from Parkin (1965a)

$$\tan \phi_\mu = 0.4 \qquad \phi_\mu = 21.8^\circ$$

$$R = 5.621 \qquad \beta = 0.310 \qquad \psi = \sqrt{2\beta} \equiv 25.1^\circ$$

substitution in equation (8) leads to $R = 6.963$. I should be grateful if the Author could establish that these solutions do fall within the compass of equation (8).'

Rowe (1970) gives the following reply:

'Taking the problem posed by Parkin and a face centred cubic array (Rowe, 1962, Fig. 8(a)) in symmetrical orientation ($\alpha = \alpha_o$, $\beta = \beta_o$)

and making one of the plan boundaries the σ_2 plane, it can be shown by spherical trigonometry that $\beta_o = 54.7$. Viewing the stack in the σ_2 direction $\alpha_o = 54.7$. Rotating the array through angle ψ and using equation (8) with $\alpha = \alpha_o + \psi$ and $\beta = \beta_o - \psi$.

$$\frac{\sigma_1}{\sigma_3} = \tan(\alpha_o + \psi) \tan(\phi_\mu + \beta_o - \psi)$$

the minimum value of σ_1/σ_3 results when

$$\psi = \frac{1}{2}(\phi_\mu + \beta_o - \alpha_o)$$

$$\left(\frac{\sigma_1}{\sigma_3}\right)_{min} = \tan^2 \frac{1}{2}\left(\alpha_o + \beta_o + \phi_\mu\right)$$

Substituting the numerical values given with $\phi_\mu = 21.8$ gives $\sigma_1/\sigma_3 = 4.86$. If Parkin's solution is 5.62 the difference might lie on the approximate treatment of higher μ terms and a previous example is given where the Author obtained a more critical value than Rennie for this reason (Rowe, 1964a). It is interesting that if $\phi_\mu = \mu = 0$ the plane strain model, in which $\alpha_o = \beta_o$, gives $\sigma_1/\sigma_3 = \tan^2 \alpha_o = 2$, in agreement with Parkin.'

Parkin (1970) recognised that the effect of lateral restraint in the intermediate principal stress direction will cause a reorientation of the critical values of α and β. Using his own results he was able to define the critical orientation of the principal stresses by the term ψ. By substituting the values of $\alpha = 54.7 + \psi$ and $\beta = 54.7 - \psi$ into Rowe's equation he has in effect minimised σ_1/σ_3 for the restricted plane strain condition.

In reply, Rowe (1970) appears to accept the effect of plane strain on the orientation of α and β but disagrees with Parkin as to the critical value of ψ. After substituting the ammended values of α and β into the stress-dilatancy equation, Rowe then differentiates this expression with respect to ψ to find the critical value of ψ which gives the minimum value of σ_1/σ_3. The critical value of ψ according to Rowe for the particular case under consideration is $10.9^o = \phi_\mu/2$, in contrast to Parkin's value of 25.1^o. Consequently Rowe obtains a lower stress ratio than Parkin.

However, Rowe's analysis is not a plane strain solution but applies to a axisymmetric compression case in which the face centred cubic array is rotated through an angle ψ about one of the horizontal axes.

The solution merely gives the stress ratio which would result if failure could occur in a specified direction corresponding to $\beta = 54.7$. An axisymmetric compression test will not fail in this direction and a plane strain test in which failure is forced to occur in this direction will not necessarily exhibit the same value of ψ as used in Rowe's analysis. Thus, Rowe (1970) failed to demonstrate that the stress-dilatancy treatment is the more critical analysis.

It is noted that Rowe's (1962) treatment of regular arrays of spheres was restricted to axisymmetric compression conditions; no plane strain analyses were given. However, the extension of the stress-dilatancy theory to random arrays, and in particular to sands, has been shown to apply to plane strain conditions if the angle of interparticle friction ϕ_μ is replaced by the empirical friction angle ϕ_{cv}, Rowe (1964b), Wightman (1967), Ismael (1969), and Tong (1970). The difference between ϕ_{cv} and ϕ_μ was attributed to restrictions on the sliding movements. Horne (1969) employed a stochastic approach to derive a theoretical relationship between ϕ_{cv} and ϕ_μ. It is possible, therefore, to provide an approximate treatment of the plane strain problem posed by Parkin (1970) by substituting ϕ_{cv} into Rowe's equation above, which then becomes

$$\frac{\sigma_1}{\sigma_3} = \tan^2 \frac{1}{2}\left(\alpha_o + \beta_o + \phi_{cv}\right) \qquad (5.17)$$

Taking $\alpha_o = \beta_o = 54.7$, and substituting $\phi_{cv} = 29.7$, Horne (1969), Fig. 18, into equation 5.17 gives $\sigma_1/\sigma_3 = 7.195$, which is in reasonable agreement with Parkin's 'stress-dilatancy' value of 6.963 considering that Horne's relationship was derived for random packings of equal spheres.

In section 5.5 it will be shown that an estimate of ϕ_{cv}, applicable to a face centred cubic array, can be obtained by using a

similar substitution technique as that employed in the stress-dilatancy treatment of sand. The value of ϕ_{cv} so obtained, for $\phi_{\mu} = 21.8^{o}$, is 30.35^{o} and leads to a value of $\sigma_1/\sigma_3 = 7.445$ when substituted into equation 5.17. The value of ϕ_{cv} corresponding to Parkin's prediction of $\sigma_1/\sigma_3 = 6.963$ is 29.1^{o}.

Although the method of modifying ϕ_{μ}, to account for the restrictions on sliding directions in plane strain tests, cannot be regarded as a rigorous analysis, it does support Parkin's interpretation of the stress-dilatancy equation. It is also noted that Rowe's value of 4.86 seems to be unrealistically low when compared with his axisymmetric compression solution for a face centred cubic array (equation 5.7a) which gives $\sigma_1/\sigma_3 = 4.67$, for $\phi_{\mu} = 21.8^{o}$.

From Table 5.1 it can be seen that the rhombic packing is much more stable than the face centred cubic packing, both in axisymmetric compression and plane strain. Also, both types of packing are stronger in plane strain than in axisymmetric compression and the increase in strength, due to the restricted lateral movement in the intermediate principal stress direction, is greater for the rhombic arrangement.

Although the face centred cubic and rhombic packings exhibit different strengths their porosities are identical (25.95%). This suggests that for regular packings, the strength-porosity relationship is not unique. However, the two types of packing are essentially the same arrangement differently orientated. This is demonstrated in Fig. 5.1 which clearly shows that, for a close packed array of spheres, the difference in the type of packing obtained is due to the arrangement of the spheres selected to form the base layer which dictates the subsequent stacking arrangement. Therefore, the different strengths exhibited by rhombic and face centred cubic packings demonstrate that the strength of regular arrays of spheres is anistropic, being dependent on the orientation of the packing with respect to the applied loadings. It is interesting to note that a similar form of strength anisotropy was

observed by Menzies (1971) who carried out axisymmetric compression tests on cuboidal samples of sand in which the orientation of the direction of deposition of the sand was varied with respect to the axis of the specimens.

Rennie (1959) and Parkin (1965) analysed close packed regular arrays of spheres whose packing orientation rotated relative to the principal stress directions until a minimum stress ratio was obtained. It is clear from Fig. 5.1 and from the solutions obtained that the lease stable orientation of the packing is that corresponding to a face centred cubic array.

The Rennie-Parkin model is of particular interest as it predicts the critical stress ratio for a range of stress conditions. It was suggested that the model was applicable to random packings which consisted of regularly packed dense zones randomly orientated in a loose matrix, and it was assumed that the collapse of the random array would occur when collapse occurred in one of the small dense zones. The relevance of the Rennie-Parkin model to random arrays will be discussed in section 5.4. However, since the analysis was based on the strength of a single dense zone within the mass the model is clearly relevant to regular packings of spheres.

The stress conditions analysed covered the range from triaxial compression to triaxial extension and if the model is considered to be applicable to a random array then the failure envelope, as depicted on an octahedral plane in principal stress space, will exhibit a six-fold symmetry. In the case of a regular packing such symmetry does not exist since, referring to Fig. 5.1, the Rennie-Parkin solutions are only applicable to the stress range from axisymmetric compression of the vertical axis (z-axis) to axisymmetric extension of either horizontal axis (x- and y-axes).

The Rennie-Parkin solution for this stress range has been calculated

for an angle of interparticle friction, $\phi_\mu = 28^\circ$ ($\mu = 0.5317$) and the results are depicted in Fig. 5.2. From Fig. 5.2 it can be seen that the model predicts that the minimum strength occurs under axi-symmetric compression conditions. The strength increases with increase in σ_2 until $\sigma_2 = (\sigma_1 + \sigma_3)/3$, but remains constant over the remaining stress range, including the triaxial extension case. The shape of the failure surface predicted by the Rennie-Parkin model has recently attracted attention as a number of recent investigations into the strength of sand under generalised stress conditions have indicated a similar variation in strength, Green (1969), Procter and Barden (1971), Lade (1972). However, the failure envelope for sand, and in particular the triaxial extension strength, at present, remains controversial, Barden (1971), Sutherland (1971).

The predicted failure envelope strictly applies only to the behaviour of close packed arrays of spheres and its validity, in this context, can be appreciated by considering the face centred cubic packing shown in Fig. 5.1. It has already been noted that the solution for the range $(\sigma_1 + \sigma_3)/3 \leq \sigma_2 \leq \sigma_1$ agrees with Leussink and Wittke's plane strain solution. Therefore this range of stress conditions must include the plane strain condition. Two interesting points arise out of the model which were not clarified in the original papers: that the triaxial extension condition should produce the same strength as the plane strain state deserves a fuller explanation, and the other limit to the stress range over which the strength is independent of the magnitude of the intermediate principal stress (i.e. when $\sigma_2 = (\sigma_1+\sigma_3)/3$) requires clarification. From an inspection of the packing arrangement shown in Fig. 5.1 it can be seen that, if $\sigma_1 = \sigma_z$ and $\sigma_2 = \sigma_y$, then under triaxial extension conditions, in which $\sigma_1 = \sigma_2$, the packing cannot deform in the y-direction since the spheres form straight rows of spheres in close contact along the y-axis. Consequently the value of the intermediate principal stress will have

no effect on the strength and since the deformation will be confined to the z–x planes then the strength obtained will correspond to the plane strain strength. Clearly this condition will apply for all values of the intermediate principal stress large enough to resist outward movement in the y-direction. Therefore, it is clear that, for a close packed regular array of spheres, there is no unique plane strain state, and the stress range over which the strength is constant corresponds to a range of plane strain states.

Although a comparison between theoretical predictions based on a regular sphere model and the behaviour of sand must necessarily be circumspective, such a comparison is provided in Fig. 5.2. The failure stress conditions obtained from the seven densest plane strain specimens and the four densest triaxial compression specimens (K_o consolidated) have been superimposed on Fig. 5.2, and show a reasonable agreement with the prediction of the regular packing model. Since some lateral yielding did occur in the intermediate principal stress direction during the plane strain tests, due to compression of the lubricated membranes, the observed values of the ratio $\sigma_2/(\sigma_1 + \sigma_3)$ should be slightly less than the true plane strain values. Taking this into account, the agreement between the test results and the Rennie–Parkin solution is all the more remarkable and cannot be dismissed as entirely fortuitous.

5.3.3. Deformation of regular arrays.

As a result of their angular definitions of the packing geometry, Leussink and Wittke (1963), and Rowe (1962), were able to predict post-failure deformation curves by substituting current values of j, or α and β, into the critical stress ratio equations (equations 5.6, 5.9, 5.12a, and 5.13a). To do this it was necessary to relate the change in the packing geometry to the overall deformation of the mass.

Leussink and Wittke (1963) predicted the theoretical stress ratio–axial strain curves for triaxial compression tests on regular packings

assembled in either the rhombic or face centred cubic arrangement. They assumed that the change in the inclination of the inter-particle contact planes, Δj, could be related to the axial strain (engineering strain) by the following expression

$$\frac{\Delta H}{H} = \frac{\Delta j}{\tan j_o} + \frac{\Delta j^2}{2} \qquad (5.18)$$

Thus, for a given axial strain the corresponding angle variation, Δj, and hence the value of j, could be obtained. By substituting the current values of j into equation 5.9 the change in stress ratio with axial strain could be predicted. A similar method was used to predict plane strain deformation curves. The theory predicted that, after failure had occurred at zero axial strain, the stress ratio decreased continously with strain, the rate of decrease being more rapid under plane strain conditions than under triaxial compression conditions.

In order to assess their theory, Leussink and Wittke (1963) performed both triaxial compression and plane strain tests on specimens composed of regularly packed balls. The experiments confirmed the relatively higher strength in plane strain but the observed maximum stress ratios only occurred after a finite strain had been applied, and the stress ratios were always less than predicted throughout a test. The discrepancies between the theory and the experimental observations were attributed to the out-of-roundness of the balls and the non-uniform deformation of the specimens due to end-restraint. It is noted that the neglect of any elastic deformation of the balls would also contribute to the disparity between the theory and the experimental results. It is also interesting to note that if the theoretical strength predictions are considered to be valid only to a first order in μ then a much improved correlation with the experimental results is obtained.

Theoretical and experimental investigations of the strength and deformation of regular arrays, under triaxial compression conditions,

was also carried out by Rowe (1962) who, as stated previously in section 5.3.1, obtained the following general formula to define the critical stress ratio.

$$\frac{\sigma_1}{\sigma_3} = \tan \alpha . \tan (\phi_\mu + \beta) \qquad (5.19)$$

By assuming that sliding occurred at all points of contact once the maximum stress ratio had been reached it was demonstrated that the dense assembly would expand during post-peak deformation, with a consequent decrease in stress ratio. The post-failure deformation was associated with a change in the packing parameters α and β, and Rowe (1962) was able to relate the instantaneous values of the two parameters with the corresponding principal strain increments by the formula

$$\frac{d\varepsilon_3}{d\varepsilon_1} = \frac{1}{2} . \tan \alpha . \tan \beta \qquad (5.20)$$

Therefore, by combining equations 5.19 and 5.20, a virtual work equation was obtained which related the work done on the specimen by the major principal stress, throughout a test, to the work done by the specimen on the minor principal stress. Using the sign convention that compressive strains are positive the equation can be expressed as

$$\frac{\sigma_1 \, d\varepsilon_1}{-2 \, \sigma_3 \, d\varepsilon_3} = \frac{\sigma_1}{\sigma_3 \left(1 - \frac{d\varepsilon_v}{d\varepsilon_1} \right)} = \frac{\tan (\phi_\mu + \beta)}{\tan \beta} \qquad (5.21)$$

The experimental results differed from the theoretical predictions in a manner similar to that observed by Leussink and Wittke (1963) and the same reasons were suggested to account for the differences.

5.3.4. Rupture plane formation.

During triaxial compression tests on regular packings of spheres,

Rowe (1962) observed that the post-failure expansion of the specimens continued until the stress ratio approached unity at some location in the assembly. At this point in the test catastrophic movement occurred, resulting in the formulation of a well defined slip band inclined at α to the minor principal plane. Thus it was concluded that the slip band was the delayed result of failure rather than the cause.

Trollope and Parkin (1964) recognised that Rennie's (1959) theory predicted that the failure plane would occur at peak stress ratio and that the inclination was dependent on the angle of interparticle friction. Consequently doubts were expressed regarding the validity of Rowe's failure mechanism. However, it is clear from the subsequent work of Parkin (1965) that Rennie's theory provided a plane strain solution, in which case Rowe's failure mechanism is not relevant, see Leussink and Wittke (1963).

It is concluded that the formation of rupture planes in regular arrays occurs at peak in plane strain tests and this is also the case for the extension range of stress conditions since the permitted deformation is in effect one of plane strain. Over the compressive range of stress conditions, however, it would appear that rupture plane formation is delayed until after failure has occurred and the delay is greatest under axisymmetric compression conditions.

5.4 The structure and deformation mechanism of random arrays.

The behaviour of random arrays of equal spheres, as distinct from sand, has received little attention. The only theories specifically related to randomly packed equal spheres appear to be those provided by Parkin (1965) and Horne (1965). The Rennie-Parkin model is restricted to strength considerations which are based on the failure of regular arrays and has been discussed in section 5.3. Horne's treatment of random arrays of equal spheres is in effect one facet of the more

general stress-dilatancy theory and as such will be dealt with in a subsequent section.

The success of any theory which purports to predict the behaviour of random arrays depends on the assumptions made regarding the structure of random arrays and the mechanism of failure. This section will be primarily concerned with the validity of these assumptions. In this respect the concepts of Rennie (1959) and Parkin (1965), Rowe (1962) and Horne (1965), Kolbuszewski (1965) and Amirsoleymani (1966) are of interest.

With the exception of Rennie (1959), there is general agreement as to the actual structure of a random array, which can be described as consisting of dense zones randomly orientated in a loose matrix and was clearly illustrated by Kolbuszewski (1965), see also section 5.2. Rennie (1959) suggested that his work was relevant to the behaviour of sand which he assumed to be composed of a large number of randomly orientated groups of particles, the structure within each group being that of a regular packing. Amirsoleymani (1966) considered the structural concept of Rennie to be merely that of a complex regular packing arrangement rather than a valid description of a random array. However, in extending Rennie's work, Parkin (1965) redefined the structure as a random arrangement of 'systones' (regular packed zones) in a chaotic matrix of loose particles. Consequently it is clear that there is essential agreement about the structural composition of random arrays.

The various conceptual models differ more in the assumptions made regarding the mechanism of failure. Rennie (1959) assumed that the collapse of one of the small regular arrays would lead to failure of the complete assembly. That a highly redundant structure such as that of a random array should collapse due to local failure of a small, unfavourably orientated, dense zone would seem to be unlikely. Rowe (1964) pointed out that in Rennie's random packing the least favourably

orientated groups would fail at an early stage of a test but this would merely lead to a redistribution of load to stronger groups and the failed group of particles would reform into a more stable orientation. Parkin (1965), in his paper, did not specify a failure mechanism for the complete assembly but simply provided the analysis of one of the regularly packed zones. Thus, he would appear to accept Rennie's assumption that failure of the mass would result from the collapse of a single weak 'systone'. However, according to Barden and Khayatt (1968), Parkin's mechanism involves the progressive re-orientation and failure of systones being accommodated by the loose infilling, until the transfer of load from failing systones cannot continue and the maximum stress ratio is reached. Rowe (1970) doubted whether the amount of rotation implied in Parkin's analysis could be accommodated in a real random assembly of particles. It has also been suggested by Barden and Khayatt (1968) that the re-orientation process would involve subtle rearrangement of particles rather than rigid body rotations.

In contrast to Rennie (1959), the stress-dilatancy theory embodies the concept of a continuously changing structure in which local failure occurs at different locations within an assembly, throughout a loading test. Since a random assembly consists of weak and strong groups of particles due to the different orientations of the inter-particle contact planes, Rowe (1962) suggested that, on first loading, the weak groups will slide and transfer load to adjacent groups thereby allowing the 'failed' group of particles to reorientate into a stronger arrangement. Consequently the structure of the assembly is progressively modified to withstand the applied loads.

The mechanism was further defined by Horne (1965) who argued that, since only a small proportion of contacts would be suitably orientated for slip to occur, sliding must occur instantaneously between groups of particles. Horne (1965) also used the concept of an induced anisotropy

to explain the ability of the assembly to withstand a continuously increasing stress ratio. Consequently, the stress-dilatancy mechanism of deformation was described as consisting of instantaneous arrested slips between the dense zones whose boundaries constantly coalesce and change thereby providing a continuous supply of new, potentially unstable, contacts. Horne (1965) noted that the mechanism required the presence of a loose matrix in order to provide local compatibility of deformation.

Kolbuszewski (1965) used the term 'macropores' to describe the loosely packed discontinuities between the dense zones in a random array, and emphasized the importance of their directional characteristics. Amirsoleymani (1966) suggested that the existence of macropores in randomly packed particles affects the stability of the assembly to such an extent that the shearing property might be governed by the structure of macropores rather than the packing of dense zones. The properties of the dense zones were not considered to be negligible since the stability of a macropore depends on the structure of the zones of densely packed particles in its immediate vicinity as well as its own structure. Barden and Khayatt (1968) considered it unrealistic to suggest that the mechanism of shear was governed by the macropores, with the dense zones playing a secondary role. In their opinion the opposite was true.

In their arguments about the relative importance of the dense zones and the loose matrix, Amirsoleymani (1966) and Barden and Khayatt (1968) do not appear to distinguish between stress and strain. In the opinion of the author the strength of a random array of particles will be governed by the dense zones, being dependent on their number, size, and internal geometry; the distribution and packing of the loose matrix will determine the deformation required to mobilize that strength. This hypothesis follows from Horne's argument that at any instant in a test only a few particles are sliding and these particles will be situated at the boundaries of the momentarily defined dense zones.

Consider a specimen of dense sand confined by the cell fluid in a triaxial apparatus. If a small deviator load is applied to the specimen, only a few particles will slide and the majority of the interparticle contacts will remain intact. The applied load will be carried by the stable particles and since the majority of these particles form the dense zones, the strength mobilized by the specimen will be governed by the properties of the dense zones. If the applied load is increased then boundary movement will occur as the specimen modifies its structure to take the additional load. If it is accepted that the structural modifications are accomplished mainly by relocation of the boundaries of the dense zones, Horne (1965), then it is clear that the distribution and orientation of the loose matrix will have a significant effect on the freedom for such movement to occur. Therefore the deformations resulting from applied loadings will be governed by the properties of the loose matrix.

5.5 Stress-dilatancy theory.

Rowe (1962) suggested that the stress-dilatancy treatment of regular arrays could be extended to random packings since the energy ratio expression, equation 5.21, did not contain the angle α, characteristic of the particular packing arrangement. Although the angle β will vary initially throughout a random array, the assumed mechanism of deformation, see section 5.4, led Rowe to suggest that the rate of internal work done would be a minimum if the contact planes on which sliding occurred were inclined at a critical angle of β. Therefore, by differentiating the left-hand side of equation 5.21 with respect to β, the critical value of β ($= 45 - \phi_\mu/2$) was obtained which, when substituted into equation 5.21, gave the following expression:

$$\frac{\sigma_1}{\sigma_3} = \left(1 - \frac{d\varepsilon_v}{d\varepsilon_1} \right) \tan^2 (45 + \phi_\mu/2) \qquad (5.22)$$

Rowe (1962) also suggested that, since deformation consists of a number of arrested slides, the above equation should also apply throughout deformation to failure.

Equation 5.22 is the basic form of the stress-dilatancy relationship and is amenable to direct experimental verification. However, the stress-dilatancy theory does not imply that a sand must necessarily obey equation 5.22 and thus subsequent experimental research has concentrated on identifying the stress conditions under which the simple stress-dilatancy equation is applicable. Before reviewing the experimental evidence, a more detailed theoretical derivation of the stress-dilatancy equation is given in the following section.

5.5.1. Principle of maximum energy transmission.

The following derivation was provided by Rowe (1971).

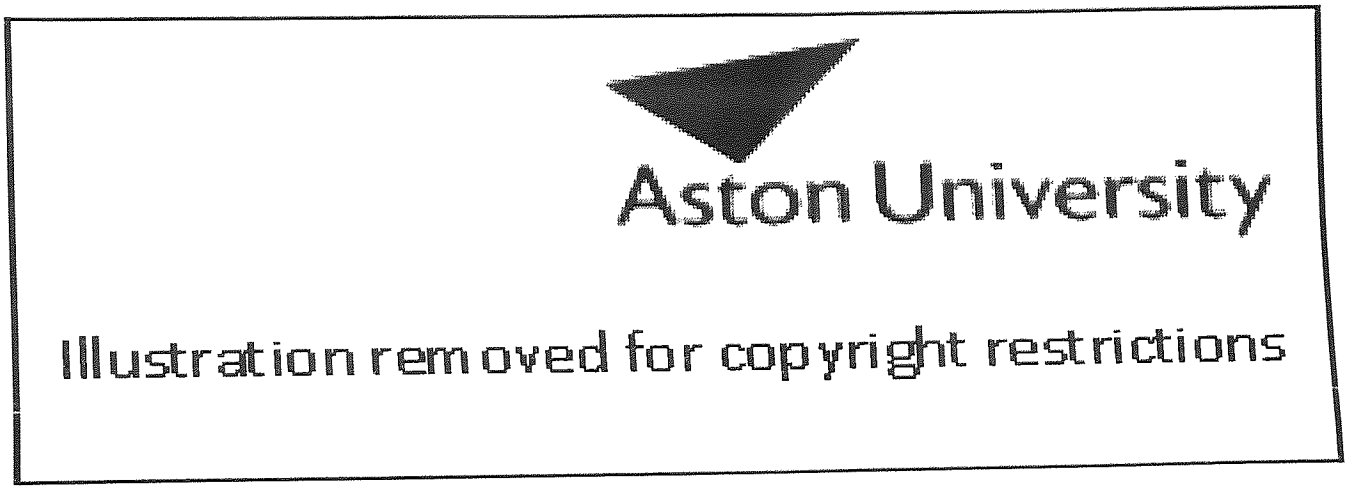

Fig. 5.3

Consider any pair of irregular particles sliding instantaneously on their interparticle contact line at β to direction 1, Fig. 5.3. L_x, L are the resultant forces in the plane of sliding at angle θ to the plane through L_1, L_3. Then

$$\frac{Lx}{L} = \tan(\phi_\mu + \beta) \tag{5.23}$$

$$\tan \beta - \frac{dl}{dx} \tag{5.24}$$

where dx and dl are incremental displacements in the directions of L_x and L.

Combining equations 5.23 and 5.24, noting $L_x = L_1$

$$\frac{L_1 dx}{-Ldl} = \frac{\tan(\phi_\mu + \beta)}{\tan \beta} = \dot{E} \tag{5.25}$$

where $\dot{E} = \dfrac{\text{Increment of work applied to contact}}{\text{Increment of work done against external forces}}$

$= \dfrac{\text{Work in}}{\text{Work out}}$, and $\dot{E}$ is an incremental energy ratio

The absolute increment of energy absorbed is

$$L_1 dx + Ldl = L_1 dx \left[1 - \frac{1}{\dot{E}}\right]$$

For a given, chosen, energy input $L_1 . dx$, the absolute energy increment is a minimum when $\dot{E}$ is a minimum. ($\dot{E}$ is merely a function of β and there is a critical β value, β_c, which makes $\dot{E}$ a minimum.)

Differentiating equation 5.25 with respect to β gives

$$\beta_c = 45 - \frac{\phi_\mu}{2}$$

and

$$\dot{E}_{min} = \tan^2\left(45 + \frac{\phi_\mu}{2}\right) = K_\mu \tag{5.26}$$

The principal strain components due to slip are denoted by ε_{1s}, ε_{2s}, and ε_{3s}. The energy input for an irregular mass of particles per unit volume in which $d\varepsilon_{1s}$ is positive, and $d\varepsilon_{2s}$, $d\varepsilon_{3s}$ are negative, is given by

$$\sum_{m=1}^{m=n_s} (L_1 dx)_m$$

where there are n_s particle pairs in sliding contact. The energy output per unit volume is given by

$$- \sum_{m=1}^{m=n_s} (Ldl)_m$$

and this is expended in both the 2 and 3 directions, if both $d\varepsilon_{2s}$ and $d\varepsilon_{3s}$ are negative.

Now $L = L_3 \cos\theta + L_2 \sin\theta$, reference Fig. 5.7

and $dl = dz \cos\theta + dy \sin\theta$

and $0 = dz \sin\theta - dy \cos\theta$

whence

$$\sum (Ldl) = \sum (L_2 dy) + \sum (L_3 dz)$$

Using equation 5.25

$$\sum_{m=1}^{m=n_s} (L_1 dx)_m = - \sum_{m=1}^{m=n_s} (\dot{E} L dl)_m$$

$$= - \left[\dot{E}_1 (Ldl)_1 + \dot{E}_2 (Ldl)_2 + \ldots \dot{E}_{ns} (Ldl)_{ns} \right]$$

The minimum possible value of the right hand side is obtained when $\dot{E}_1$ $\dot{E}_2 \ldots \dot{E}_n$ are all at K_μ (equation 5.26) whence

$$\sum_{1}^{n_s} (L_1 dx)_m = - K_\mu \sum_{1}^{n_s} (Ldl)_m = - K_\mu \left[\sum_{1}^{n_s} (L_2 dy)_m + \sum_{1}^{n_s} (L_3 dz)_m \right]$$

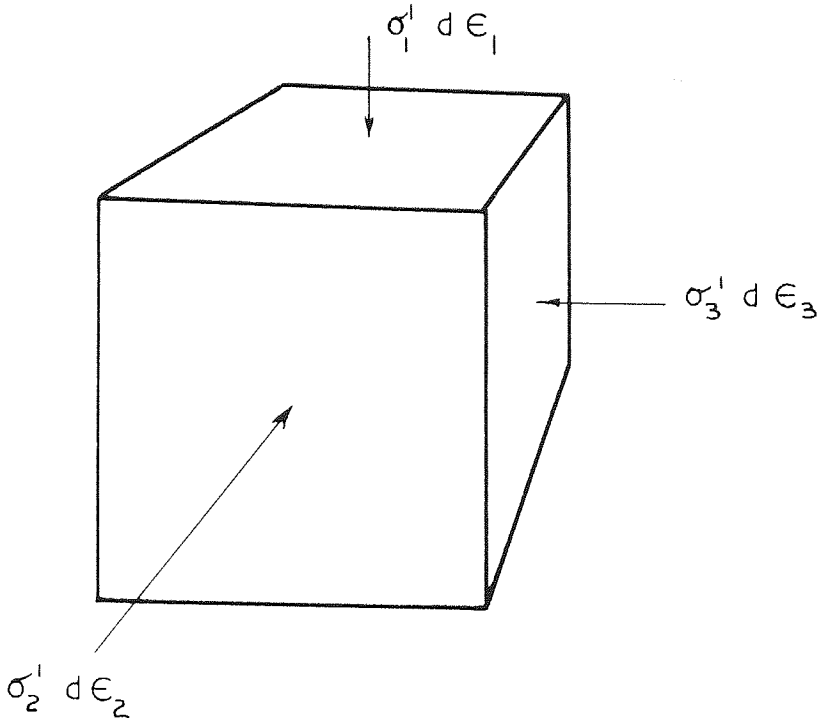

Fig. 5.4

Now

$$\sum_{1}^{n_s} \left(L_1 dx \right)_m = \sigma_1 d\varepsilon_{1s}$$

the energy supplied per unit volume in direction 1, Fig. 5.4, and

$$- \left[\sum_{1}^{n_s} \left(L_2 dy \right)_m + \sum_{1}^{n_s} \left(L_3 dz \right)_m \right] = - \left(\sigma_2 \, d\varepsilon_{2s} + \sigma_3 \, d\varepsilon_{3s} \right)$$

the work done per unit volume in direction 2 and 3.

Therefore

$$\frac{\sigma_1 \, d\varepsilon_{1s}}{- \left(\sigma_2 \, d\varepsilon_{2s} + \sigma_3 \, d\varepsilon_{3s} \right)} = K_\mu \qquad (5.27)$$

Assuming small strain increments, the volume change per unit volume, $d\varepsilon_{vs}$ is given by

$$d\varepsilon_{vs} = d\varepsilon_{1s} + d\varepsilon_{2s} + d\varepsilon_{3s}$$

and

$$\left(1 - \frac{d\varepsilon_{vs}}{d\varepsilon_{1s}} \right) = \frac{- \left(d\varepsilon_{2s} + d\varepsilon_{3s} \right)}{d\varepsilon_{1s}}$$

Using equation 5.27

$$\frac{\sigma_1}{\sigma_3 \left[1 - \left(\frac{d\varepsilon_v}{d\varepsilon_1}\right)_s - \frac{d\varepsilon_{2s}}{d\varepsilon_{1s}} \left(\frac{\sigma_2}{\sigma_3} - 1 \right) \right]} = K_\mu$$

For the triaxial compression test $\sigma_2 = \sigma_3$

For plane strain

$$\frac{d\varepsilon_{2s}}{d\varepsilon_{1s}} = - \frac{d\varepsilon_{r2e}}{d\varepsilon_{1s}}$$

where ε_{r2e} is the resultant elastic strain in direction 2.

Pending an examination of the elastic parameters this ratio is taken approximately equal to 0.

Hence for both cases

$$\frac{\sigma_1}{\sigma_3 \left(1 - \left(\frac{d\varepsilon_v}{d\varepsilon_1}\right)_s \right)} = K_\mu \qquad (5.28)$$

In the above treatment, elastic and plastic deformation of the grains, crushing and cracking are all ignored. The occurrence of rolling is considered to be insignificant and equation 5.28 only strictly applies to slip strains, resulting from rigid body sliding between groups of particles, obeying the principle of maximum energy transmission. In order to account for test conditions under which the minimum energy criterion does not apply Rowe (1962) substituted the empirical friction angle ϕ_f for ϕ_μ, and specified the limits of ϕ_f as $\phi_\mu \leq \phi_f \leq \phi_{cv}$. Equation 5.28 was therefore modified to

$$\frac{\sigma_1}{\sigma_3} = \left(1 - \frac{d\varepsilon_v}{d\varepsilon_1} \right) \tan^2 (45 + \phi_f/2) \qquad (5.29)$$

where ϕ_f is the empirical friction angle which fits the experimental observations.

An alternative derivation of equation 5.28 was provided by Horne

(1955) who also introduced the concept of an induced anisotropy.

Although the angle α is not contained in the energy ratio expression, equation 5.21, Rowe's (1962) treatment of regular packings appears to depend on a valid physical interpretation of the 'α planes'. The physical interpretation is clear in the case of regular packings but it is less easy to understand for random assemblies. Horne (1965) recognised that it is possible to trace an entirely solid path through an array of spheres in the general direction of any one of the principal stress directions. By dividing the length of the path by the number of particles traversed by the path, Horne (1965) obtained the mean distance traversed per particle which he termed the 'mean projected solid path', (m.p.s.p.), denoted by the symbol m, see Horne (1965), Fig. 4. (It is noted that later references to Horne (1965) have frequently defined the m.p.s.p. incorrectly as 'the ratio of the number of particles required to trace a solid path parallel to a principal stress direction, to the length of the path itself', Parikh (1967), Barden and Khayatt (1968).). If the m.p.s.p. in the direction of the major principal stress is m_1, and m_2 and m_3 are the m.p.s.p.'s in the other two principal stress directions, then the ratios m_1/m_2, m_1/m_3, and m_2/m_3 describe the degree of anisotropy of the packing.

Horne (1965) related the m.p.s.p.'s to the principal strain increments and demonstrated that, for regular arrays, the ratio $m_1/m_3 = \tan \alpha$, the packing characteristic used by Rowe (1962). This implies that the ratios of the m.p.s.p.'s will suitably define the packing characteristics of random arrays.

Horne's (1965) assumed mechanism of deformation of a random array is one of continual formation and destruction of particle contacts. By assuming that after a certain initial period the resulting state of anisotropy is dependent only on the relative distribution of new contacts, and that all the initial contacts have been destroyed, Horne (1965) was able to derive the following relationships for triaxial

compression conditions.

$$\frac{\sigma_1}{\sigma_3} = \frac{4}{\pi} \cdot \frac{m_1}{m_3} \cdot \tan\left(\frac{\pi}{4} + \frac{\phi_\mu}{2}\right) \qquad (5.30)$$

and

$$\frac{d\varepsilon_3}{d\varepsilon_1} = -\frac{2}{\pi} \cdot \frac{m_1}{m_3} \cdot \tan\left(\frac{\pi}{4} - \frac{\phi_\mu}{2}\right) \qquad (5.31)$$

It was further assumed that at the state of maximum dilatation, the only contacts existing are those which occur at the maximum frequency. Thus, by assuming that these are the only contacts, Horne (1965) was able to derive the following limits.

$$\left(\frac{m_1}{m_3}\right)_{max} = \frac{\pi}{2} \tan\left(\frac{\pi}{4} + \frac{\phi_\mu}{2}\right)$$

and hence from equations 5.30 and 5.31

$$\left(\frac{\sigma_1}{\sigma_3}\right)_{max} = 2 \tan^2\left(\frac{\pi}{4} + \frac{\phi_\mu}{2}\right)$$

and

$$\left(\frac{d\varepsilon_3}{d\varepsilon_1}\right)_{max} = -1$$

or

$$\left(1 - \frac{d\varepsilon_v}{d\varepsilon_1}\right)_{max} = 2$$

5.5.2. Determination of the limiting values of ϕ_f

Rowe (1964a) described the parameter ϕ_f as the value which fits the experimental observations and suggested that its value was limited to the range $\phi_\mu \leq \phi_f \leq \phi_{cv}$, where ϕ_{cv} is the angle of internal

shearing resistance corresponding to the critical void ratio state. Therefore, in order to assess the validity of equation 5.29 it is necessary to determine the values of ϕ_μ and ϕ_{cv} for the sand tested.

The angle of interparticle friction, ϕ_μ, depends on the nature of the parent mineral, the properties of the particle surface, and the size of the load per particle. The absolute verification of the stress-dilatancy theory depends on a reliable independent measurement of ϕ_μ and this would appear possible using some form of friction slider technique. However, the results of such tests are extremely sensitive to the actual test conditions and the method of interpretation. No particular technique has found general approval and consequently no standard method of determining ϕ_μ has yet been evolved. Nevertheless, Rowe (1962) and later co-workers have favoured the original method used by Rowe (1962) in which the angle of interparticle friction, ϕ_μ, was measured by sliding a mass of particles over a block of the same mineral in a modified shear box. Details of the apparatus and the testing techniques employed were provided by Tong (1970).

The upper limit to ϕ_f, ϕ_{cv} was originally obtained by fitting equation 5.29 to the observed stress ratio at the ultimate constant volume condition in a triaxial compression test. However, a theoretical relationship between ϕ_{cv} and ϕ_μ was obtained by Horne (1969).

Horne's (1965) concept of induced anisotropy was based on the assumption that the principle of maximum energy transmission was not invalidated. However, Horne (1969) suggested that with the increased degree of dilation* that occurs after failure the average size of the instantaneous groups of particles which are sliding will decrease. This will lead to sliding occurring at angles other than the preferred angle, $\beta = 45 - \phi_\mu/2$, which will destroy the state of high anisotropy previously attained. It was assumed that the sliding directions are limited to the range $\beta_2 \leq \beta \leq \beta_1$ where β_1 is the maximum

* amount of expansion

inclination at which sliding is physically possible and β_2 is the angle that satisfies the constant volume condition. By assuming that the intensity of sliding at any one instant is constant for all values of β within these limits, it was possible to relate β_2 to β_1 by the expression

$$2\,\beta_1 + \sin 2\,\beta_1 + 2\cos 2\,\beta_1 = 2\,\beta_2 + \sin 2\,\beta_2 + 2\cos 2\,\beta_2$$

where $\beta_1 = 45 - \phi_\mu$

In order to determine the stress ratio at the ultimate constant volume condition it was necessary to make the additional assumption that the mean force between sliding contacts is constant for all values of β. The stress conditions at the ultimate constant volume state were given by the equation

$$\frac{\sigma_1}{\sigma_1 - \sigma_3} = \frac{\cot \phi_\mu}{3}\left[\frac{\cos^3\beta_2 - \cos^3\beta_1}{\sin\beta_1 - \sin\beta_2}\right] + 1 - \frac{1}{3}\left(\sin^2\beta_1 + \sin\beta_1 \sin\beta_2 + \sin^2\beta_2\right) \tag{5.32}$$

The stress ratio at the constant volume condition is also given by

$$\frac{\sigma_1}{\sigma_3} = \tan^2\left(45 + \frac{\phi_{cv}}{2}\right) \tag{5.33}$$

Therefore, from equations 5.32 and 5.33, the relationship between ϕ_{cv} and ϕ_μ was obtained, which was then expressed in graphical form. The theoretical values of ϕ_{cv} were compared with previous expressions provided by Caquot (1934) and Bishop (1954).

Caquot (1934) assumed that sliding occurred on all the tangent planes of a spherical surface and derived an equation for plane strain conditions:

$$\tan \phi_{cv} = \frac{\pi}{2} \cdot \mu \tag{5.34}$$

From an analysis of triaxial compression and plane strain conditions based on energy considerations, Bishop (1954) obtained the

following approximate expressions

For triaxial compression

$$\sin \phi_{cv} = \frac{15\mu}{10 + 3\mu} \tag{5.35}$$

and for plane strain, assuming $\sigma_2 = (\sigma_1 + \sigma_3)/2$

$$\sin \phi_{cv} = \frac{3}{2}\cdot\mu \tag{5.36}$$

In order to extend the stress-dilatancy theory to triaxial compression tests on sands it was necessary to introduce the parameter ϕ_f, to account for conditions in which the sliding directions deviate from the preferred direction for maximum energy transmission. Since no fundamental theoretical analysis of the plane strain condition has been provided by the stress-dilatancy theory, the plane strain stress-dilatancy solution has to be obtained empirically. Rowe (1969) suggested that the form of the stress-dilatancy equation given by equation 5.29 could be retained for plane strain conditions by taking $\phi_f = \phi_{cv}$. If a similar substitution technique is applied to Rowe's (1962) triaxial compression solutions for regular packings then an analogous plane strain solution can be obtained. By equating the analogous solution to the corresponding true plane strain solution a relationship between ϕ_{cv} and ϕ_μ can be obtained.

Although the Rennie-Parkin solutions have been shown to give the most critical stress ratios the form of the solutions is not suitable for the present treatment. Since Rowe's (1962) triaxial compression solutions for regular packings are identical to those of Leussink and Wittke (1963) it is convenient to use Leussink and Wittke's face centred cubic solutions. Therefore, if μ in equation 5.10a is replaced by $\mu_{cv} = \tan \phi_{cv}$ and the modified form is equated to Leussink and Wittke's plane strain solution, equation 5.12b, then the following expression is obtained

$$\frac{1 + \mu_{cv}}{1 - \mu_{cv}} = \frac{\sqrt{3} + \sqrt{2}\,\mu}{\sqrt{3} - 2\sqrt{2}\,\mu}$$

therefore

$$\mu_{cv} = \frac{3\mu}{\sqrt{6} - \mu} \qquad (5.37)$$

Since the Rennie-Parkin model predicts more critical strengths, and the difference is greater for the plane strain case, the above equation would be expected to overestimate ϕ_{cv}. This is especially true if Rennie's (1959) limitations on such solutions is accepted. A possible lower limit to ϕ_{cv} can be estimated by applying the same procedure to the approximate solutions given in Table 5.1.

Thus $$2 + 4\,\mu_{cv} = 2 + 2\sqrt{6}\,\mu$$

and $$\mu_{cv} = \sqrt{\frac{3}{2}} \cdot \mu \qquad (5.38)$$

All the above solutions are depicted in Fig. 5.5 together with the experimental values provided by Parikh (1967), Fig. 7.1, and Tong (1970), Table 6.1. Parikh (1967) obtained estimates of ϕ_{cv} from triaxial compression tests which were continued until an approximate constant volume condition was reached; thus ϕ_{cv} could be determined by a slight extrapolation. Tong (1970) performed plane strain tests and observed that ϕ_f was approximately constant throughout pre-peak deformation and independent of initial porosity. Assuming that $\phi_f = \phi_{cv}$, Tong (1970) found that ϕ_{cv} decreased with increase in cell pressure. The range of ϕ_{cv} values obtained, corresponding to a cell pressure range 14 - 345 kN/m^2, are indicated on Fig. 5.5. It can be seen from Fig. 5.5 that, although the best correlation with the experimental values is given by Horne's relationship, equation 5.37 and 5.38 provide a simple means of estimating the likely range of ϕ_{cv} values in plane strain tests.

No experimental work was carried out in the course of this research program to obtain an independent measurement of ϕ_μ. Therefore it was necessary to refer to Rowe (1962) to obtain a value of ϕ_μ for the sand tested, against which the triaxial compression behaviour could be compared.

The sand used in the tests reported in previous chapters was a fine quartz sand, passing No. 100 and retained on No. 300 B.S. sieves. From Rowe's (1962) Fig. 3 the limits to ϕ_μ for this range of particle sizes are $27^\circ - 29^\circ$. It was also noted that the sand used had similar physical properties to the R. Welland sand used by Parikh (1967). Therefore, Parikh's values of $\phi_\mu = 28^\circ$ and $\phi_{cv} = 35^\circ$ have been used to interpret the tests reported in Chapters 3 and 4, in terms of the stress-dilatancy theory.

5.5.3. Evaluation of test data in terms of the stress-dilatancy theory.

The stress-dilatancy equation can be expressed as

$$R = DK \qquad (5.39)$$

where $R = \sigma_1/\sigma_3$ = principal effective stress ratio

$D = (1 - d\varepsilon_v/d\varepsilon_1)$ = dilatancy factor

$K = \tan^2(45 + \phi_f/2)$ and $\phi_\mu \leq \phi_f \leq \phi_{cv}$

Thus, the performance of particulate material in terms of the stress-dilatancy theory can be conveniently assessed by presenting the experimental results in the form of a graph of R against D. Comparison can then be made with the theoretical limits K_μ and K_{cv} represented by straight lines through the origin. According to Rowe (1964a), the K_μ and K_{cv} lines represent the lower and upper limits of energy absorbed in internal friction for a given energy input. The lower limit K_μ is only achieved if the maximum energy transmission principle is adhered to and since this implies large group movement, Horne (1965) suggested that deviations from K_μ will occur when particle groups are small as sliding will then occur in other than the

preferred direction, β_c. The present research has been interpreted in terms of the stress-dilatancy theory but, before the results are discussed, a brief summary of previous experimental findings is provided.

The stress-dilatancy relationship was verified experimentally by Rowe (1962), (1964a), for a wide range of cohesionless materials tested under triaxial compression conditions for constant σ_3 stress paths. It was observed that initially dense specimens followed the lower limit K_μ almost up to the peak stress ratio. During post-peak deformation, as the dilatancy factor decreased, K increased to approach the upper limit K_{cv} at D = 1, corresponding to the critical void ratio state. Initially loose specimens generally indicated a tendency towards the K_{cv} line throughout deformation.

Barden and Khayatt (1966), (1968), investigated the effect of stress path on the stress-dilatancy behaviour in triaxial compression tests. The measured total strains were treated as slip strains and from the experimental results it was concluded that, for virgin loading in triaxial compression tests, the pre-peak behaviour of dense sand obeyed the principle of maximum energy transmission, except possibly at very small strains where elastic strains are significant. The greatest departure from the K_μ line occurred at small strains in constant axial stress tests in which the mean stress was decreasing. Rowe (1971) concluded that good agreement with the K_μ line is obtained for the stress path σ_3 constant, σ_1 increasing, even without isolation of the elastic components which are relatively small; for the stress path σ_1 constant, σ_3 decreasing, good agreement is only obtained after isolation of the elastic strains.

Rowe (1964b) reanalysed the plane strain data provided by Cornforth (1961), (1964), in terms of the stress-dilatancy theory and noted that the experimental results followed the K_{cv} line throughout deformation. This observation was confirmed by Wightman (1967), Ismael (1969), and Tong (1970), for a variety of cohesionless materials. It

was found that good agreement with the K_{cv} line was obtained throughout deformation irrespective of the initial porosity. The difference between plane strain and triaxial compression behaviour was attributed to the restrictions on particle movement enforced by the plane strain condition. Such restrictions cause sliding to occur in directions other than the preferred direction, β_c , and thus, since plane strain permits a minimum degree of freedom for particle movement, the range of sliding directions will be a maximum and the corresponding energy absorbed in internal friction will be a maximum, with $\phi_f = \phi_{cv}$.

Tong (1970) demonstrated that the effect of stress path on the plane strain behaviour of sand was similar to that observed for triaxial compression tests, Barden and Khayatt (1968).

Ismael (1969) investigated the effect of confining pressure on the stress-dilatancy behaviour of sand for both triaxial compression and plane strain conditions. It was found that, for triaxial compression conditions, the frictional component, K, increased towards the K_{cv} limit with increase in confining pressure. This phenomenon was attributed to grain crushing which results in random sliding directions and an increase in the amount of energy absorbed in internal friction. Since crushing also produces comprehensive volume changes, the dilatancy component, D, decreased with increase in confining pressure. Under plane strain conditions the frictional component, K_{cv}, was found to be unaffected by confining pressure and an increase in confining pressure merely reduced the dilatancy component, D.

Rowe (1971) considered that one of the most significant features of the stress-dilatancy behaviour of cohesionless material, demonstrated by Rowe (1962), was that 'the stress-dilatancy relation holds true on reload paths of increasing R even though the absolute strains are completely different in size'. Lee (1966), from triaxial compression tests on feldspar sand, observed that, although reloading during pre-peak deformation gave similar plots to those obtained during virgin

loading, the correlation was not as good as that obtained by Rowe (1962). Lee (1966) also suggested that the minimum energy criterion was not closely obeyed on reloading during post-peak deformation. Khayatt (1967), however, published stress-dilatancy plots for a number of post-peak reloads which showed excellent agreement with the K_μ line.

With reference to pre-peak reload paths, Barden and Khayatt (1966) concluded that the K_μ line was approached more closely on second or even on third loadings. This was taken to indicate that slips continued to predominate over elastic deformations since the data would deviate markedly from the K_μ, K_{cv} limits if the elastic strains became predominant. However, in extending their work to other stress paths, Barden and Khayatt (1968) observed that, in general, there was little agreement with the stress-dilatancy equation when reloading during pre-peak deformation. It was observed that in the constant σ_3 tests the value of K depended upon the value of the stress ratio from which the unloading had been commenced: the lower the R value the more K exceeded K_μ. It was therefore concluded that deformation during pre-peak reloading paths was not dominated by slips and probably included a large proportion of elastic strains.

Wightman (1967) investigated the reloading behaviour of sands in plane strain tests. Although the post-peak reloading behaviour indicated good agreement with the K_{cv} line, the pre-peak reloading data indicated K values much higher than K_{cv} until the maximum previous value of stress ratio was reached. Wightman (1967) noted that the stress-dilatancy plots obtained from the pre-peak reloads were similar to those obtained by El-Sohby (1964) for constant stress ratio tests in which elastic strains were shown to be appreciable.

The above experimental investigations demonstrate the validity of the stress-dilatancy theory for a wide range of test conditons, especially with regard to the behaviour during virgin loading.

Reloading behaviour, however, would appear to be somewhat ambiguous, especially during pre-peak deformation. It is, therefore, of particular interest to re-examine the stress-dilatancy performance of particulate material during reloading since it is imperative that the relative importance of elastic strains is clarified.

Typical stress-dilatancy plots obtained from the Ko consolidated triaxial compression tests, Chapter 3, are shown in Figs. 5.6 - 5.11. The results of the two tests on dense specimens, Fig. 5.6 and 5.7, indicate a value of $\phi_\mu = 28^o$, agreeing with Rowe's (1962) prediction for the sand fraction tested in this research program. As noted by other research workers, the loose specimens do not correlate with the K_μ line to the same extent as do the dense specimens. However, allowing for possible errors in the initial readings, the results are in excellent agreement with the stress-dilatancy predictions, from the start of the shear stage. Figs. 5.6 and 5.7 indicate that the value of K increased as D decreased during post-peak deformation and it would appear that the K_{cv} line was reached well before the critical void ratio state was attained. However, it was observed that edge discontinuities were initiated in the Ko consolidated specimens due to overlapping of the platens, section 3.6. The discontinuities tended to occur at about 9% axial strain and thus the specimens cannot be considered to represent homogeneous elements of soil beyond this stage of the tests. Consequently the stress-dilatancy plots for these tests are only reliable up to 9% axial strain.

The stress-dilatancy behaviour of the ambient consolidated triaxial compression tests is shown in Figs. 5.12 - 5.16. For the cyclic tests, Figs. 5.14 - 5.16, only the virgin loading portions of the tests are shown. It can be seen that, although the experimental data exhibited the characteristic behaviour pattern associated with the stress-dilatancy theory, the minimum energy line corresponding to $\phi_\mu = 28^o$ was not attained. As shown in Figs. 5.12 - 5.16, the experimental

results of the ambient consolidated triaxial compression tests appear to indicate a value of $\phi_\mu = 30^\circ$. It is noted that, using the method suggested by Bishop (1971), the ambient consolidated tests also indicated a value of $\phi_{cv} = 37^\circ$ which was 2° higher than that indicated by the Ko consolidated triaxial compression tests, Fig. 3.7.

It has already been pointed out in Chapters 3 and 4 that one of the anomalous features of this research program was the apparent difference in strength exhibited by the two series of triaxial compression tests. In order to clarify this issue, additional tests were performed, see Chapter 3, calibrations of measuring devices were checked, and the analyses of the test results were scrutinized; but no explanation was discovered. Whilst it is possible that both sets of test results are valid, the stress-dilatancy plots provided in this chapter would appear to provide some circumstantial evidence to suggest that the Ko consolidated series of tests is more reliable since the ϕ_μ and ϕ_{cv} values indicated by the test results are in better agreement with the predictions of Rowe (1962) and the experimental work on R. Welland sand (which has similar physical properties to the sand tested in this research program). Nevertheless, it must be stressed that no conclusive evidence was found to support either set of results.

In order to clarify the comparison between reload and virgin loading behaviour, the experimental data from a number of reloading paths, shown in Figs. 5.17 - 5.19, have been compared with a K_μ line corresponding to $\phi_\mu = 30^\circ$, as indicated by the ambient consolidated triaxial compression tests. From the data shown in Figs. 5.17 - 5.19 it is clear, in retrospect, that greater accuracy in strain measurements during cyclic loading in triaxial compression tests is required before any definitive conclusions can be drawn. Nevertheless, the reload data shown are sufficient to identify general trends.

The behaviour pattern obtained during two pre-peak reloads is shown in Fig. 5.17. The reloading behaviour shown, for the second

reload in test TC 15 and the third reload in test TC 17, is typical of the reloading behaviour observed during all the pre-peak cycles which were unloaded to approximate ambient stress conditions. Notwithstanding the erratic nature of the reloading behaviour shown in Fig. 5.17, it is clear that there is a definite tendency towards the minimum energy line indicated by the virgin loading behaviour.

During test TC 18 four cycles of unloading and reloading were applied and the data from the third and fourth reloads are plotted in Fig. 5.18. The third unload-reload cycle was applied during pre-peak deformation at an axial strain of 4% whereas the fourth cycle was unloaded at 16.5% axial strain, well past the point at which the maximum stress ratio had been reached. It would appear that a similar correlation with the K_μ line corresponding to $\phi_\mu = 30^o$ is obtained during both pre-peak and post-peak reloadings.

The reloading data from the second and third cycles applied during test TC 13 are shown in Fig. 5.19. Both cycles were performed during pre-peak deformation but the second cycle was only partially unloaded (to a stress ratio of 2.5). It is clear that the behaviour during the second reload was significantly different from the reloading behaviour exhibited by cycles which were unloaded to approximate ambient stress conditions. The deviation from the K_μ and K_{cv} limits shown by the second reload data suggests the existence of appreciable elastic deformation. It would seem unlikely that the elastic strains should be greater after partial unloading than after an almost complete removal of the deviator stress. Therefore, it is presumed that the slip strains are less if a specimen is only partially unloaded before reloading is commenced.

Representative data obtained from the plane strain tests performed using flexible side platens, Chapter 4, are shown in Figs. 5.20 - 5.33 and reloading behaviour is illustrated in Figs. 5.32 and 5.33. The agreement with the upper K_{cv} limit, obtained during virgin loading,

confirms that, under plane strain conditions, the value of K in equation 5.39 is equal to K_{cv} throughout deformation irrespective of initial porosity.

The stress-dilatancy behaviour illustrated in Figs. 5.20 - 5.31 is remarkably similar to the stress-dilatancy plots obtained from plane strain tests on R. Welland sand by Wightman (1967), Ismael (1969), an Tong (1970). Since these research workers employed rigid side platens to maintain plane strain deformation the stress-dilatancy plots obtained from the present research clearly demonstrate that the flexible side platens provided an adequate simulation of plane strain conditions.

Typical stress-dilatancy plots obtained during reloading in plane strain tests are shown in Figs. 5.32 and 5.33. Both the tests illustrated, PS 21 and PS 25, included a post-peak cycle of loading in addition to three cycles applied during pre-peak deformation. The results show a complete lack of correlation with the K_{cv} line until the stress ratio attains the value from which the specimen had been unloaded. The deformation pattern shown in Figs. 5.32 and 5.33 is similar to that observed by Wightman (1967) during pre-peak reloading in plane strain tests. However, unlike Wightman, the author found no significant difference between pre-peak and post-peak behaviour, as is evident from Figs. 5.32 and 5.33.

It would appear that Rowe's (1971) statement, that the stress-dilatancy relationship also applies to reloading behaviour, is not of general validity. Thus the conditions under which reloading exhibits stress-dilatancy behaviour requires further examination. From the results of the present research program it would appear that the distinction, between the reloading cases which conform to the stress-dilatancy rule and those which do not, is the degree of unloading applied. During the cyclic plane strain tests the specimens were unloaded to $R \simeq 1/K_o$. This was true also of the second cycle of

loading applied in test TC 13 which exhibited a similar pattern of deformation to the plane strain tests during reloading, see Fig. 5.19. All the other cycles of loading applied during the triaxial compression tests involved unloading to approximate ambient stress conditions which resulted in reasonable correlation with the stress-dilatancy relation during subsequent reloading. Previous experimental work which indicated good correlation with the stress-dilatancy relationship during reloading, Rowe (1962), Lee (1966), Barden and Khayatt (1966), (1968), was restricted to cases in which the specimens had been unloaded to approximate ambient stress conditions.

The conclusion that the stress-dilatancy rule is only obeyed on reloading if the specimen has been unloaded to $R \simeq 1$ is also supported by Wightman's (1967) plane strain results. Wightman's pre-peak cycles only involved unloading to $R = 1/K_o$ and the subsequent reloading behaviour indicated appreciable elastic deformation present; the post-peak cycles reported, which gave good correlation with the stress-dilatancy rule, were unloaded to a stress ratio close to unity.

During virgin loading the structure of a specimen of sand is continually modified to carry the increasing stress ratio. The deformation is composed of a combination of elastic strains and rigid body slip movements but, as shown by the stress-dilatancy theory, the slip strains generally predominate.

If the stress ratio is reduced by unloading the specimen then the previously developed structure should be relatively unaffected by the small elastic strains which will result from the release of stored elastic energy in the particles. This being so, the subsequent reloading of the specimen should result in similar small deformations since the structure is preconditioned to carry a higher stress ratio. As the previous maximum value of R is attained the structure will once more start to readjust and slip strains will again become predominant. If, however, interparticle slips occur during unloading as

a result of the release of energy then the locations at which the slips occur will be susceptible to interparticle slip movement when the specimen is reloaded.

It has been shown in this section that the stress-dilatancy relationship is only obtained during reloading if the specimen has been unloaded to approximate ambient stress conditions. Furthermore, the test results, Appendix C, show that the stress ratio - axial strain curves during unloading do not exhibit any significant curvature until very low stress ratios are reached. Therefore, it would appear that slip strains only become significant during unloading when the stress ratio approaches unity.

According to continuum mechanics theory the separation of elastic and plastic deformation can be obtained by simply subtracting the elastic rebound from the total deformation. As a result of previous experimental investigations into the reloading behaviour of sands, Rowe (1962), Lee (1966), Barden and Khayatt (1966), (1968), it has been suggested that this simple approach cannot be used to separate the elastic and slip components for particulate material, except in the case of constant stress ratio tests, Rowe (1971). However, the evidence to support this supposition is largely based on the results of tests in which the specimens were unloaded to ambient stress conditions.

Soil insitu exists under an anisotropic stress system and, in general, is unlikely to experience complete unloading to an all-round pressure. Consequently, it may be more appropriate to consider the experimental evidence obtained during reloading following partial unloading. In this case, from the present research program and from the results of Wightman's (1967) plane strain tests, it would appear that some form of elastic treatment of the reloading behaviour may be possible. Therefore, in developing deformation theories to analyse boundary value problems it would seem to be more relevant that the stress-dilatancy relationship is not obeyed during reloading after

partial unloading rather than the observation that the stress-dilatancy relationship applies to reloading when the specimen has been previously unloaded to ambient stress conditions.

5.5.4. Components of shear strength.

The stress-dilatancy equation separates the strength of a particulate material into two components: a frictional component, K, and a component due to expansion, D. Rowe (1964a) suggested that the dilatancy factor, D, isolated the effect of structure. In his treatment of regular packings Rowe (1962) identified tan α as a structural parameter. However, the structural parameter should only be related to the internal geometry and not be associated with interparticle friction.

From triaxial compression tests on different particulate materials, Parikh (1967) found that tan α increased with interparticle friction (as predicted by stress-dilatancy theory) whereas D was essentially unaffected. This finding was corroborated by tests on R. Welland sand in which ϕ_μ was varied by changing the pore fluid. Therefore, Parikh (1967) concluded that the dilatancy factor can be regarded as a fundamental component of shear strength which identifies the effect of structure.

Bent Hansen (1958) introduced the term 'angle of dilatation', ν to identify the component of strength due to change in volume. Davis (1967) recognised that the relationship between ν and the strain rates was analogous to the relation between ϕ and stress ratio, since ν is related to D in the following manner.

$$D = \tan^2 \left(45 + \frac{\nu}{2}\right)$$

Therefore the stress-dilatancy equation, equation 5.39, can also be expressed as

$$\tan^2 \left(45 + \frac{\phi}{2}\right) = \tan^2 \left(45 + \frac{\nu}{2}\right) \cdot \tan^2 \left(45 + \frac{\phi_f}{2}\right) \qquad (5.40)$$

The values of R, D and K at failure in the triaxial compression and plane strain tests are plotted against initial porosity in Fig. 5.34. The alternative geometric parameters ϕ, ν and ϕ_f are shown in Fig. 5.35. From both figures it is clear that the difference in strength between plane strain and triaxial compression tests is essentially due to the difference in the frictional component K, since the structural parameter D is similar for both conditions. In plane strain $K = K_{cv}$, independent of porosity, but in triaxial compression K decreases with porosity to approach the K_μ value at minimum porosity.

The results shown in Fig. 5.35 indicate a value of ϕ_{cv} slightly higher than Horne's value of 35° but not as high as indicated by Fig. 4.22 ($\phi_{cv} = 38^\circ$) using Bishop's (1971) suggestion. The mean value of ϕ_{cv} obtained from the conditions of failure, Fig. 5.35, is 36.12°. The disagreement with the value obtained from Fig. 4.22 is probably partly due to the extrapolative nature of Bishop's method. However, no satisfactory method of sample preparation has yet been developed which will ensure uniform deformation of loose specimens of sand. Therefore, even when no extrapolation is required, Bishop's method tends to rely on the least reliable data.

Although the mean value of ϕ_{cv} obtained from the failure conditions is only based on the data from one point in each test, the experimental stress-dilatancy plots obtained from the plane strain test results correlate equally well with a value of ϕ_{cv} equal to either 35° or 36°. Consequently, from the results of the present research program, it is not possible to define the ϕ_{cv} value in plane strain with sufficient accuracy to make any conclusive statements regarding the possible difference between ϕ_{cv} in plane strain and triaxial compression.

From his theoretical treatment of random packings of equal spheres, Horne (1965) was able to predict that, for triaxial compression conditions, the maximum value of D = 2. No prediction was made for plane strain conditions. Fig. 5.34 indicates that the dilatancy factor at failure is

similar in plane strain and triaxial compression: increasing with decrease in porosity towards the theoretical limit of 2 at minimum porosity. Although Barden and Khayatt (1968) demonstrated that the maximum rate of dilatation in plane strain should be similar to the value obtained in triaxial compression it was suggested that there was no theoretical reason why the two values should be equal. However, the theoretical analysis of regular packings implies that D should be unaffected by restraint in the intermediate principal stress direction.

As shown in section 5.3.2. the strength of a regular array is the same in triaxial compression and plane strain if $\mu = 0$. Since the strength of an ideal frictionless particulate material will result solely from the effect of volume change this implies that the structural parameter D, at failure, will be the same in both cases. Furthermore, the strength of the densest arrangement of equal spheres with zero interparticle friction was shown to be equal to 2 for both triaxial compression and plane strain. Considering the loosest possible regular packing of equal spheres, simple cubic, the stress ratio at failure for zero friction is equal to 1. Therefore, the treatment of regular arrays implies that, at failure, D is the same in plane strain and triaxial compression, and for both cases $1 \leq D \leq 2$ depending on the packing geometry.

It is noted that the test results, in fact, indicate that, at failure in plane strain, D is slightly higher than in triaxial compression. However, it will be recalled that in triaxial compression the maximum rate of dilatation does not occur at peak and that the stress-dilatancy plots indicated that K tended to increase above the minimum value as D approached its maximum value. Lee (1968) presented data (Lee's Fig. 4.83) which suggests that the curvature of the stress-dilatancy plot, usually observed just prior to peak, is due to slight non-uniform deformation of the specimen. Consequently further improvements in testing techniques may well confirm that the rate of

dilatation at failure is identical in both triaxial compression and plane strain.

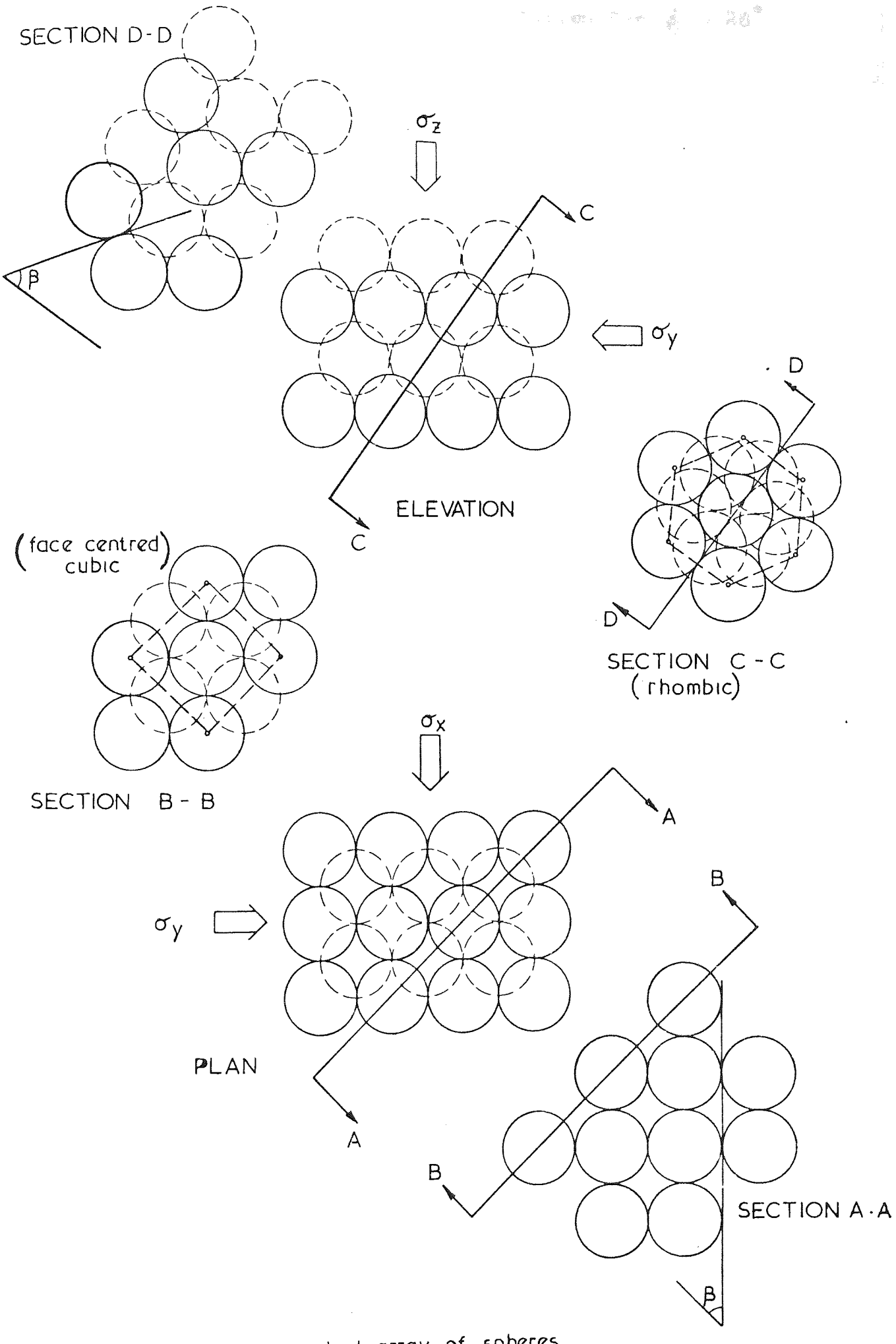

Fig. 5.1 Close packed array of spheres

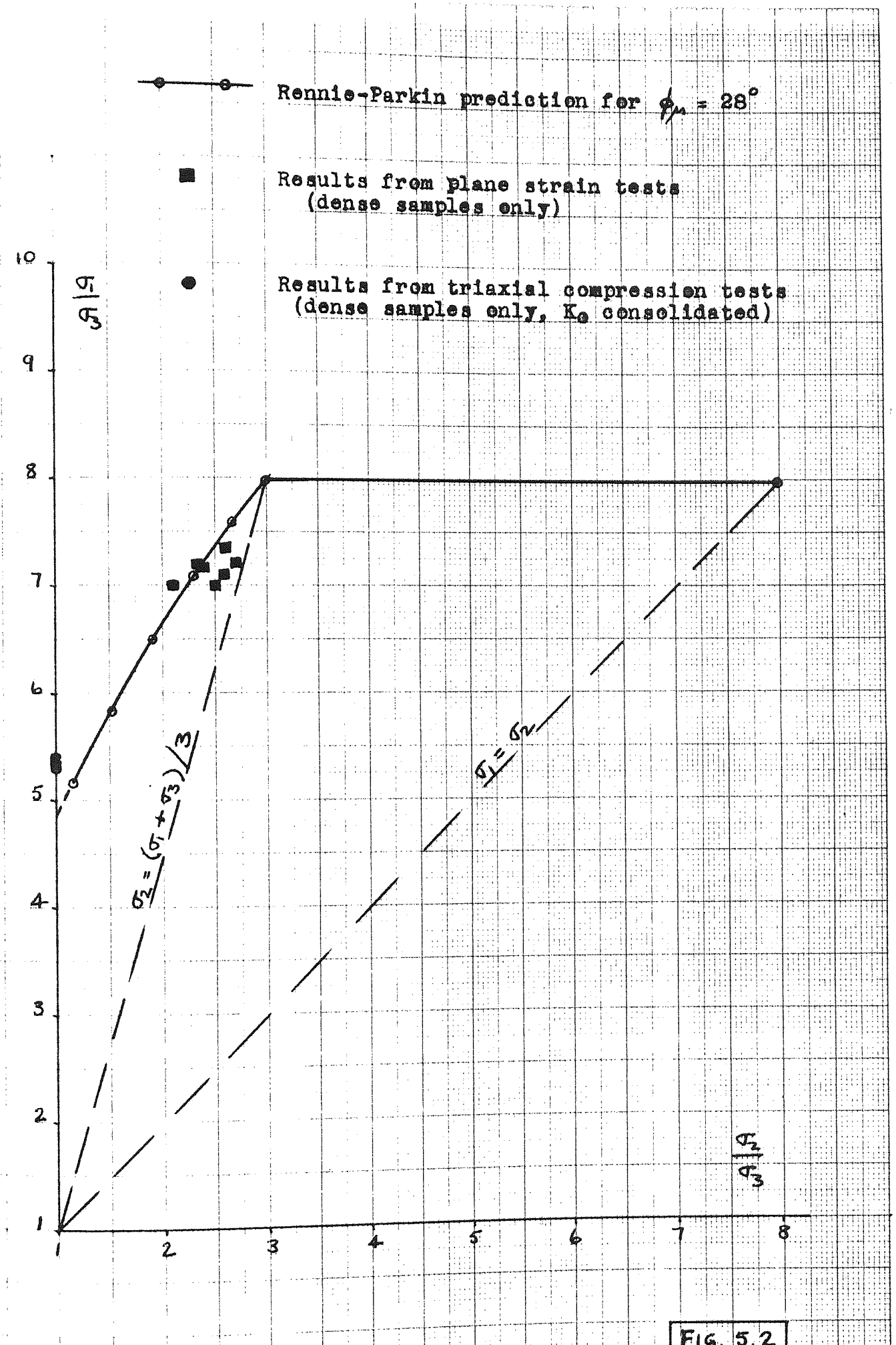
Rennie-Parkin prediction for $\phi_m = 28°$
Results from plane strain tests (dense samples only)
Results from triaxial compression tests (dense samples only, K_o consolidated)
$\frac{\sigma_1}{\sigma_3}$
$\frac{\sigma_2}{\sigma_3}$
$\sigma_2 = (\sigma_1 + \sigma_3)/3$
$\sigma_1 = \sigma_2$
1
2
3
4
5
6
7
8
9
10

FIG. 5.2

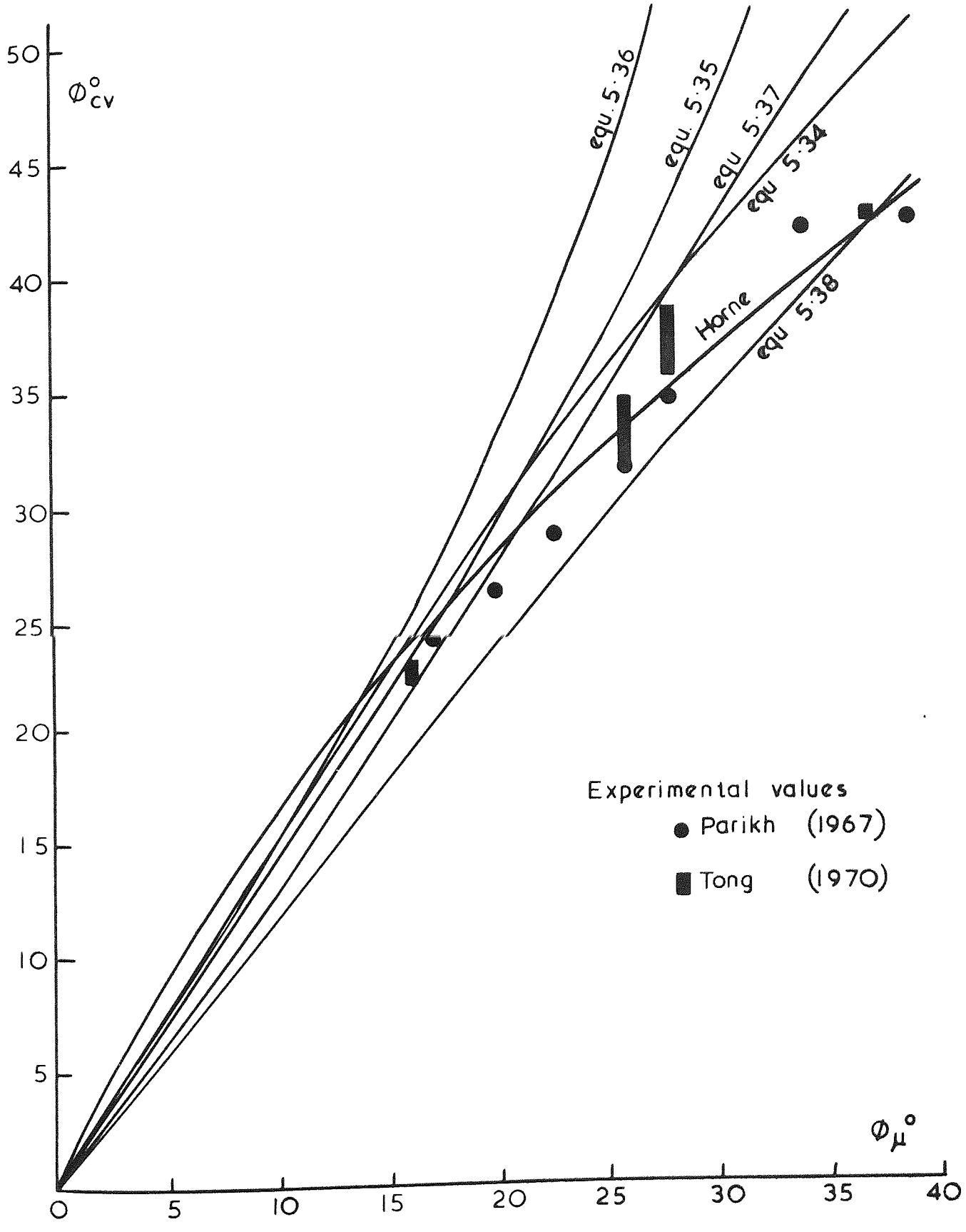
50
45
40
35
30
25
20
15
10
5
0
5
10
15
20
25
30
35
40
ϕ°_{cv}
ϕ_{μ}°
equ. 5·36
equ. 5·35
equ. 5·37
equ 5·34
equ 5·38
Horne
Experimental values
Parikh (1967)
Tong (1970)

Fig. 5·5

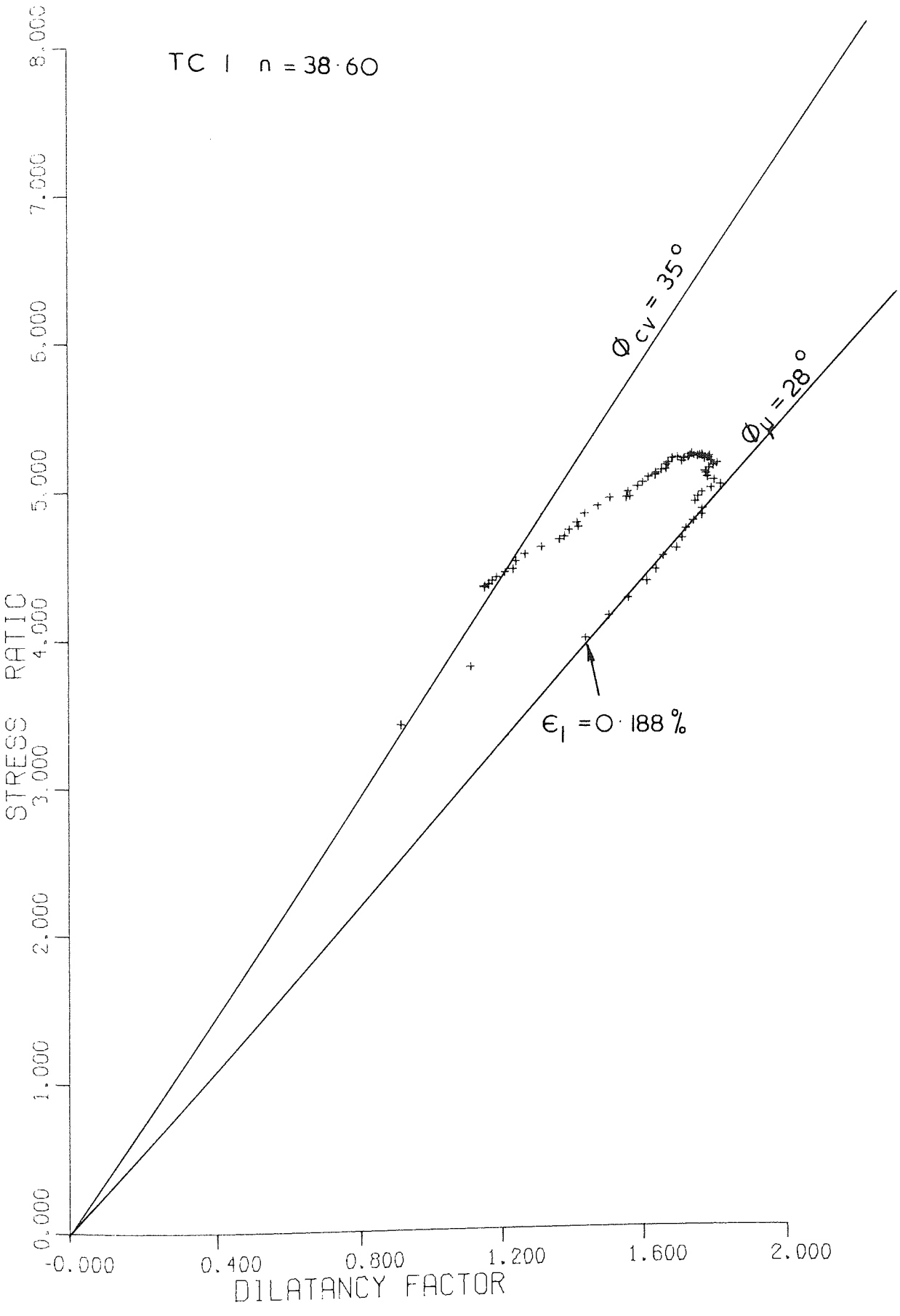
TC 1 n = 38·60
STRESS RATIO
DILATANCY FACTOR
0.000
1.000
2.000
3.000
4.000
5.000
6.000
7.000
8.000
-0.000
0.400
0.800
1.200
1.600
2.000
$\phi_{cv} = 35°$
$\phi_{\mu} = 28°$
$\epsilon_1 = 0 \cdot 188\,\%$

Fig 5·6

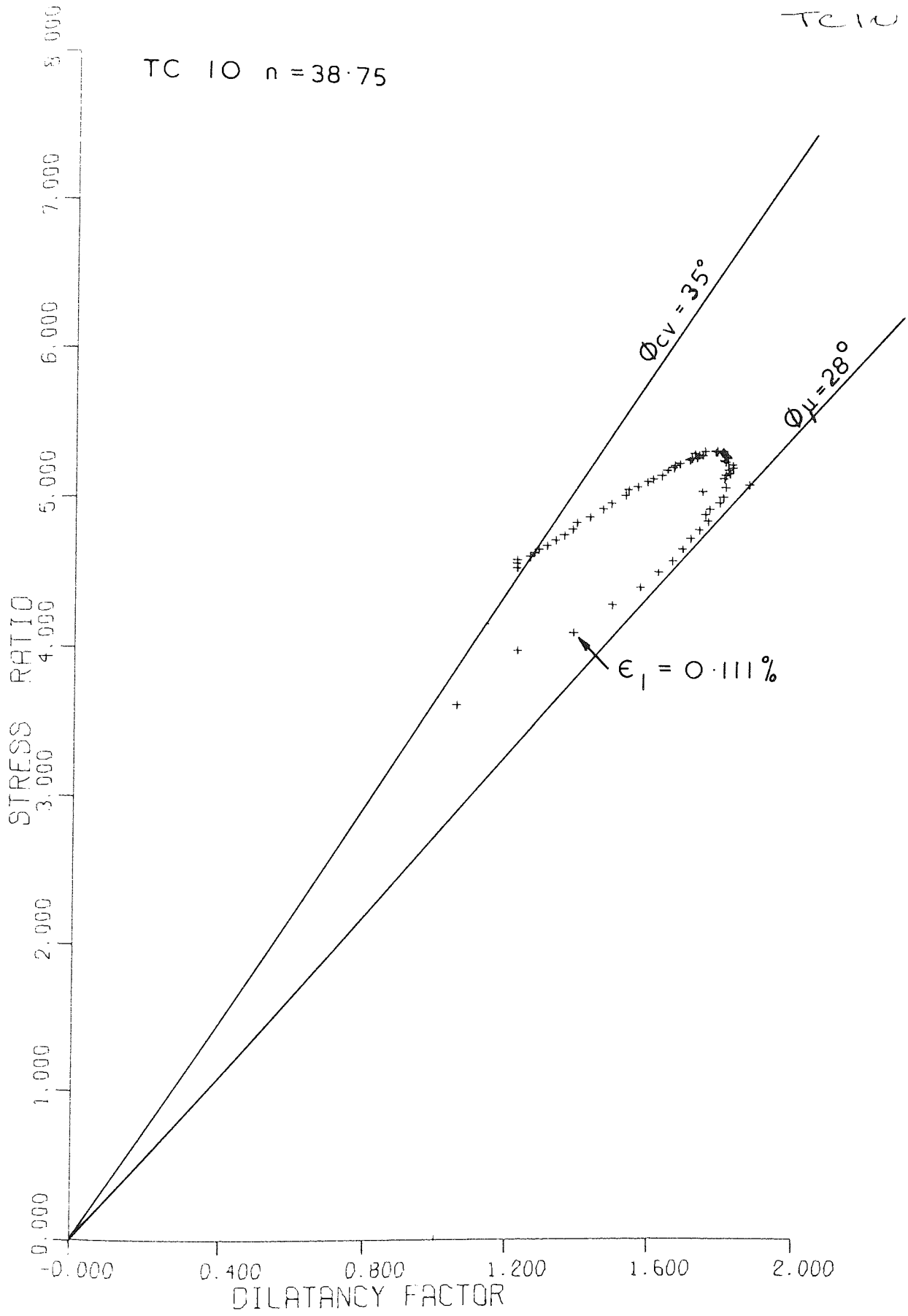
TC 10 n = 38·75
TC 10
$\phi_{cv} = 35°$
$\phi_{\mu} = 28°$
$\epsilon_1 = 0·111\%$
STRESS RATIO
0.000
1.000
2.000
3.000
4.000
5.000
6.000
7.000
8.000
-0.000
0.400
0.800
1.200
1.600
2.000
DILATANCY FACTOR

Fig. 5·7

TC 8

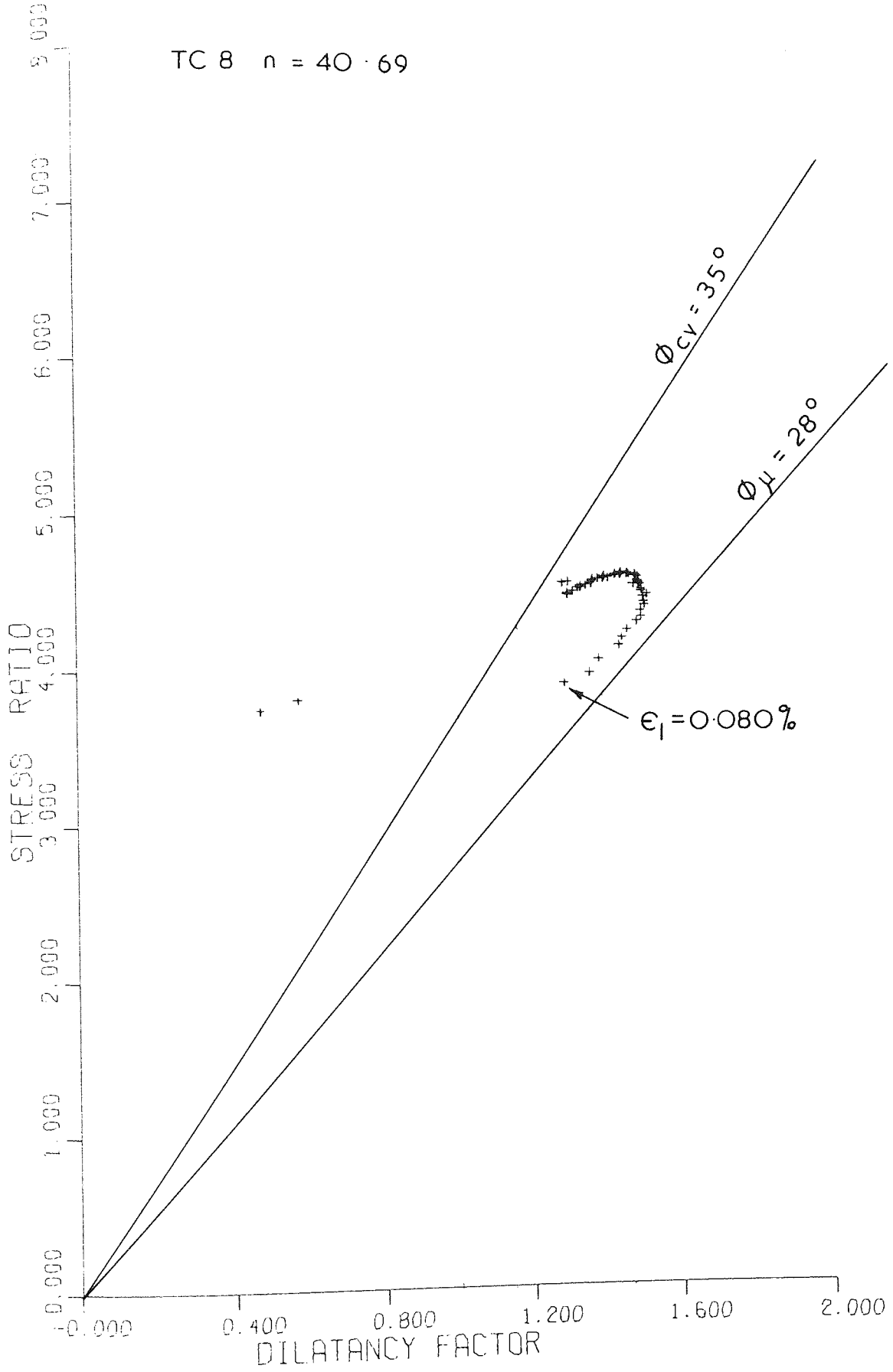
TC 8 n = 40 · 69
STRESS RATIO
DILATANCY FACTOR
0.000
1.000
2.000
3.000
4.000
5.000
6.000
7.000
8.000
-0.000
0.400
0.800
1.200
1.600
2.000
$\phi_{cv} = 35°$
$\phi_{\mu} = 28°$
$\epsilon_1 = 0.080\%$

Fig. 5·8

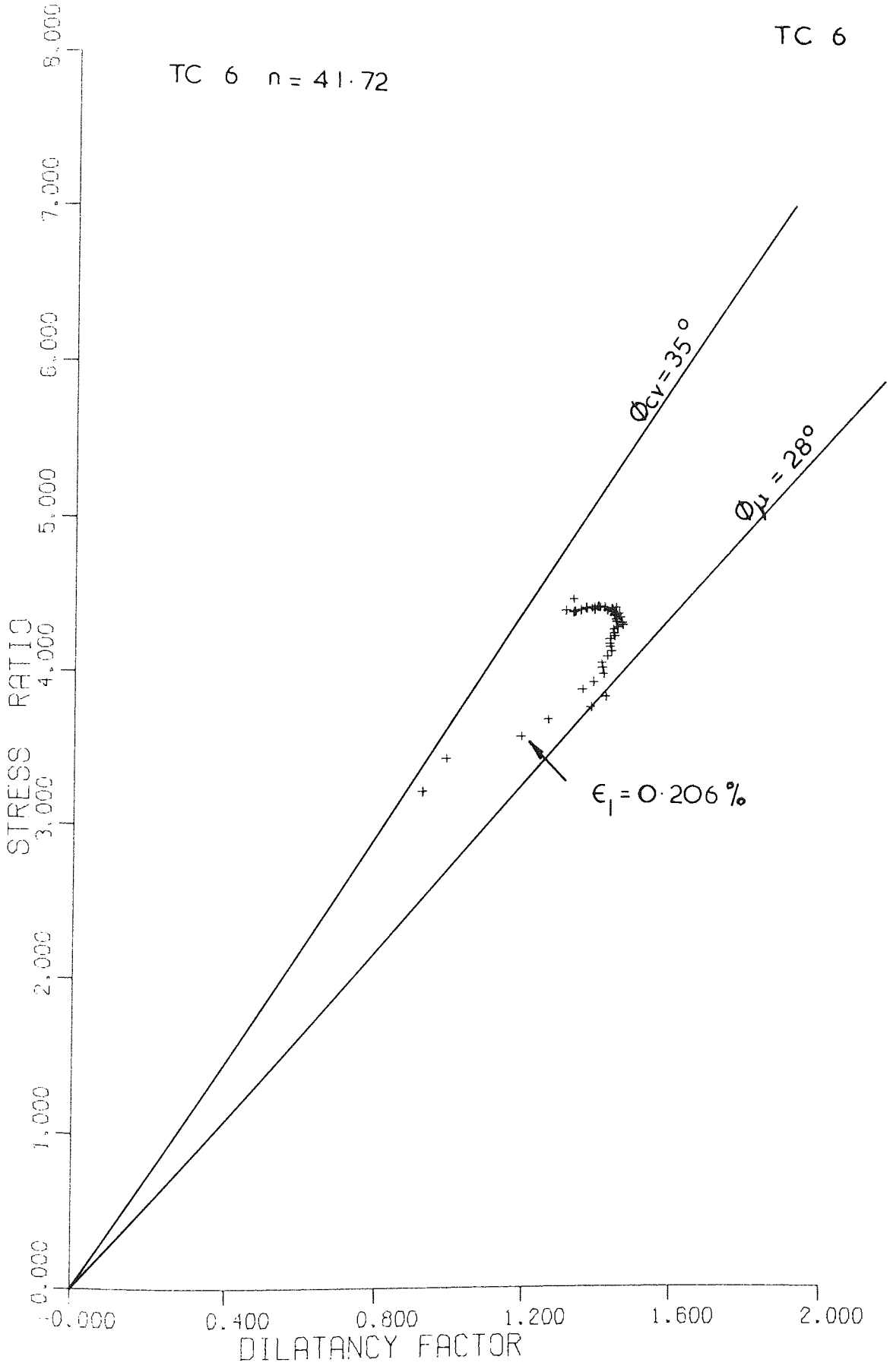
TC 6
TC 6 n = 41·72
STRESS RATIO
DILATANCY FACTOR
0.000
1.000
2.000
3.000
4.000
5.000
6.000
7.000
8.000
-0.000
0.400
0.800
1.200
1.600
2.000
$\phi_{cv} = 35°$
$\phi_{\mu} = 28°$
$\epsilon_1 = 0·206\ \%$

Fig. 5·9

TC5

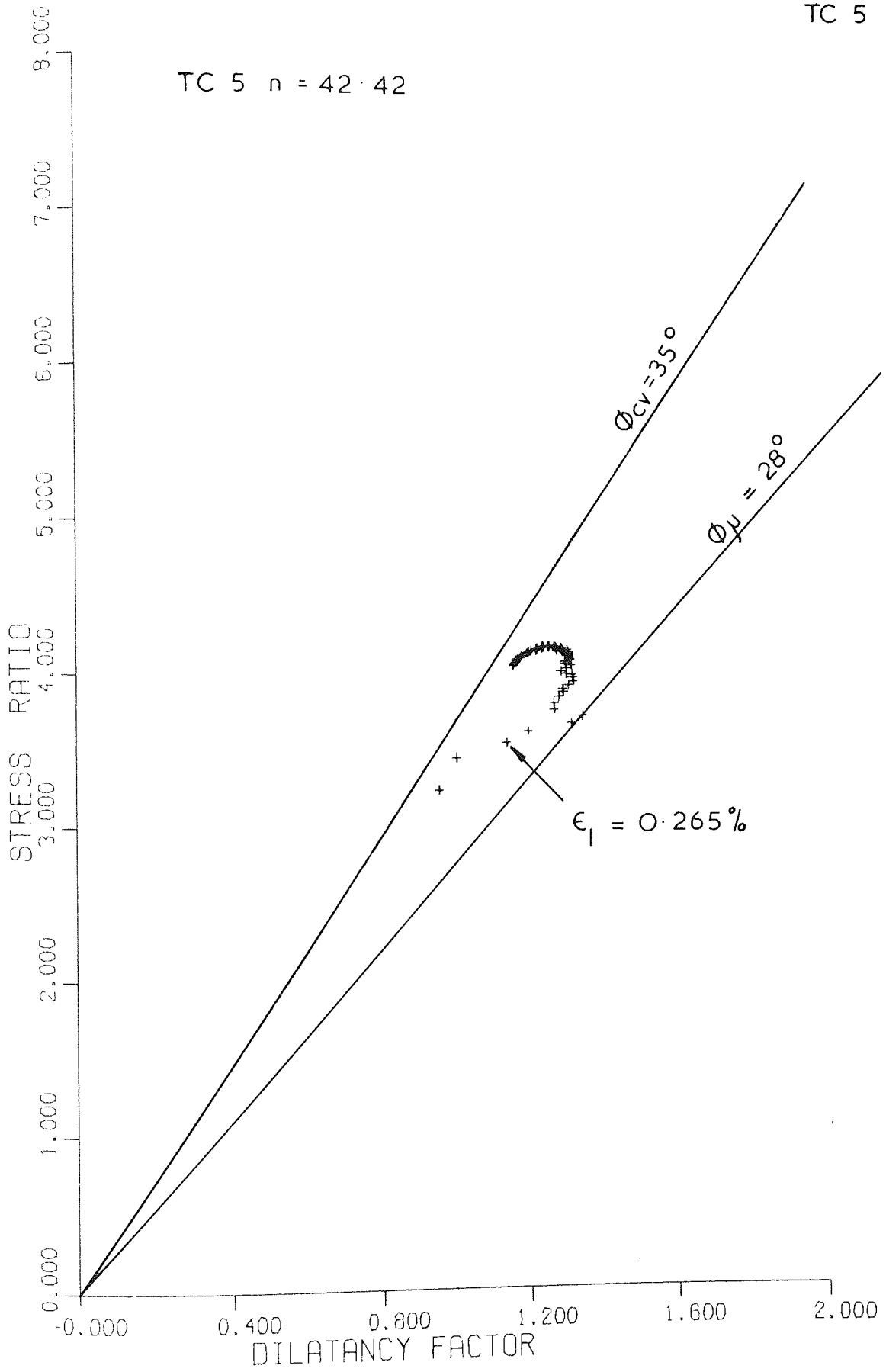
TC 5
TC 5 n = 42·42
STRESS RATIO
0.000
1.000
2.000
3.000
4.000
5.000
6.000
7.000
8.000
-0.000
0.400
0.800
1.200
1.600
2.000
DILATANCY FACTOR
Øcv=35°
Øμ = 28°
ε1 = 0·265%

Fig. 5·10

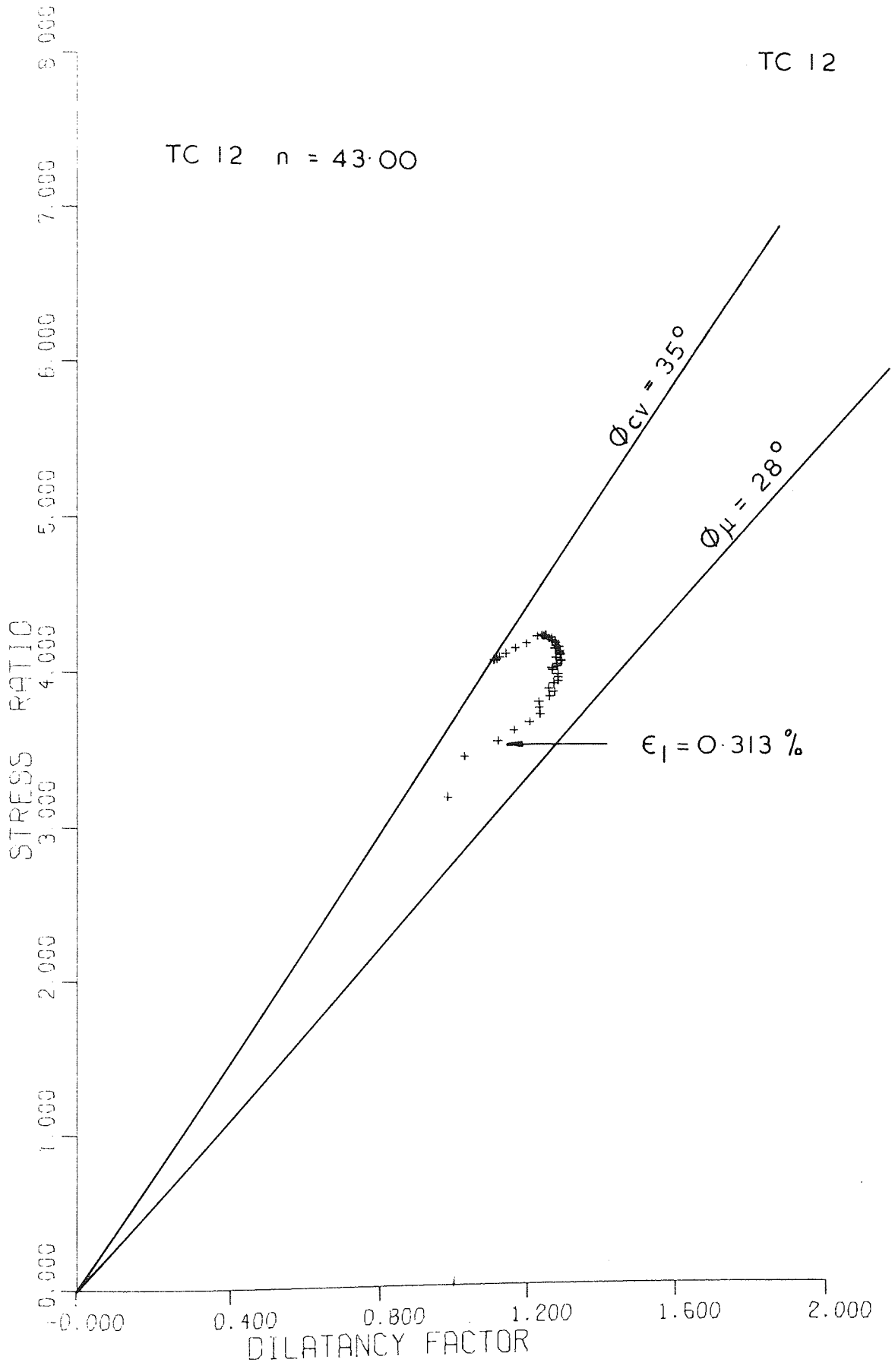
TC 12
TC 12 n = 43·00
$\phi_{cv} = 35°$
$\phi_{\mu} = 28°$
$\epsilon_1 = 0·313\ \%$
STRESS RATIO
0.000
1.000
2.000
3.000
4.000
5.000
6.000
7.000
8.000
-0.000
0.400
0.800
1.200
1.600
2.000
DILATANCY FACTOR

Fig. 5·11

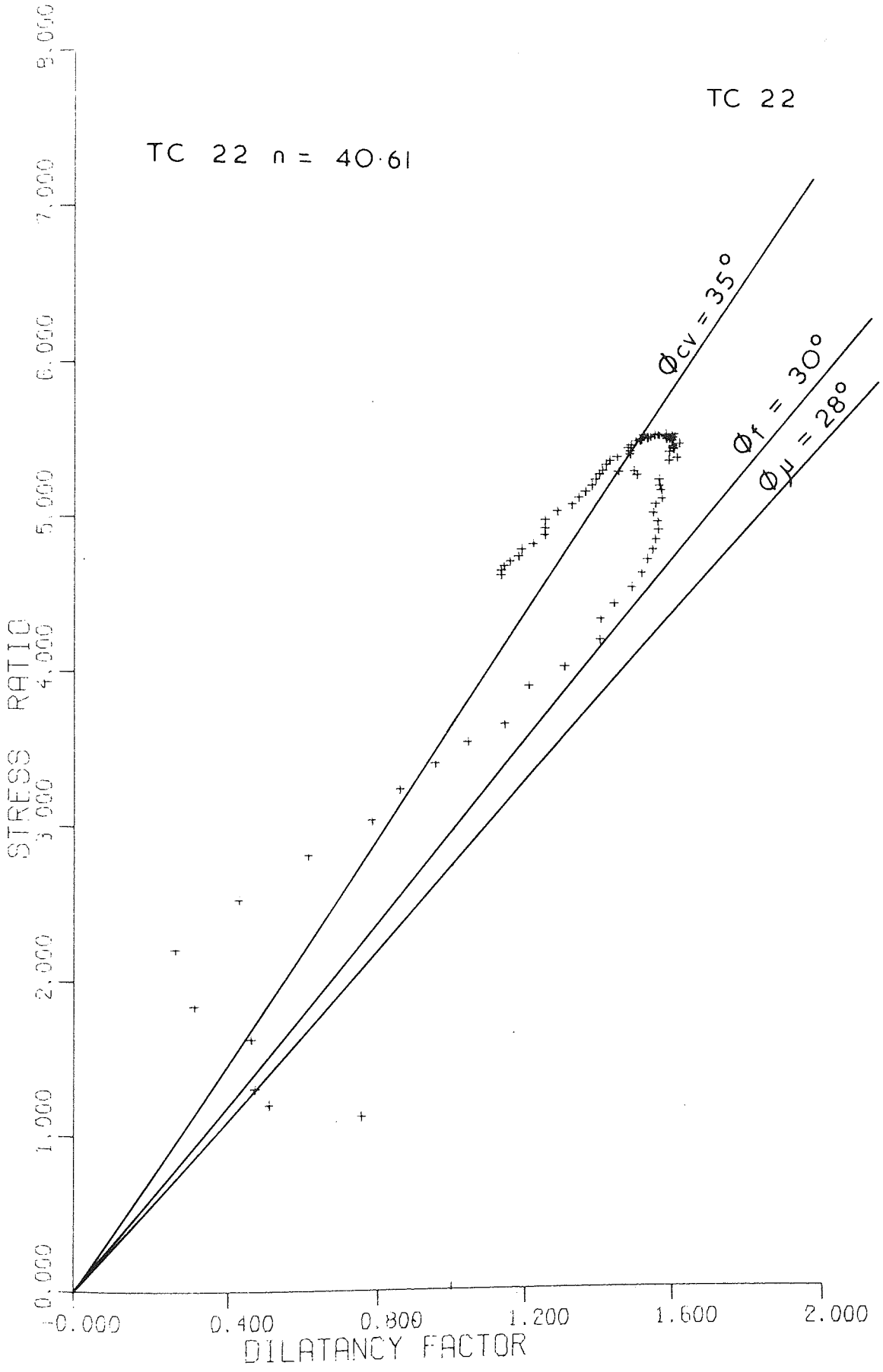
TC 22
TC 22 n = 40·61
$\phi_{cv} = 35°$
$\phi_f = 30°$
$\phi_\mu = 28°$
STRESS RATIO
0.000
1.000
2.000
3.000
4.000
5.000
6.000
7.000
8.000
0.000
0.400
0.800
1.200
1.600
2.000
DILATANCY FACTOR

Fig. 5·12

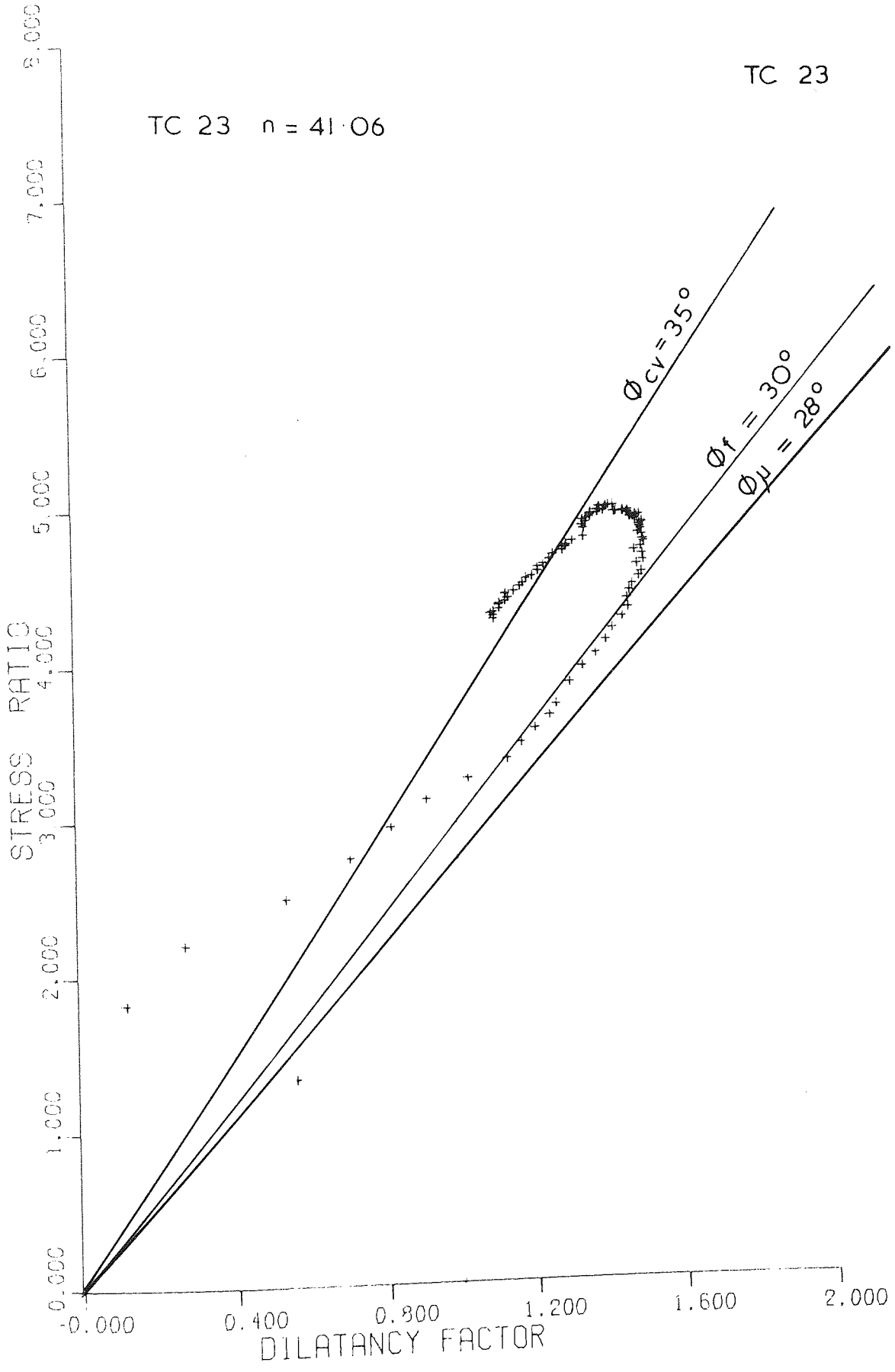
TC 23
TC 23 n = 41·06
STRESS RATIO
DILATANCY FACTOR
0.000
1.000
2.000
3.000
4.000
5.000
6.000
7.000
8.000
-0.000
0.400
0.800
1.200
1.600
2.000
Ø cv = 35°
Øf = 30°
Øμ = 28°

Fig. 5·13

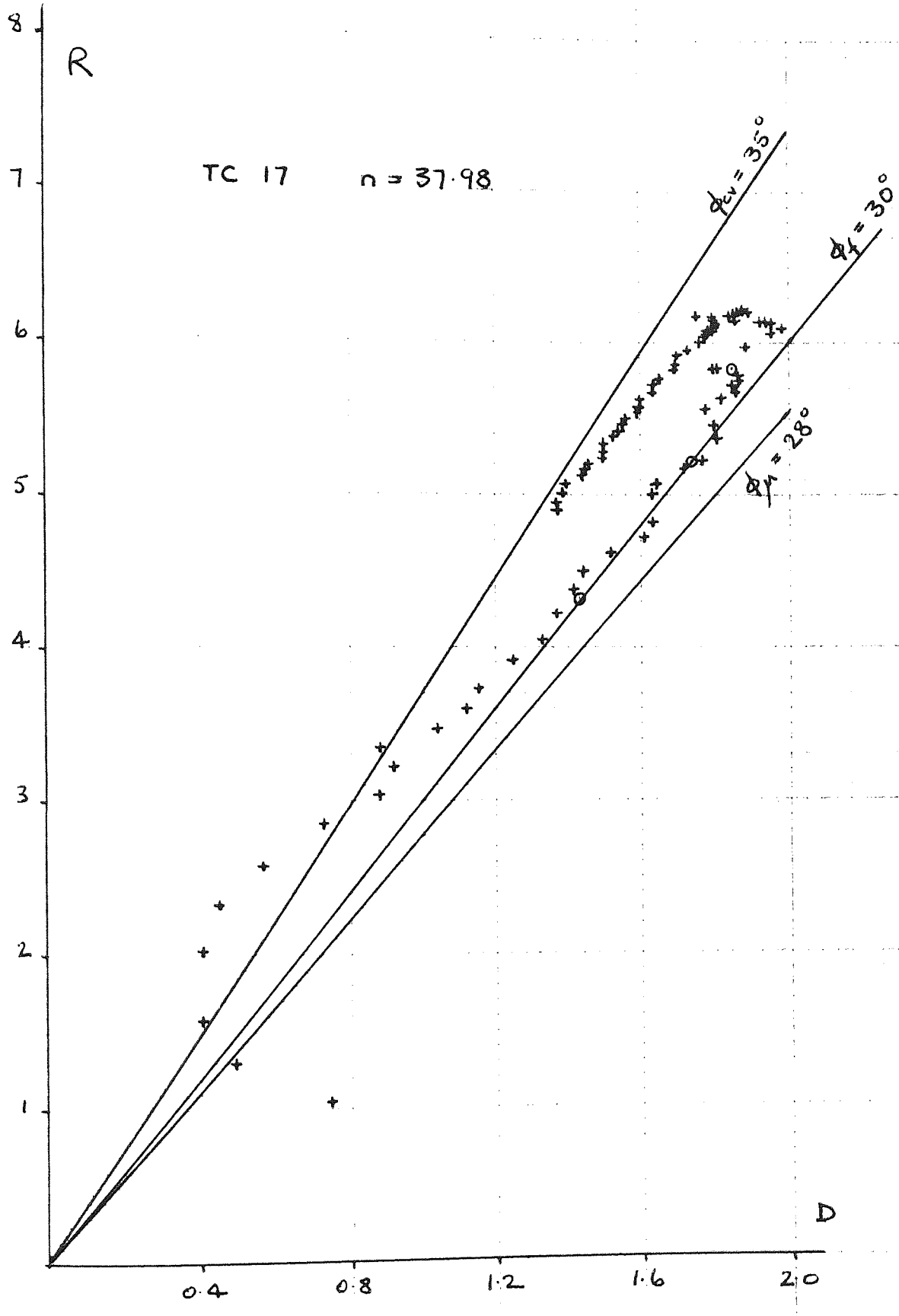

FIG. 5.14

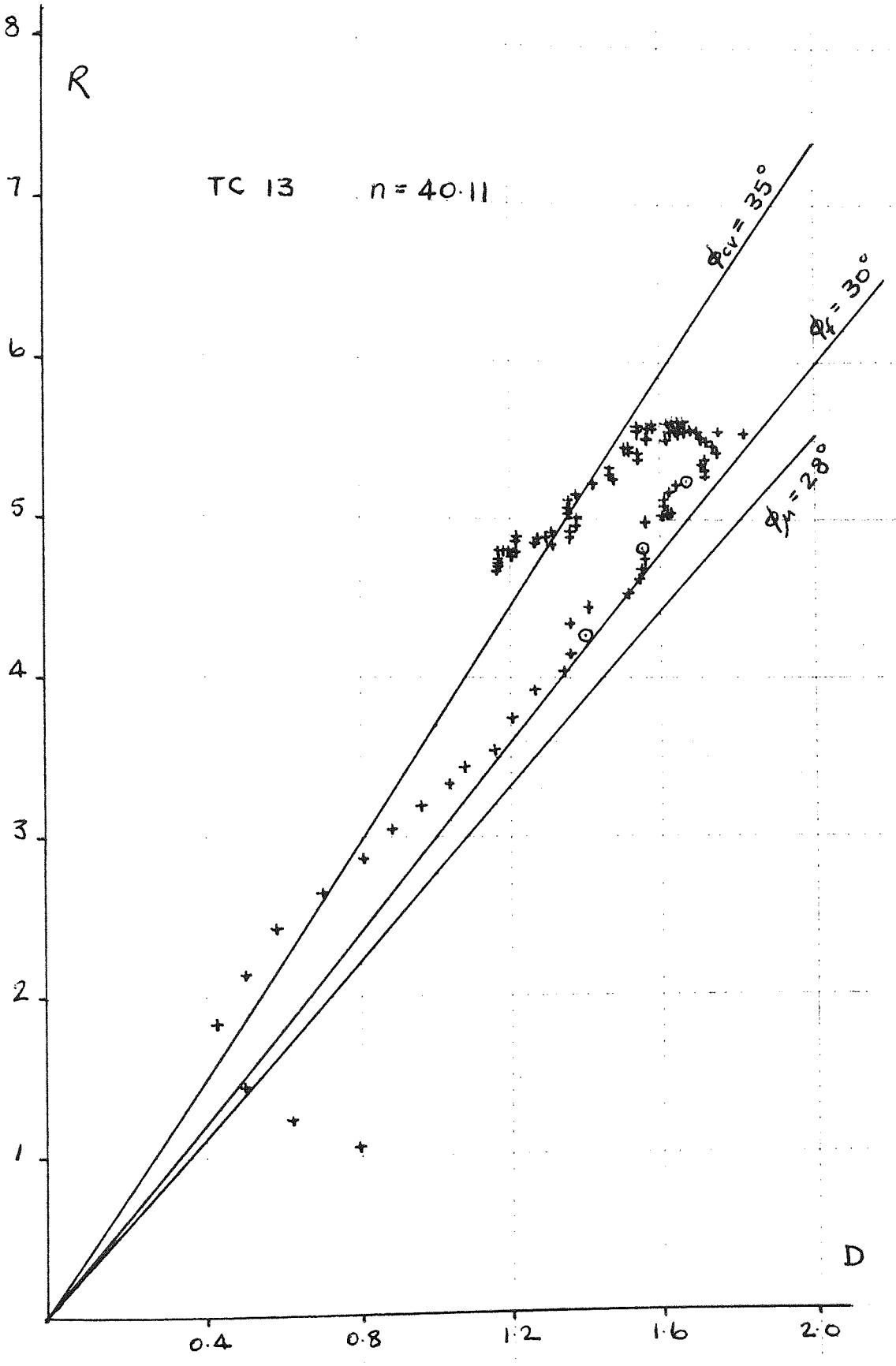

FIG. 5.15

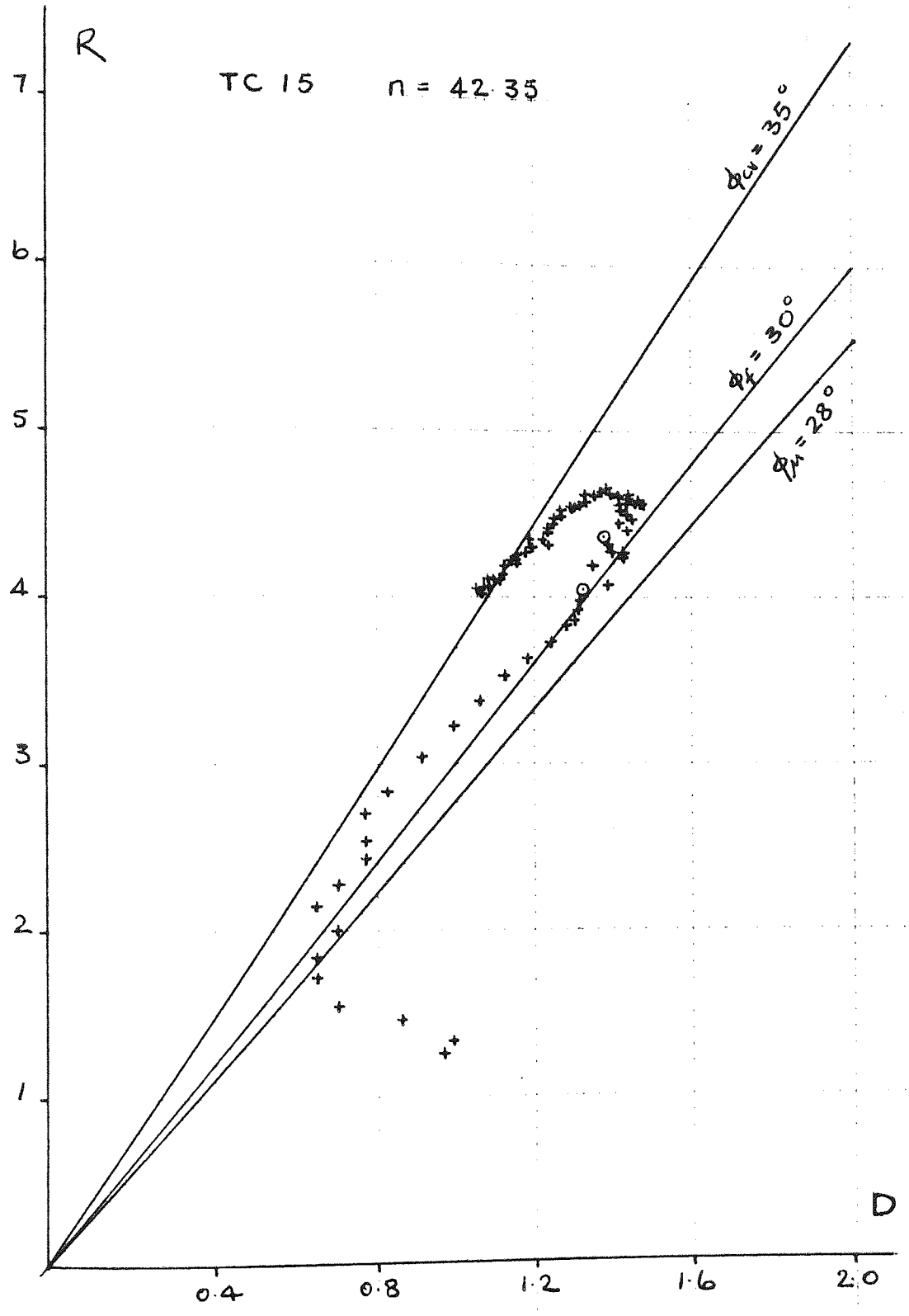

FIG. 5.16

FIG. 5.17

TC 15

2ND. RELOAD

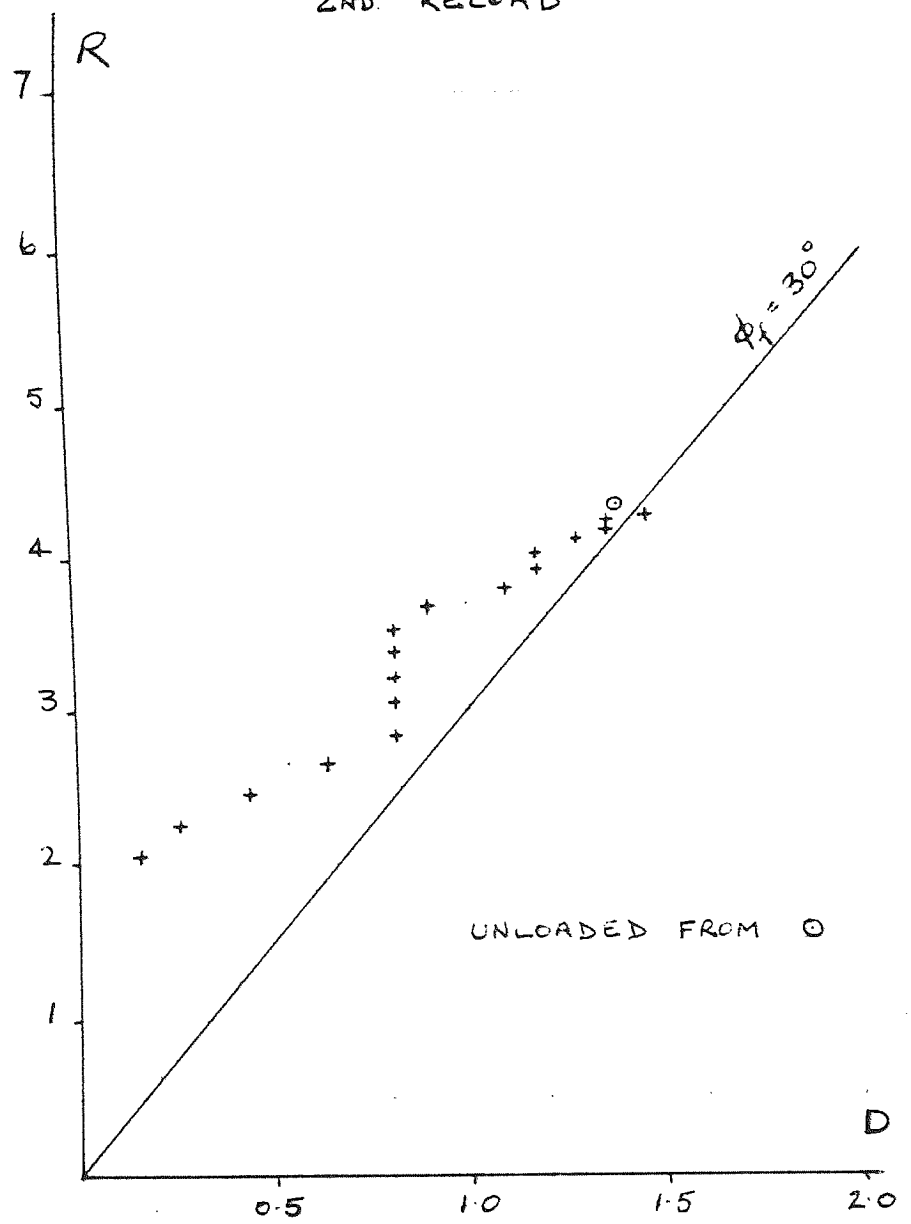

TC 17

3RD. RELOAD

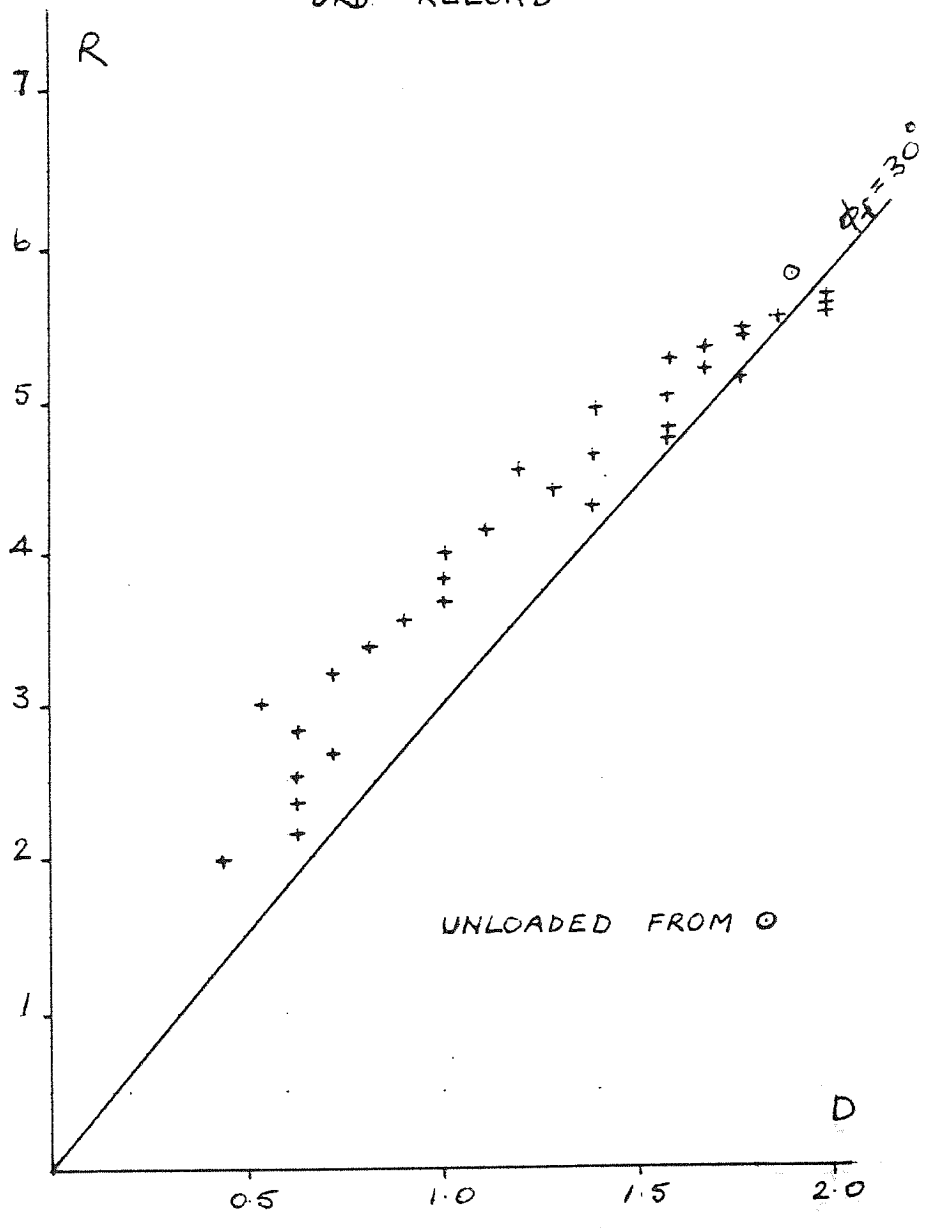

FIG. 5.18

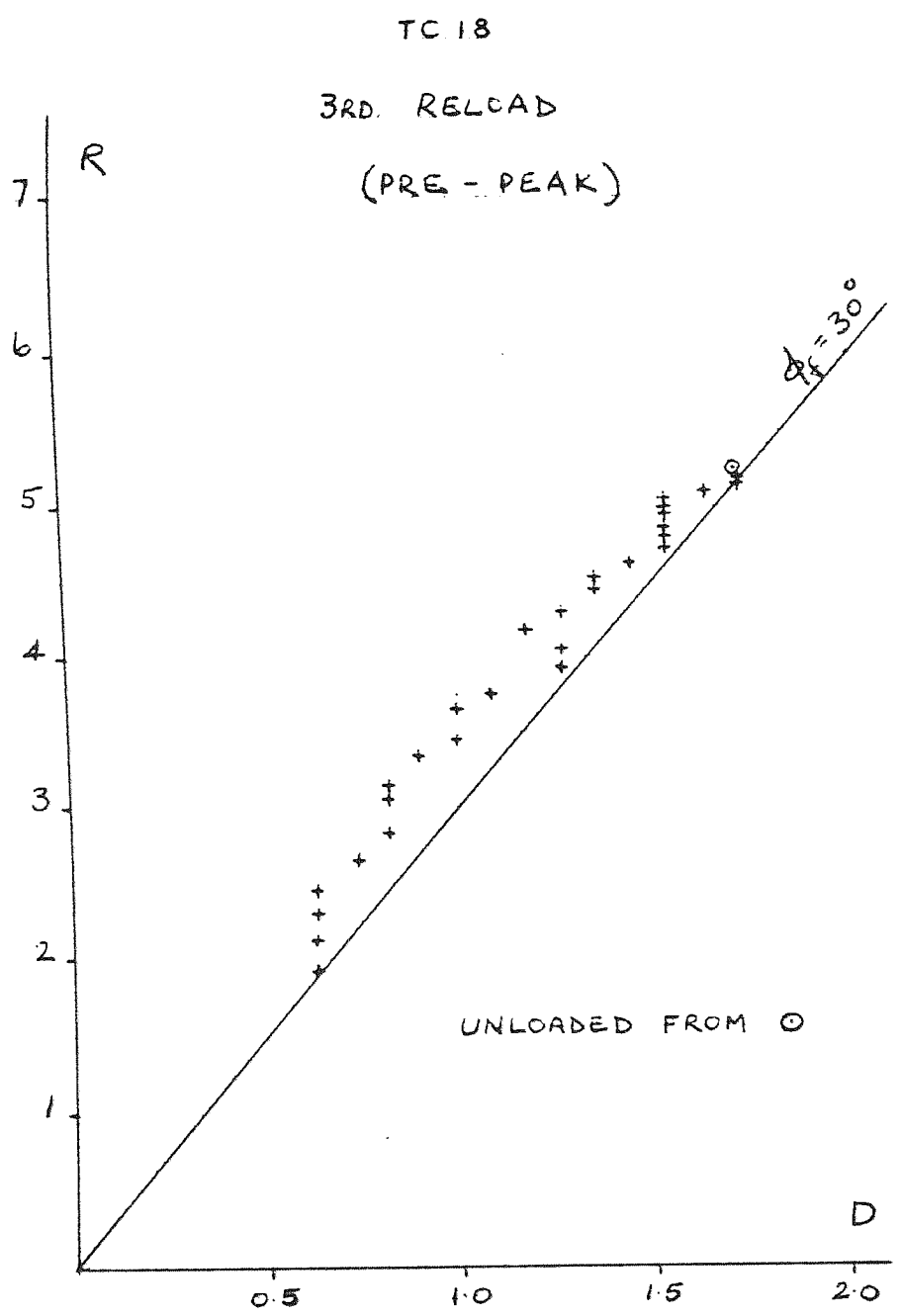
TC 18
3RD. RELOAD
(PRE - PEAK)
R
D
$\phi_f = 30^\circ$
UNLOADED FROM ⊙
1
2
3
4
5
6
7
0·5
1·0
1·5
2·0

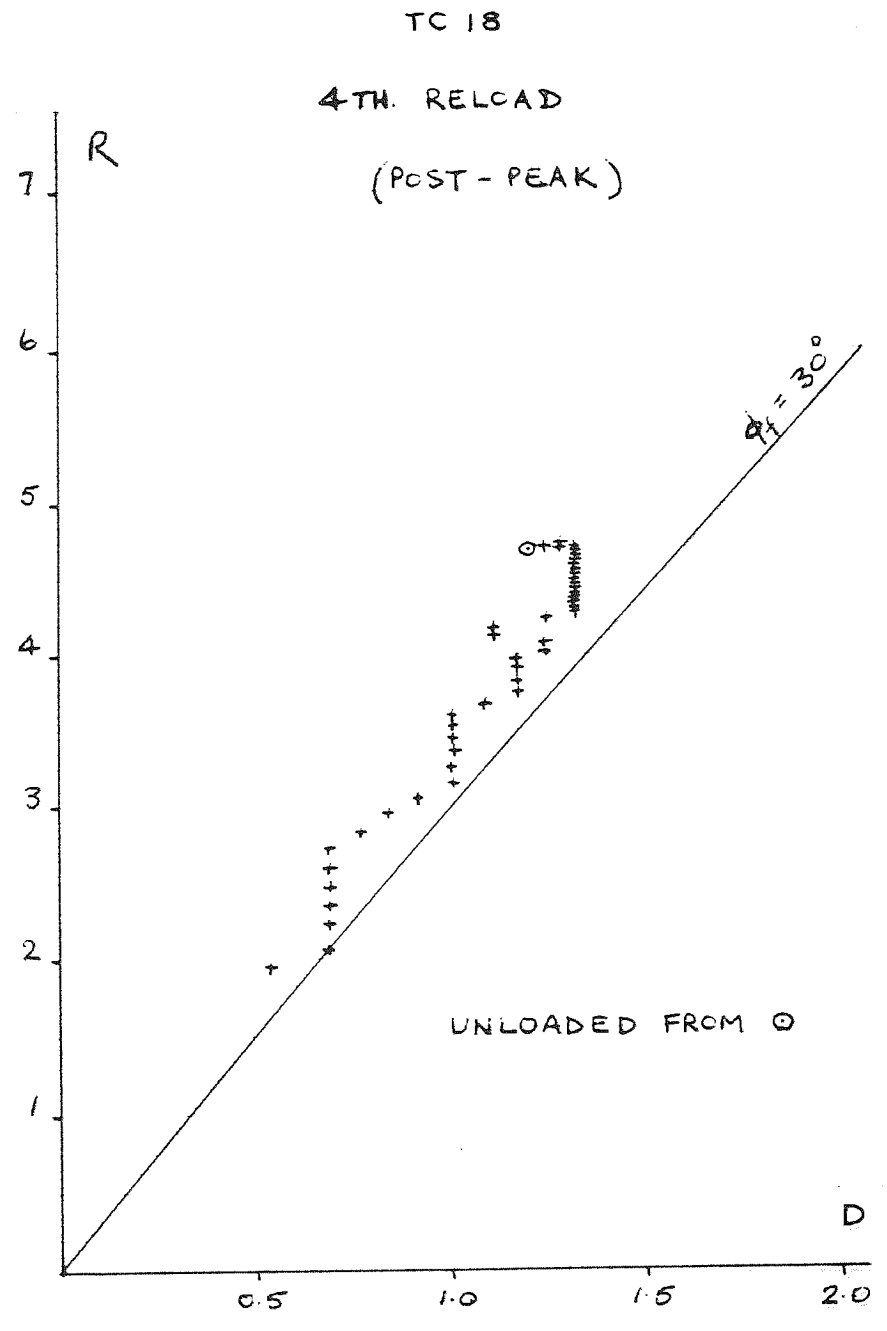
TC 18
4TH. RELOAD
(POST - PEAK)
R
D
$\phi_f = 30^\circ$
UNLOADED FROM ⊙
1
2
3
4
5
6
7
0·5
1·0
1·5
2·0

FIG. 5.19

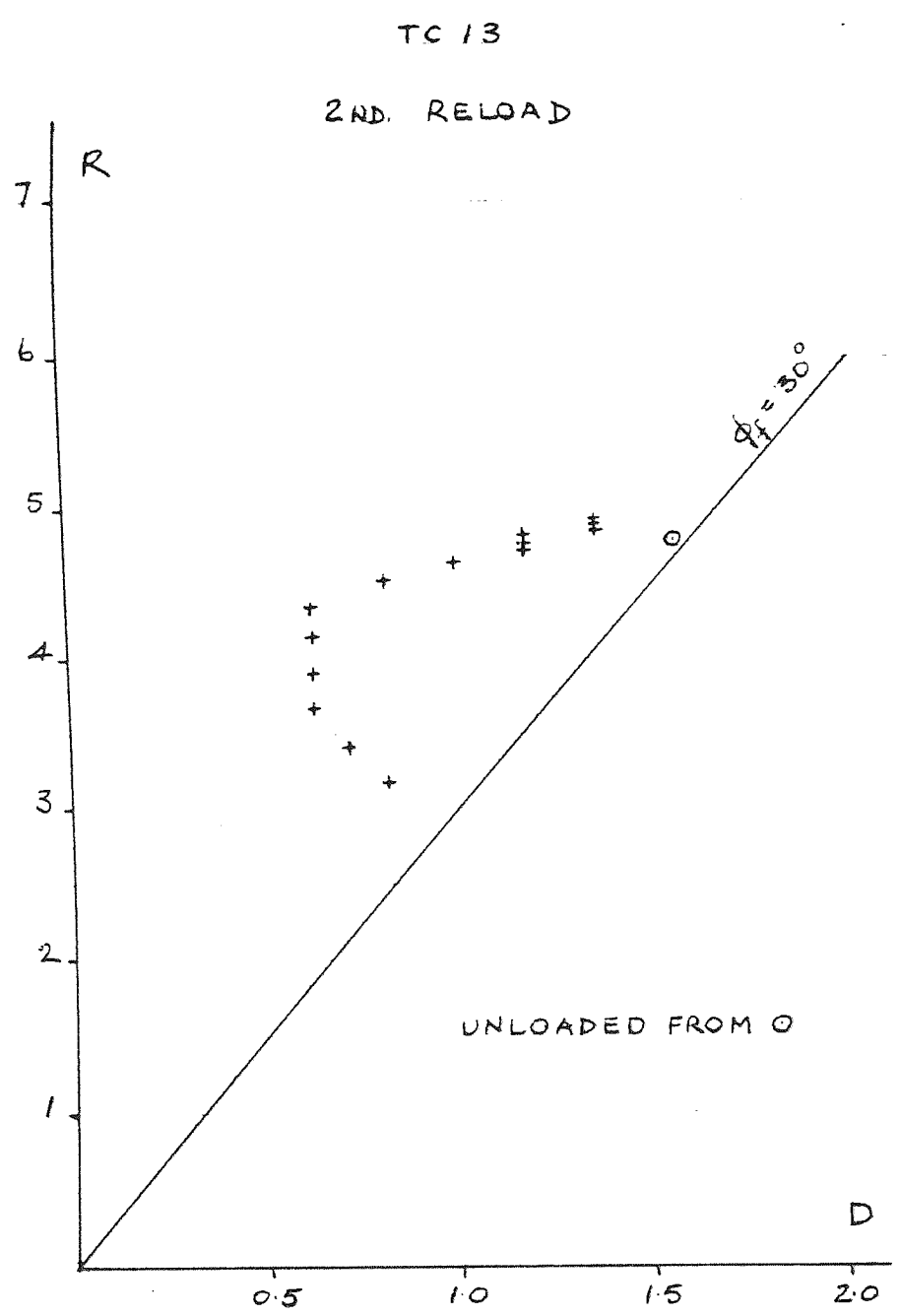
TC 13
2ND. RELOAD
R
7
6
5
4
3
2
1
$\phi_f = 30^\circ$
UNLOADED FROM O
D
0·5
1·0
1·5
2·0

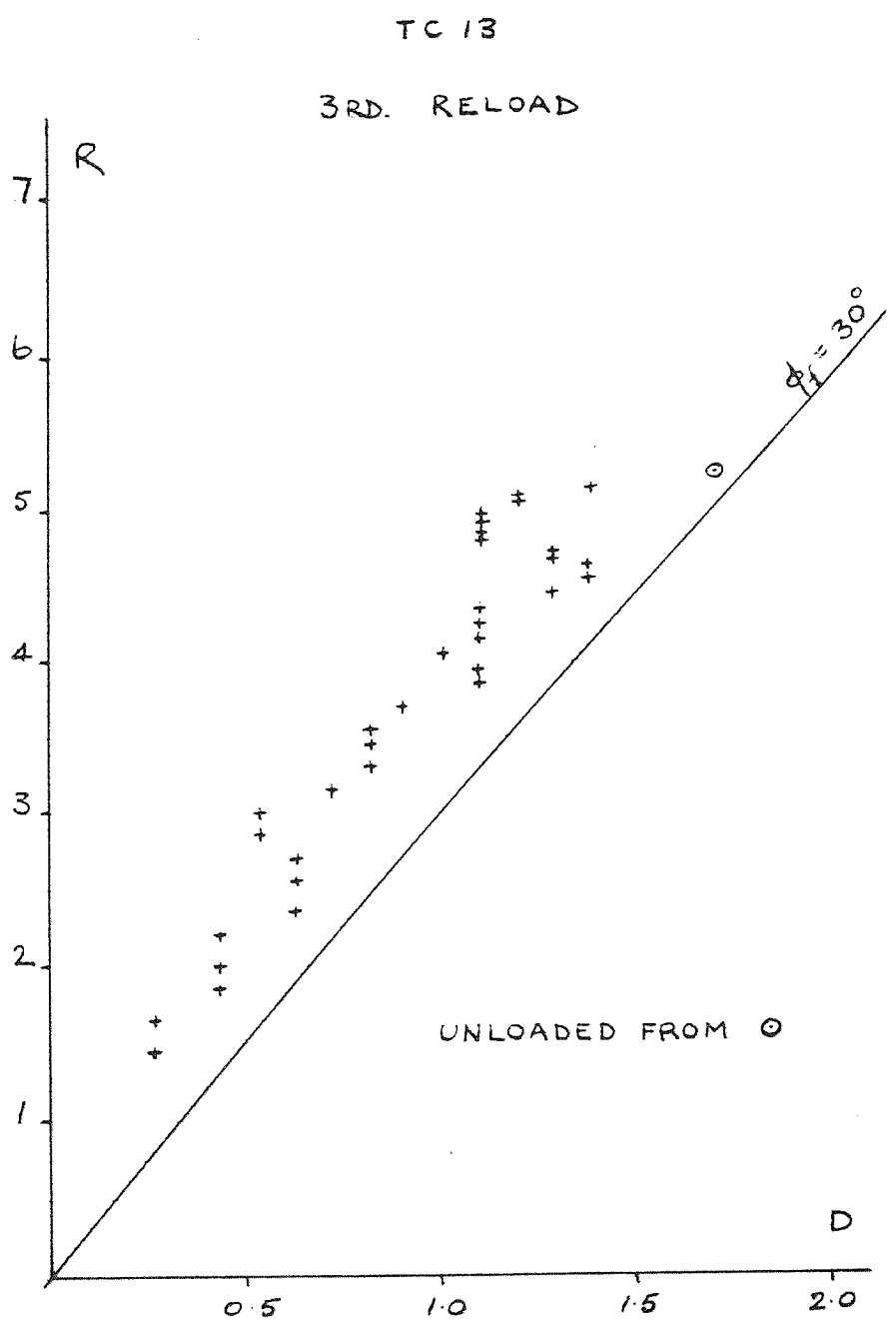
TC 13
3RD. RELOAD
R
7
6
5
4
3
2
1
$\phi_f = 30^\circ$
UNLOADED FROM O
D
0·5
1·0
1·5
2·0

P.S. 2

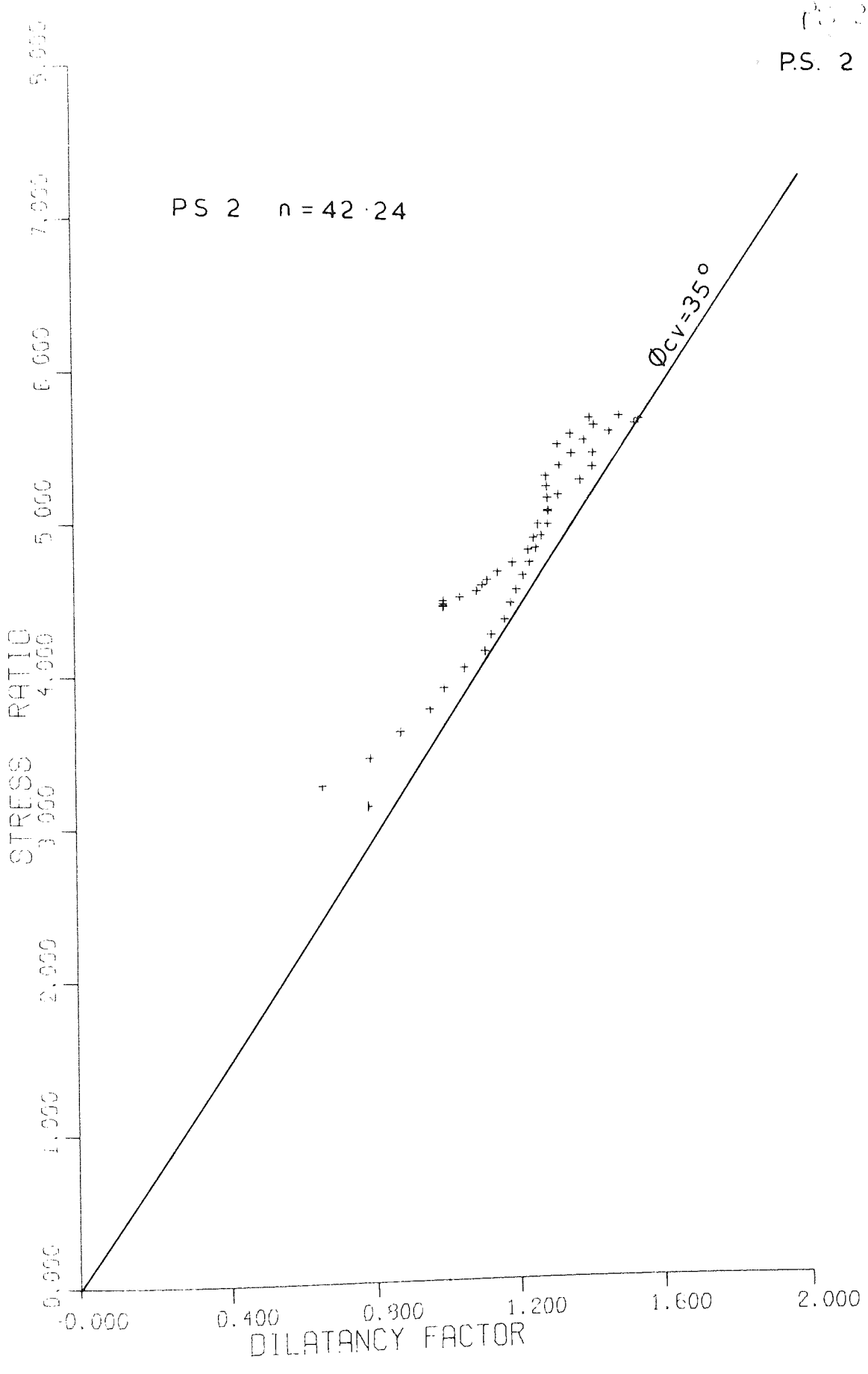
PS 2 n = 42 24
Øcv=35°
STRESS RATIO
5.000
4.000
3.000
2.000
-0.000
0.400
0.800
1.200
1.600
2.000
DILATANCY FACTOR

Fig. 20

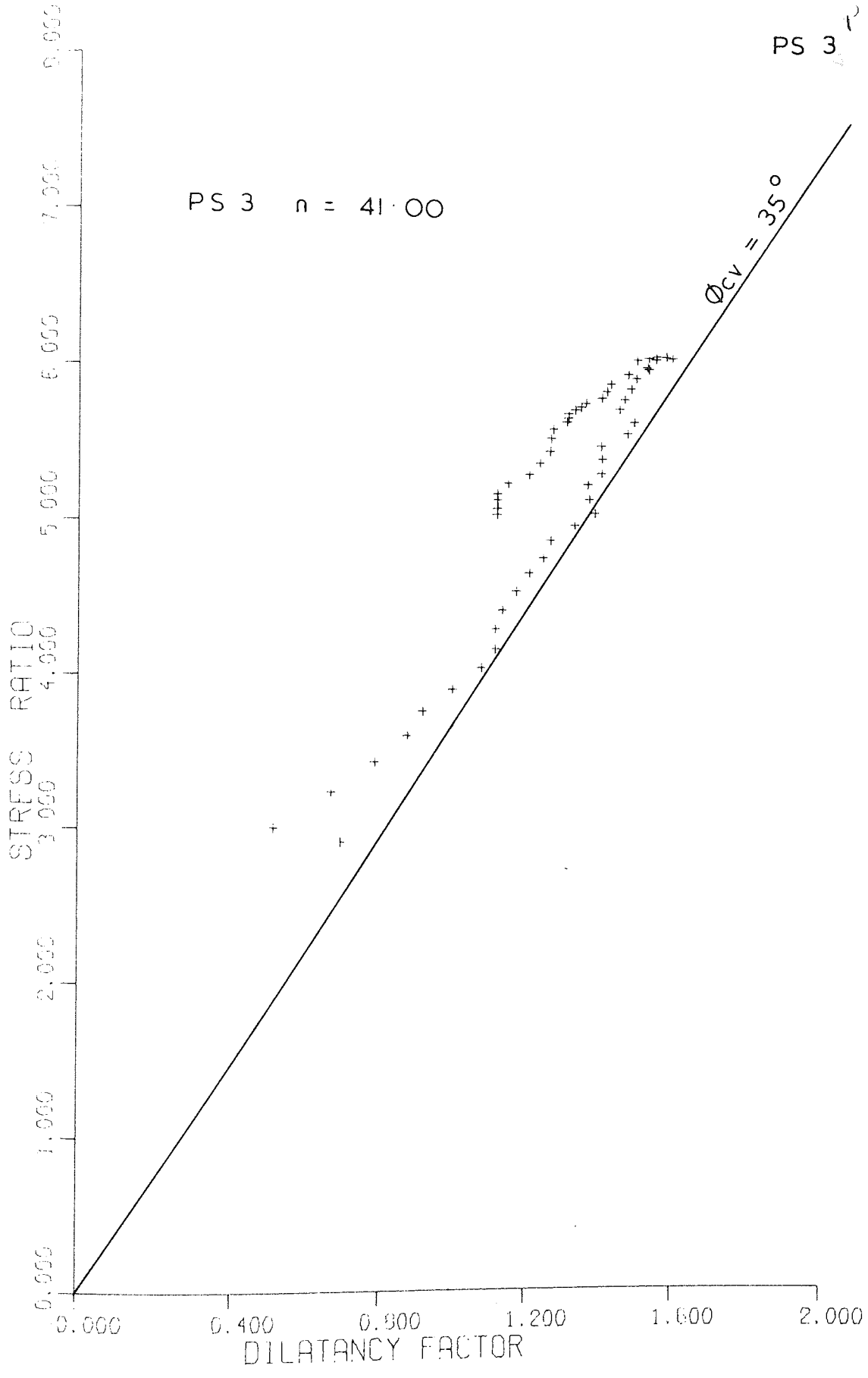
PS 3
PS 3 n = 41.00
Øcv = 35°
STRESS RATIO
0.000
1.000
2.000
3.000
4.000
5.000
6.000
7.000
8.000
0.000
0.400
0.800
1.200
1.600
2.000
DILATANCY FACTOR

Fig. 5.21

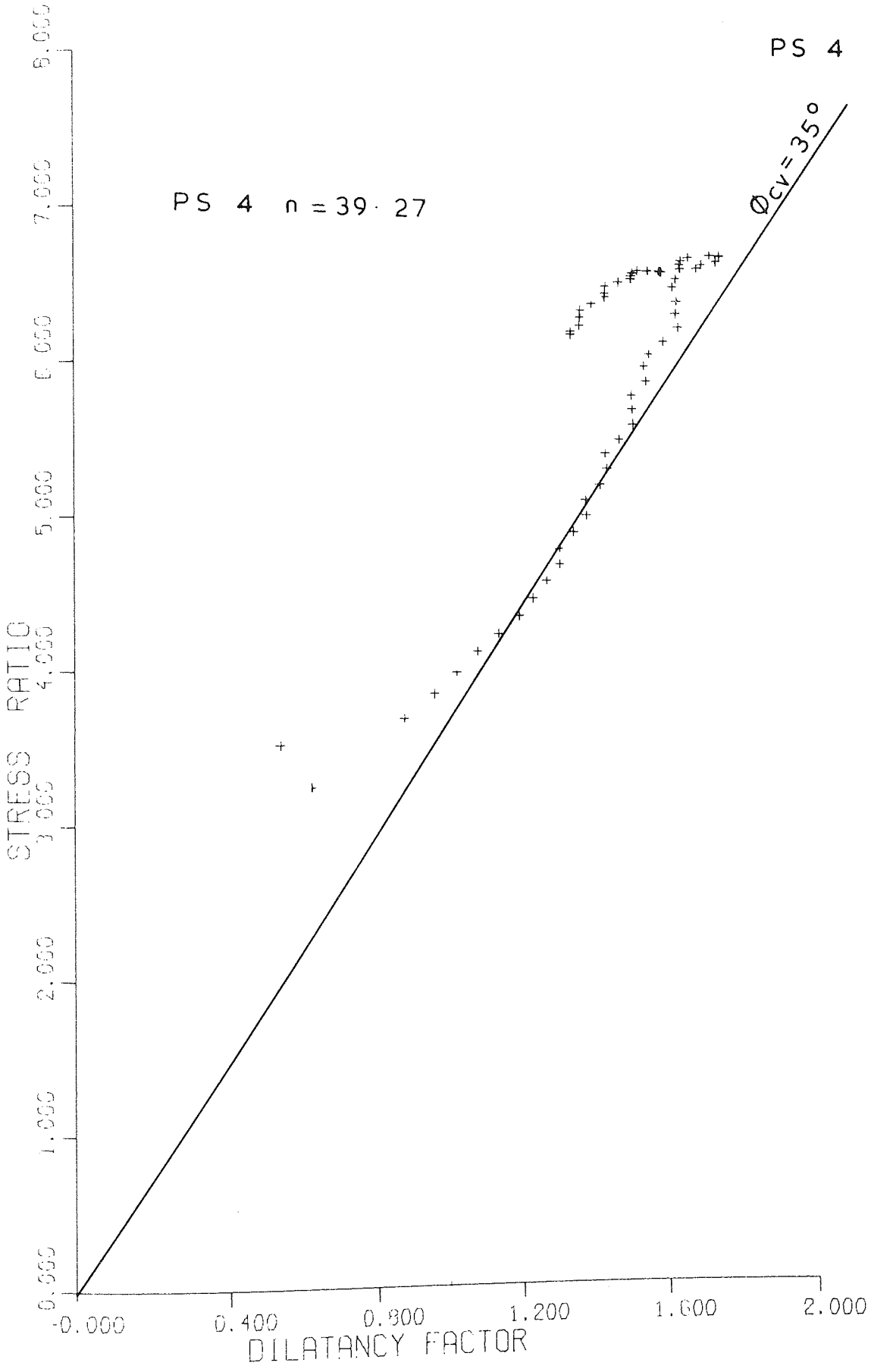
PS 4
PS 4 n = 39.27
Øcv = 35°
STRESS RATIO
DILATANCY FACTOR
-0.000
0.400
0.800
1.200
1.600
2.000

Fig. 5·22

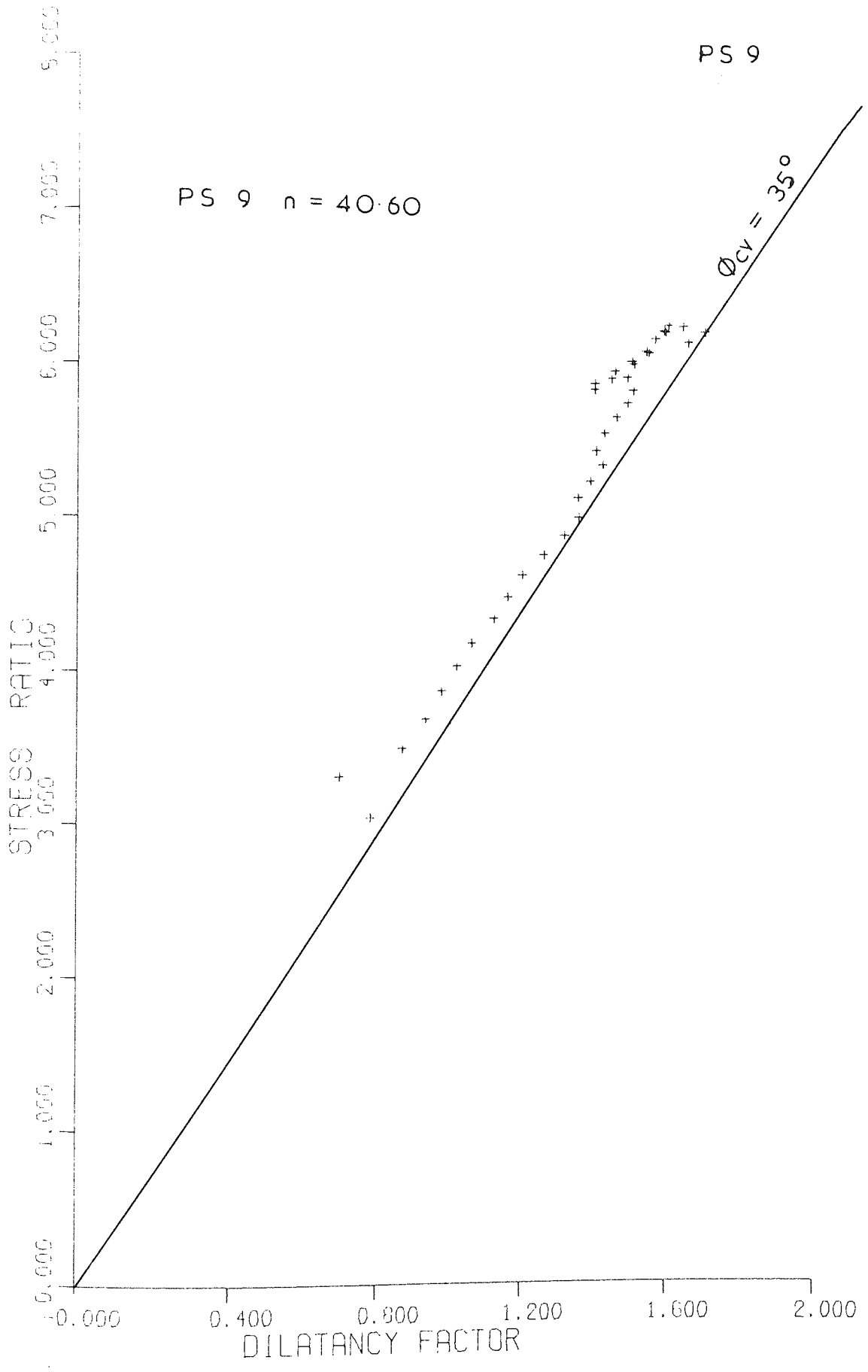
PS 9
PS 9 n = 40·60
ϕ_{cv} = 35°
STRESS RATIO
0.000
1.000
2.000
3.000
4.000
5.000
6.000
7.000
0.000
0.400
0.800
1.200
1.600
2.000
DILATANCY FACTOR

Fig. 5·23

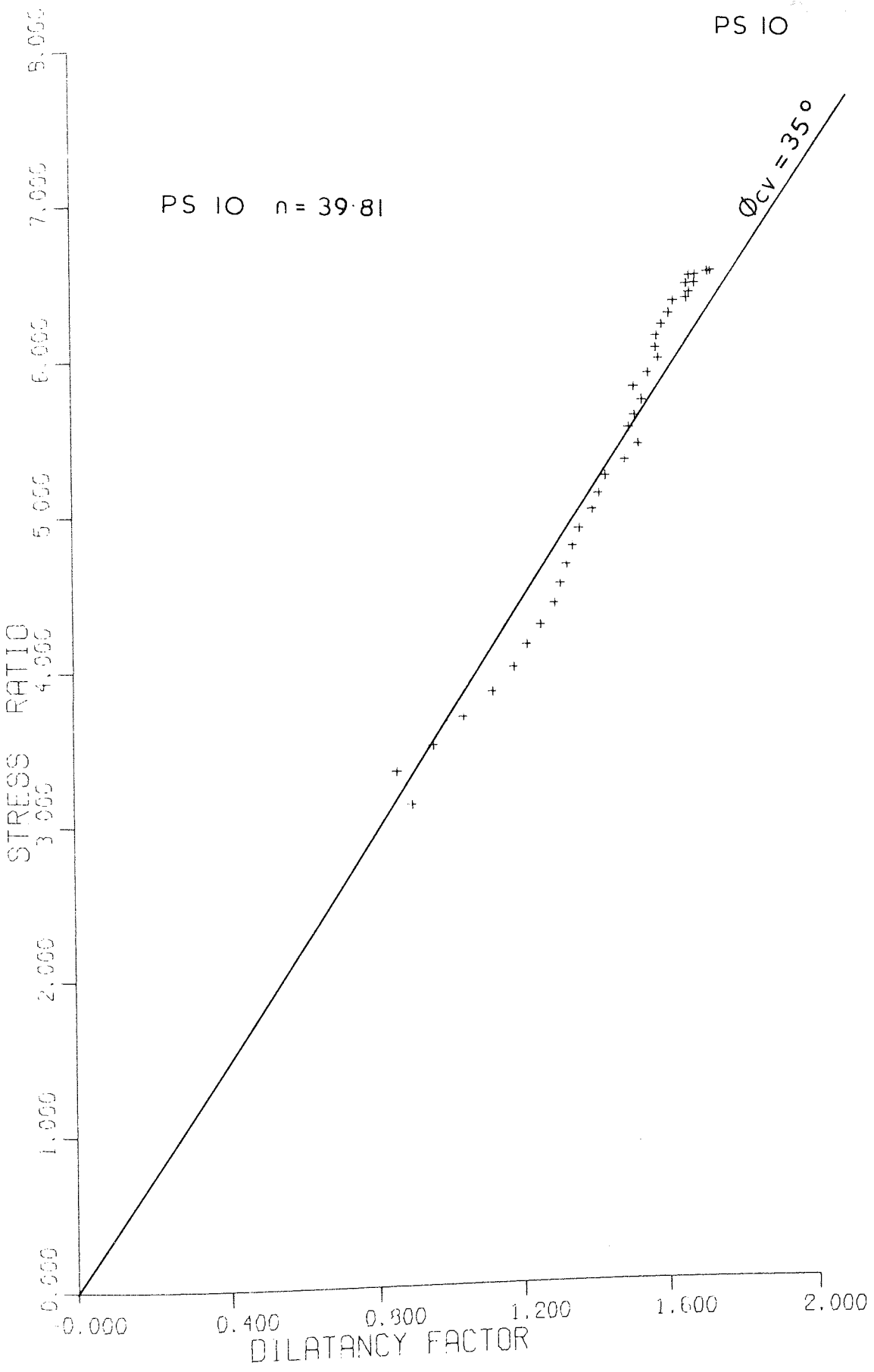
PS 10
PS 10 n = 39·81
Øcv = 35°
STRESS RATIO
1.000
2.000
3.000
4.000
5.000
6.000
7.000
0.000
0.400
0.800
1.200
1.600
2.000
DILATANCY FACTOR

Fig 5·24

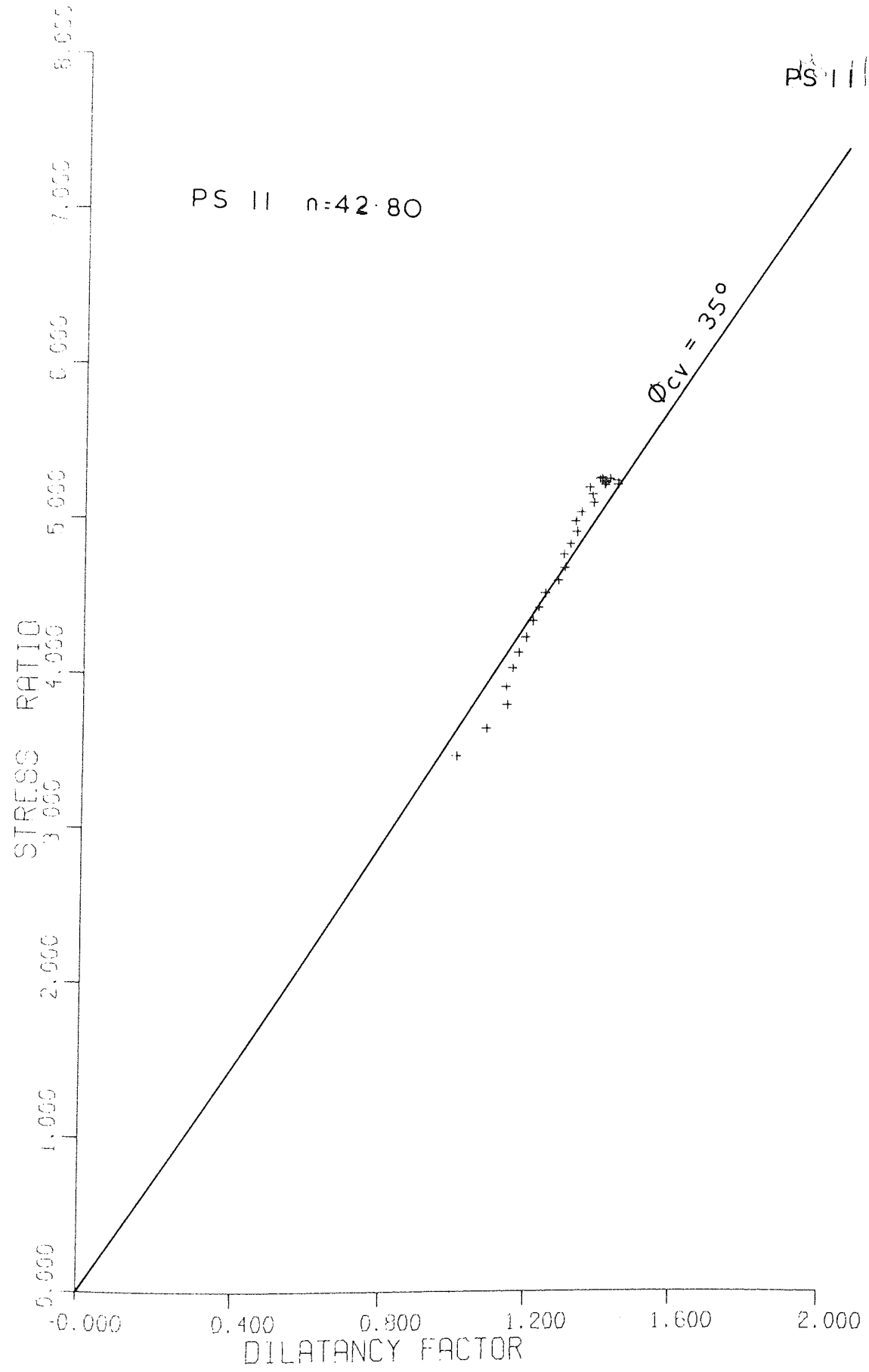
PS II
PS II n=42·80
Øcv = 35°
STRESS RATIO
5.000
4.000
3.000
2.000
1.000
0.000
-0.000
0.400
0.800
1.200
1.600
2.000
DILATANCY FACTOR

Fig 5·25

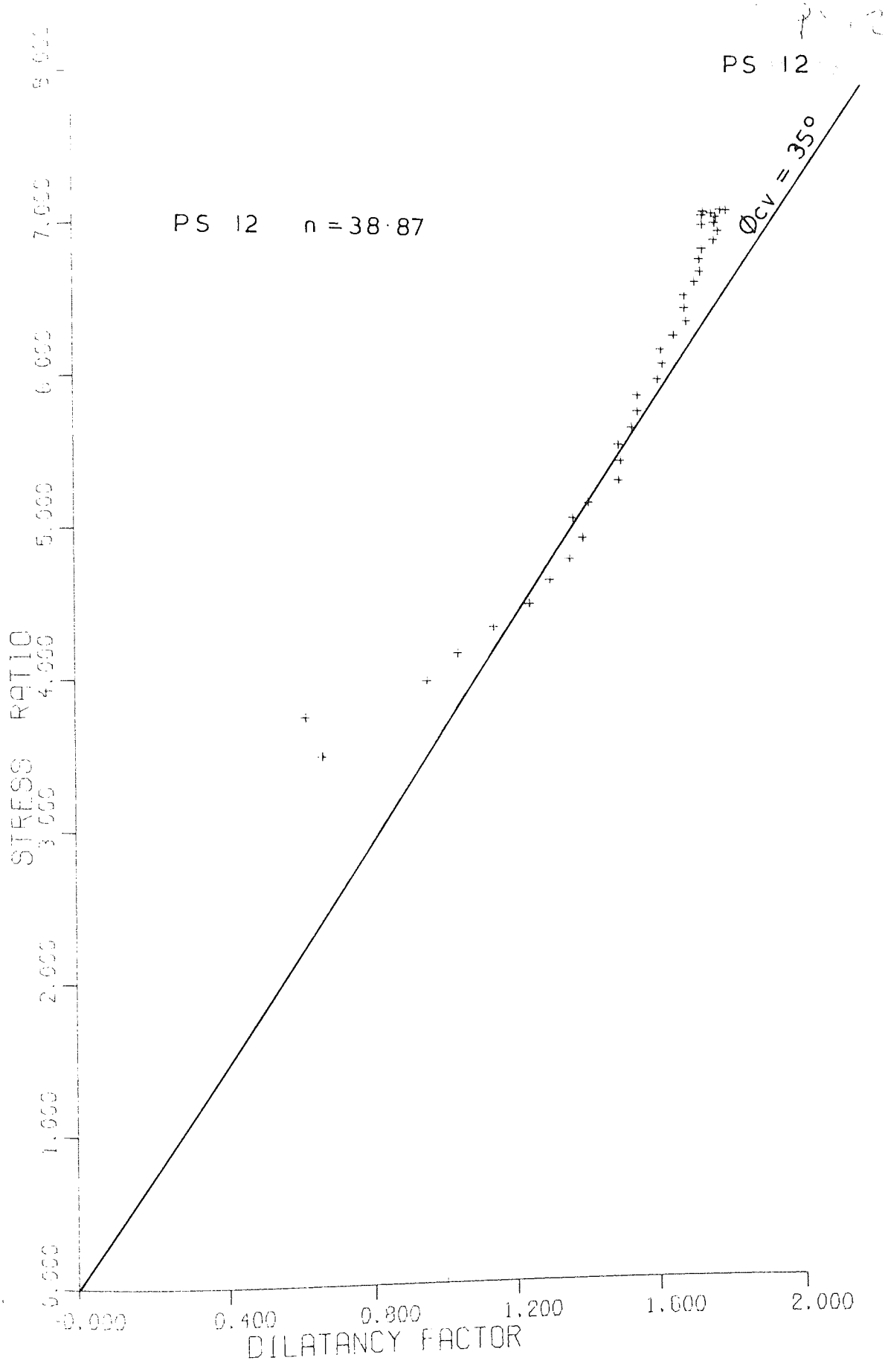
PS 12
PS 12 n = 38·87
Øcv = 35°
STRESS RATIO
4.000
3.000
2.000
1.000
0.000
0.400
0.800
1.200
1.600
2.000
DILATANCY FACTOR

Fig. 5·26

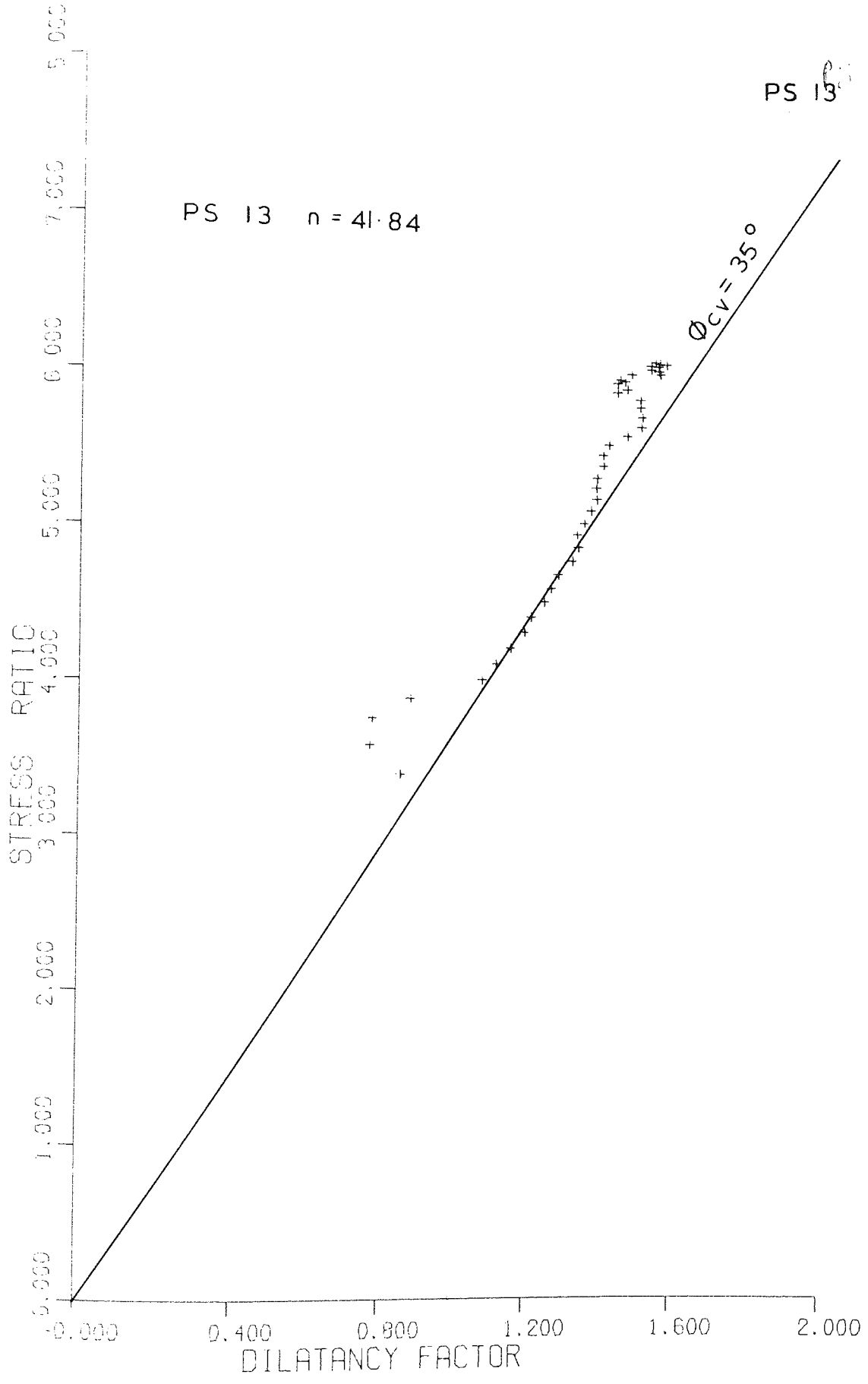
PS 13
PS 13 n = 41·84
Øcv = 35°
STRESS RATIO
5.000
4.000
3.000
2.000
1.000
0.000
-0.000
0.400
0.800
1.200
1.600
2.000
DILATANCY FACTOR

Fig. 5·27

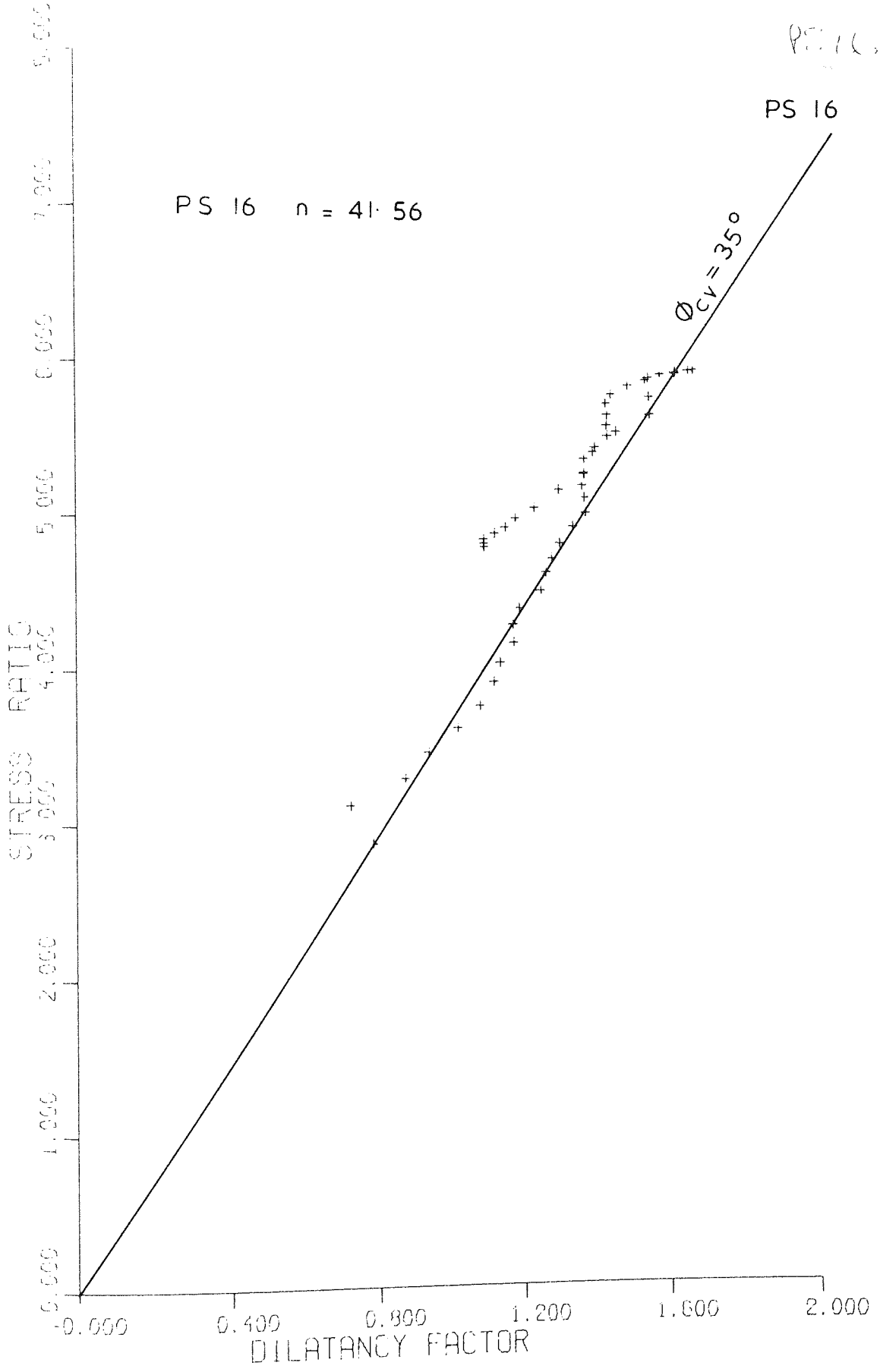
PS 16
PS 16 n = 41· 56
$\phi_{cv} = 35°$
STRESS RATIO
DILATANCY FACTOR
-0.000
0.400
0.800
1.200
1.600
2.000

Fig 5·28

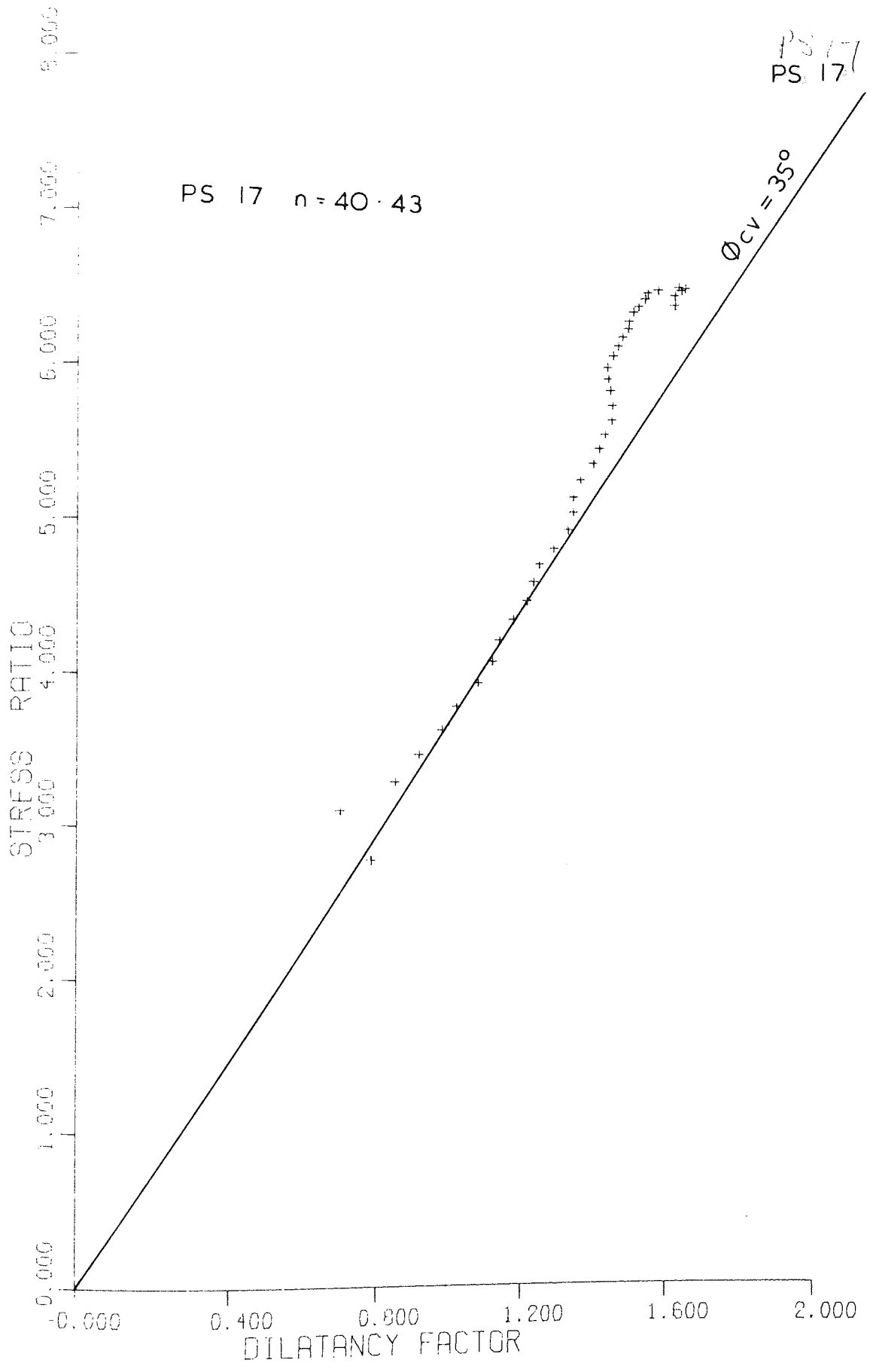
PS 17
PS 17 n = 40 · 43
$\phi_{cv} = 35°$
STRESS RATIO
0.000
1.000
2.000
3.000
4.000
5.000
6.000
7.000
8.000
-0.000
0.400
0.800
1.200
1.600
2.000
DILATANCY FACTOR

Fig 17

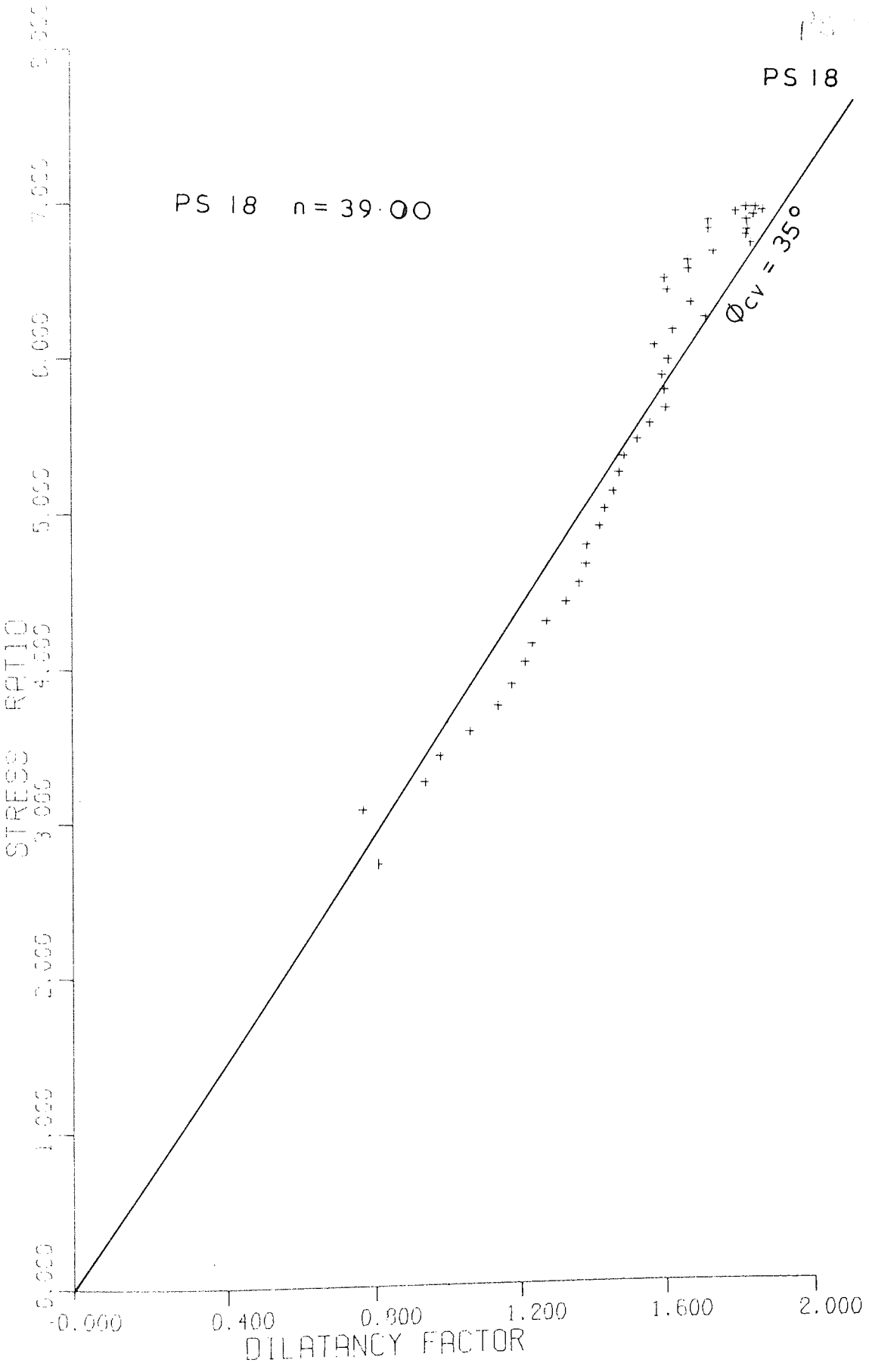
PS 18
PS 18 n = 39.00
$\phi_{cv} = 35°$
STRESS RATIO
DILATANCY FACTOR
-0.000
0.400
0.800
1.200
1.600
2.000

Fig · 5 · 30

PS 20

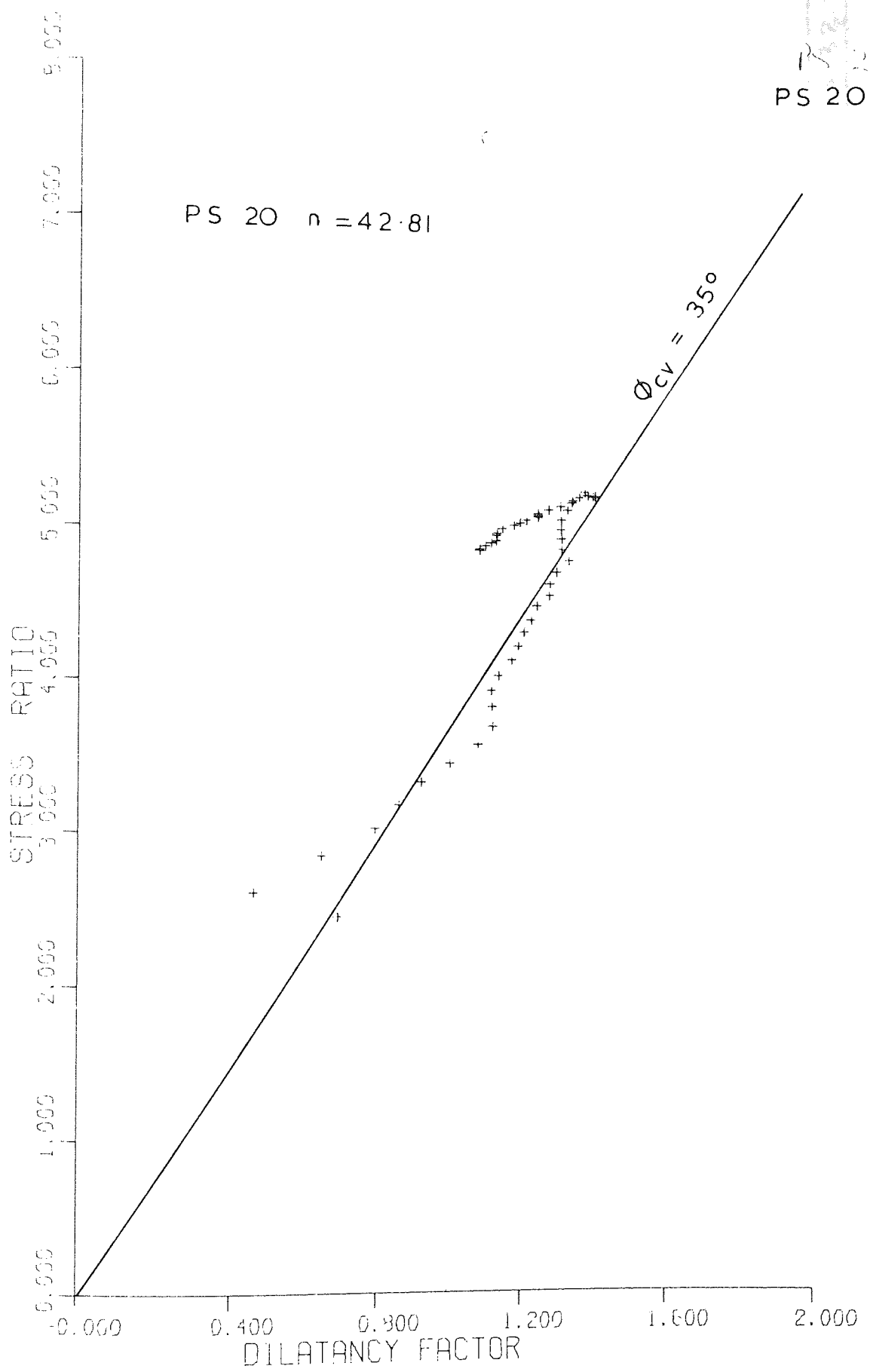
PS 20 n = 42·81
ϕ_{cv} = 35°
STRESS RATIO
DILATANCY FACTOR
-0.000
0.400
0.800
1.200
1.600
2.000

Fig 5·31

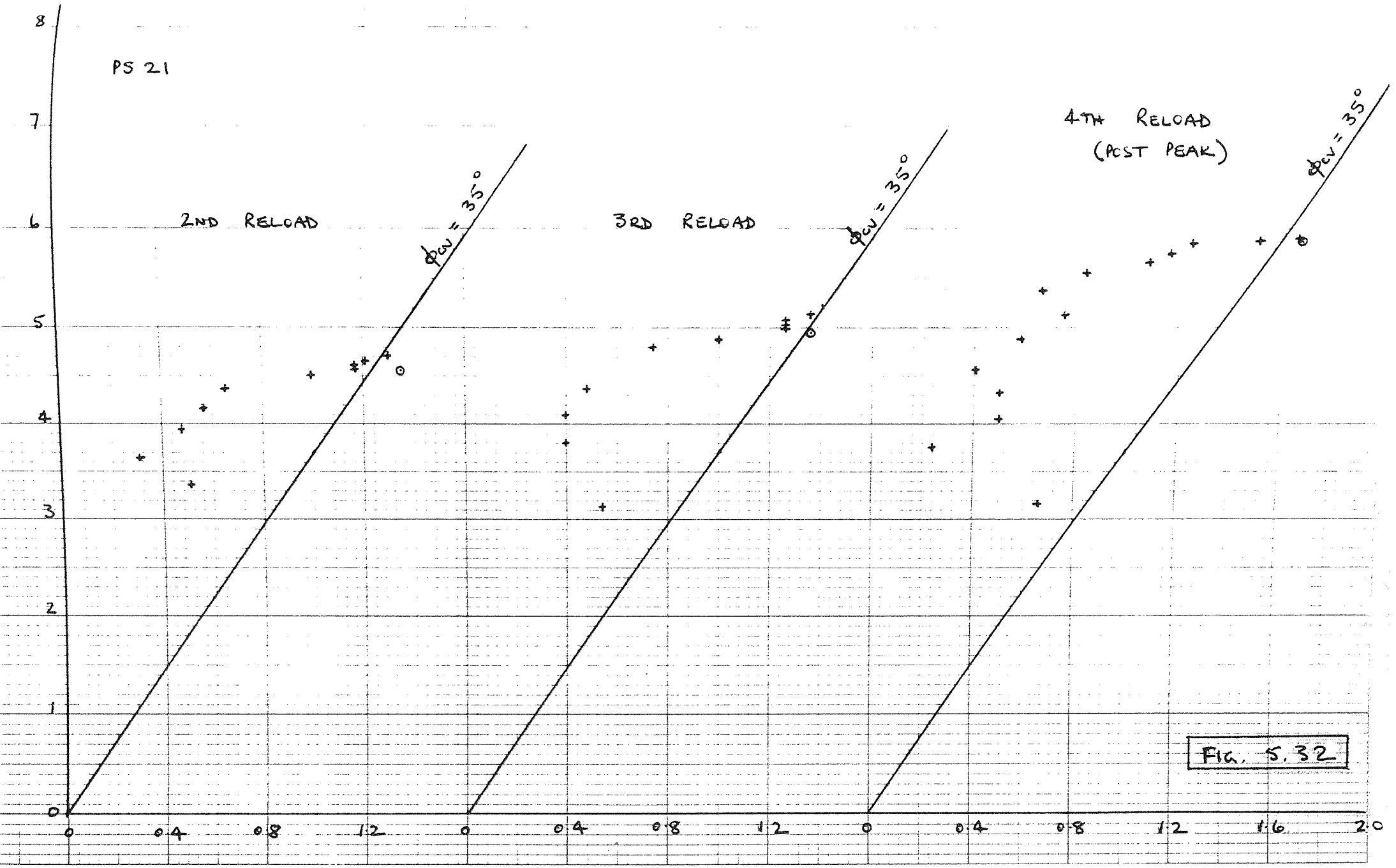
PS 21
2ND RELOAD
3RD RELOAD
4TH RELOAD
(POST PEAK)
$\phi_{cv} = 35°$
$\phi_{cv} = 35°$
$\phi_{cv} = 35°$
0
1
2
3
4
5
6
7
8
0
0.4
0.8
1.2
0
0.4
0.8
1.2
0
0.4
0.8
1.2
1.6
2.0

Fig. 5.32

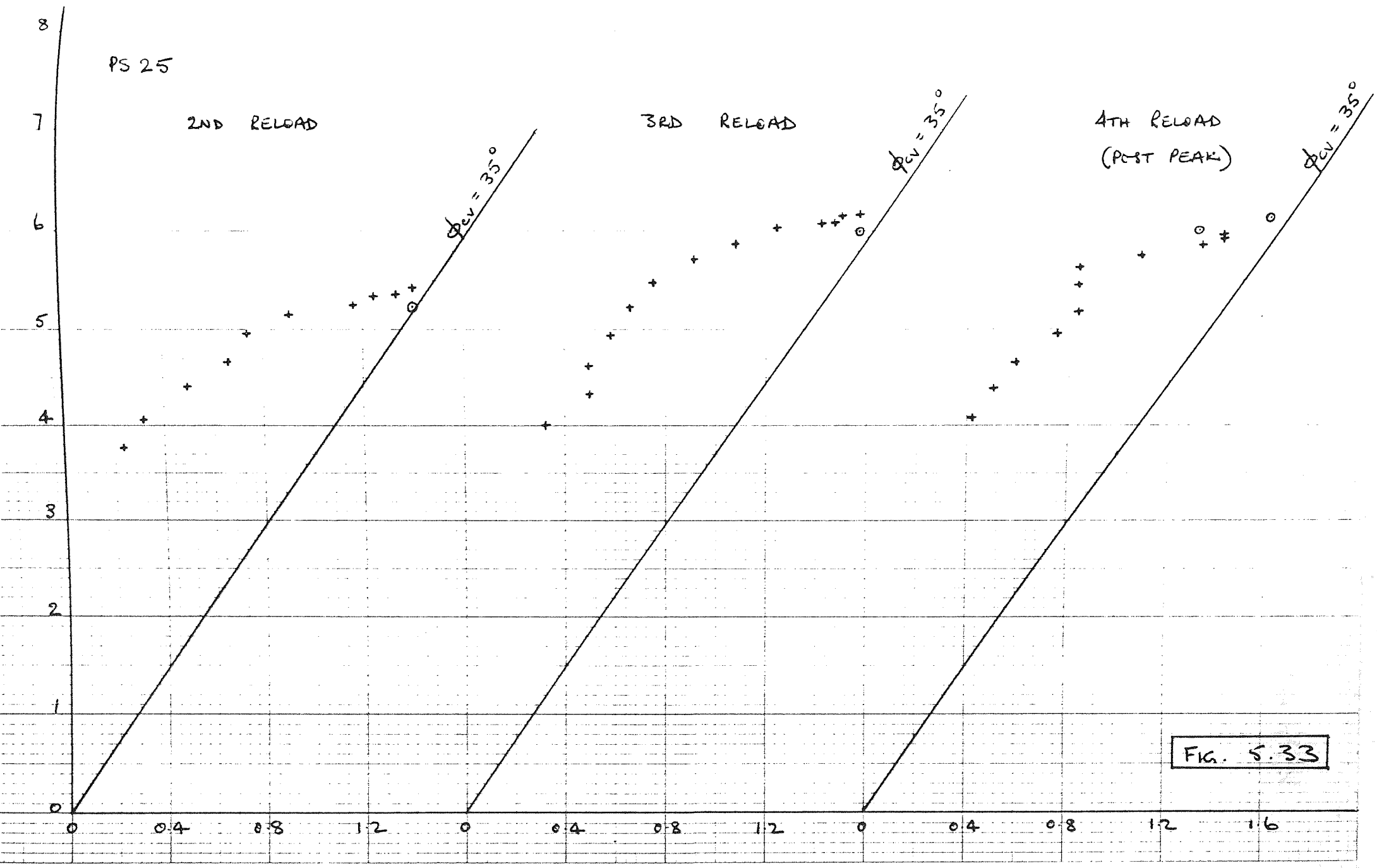
PS 25
2ND RELOAD
3RD RELOAD
4TH RELOAD
(POST PEAK)
$\phi_{cv} = 35°$
$\phi_{cv} = 35°$
$\phi_{cv} = 35°$
8
7
6
5
4
3
2
1
0
0
0·4
0·8
1·2
0
0·4
0·8
1·2
0
0·4
0·8
1·2
1·6

FIG. 5.33

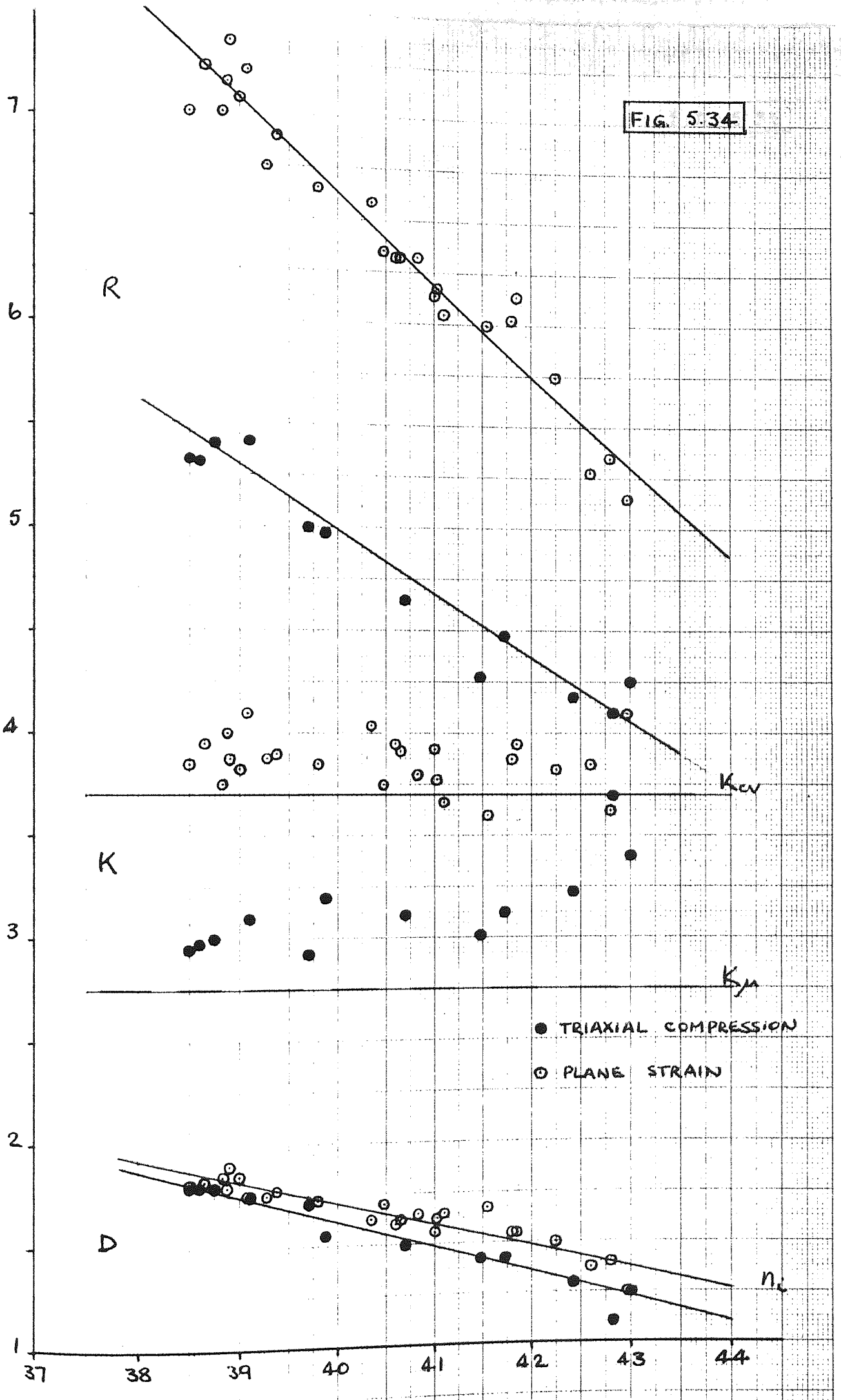
FIG. 5.34
R
K
D
7
6
5
4
3
2
1
37
38
39
40
41
42
43
44
K_{cv}
K_{pl}
n_i
TRIAXIAL COMPRESSION
PLANE STRAIN

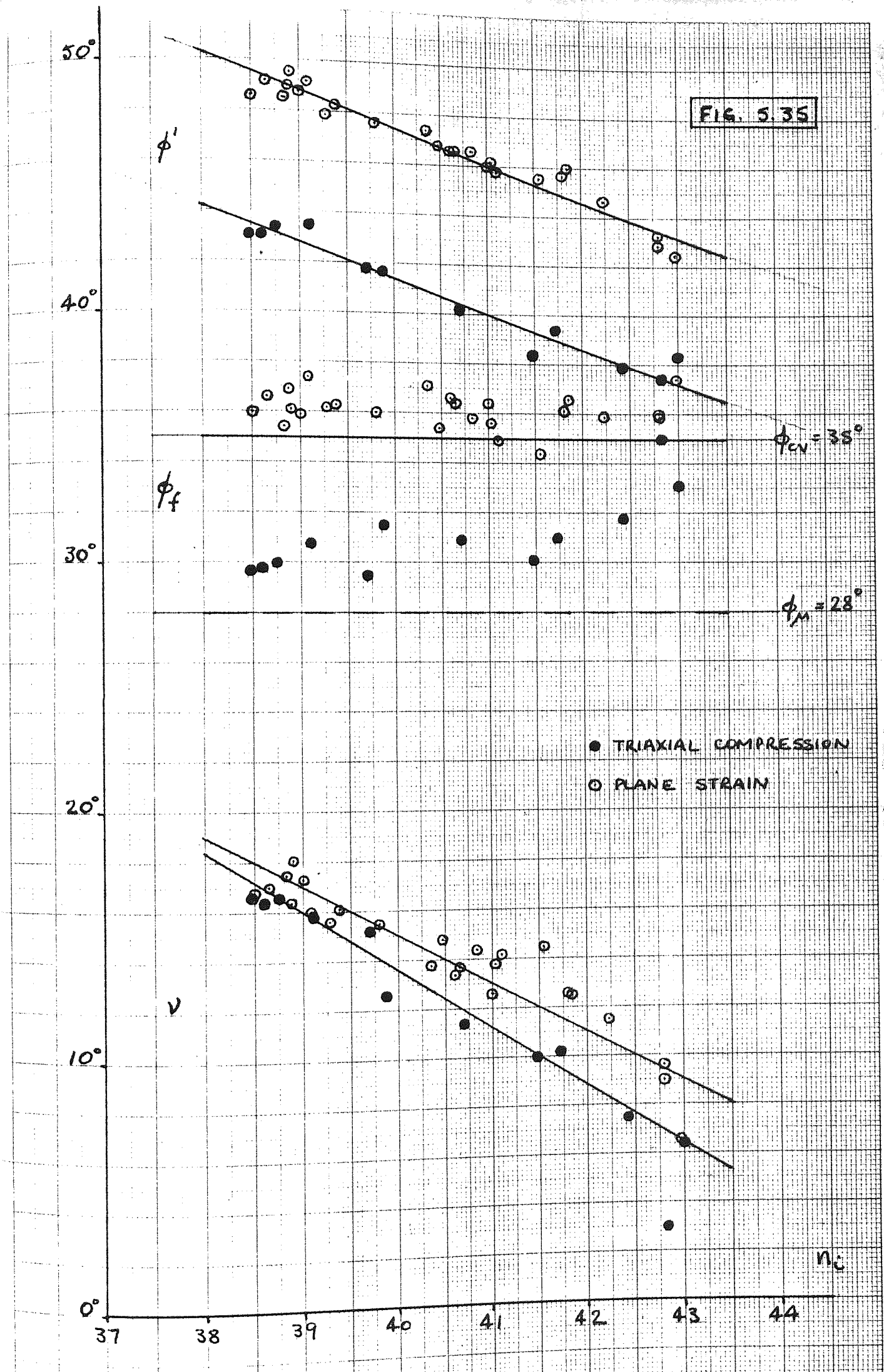
FIG. 5.35
50°
40°
30°
20°
10°
0°
ϕ'
ϕ_f
ν
$\phi_{CV} = 35°$
$\phi_M = 28°$
● TRIAXIAL COMPRESSION
○ PLANE STRAIN
37
38
39
40
41
42
43
44
n_c

CHAPTER SIX

6. PARABOLIC AND HYPERBOLIC STRESS-STRAIN FUNCTIONS.

6.1. Introduction

The rigorous analysis of boundary value problems requires the formulation of a general, physically sound, mathematical theory which will accurately predict the stress-strain behaviour of the material under the imposed boundary conditions. The most successful theoretical treatment of the deformation of sand has been provided by the stress-dilatancy theory, Rowe (1962), Horne (1965), see Chapter 5. However, although the stress-dilatancy theory provides a sound physical explanation of the deformation process, and leads to certain predictions which have been verified experimentally, the theory fails to predict the shape of the stress-strain curve, Horne (1965). The development of a stress-strain law is also complicated by the presence of elastic strains the treatment of which would appear to be complex, Rowe (1971). Even if a theoretical stress-strain relationship was to be obtained it would incorporate material properties which would have to be determined from tests on the specific material under investigation. Thus, if the form of the relationship is complex, as anticipated, it may be more expedient to adopt a purely empirical approach.

The most convenient empirical treatment is to fit mathematical functions to the observed behaviour. Several empirical formulae have been used to fit stress-strain curves including hyperbolic, parabolic, exponential, and spline functions. Examples of these have already been given in Chapter 3. The ability of simple hyperbolic and parabolic functions to describe the triaxial compression and plane strain stress-strain curves obtained in this research program will be assessed in the following sections.

6.2. Hyperbolic deformation parameters.

6.2.1. A simple hyperbolic function.

Kondner (1963) and Kondner and Zelasko (1963) demonstrated that the non-linear pre-peak deformation characteristics of soils could be described by a simple two-constant hyperbolic function of the form

$$\sigma_1 - \sigma_3 = \frac{\varepsilon_1}{a + b\,\varepsilon_1} \qquad (6.1)$$

Transformation of equation 6.1 to the linear form

$$\frac{\varepsilon_1}{\sigma_1 - \sigma_3} = a + b\,\varepsilon_1 \qquad (6.2)$$

permitted the two constants, a and b, to be obtained graphically. The constants, a and b, were shown to be equal to the reciprocals of the initial tangent modulus and the ultimate value of deviator stress respectively. Barden and Khayatt (1968) suggested that the principal effective stress ratio was a more relevant parameter than the deviator stress, and suggested the following alternative equation:

$$R = \frac{\varepsilon_1}{a + b\,\varepsilon_1} \qquad (6.3)$$

Applications of both equation 6.1 and equation 6.3 are limited to specimens which have been consolidated under ambient stress conditions. In addition, equation 6.3 is incorrect as it predicts the initial stress ratio to be zero instead of unity.

In the analysis of the results presented in this thesis the principal stress ratio has been used since the shearing behaviour of sand is frictional rather than plastic. In addition, it is anticipated that the hyperbolic constants will vary less with confining stress since the principal effective stress ratio is less affected by confining stress than the deviator stress.

Kondner's equation (equation 6.1) has, therefore, been modified to provide for an initial stress condition and the modified form has been rearranged to give an equation for the principal effective stress ratio.

Rewriting equation 6.1 to allow for an initial stress condition,

$$(\sigma_1 - \sigma_3) = (\sigma_1 - \sigma_3)_o + \frac{\varepsilon_1}{a + b\,\varepsilon_1} \quad \text{for } \sigma_3 = \text{const.} \qquad (6.4)$$

where $(\sigma_1 - \sigma_3)_c$ is the deviator stress at $\varepsilon_1 = o$.

Dividing equation 6.4 by σ_3 gives

$$R = R_o + \frac{\varepsilon_1}{A + B\,\varepsilon_1} \qquad (6.5)$$

where $A = a.\,\sigma_3$ and $B = b.\,\sigma_3$

Equation 6.5 is in the form used to quantify the deformation curves obtained from the present research program. In order to determine the constants A and B the following linear form of equation 6.5 was used:

$$\frac{\varepsilon_1}{(R-R_o)} = A + B\,\varepsilon_1 \qquad (6.6)$$

6.2.2. Triaxial compression deformation curves.

Figs. 6.1 – 6.4 provide a representative sample of the experimental results expressed in the form given by Equation 6.6, and include both tests which were K_o consolidated and tests which were consolidated under ambient stress conditions, including cyclic tests. For the analysis of the cyclic test results only the virgin loading portions of the experimental curves were used. The correlation between the experimental results and the hyperbolic assumption was extremely good for all the tests. The greatest difference occurred during the first 1% strain and it was noticed that in the majority of the tests the experimental results were initially below the fitted straight line, thus indicating a greater degree of non-linearity than the hyperbolic approximation. The few tests which did not show this were ambient consolidated tests which, presumably, were subject to slight initial specimen non-uniformities.

Further examples of the close agreement between the experimental results and the hyperbolic assumption are shown in Fig. 6.5 and Fig. 6.6, in which both the experimental results and the predicted stress ratio–axial strain curves obtained from equation 6.5 are plotted. Three

examples of the K_o consolidated tests are given in Fig. 6.5 and two ambient consolidated tests are shown in Fig. 6.6. Both figures show the good correlation between the hyperbolic function and the experimental results. For all the monotonic tests performed the maximum error in the stress ratio predicted by the hyperbolic curves was $\pm$ 1%, between 1% axial strain and failure. As can be seen from the test results in Appendix C, the experimental curve subsequent to a cycle of load did not always exactly coincide with the anticipated virgin loading curve. Nevertheless, for the cyclic tests, the hyperbolic predictions were usually within $\pm$ 2.5% of the experimental results, after the initial 1% axial strain.

The hyperbolic constants obtained from all the triaxial compression tests are summerized in Fig. 6.7. The parameters A and B have been plotted against initial porosity in Fig. 6.7a and 6.7b respectively. Anticipating the experimental results, one would expect the initial stiffness to decrease with initial density and this is confirmed by the K_o consolidated test results which show an increase in A with increase in initial porosity. One would also expect the initial modulus to decrease with initial stress ratio increase and the difference between the K_o consolidated test results and the ambient consolidated test results supports this. What is interesting is that, allowing for experimental scatter, the initial deformation modulus, as deduced from equation 6.6, would appear to be independent of initial porosity, for specimens which have been consolidated under ambient stress conditions. However, the initial porosity does affect the rate of change of stiffness and thus, when more conventional methods of determining the deformation modulus are used an apparent dependence on initial porosity is obtained.

Since the parameter B is equal to the inverse of the difference between the ultimate and initial stress ratios the results shown in

Fig. 6.7b are as expected. The increase in B for the K_o consolidated tests is much greater than for the ambient consolidated tests but this largely due to the reciprocal nature of the parameter B.

6.2.3. Plane strain deformation curves.

Figs. 6.8 - 6.10 provide three typical examples of plane strain test results transformed so as to obtain the hyperbolic parameters A and B. It can be seen that, although the transformed plots are non-linear over the initial 1% range of axial strain, an hyperbola can be reasonably assumed to fit the subsequent range of pre-peak deformation. Although the plane strain results do not appear to correlate with a linear transformed plot to the same extent as do the triaxial compression test results, Figs. 6.1 - 6.4, this is simply due to the small strains required to mobilize peak strength in plane strain. Both plane strain and triaxial compression tests exhibited a lack of agreement with the hyperbolic assumption over the initial 1% range of axial strain.

Examples of the accuracy with which the fitted hyperbolic functions predicted the experimental results can be seen in Fig. 6.11. The correlation between the hyperbolic curves and the test results was generally good until just prior to failure although the hyperbolae always underestimated the stress ratios developed at small strains.

Fig. 6.12a and Fig. 6.12b show the variation of the plane strain hyperbolic parameters A and B with initial porosity. The corresponding triaxial compression values (obtained from the K_o consolidated tests) are indicated by broken lines. Fig. 6.12a indicates that the initial stiffness of sand is greater in plane strain than in triaxial compression, although the difference is small for dense specimens.

6.2.4. Limitations.

If hyperbolic functions of the form used in this section are to be employed in the analyses of boundary value problems then the most

serious limitation is the lack of correlation with experimental results in the small strain region. In the many problems in which the working load is never more than half the failure load the deformations will be overestimated. For a more accurate representation of experimental data it is, therefore, worthwhile considering alternative mathematical functions to describe the early part of the stress ratio–axial strain curve.

Since the experimental results of both plane strain and triaxial compression tests indicated a possible parabolic R-ε_1 relationship at small strains the expressions suggested by Brinch Hansen (1963) were also considered. The equations were given as

$$(\sigma_1 - \sigma_3) = \left(\frac{\varepsilon_1}{a - b\varepsilon_1}\right)^{\frac{1}{2}} \tag{6.7}$$

and

$$(\sigma_1 - \sigma_3) = \frac{\sqrt{\varepsilon_1}}{a - b\varepsilon_1} \tag{6.8}$$

Expressing the above two equations in terms of stress ratio and allowing for an initial stress ratio condition:

$$R = R_o + \left(\frac{\varepsilon_1}{A - B\varepsilon_1}\right)^{\frac{1}{2}} \tag{6.9}$$

and

$$R = R_o + \frac{\sqrt{\varepsilon_1}}{A - B\varepsilon_1} \tag{6.10}$$

The parameters A and B in equations 6.9 and 6.10 were obtained in a similar manner to that used to determine the hyperbolic parameters.

Test PS 2 has been used to illustrate the correlation obtained between the experimental results and both the parabolic and hyperbolic assumptions. The test results obtained from test PS 2 were plotted in the various forms necessary to obtain the values of A and B in equations 6.5, 6.9, and 6.10, as shown in Fig. 6.13. None of the expressions gave a linear relationship for the complete pre-peak deformation range. Nevertheless, straight line approximations have been fitted to the experimental results, as shown in Fig. 6.13. Using the

parabolic parameters so obtained, it was found that there was no significant difference in the stress ratios predicted by the two parabolic expressions. Therefore, only the predictions given by equation 6.10 have been used to provide a comparison with the hyperbolic predictions and the experimental results.

The comparison with the experimental results is shown in Fig. 6.14. It can be seen that, in contrast to the hyperbolic function, the parabolic equation overestimated the stress ratios at small strains; neither the parabolic nor the hyperbolic function adequately predicted the initial part of the stress ratio–axial strain curve. Although an expression corresponding to the arithmetic mean of the two equations, 6.5 and 6.10, gave reasonable results, a much simpler parabolic function was subsequently found which accurately predicted the stress ratios at small strains.

6.3. Parabolic deformation parameters.

The inability of the hyperbolic function to accurately predict the stress ratios over the initial 1% axial strain range is most serious in the case of plane strain deformation since this constitutes the working range of many practical problems. Furthermore, with the introduction of sophisticated experimental techniques to determine internal strain patterns, Roscoe et al (1963), Butterfield et al (1970), the accurate prediction of the stress–strain relation at small strains in elemental plane strain tests is essential to the understanding of the behaviour of soil, and the interaction between soil and structure, in two dimensional model tests. Consequently, further attempts to obtain a more accurate mathematical representation of the stress–strain relationship were initially concentrated on re-analysing the plane strain test results.

6.3.1. A simple parabolic function.

Empirical formulae have been used to represent the stress–strain

curves of metals. As an example, Hill (1950) gives the following power law

$$\sigma = a + b\varepsilon^{c} \tag{6.11}$$

where a, b, c are described as arbitrary constants. Polakowski and Ripling (1966) suggest that the tensile stress-strain curves in the plastic region of most ductile materials can be approximated by the following form of equation

$$\sigma = K\varepsilon^{n} \tag{6.12}$$

where K and n are referred to as the strength coefficient and the strain-hardening exponent respectively. The equation is represented by a straight line on a log-log plot of stress against strain where K is then the intercept at $\varepsilon = 1$ and n is the slope of the line.

The possibility that a similar relationship could describe the plane strain deformation of sand was investigated and it was found that the shape of the stress ratio-axial strain curves were accurately represented by the following parabolic function:

$$R = R_{o} + M\varepsilon_{1}^{r} \tag{6.13}$$

and the instantaneous tangent to the curve is given by

$$\frac{dR}{d\varepsilon_{1}} = Mr\,\varepsilon_{1}^{r-1} \tag{6.14}$$

Substituting $\varepsilon = 1$ in equations 6.13 and 6.14

$$(R - R_{o})_{\varepsilon_{1} = 1} = M \tag{6.15}$$

and

$$\left(\frac{dR}{d\varepsilon_{1}}\right)_{\varepsilon_{1} = 1} = Mr \tag{6.16}$$

Thus from equations 6.15 and 6.16 the parameters M and r are identified as

M = secant modulus at 1% strain

r = ratio of tangent modulus to secant modulus at 1% strain.

6.3.2. Correlation with experimental results.

The plane strain results were examined to assess whether a linear

relationship could be obtained by plotting to logarithmic scales. Typical examples of the agreement with the parabolic assumption so obtained are shown in Fig. 6.15 which clearly indicates that the stress ratio–axial strain curves can be approximated by parabolae over most of the pre–peak deformation range. As a result of the good correlation shown in Fig. 6.15, the triaxial compression test results were also re–analysed in a similar manner. The K_o consolidated test series yielded results which were in good agreement with the parabolic assumption over the initial 2% axial strain range, Fig. 6.16, but a poor correlation was obtained when the ambient consolidated test results were analysed as is evident from Fig. 6.17.

The secant modulus, M, can be obtained directly from the log–log plot but it is worthwhile checking the value by plotting a graph of $R - R_o$ against ε_1^r, as illustrated in Figs. 6.18 and 6.19. Although the anticipated straight line through the origin was generally obtained, a few tests, for example test TC 6 in Fig. 6.19, indicated that a small origin correction was required and, therefore, the initial stress ratios in these tests were correspondingly adjusted.

The accuracy with which the plane strain experimental results were predicted by the simple parabolic function is illustrated in Fig.6.20. The parabolic function clearly provides a very accurate representation of the test results until just before failure occurs. Generally over this range the percentage error in the stress ratio predictions was within $\pm$ 0.3%, as calculated. For the tests performed, this corresponded to a difference of less than 1 kN/m^2 between the measured and predicted values of deviator stress.

The parabolic parameters M and r obtained from both the plane strain tests and the K_o consolidated triaxial compression tests are plotted against initial porosity in Fig. 6.21. Fig. 6.21a indicates that the parameter r, which describes the 'strain hardening' effect, is independent of initial porosity for both triaxial compression and plane

strain conditions. It is also clear that the stress ratio–axial strain curves are more linear in plane strain than in triaxial compression. As would be expected, the secant modulus, M, is shown to increase with initial density, Fig. 6.21b, and to be greater in plane strain than in triaxial compression. The results shown in Fig. 6.21b suggest that the variation of M with porosity is similar for both test conditions.

Although the appreciable scatter in the M values shown in Fig. 6.21b may be partly attributed to deviations from the zero lateral strain condition during consolidation, it may also be the result of variations in the macropore structure, section 5.4. Since the deformation required to mobilize resistance to load will be controlled by the distribution and orientation of the macropores the consistency usually associated with strength parameters may not be obtainable when evaluating deformation parameters.

6.4. Combined parabolic–hyperbolic treatment.

The ability of simple hyperbolic and parabolic functions to represent experimental stress–strain curves has been assessed in sections 6.2 and 6.3. Both mathematical functions failed to provide an accurate representation of the test data over the complete range of pre–peak deformation. However, it was shown that the two functions yielded accurate predictions for different stages of deformation: the hyperbolic function gave accurate predictions of stress ratio except during the initial 1% range of axial strain but the initial deformation stage was accurately represented by the simple parabolic function.

The comparison of experimental results with the predictions of both the hyperbolic and parabolic functions is shown in Figs. 6.22 – 6.26. These figures illustrate the way in which the experimental results follow the parabolic curve initially and then change to follow the hyperbolic curve until the failure condition is approached. Although the plane strain results are reasonably represented by the parabolic

function alone it is clear from Figs. 6.25 and 6.26 that the triaxial compression results can be usefully represented by a combination of both functions.

Examination of the parabolic and hyperbolic curves deduced from the experimental results of each test showed that the two functions were related, as illustrated in Fig. 6.27. The stress ratios predicted by the parabolic function were at no stage of deformation less than those predicted by the hyperbolic function. Furthermore, the parabolic curve became tangential to the hyperbolic curve at a certain value of axial strain, ε_1^*, which coincided with the point at which the experimental results transferred from one curve to the other. Consequently, since the two functions predict the same stress ratio and tangent modulus at $\varepsilon_1 = \varepsilon_1^*$ the value of ε_1^* can be determined from equations 6.5 and 6.13.

Equating equations 6.5 and 6.13:

$$\frac{\varepsilon_1^*}{A + B\,\varepsilon_1^*} = M\,\varepsilon_1^{*r} \qquad (6.17)$$

Differentiating equations 6.5 and 6.13 with respect to axial strain and then equating:

$$\left(\frac{A}{A + B\,\varepsilon_1^*}\right)^2 = Mr\,\varepsilon_1^{*r-1} \qquad (6.18)$$

Multiplying equation 6.18 by ε_1^*/r and dividing by equation 6.17:

$$\frac{A}{r\left(A + B\,\varepsilon_1^*\right)} = 1 \qquad (6.19)$$

Thus

$$\varepsilon_1^* = \frac{A}{B} \cdot \frac{(1 - r)}{r} \qquad (6.20)$$

It is, therefore, concluded that the pre-peak stress ratio–axial strain curves of both plane strain and K_o consolidated triaxial compression tests on sand are accurately predicted by the following

combined parabolic-hyperbolic specification:

$$R = R_o + M \varepsilon_1^{\,r} \qquad \text{for} \quad \varepsilon_1 \leq \frac{A}{B} \cdot \frac{(1 - r)}{r}$$

and

$$R = R_o + \frac{\varepsilon_1}{A + B \varepsilon_1} \qquad \text{for} \quad \varepsilon_1 \geq \frac{A}{B} \cdot \frac{(1 - r)}{r}$$

The parabolic and hyperbolic parameters obtained from the plane strain and K_o consolidated triaxial compression tests are summarized in Tables 6.1 and 6.2, together with the calculated values of ε_1^*. The factor of safety against failure, corresponding to the strain at which the transition from parabolic to hyperbolic behaviour occurs, is also provided, assuming that

$$F = \frac{(R-R_o)_{max}}{(R-R_o)_{\varepsilon_1 = \varepsilon_1^*}} \tag{6.21}$$

It is clear that for most practical problems, in which the factor of safety is never less than 1.5, the stress ratio-axial strain relationship can be represented by the parabolic function alone.

Table 6.1. PARABOLIC AND HYPERBOLIC PARAMETERS

(Triaxial compression)

TEST NO	POROSITY	A	B	M	r	ε_1*	F
TC 1	38.60	0.33	0.428	1.26	0.3743	1.29	1.34
TC 2	39.70	0.44	0.632	0.93	0.3520	1.28	1.34
TC 3	42.83	1.80	0.980	0.43	0.4563	2.19	1.37
TC 4	39.87	0.65	0.578	0.83	0.3802	1.83	1.34
TC 5	42.42	0.88	0.930	0.55	0.4350	1.23	1.56
TC 6	41.72	0.70	0.673	0.82	0.3630	1.83	1.21
TC 7	41.47	0.60	0.688	0.79	0.3876	1.38	1.27
TC 8	40.69	0.75	0.944	0.69	0.3760	1.32	1.16
TC 9	39.09	0.48	0.454	1.09	0.4036	1.56	1.35
TC 10	38.75	0.44	0.478	1.13	0.3566	1.66	1.29
TC 11	38.48	0.43	0.540	1.10	0.3814	1.29	1.30
TC 12	43.00	1.00	0.803	0.64	0.3582	2.23	1.24

Table 6.2. PARABOLIC AND HYPERBOLIC PARAMETERS

(Plane strain)

TEST NO	POROSITY	A	B	M	r	ε_1^*	F
PS 1	41.10	0.412	0.203	1.63	0.6833	0.94	1.46
PS 2	42.24	0.417	0.164	1.73	0.6553	1.34	1.24
PS 3	41.00	0.335	0.145	-	-	-	-
PS 4	39.27	0.425	0.100	1.95	0.7250	1.61	1.27
PS 5	40.48	0.430	0.098	1.95	0.7265	1.65	1.35
PS 6	41.02	0.442	0.120	1.63	0.7684	1.11	1.83
PS 7	42.98	0.358	0.220	1.75	0.6204	1.00	1.43
PS 8	38.51	0.351	0.106	2.20	0.7018	1.41	1.50
PS 9	40.60	0.293	0.138	2.38	0.7156	0.84	1.56
PS 10	39.81	0.342	0.129	2.23	0.7066	1.10	1.47
PS 11	42.80	0.418	0.250	1.51	0.7173	0.66	1.66
PS 12	38.87	0.293	0.137	2.36	0.6420	1.19	1.39
PS 13	41.84	0.470	0.166	1.59	0.6747	1.37	1.39
PS 14	39.07	0.382	0.129	1.96	0.7303	1.09	1.63
PS 15	40.83	0.370	0.130	2.03	0.6793	1.34	1.43
PS 16	41.56	0.340	0.158	2.00	0.6969	0.94	1.62
PS 17	40.34	0.330	0.114	2.28	0.6947	1.27	1.41
PS 18	39.00	0.355	0.090	2.26	0.7466	1.34	1.54
PS 19	38.66	0.290	0.095	2.67	0.6516	1.63	1.27
PS 20	42.81	0.338	0.182	1.95	0.6337	1.07	1.38

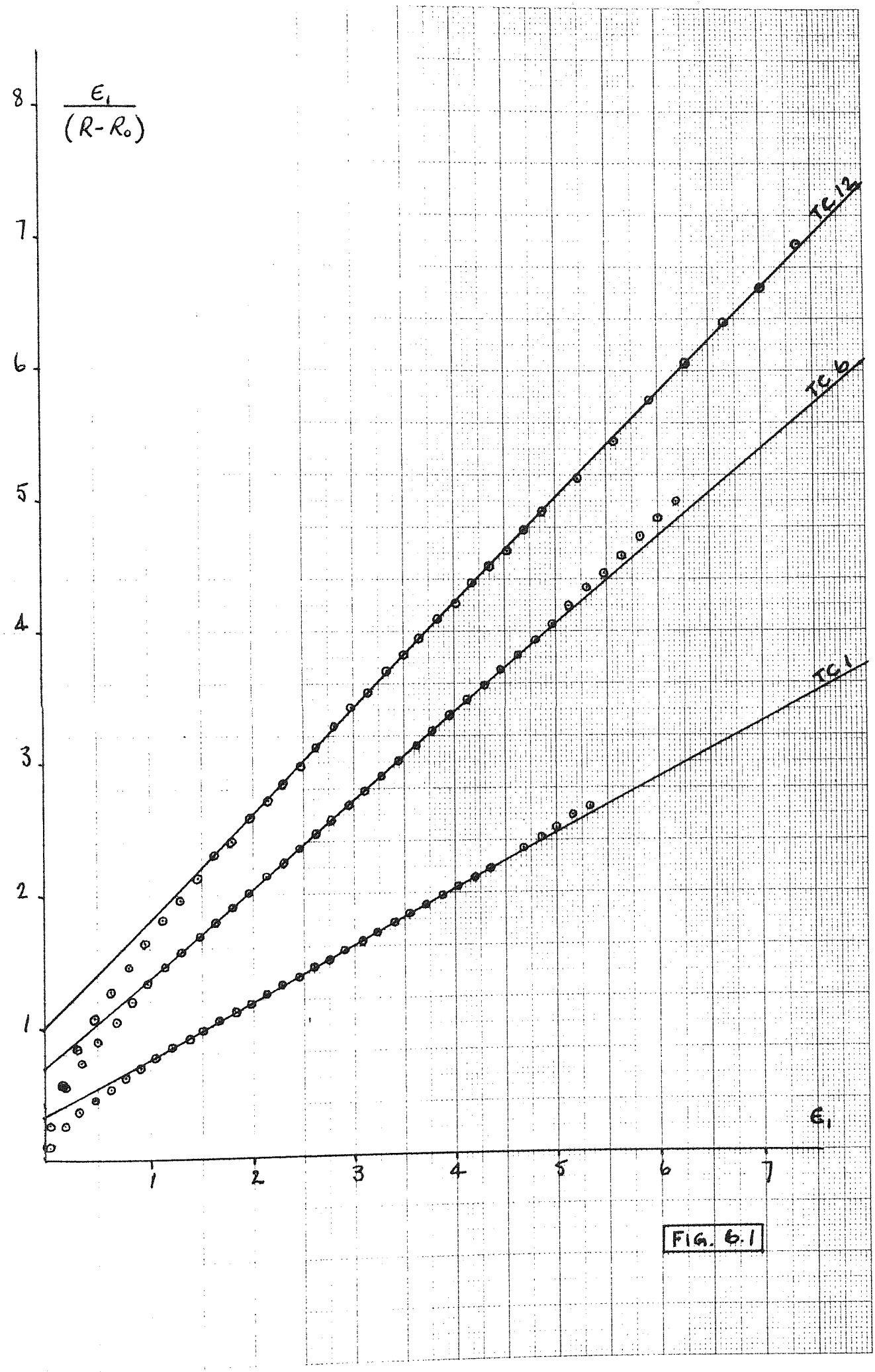

FIG. 6.1

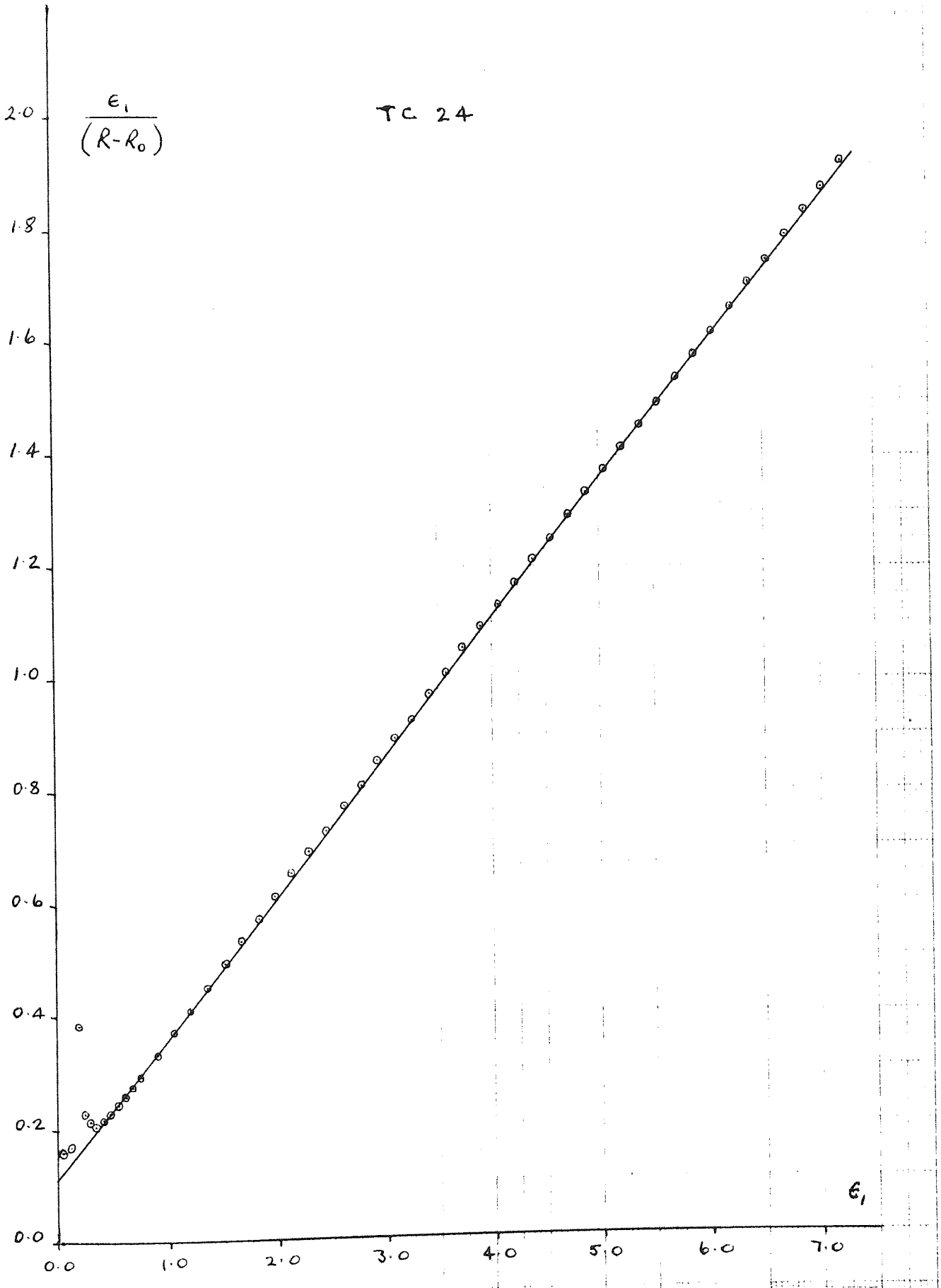
$\frac{\epsilon_1}{(R-R_0)}$
TC 24
2·0
1·8
1·6
1·4
1·2
1·0
0·8
0·6
0·4
0·2
0·0
0·0
1·0
2·0
3·0
4·0
5·0
6·0
7·0
ϵ_1

FIG. 6.2

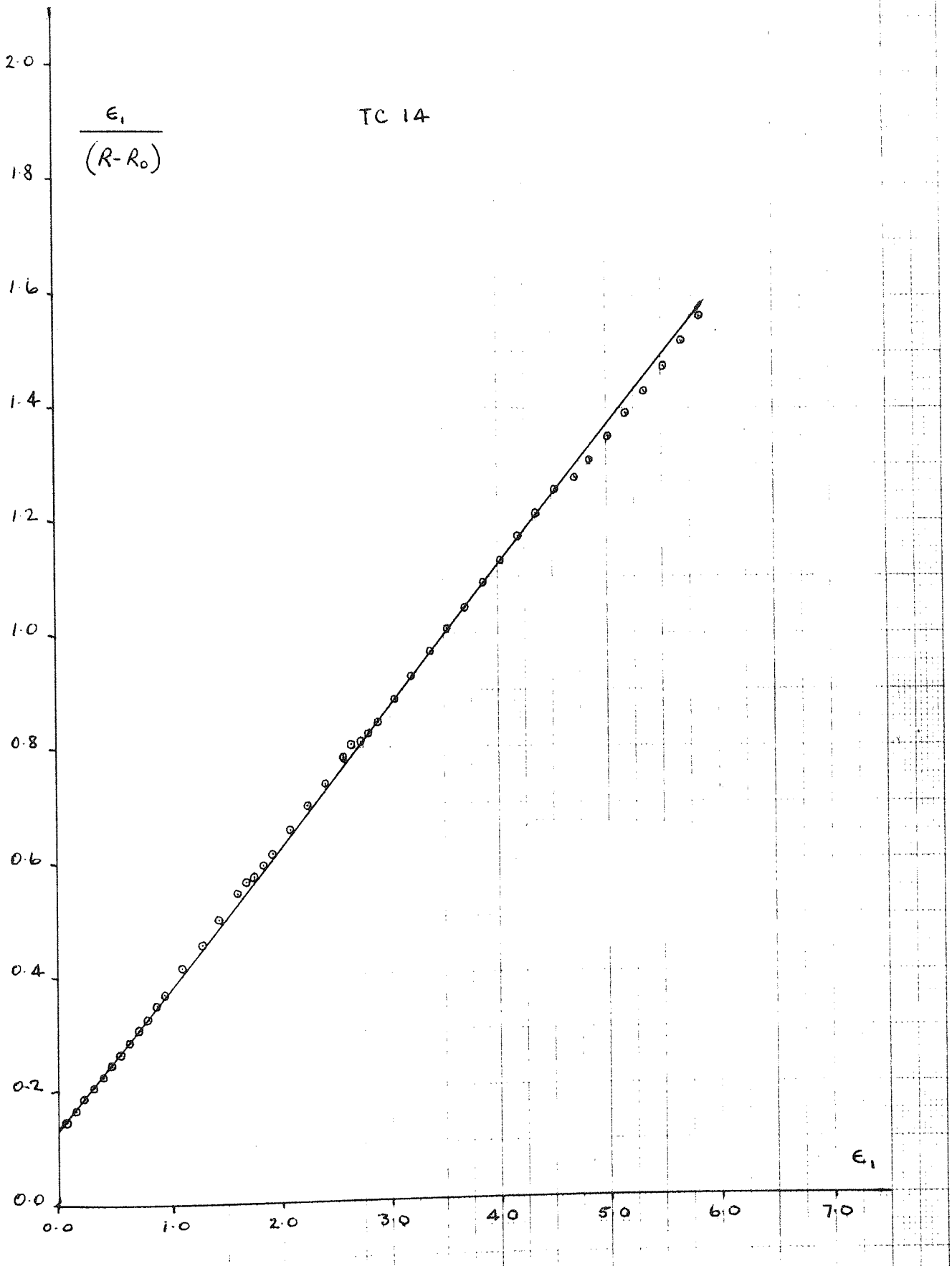
TC 14
$\frac{\epsilon_1}{(R-R_0)}$
2·0
1·8
1·6
1·4
1·2
1·0
0·8
0·6
0·4
0·2
0·0
0·0
1·0
2·0
3·0
4·0
5·0
6·0
7·0
ϵ_1

FIG. 6.3

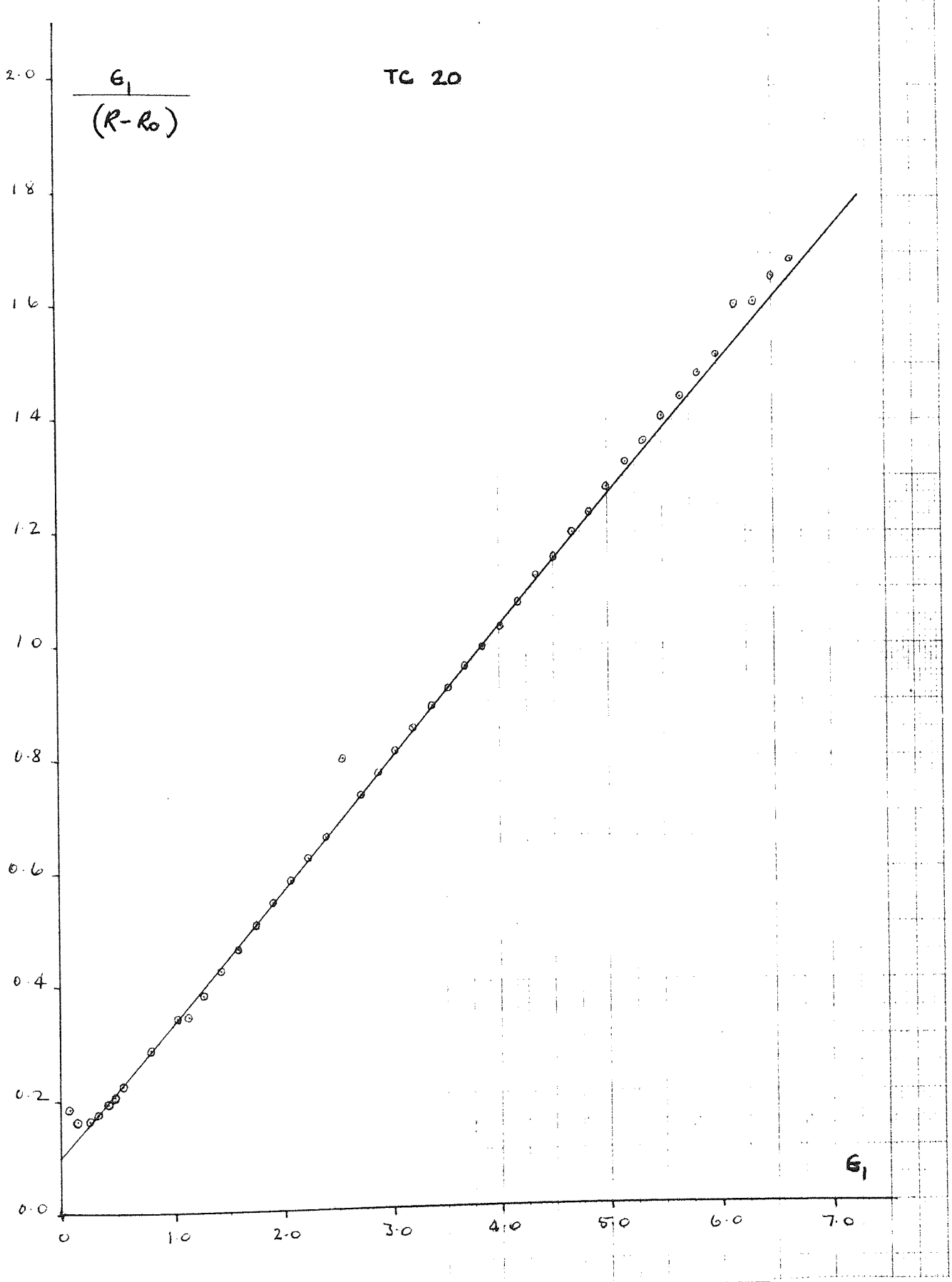
TC 20
$\frac{G_1}{(R-R_0)}$
2·0
1·8
1·6
1·4
1·2
1·0
0·8
0·6
0·4
0·2
0·0
0
1·0
2·0
3·0
4·0
5·0
6·0
7·0
G_1

FIG. 6.4

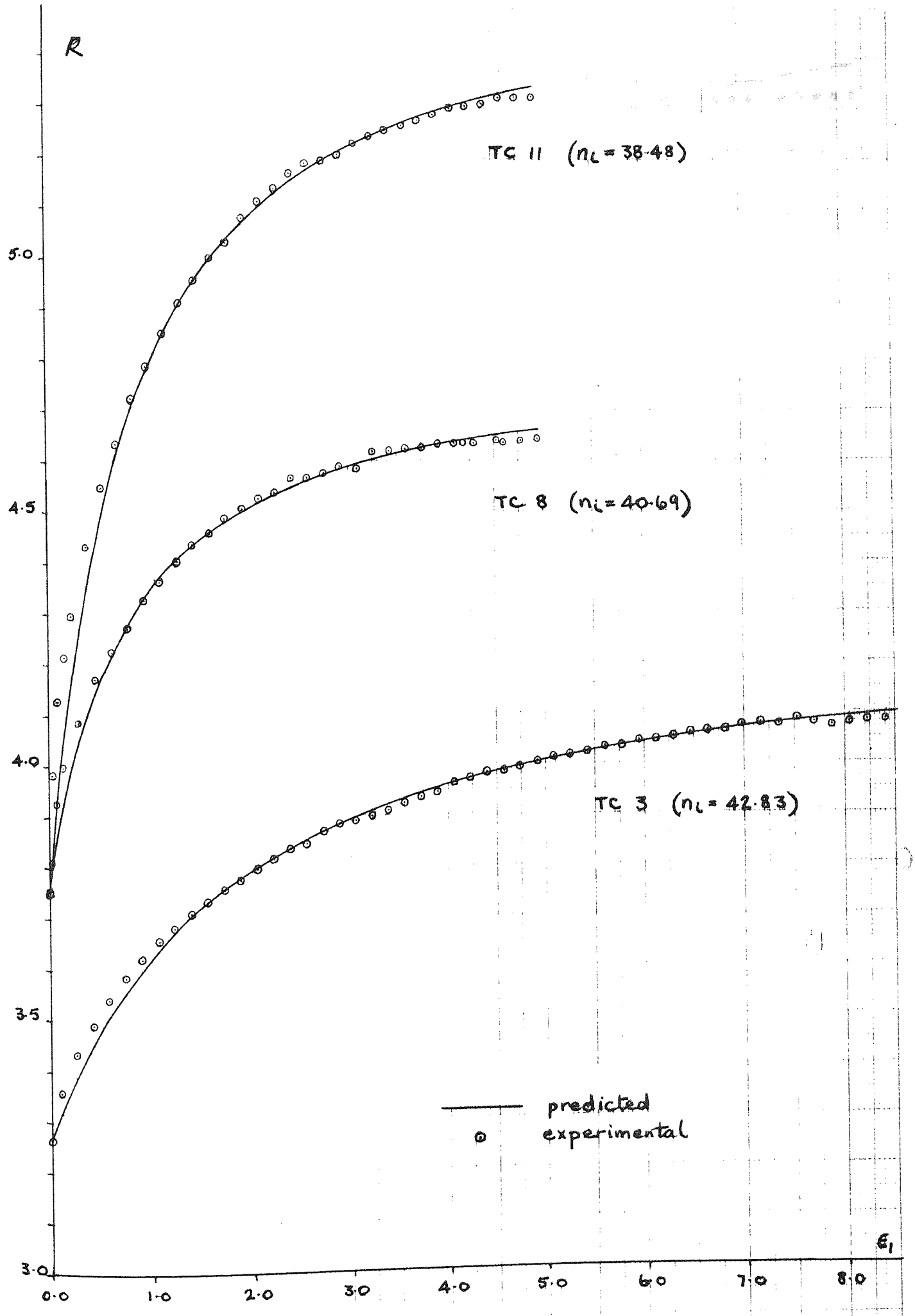
R
TC 11 (n_L = 38·48)
TC 8 (n_L = 40·69)
TC 3 (n_L = 42·83)
predicted
experimental
ϵ_1
5·0
4·5
4·0
3·5
3·0
0·0
1·0
2·0
3·0
4·0
5·0
6·0
7·0
8·0

FIG. 6.5

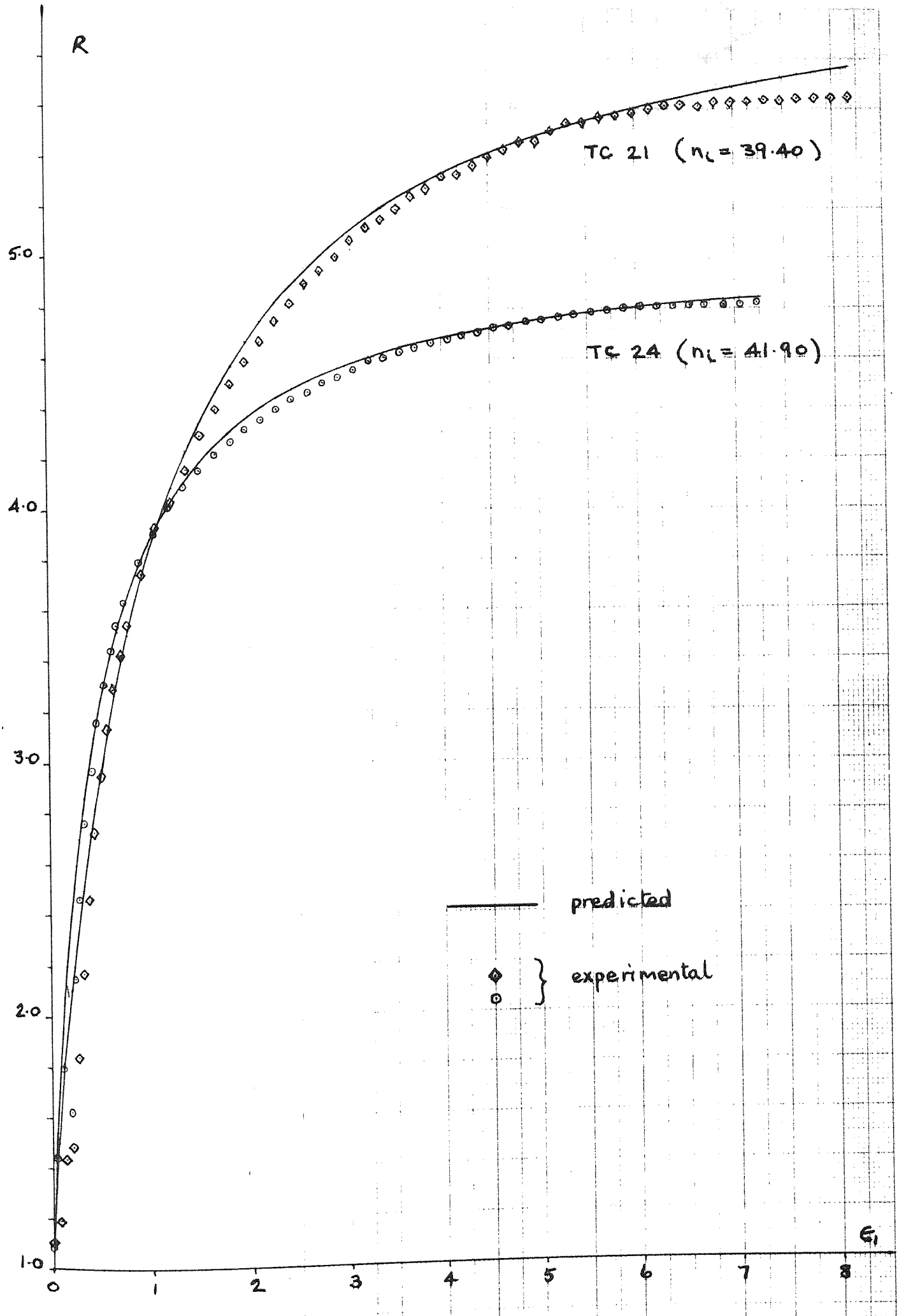
R
TC 21 (n_L = 39.40)
TC 24 (n_L = 41.90)
5.0
4.0
3.0
2.0
1.0
0
1
2
3
4
5
6
7
8
ϵ_1
predicted
experimental

FIG. 6.6

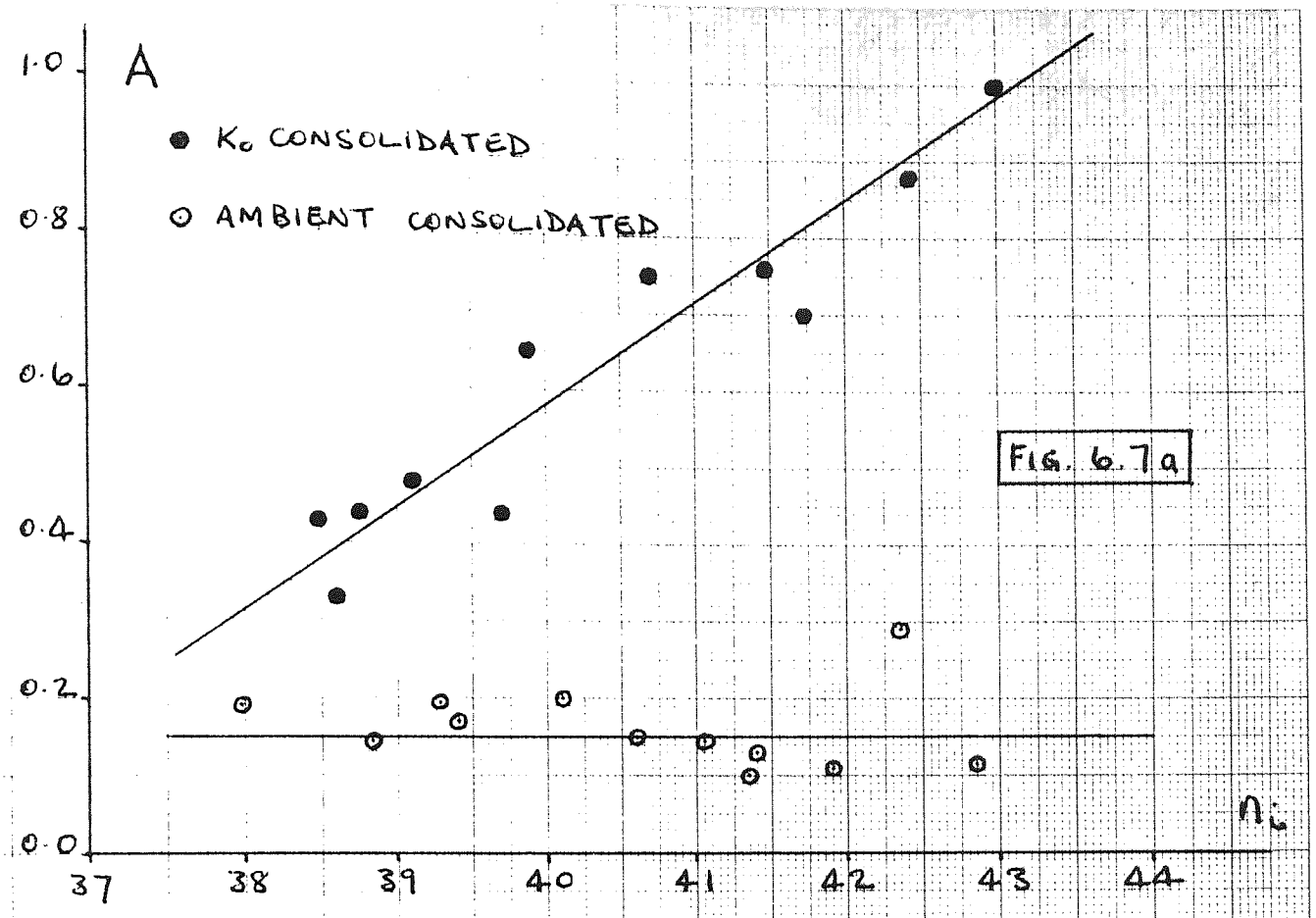

Fig. 6.7a

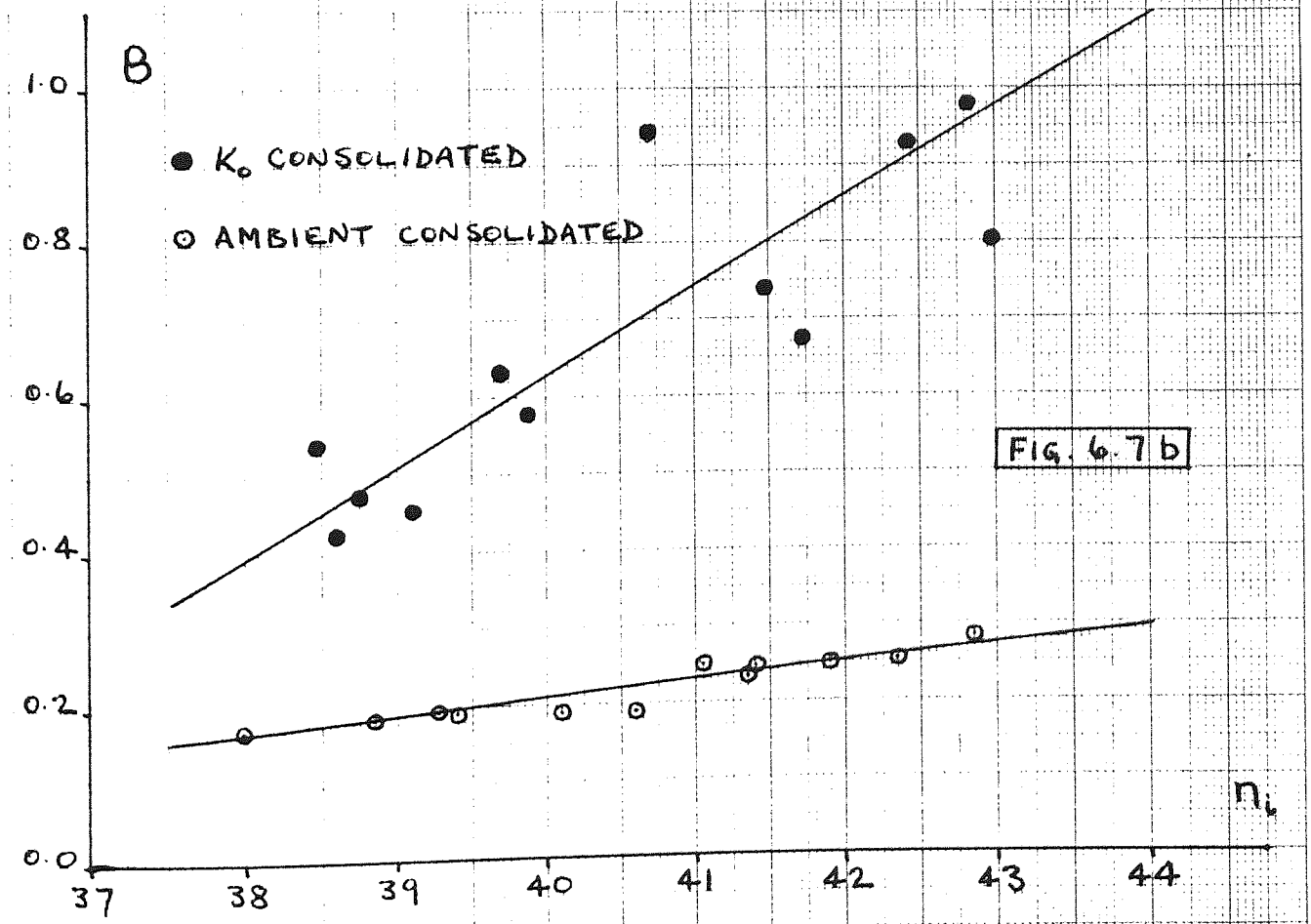

Fig. 6.7b

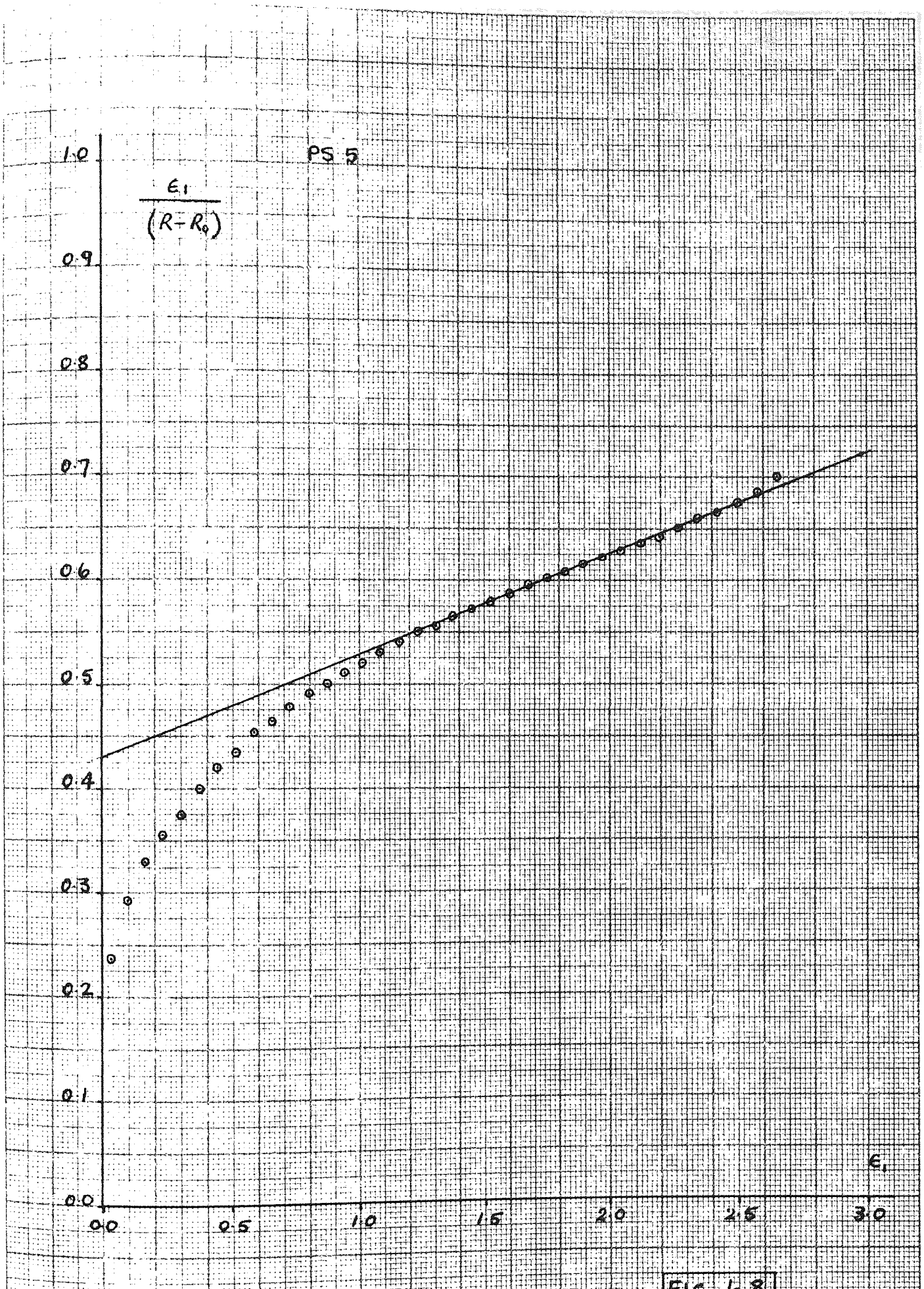
PS 5
$\frac{\epsilon_1}{(R-R_0)}$
1.0
0.9
0.8
0.7
0.6
0.5
0.4
0.3
0.2
0.1
0.0
0.0
0.5
1.0
1.5
2.0
2.5
3.0
ϵ_1

FIG. 6.8

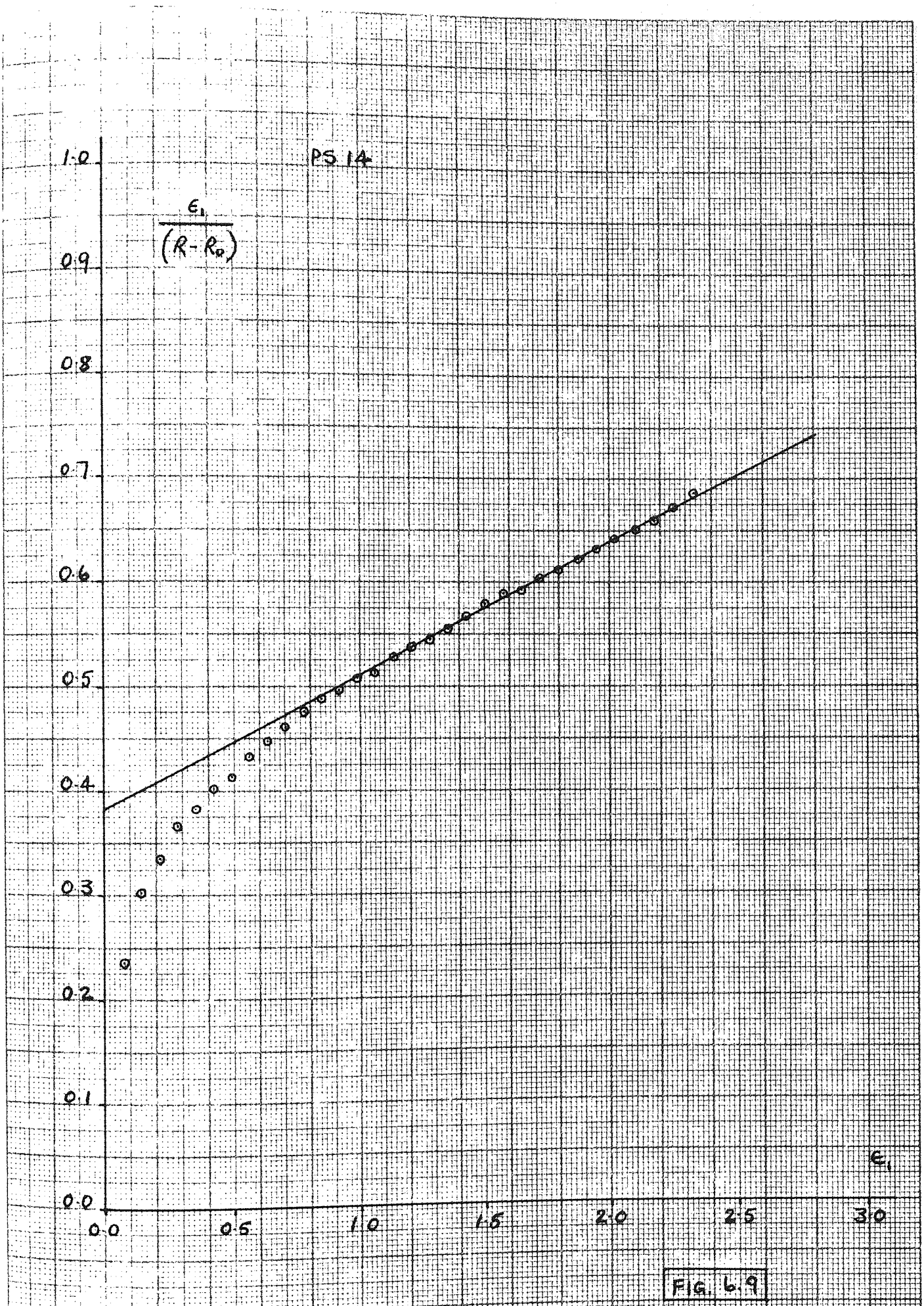
PS 14
$\frac{\epsilon_1}{(R-R_0)}$
1.0
0.9
0.8
0.7
0.6
0.5
0.4
0.3
0.2
0.1
0.0
ϵ_1
0.0
0.5
1.0
1.5
2.0
2.5
3.0

FIG. 6.9

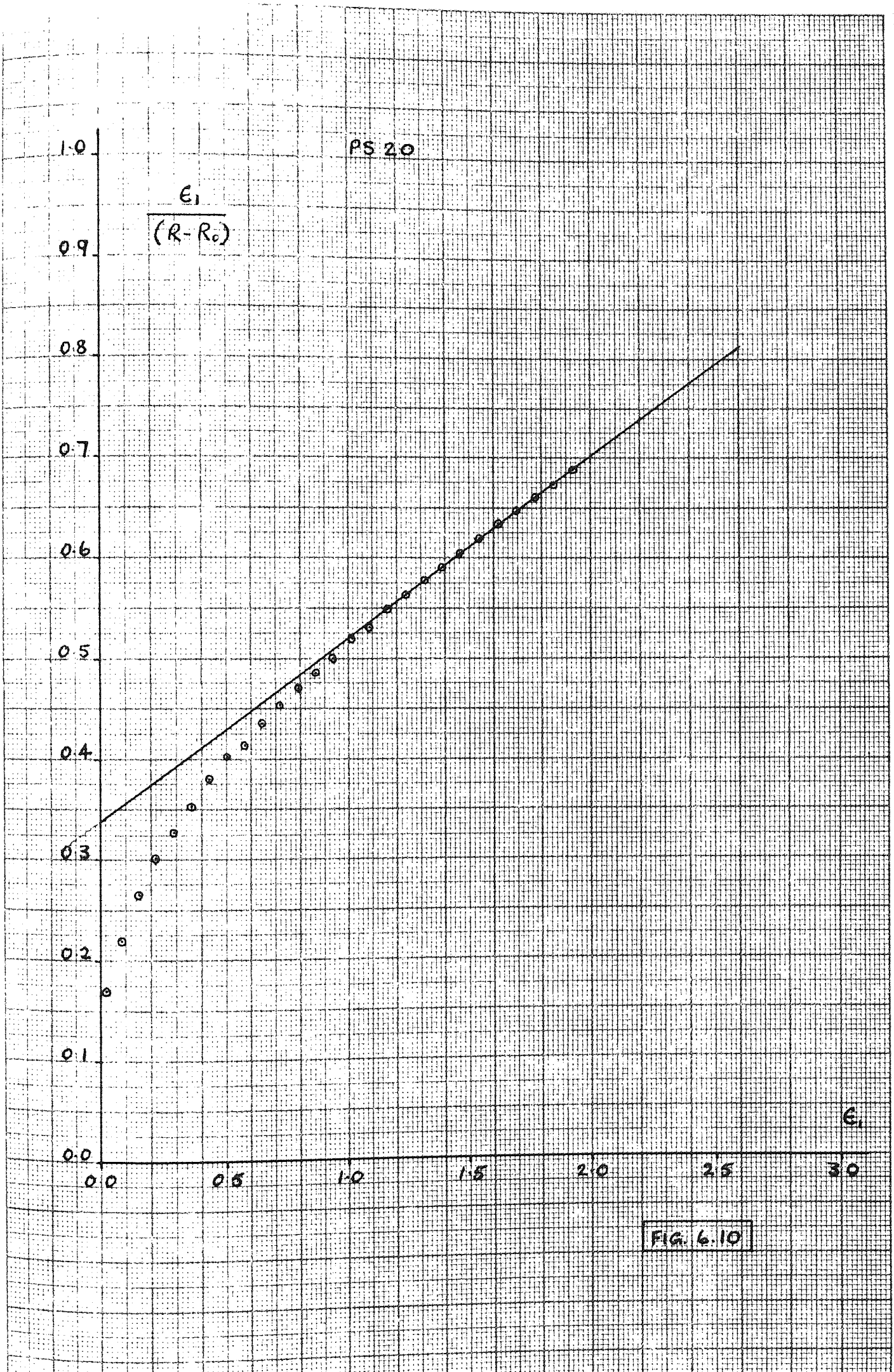
PS 20
$\frac{\epsilon_1}{(R-R_0)}$
1·0
0·9
0·8
0·7
0·6
0·5
0·4
0·3
0·2
0·1
0·0
0·0
0·5
1·0
1·5
2·0
2·5
3·0
ϵ_1

FIG. 6.10

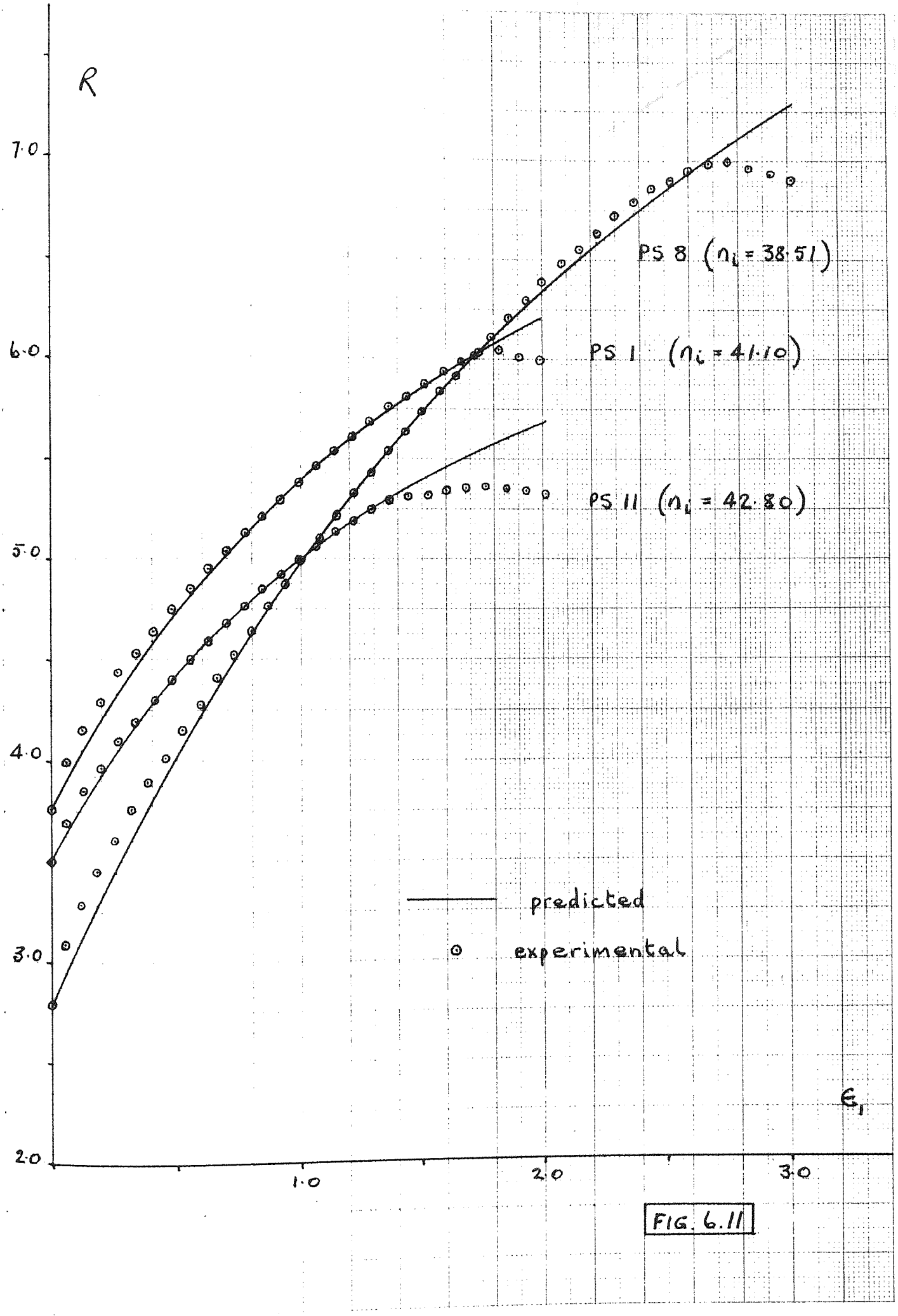
R
7·0
6·0
5·0
4·0
3·0
2·0
1·0
2·0
3·0
ϵ_1
PS 8 (n_i = 38·51)
PS 1 (n_i = 41·10)
PS 11 (n_i = 42·80)
predicted
experimental

FIG. 6.11

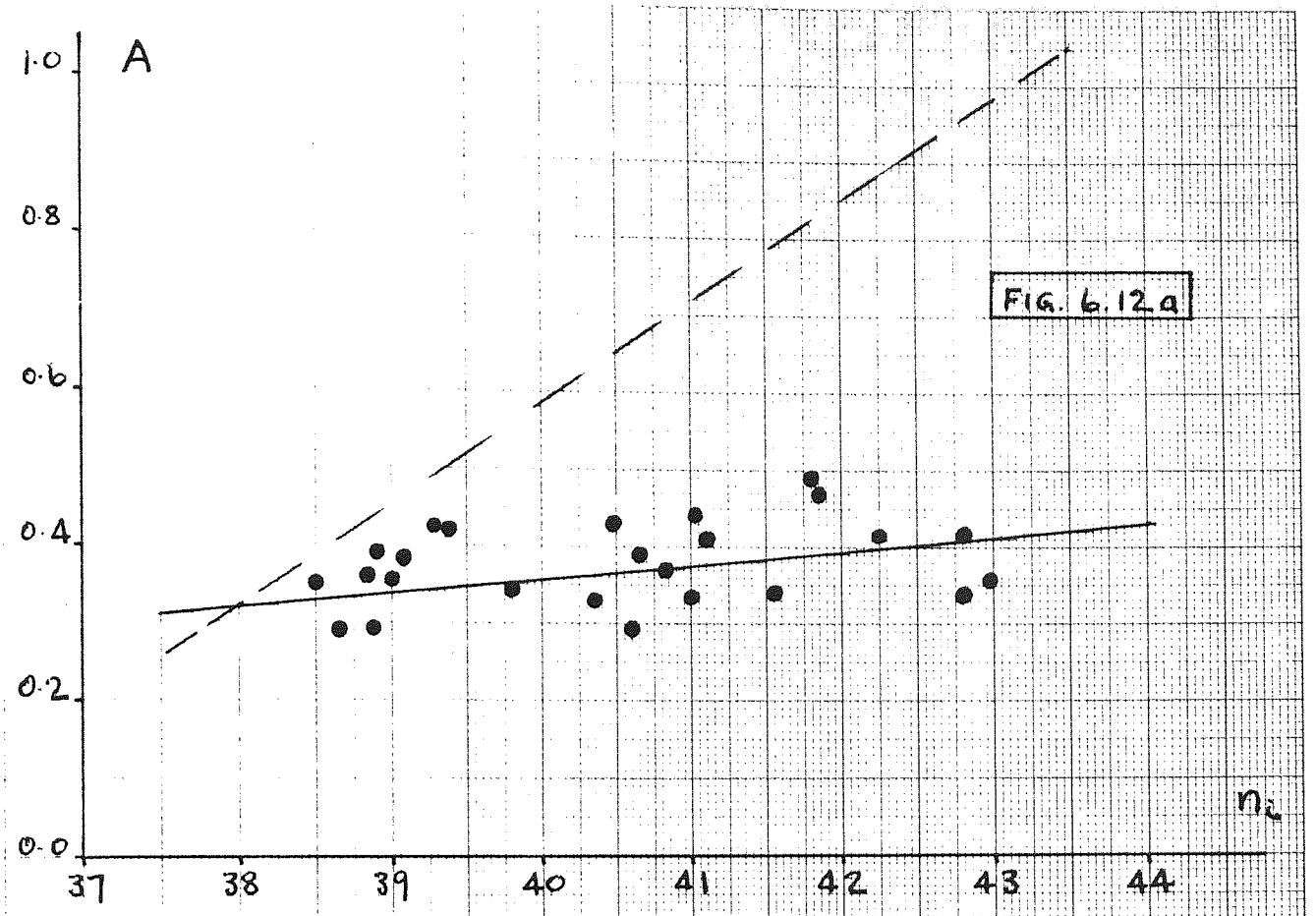

FIG. 6.12a

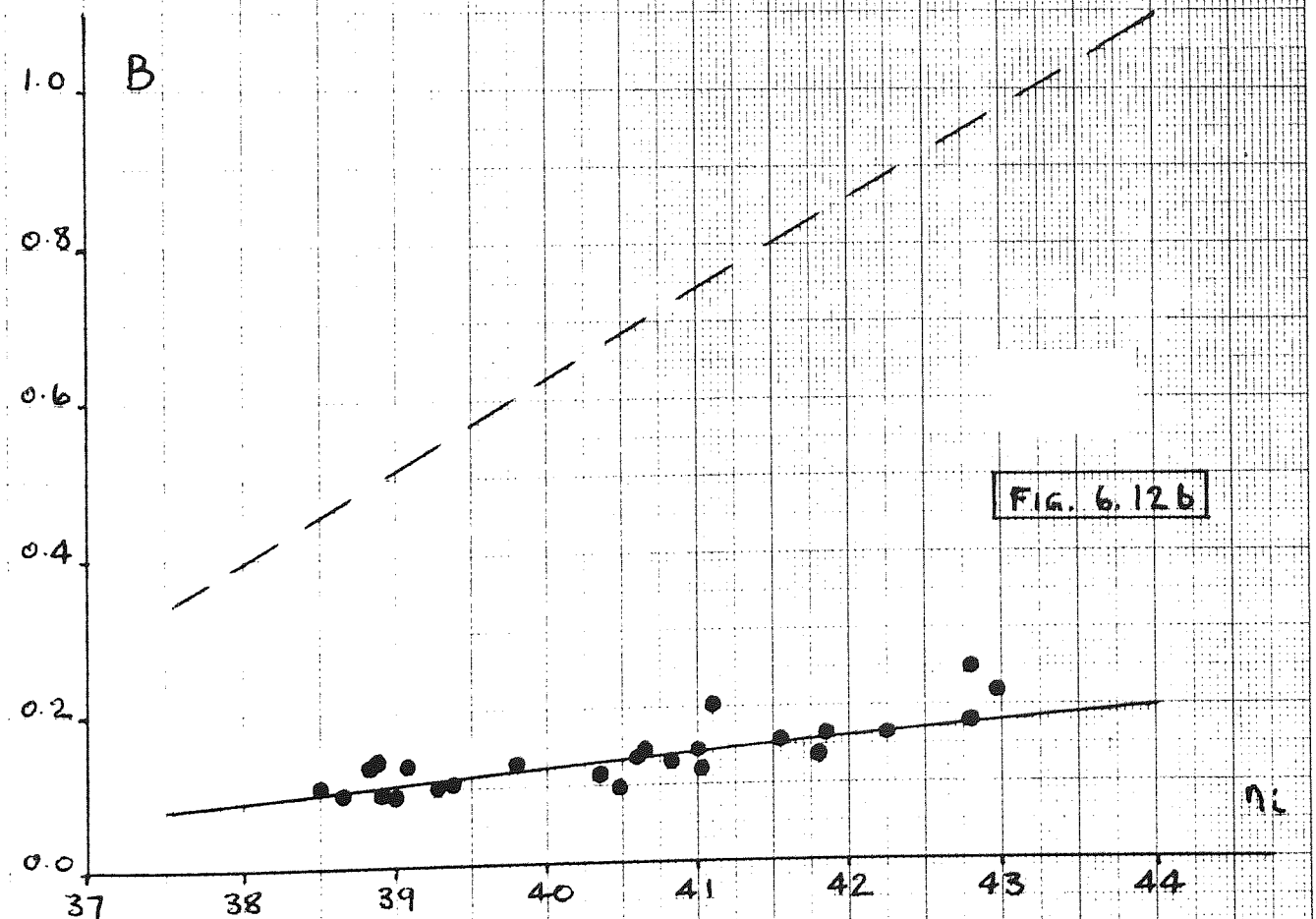

FIG. 6.12b

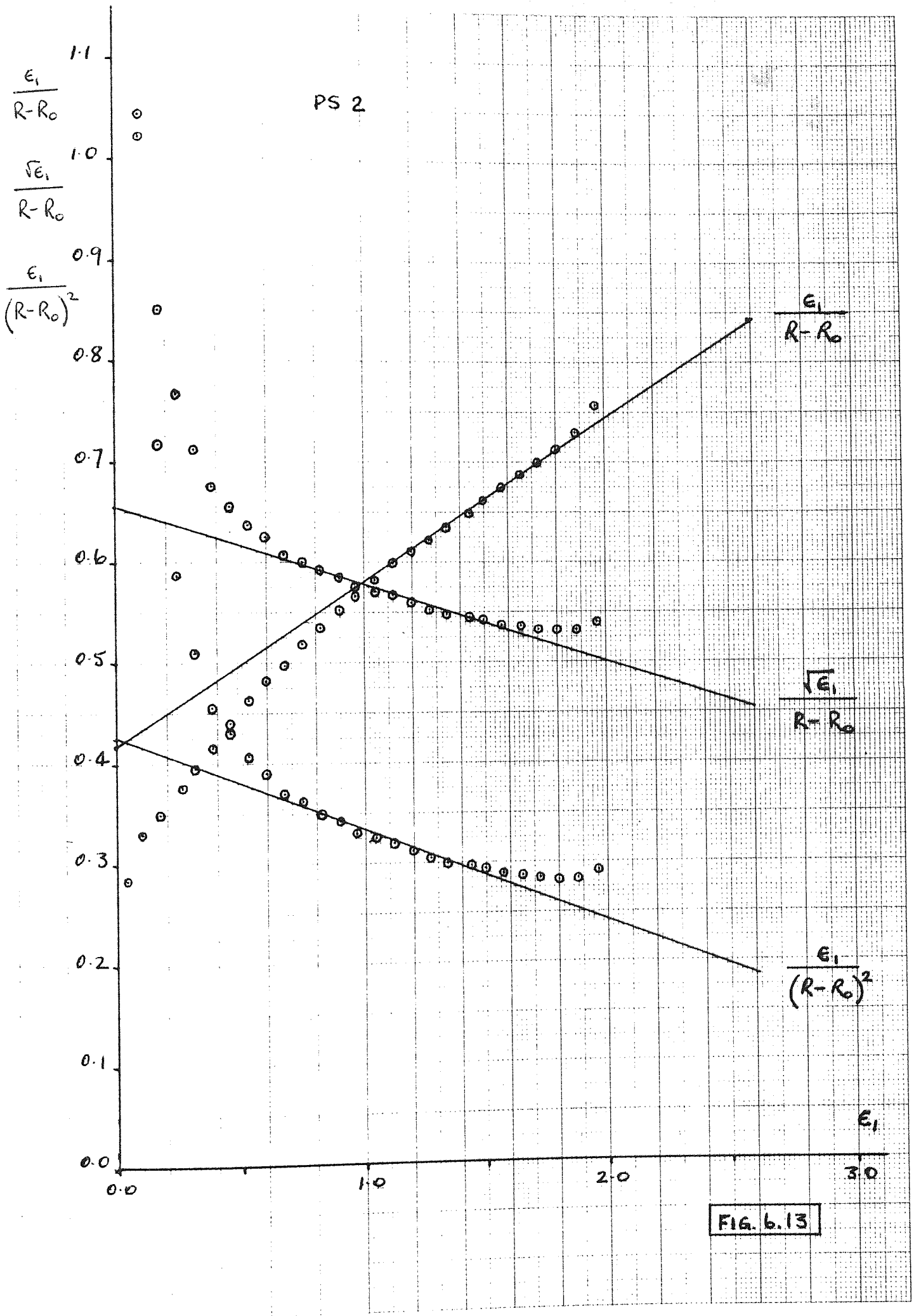
PS 2
$\frac{\epsilon_1}{R-R_0}$
$\frac{\sqrt{\epsilon_1}}{R-R_0}$
$\frac{\epsilon_1}{(R-R_0)^2}$
1.1
1.0
0.9
0.8
0.7
0.6
0.5
0.4
0.3
0.2
0.1
0.0
0.0
1.0
2.0
3.0
ϵ_1
$\frac{\epsilon_1}{R-R_0}$
$\frac{\sqrt{\epsilon_1}}{R-R_0}$
$\frac{\epsilon_1}{(R-R_0)^2}$

FIG. 6.13

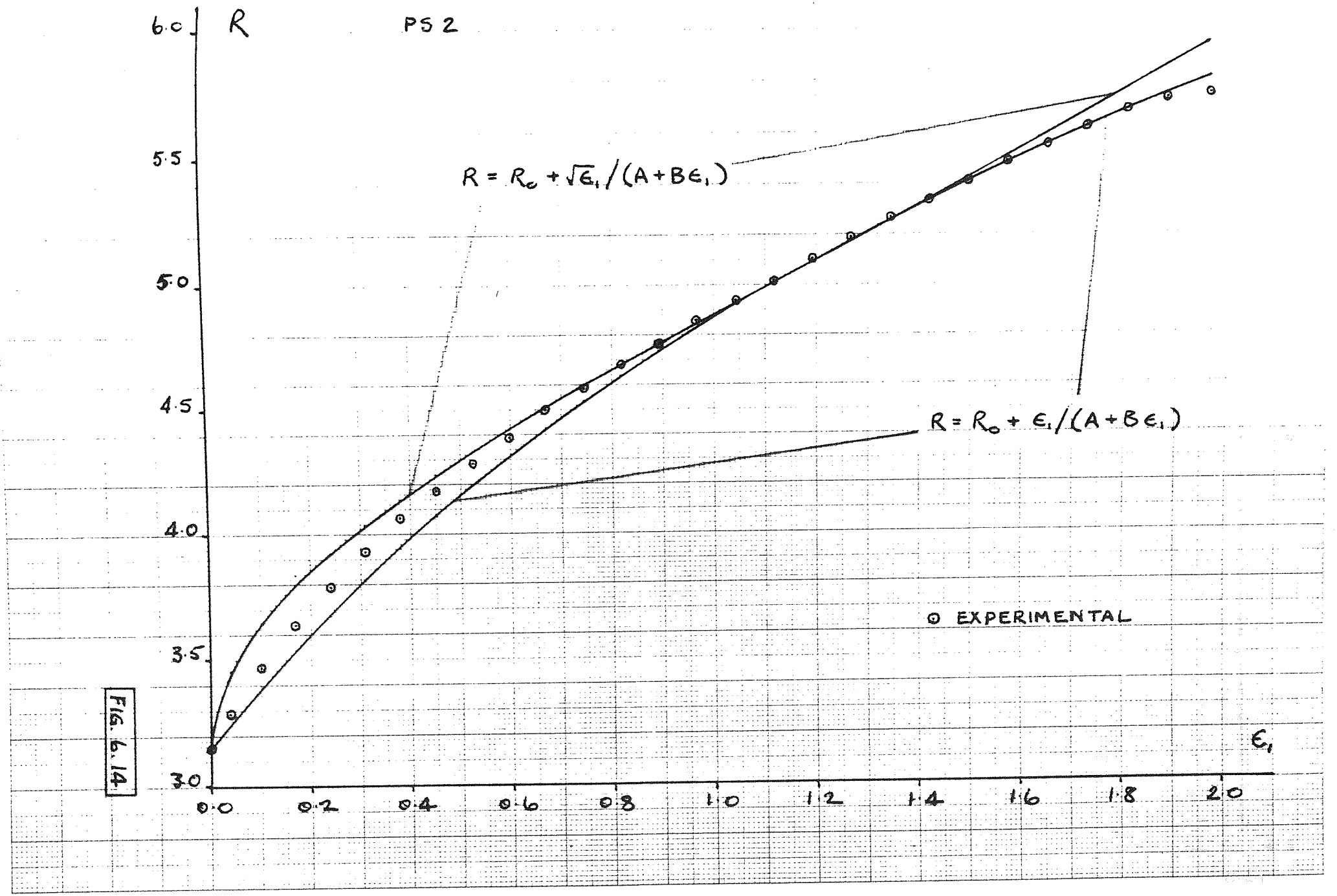
R
PS 2
6·0
5·5
5·0
4·5
4·0
3·5
3·0
0·0
0·2
0·4
0·6
0·8
1·0
1·2
1·4
1·6
1·8
2·0
ϵ_1
$R = R_o + \sqrt{\epsilon_1}/(A + B\epsilon_1)$
$R = R_o + \epsilon_1/(A + B\epsilon_1)$
⊙ EXPERIMENTAL

Fig. 6.14

FIG. 6.15

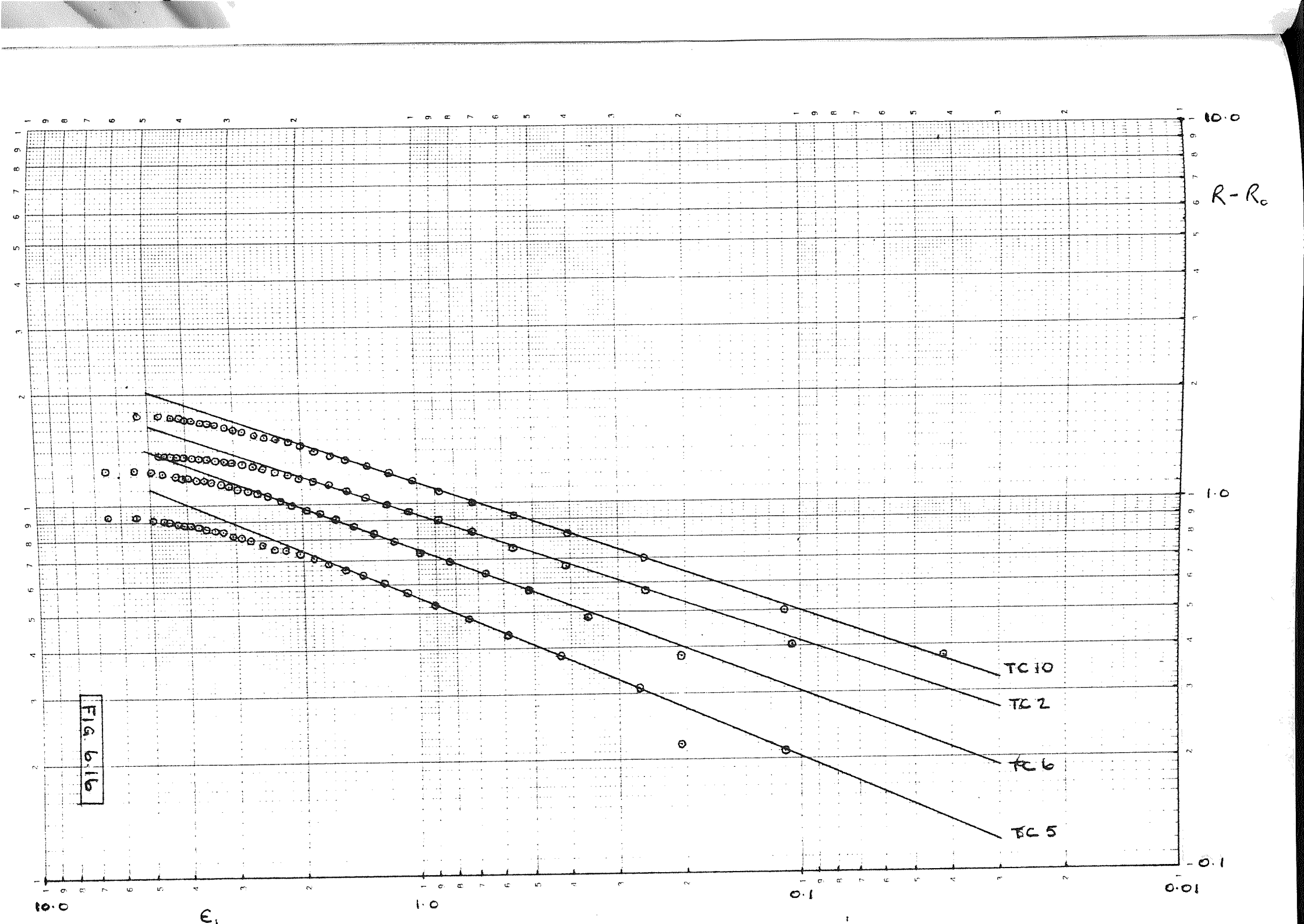

FIG. 6.16

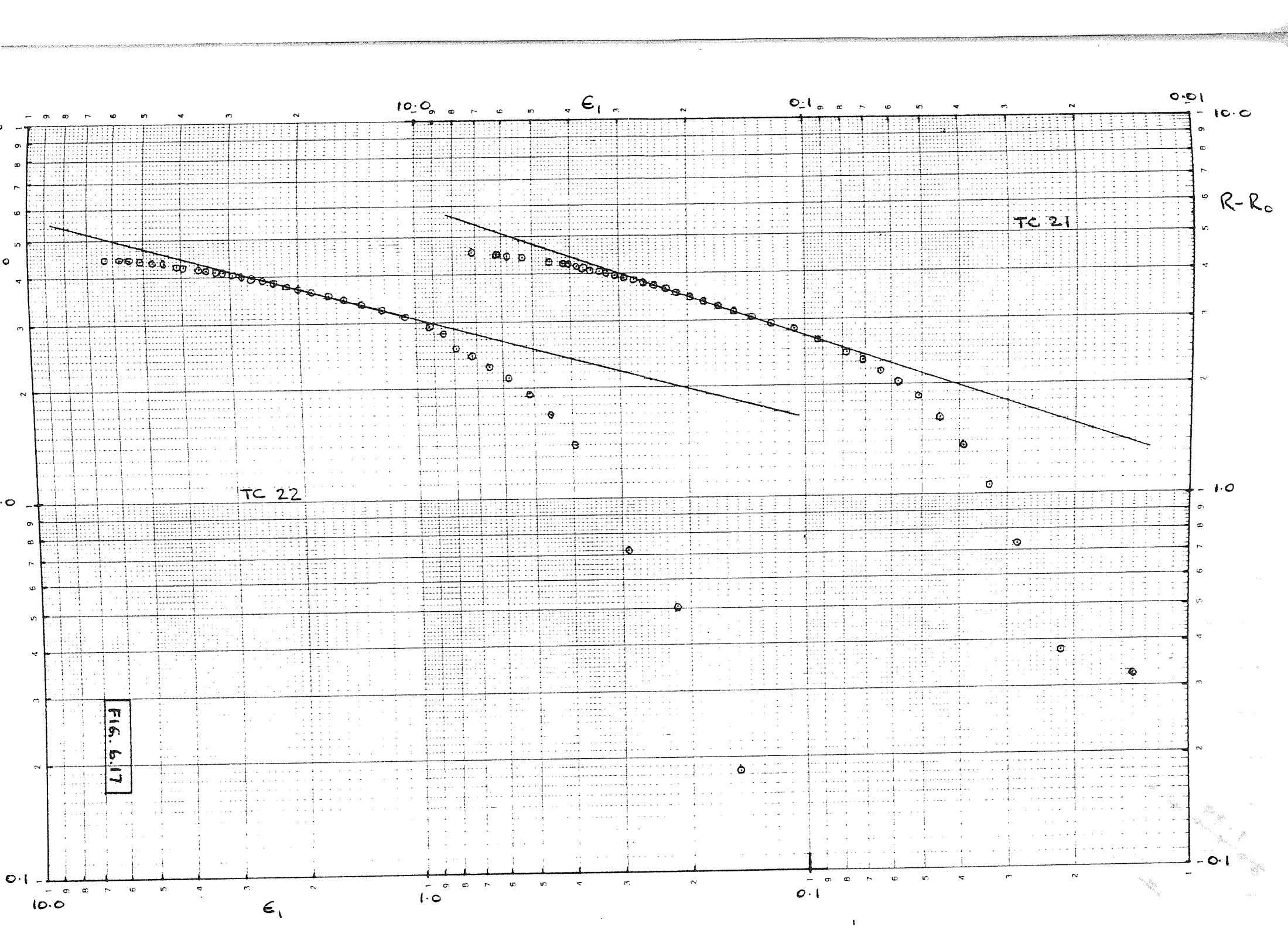
10·0
ϵ_1
0·1
0·01
10·0
$R-R_0$
TC 21
TC 22
1·0
0·1
10·0
ϵ_1
1·0
0·1
-0·1

FIG. 6.17

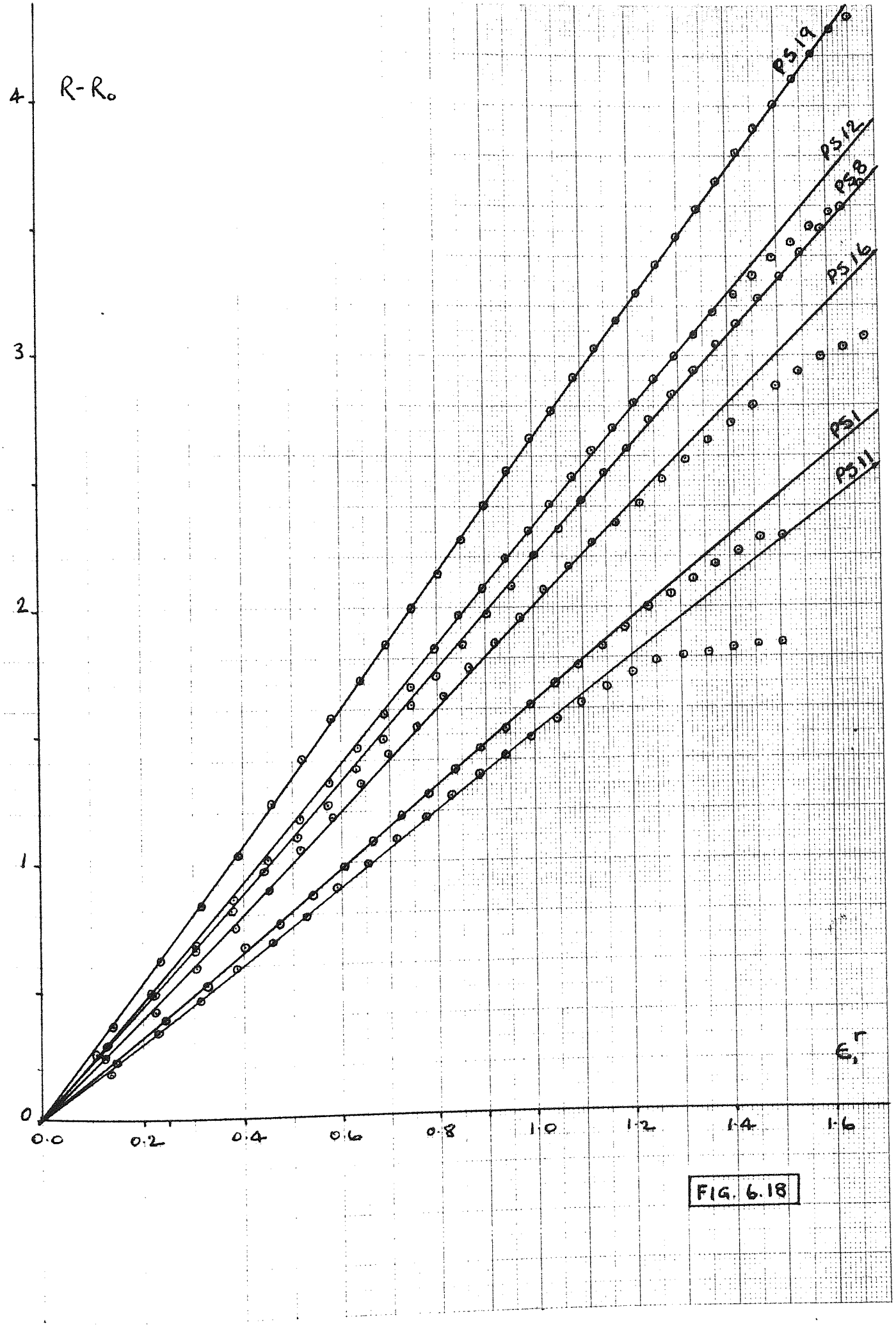

FIG. 6.18

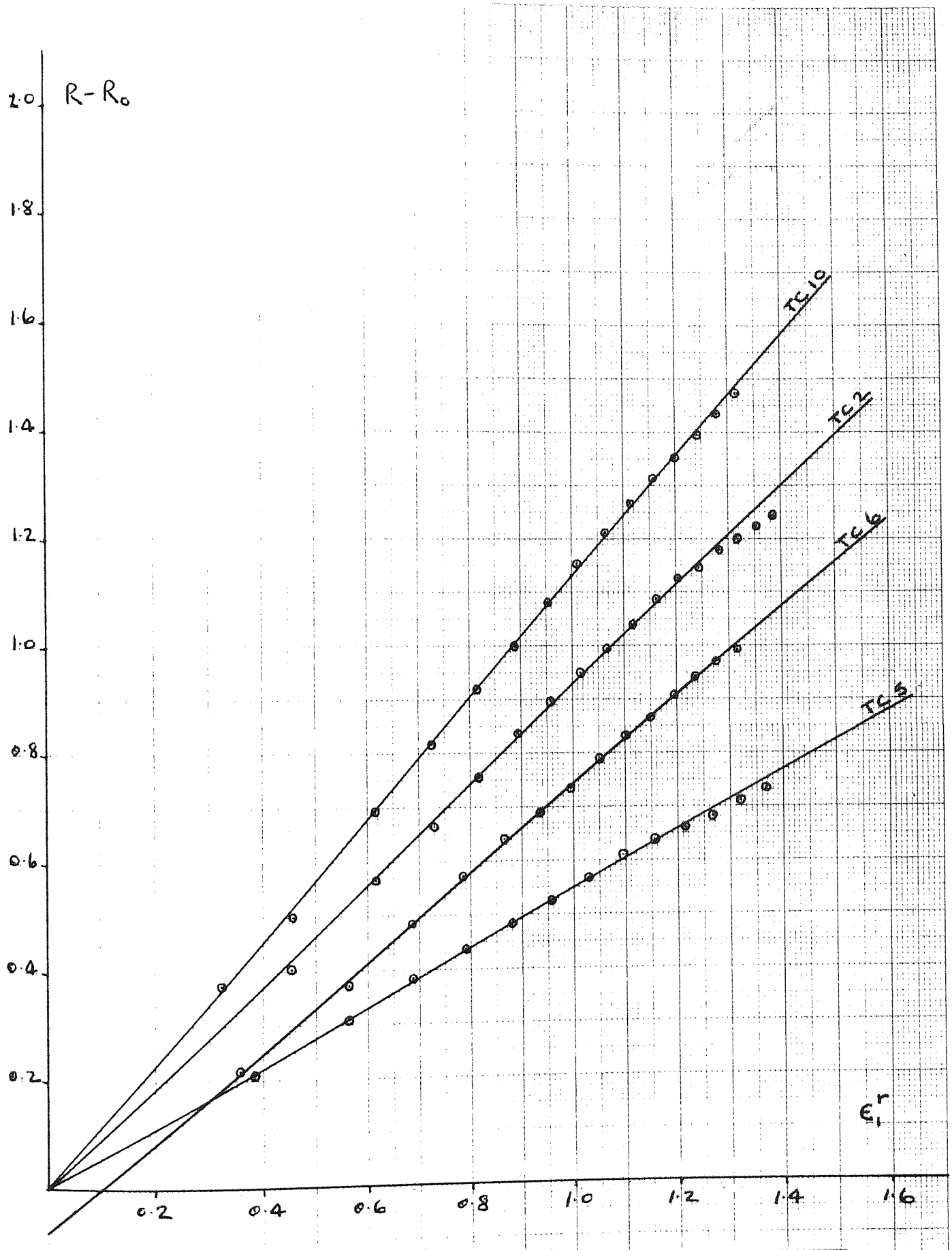
R - R₀
2·0
1·8
1·6
1·4
1·2
1·0
0·8
0·6
0·4
0·2
TC 10
TC 2
TC 6
TC 5
ϵ_1^r
0·2
0·4
0·6
0·8
1·0
1·2
1·4
1·6

FIG. 6.19

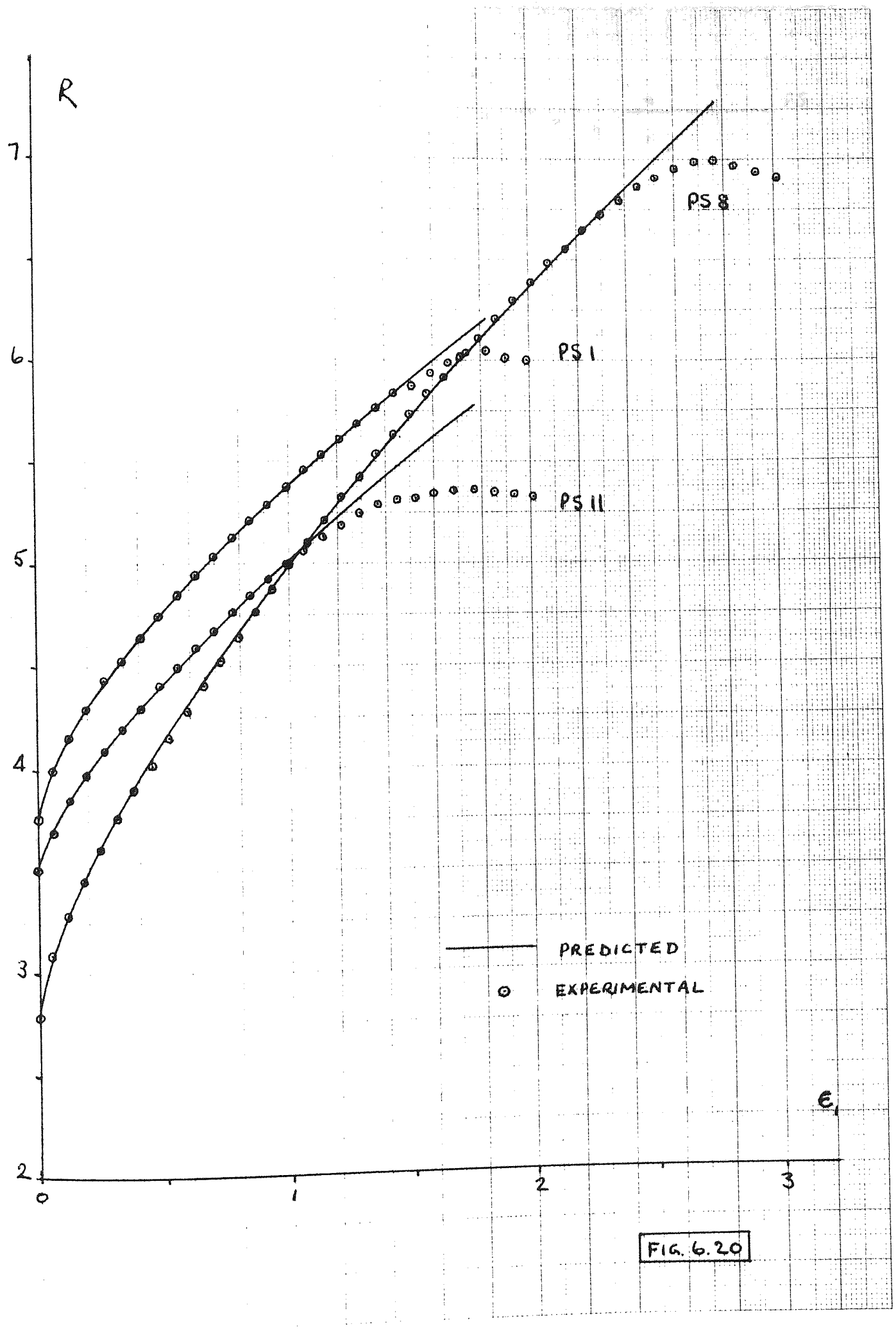
R
7
6
5
4
3
2
0
1
2
3
ϵ_1
PS 8
PS 1
PS 11
PREDICTED
EXPERIMENTAL

FIG. 6.20

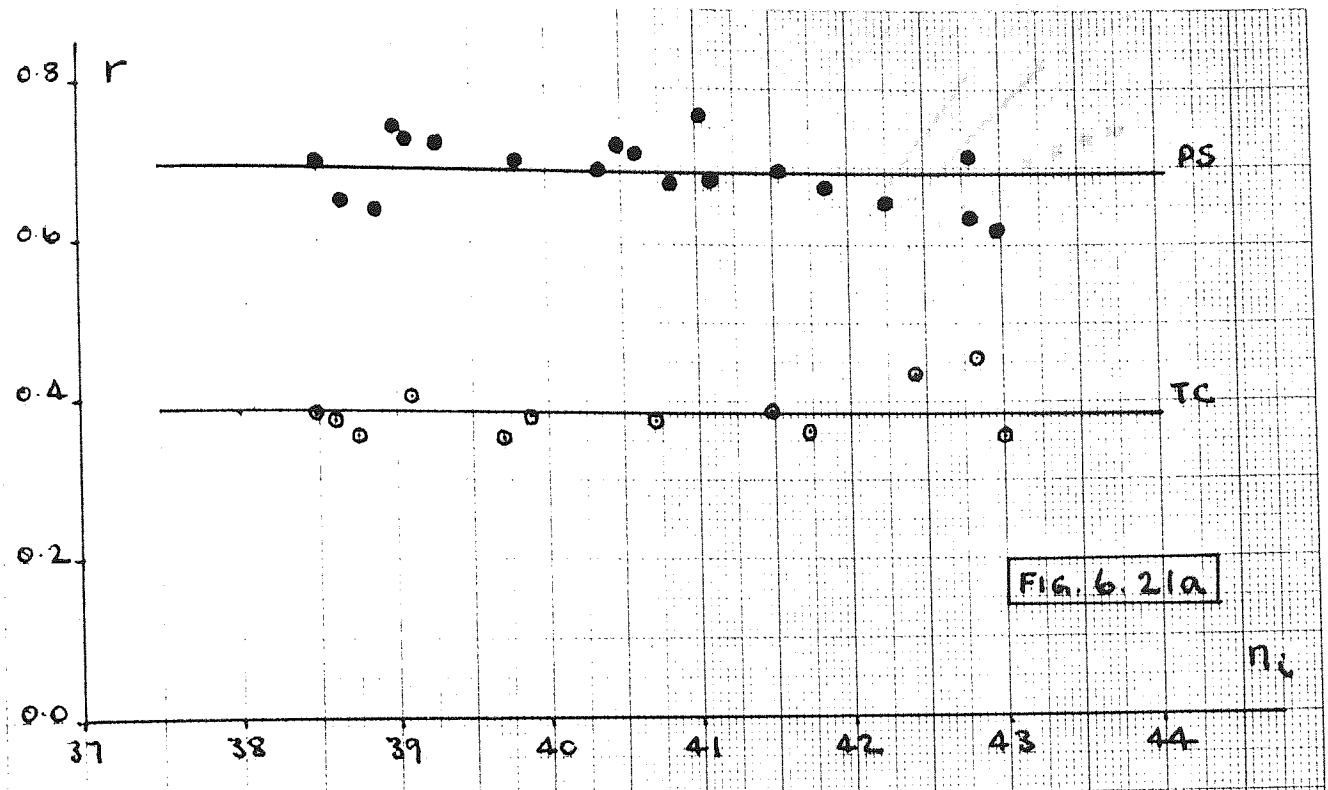

Fig. 6.21a

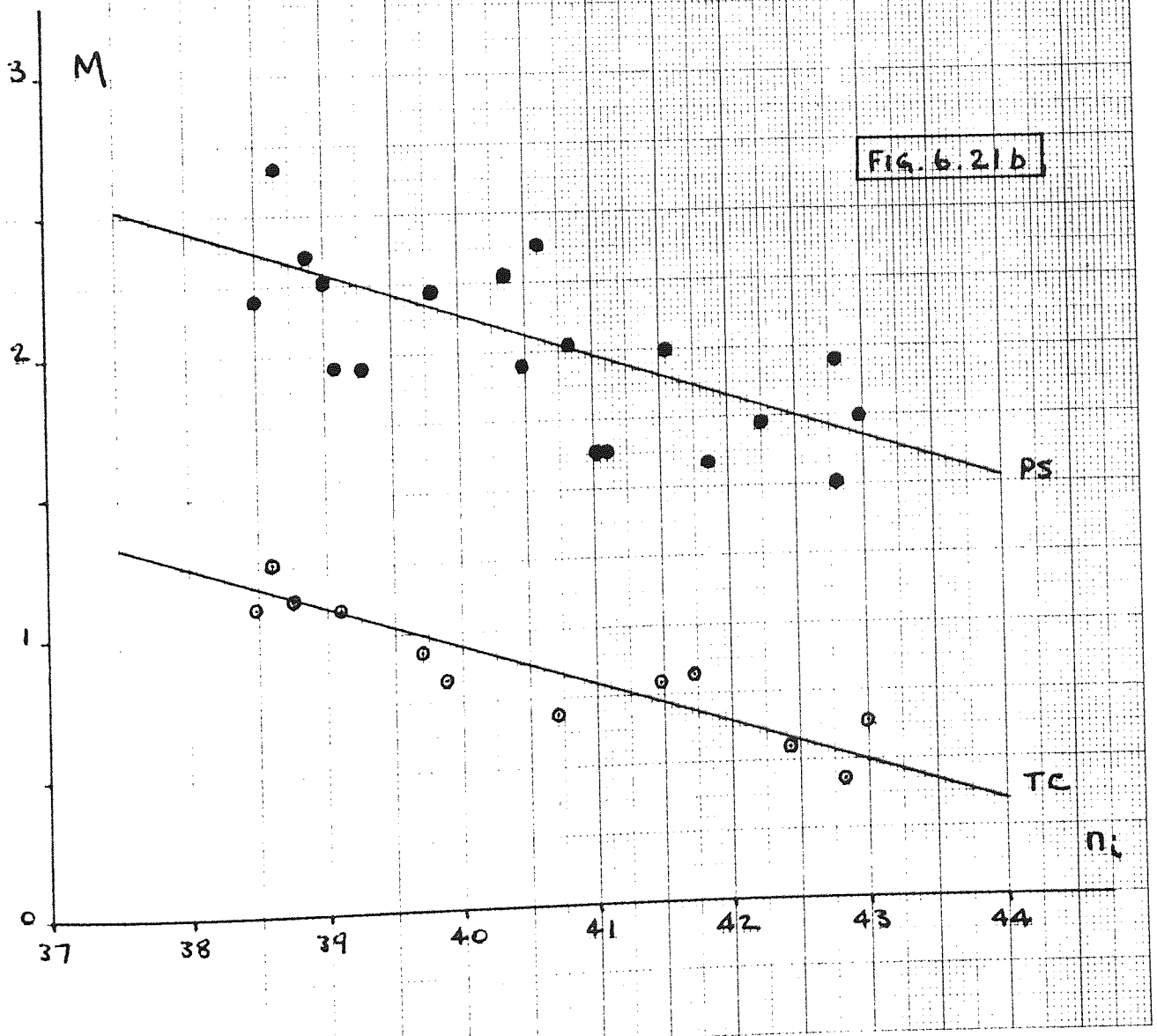

Fig. 6.21b

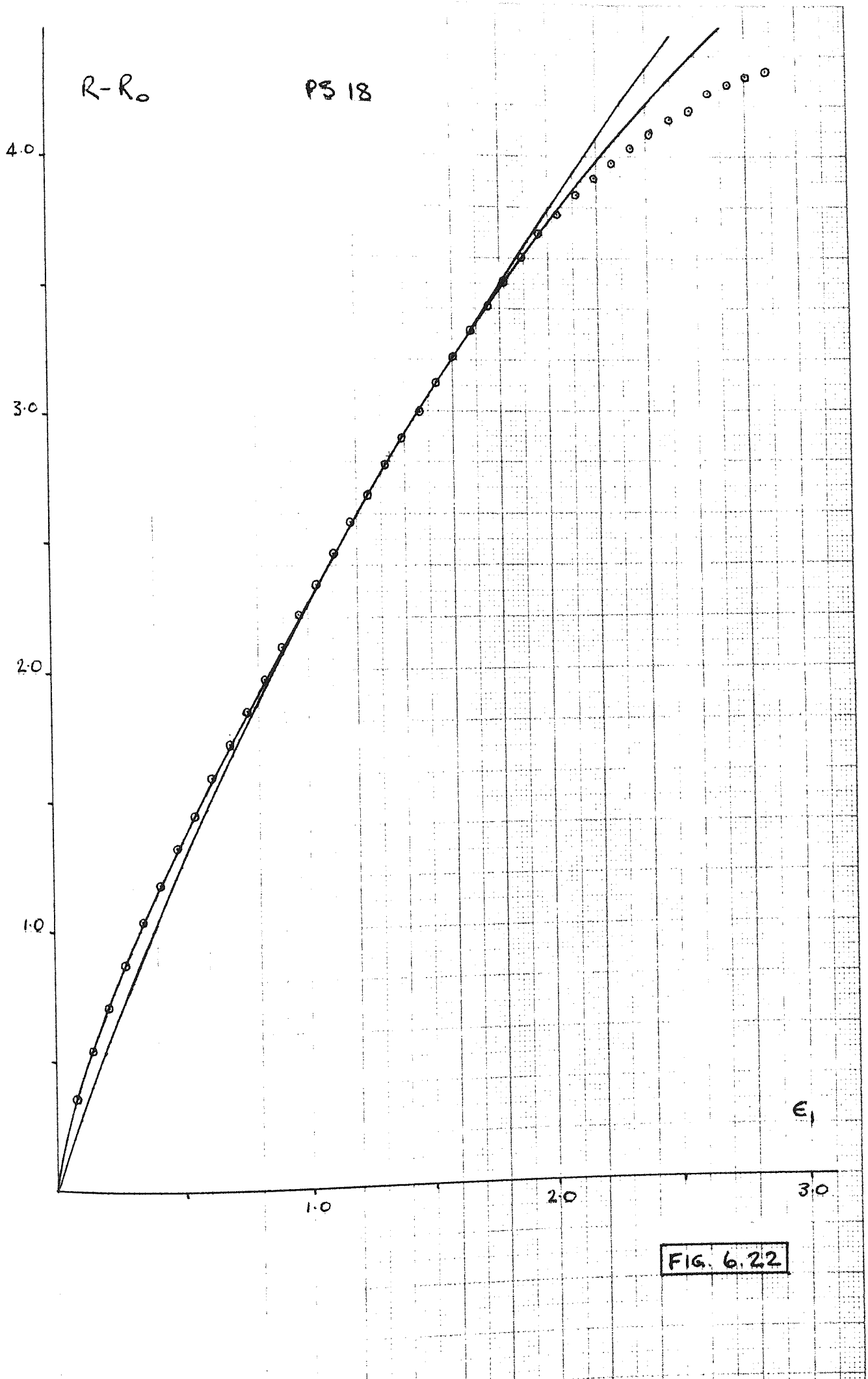

FIG. 6.22

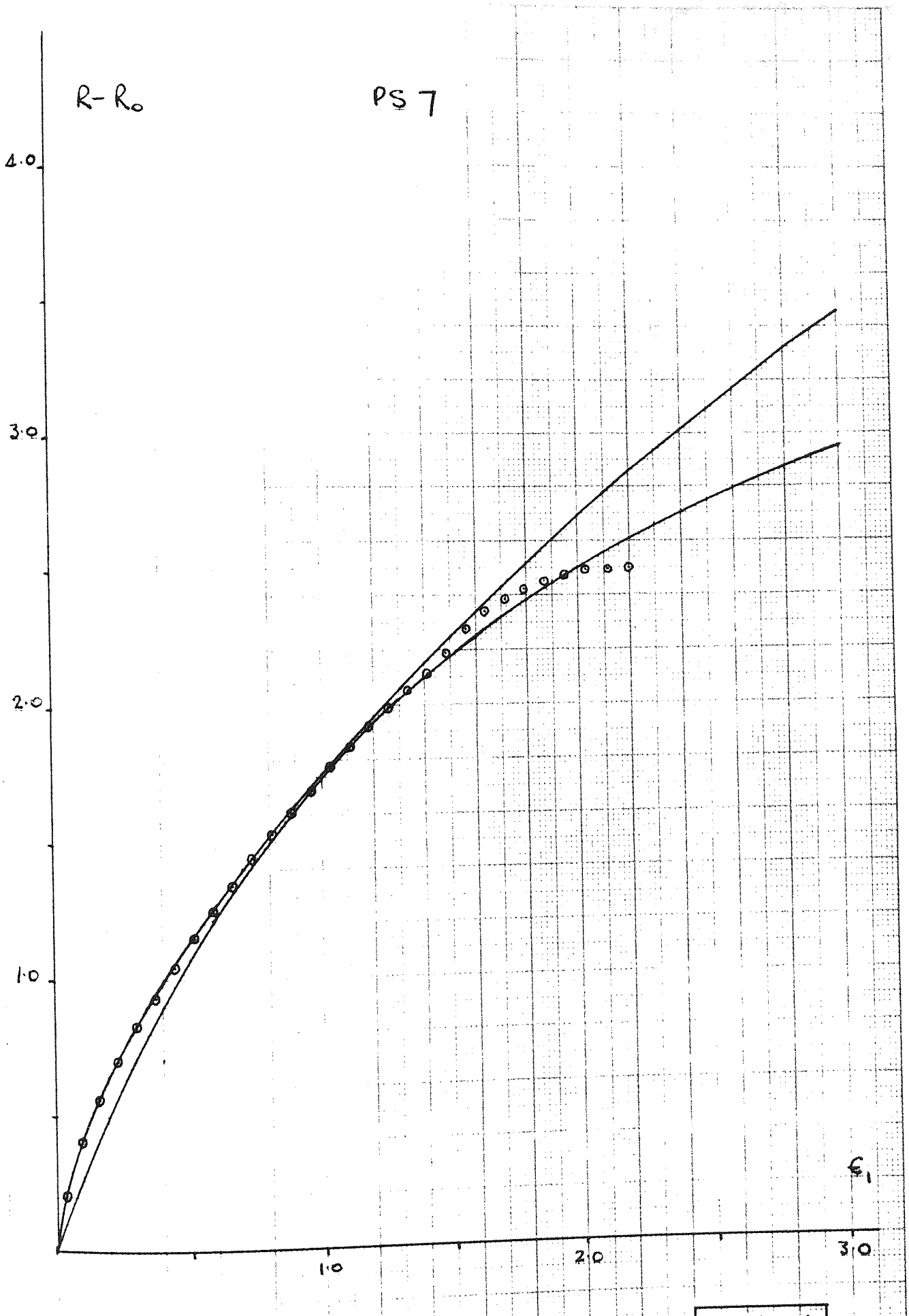

FIG. 6.24

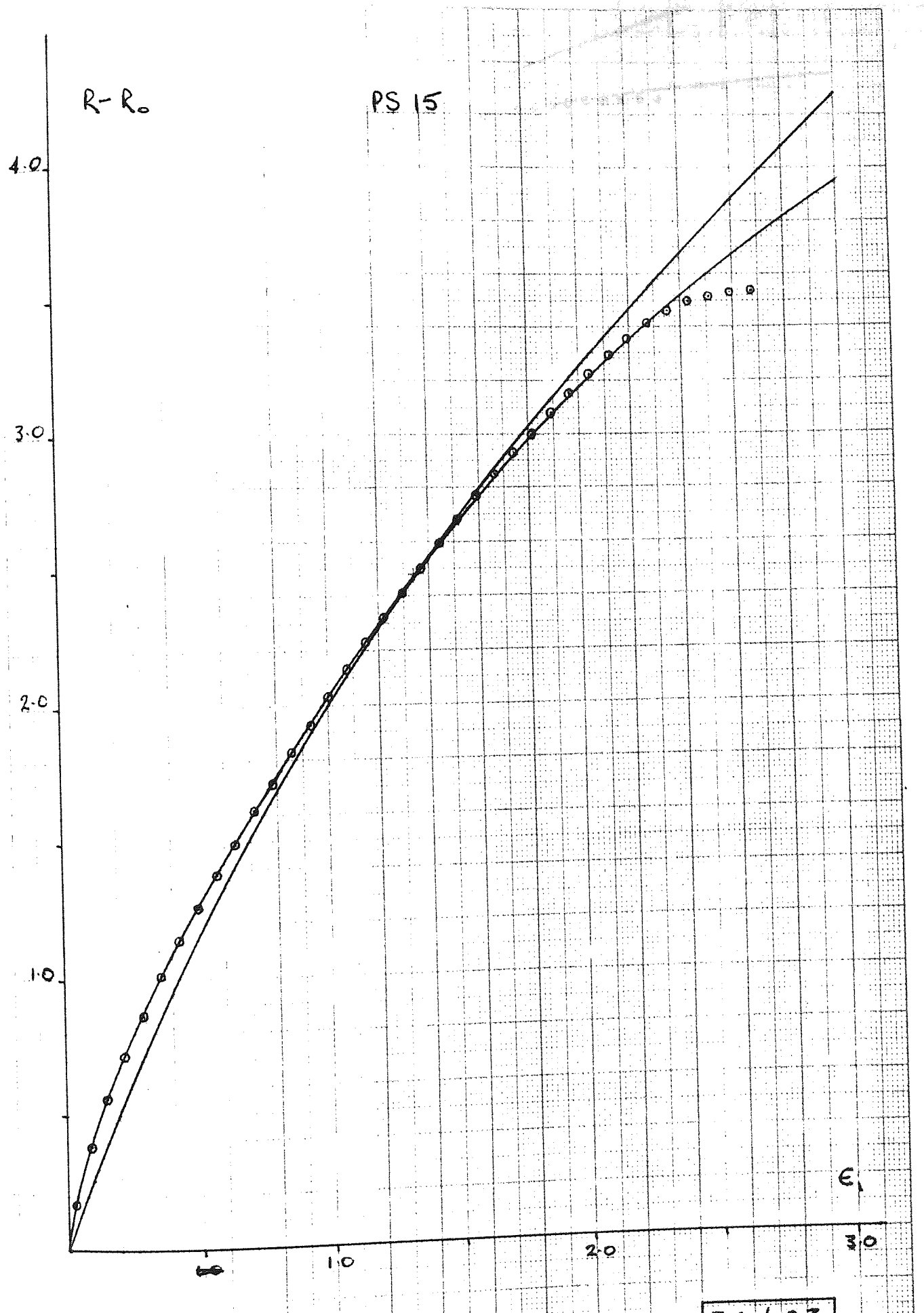

FIG. 6.23

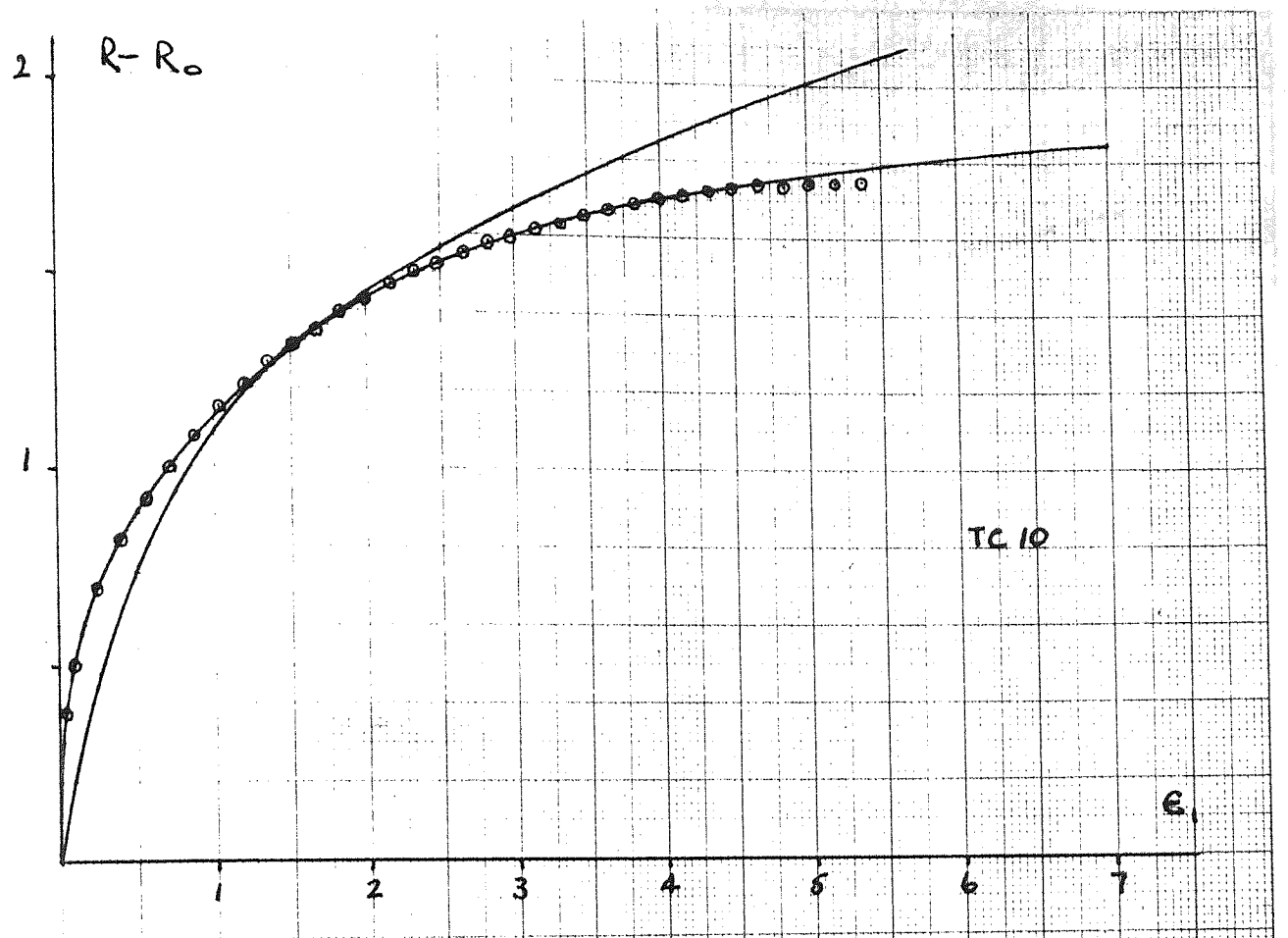

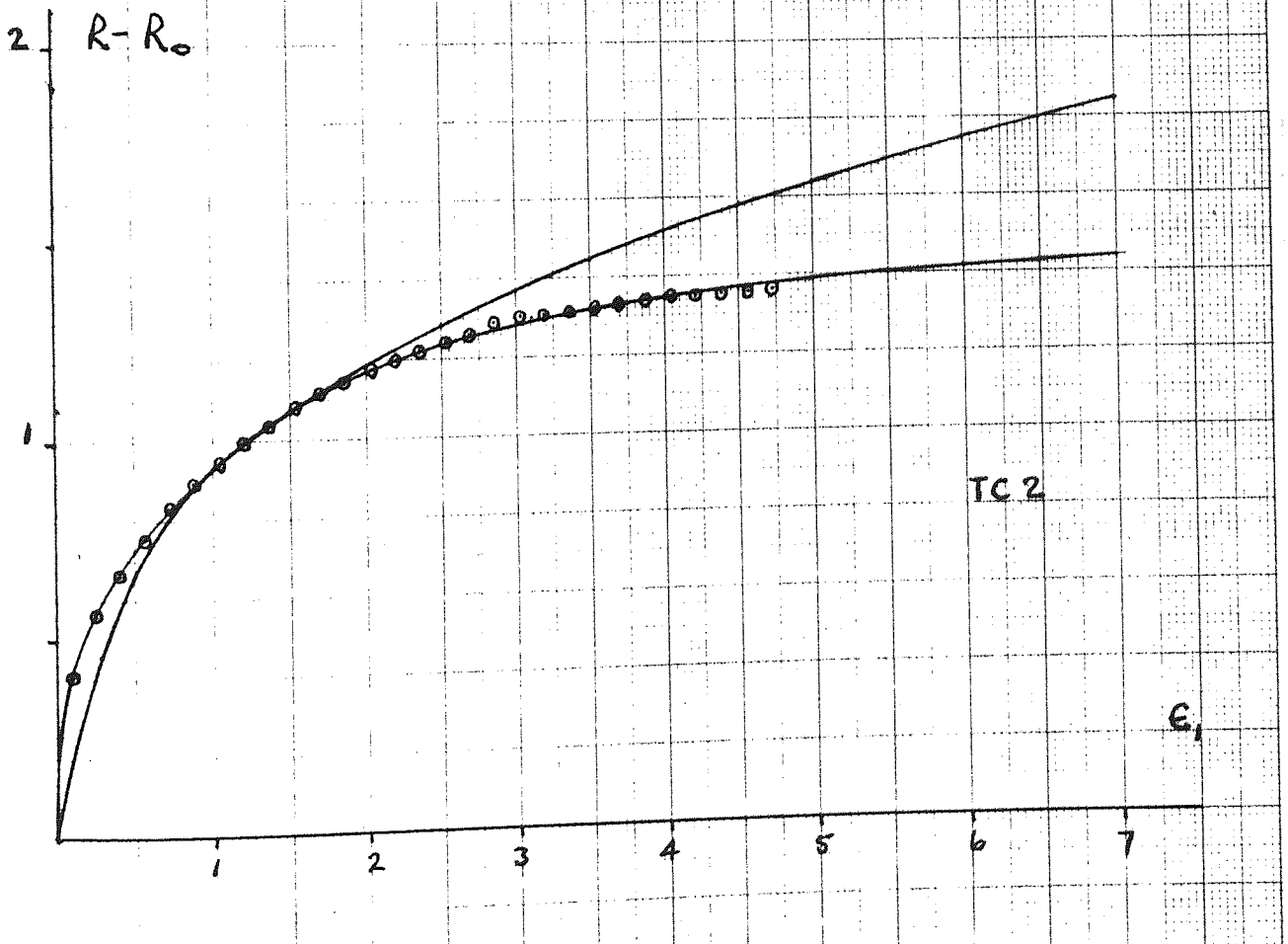

FIG. 6.25

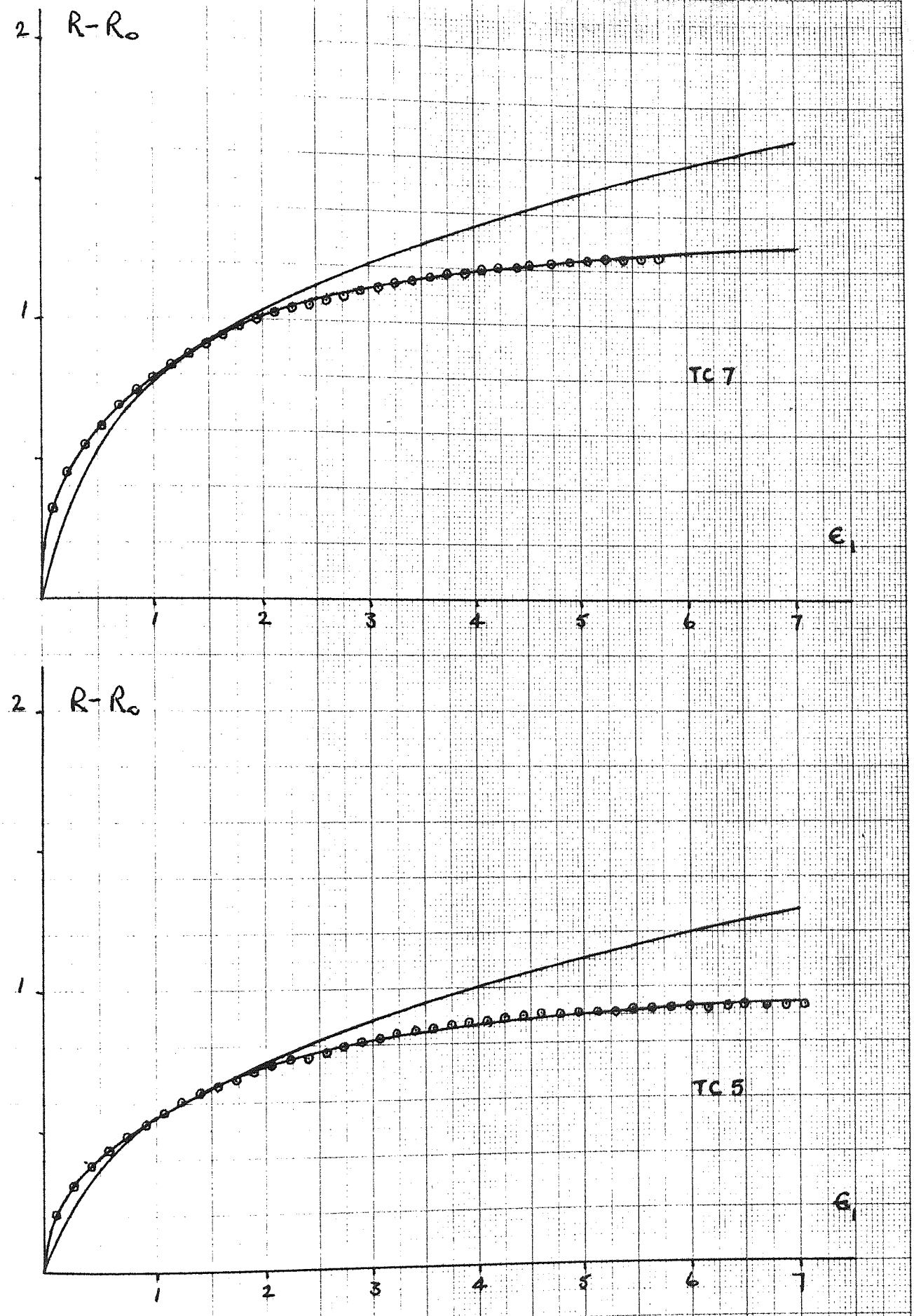

FIG. 6.26

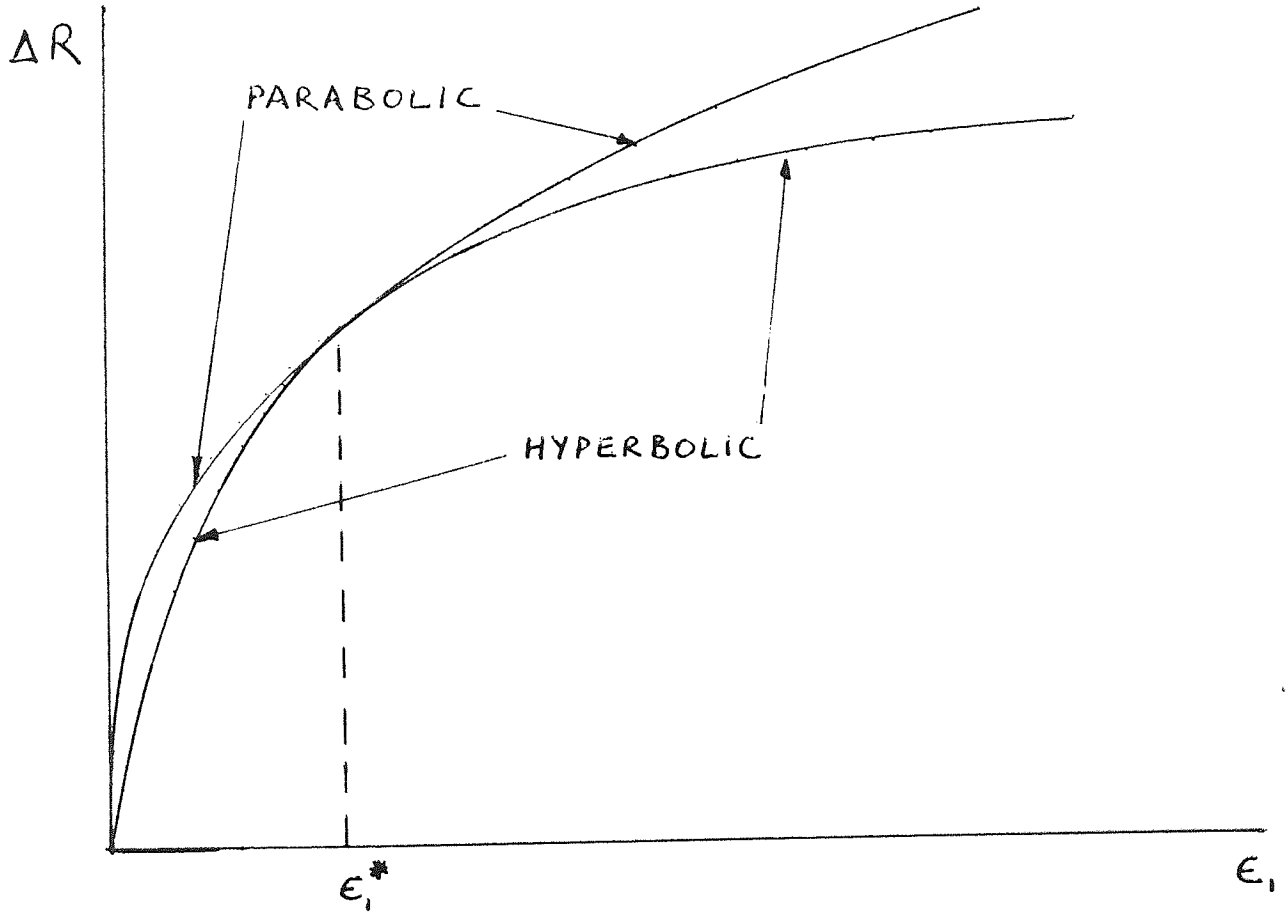

FIG. 6.27

CHAPTER SEVEN

7. PREDICTION OF THE INTERMEDIATE PRINCIPAL STRESS IN PLANE STRAIN.

7.1. Introduction

In this research program an attempt has been made to measure the intermediate principal stress during the plane strain deformation of sand. The results of the plane strain tests have been presented and discussed in Chapter 4. The differences in specimen behaviour exhibited under plane strain and triaxial compression conditions are due to restrictions on particle movement as a result of constraining the plane strain specimens in one orthogonal direction. Consequently the principal stress acting in the zero lateral strain direction attains a value which is intermediate between the other two principal stresses. Previous research has failed to incorporate the intermediate principal stress into any fundamental soil mechanics theory; existing expressions for σ_2 in plane strain have either been based on the assumption of isotropic elastic theory or have been purely empirical, Wood (1958), Cornforth (1961), Wade (1963), Bishop (1966), Green (1969).

The most successful theoretical treatment of the behaviour of sand has been provided by the stress-dilatancy theory, Rowe (1962), Horne (1965). However, workers in this field have generally ignored the intermediate principal stress in plane strain since it does not appear in the stress-dilatancy equation $R = D.K_{cv}$, Wightman (1967), Ismael (1969), Tong (1970). The object of this chapter is to rectify this omission.

It is postulated that, in plane strain, the intermediate principal stress is related to the slip planes in a unique manner, irrespective of the type of material. The theory is based on the interpretation of Mohr's circles and is a logical extension of the theory of ideal isotropic rigid-plastic material.

7.2. Rigid-plastic model.

Since the volume of an element of ideal, isotropic, rigid-plastic material does not alter, each incremental distortion in a state of plane strain consists of a pure shear, and the state of stress at each point can be represented by a pure shear stress together with a hydrostatic pressure, Hill (1950). The intermediate principal stress, normal to the planes of flow, can therefore be expressed in terms of principal stresses as

$$\sigma_2 = 0.5 \left(\sigma_1 + \sigma_3 \right) \qquad (7.1)$$

The above can be illustrated by Mohr's circles of stress and strain-increment as shown in Fig. 7.1. For an isotropic rigid-plastic material undergoing plane strain deformation, the principal axes of stress and strain-increment coincide. Consequently the directions of maximum shear stress coincide with the directions of maximum shear strain-increment and are inclined at 45° to the major principal plane. As shown by the Mohr's circle of strain-increment in Fig. 7.1, these characteristic directions, known as slip-lines in the classical theory of plasticity, are also directions of zero extension.

It is evident from Fig. 7.1 that the intermediate principal stress is equal to the normal stress acting on the slip planes. However, there is a uniqueness about the ideal rigid-plastic model which obscures the logical extension of the mathematical theory of plasticity to account for the mechanical behaviour of particulate material. The ideal, isotropic, rigid-plastic material possesses the following directional characteristics: the principal axes of stress and strain-increment coincide; the planes on which the limiting stress state applies are planes of zero extension; the limiting stress planes are also the planes on which physical slip occurs. None of these conditions will necessarily apply to materials other than the ideal, isotropic, rigid-plastic material. Indeed, Hill (1950), p. 336,

states that, for anisotropic metals, ' the characteristics for the stresses and velocities are the same, and that they are the slip-lines, or directions of maximum shear strain-rate; these are not, in general, maximum shear-stress directions.' It is thus implied that the principal axes of stress and strain-increment do not necessarily coincide for anisotropic materials. It is interesting to note that non-coincidence of principal stress and strain-increment directions was one of the features of Parkin's (1965) analytical solution for the strength of regular close-packed spheres. Consequently, when attempting to apply the theory of ideally plastic solids to soil behaviour it is necessary to identify the directional characteristics of the theoretical model and to ensure that the implications of the theory are consistent with the observed mechanical behaviour of soil.

7.3. Mohr-Coulomb models.

Many attempts have been made to develop a mathematical theory of plasticity which is consistent with the mechanical behaviour of soil; see for example, Drucker et al (1955), de Jong (1958), Cox (1963), Spencer (1964), Mandl and Fernandez Luque (1970). The various theoretical models have been discussed by Spencer (1964), and Mandl and Fernandez Luque (1970). All the existing theories are based on the Mohr-Coulomb failure criterion but adopt different kinematic assumptions; none of the theories predict strain fields which are consistent with the observed deformation of sand. It is not the object of this chapter to develop an alternative mathematical theory of plasticity for sand but it is the intention to consider certain ideal particulate materials and to identify the corresponding Mohr-Coulomb interpretations, from which mathematical theories of plasticity may be developed.

7.3.1. A Non-dilatant/frictional model.

The material described is assumed to be volumetrically incompressible and to derive its strength solely from friction between

the particles. The Mohr's circles of stress and strain-increment are shown in Fig. 7.2, assuming that the axes of stress and strain-increment coincide. The model is the one used by Cox (1963) to formulate a non-associated flow rule. Since the volume is constant, $\phi = \phi_{cv}$, and the failure plane, AB, is also the plane of interparticle slip, being inclined at an angle of $45^{o} + \phi_{cv}/2$ to the major principal plane. The lines of zero extension, AC, however, are inclined at an angle of $\phi_{cv}/2$ to the failure plane and it is clear that non-coincidence of stree and velocity characteristics is a necessary consequence of the assumption of coincidence of principal stress and strain-increment directions for this material.

Although soils exhibit volume changes during shear the above model would appear to be relevant to the critical state strength attained at large strains when the soil is deforming at constant volume.

7.3.2. A non-frictional/dilatant model.

It was shown in the previous section that, for a non-dilatant Mohr-Coulomb material, the assumption of coincidence of principal stress and strain-increment directions was incompatible with coincidence of stress and velocity characteristics. This is generally true for a dilatant Mohr-Coulomb material also. However, the 'associated flow rule' model of Drucker et al (1952) is a special case of a Mohr-Coulomb model in which this incompatibility does not arise. For the model, normality is applied (incorrectly) to the failure envelope as if it were a yield locus, and St. Venant's hypothesis is assumed; the consequence is that volumetric expansion is a feature of the model as illustrated in Fig. 7.3.

The predicted rates of dilatation, however, are far in excess of those normally encountered in particulate materials. As can be seen from Fig. 7.3. the angle of dilatation, ν, is equal to the angle of internal shearing resistance, ϕ; thus

$$\frac{\sigma_1}{\sigma_3} = \frac{-d\varepsilon_3}{d\varepsilon_1} \qquad (7.2a)$$

and $$\sigma_1 \, d\varepsilon_1 + \sigma_3 \, d\varepsilon_3 = 0 \qquad (7.2b)$$

Equation 7.2b demonstrates that no energy is dissipated internally. This observation was also made by Harkness (1972) who pointed out that the 'associated flow rule' model corresponds to the behaviour of a 'frictionless dilating material that is incapable of dissipating energy' and further added that the frictionless dilating material 'is not really exhibiting plastic yield, but is merely an engine for transferring energy from one boundary to another.'

The frictionless nature of the 'associated flow rule' model can also be demonstrated by comparing the flow rule (equation 7.2a) with the stress–dilatancy flow rule

$$\frac{\sigma_1}{\sigma_3} = \frac{-d\varepsilon_3}{d\varepsilon_1} \cdot \tan^2 \left(45 + \phi_{cv}/2 \right) \qquad (5.29 \text{ bis})$$

The experimental verification of the stress–dilatancy flow rule has been demonstrated for a variety of particulate materials, see Chapter 5, and it is clear from the comparison of equations 7.2a and 5.29 that the Mohr–Coulomb model illustrated in Fig. 7.3 corresponds to the behaviour of a particulate material with zero interparticle friction. Hence, since $K_{cv} = 1$, $\beta = 45^\circ$ and, as shown in Fig. 7.3, the limiting stress plane, AB, does not coincide with the interparticle slip plane, AC. Furthermore, since $\tan \alpha = D$ according to the stress–dilatancy theory, the rupture plane, AD, is not inclined in the direction of zero extension.

7.3.3. Stress-dilatancy model.

The stress-dilatancy interpretation of Mohr's circles of stress was provided by Rowe (1971b) and is shown in Fig. 7.4, together with the corresponding Mohr's circle of strain increment. The strain-rate circle is similar to that of the frictionless Mohr-Coulomb material, Fig. 7.3, but the predicted rates of dilatation correlate with experimental evidence for sand; the stress circles require further explanation.

The conventional stress circle of diameter $(\sigma_1 - \sigma_3)$ represents the actual stress conditions at failure for the dilating material. The small stress circle of diameter $(\sigma_1/D - \sigma_3)$ represents the stress conditions for the same material deforming at constant volume. Therefore, the small circle, which can be conveniently described as the friction circle, is the 'Mohr's circle for the material modified for no dilation', Rowe (1971b). Consequently, the failure envelope to the friction circle is inclined at an angle of ϕ_{cv} and corresponds to the non-dilatant Mohr-Coulomb model shown in Fig. 7.2. As the deviator stress increases during a test the conventional stress circle increases in size, being smaller than the friction circle during volumetric compression and larger when expanding.

The stress-dilatancy theory predicts that $\phi_f = \phi_{cv}$ throughout deformation in plane strain tests and this was substantiated by the experimental results presented in Chapter 5. Therefore, the friction circle is invariant throughout a test. Furthermore, it is a basic tenet of the stress-dilatancy theory that sliding occurs on interparticle contact planes inclined at a critical inclination to the major principal stress direction, β_c. This is illustrated by the slip planes indicated by the friction circle. Since the interparticle slip behaviour occurs throughout deformation, with ϕ_f constant in plane strain, the stresses acting on the slip planes of the dilating material can be obtained by

extrapolation as shown in Fig. 7.4.

Further aspects of the stress-dilatancy model are also shown in Fig. 7.4. Although slip occurs between particles on the β planes, these planes are not continuous since the sliding particles interlock with neighbouring particles which are stable. Consequently, when rupture planes form, the rupture surface is saw-toothed, as illustrated by Rowe (1962), although the particles slip along β planes the overall inclination of the rupture planes coincide with the α planes, Rowe (1962), (1964b), α being defined by the expression

$$\tan \alpha = D. \tan (45 + \phi_{cv}/2) \qquad (7.3)$$

The α plane, deduced from equation 7.3 is shown in Fig. 7.4 and it can be seen that the same ratio of shear stress to normal stress is applied to both α and β planes. It is also noted that the stress-dilatancy model predicts that no two 'characteristic' directions coincide: the planes of limiting stress conditions, slip, rupture, and zero extension, are all orientated at different inclinations to the major principal stress plane. Consequently the stress-dilatancy model is much more complex than the simple ideal rigid-plastic model, Fig. 7.1.

The complications arise from the effects of both the particulate structure and the friction between the particles. The frictional and structural components of the shear strength of sand have been discussed in Chapter 5 and it is in this context that the models illustrated in Figs. 7.2 and 7.3 are of interest. The frictional component of shear strength can be described by the non-dilatant/frictional model shown in Fig. 7.2 whereas the structural component is represented by the non-frictional/dilatant model, Fig. 7.3. It is interesting to note that it is the interparticle friction rather than the particulate structure that causes the lack of coincidence between the limiting stress planes and the lines of zero-extension.

7.4. The intermediate principal stress in plane strain.

The hypothesis put forward in this chapter is that the intermediate principal stress in plane strain is equal to the normal stress acting on the slip planes. This is rigorously true for ideal rigid-plastic material. Since the internal geometry of random packings is similar to that of polycrystalline metals, the interparticle slip mechanism is analogous to the slip planes within the grains of a polycrystalline metal. Thus, the present hypothesis is a logical extension to the theory of rigid-plastic material. As shown in Fig. 7.4, the relationship between the Mohr's stress circle for a dilating material and the Mohr's stress circle corresponding to constant volume conditions is explained by the stress-dilatancy theory which, therefore, provides a rational basis for the following theoretical development.

The stress-dilatancy model illustrated in Fig. 7.4 is also shown in Fig. 7.5; but only the details relevant to the following theoretical treatment are shown.

From Fig. 7.5

$$AB = (\sigma_1 - \sigma_3) \cos (45^\circ + \phi_{cv}/2)$$

therefore

$$EB = (\sigma_1 - \sigma_3) \sin (45^\circ + \phi_{cv}/2) \cos (45^\circ + \phi_{cv}/2)$$

but

$$EB = (\sigma_2 - \sigma_3) \tan (45^\circ + \phi_{cv}/2)$$

Therefore

$$\frac{\sigma_2 - \sigma_3}{\sigma_1 - \sigma_3} = \cos^2 (45^\circ + \phi_{cv}/2) \qquad (7.10)$$

and

$$\frac{\sigma_2}{\sigma_3} = \frac{\sigma_1}{\sigma_3} \cdot \cos^2 (45^\circ + \phi_{cv}/2) + \sin^2 (45^\circ + \phi_{cv}/2) \qquad (7.11)$$

Using the relationships

$$\frac{\sigma_1}{\sigma_3} = D.K_{cv}$$

$$\cos^2 (45^\circ + \phi_{cv}/2) = 1/(K_{cv} + 1)$$

$$\sin^2 (45^\circ + \phi_{cv}/2) = K_{cv}/(K_{cv} + 1)$$

the following expressions are obtained

$$\frac{\sigma_2}{\sigma_3} = \frac{K_{cv}(D + 1)}{(K_{cv} + 1)} \qquad (7.12)$$

$$\frac{\sigma_1}{\sigma_2} = \frac{D\ (K_{cv} + 1)}{(D + 1)} \qquad (7.13)$$

$$\frac{\sigma_2}{(\sigma_1 + \sigma_3)} = \frac{K_{cv}(D + 1)}{(K_{cv} + 1)\ (DK_{cv} + 1)} \qquad (7.14)$$

$$\frac{\sigma_2 - \sigma_3}{\sigma_1 - \sigma_3} = \frac{1}{(K_{cv} + 1)} \qquad (7.15)$$

The predictions given by the above theoretical expressions are illustrated in Fig. 7.6–7.9. Since, for sand, $1 \leq D \leq 2$, the theory predicts a range of values for specific values of ϕ_{cv}. Fig. 7.6 shows the predicted range of σ_1/σ_3 for different values of ϕ_{cv}. This, of course, is the familiar stress–dilatancy relationship and requires no further comment. The minor principal stress ratio, σ_2/σ_3, as predicted by equation 7.12, is shown in Fig. 7.7. The minor principal stress ratio increases with both D and ϕ_{cv} but, unlike the major principal stress ratio, the rate of increase decreases with increase in ϕ_{cv}, for a given D. Equation 7.14 is illustrated in Fig. 7.8 and shows that the ratio $\sigma_2/(\sigma_1 + \sigma_3)$ decreases with both D and ϕ_{cv}.

When $\phi_{cv} = 0$ then $\sigma_2 = 0.5\ (\sigma_1 + \sigma_3)$ irrespective of D. Fig. 7.9 is of special interest as it predicts that the plane strain value of Bishop's (1966) parameter $b = (\sigma_2 - \sigma_3)/(\sigma_1 - \sigma_3)$ is independent of D, and therefore initial porosity, equal to 0.5 when $\phi_{cv} = 0$, and decreases as ϕ_{cv} increases.

Since the Mohr-Coulomb models illustrated in Figs. 7.2 and 7.3 apply to the shear strength components of sand the stress ratios for a frictionless particulate material and a particulate material deforming at constant volume can be obtained by substituting K = 1 and D = 1, respectively, in equations 7.12 - 7.15. The sets of equations corresponding to the Mohr-Coulomb models illustrated in Figs. 7.2 - 7.4 are given in Table 7.1.

Table 7.1.

stress ratio	incompressible model	frictionless model	stress-dilatancy model
$\frac{\sigma_1}{\sigma_3}$	K	D	DK
$\frac{\sigma_1}{\sigma_2}$	$\frac{(K+1)}{2}$	$\frac{2D}{(D+1)}$	$\frac{D(K+1)}{(D+1)}$
$\frac{\sigma_2}{\sigma_3}$	$\frac{2K}{(K+1)}$	$\frac{(D+1)}{2}$	$\frac{K(D+1)}{(K+1)}$
$\frac{\sigma_2}{\sigma_1+\sigma_3}$	$\frac{2K}{(K+1)^2}$	$\frac{1}{2}$	$\frac{K(D+1)}{(K+1)\ (DK+1)}$
$\frac{\sigma_2-\sigma_3}{\sigma_1-\sigma_3}$	$\frac{1}{(K+1)}$	$\frac{1}{2}$	$\frac{1}{(K+1)}$

The predictions of the incompressible Mohr-Coulomb model are of special interest since they can be considered to apply to the critical state strength of sand. It is noted that the theory does not predict that the intermediate principal stress is equal to the mean of the other two principal stresses at this stage of a test, as might be anticipated from the theory of incompressible rigid-plastic material. In fact it can be seen from Table 7.1 that, for a particulate material such as sand, it is the friction between the particles, not the dilatation, which causes the intermediate principal stress to be less that that predicted by rigid-plastic theory.

The expressions given in Table 7.1 for constant volume conditions (D = 1) can also be expressed in terms of ϕ_{cv} as shown below

$$\frac{\sigma_1}{\sigma_3} = \tan^2 (45^\circ + \phi_{cv}/2) \qquad (7.16)$$

$$\sigma_2 = \sigma_3 \ (1 + \sin \phi_{cv}) \qquad (7.17)$$

$$\sigma_2 = \sigma_1 \ (1 - \sin \phi_{cv}) \qquad (7.18)$$

$$\frac{\sigma_2}{\sigma_1 + \sigma_3} = \frac{\cos^2 \phi_{cv}}{2} \qquad (7.19)$$

$$\frac{\sigma_2 - \sigma_2}{\sigma_1 - \sigma_3} = \cos^2 (45^\circ + \phi_{cv}/2) \qquad (7.20)$$

It is interesting to note that equations 7.18 and 7.19 are identical to the expressions given by Wade (1963) and Bishop (1966) for $\phi = \phi_{cv}$, see section 4.2. The equations derived by Wade (1963) and Bishop (1966) were based on the experimental observation of Wood (1958) that, in plane strain, $\sigma_2 \simeq K_o.\sigma_1$, and the approximate relationship $K_o = 1 - \sin \phi$, Jaky (1944). Neither Wade (1963) nor Bishop (1966) appear to have

recognised that their empirical expressions implied that the intermediate principal stress in plane strain was equal to the normal stress acting on the failure planes.

7.5. Correlation with experimental results.

7.5.1. Stress conditions at failure in plane strain.

Superimposed on Figs. 7.6 - 7.9 are the experimental results obtained by Cornforth (1961), at failure, in his plane strain tests on Brasted sand. From Cornforth's (1961) Fig. 8-19, the relevant value of $\phi_{cv} = 32.8^{o}$ and the series of tests covered the dilatancy range $1.07 \leq D_f \leq 1.67$. If the true values of σ_2 were underestimated in Cornforth's tests, as suggested by Green (1969), then it is clear that the results are in excellent agreement with the theoretical predictions of equations 7.12 - 7.15.

A more detailed comparison can be made with the results of the plane strain tests reported in Chapter 4. The experimental results obtained from the plane strain tests (flexible side platens), at failure, are plotted against initial porosity in Figs. 7.10 and 7.11. Ideally, the stress ratios predicted by equations 7.12 - 7.15 should be determined from the measured values of D and K. However, although the experimental scatter in D, at failure, was acceptable, the measured values of σ_1/σ_3, at failure, were thought to be more reliable. Consequently, the theoretical calculations have been based on the empirical linear relationship between σ_1/σ_3 and initial porosity shown in Fig. 7.10, which is identical to that given in Fig. 4.6a. Taking the mean value of ϕ_{cv} obtained at failure in the plane strain tests as 36^{o}, see section 5.5.4, D_f was predicted using the stress-dilatancy equation $R = DK$. The predicted variation of D_f with initial porosity is shown in Fig. 7.10 and clearly provides a satisfactory representation of the measured values.

The predicted stress ratios given by equations 7.12 - 7.15 are compared with the experimental results in Fig. 7.11. Although the agreement is generally very satisfactory the correlation for the dense specimens is obscured by the scatter in the experimental results. The postulated relationship between the intermediate principal stress and the interparticle slip planes is effectively assessed by comparing the predictions of equation 7.12 with the measured values of the minor principal stress ratio, σ_2/σ_3, as shown in Fig. 7.11. Generally, the experimental results were predicted by the theory to an accuracy of $\pm$ 10%. The exceptions were tests PS 18 (n_i = 39.00%), PS 19 (n_i = 38.66%), and PS 22 (n_i = 38.89%), and it would appear that the intermediate principal stress was significantly overestimated in these tests. With the exception of these tests the overall correlation between the experimental results and the theoretical predictions shown in Fig. 7.11 is extremely good.

As a result of the experimental scatter obtained from the tests on dense specimens an empirical assessment of the trends shown in Fig. 7.11 suggested that there were two possible stress ratios which were unaffected by porosity: σ_1/σ_2 or $\sigma_2/(\sigma_1 + \sigma_3)$, see section 4.5.2. However, on the basis of the theory developed in this chapter, both of these stress ratios are dependent on the rate of dilatation and the only stress ratio which is independent of D, and therefore independent of porosity, is the ratio $(\sigma_2 - \sigma_3)/(\sigma_1 - \sigma_3)$, given by equation 7.15.

7.5.2. Development of the intermediate principal stress during plane strain deformation.

From the comparison with the experimental results given in the previous section it is evident that the theory developed in section 7.3.1 accurately predicts the stress conditions at failure in plane strain tests on sands. Since equations 7.12 - 7.15 were derived from the stress-dilatancy theory one might expect that they should also apply during pre-peak deformation.

Whether the theory predicts the development of the intermediate principal stress during plane strain deformation or not can be assessed by plotting σ_2/σ_3 against $(D + 1)$. According to equation 7.12 the experimental points should lie on a straight line passing through the origin. The results of test PS 9, when plotted in this manner, are illustrated in Fig. 7.12. The lack of agreement with the theoretical predictions, except at or close to failure, shown in Fig. 7.12 was typical of that obtained from the results of the other plane strain tests performed. Fig. 7.12 shows that the experimental points lie significantly below the theoretical line during the initial stage of the test but approach the theoretical line as the test proceeds until reasonable agreement is obtained as failure is approached.

The lack of agreement with the theory shown in Fig. 7.12 may be attributed to experimental deficiencies, limitations of the theory, or both. Aside from any uncertainties as to whether or not the flexible side platens accurately measure the intermediate principal stress, the measured values of σ_2 will be less than the true plane strain values as a result of the compressibility of the lubricated membranes. Attempts to compensate for such lateral movement by applying a controlled rate of inward movement of the side platens have not been successful, Reades (1972). However, even if the condition of zero lateral strain in the intermediate principal stress direction was achieved, a satisfactory correlation may not be obtained due to theoretical limitations.

The theory ignores elastic deformations and consequently implies higher stress ratios than would be measured in a true plane strain test. Due to elastic compression of the particles the measured rates of dilatation will also be low. However, the effect of errors in D can, to some extent, be eliminated by plotting the results in terms of equation 7.13, as shown in Fig. 7.13. The results shown in Fig. 7.13 suggest that, if the theory is valid during plane strain deformation, the lack of correlation with the experimental results is primarily due to

experimental deviations from the true plane strain condition.

It is concluded that the results of the plane strain tests reported in Chapter 4 do not agree with the theoretical predictions until failure is approached. However, a final appraisal of the theory must await the development of more sophisticated plane strain testing techniques.

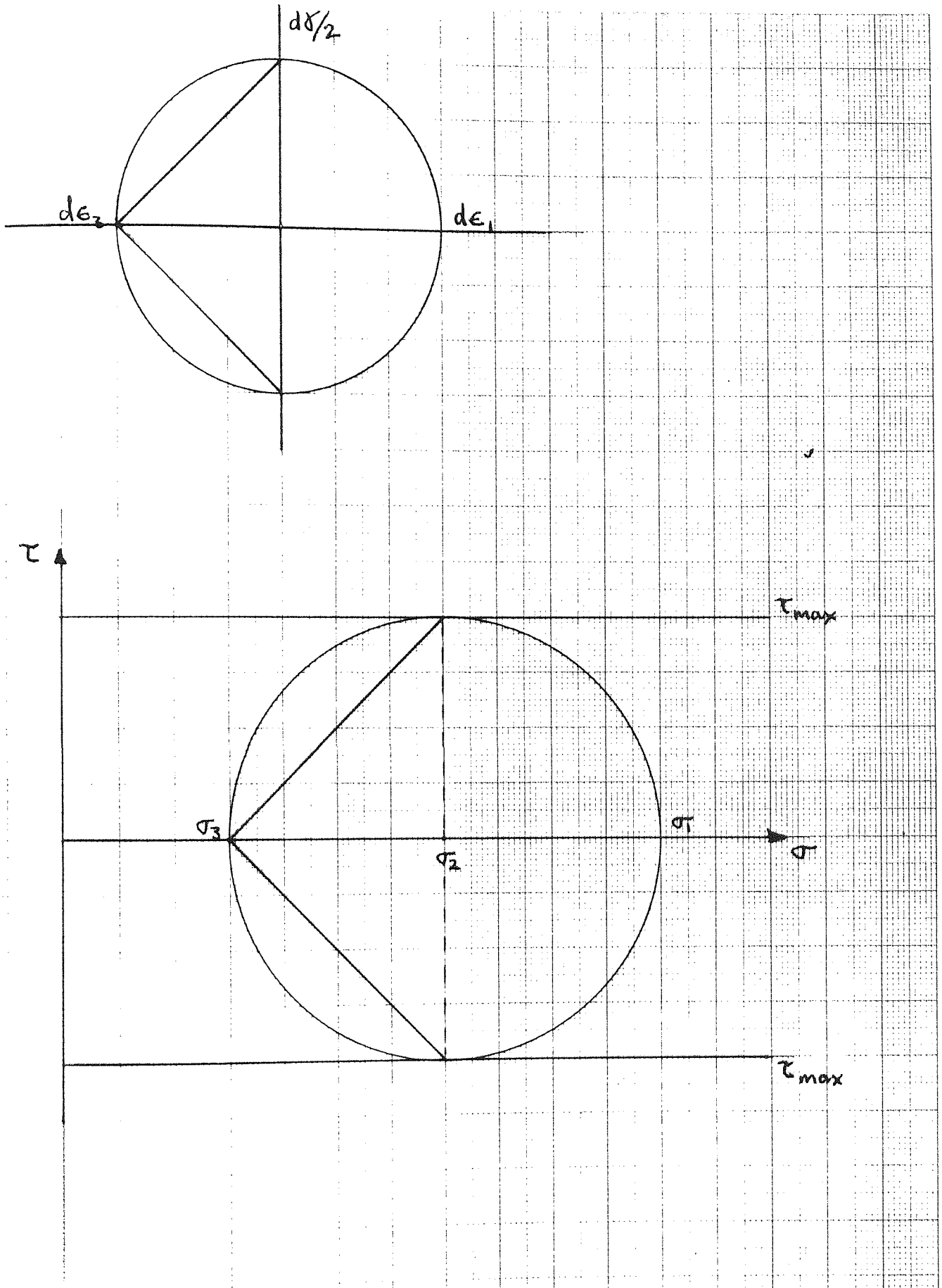

RIGID-PLASTIC MODEL

FIG. 7.1

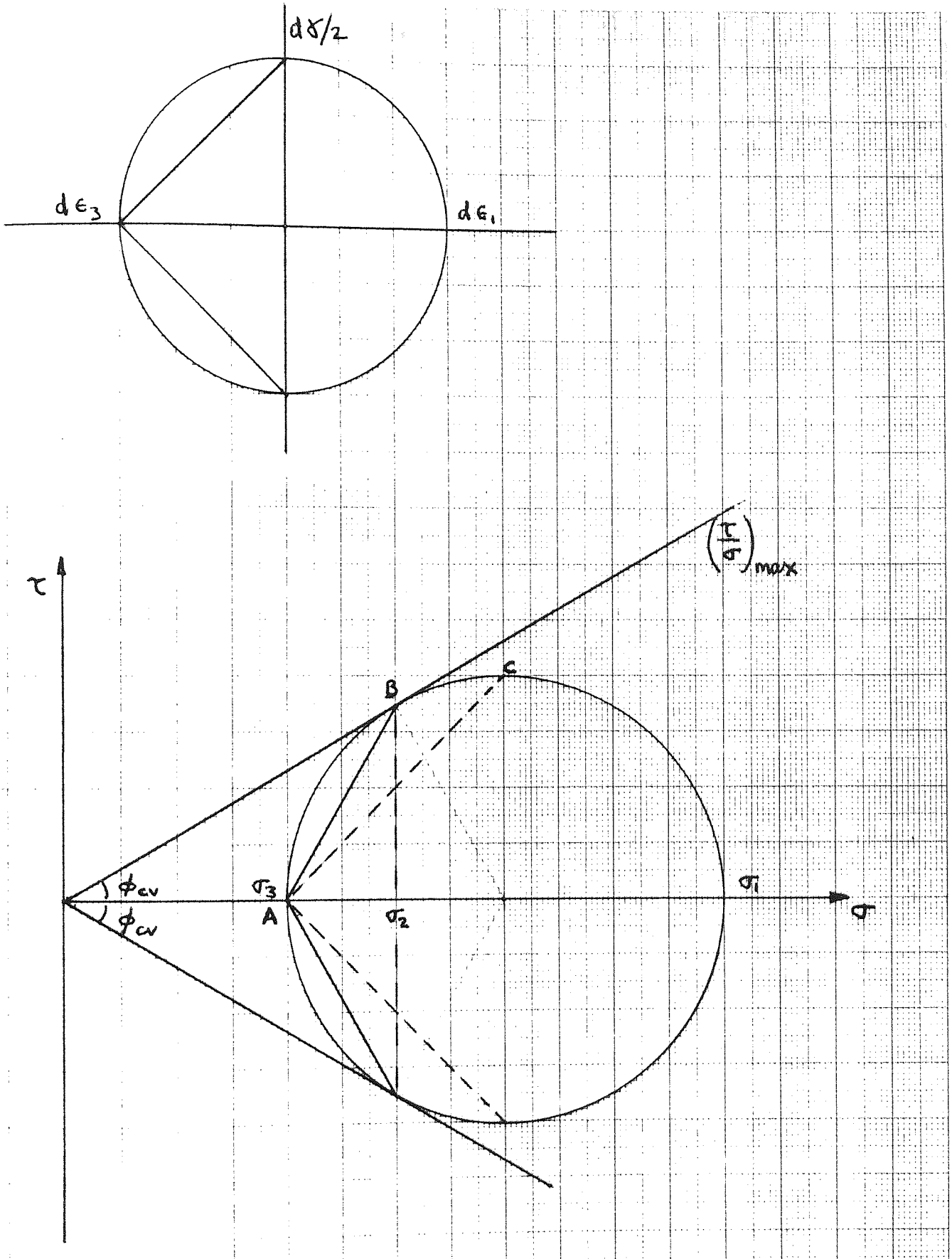

NON-DILATANT/FRICTIONAL MODEL

FIG. 7.2

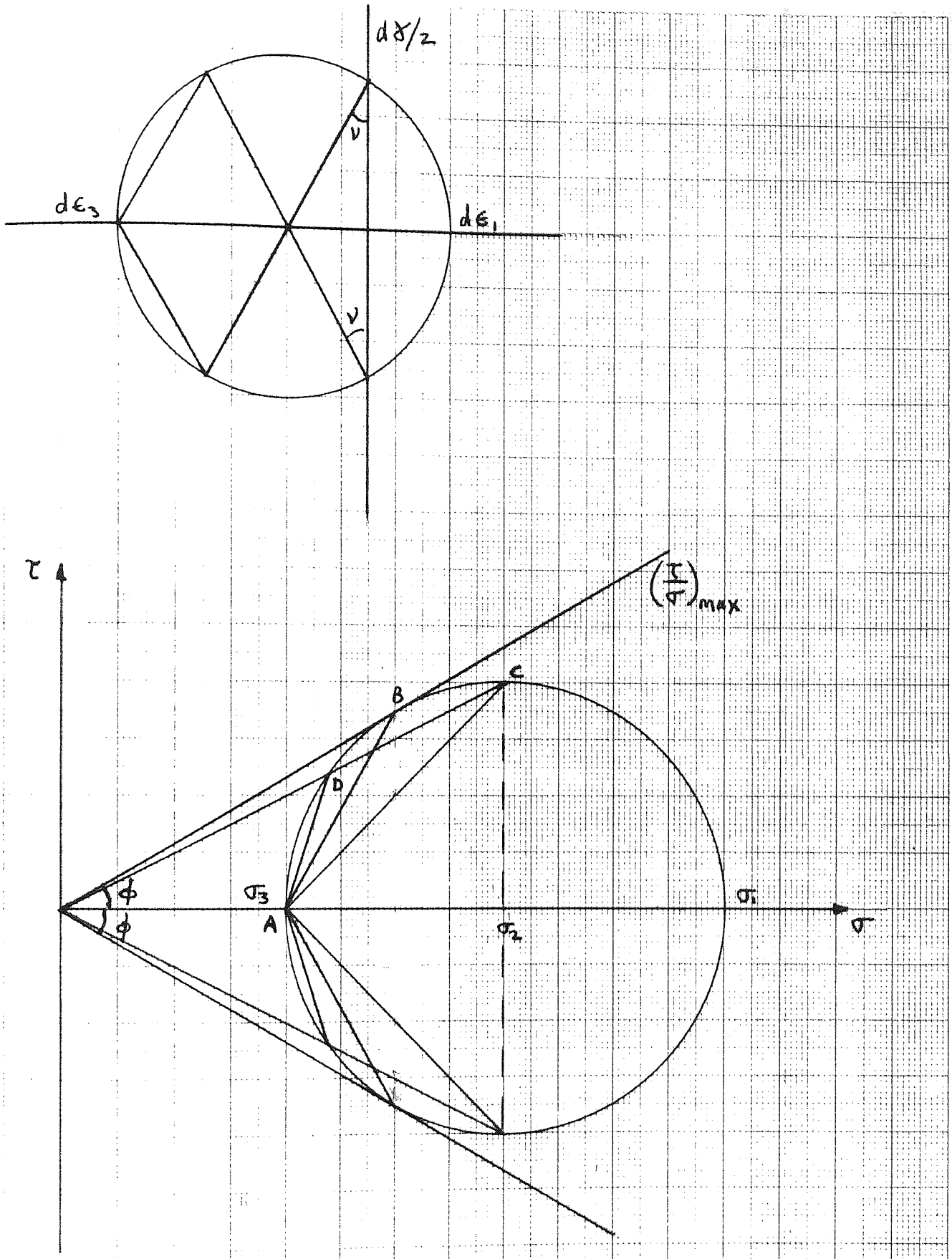

NON-FRICTIONAL / DILATANT MODEL

FIG. 7.3

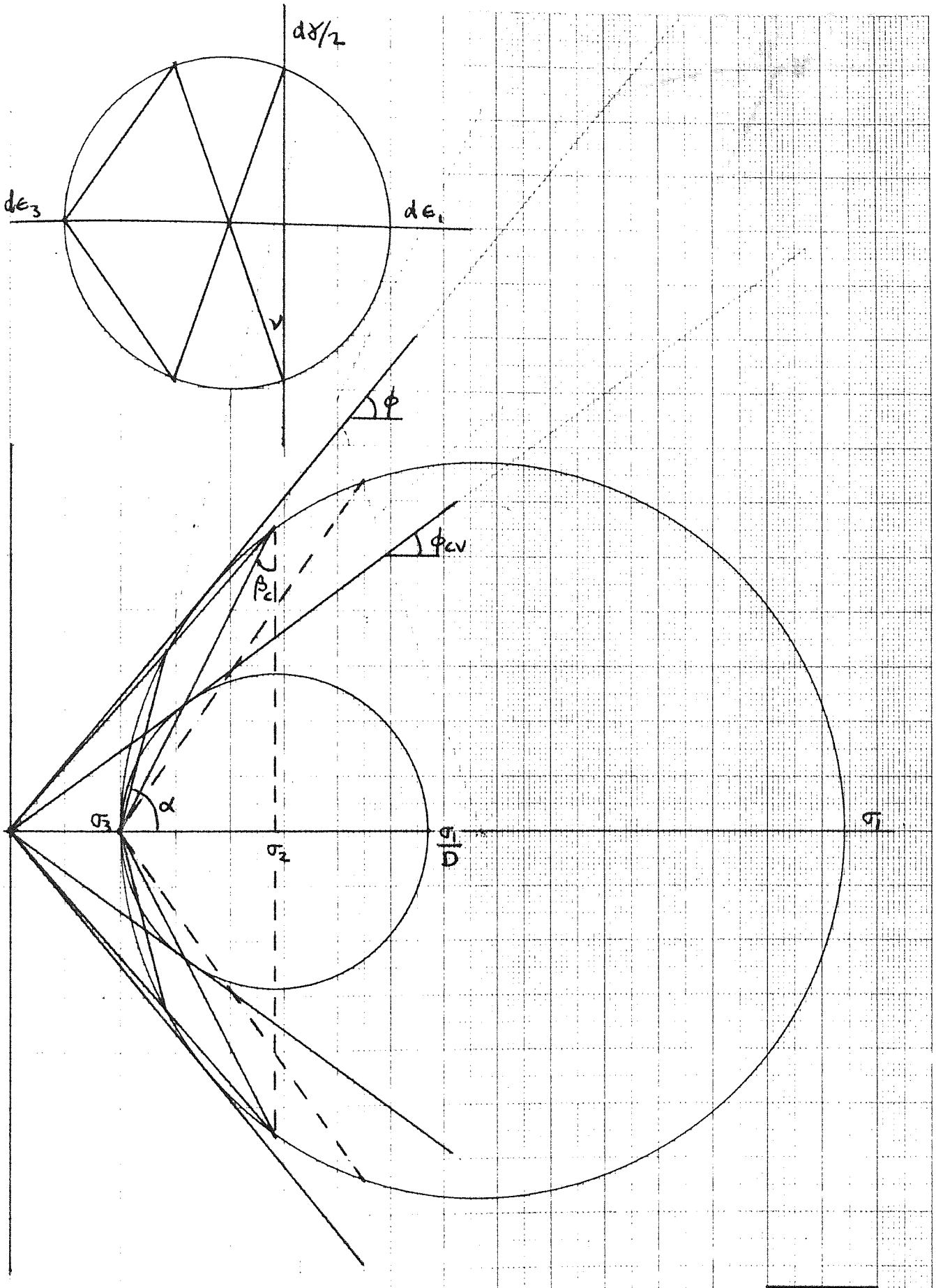

STRESS DILATANCY MODEL

FIG. 7.4

FIG. 7·5

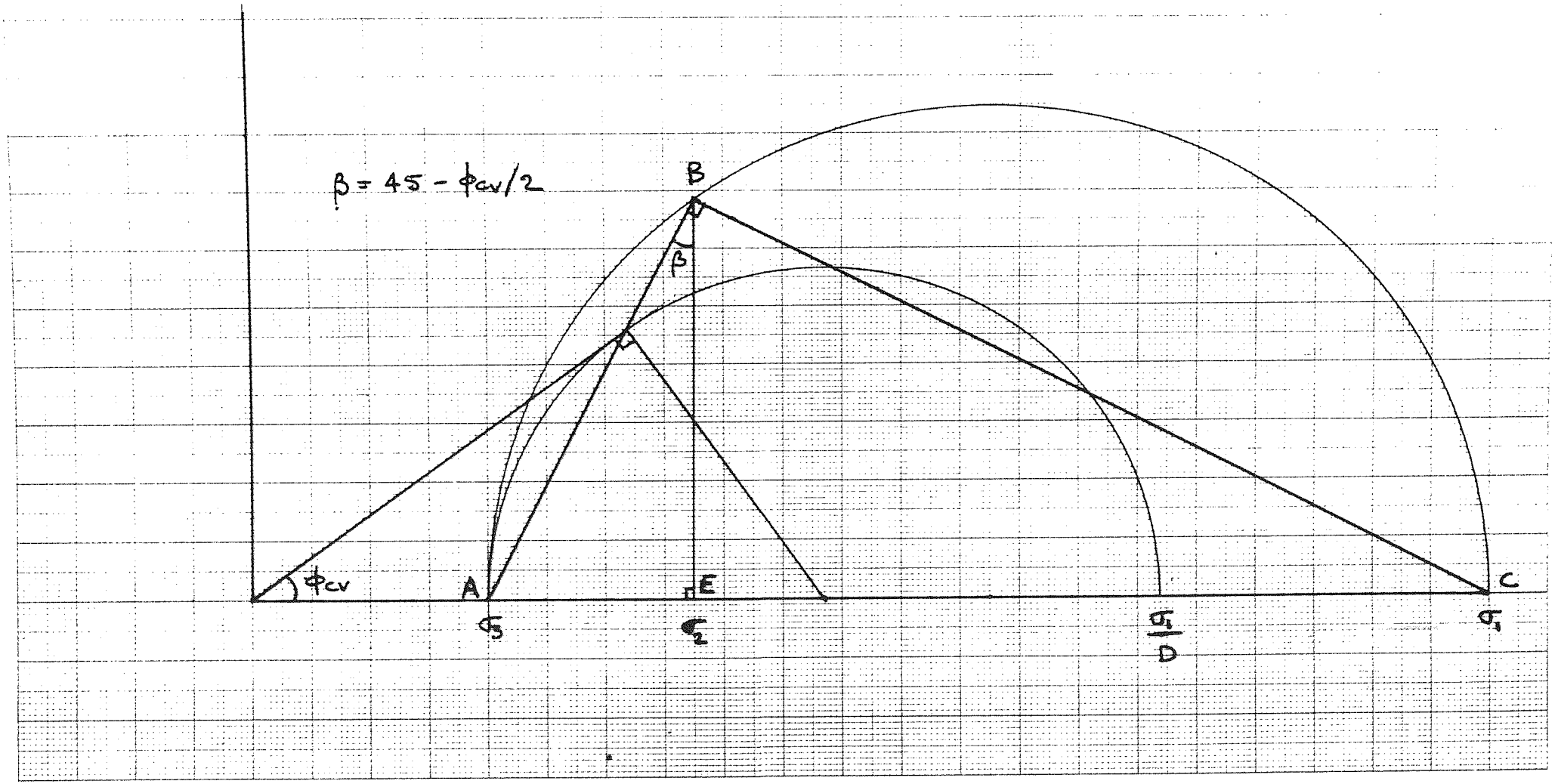

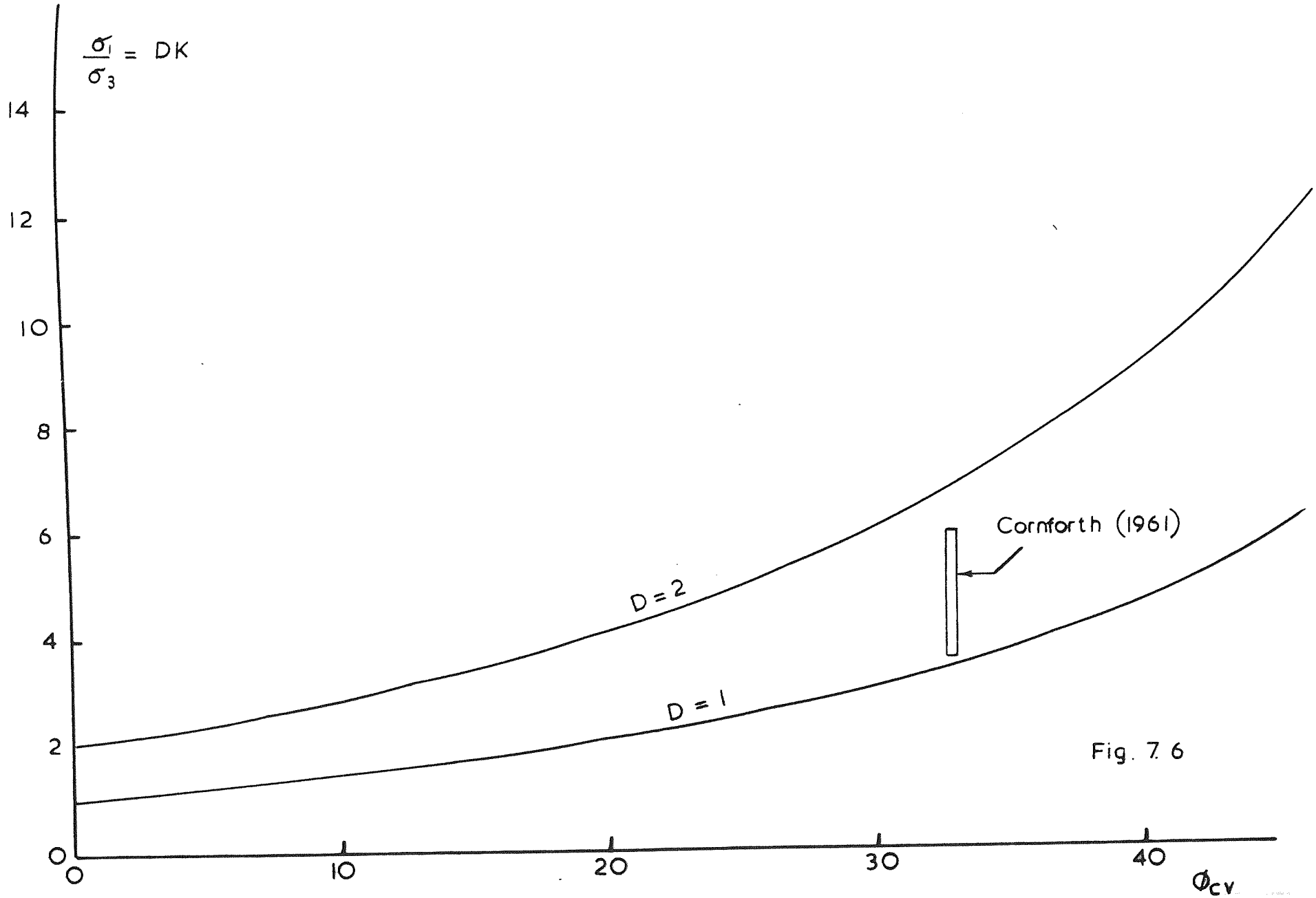
$\frac{\sigma_1}{\sigma_3}$ = DK
14
12
10
8
6
4
2
0
0
10
20
30
40
ϕ_{cv}
D = 2
D = 1
Cornforth (1961)

Fig. 7.6

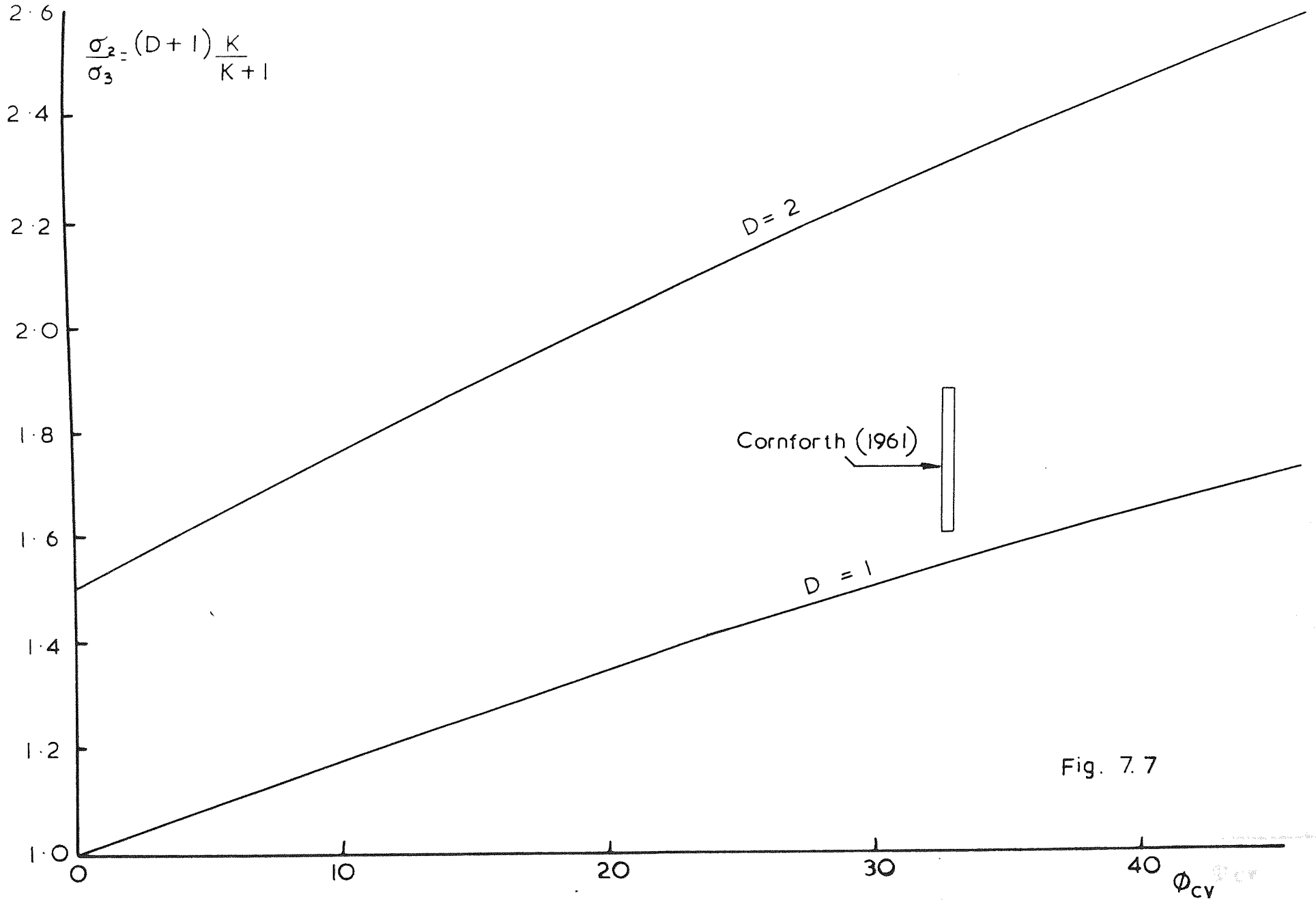
$\frac{\sigma_2}{\sigma_3} = (D+1)\frac{K}{K+1}$
2·6
2·4
2·2
2·0
1·8
1·6
1·4
1·2
1·0
D = 2
D = 1
Cornforth (1961)
0
10
20
30
40
ϕ_{cv}

Fig. 7.7

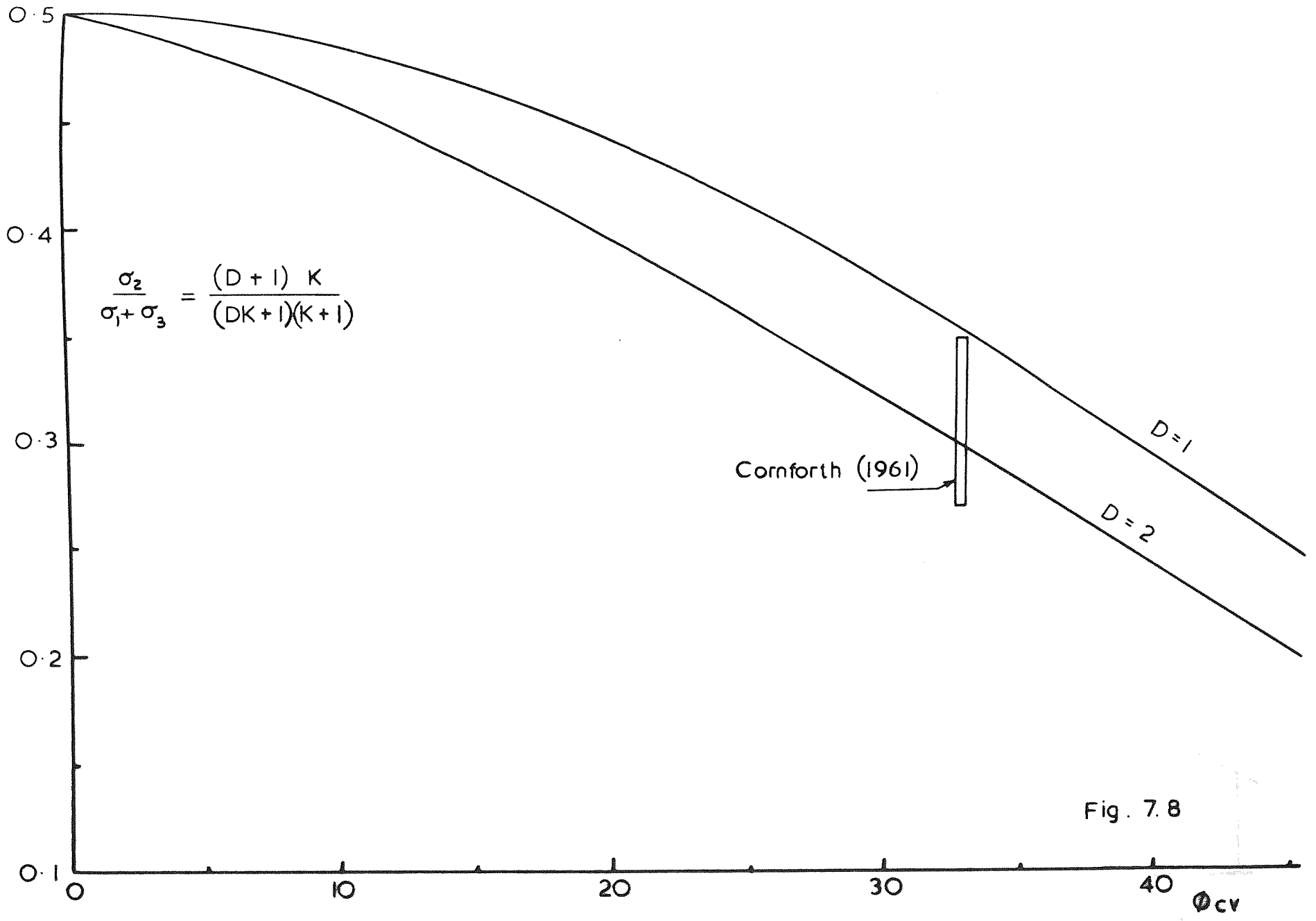
0·5
0·4
0·3
0·2
0·1
0
10
20
30
40
ϕ_{cv}
$\frac{\sigma_2}{\sigma_1+\sigma_3} = \frac{(D+1)\ K}{(DK+1)(K+1)}$
D=1
D=2
Cornforth (1961)

Fig. 7.8

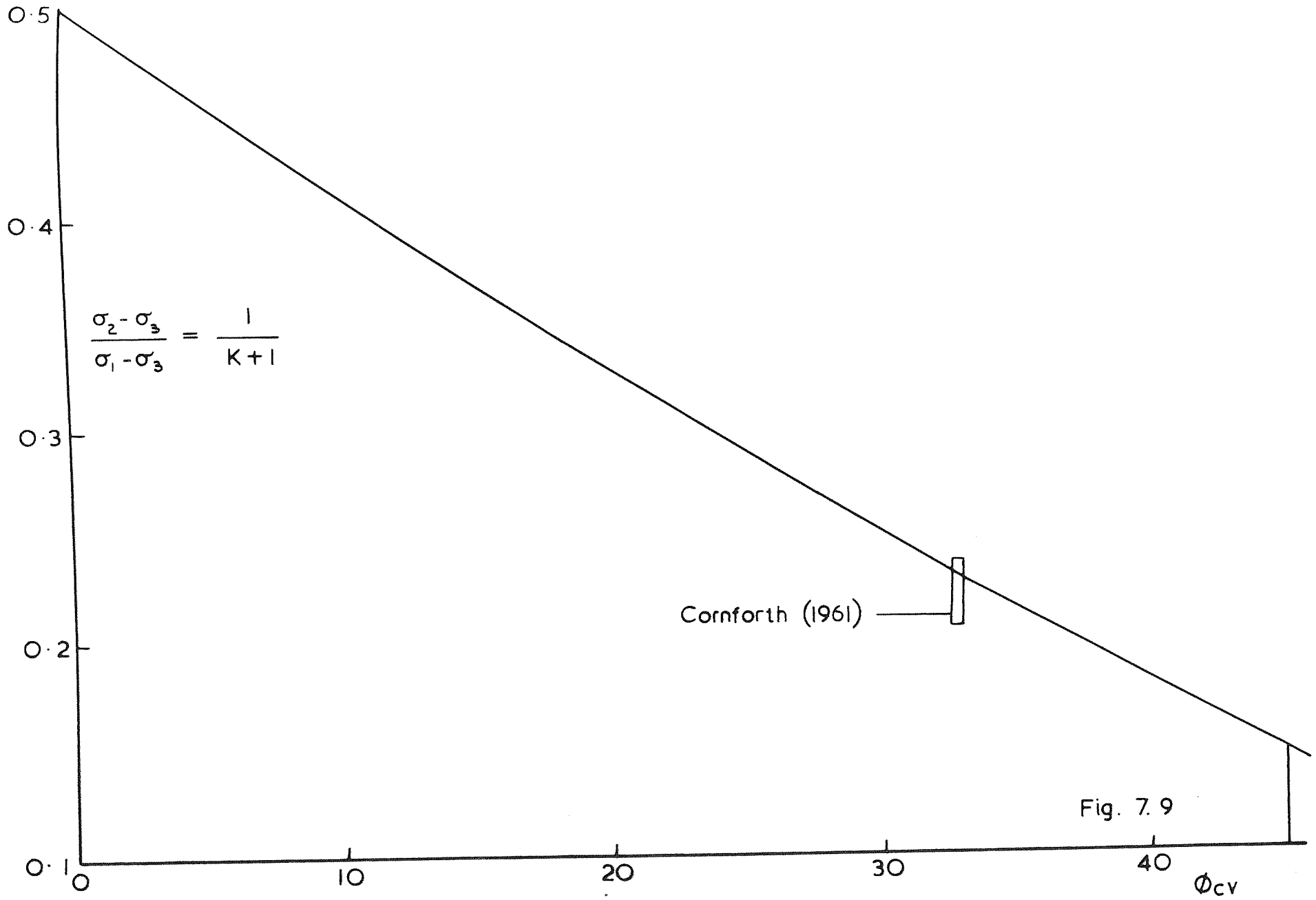
0·5
0·4
0·3
0·2
0·1
0
10
20
30
40
ϕ_{cv}
$\frac{\sigma_2 - \sigma_3}{\sigma_1 - \sigma_3} = \frac{1}{K+1}$
Cornforth (1961)

Fig. 7.9

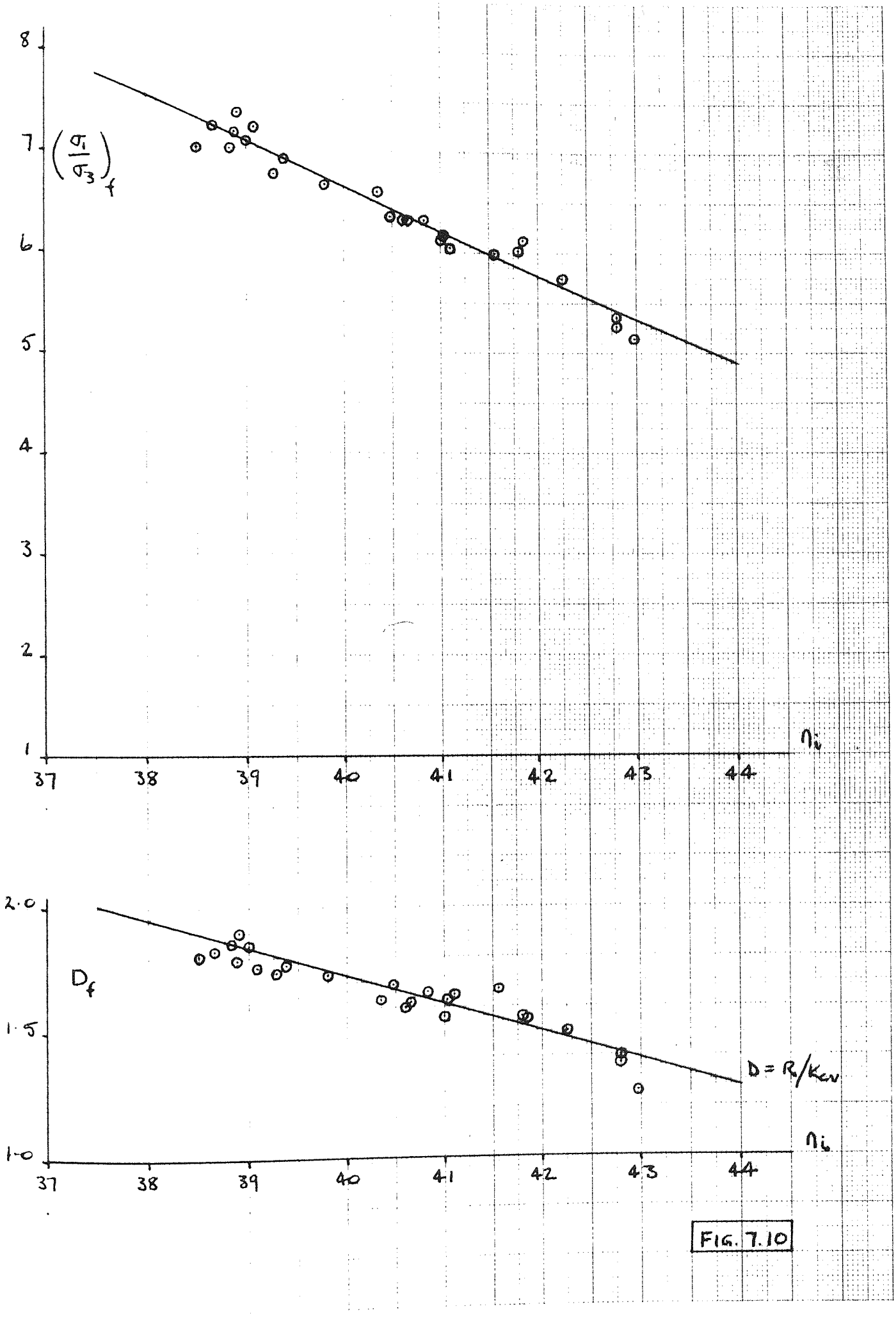
8
7
6
5
4
3
2
1
$\left(\frac{\sigma_1}{\sigma_3}\right)_f$
37
38
39
40
41
42
43
44
n_i
2·0
1·5
1·0
D_f
$D = R/K_{cv}$
n_i

FIG. 7.10

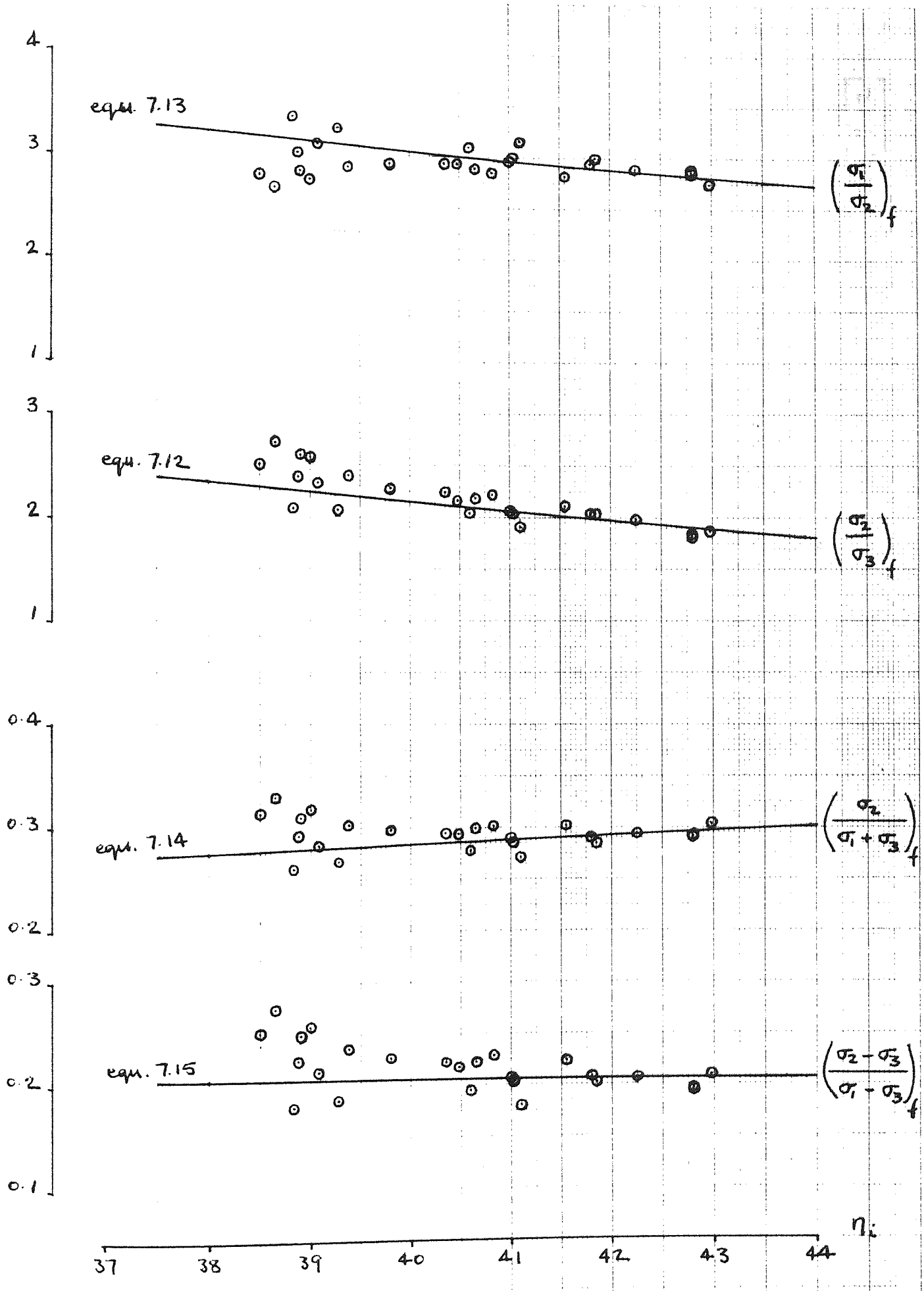
4
3
2
1
eqn. 7.13
$\left(\frac{\sigma_1}{\sigma_2}\right)_f$
3
2
1
eqn. 7.12
$\left(\frac{\sigma_2}{\sigma_3}\right)_f$
0·4
0·3
0·2
eqn. 7.14
$\left(\frac{\sigma_2}{\sigma_1+\sigma_3}\right)_f$
0·3
0·2
0·1
eqn. 7.15
$\left(\frac{\sigma_2-\sigma_3}{\sigma_1-\sigma_3}\right)_f$
η_i
37
38
39
40
41
42
43
44

FIG. 7.11

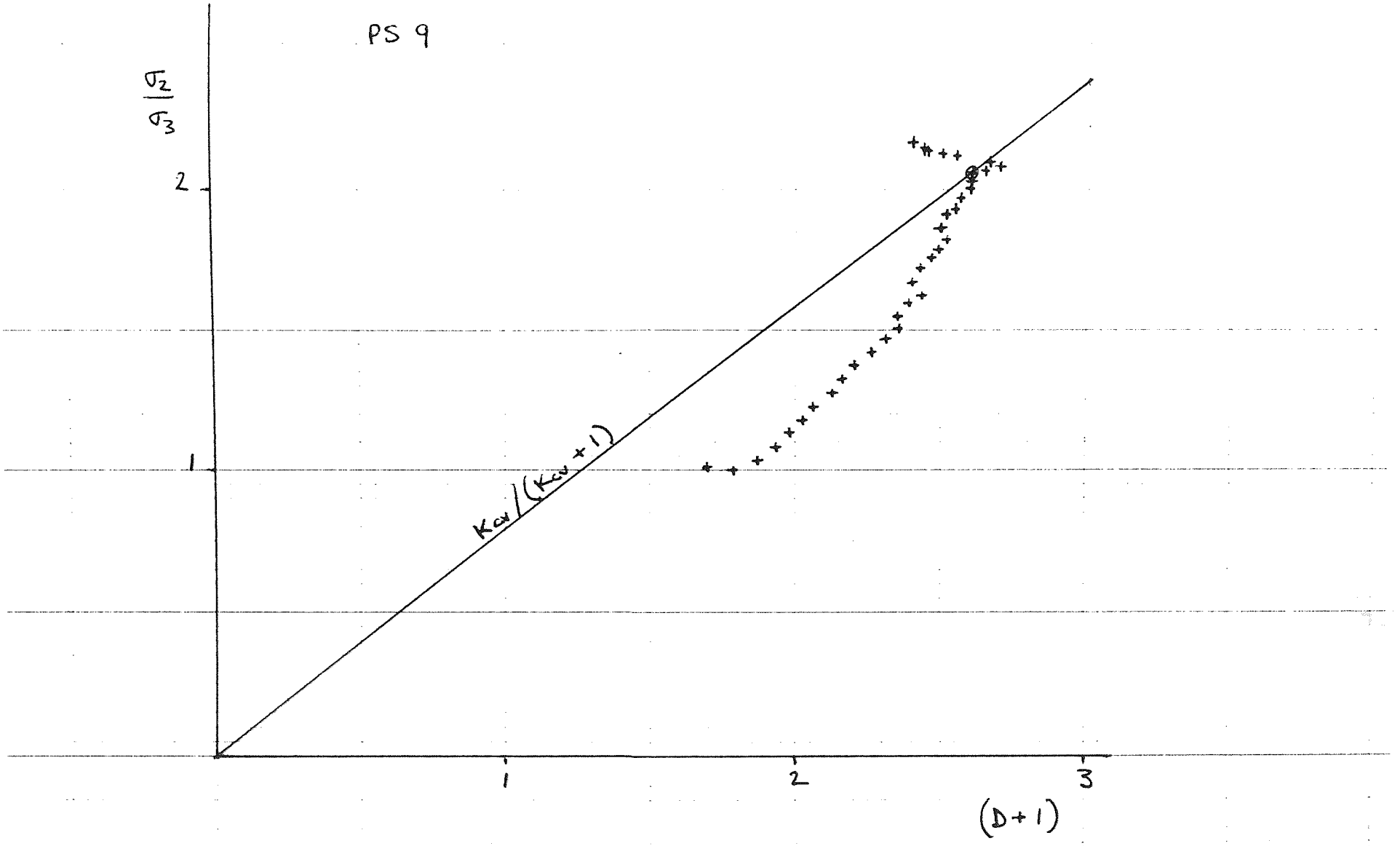

FIG. 7.12

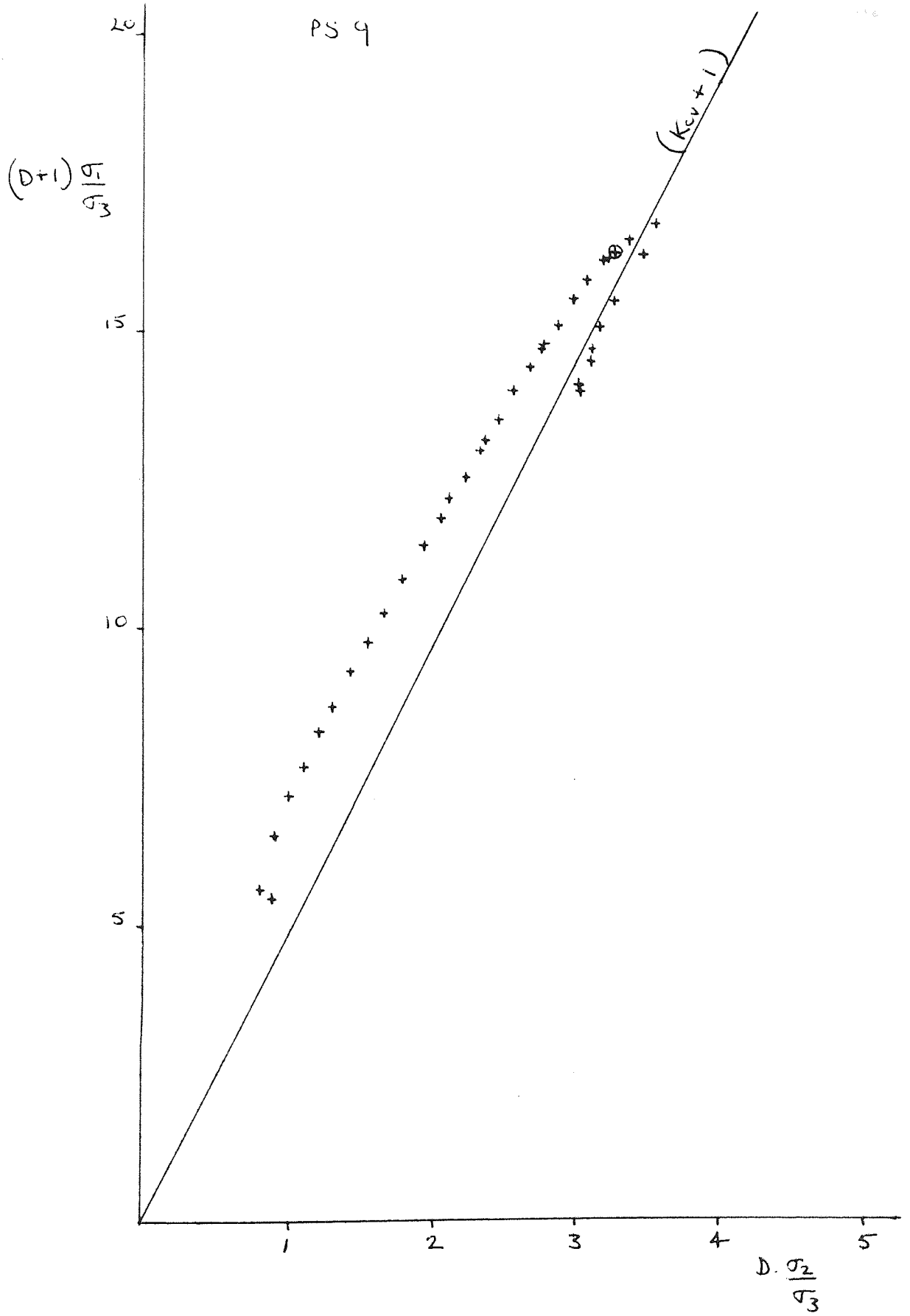
20
15
10
5
1
2
3
4
5
$(D+1)\frac{\sigma_1}{\sigma_3}$
$(K_{cv}+1)$
D. $\frac{\sigma_2}{\sigma_3}$

FIG. 7.13

CHAPTER EIGHT

8. CONCLUDING REMARKS

An experimental investigation of the plane strain and axi-symmetric compression behaviour of a fine sand has been reported in this thesis. The experimental results have also been assessed in the light of certain theoretical considerations. Throughout the text comments and conclusions have been provided where appropriate and it is, therefore, only necessary to add a few closing remarks in this final chapter.

The apparatus used in the experimental work has been described in Chapter 2, together with the method of sample preparation adopted. The experimental program was greatly assisted by the vibratory technique used to control the initial porosity of the specimens. This, together with the other techniques used in the preparation of test specimens, provided a quick, simple, and effective means of preparing homogeneous specimens of sand. The degree of control afforded by the vibratory technique was highly encouraging and it is recommended that the technique be adopted for future experimental work on sands. That the specimens subsequently deformed uniformly when tested in the new apparatus was demonstrated by photographs and by end of test measurements, and is also implied by the smooth stress-strain curves presented in Appendix C.

A novel feature of the apparatus design was the method used to simulate the plane strain condition. Exact experimental reproduction of the mathematical concept of plane strain would appear to be intractable due to the requirement that the strain in one orthogonal direction must be prevented without inducing shear stresses on the planes normal to that direction. All apparatuses which have purported

to apply plane strain conditions to specimens of sand have, in fact, either induced significant side friction or have permitted lateral movement due to the compressibility of the lubricated membranes used to prevent side friction. Consequently, it is only possible to assess whether the simulation provided by the flexible side platens is comparable with the plane strain simulation afforded by rigid side platens.

Although the plane strain test results obtained using rigid side platens indicated slightly different strengths, and significantly smaller axial strains to failure, compared with the results of the tests employing flexible side platens, reservations were expressed in Chapter 4 concerning the reliability of the test results obtained using rigid side platens. Indeed, when compared with the results of conventional plane strain tests reported by other investigators the plane strain simulation provided by the flexible side platens would appear to be reasonably satisfactory. This is especially true when compared with the results obtained by Tong (1970) who conducted tests on a fine sand the physical properties of which were very similar to those of the sand tested in this research program. It is, therefore, concluded that a reasonable plane strain simulation can be obtained using flexible side platens of the type described in Chapter 2 and that these provide a simple means of estimating the intermediate principal stress.

The present research program forms part of a continuing study of the plane strain behaviour of soils and much of the work presented in this thesis could be supplemented by further additional tests to corroborate the comments and conclusions which have been provided in the various chapters. However, two aspects of the present work, in particular, recommend themselves as topics for future research, namely, the curve fitting technique presented in Chapter 6, and the theoretical development provided in Chapter 7.

In the absence of a physically sound, theoretical stress-strain relationship, the combined parabolic-hyperbolic curve fitting technique described in Chapter 6 provides a useful and accurate method of quantifying the pre-peak deformational behaviour of sand. An obvious extension to the work presented in Chapter 6 would be to examine the effect of confining stress and stress path on the parabolic and hyperbolic parameters contained in the mathematical representation. Furthermore, since it was demonstrated in Chapter 6 that both plane strain and axi-symmetric compression test results are accurately represented by a combination of parabolic and hyperbolic curves, the technique may be extended to cover compressive stress states intermediate between these two conditions. In any future work along these lines it will be of particular interest to determine the extent to which complex loading paths can be accommodated into the combined parabolic-hyperbolic treatment.

It was concluded in Chapter 7 that the theory developed therein accurately predicts the stress conditions at failure in plane strain. However, further experimental evidence is required to demonstrate that the theory can be extended to other particulate materials such as glass ballotini and angular sands. It was also suggested that significant improvements in present day plane strain testing techniques are required before a proper assessment can be made of the ability of the theory to predict the intermediate principal stress during plane strain deformation. Therefore, the development of a more sophisticated plane strain apparatus capable of permitting inward movement of the side platens to compensate for the compressibility of the lubrication system used to prevent side friction, together with an examination of the effect of lateral movement on the intermediate principal stress developed, would provide a valuable contribution to the evaluation, and possible extension, of the theory developed in Chapter 7.

APPENDIX A

A. EVALUATION OF EXISTING APPARATUS.

A.1. Review of previous work.

A.1.1. Apparatus.

An apparatus was developed by Dyson (1970) in which the three mutually orthogonal stresses could be independently varied. Details of the apparatus are shown in Fig. A.1 and Fig. A.2. Tests were performed on cuboidal samples of saturated sand 4 in. high and $2\frac{1}{4}$ in. square in cross-section. The specimen was enclosed in a latex rubber membrane which was manufactured to exact dimensions so as to provide a snug fit to the specimen and the axial platens. The membrane was sealed at the base between the two halves of the bottom stress-cell, and by O-rings in the normal manner at the top.

The apparatus was fully enclosed within a conventional triaxial cell and de-aired water was used to apply the stress to one pair of vertical faces. The stress on the other two vertical faces was applied through two identical 'side stress-cells', see Fig. A.1a. Each side stress-cell consisted of a stainless steel side frame and back plate, fixed securely together to form a hollow rigid compartment. A latex rubber membrane fitted snugly inside the compartment so as to completely cover the opening on the active face of the assembly. Sealing was achieved using rubber gaskets between the side frame and the back plate. The compartments were water-filled and pressurized to provide a uniform stress on the sample faces, and the pair of compartments were interconnected to ensure equal pressures. Silicone grease was smeared onto the sample/stress-cell interfaces to reduce friction. Having been placed in position against two opposite faces of the specimen, the two side stress-cells were connected together with four stainless steel tie bars, screwed to the top and bottom of the side frames. The pressures

applied to the side stress-cells could be applied manually using a screw-piston or by a self-compensating mercury pressure control system. For 'plane strain' tests the side stress-cells were connected to a conventional null indicator system.

Instead of conventional rigid axial platens, axial stress-cells were used to measure the axial stress at the top and the bottom faces of the specimen. The 'top stress-cell' (Fig. A.1b) was cuboidal in shape, with a cylindrical upstand to which the specimen membrane could be easily sealed using O-rings. A recess was machined in the active face and then covered with a soft rubber diaphragm, glued to the peripheral flange. Two holes were drilled to connect the hollow compartment to the top of the cylindrical upstand. One hole was used to fill the recess with de-aired water and the other hole was fitted with a de-airing screw. The hollow compartment was connected to a transducer block via polythene capillary tubing and a duct in the cell base. Drainage was facilitated by filter paper drains connected to rectangular bauxilite porous stones set into a peripheral channel in the stress-cell and connected to a top drainage tube.

The bottom stress-cell (Fig. A.1c and A.1d) was screwed into the base of the cell and consisted of two sections between which the specimen membrane was sealed. The upper section was recessed, in a manner similar to the top stress-cell, and a rubber diaphragm was glued to the peripheral flange. In order to protect the diaphragm during the dismantling of the specimen, the upper section was dipped in latex which, when dried, provided adequate protection. The hollow compartment was connected to a transducer block via a central hole in the bottom stress-cell and a duct in the cell base. No separate de-airing hole was provided in the bottom stress-cell thus complicating the de-airing and setting up procedure, nor was any provision made to drain the sample from the base.

The principle of the stress-cell action was that a pressure applied directly to the diaphragm would be transmitted, with negligible volume change, to the confined de-aired water and hence measured by the pressure transducer. Since two axial stress-cells were used, top and bottom, two measurements of axial stress were obtained. The two measurements were generally dissimilar. Dyson showed that the difference in the measured pressures at the top and the base of the sample was mainly due to the difference in cross-sectional area at the sample/platen interfaces. Although the area covered by the flexible diaphragm was never more than 80% of the area of the specimen it was assumed that end lubrication would ensure that any stress variations, due to the rigidity of the peripheral flange, would be small. End lubrication was provided by a single 0.01 in. thick lubricated rectangular rubber membrane placed on the face of each axial stress-cell.

The transducers were connected to an oscillograph and the axial stresses were determined from the movement of the galvanometer trace on the recording paper. The two lateral stresses were measured using Bourdon gauges. Axial deformation was determined by a dial gauge, reading to 0.01 in., attached to the cross-beam of the loading machine and bearing on a pedestal fixed to the top of the cell. Volume change of the specimen was recorded by a 50 ml. burette.

A.1.2. Test results.

All the tests performed were drained tests on saturated samples of coarse sand, passing No. 14 and retained on No. 25 B.S. sieves. The majority of the tests were triaxial compression and 'plane strain' tests, for a range of initial porosities. In addition, a few tests were carried out on dense specimens in which the three mutually orthogonal stresses and strains were different.

These last tests were termed 'intermediate stress tests' and were designed to permit the intermediate principal stress to be independently

varied in order to study the effect it had on the failure envelope. The tests were conducted in three stages. The first stage consisted of ambient consolidation to a predetermined level. Then, with the cell pressure constant, the sample was axially loaded and, using the axial stress–cell readings, the side stress–cell pressures were adjusted to maintain an equal increase with the axial stress. When the desired value of the intermediate principal stress was reached the side stress–cell pressures were then maintained constant at that value whilst the sample was sheared under a constant rate of axial deformation. Six tests were performed at different side stress–cell pressures and the variation in strength obtained is shown in Fig. A.3.

The 'plane strain' tests included both loading and unloading tests. The maximum ratio of major to minor principal stress was unaffected by the stress path but other stress ratios, which incorporated the intermediate principal stress, were sensitive to the stress path followed. Strains to failure in the 'plane strain' tests were found to be comparable with those in triaxial compression tests. The stress–strain curves were unusual in that the major principal stress curve exhibited points of contraflexure and there was a corresponding delay in the increase in the intermediate principal stress. Examples of typical stress–strain curves are shown in Fig. A.4 and Fig. A.5.

A comparison of stress–strain curves for triaxial compression and 'plane strain' tests indicated that there was no significant difference until the increased rate of change of the intermediate principal stress occurred. Dyson concluded that the samples did not deform under plane strain conditions throughout the tests and this was caused by apparatus deficiencies at low axial strains, due to exposure of the side stress–cell membranes and possible limitations in the manual control of the mercury null indicator. The difference in strength (ϕ max) between 'plane strain' tests and triaxial compression tests was found to increase with decrease in initial porosity, to a maximum of 7^{o} at minimum porosity.

In order to assess the performance of the apparatus, triaxial compression tests were carried out on cuboidal samples, both with and without the side stress-cells in position, and on cylindrical samples using either rigid platens or cylindrical stress-cells. Using the mean of the axial stress-cell readings it was found that the peak strengths of cuboidal and cylindrical triaxial compression specimens were very similar over the range of initial porosities tested. The majority of the triaxial compression tests were performed using both an external proving ring and axial stress-cells. A comparison of peak strengths based on proving ring readings showed agreement between cylindrical specimens and conventional cylindrical triaxial compression tests using rigid platens, but cuboidal specimens gave higher strengths. In tests where both proving ring measurements and axial stress-cells were used the former gave values of peak stress ratio up to 13% higher than the peak stress ratio deduced from axial stress-cell readings. The difference varied randomly but the difference in ϕ max tended to be between 2° and 3°. Dyson concluded that the difference was due to bush friction which varied with axial deformation. The values of peak stress ratio deduced from the two methods did not occur simultaneously. The stress-cells consistently reached a maximum stress at a smaller strain.

A.1.3. Comments.

Although the apparatus nominally achieved the object of permitting the intermediate principal stress to be varied, deficiencies due to the rigidity of the edges of the stress-cells and the limitations on the magnitude of stress existed. An assessment of the complete test program indicated that numerous deficiencies existed in both technique and mensural precision. Further testing of the apparatus was therefore necessary.

In view of the random difference between the axial stress-cell readings and the external proving ring readings, as observed by Dyson,

priority was given to a reassessment of the axial stress-cells. A series of triaxial compression tests was conducted to fulfil this objective.

A.2. Modifications.

In order to eliminate uncertainties due to bush friction it was necessary to measure the axial load inside the cell and for this purpose a load cell was used. This was the same load cell that was subsequently used in the main research program and so the larger confining cell, described in Chapter 2, was also required.

From the stress-dilatancy plots of Dyson's results it was apparent that a significant improvement in the accuracy of measurement was necessary. Consequently, the dial gauge, volume change system, and datalogger described in Chapter 2 were used in this series of triaxial compression tests.

A close inspection of Dyson's test results and photographs indicated that the desired uniformity of deformation was not in fact achieved. In a preliminary series of tests, not reported in this thesis, the limitations of uniform deformation were confirmed. Further preliminary tests were performed in an attempt to improve end lubrication.

Instead of a single lubricated membrane, as used by Dyson, two lubricated membranes were used, top and bottom, but the improvement was marginal. Although the degree of bulging was not excessive, end of test measurements of the specimen dimensions indicated that in most tests either one or both ends of the specimen had not expanded laterally at all.

It was thought that restraint may have been due to the pre-formed edges of the sample membrane which was shaped to fit the initial platen-sample dimensions. The membrane mould was altered so as to remove the pre-formed edges, the modified membranes being stretched over the platens in subsequent tests. However, no improvement in the resultant deformation was noticeable.

The lubricated membranes at the base of the specimen had been placed in the same manner as carried out by Dyson, that is, with the specimen mould in position, the membrane was lowered down onto the bottom stress-cell under water. This procedure was adopted in order to prevent air bubbles becoming trapped between the membranes and the stress-cell. However, the membranes were necessarily undersize and thus permitted grains on the perimeter of the specimen to be directly in contact with the unlubricated protective cover to the bottom stress-cell. Consequently the inside of the protective latex cover was greased before it was fitted over the top half of the bottom stress-cell and a significant improvement in the expansion of the sample at the base was achieved, although it was not completely satisfactory. No improvement was achieved at the top of the specimen.

Measurements of sample dimensions before and after the tests showed that the specimens bulged and it was concluded that the limited freedom from end restraint was due to the non-rigid, non-planar interfaces between the specimen and the stress-cells. Since the interfaces were not planar, the specimen end faces being slightly convex, particles at the ends of the specimen would have to de excess work against the specimen to overcome friction.

A.3. Test results.

The performance of the axial stress-cells was investigated in a series of triaxial compression tests conducted over a range of initial porosities. Many of the tests were terminated soon after the consolidation stage when it became apparent that one of the stress-cells, usually the bottom stress-cell, had sprung a leak sufficient to cause complete collapse of the stress-cell diaphragm.

Only a few tests were apparently successful and the test results are shown in Fig. A.6-A.11. Fig. A.6a-A.11a show axial stress as deduced from both the stress-cell readings and load cell readings, plotted

against axial strain. Fig. A.6b–A.11b show axial stresses recorded by the stress-cells plotted against the axial stress as calculated from the load cell readings. Details of initial cross-sectional areas and subsequent lateral strains for the tests are given in Fig. A.12.

Although the tests described in this section were 'successful' in comparison with the many other tests carried out using the axial stress-cells, there still existed in these tests some obvious discrepancies. In both test SC 10 (Fig. A.8) and test SC 14 (Fig. A.10) it is clear that the bottom stress-cell sprung a leak during the tests. In the former the leak was a minor one and occurred during the shear stage at an axial strain of 1.5%. In the latter the leak was much greater and occurred during the consolidation stage. Consequently the bottom stress-cell pressures in these two tests are ignored. In test SC 8 (Fig. A.6) the top stress-cell was extremely low and it was suspected that the stress-cell was not completely de-aired. Therefore the results of the top stress-cell readings for this test are considered to be erroneous.

It is apparent from the six tests reported that any agreement between the two stress-cell pressures and the load cell deduced axial stress is entirely fortuitous. Although uncertainties exist in the value of axial stress, as deduced from the load cell readings (due to variations in cross-sectional area), the results so obtained can be regarded as the standard against which the stress-cell pressures can be compared. Therefore in Figs. A.6a–A.11a the curves obtained from load cell readings will be referred to as 'standard curves'.

It can be seen that, in general, the top and bottom stress-cell pressures started to diverge at the start of the consolidation stage. The exception was test SC 10 (Fig. A.8) and this test specimen, unlike the others tested, had little if any variation in cross-sectional area. However, in the other tests, although the cross-sectional area at the base tended to be greater than at the top of the specimen, the stress recorded at the base also tended to be greater than that given by the

top stress-cell. This is contrary to what would be expected and indicates that the difference is not due solely to variation in cross-sectional area of the specimens. No satisfactory explanation for the observed phenomena was found.

Figs. A.6a-A.11a together with Fig. A.12 show that the curves obtained from the stress-cell pressures were similar in shape to the standard curves provided that restraint occurred at the end of the specimen. If the end of the specimen expanded significantly then the resultant stress-strain curve tended to reach a maximum early in the shear stage (at about 2% axial strain) and thereafter remained relatively constant.

A.4. Conclusions.

Ignoring the unexplained differences which occurred during consolidation, it would appear that the stress-cell pressures were only acceptable if restraint occurred at the ends; and this is undesirable because of the associated non-uniform deformation of the specimen. The importance of end expansion was emphasized in Chapter 2. However, when a reasonable amount of end expansion did occur in the tests the stress-cells gave stress-strain curves which diverged from the standard curves as soon as the end area of the specimen became greater than the initial area at the start of the test.

It is concluded that if the specimen expands at the ends then the increase in load during the test is transferred to the rigid flange with little if any increase in the water pressure in the cells. Thus it appears that the assumption made by Dyson (1970), that the lubrication of the rigid flange will ensure that stress variations over the face of the stress-cell are small, is incorrect.

As a result of the above tests a new apparatus, described in Chapter 2, was used for the main research program.

FIG. A. 1(b)
TOP STRESS-CELL

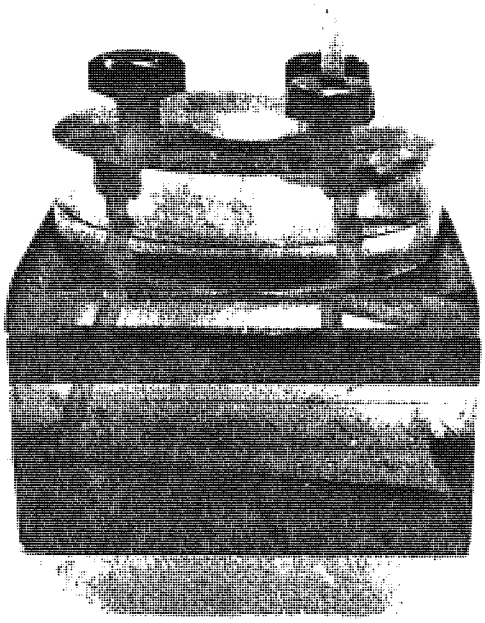

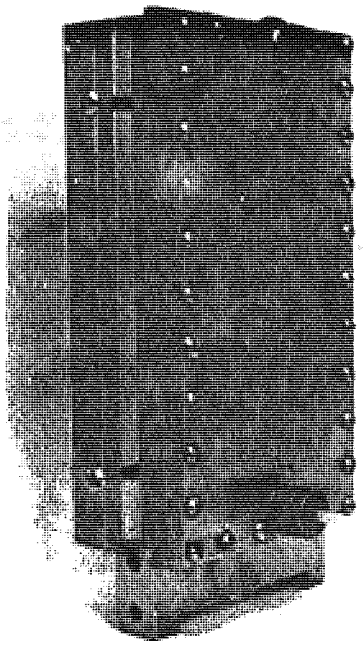

FIG. A. 1(a)
SIDE STRESS-CELLS

FIG. A. 1(c)
BOTTOM STRESS-CELL
UPPER AND LOWER SECTIONS

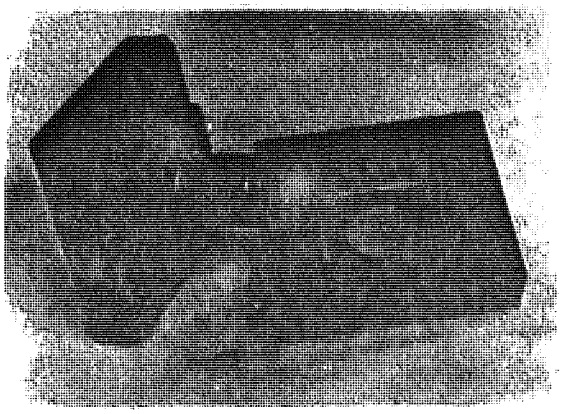

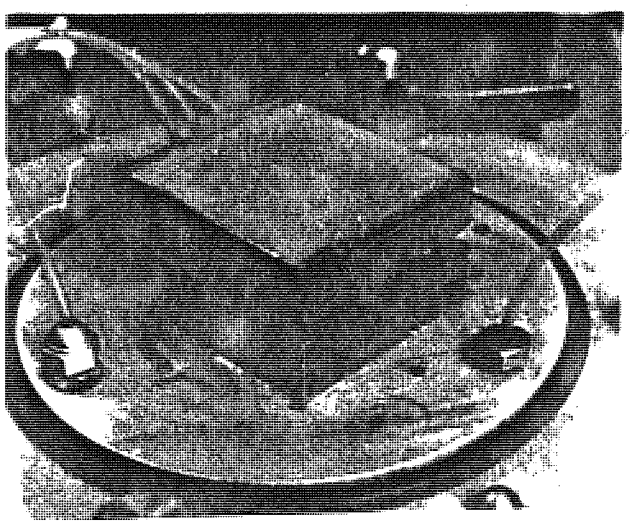

FIG. A. 1(d)
BOTTOM STRESS-CELL
ASSEMBLED WITHOUT
SPECIMEN MEMBRANE

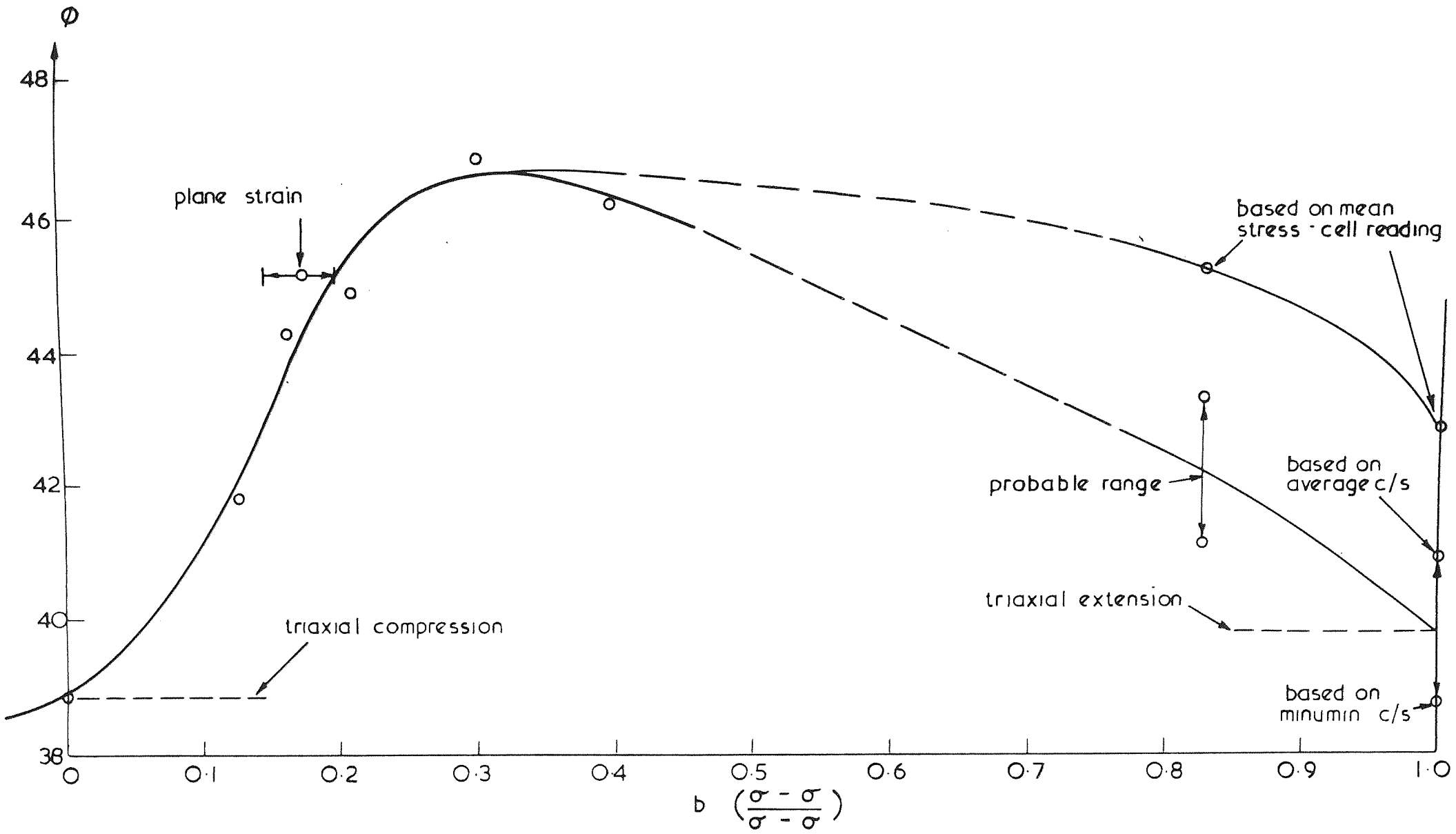
Φ
48
46
44
42
40
38
plane strain
triaxial compression
based on mean
stress - cell reading
probable range
based on
average c/s
triaxial extension
based on
minumin c/s
0
0·1
0·2
0·3
0·4
0·5
0·6
0·7
0·8
0·9
1·0
b (σ - σ / σ - σ)

Fig. A 3

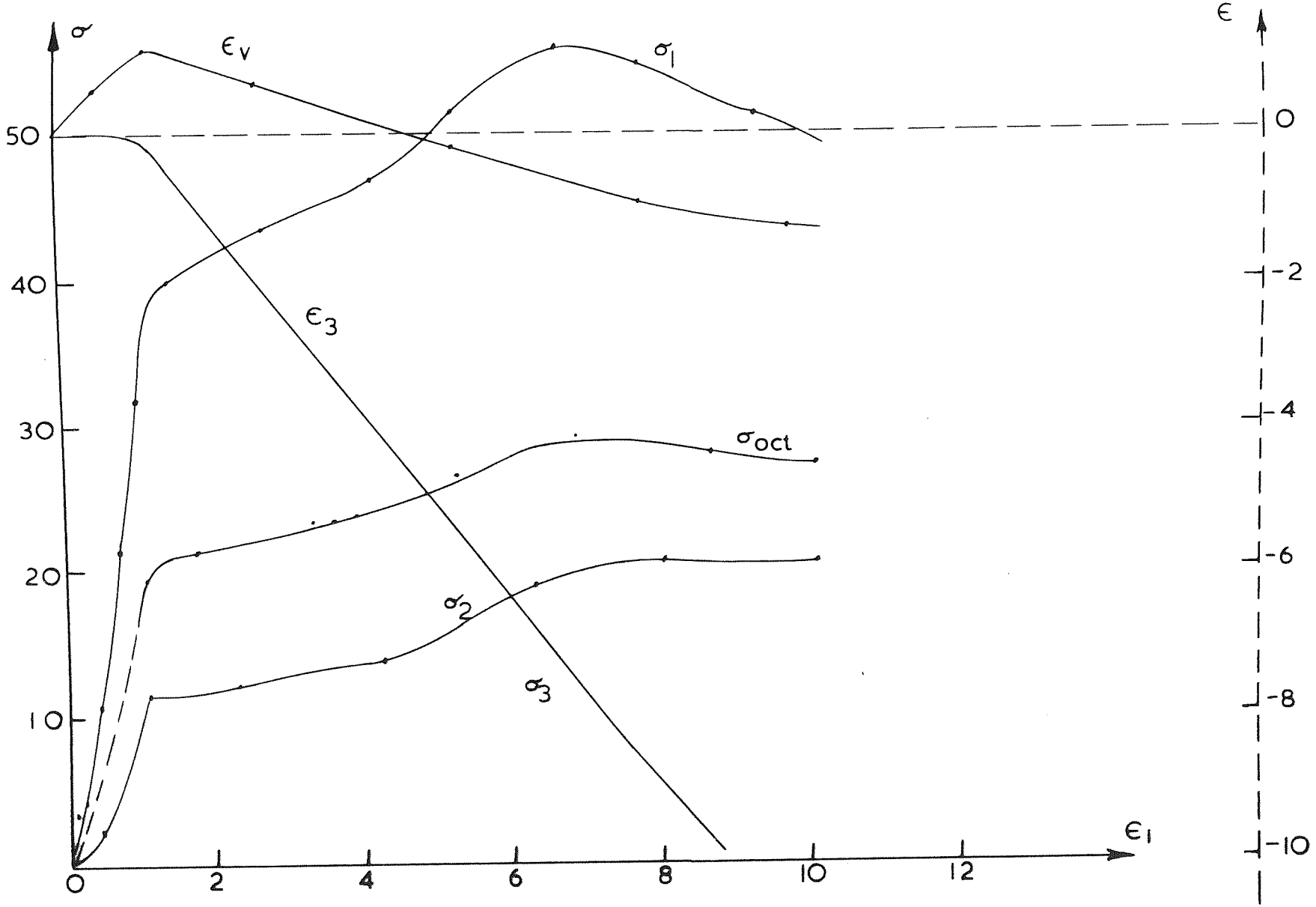
σ
ε
ϵ_v
σ_1
ϵ_3
σ_{oct}
σ_2
σ_3
ϵ_1
50
40
30
20
10
0
2
4
6
8
10
12
0
-2
-4
-6
-8
-10

Fig. A4

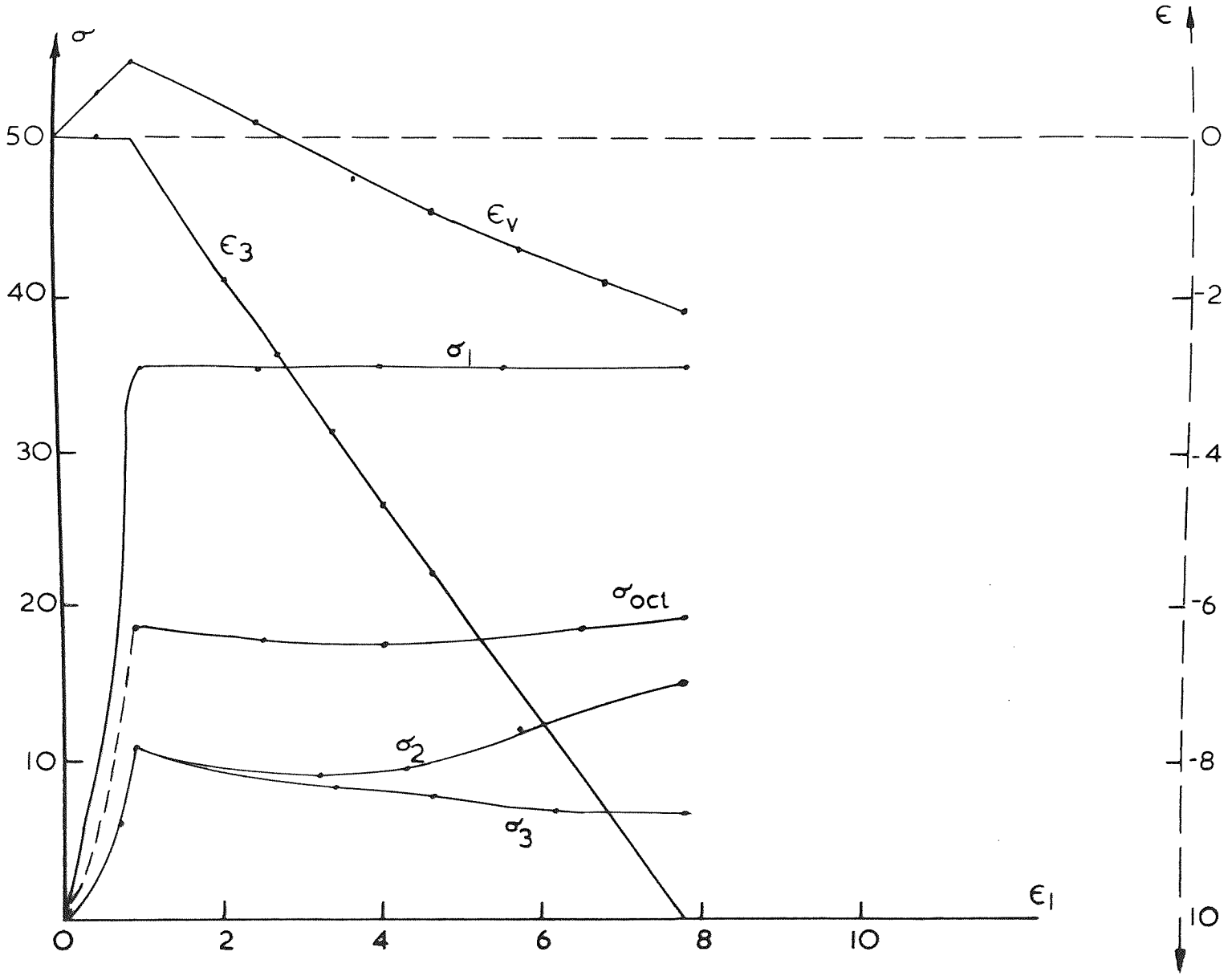
σ
ε
50
40
30
20
10
0
-2
-4
-6
-8
10
ϵ_v
ϵ_3
σ_1
σ_{oct}
σ_2
σ_3
ϵ_1
0
2
4
6
8
10

Fig . A 5

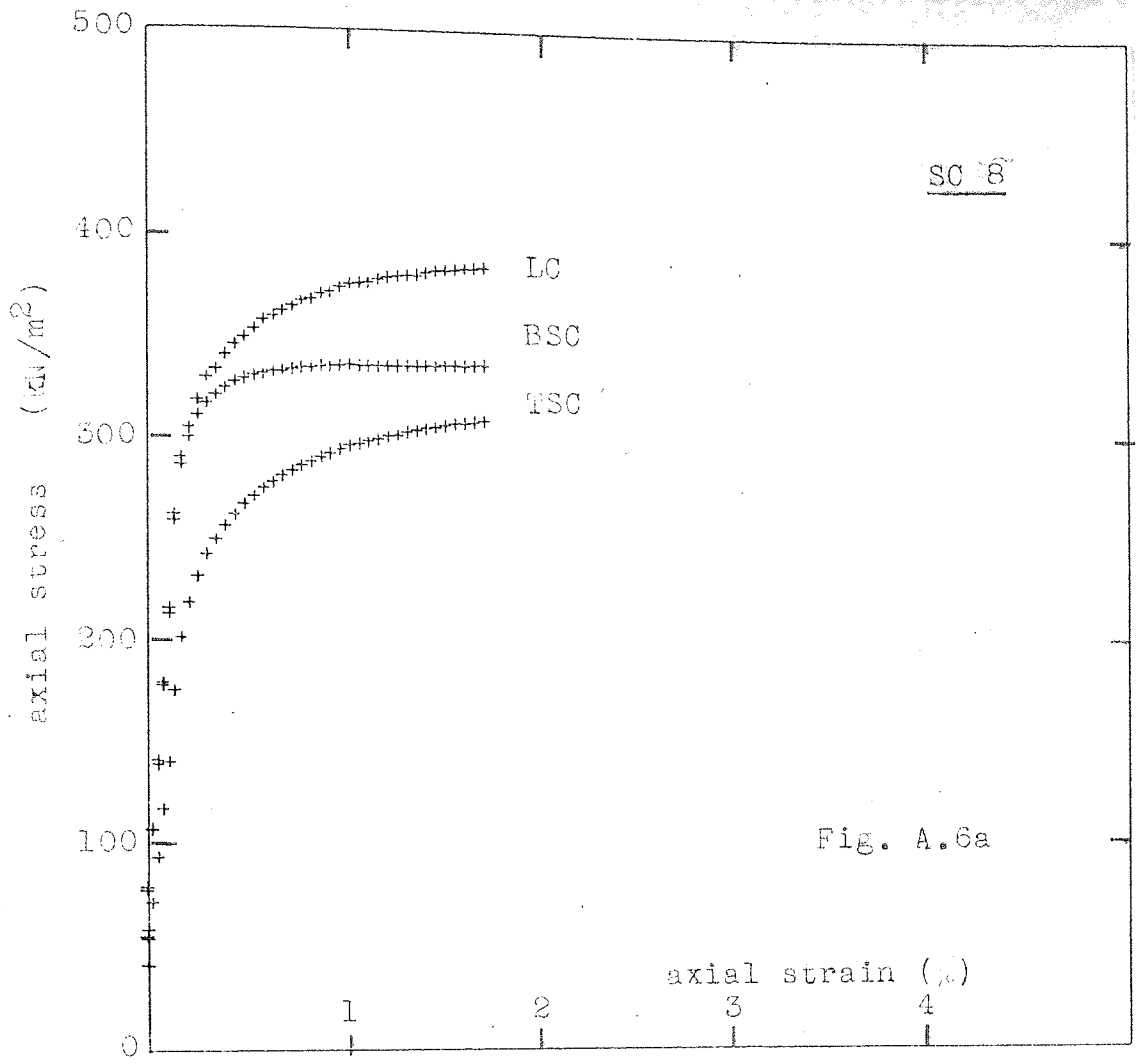

Fig. A.6a

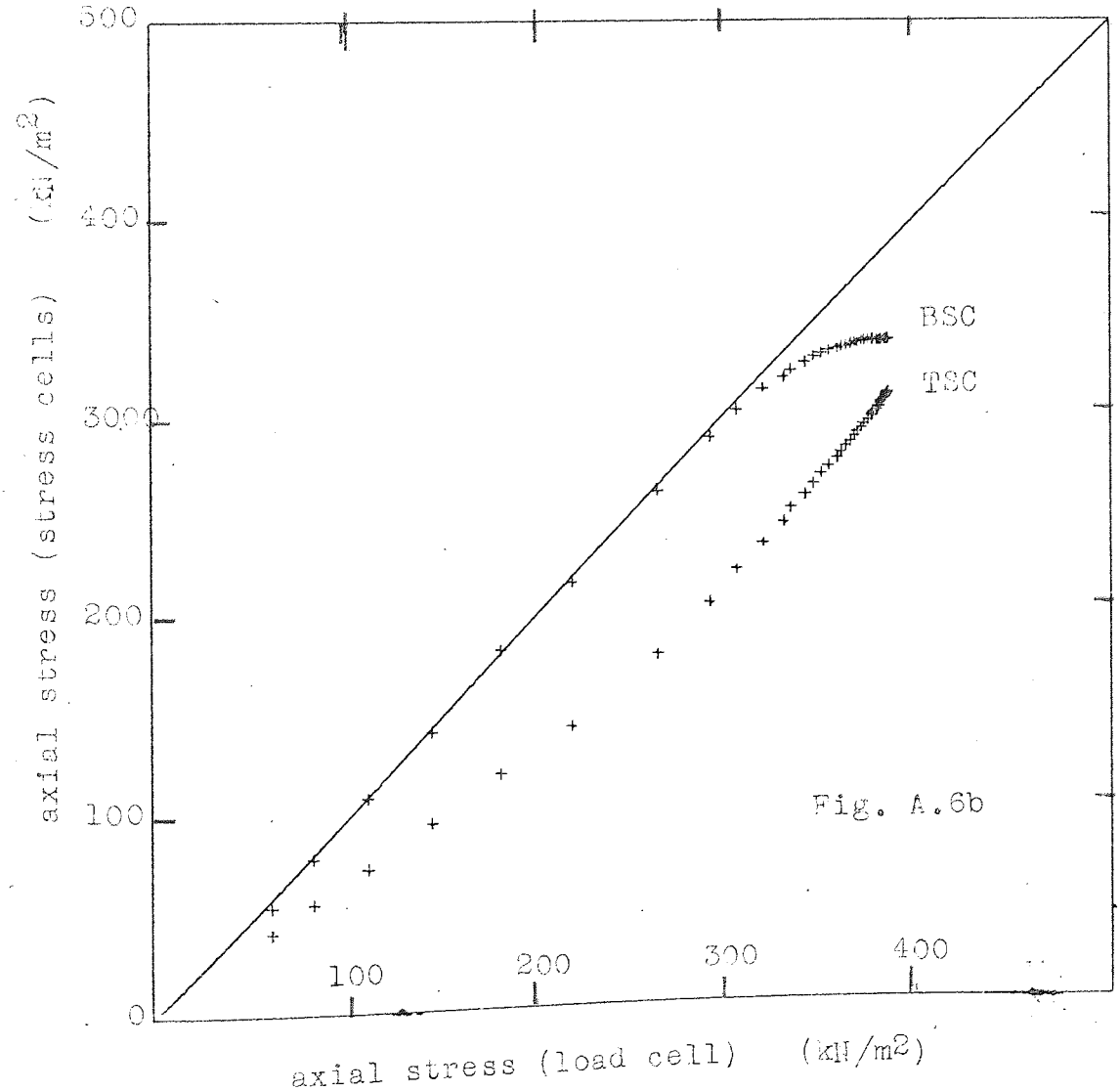

Fig. A.6b

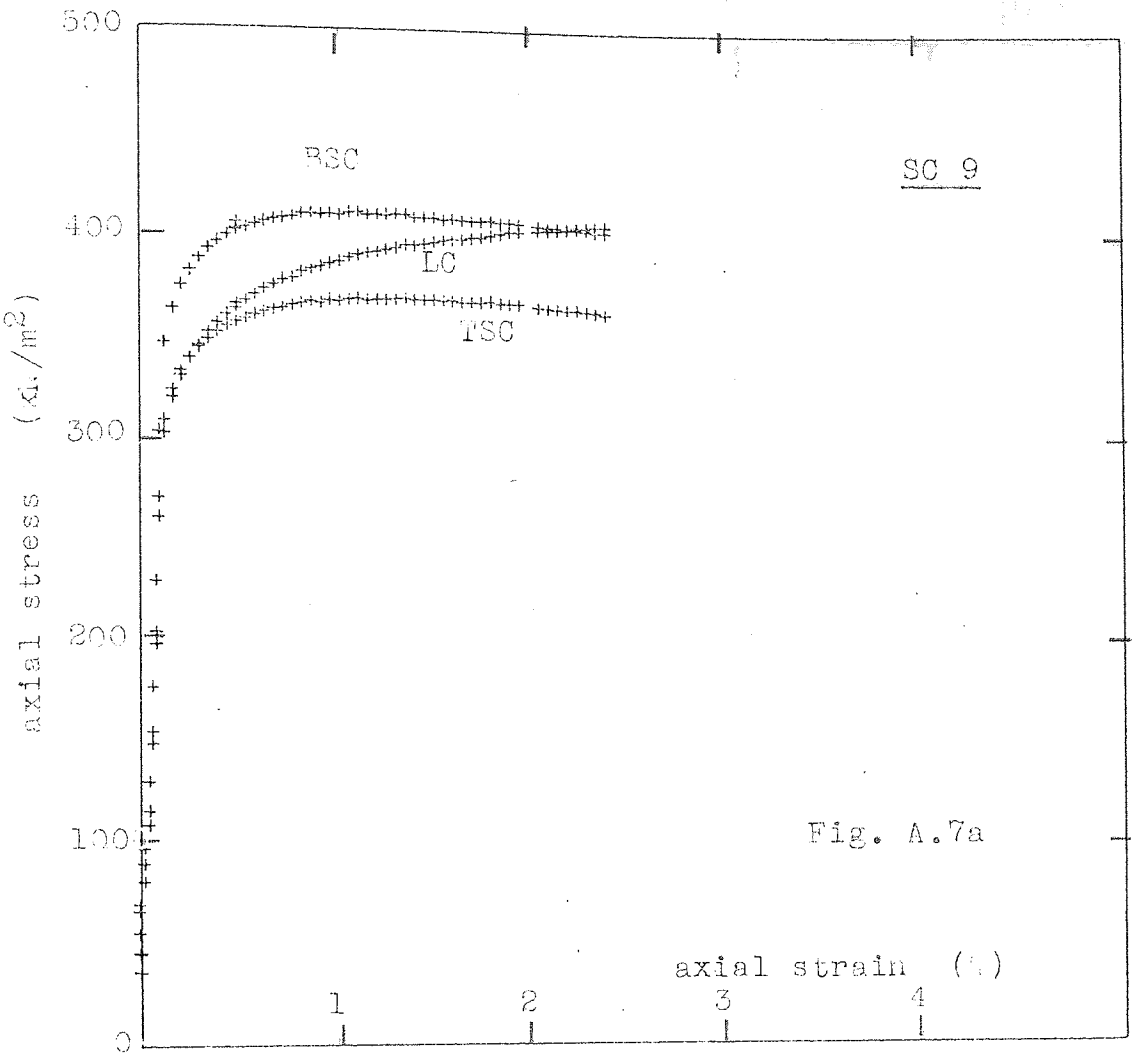

Fig. A.7a

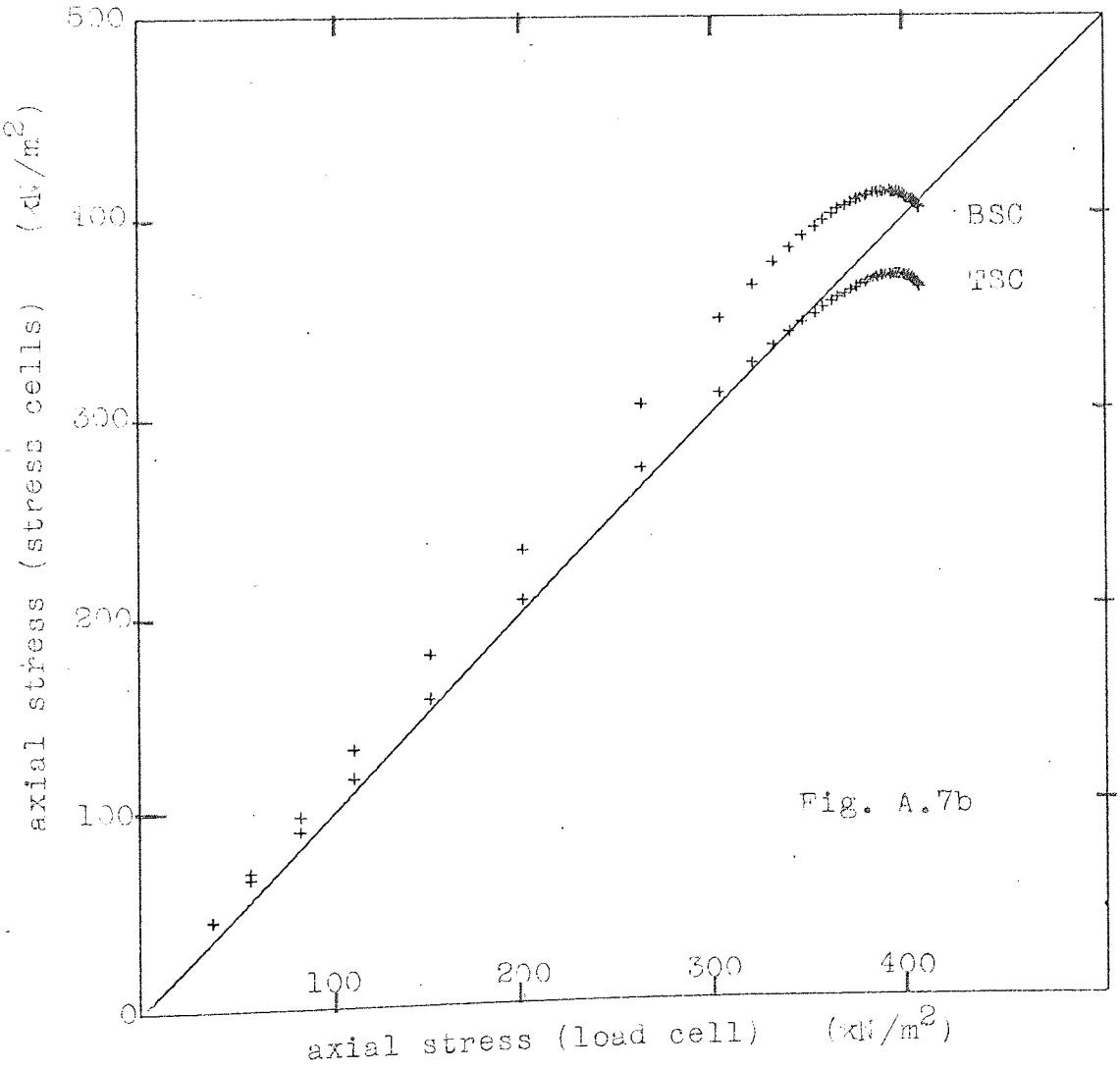

Fig. A.7b

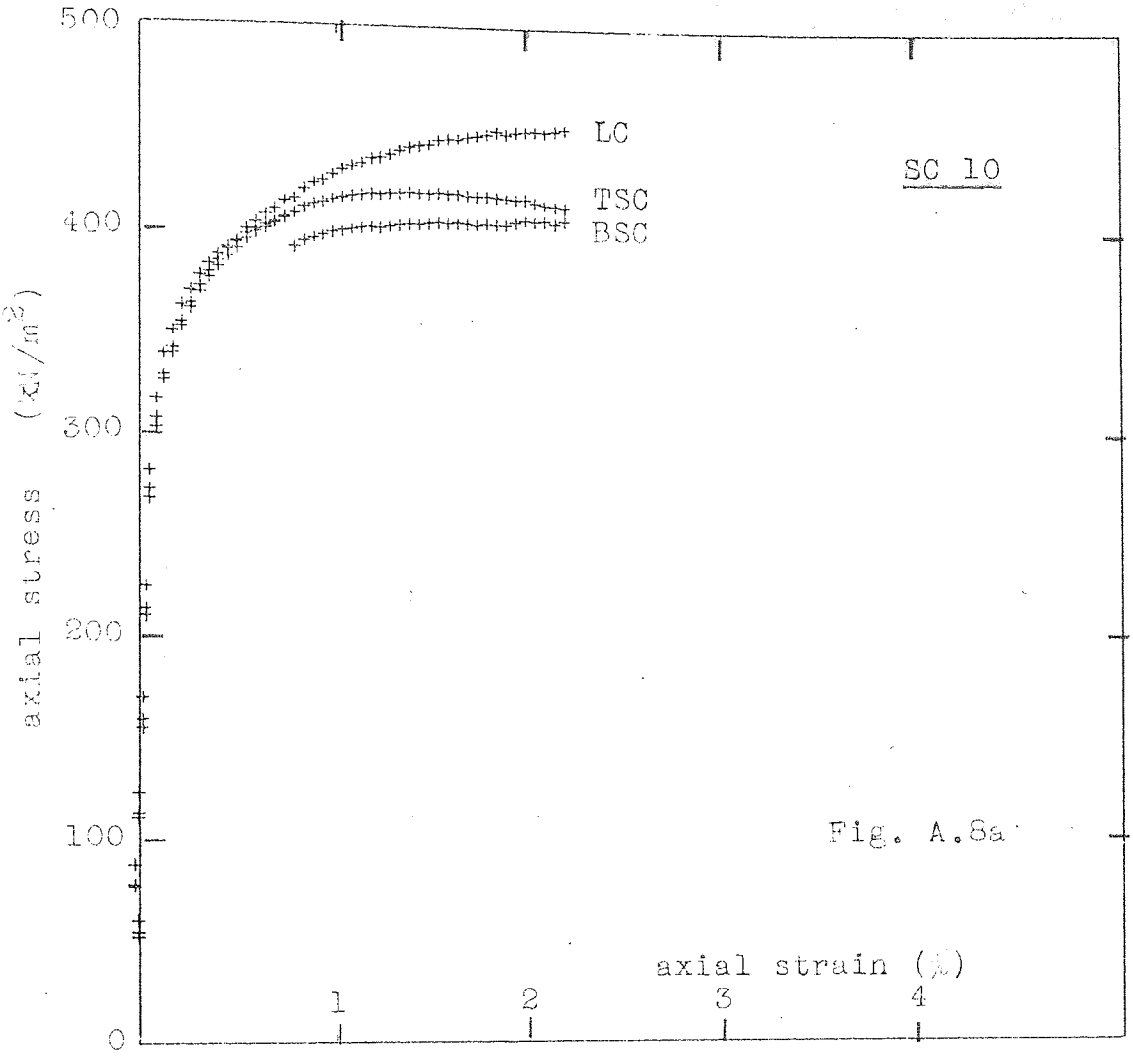

Fig. A.8a

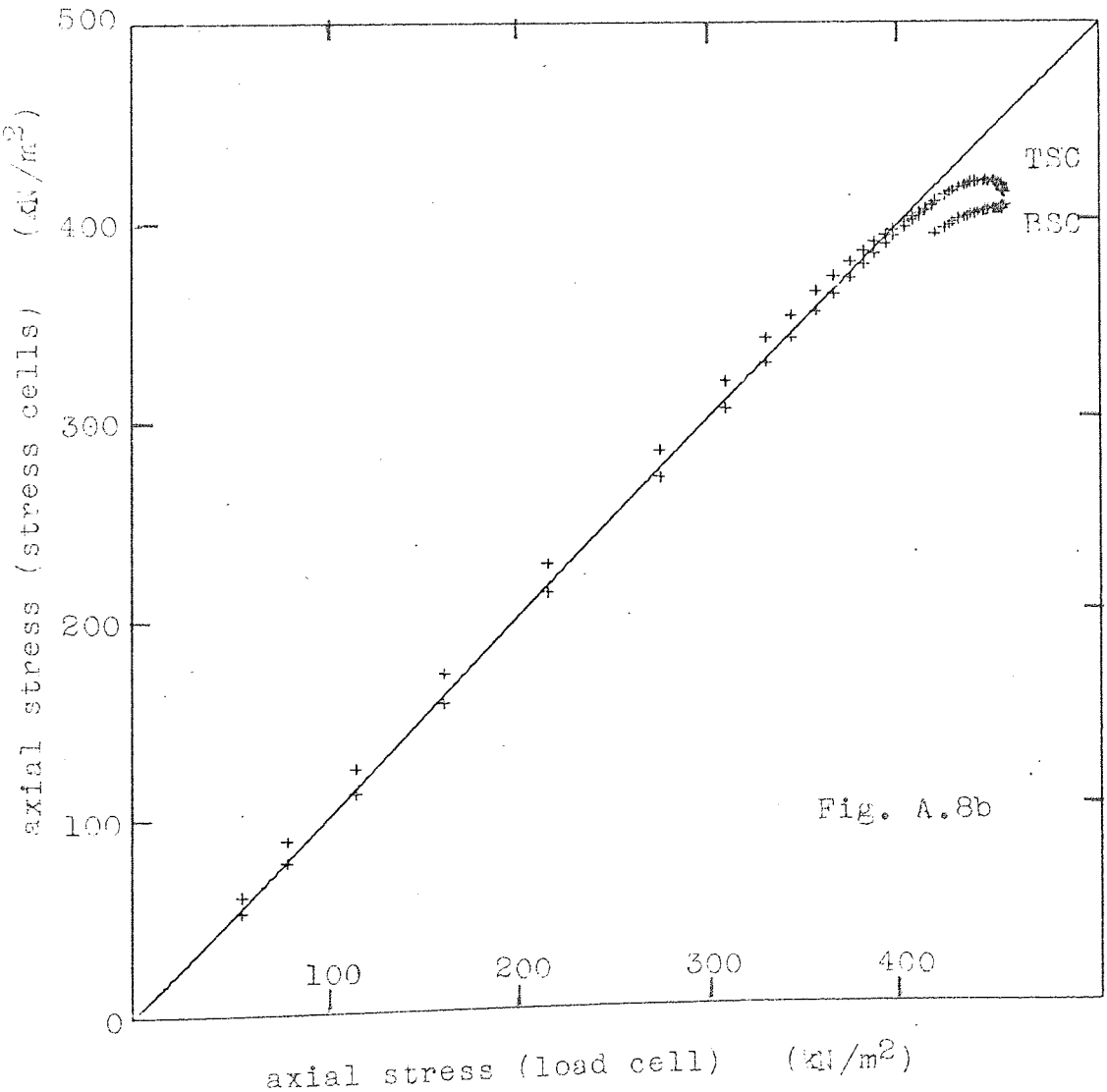

Fig. A.8b

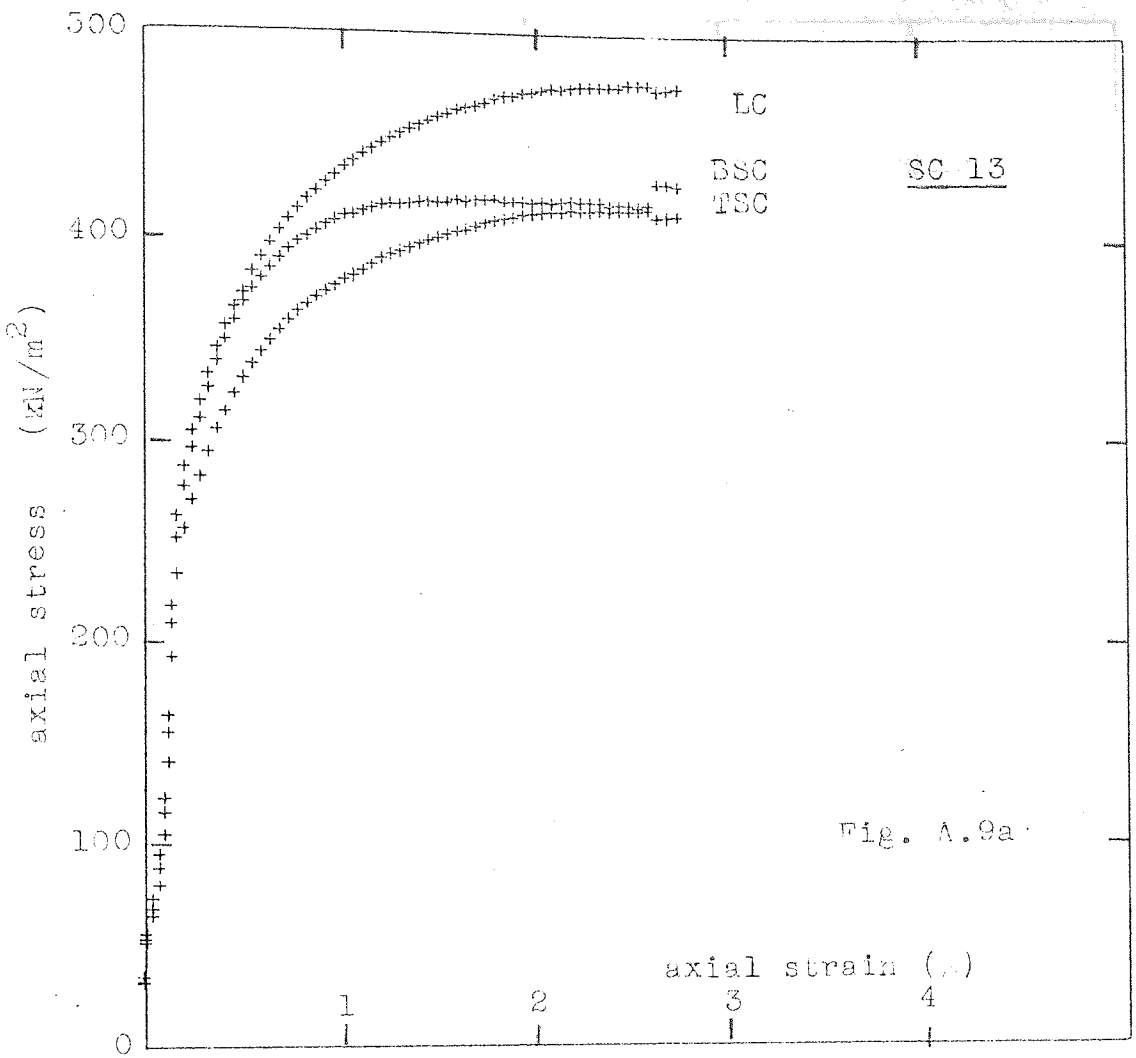

Fig. A.9a

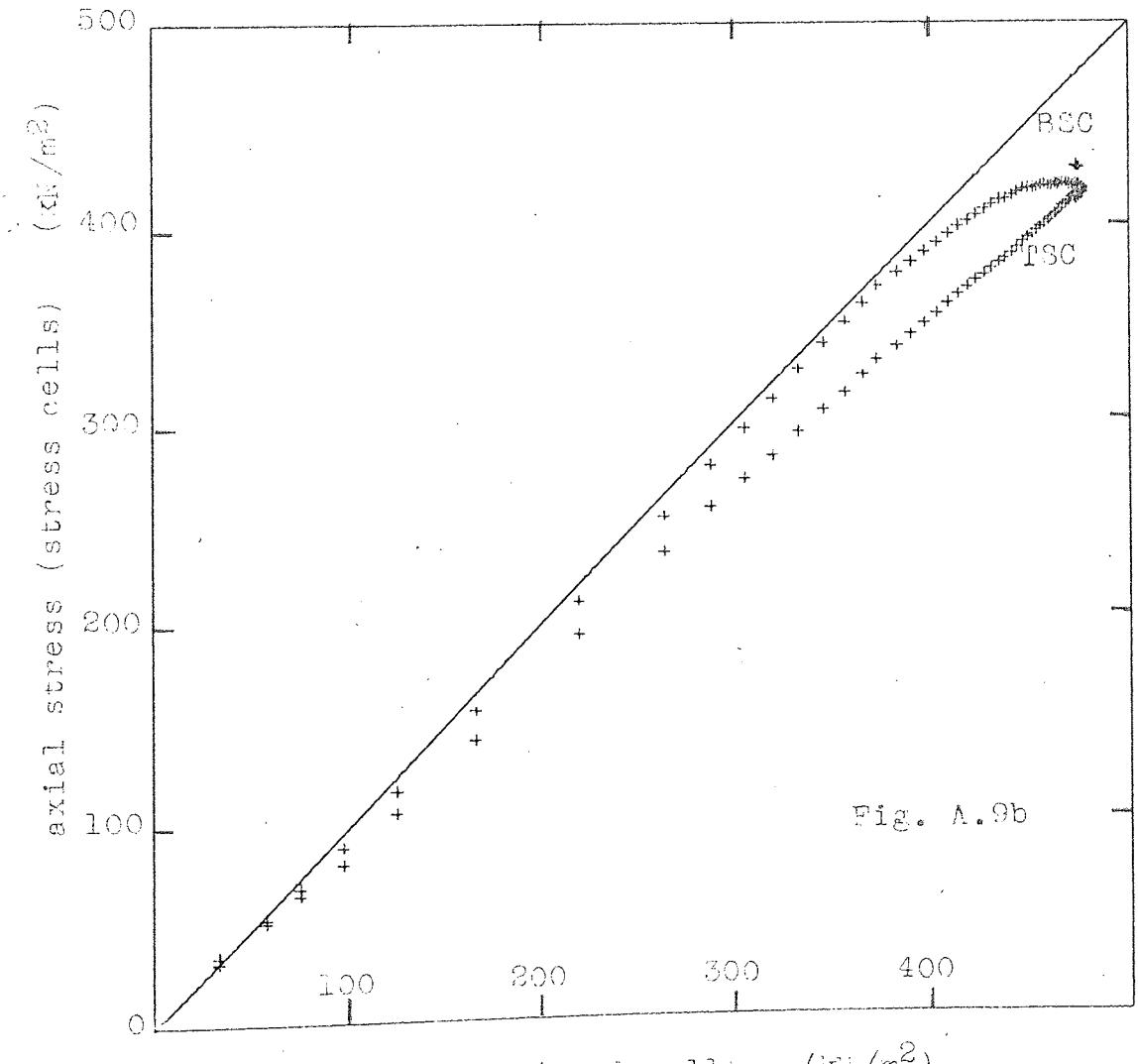

Fig. A.9b

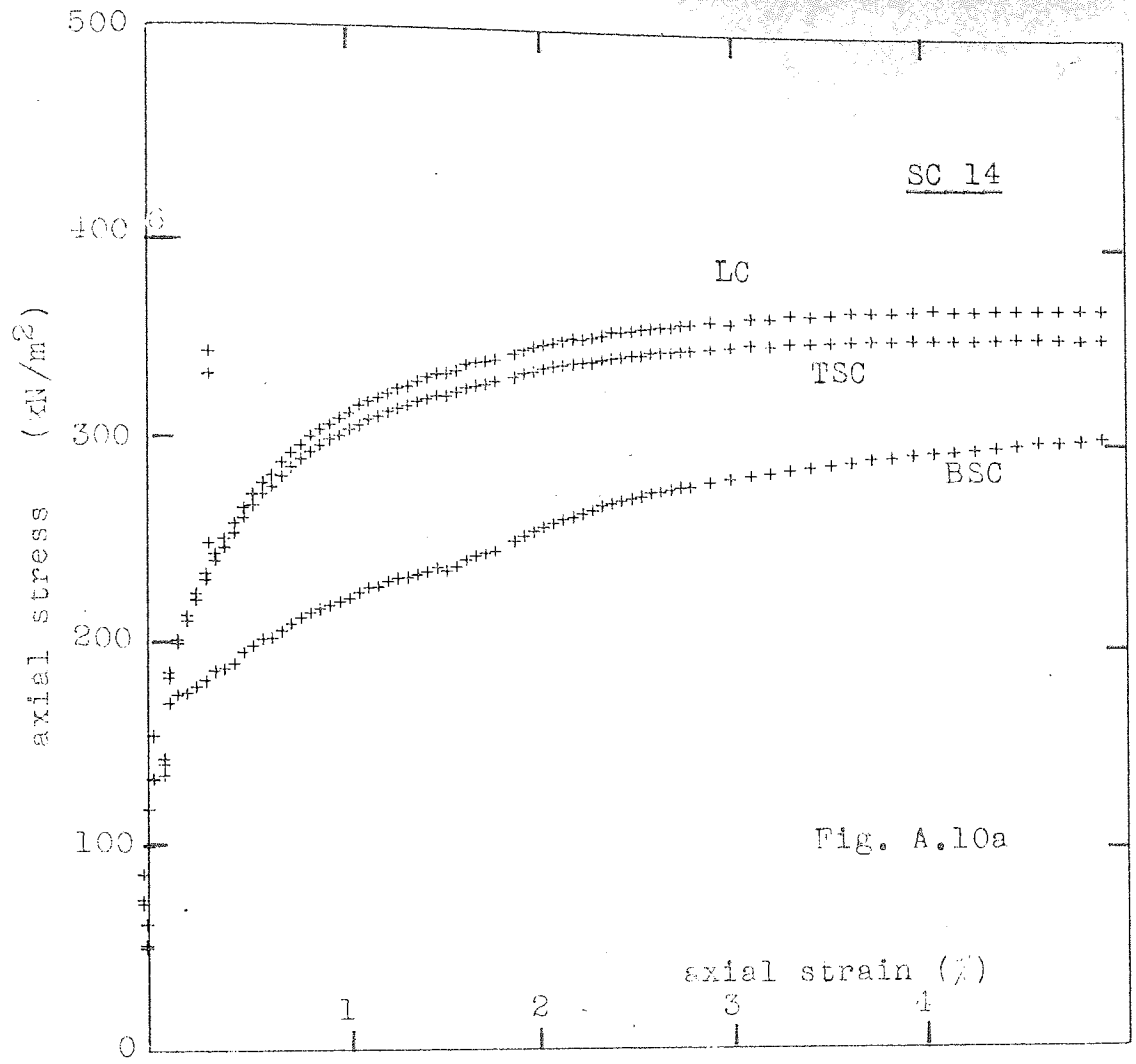

Fig. A.10a

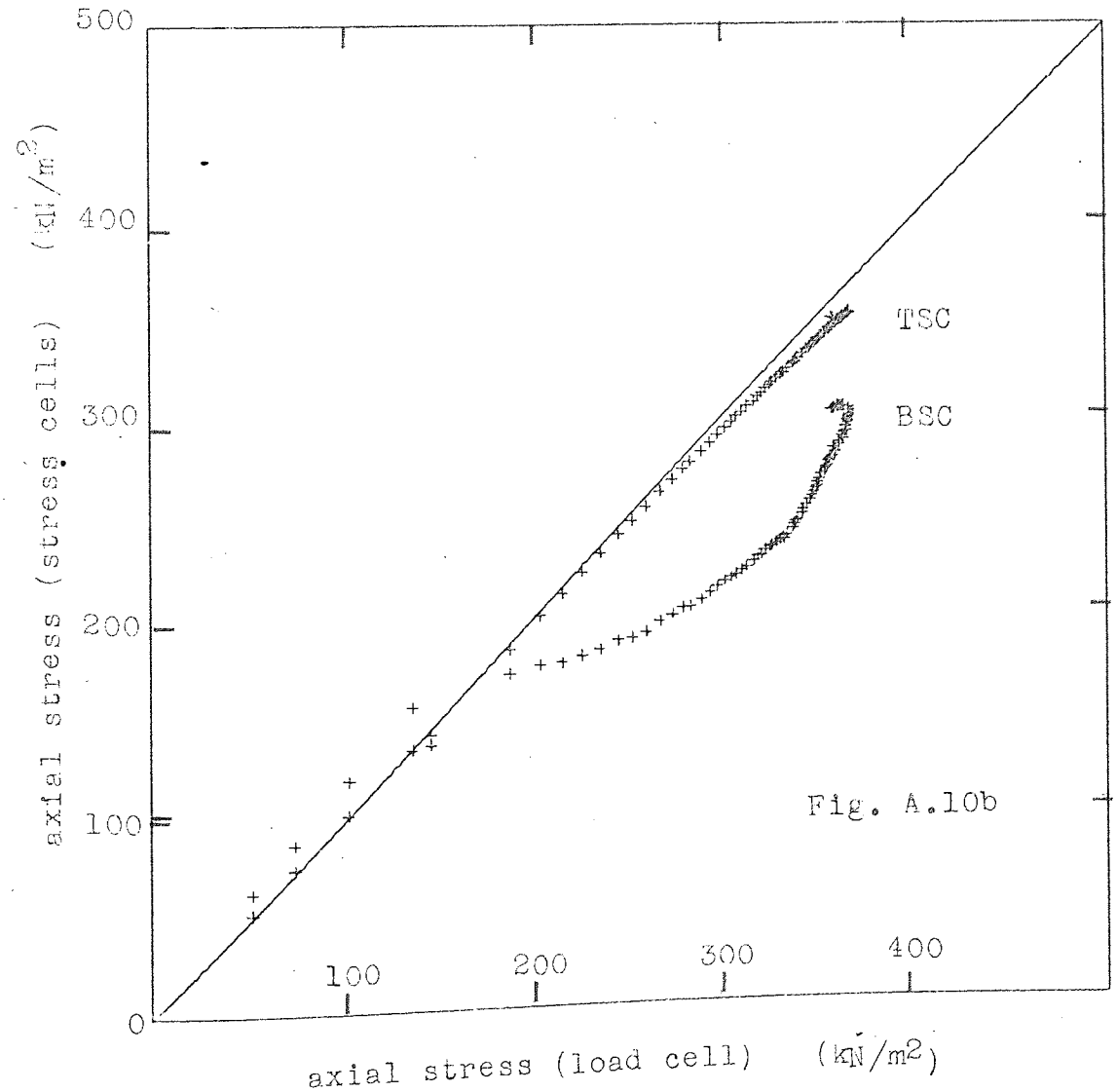

Fig. A.10b

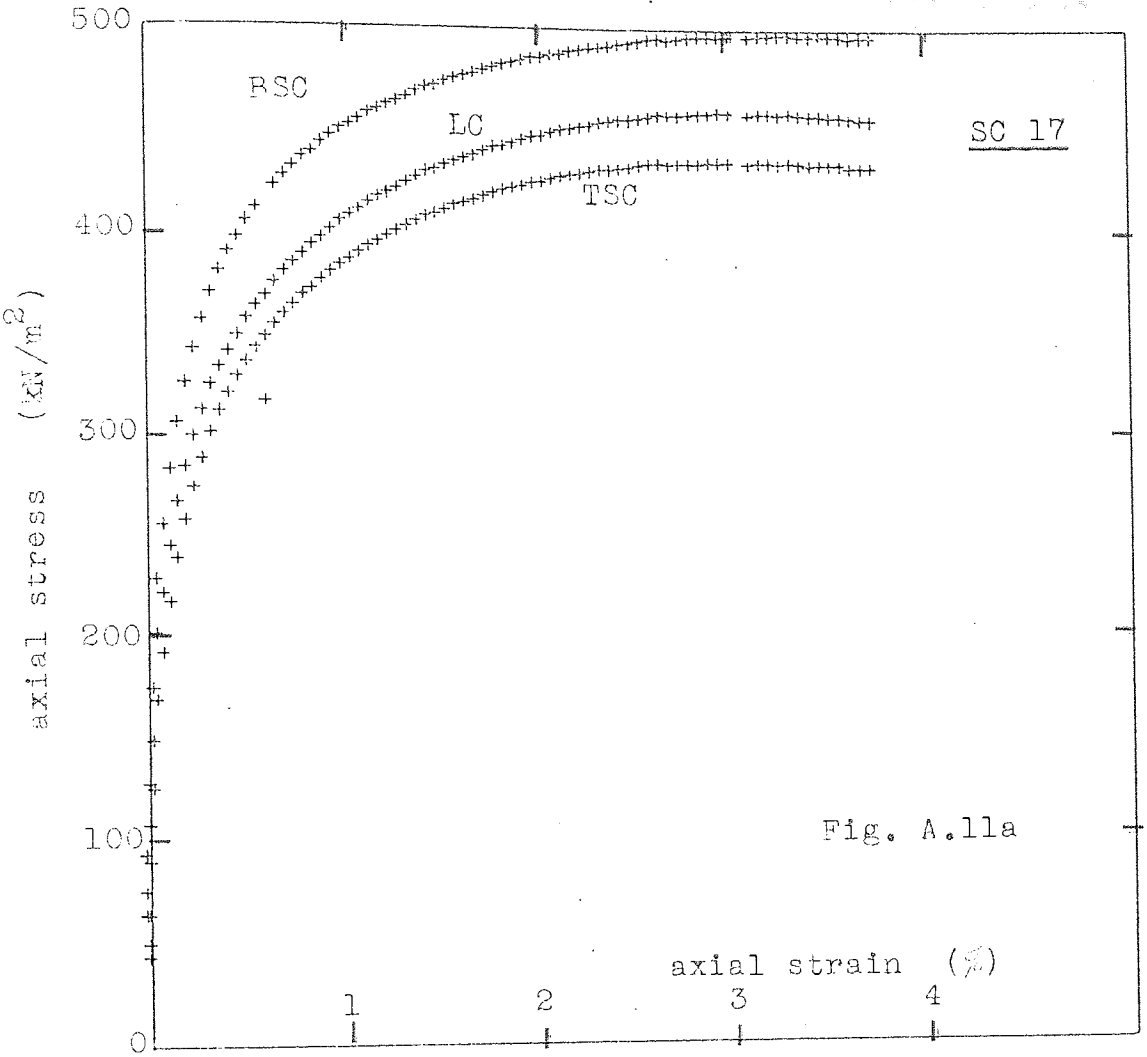

Fig. A.11a

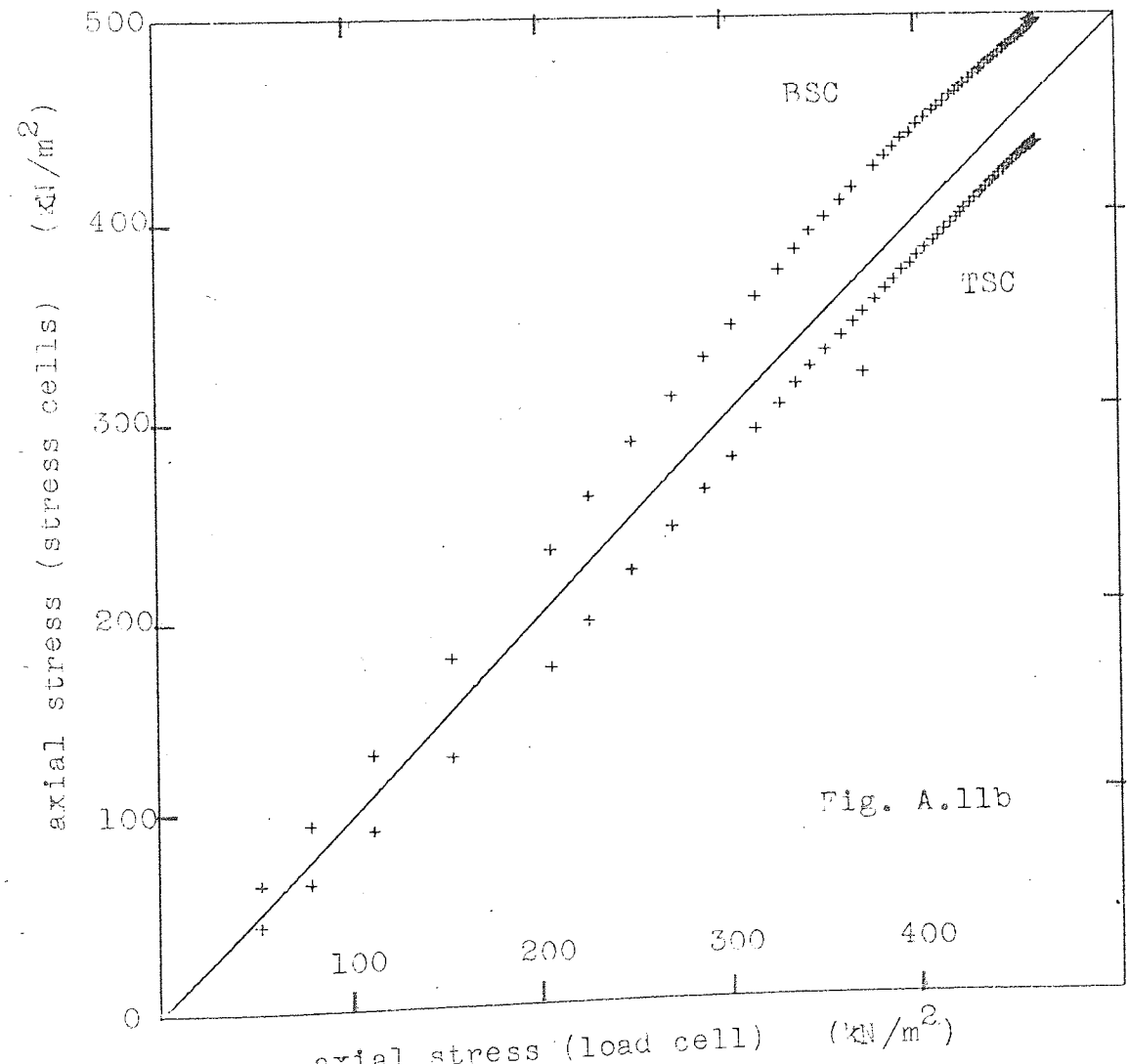

Fig. A.11b

TEST	POSITION	INITIAL CROSS-SECTIONAL AREA (mm^2)	LATERAL STRAIN (%)	
SC8	TOP	3385	-0.23	
	MID-HEIGHT	3425	-	*
	BASE	3435	-4.12	
SC9	TOP	3381	-2.27	
	MID-HEIGHT	3406	-	*
	BASE	3413	-1.33	
SC10	TOP	3387	-1.66	
	MID-HEIGHT	3398	-3.76	
	BASE	3399	-1.46	
SC13	TOP	3385	-1.65	
	MID-HEIGHT	3414	-3.00	
	BASE	3420	-2.08	
SC14	TOP	3286	-	*
	MID-HEIGHT	3359	-	*
	BASE	3387	-	*
SC17	TOP	3382	-2.83	
	MID-HEIGHT	3423	-4.91	
	BASE	3426	-2.87	

* No final measurements taken

Fig. A. 12

APPENDIX B

B. CALIBRATIONS AND CORRECTIONS

B.1. Axial load cell calibration

A Wykeham Farrance 1000 lbf (4.448 kN) Load Cell Type WF/17001 was used to measure the deviator load in all the tests reported. The load cell was calibrated against a 1000 lbf (4.448 kN) high tensile steel proving ring at regular intervals throughout the testing program. The manufacturer's specification quoted a nominal output of 20 mV at full rated load when energised at 10 V. No significant difference was found between the results of the calibration tests and the manufacturer's rating. The calibration curves obtained were linear and exhibited no hysteresis effect.

Although no zero drift was observed between the start and finish of an individual test there was a gradual drift of the zero reading over the complete testing program. This small problem was easily resolved by noting the zero reading at the start and end of each test.

B.2. Flexible side platen calibration

The cell pressure and the pressure recorded by the flexible side platens were measured by Bell and Howell pressure transducers which were calibrated against a Budenberg dead weight tester. The calibration curves were linear and no hysteresis was observed.

Having calibrated the pressure transducers, the side platen transducer was connected to the two flexible side platens which were then de-aired. The flexible side platens were then positioned inside the triaxial cell and the cell was filled with de-aired water. The cell pressure was raised in increments of 20 kN/m^2 up to a maximum of 300 kN/m^2 using the calibrated cell pressure transducer output as a guide. The pressures recorded by the side platen transducer were noted and the

calibration curve obtained was found to be identical to that obtained when the transducer was calibrated in isolation from the side platens.

The calibration of the pressure transducers was checked periodically and found to be constant. No zero drift was observed over the entire testing period.

B.3. Axial strain correction calibrations.

In all the tests performed, corrections were applied to the measured axial strains in an attempt to account for the compressibility of the axial load cell, compression of the lubricated membranes, and the squeezing out of the silicone grease under load. Therefore, at the start of the testing program, calibration tests were performed to determine the effect of each of these sources of error.

B.3.1. Compressibility of axial load cell.

The compressibility of the axial load cell was calibrated in a Denison Universal Testing Machine and the results of the calibration test are shown in Fig. B.1. It can be seen that the load-deflection curve was non-linear and exhibited a slight hysteresis effect. Since the maximum load recorded in the experiments was never more than 2 kN the hysteresis was neglected. By plotting the load to the power 2/3 a linear calibration curve was obtained, as is shown in Fig. B.2.

B.3.2. Compressibility of load cell and lubricated membranes.

The combined compressibility of the load cell and lubricated membranes was measured by conducting a 'triaxial compression test' on a dummy steel specimen. For this purpose the triaxial cell was not filled with water.

Having set up the dummy specimen ready for testing, the motor was switched on at a very slow rate of feed and the load cell output readings were noted for every 0.01 mm deflection on the dial gauge. When the load reached the anticipated maximum working load the motor

was switched off, the pedestal was lowered by hand, and the apparatus was dismantled. Any excess grease which had been squeezed out under load was removed. The apparatus was then re-assembled using the same lubricated membranes and a second calibration test was performed. The results of the two calibration tests are shown in Fig. B.3 in which the calibration curve for the load cell alone is also shown.

It is evident from Fig. B.3 that, if the excess silicone grease is removed prior to testing, the initial compression is essentially due to the compressibility of the load cell, and the subsequent combined compression of the load cell and the lubricated membranes results in a linear load-deflection curve. The difference between the first and second loading curves is due to squeezing out of the excess grease which occurred during the early part of the first calibration test.

For the tests on sand reported in this thesis the excess grease was removed from the lubricated membranes at the start of the sample preparation procedure, see section 2.4.4. Two additional calibration tests were performed using the dummy steel specimen for which the excess grease had been removed using the same technique. The results of these additional tests are shown in Fig. B.4 and are compared with the line representing the second loading curve shown in Fig. B.3. Although the results of the two additional tests differed somewhat, it was thought that the straight line shown in Fig. B.4 provided a reasonable estimate of the correction to be applied to the dial gauge readings, for deviator loads greater than 250 N. For loads less than 250 N the correction for the load cell alone was used, see Fig. B.2.

B.3.3. Compression of load cell and lubricated membranes during cyclic loading.

A further calibration test was performed in which the dummy steel specimen was loaded, unloaded, and reloaded. The results are shown in Fig. B.5. During virgin loading the rate of compression was similar to that given by the straight line in Fig. B.4. On unloading the specimen

there was an immediate fall off in load without any extension followed by a rate of extension that was compatible with the compressibility of the load cell alone, until unloading was nearly complete. It would appear that extension of the lubricated membranes only occurred after the deviator load had been virtually removed and that, on reloading, the lubricated membranes compressed first, followed by compression of the load cell.

Although the behaviour immediately following a reversal of load was not clear the axial strain corrections to be applied during a cycle of load were initially based on the calibration of the load cell alone. However, when the corrections were applied to the test results nonsensical values of strain were obtained and further attempts to apply a correction to the axial strain data during cycles of load were abandonded.

Clearly the corrections to be applied to the axial strains during cycles of loading are relatively large and it is therefore suggested that, for future work in which cycles of load are applied, a rigid load cell similar to the one used by Tong (1970) may be more appropriate than the flexible load cell used in this research program.

B.4. Volumetric strain corrections.

The measurement of volumetric deformation of cohesionless soils, if based on the volume of pore-fluid entering or leaving the specimen, is susceptible to errors resulting from penetration of the rubber sheath into the voids under pressure, Newland and Allely (1959). The apparent volume change exceeds the true volume change of the specimen by an amount dependent upon the size and shape of the particles, the magnitude of the differential pressure across the sheath, the thickness of the sheath, and the shape and size of the specimen.

In the present experimental research program the effect of membrane penetration was minimised rather than calibrated for, by testing a fine

sand enclosed in a relatively thick (0.375 mm) sheath, under drained conditions at a relatively low (100 kN/m^2) cell pressure. Consequently no corrections have been made to the volume change measurements recorded during the tests.

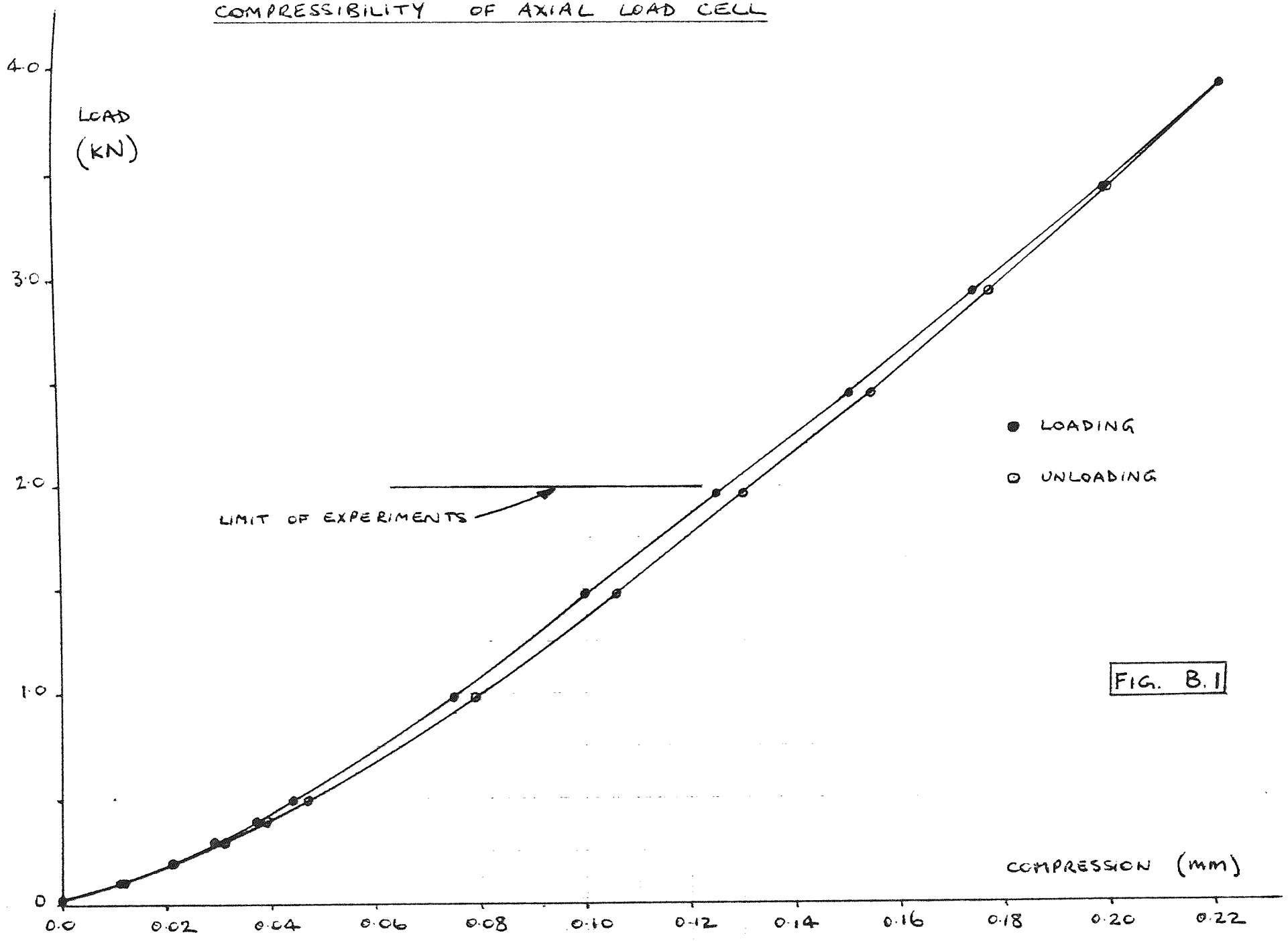
COMPRESSIBILITY OF AXIAL LOAD CELL
LOAD (kN)
4·0
3·0
2·0
1·0
0
LIMIT OF EXPERIMENTS
LOADING
UNLOADING
COMPRESSION (mm)
0·0
0·02
0·04
0·06
0·08
0·10
0·12
0·14
0·16
0·18
0·20
0·22

FIG. B.1

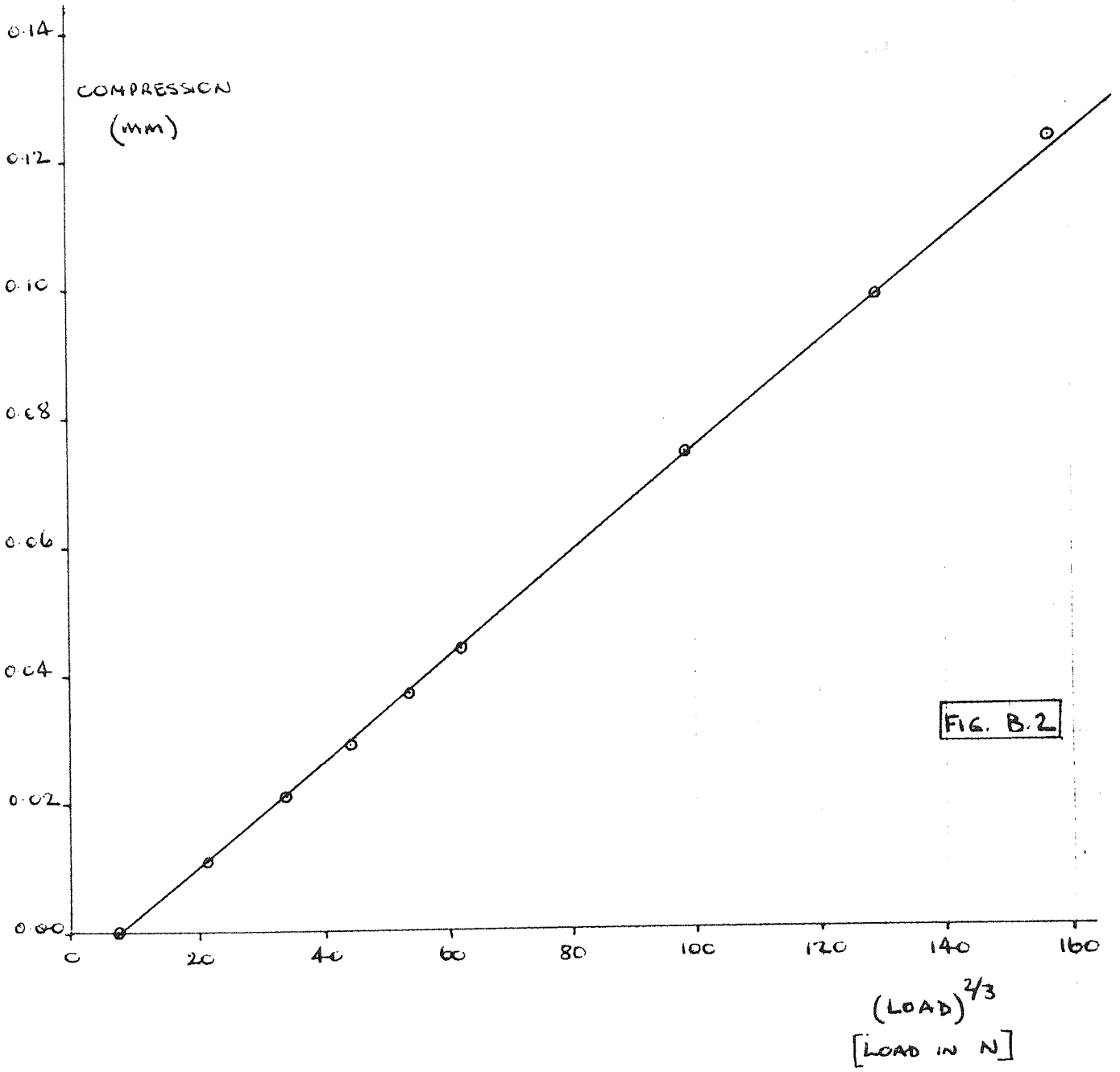

FIG. B.2

CORRECTION FOR COMPRESSION OF AXIAL LOAD CELL

$$\Delta = 0.000081 . W^{2/3}$$

where Δ = correction to be applied in cm

W = deviator load in N

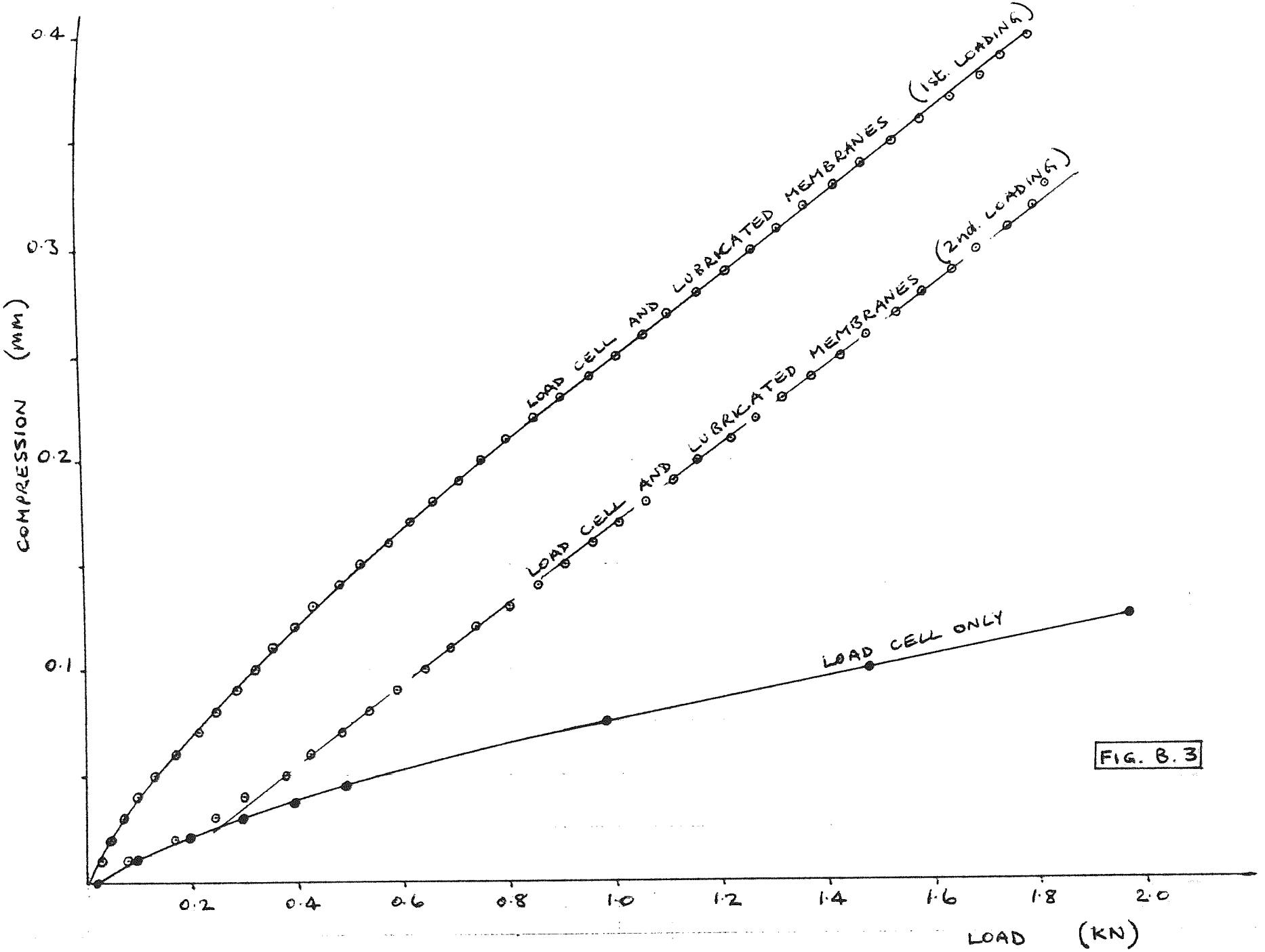
0.4
0.3
0.2
0.1
COMPRESSION (MM)
LOAD CELL AND LUBRICATED MEMBRANES (1st. LOADING)
LOAD CELL AND LUBRICATED MEMBRANES (2nd. LOADING)
LOAD CELL ONLY
0.2
0.4
0.6
0.8
1.0
1.2
1.4
1.6
1.8
2.0
LOAD (KN)

FIG. B.3

CORRECTION FOR COMPRESSION OF LOAD CELL AND LUBRICATED MEMBRANES

$$\Delta = 0.0001925\,(W - 250) + 0.0038$$

where

Δ = correction to be applied in cm

W = deviator load in N

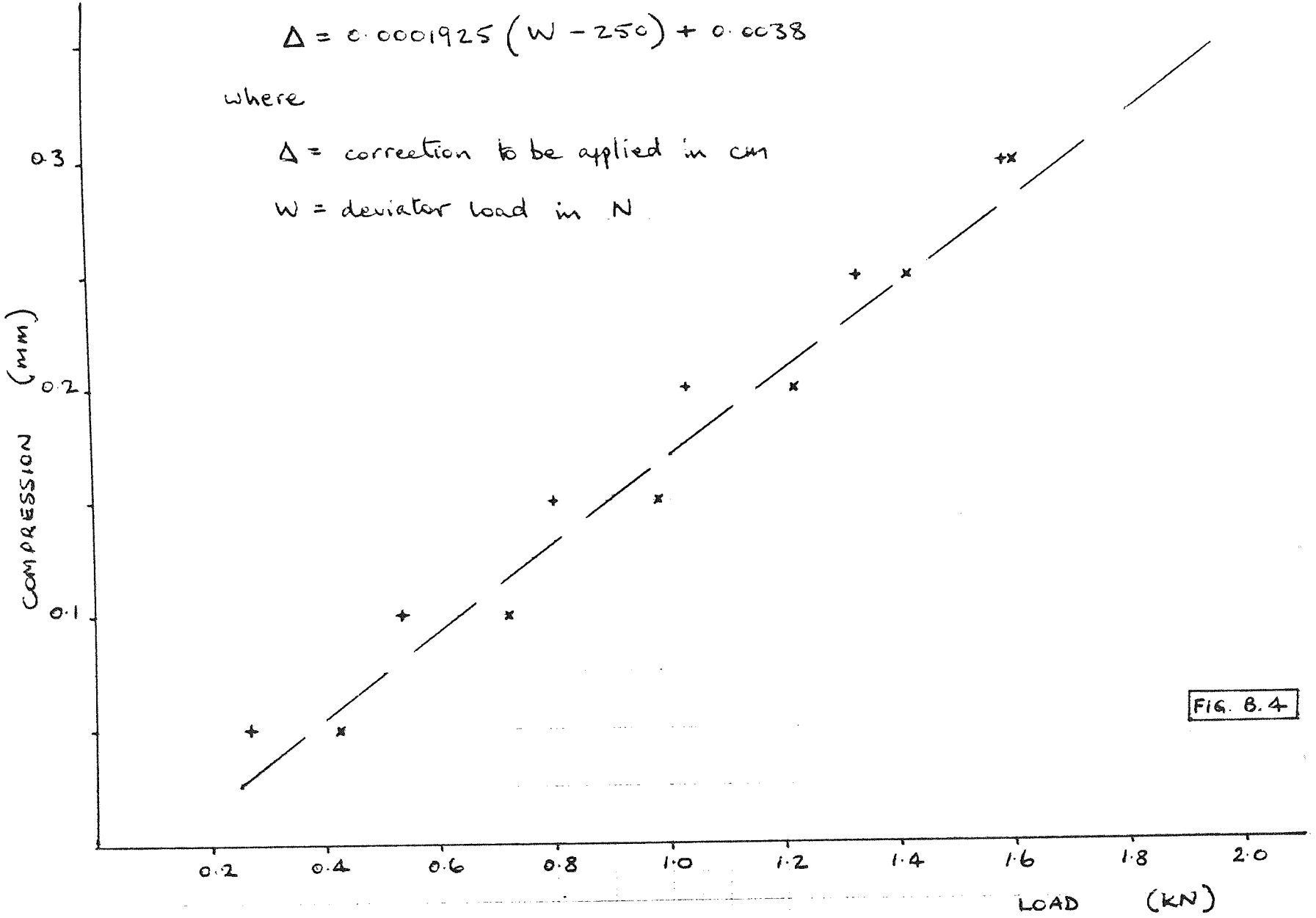

FIG. 8.4

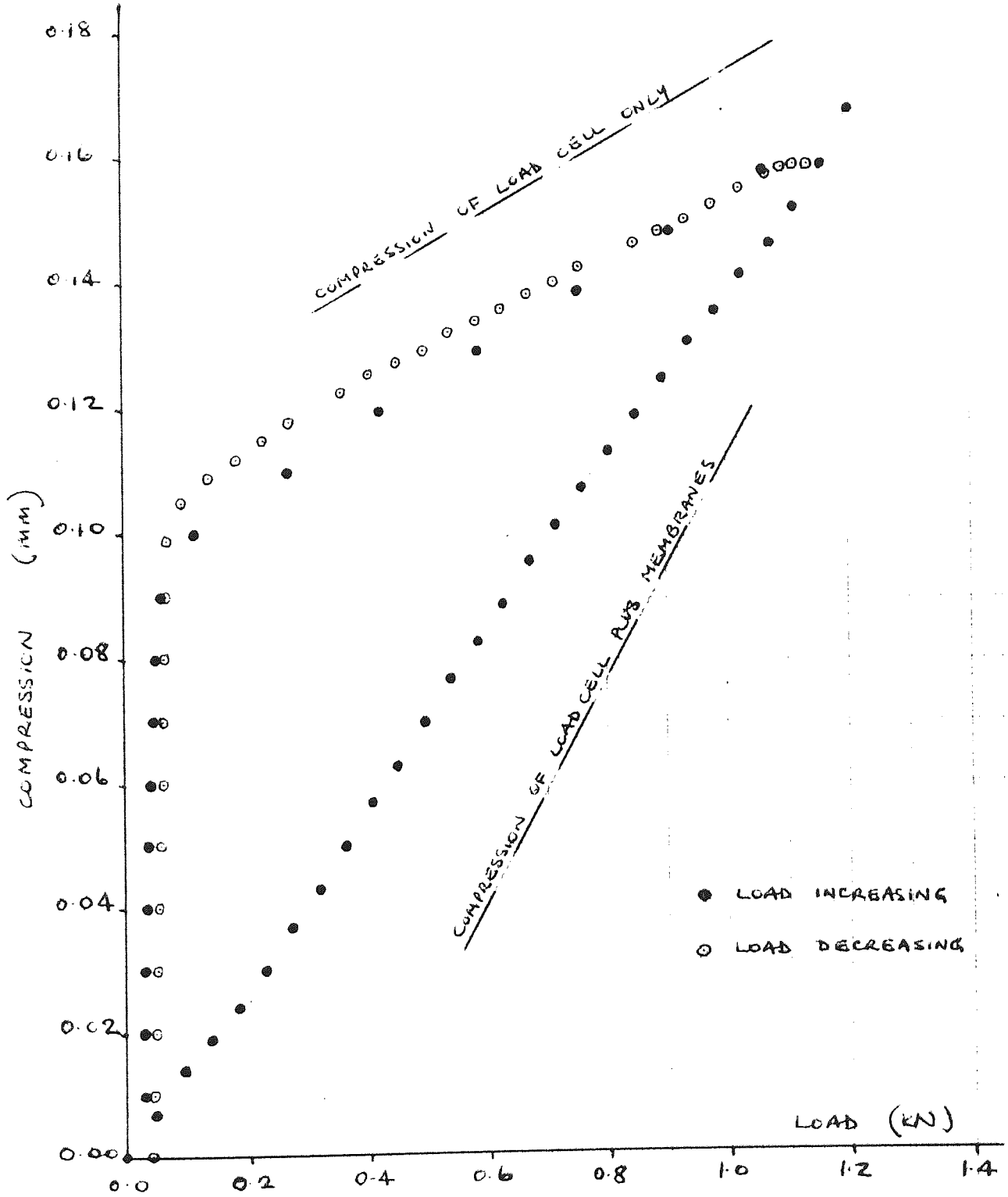
0·18
0·16
0·14
0·12
0·10
0·08
0·06
0·04
0·02
0·00
COMPRESSION (MM)
0·0
0·2
0·4
0·6
0·8
1·0
1·2
1·4
LOAD (KN)
COMPRESSION OF LOAD CELL ONLY
COMPRESSION OF LOAD CELL PLUS MEMBRANES
LOAD INCREASING
LOAD DECREASING

FIG. 8.5

APPENDIX C

TRIAXIAL COMPRESSION TESTS

Test Number	Initial Porosity	Axial Strain at Failure	Maximum Dilatancy Factor	Maximum Stress Ratio	Angle of Internal Shearing Resistance
TC 1	38.60	4.35	1.88	5.31	43.1
TC 2	39.70	4.04	1.74	4.99	41.8
TC 3	42.83	7.17	1.11	4.10	37.5
TC 4	39.87	4.49	1.57	4.97	41.7
TC 5	42.42	5.12	1.32	4.13	37.9
TC 6	41.72	5.22	1.46	4.48	39.4
TC 7	41.47	5.25	1.46	4.28	38.4
TC 8	40.69	3.25	1.51	4.64	40.2
TC 9	39.09	4.11	1.78	5.41	43.5
TC 10	38.75	4.68	1.83	5.40	43.4
TC 11	38.48	4.58	1.87	5.32	43.1
TC 12	43.00	7.00	1.30	4.26	38.3
TC 13	40.11	7.99	1.72	5.64	44.3
TC 14	41.41	6.19	1.46	5.07	42.1
TC 15	42.35	8.80	1.48	4.65	40.2
TC 16	38.83	5.74	1.79	5.97	45.5
TC 17	37.98	7.74	1.96	6.23	46.3
TC 18	39.28	7.59	1.75	5.78	44.8
TC 19	42.84	7.36	1.53	4.68	40.4
TC 20	41.34	6.34	1.66	4.95	41.6
TC 21	39.40	8.16	1.79	5.65	44.4
TC 22	40.61	6.28	1.62	5.60	44.2
TC 23	41.06	7.71	1.51	5.05	42.0
TC 24	41.90	5.88	1.41	4.82	41.0

TC 1
VOL. STRAIN X10-1
0.000
-0.200
-0.400
-0.600
-0.800
-1.000
-1.200
AXIAL STRAIN X10-1
0.000
0.200
0.400
0.600
0.800
1.000
1.200
1.400
1.600
1.800
STRESS RATIO
1.000
2.000
3.000
4.000
5.000
6.000
7.000

TC 2

STRESS RATIO

1.000
2.000
3.000
4.000
5.000
6.000
7.000

AXIAL STRAIN X10-1

0.000
0.200
0.400
0.600
0.800
1.000
1.200
1.400
1.600
1.800

VOL. STRAIN %

0.200
-0.400
-0.600
-0.800
-1.000
-1.200

TC 3
STRESS RATIO
1.000
2.000
3.000
4.000
5.000
6.000
7.000
AXIAL STRAIN X10-1
0.000
0.200
0.400
0.600
0.800
1.000
1.200
1.400
1.600
1.800
VOL. STRAIN X10-1
0.000
-0.200
-0.400
-0.600
-0.800
-1.000
-1.200

TC 4

VOL. STRAIN X10-1
0.000
-0.200
-0.400
-0.600
-0.800
-1.000
-1.200
1.800
1.600
1.400
1.200
1.000
0.800
0.600
0.400
0.200
0.000
AXIAL STRAIN X10-1
STRESS RATIO
1.000
2.000
3.000
4.000
5.000
6.000
7.000

TC 5
STRESS RATIO
7.000
6.000
5.000
4.000
3.000
2.000
1.000
AXIAL STRAIN X10-1
0.000
0.200
0.400
0.600
0.800
1.000
1.200
1.400
1.600
1.800
VOL. STRAIN X10-1
0.000
-0.200
-0.400
-0.600
-0.800
-1.000
-1.200

TC 6
STRESS RATIO
1.000
2.000
3.000
4.000
5.000
6.000
7.000
AXIAL STRAIN X10⁻¹
0.000
0.200
0.400
0.600
0.800
1.000
1.200
1.400
1.600
1.800
VOL. STRAIN X10⁻¹
0.000
-0.200
-0.400
-0.600
-0.800
-1.000
-1.200

TC 7
STRESS RATIO
1.000
2.000
3.000
4.000
5.000
6.000
7.000
AXIAL STRAIN X10-1
0.000
0.200
0.400
0.600
0.800
1.000
1.200
1.400
1.600
1.800
VOL. STRAIN X10-1
0.000
-0.200
-0.400
-0.600
-0.800
-1.000
-1.200

TC8
STRESS RATIO
1.000
2.000
3.000
4.000
5.000
6.000
7.000
AXIAL STRAIN X10-1
0.000
0.200
0.400
0.600
0.800
1.000
1.200
1.400
1.600
1.800
VOL. STRAIN X10-1
0.000
-0.200
-0.400
-0.600
-0.800
-1.000
-1.200

STRESS RATIO
1.000
2.000
3.000
4.000
5.000
6.000
7.000
AXIAL STRAIN X10-1
0.000
0.200
0.400
0.600
0.800
1.000
1.200
1.400
1.600
1.800
VOL. STRAIN X10-1
0.000
-0.200
-0.400
-0.600
-0.800
-1.000
-1.200

TC 6

TC 10

VOL. STRAIN X10⁻¹
0.000
-0.200
-0.400
-0.600
-0.800
-1.000
-1.266
AXIAL STRAIN X10⁻¹
0.000
0.200
0.400
0.600
0.800
1.000
1.200
1.400
1.600
1.800
STRESS RATIO
1.000
2.000
3.000
4.000
5.000
6.000
7.000

TC 11
VOL. STRAIN X10⁻¹
0.000
-0.200
-0.400
-0.600
-0.800
-1.000
-1.200
1.800
1.600
1.400
1.200
1.000
0.800
0.600
0.400
0.200
0.000
AXIAL STRAIN X10⁻¹
STRESS RATIO
1.000
2.000
3.000
4.000
5.000
6.000
7.000

TC 12
VOL. STRAIN X10-1
0.000
-0.200
-0.400
-0.600
-0.800
-1.000
-1.200
AXIAL STRAIN X10-1
0.000
0.200
0.400
0.600
0.800
1.000
1.200
1.400
1.600
1.800
STRESS RATIO
1.000
2.000
3.000
4.000
5.000
6.000
7.000

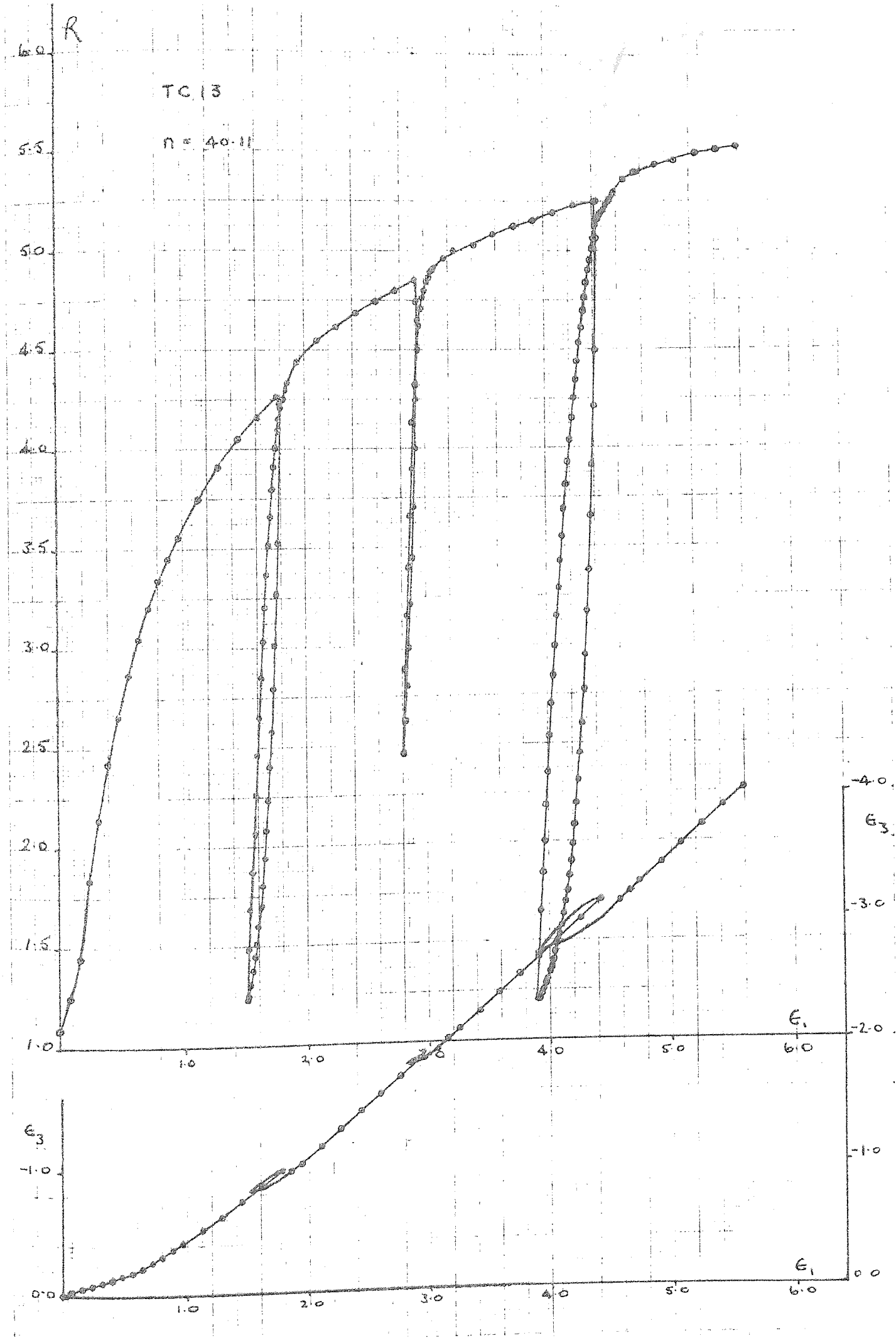
R
TC 13
n = 40·11
6·0
5·5
5·0
4·5
4·0
3·5
3·0
2·5
2·0
1·5
1·0
1·0
2·0
3·0
4·0
5·0
6·0
ε1
ε3
-4·0
-3·0
-2·0
-1·0
0·0
ε3
-1·0
0·0
1·0
2·0
3·0
4·0
5·0
6·0
ε1

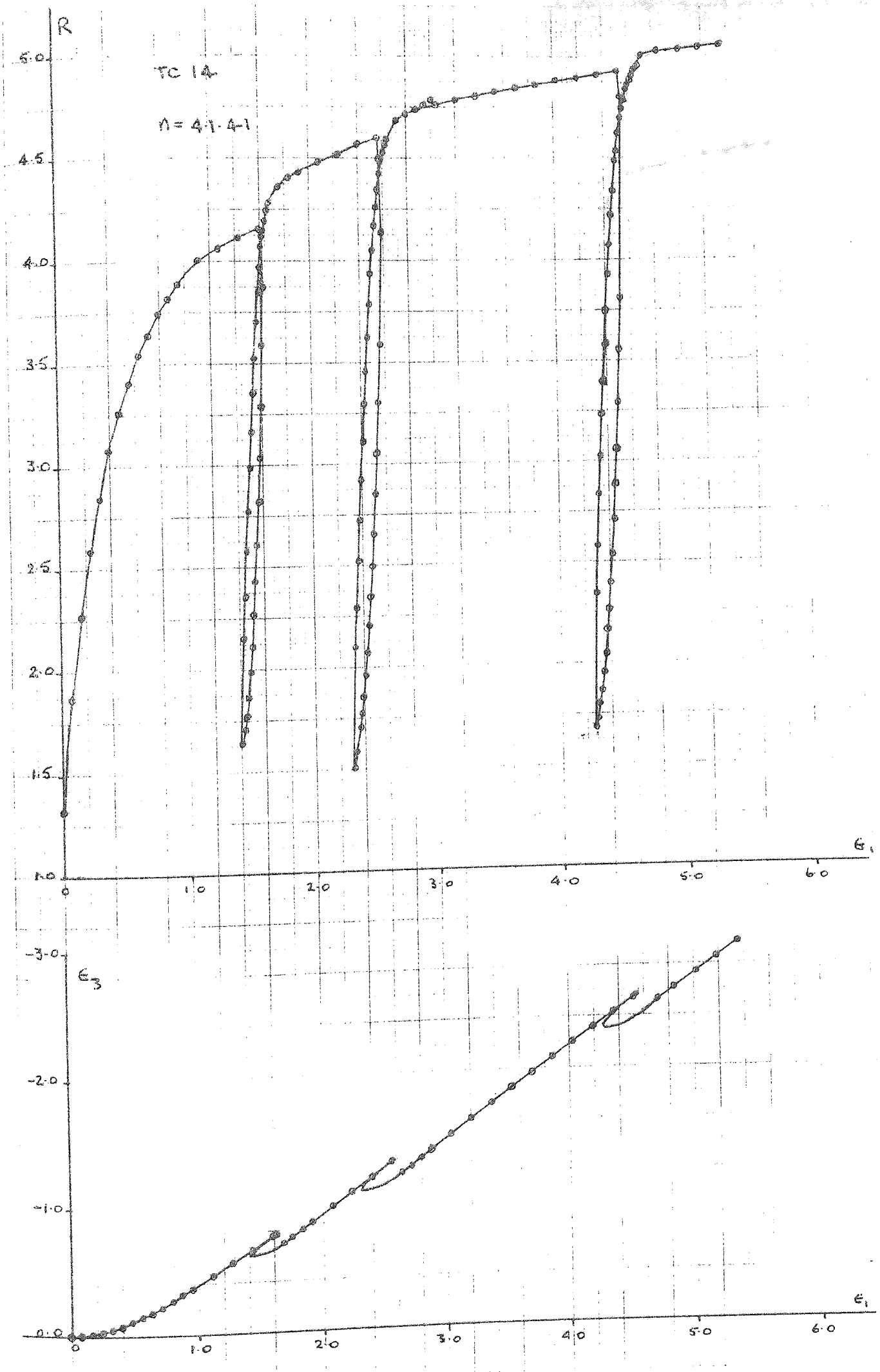
R
TC 14
n = 4·1 · 4·1
5·0
4·5
4·0
3·5
3·0
2·5
2·0
1·5
1·0
0
1·0
2·0
3·0
4·0
5·0
6·0
ε1
-3·0
-2·0
-1·0
0·0
ε3

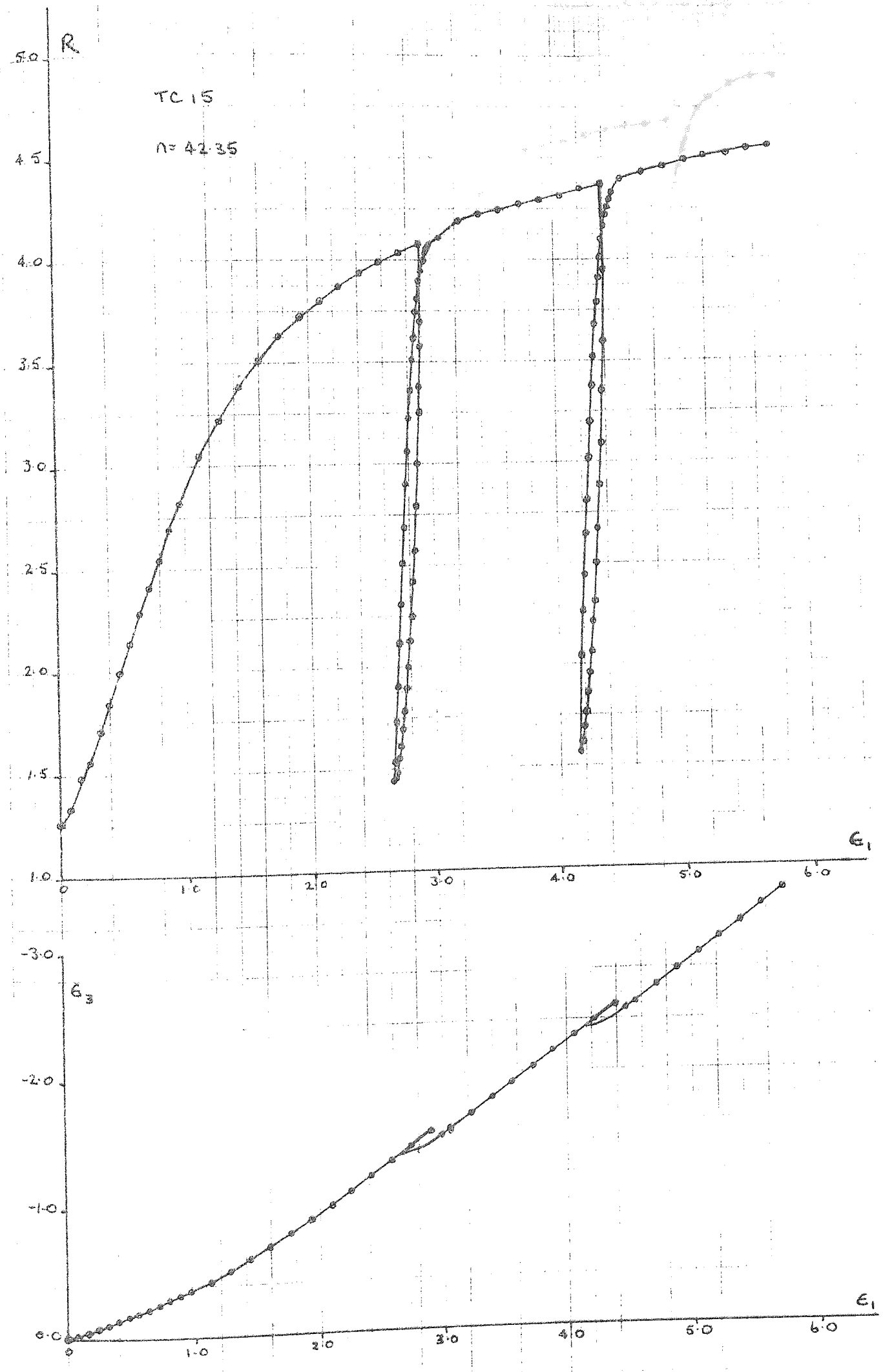
R
TC 15
n= 42.35
5.0
4.5
4.0
3.5
3.0
2.5
2.0
1.5
1.0
0
1.0
2.0
3.0
4.0
5.0
6.0
ϵ_1
-3.0
-2.0
-1.0
0.0
σ_3
0
1.0
2.0
3.0
4.0
5.0
6.0
ϵ_1

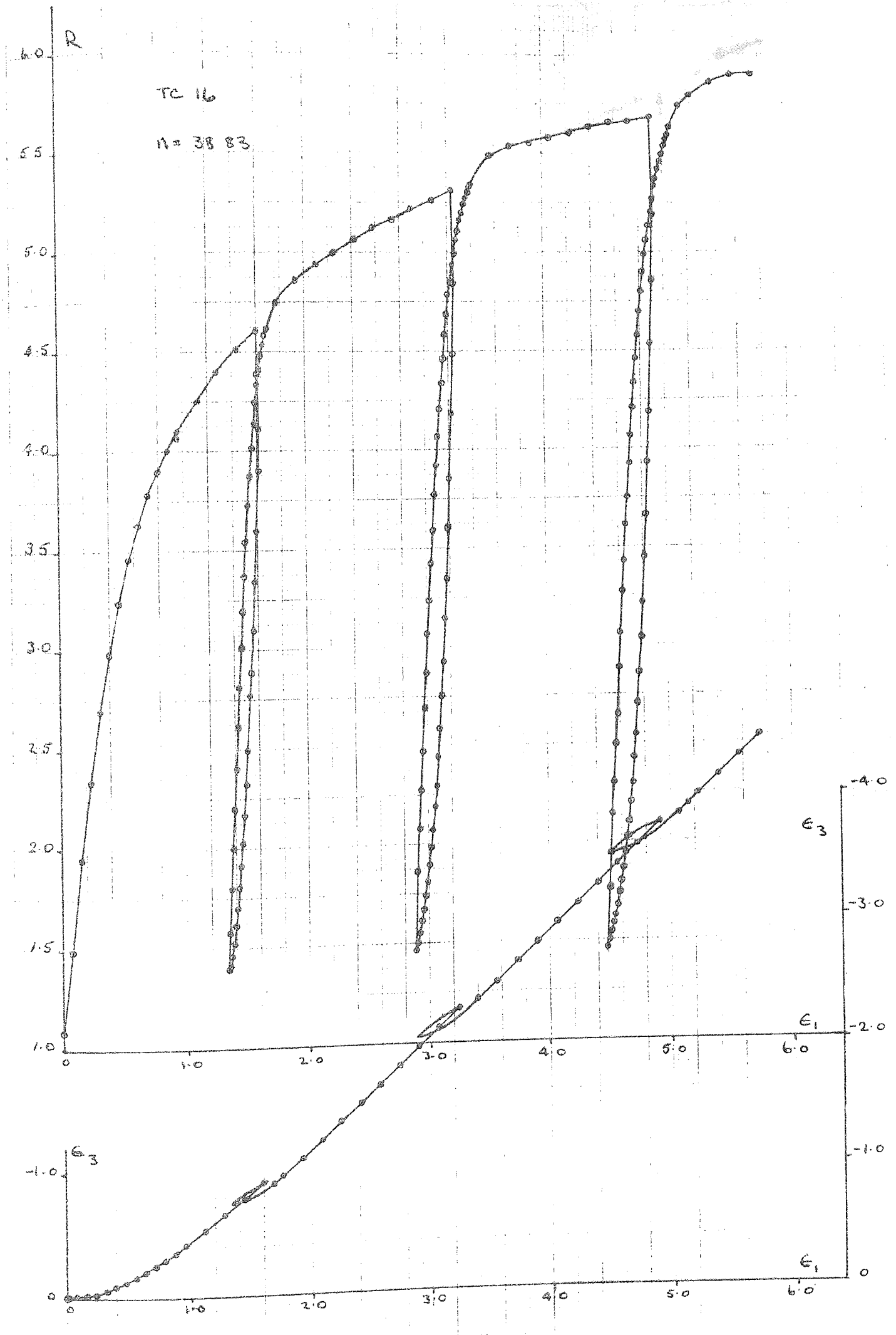
R
TC 16
11 = 38 83
6.0
5.5
5.0
4.5
4.0
3.5
3.0
2.5
2.0
1.5
1.0
0
1.0
2.0
3.0
4.0
5.0
6.0
ϵ_3
ϵ_1
-4.0
-3.0
-2.0
-1.0
0
-1.0

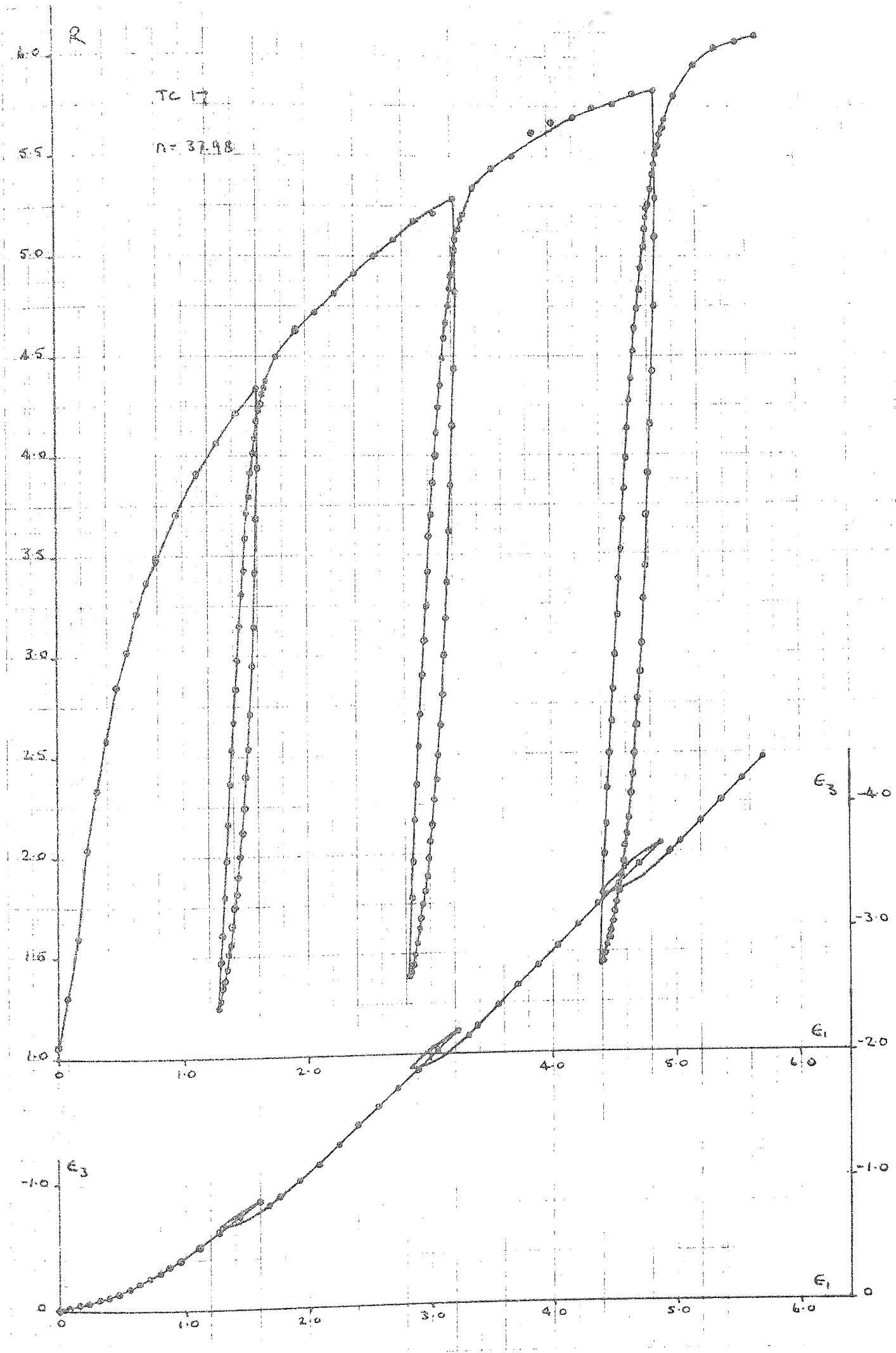
R
TC 1-7
n = 37.98
6.0
5.5
5.0
4.5
4.0
3.5
3.0
2.5
2.0
1.5
1.0
0
1.0
2.0
4.0
5.0
6.0
ϵ_3
-4.0
-3.0
-2.0
ϵ_1
-1.0
0
ϵ_3
-1.0
0
1.0
2.0
3.0
4.0
5.0
6.0
ϵ_1

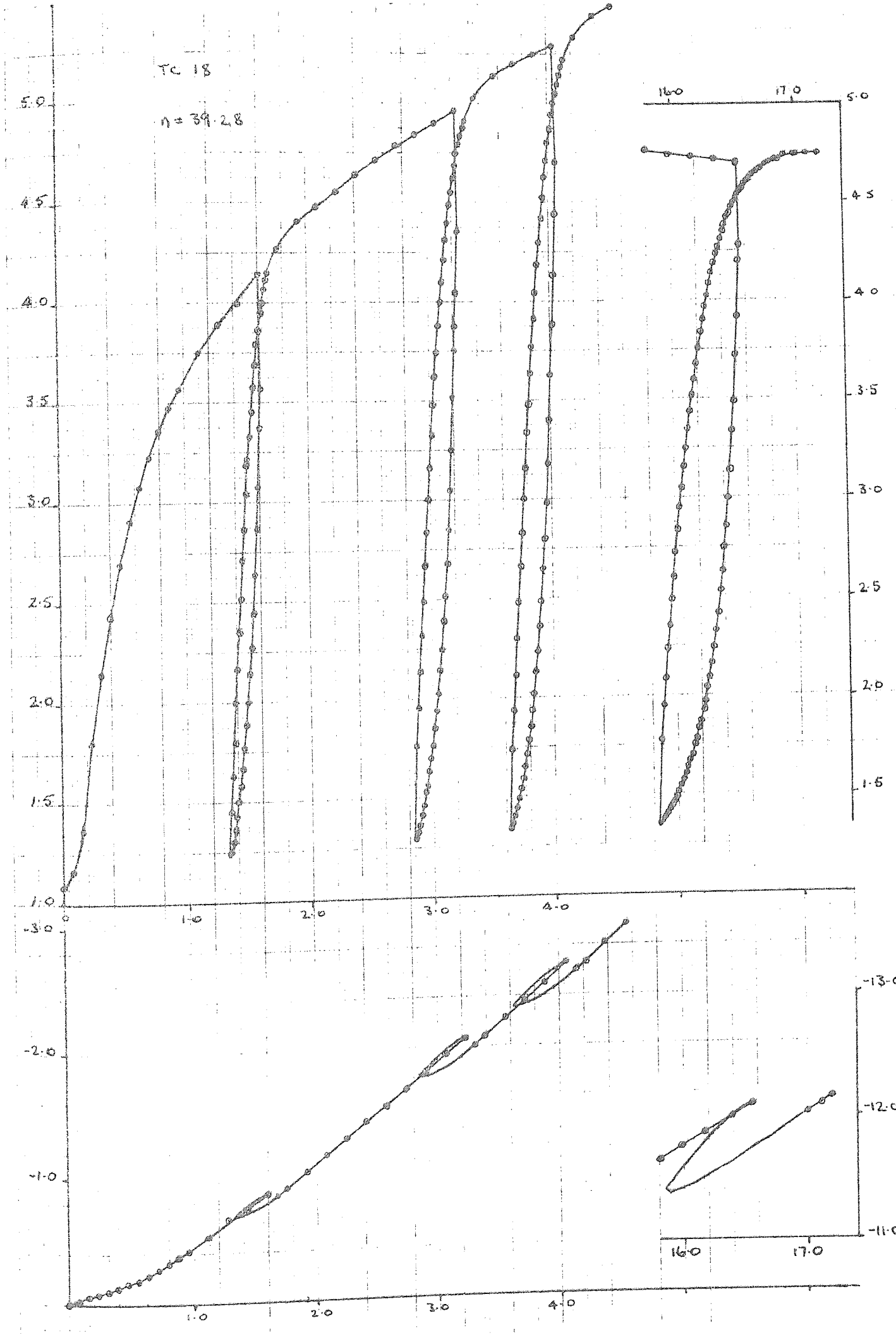
Tc 18
n = 39.28
5.0
4.5
4.0
3.5
3.0
2.5
2.0
1.5
1.0
1.0
2.0
3.0
4.0
16.0
17.0
-3.0
-2.0
-1.0
-13.0
-12.0
-11.0

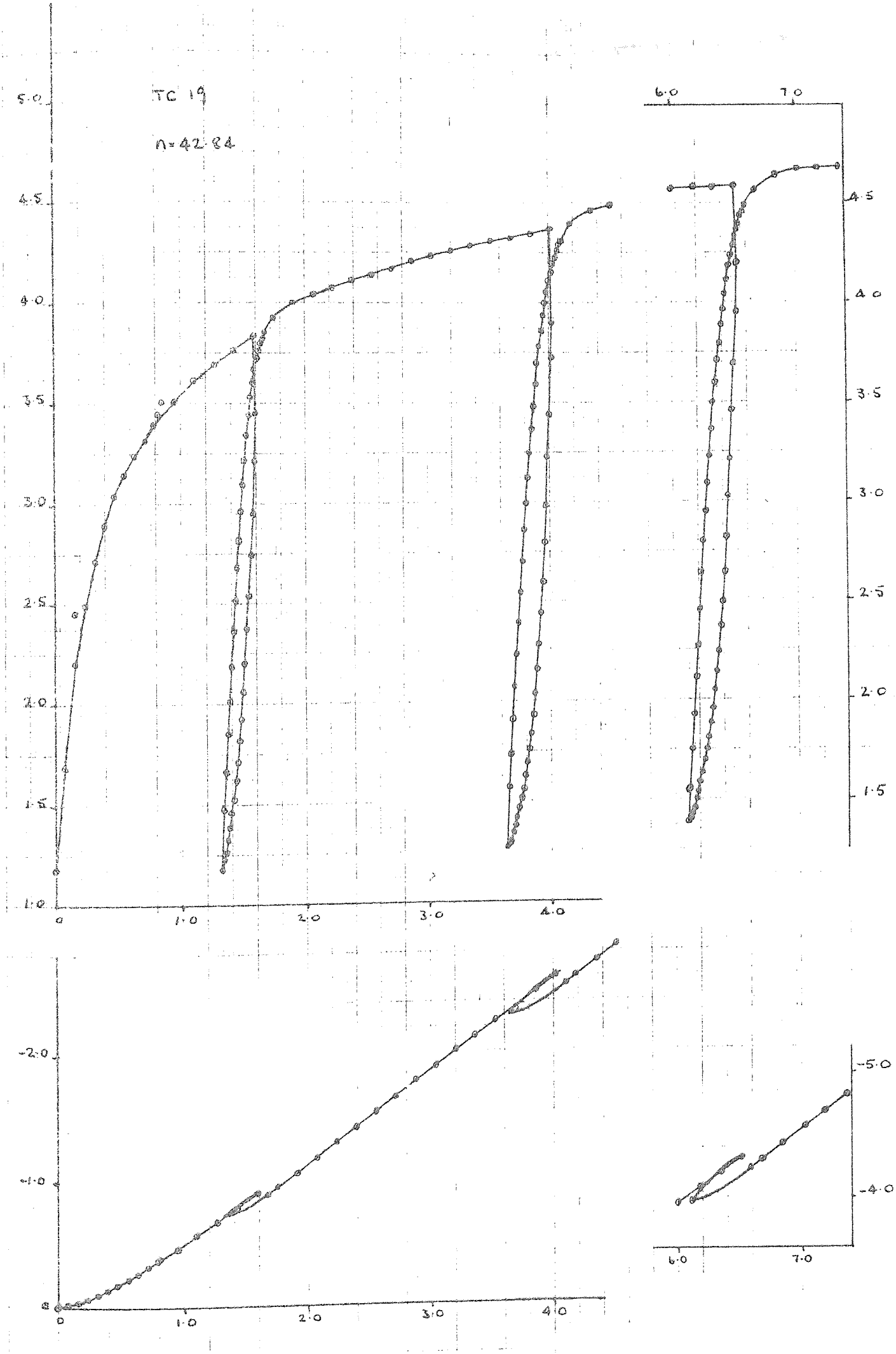
TC 19
n=42·84
5·0
4·5
4·0
3·5
3·0
2·5
2·0
1·5
1·0
0
1·0
2·0
3·0
4·0
6·0
7·0
-2·0
-1·0
-5·0
-4·0

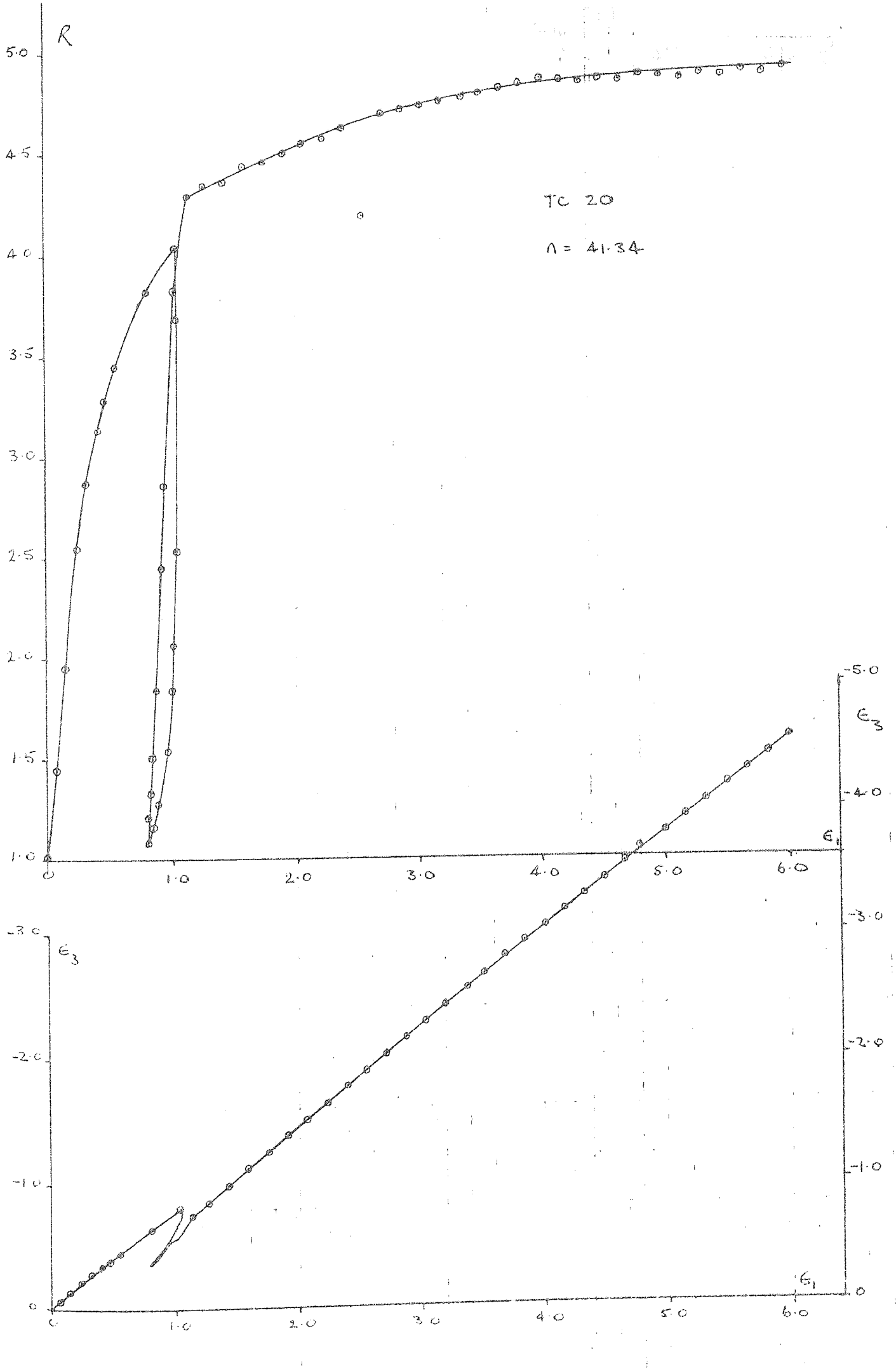
R
5·0
4·5
4·0
3·5
3·0
2·5
2·0
1·5
1·0
0
1·0
2·0
3·0
4·0
5·0
6·0
TC 20
Λ = 41·34
ε3
ε1
-5·0
-4·0
-3·0
-2·0
-1·0
0

TC 21
STRESS RATIO
1.000
2.000
3.000
4.000
5.000
6.000
7.000
AXIAL STRAIN X10⁻¹
0.000
0.200
0.400
0.600
0.800
1.000
1.200
1.400
1.600
1.800
VOL. STRAIN X10⁻¹
0.000
-0.200
-0.400
-0.600
-0.800
-1.000
-1.200

TC 22
VOL. STRAIN X10-1
0.000
-0.200
-0.400
-0.600
-0.800
-1.000
-1.200
1.800
1.600
1.400
1.200
1.000
0.800
0.600
0.400
0.200
0.000
AXIAL STRAIN X10-1
STRESS RATIO
1.000
2.000
3.000
4.000
5.000
6.000
7.000

TC 23
VOL. STRAIN X10-1
0.000
-0.200
-0.400
-0.600
-0.800
-1.000
-1.200
1.800
1.600
1.400
1.200
1.000
0.800
0.600
0.400
0.200
AXIAL STRAIN X10-1
STRESS RATIO
1.000
2.000
3.000
4.000
5.000
6.000
7.000

TC 24
VOL. STRAIN X10-1
0.000
-0.200
-0.400
-0.600
-0.800
-1.000
-1.200
1.800
1.600
1.400
1.200
1.000
0.800
0.600
0.400
0.200
0.000
AXIAL STRAIN X10-1
STRESS RATIO
1.000
2.000
3.000
4.000
5.000
6.000
7.000

PLANE STRAIN TESTS

(rigid side platens)

Test Number	Initial Porosity	Axial Strain at Failure	Maximum Dilatancy Factor	Maximum Stress Ratio	Angle of Internal Shearing Resistance
PSR 1	41.22	0.76	1.40	5.76	44.8
PSR 2	38.91	0.88	1.73	6.86	48.2
PSR 3	40.29	0.82	1.59	5.79	44.9
PSR 4	40.40	1.05	1.52	6.16	46.1
PSR 5	39.48	0.94	1.62	6.37	46.8
PSR 6	39.74	1.35	1.57	6.21	46.3
PSR 7	43.37	1.99	1.29	4.88	41.3
PSR 8	42.85	2.01	1.30	5.17	42.5
PSR 9	39.30	1.48	1.82	6.52	47.2
PSR 10	38.37	1.73	1.83	6.99	48.6

PSR.I

STRESS RATIO
0.000
1.000
2.000
3.000
4.000
5.000
6.000
7.000
8.000
9.000
AXIAL STRAIN
0.000
1.000
2.000
3.000
4.000
5.000
6.000
VOL. STRAIN
0.000
-1.000
-2.000
-3.000
-4.000
-5.000
-6.000

PSR 2

STRESS RATIO
0.000
1.000
2.000
3.000
4.000
5.000
6.000
7.000
8.000
9.000
AXIAL STRAIN
0.000
1.000
2.000
3.000
4.000
5.000
6.000
VOL STRAIN
0.000
-1.000
-2.000
-3.000
-4.000
-5.000
-6.000

PSR 3

STRESS RATIO
0.000
1.000
2.000
3.000
4.000
5.000
6.000
7.000
8.000
9.000
AXIAL STRAIN
0.000
1.000
2.000
3.000
4.000
5.000
6.000
VOL. STRAIN
0.000
-1.000
-2.000
-3.000
-4.000
-5.000
-6.000

PSR 4

PSR 5
STRESS RATIO
0.000
1.000
2.000
3.000
4.000
5.000
6.000
0.000
1.000
2.000
3.000
4.000
5.000
6.000
AXIAL STRAIN
-6.000
-5.000
-4.000
-3.000
-2.000
-1.000
0.000
LATERAL STRAIN

PSR 5

STRESS RATIO
AXIAL STRAIN
VOL. STRAIN
0.000
1.000
2.000
3.000
4.000
5.000
6.000
-1.000
-2.000
-3.000
-4.000
-5.000
-6.000

PSR 6

STRESS RATIO
AXIAL STRAIN
VOL. STRAIN
0.000
1.000
2.000
3.000
4.000
5.000
6.000
-1.000
-2.000
-3.000
-4.000
-5.000
-6.000

PSR 7

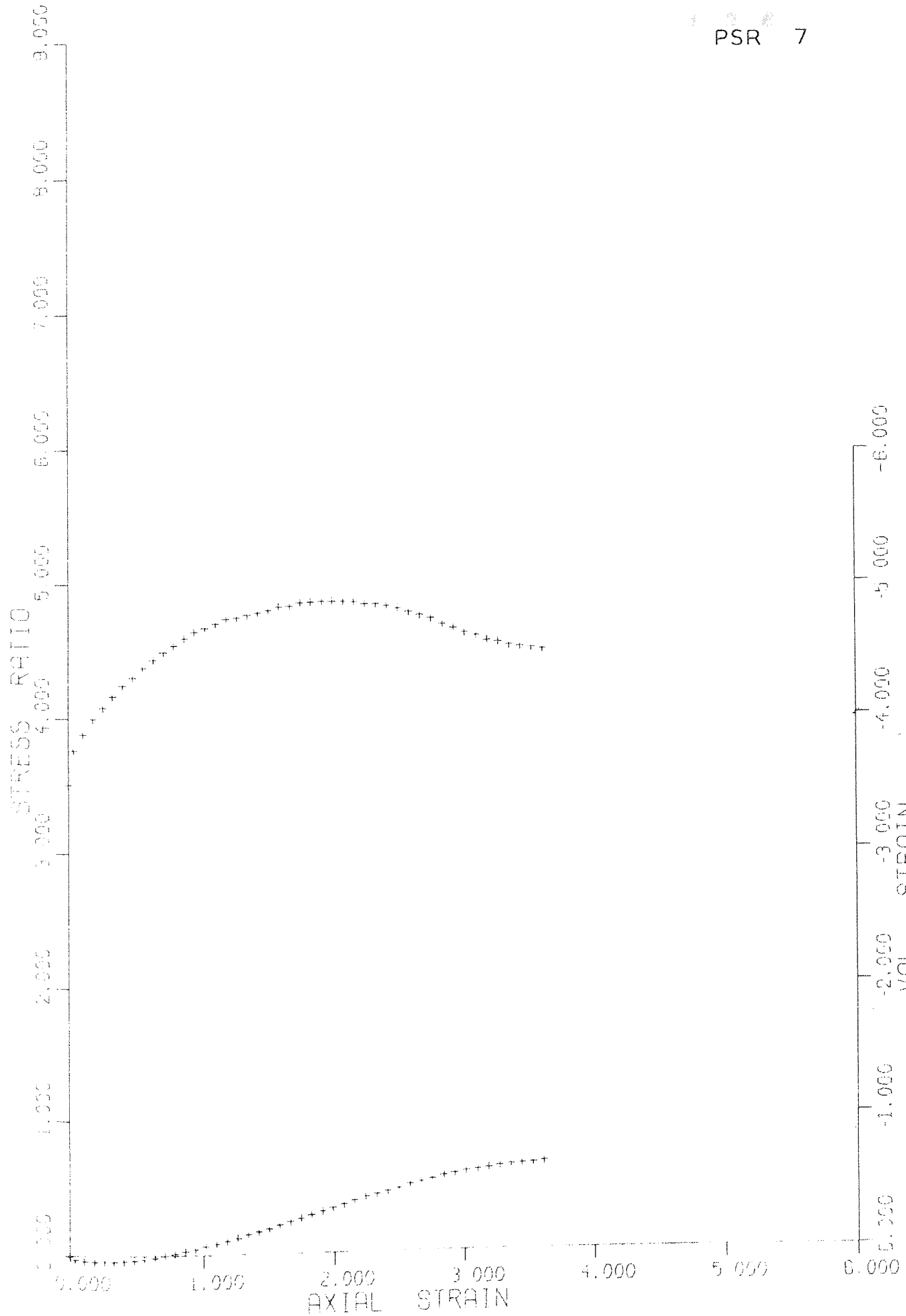
STRESS RATIO
0.000
1.000
2.000
3.000
4.000
5.000
6.000
7.000
8.000
9.000
AXIAL STRAIN
0.000
1.000
2.000
3.000
4.000
5.000
6.000
VOL. STRAIN
-6.000
-5.000
-4.000
-3.000
-2.000
-1.000
0.000

PSR 8

STRESS RATIO
AXIAL STRAIN
VOL. STRAIN
0.000
1.000
2.000
3.000
4.000
5.000
6.000
-1.000
-2.000
-3.000
-4.000
-5.000
-6.000

PSR 9

STRESS RATIO
0.000
1.000
2.000
3.000
4.000
5.000
6.000
7.000
8.000
9.000
AXIAL STRAIN
0.000
1.000
2.000
3.000
4.000
5.000
6.000
VOL. STRAIN
-6.000
-5.000
-4.000
-3.000
-2.000
-1.000
0.000

PSR 10

STRESS RATIO
0.000
1.000
2.000
3.000
4.000
5.000
6.000
7.000
8.000
9.000
AXIAL STRAIN
0.000
1.000
2.000
3.000
4.000
5.000
6.000
VOL. STRAIN
-6.000
-5.000
-4.000
-3.000
-2.000
-1.000
0.000

PSR.I

STRESS RATIO
0.000
1.000
2.000
3.000
4.000
5.000
6.000
7.000
8.000
9.000
AXIAL STRAIN
0.000
1.000
2.000
3.000
4.000
5.000
6.000
VOL. STRAIN
0.000
-1.000
-2.000
-3.000
-4.000
-5.000
-6.000

PSR 2

STRESS RATIO
AXIAL STRAIN
VOL STRAIN
0.000
1.000
2.000
3.000
4.000
5.000
6.000
7.000
8.000
9.000
-1.000
-2.000
-3.000
-4.000
-5.000
-6.000

PSR 3

STRESS RATIO
0.000
1.000
2.000
3.000
4.000
5.000
6.000
7.000
8.000
9.000
AXIAL STRAIN
0.000
1.000
2.000
3.000
4.000
5.000
6.000
VOL. STRAIN
0.000
-1.000
-2.000
-3.000
-4.000
-5.000
-6.000

PSR 4

STRESS RATIO
0.000
1.000
2.000
3.000
4.000
5.000
6.000
7.000
8.000
9.000
AXIAL STRAIN
0.000
1.000
2.000
3.000
4.000
5.000
6.000
-6.000
-5.000
-4.000
-3.000
-2.000
-1.000
0.000

PSR 5

STRESS RATIO
0.000
1.000
2.000
3.000
4.000
5.000
6.000
7.000
8.000
0.000
1.000
2.000
3.000
4.000
5.000
AXIAL STRAIN
VOLT. STRAIN
0.000
-1.000
-2.000
-3.000
-4.000
-5.000
-6.000

PSR 6

STRESS RATIO
AXIAL STRAIN
VOL. STRAIN
0.000
1.000
2.000
3.000
4.000
5.000
6.000
-1.000
-2.000
-3.000
-4.000
-5.000
-6.000

PSR 7

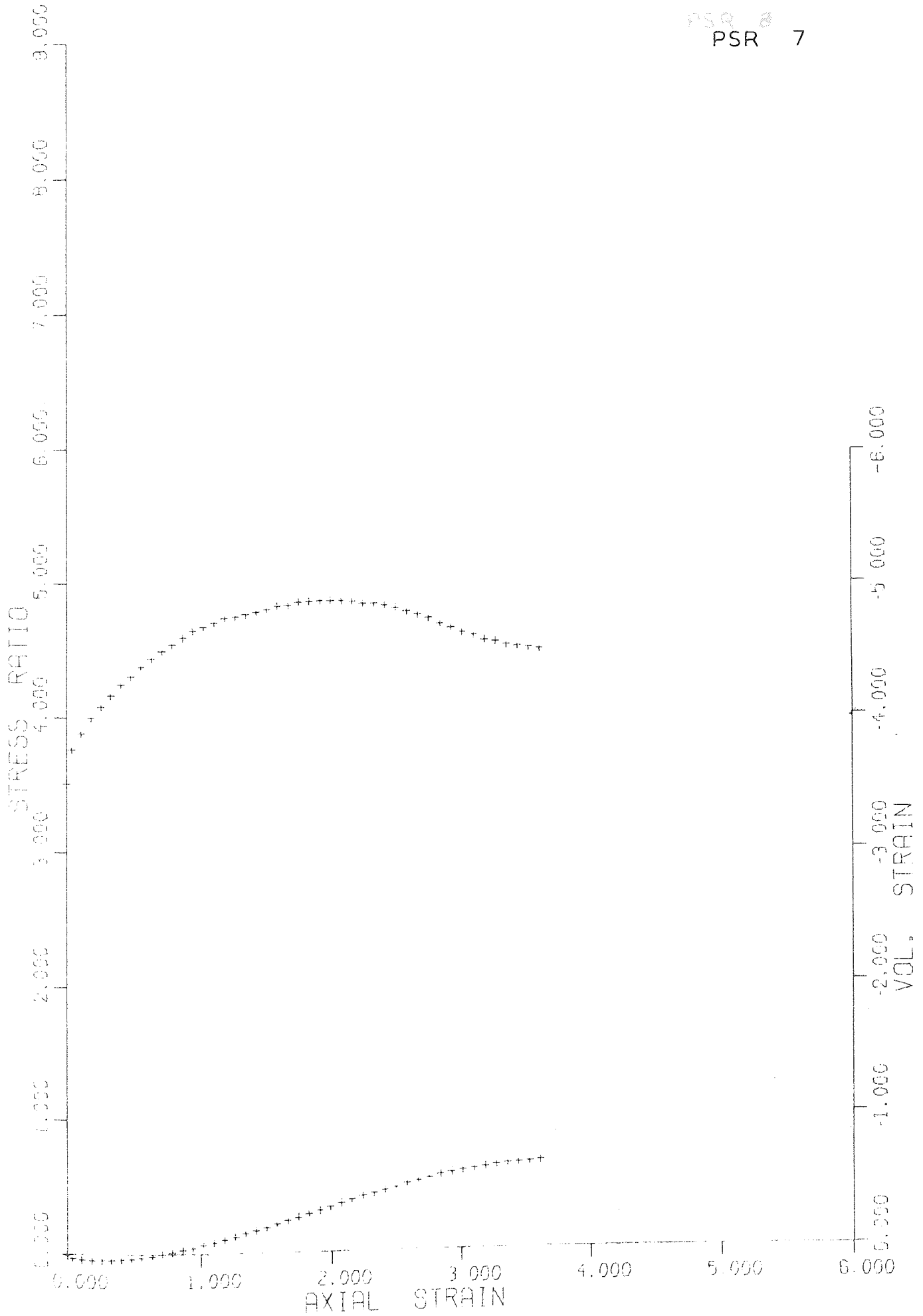
STRESS RATIO
0.000
1.000
2.000
3.000
4.000
5.000
6.000
7.000
8.000
9.000
AXIAL STRAIN
0.000
1.000
2.000
3.000
4.000
5.000
6.000
VOL. STRAIN

PSR 8

STRESS RATIO
0.000
1.000
2.000
3.000
4.000
5.000
6.000
7.000
8.000
AXIAL STRAIN
0.000
1.000
2.000
3.000
4.000
5.000
6.000
VOL. STRAIN
0.000
-1.000
-2.000
-3.000
-4.000
-5.000
-6.000

PSR 9

STRESS RATIO
9.000
8.000
7.000
6.000
5.000
4.000
3.000
2.000
1.000
0.000
AXIAL STRAIN
0.000
1.000
2.000
3.000
4.000
5.000
6.000
VOL. STRAIN
-6.000
-5.000
-4.000
-3.000
-2.000
-1.000
0.000

PSR 10

STRESS RATIO
9.000
8.000
7.000
6.000
5.000
4.000
3.000
2.000
1.000
0.000
AXIAL STRAIN
0.000
1.000
2.000
3.000
4.000
5.000
6.000
VOL. STRAIN
-6.000
-5.000
-4.000
-3.000
-2.000
-1.000
0.000

PLANE STRAIN TESTS

(flexible side platens)

Test Number	Initial Porosity	Axial Strain at Failure	Maximum Dilatancy Factor	$\left(\sigma_1/\sigma_3\right)_f$	$\left(\sigma_2/\sigma_3\right)_f$	Angle of Internal Shearing Resistance
PS 1	41.10	1.82	1.65	6.05	1.91	45.7
PS 2	42.24	1.96	1.50	5.74	1.98	44.7
PS 3	41.00	2.31	1.56	6.13	2.07	46.0
PS 4	39.27	2.51	1.74	6.76	2.07	47.9
PS 5	40.48	2.66	1.69	6.36	2.16	46.7
PS 6	41.02	2.60	1.63	6.17	2.06	46.1
PS 7	42.98	2.20	1.26	5.16	1.87	42.5
PS 8	38.51	2.76	1.81	6.99	2.51	48.6
PS 9	40.60	1.87	1.60	6.33	2.04	46.7
PS 10	39.81	2.36	1.73	6.66	2.28	47.6
PS 11	42.80	1.77	1.40	5.36	1.86	43.3
PS 12	38.87	2.41	1.79	7.16	2.39	49.0
PS 13	41.84	2.60	1.55	6.14	2.04	46.0
PS 14	39.07	2.33	1.76	7.21	2.33	49.2
PS 15	40.83	2.67	1.66	6.33	2.22	46.6
PS 16	41.56	2.17	1.67	5.99	2.12	45.6
PS 17	40.34	2.57	1.63	6.59	2.24	47.4
PS 18	39.00	2.89	1.85	7.08	2.57	48.8
PS 19	38.66	3.21	1.83	7.22	2.71	49.2
PS 20	42.81	1.93	1.37	5.27	1.84	42.9
PS 21	41.79	2.44	1.56	6.03	2.05	45.7
PS 22	38.89	3.10	1.90	7.36	2.59	49.5
PS 23	39.37	3.11	1.77	6.90	2.40	48.3
PS 24	40.66	2.87	1.62	6.33	2.19	46.6
PS 25	38.83	2.47	1.86	6.99	2.08	48.6

PS 1
STRESS RATIO
9.000
8.000
7.000
6.000
5.000
4.000
3.000
2.000
1.000
0.000
-6.000
-5.000
-4.000
-3.000
-2.000
-1.000
0.000
1.000
2.000
3.000
4.000
5.000
6.000

PS 2
STRESS RATIO
9.000
8.000
7.000
6.000
5.000
4.000
3.000
2.000
1.000
0.000
-6.000
-5.000
-4.000
-3.000
-2.000
-1.000
0.000
0.000
1.000
2.000
3.000
4.000
5.000
6.000
AXIAL STRAIN

PS 3
STRESS RATIO
9.000
8.000
7.000
6.000
5.000
4.000
3.000
2.000
1.000
0.000
0.000
1.000
2.000
3.000
4.000
5.000
6.000
AXIAL STRAIN
-6.000
-5.000
-4.000
-3.000
-2.000
-1.000
0.000

PS 4

STRESS RATIO
0.000
1.000
2.000
3.000
4.000
5.000
6.000
7.000
8.000
9.000
-6.000
-5.000
-4.000
-3.000
-2.000
-1.000
0.000
1.000
2.000
3.000
4.000
5.000
6.000

PS 5

STRESS RATIO
AXIAL STRAIN
1.000
2.000
3.000
4.000
5.000
-1.000
-2.000
-3.000
-4.000
-5.000
-6.000

PS 6

STRESS RATIO
AXIAL STRAIN
0.000
1.000
2.000
3.000
4.000
5.000
6.000
9.000
8.000
7.000
6.000
5.000
4.000
3.000
2.000
1.000
0.000
-9.000
-5.000
-4.000
-3.000
-2.000
-1.000
0.000

PS 7
STRESS RATIO
9.000
8.000
7.000
6.000
5.000
4.000
3.000
2.000
1.000
0.000
1.000
2.000
3.000
4.000
5.000
6.000
AXIAL STRAIN
-6.000
-5.000
-4.000
-3.000
-2.000
-1.000
0.000

PS 8

STRESS RATIO
0.000
1.000
2.000
3.000
4.000
5.000
6.000
7.000
8.000
9.000
AXIAL STRAIN
0.000
1.000
2.000
3.000
4.000
5.000
6.000
-1.000
-2.000
-3.000
-4.000
-5.000
-6.000

PS 9

STRESS RATIO
0.000
1.000
2.000
3.000
4.000
5.000
6.000
7.000
8.000
9.000
AXIAL STRAIN
0.000
1.000
2.000
3.000
4.000
5.000
6.000
-1.000
-2.000
-3.000
-4.000
-5.000
-6.000

PS 10
STRESS RATIO
0.000
1.000
2.000
3.000
4.000
5.000
6.000
7.000
8.000
9.000
AXIAL STRAIN
0.000
1.000
2.000
3.000
4.000
5.000
6.000
-1.000
-2.000
-3.000
-4.000
-5.000
-6.000

PS II

STRESS RATIO
0.000
1.000
2.000
3.000
4.000
5.000
6.000
7.000
8.000
9.000
0.000
1.000
2.000
3.000
4.000
5.000
6.000
AXIAL STRAIN
-1.000
-2.000
-3.000
-4.000
-5.000
-6.000

PS 12
STRESS RATIO
0.000
1.000
2.000
3.000
4.000
5.000
6.000
7.000
8.000
9.000
AXIAL STRAIN
0.000
1.000
2.000
3.000
4.000
5.000
6.000
-1.000
-2.000
-3.000
-4.000
-5.000
-6.000

PS 13

STRESS RATIO
0.000
1.000
2.000
3.000
4.000
5.000
6.000
7.000
8.000
9.000
AXIAL STRAIN
0.000
1.000
2.000
3.000
4.000
5.000
6.000
-1.000
-2.000
-3.000
-4.000
-5.000
-6.000

PS 14
STRESS RATIO
9.000
8.000
7.000
6.000
5.000
4.000
3.000
2.000
1.000
0.000
-6.000
-5.000
-4.000
-3.000
-2.000
-1.000
0.000
0.000
1.000
2.000
3.000
4.000
5.000
6.000
AXIAL STRAIN

PS 15

STRESS RATIO
0.000
1.000
2.000
3.000
4.000
5.000
6.000
7.000
8.000
9.000
AXIAL STRAIN
0.000
1.000
2.000
3.000
4.000
5.000
6.000
-1.000
-2.000
-3.000
-4.000
-5.000
-6.000

PS 16

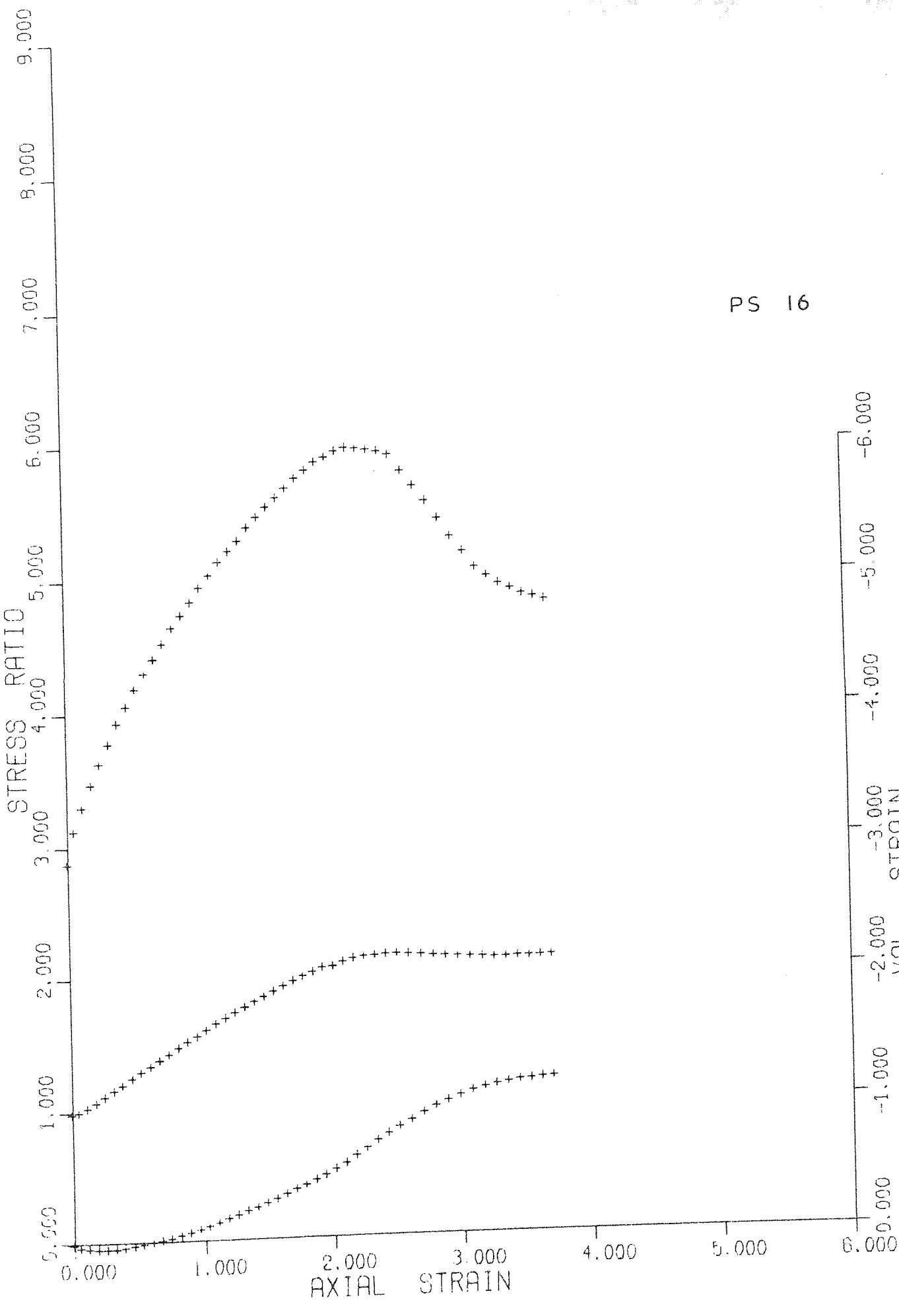
STRESS RATIO
9.000
8.000
7.000
6.000
5.000
4.000
3.000
2.000
1.000
0.000
0.000
1.000
2.000
3.000
4.000
5.000
6.000
AXIAL STRAIN
-6.000
-5.000
-4.000
-3.000
-2.000
-1.000
0.000

PS 17

STRESS RATIO
0.000
1.000
2.000
3.000
4.000
5.000
6.000
7.000
8.000
9.000
AXIAL STRAIN
0.000
1.000
2.000
3.000
4.000
5.000
6.000
-1.000
-2.000
-3.000
-4.000
-5.000
-6.000

PS 18
STRESS RATIO
0.000
1.000
2.000
3.000
4.000
5.000
6.000
7.000
8.000
9.000
AXIAL STRAIN
0.000
1.000
2.000
3.000
4.000
5.000
6.000
VOL. STRAIN
0.000
-1.000
-2.000
-3.000
-4.000
-5.000
-6.000

PS 19
STRESS RATIO
9.000
8.000
7.000
6.000
5.000
4.000
3.000
2.000
1.000
-6.000
-5.000
-4.000
-3.000
-2.000
-1.000
STRAIN
AXIAL STRAIN

PS 20
STRESS RATIO
9.000
8.000
7.000
6.000
5.000
4.000
3.000
2.000
1.000
0.000
0.000
1.000
2.000
3.000
4.000
5.000
6.000
AXIAL STRAIN
-6.000
-5.000
-4.000
-3.000
-2.000
-1.000
0.000

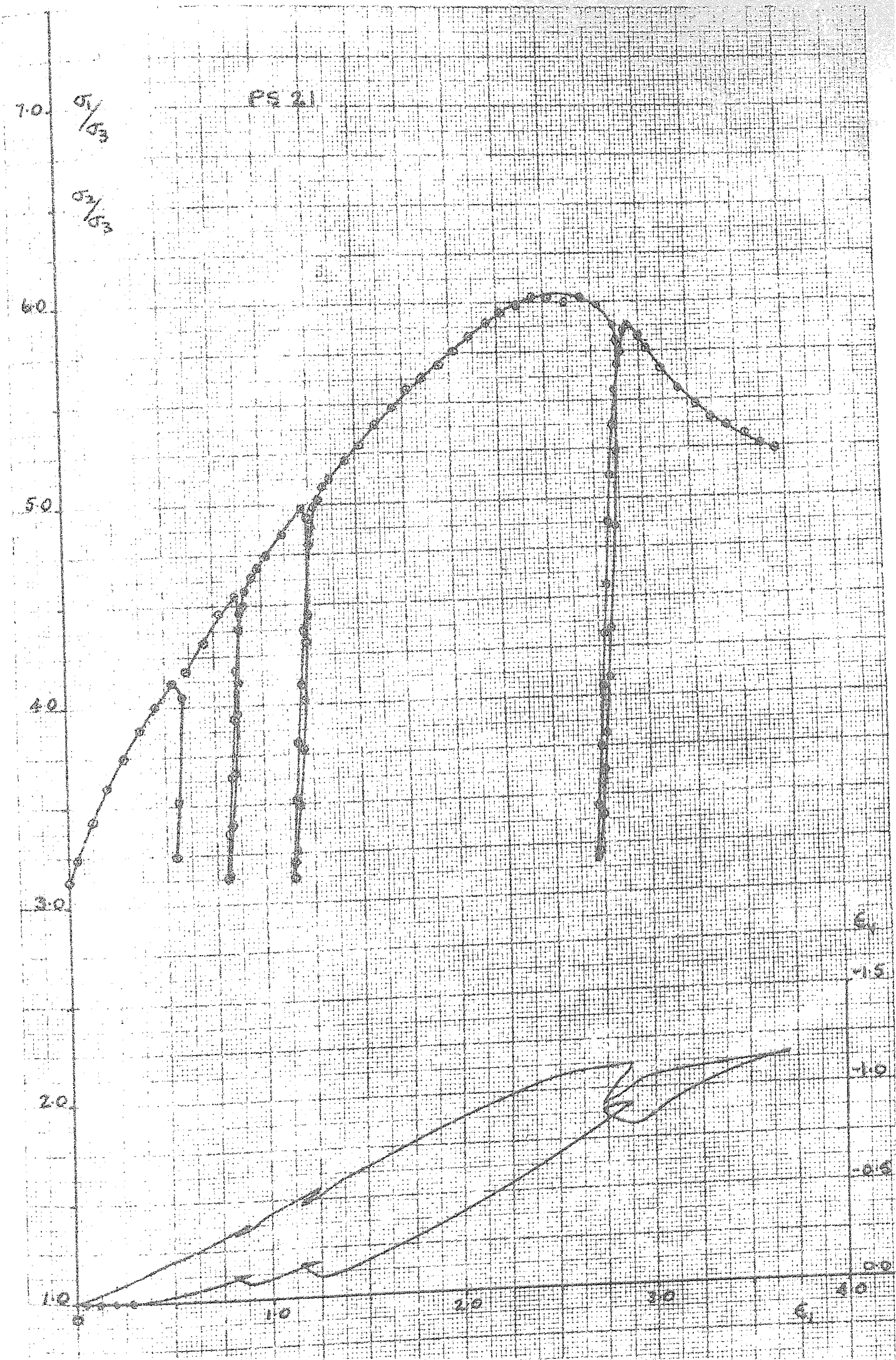
PS 21
σ1/σ3
σ2/σ3
7.0
6.0
5.0
4.0
3.0
2.0
1.0
1.0
2.0
3.0
4.0
ε1
εv
-1.5
-1.0
-0.5
0.0

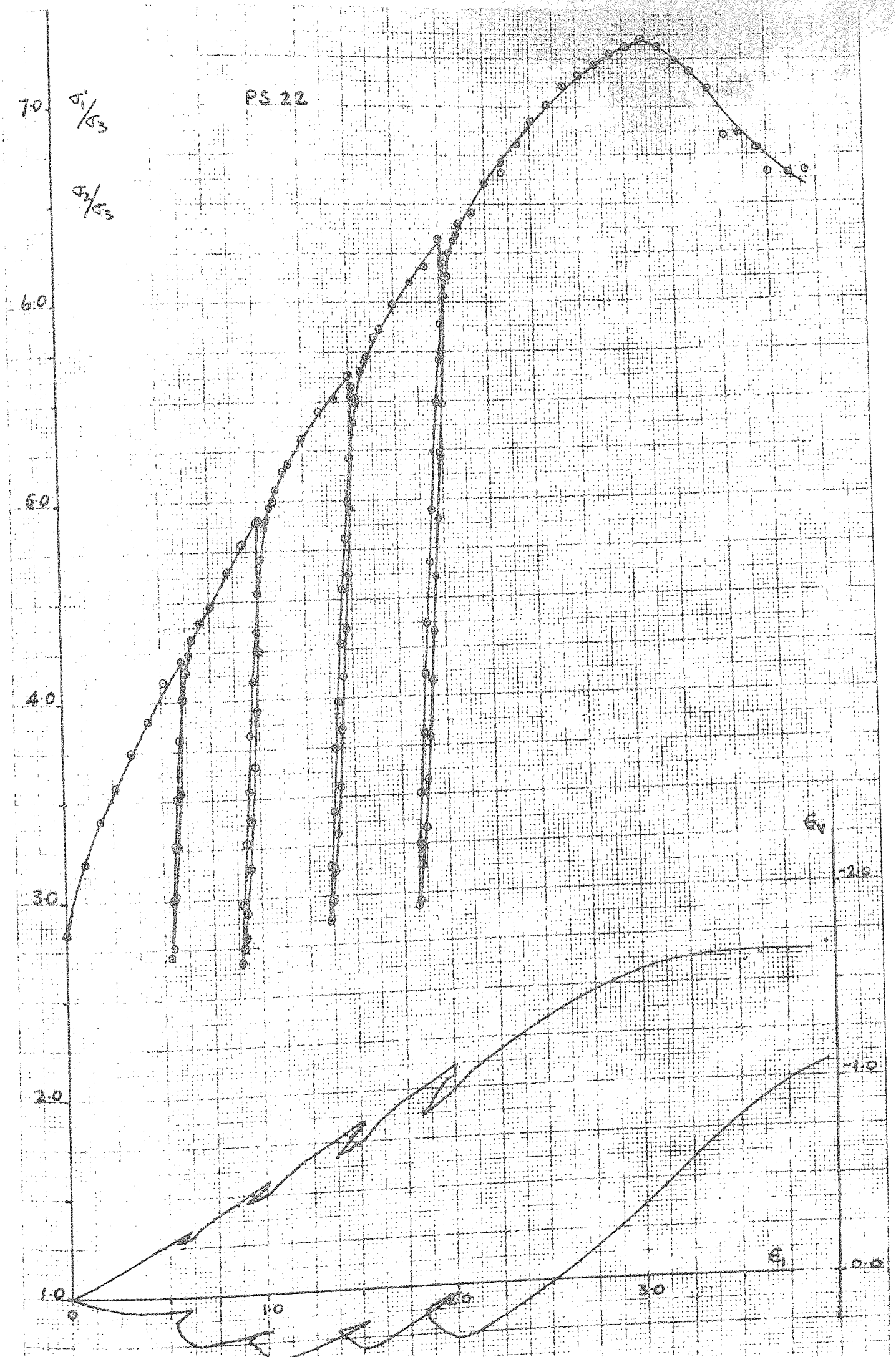
PS 22
σ1/σ3
σ2/σ3
7.0
6.0
6.0
4.0
3.0
2.0
1.0
0
1.0
2.0
3.0
εv
-2.0
-1.0
ε1
0.0

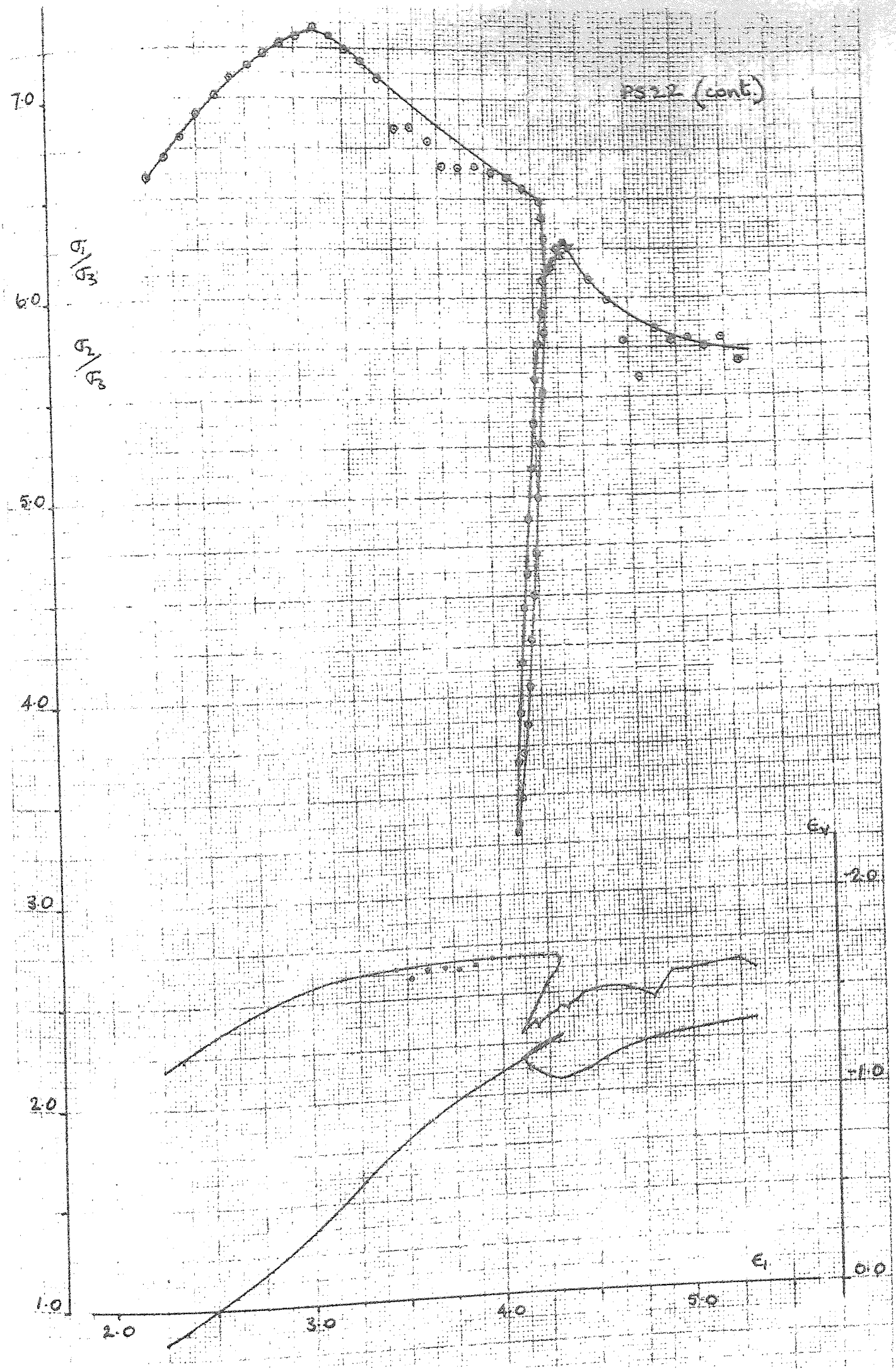
PS 22 (cont.)
σ_1/σ_3
σ_2/σ_3
7.0
6.0
5.0
4.0
3.0
2.0
1.0
ϵ_v
2.0
1.0
0.0
ϵ_1
2.0
3.0
4.0
5.0

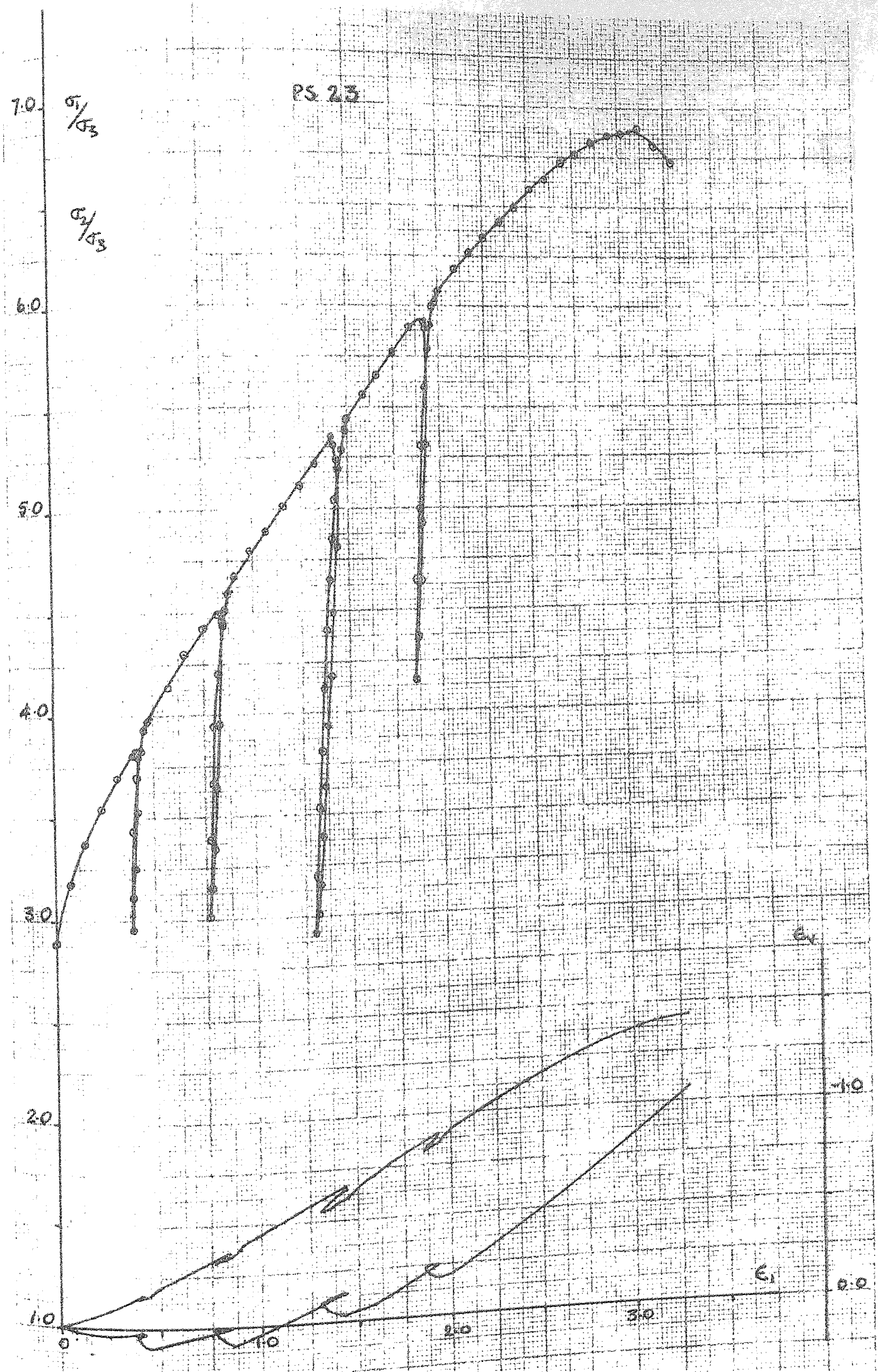
PS 23
σ_1/σ_3
σ_2/σ_3
7.0
6.0
5.0
4.0
3.0
2.0
1.0
0
1.0
2.0
3.0
ϵ_1
0.0
-1.0
ϵ_v

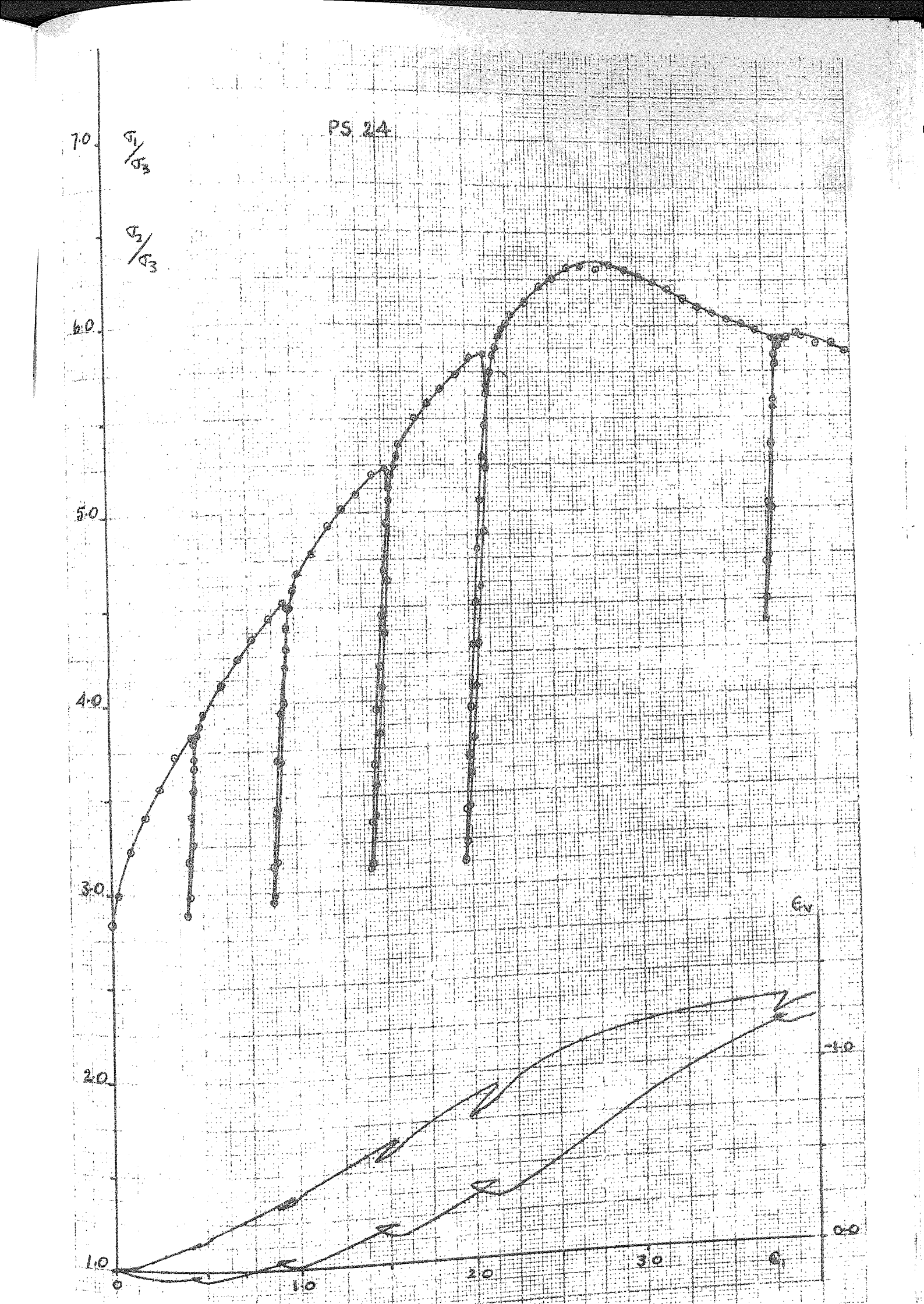
PS 24
7.0
σ_1/σ_3
σ_2/σ_3
6.0
5.0
4.0
3.0
2.0
1.0
0
1.0
2.0
3.0
ε_1
ε_v
-1.0
0.0

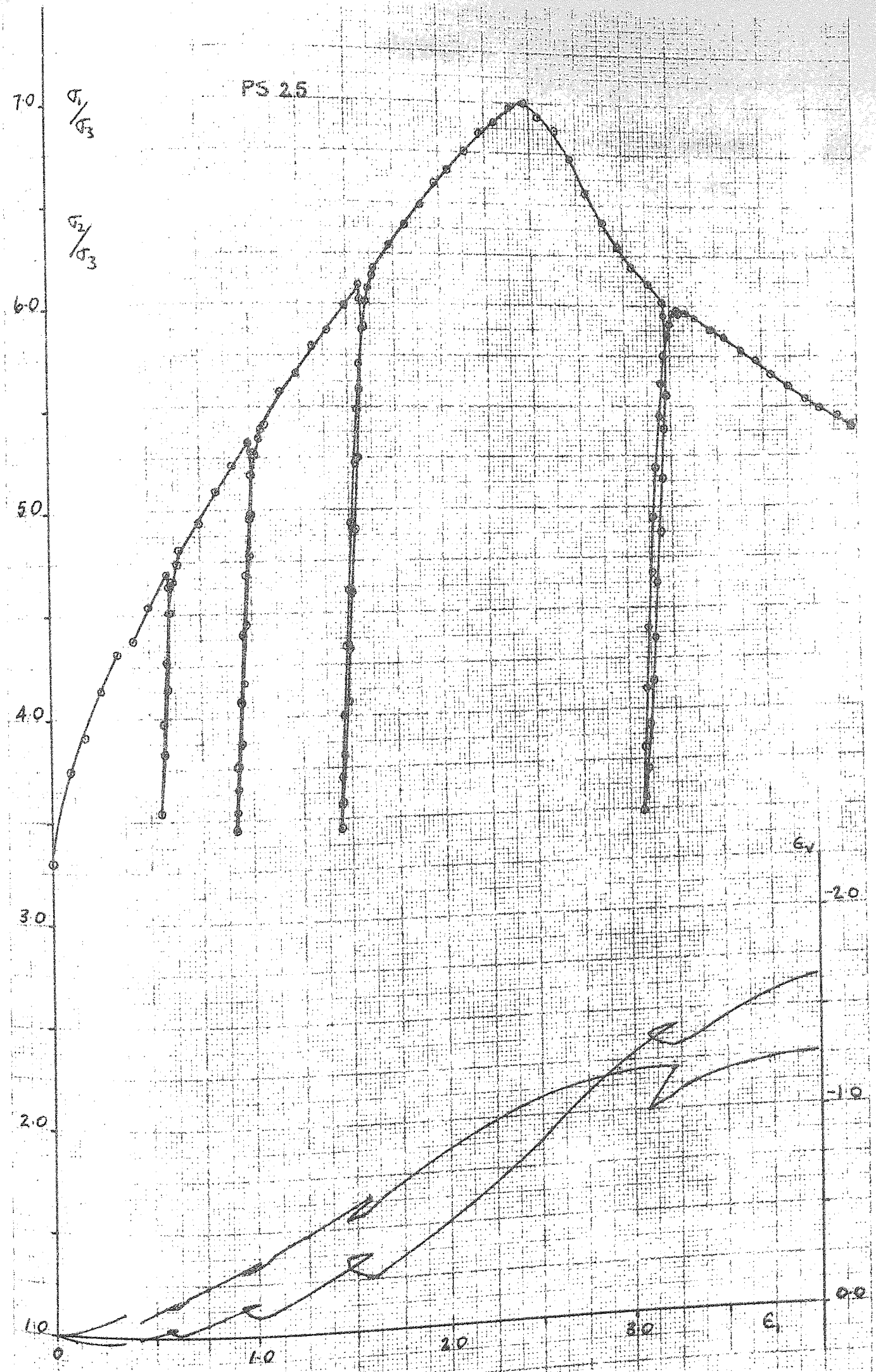
PS 2.5
σ_1/σ_3
σ_2/σ_3
7.0
6.0
5.0
4.0
3.0
2.0
1.0
0
1.0
2.0
3.0
ϵ_1
ϵ_v
-2.0
-1.0
0.0

REFERENCES

ALYANAK, I. (1961)
'Vibration of sands with special reference to the minimum porosity test for sands.'
Proc. Midland Soil Mech. & Found. Eng. Soc., Vol. 4, pp 37 -72.

AMIRSOLEYMANI, T. (1966)
'Packing of granular materials with special reference to triaxial testing.'
Ph.D. Thesis, University of Birmingham.

ANDRAWES, K.Z. (1964)
'The behaviour of particulate materials in the at rest state.'
M.Sc. Thesis, University of Manchester.

ARTHUR, J.R.F. and DUNSTAN, T. (1970)
'Radiological techniques developed to describe particle packing.'
Powder Technology, March 1970, pp 195 -207.

BARDEN, L. (1971)
Discussion on Session 3,
Proc. Roscoe Mem. Symp., Cambridge, pp 375 -376.

BARDEN, L. and KHAYATT, A.J. (1966)
'Incremental strain rate ratios and strength of sand in the triaxial test.'
Geotechnique, 16, No 4, pp 338 -357.

BARDEN, L. and KHAYATT, A.J. (1968)
'Incremental stress-strain relations for sand.'
Research Report No. 5, University of Manchester.

BENNETT, D.H. (1969)
'Three dimensional stress test.'
Speciality Session 16,
Proc. 7th Int. Conf. Soil Mech. & Found. Eng., Vol. 3, p 519.

BENT HANSEN, J. (1958)
'Line ruptures regarded as narrow rupture zones: basic equation based on kinematic considerations.'
Proc. Brussels Earth Pressure Conf., Vol. 1, pp 39 -49.

BIAREZ, J. (1961)
'Contribution a l'etude des properties mecaniques sols et des materiaux pulverulents.'
D.Sc. Thesis, Grenoble University.

BISHOP, A.W. (1948)
'A large shear box for testing sands and gravels.'
Proc. 2nd Int. Conf. Soil Mech. & Found. Eng., Vol. 1, pp 207 - 211.

BISHOP, A.W. (1950)
'Summarised proceedings of a conference on stress analysis.'
Brit. J. App. Phys., 1, pp 241 - 251.

BISHOP, A.W. (1954)
Correspondence on Penman (1953).
Geotechnique, 4, No 1, pp 43 - 45.

BISHOP, A.W. (1958)
'Test requirements for measuring the coefficient of earth pressure at rest.'
Proc. Brussels Earth Pressure Conf., Vol. 1, pp 2 - 14.

BISHOP, A.W. (1966)
'The strength of soils as engineering materials.'
Geotechnique, 16, No 2, pp 91 - 128.

BISHOP, A.W. (1971)
'Shear strength parameters for undisturbed and remoulded soil specimens.'
Proc. Roscoe Mem. Symp., Cambridge, pp 3 - 58.

BISHOP, A.W. and ELDIN, A.K.G. (1953)
'The effect of stress history on the relation between and porosity in sand.'
Proc. 3rd Int. Conf. Soil Mech. & Found. Eng., Vol. 1, pp 126 - 130.

BISHOP, A.W. and GREEN, G.E. (1965)
'The influence of end restraint on the compression strength of a cohesionless soil.'
Geotechnique, 15, No 3, pp 243 - 266.

BISHOP, A.W. and HENKEL, D.J. (1953)
'The pore pressure changes during shear in two undisturbed clays.'
Proc. 3rd Int. Conf. Soil Mech. & Found. Eng., Vol. 1, pp 94 - 99.

BISHOP, A.W. and HENKEL, D.J. (1957)
'The measurement of soil properties in the triaxial test.'
Edward Arnold, London.

BISHOP, A.W., WEBB, D.L. and SKINNER, A.E. (1965)
'Triaxial tests on soil at elevated cell pressures.'
Proc. 6th Int. Conf. Soil Mech. & Found. Eng., Vol. 1, pp 170 - 174.

BJERRUM, L. and KUMMENEJE, O. (1961)
'Shearing resistance of sand samples with circular and rectangular cross-sections.'
Norwegian Geotechnical Inst. Publn. No. 44.

BRANSBY, P.L. (1968)
'Stress and strain in sand caused by rotation of a model wall.'
Ph.D. Thesis, University of Cambridge.

BRANSBY, P.L. (1971)
Discussion on Session 2.
Proc. Roscoe Mem. Symp., Cambridge, pp 255 - 258.

BRINCH HANSEN, J. (1963)
Discussion of Kondner (1963).
J. Soil Mech. & Found. Eng. Div., ASCE, 89, SM 4, pp 241 - 242.

BRINCH HANSEN, J. (1965)
'Some stress-strain relationships for soils.'
Proc. 6th Int. Conf. Soil Mech. & Found. Eng., Vol. 1, pp 231 - 234.

BRUMUND, W.F. and LEONARDS, G.A. (1972)
'Subsidence of sand due to surface vibration.'
J. Soil Mech. & Found. Eng. Div., ASCE, 98, SM 1, pp 27 - 41.

BUTTERFIELD,R., HARKNESS,R.M. and ANDRAWES,K.Z. (1970)
'A stereo-photogrammetric method for measuring displacement fields.'
Geotechnique, 20, No 3, pp 308 - 314.

CAQUOT,A. (1934)
'Equilibre des massifs a frottement interne.'
Stabilite des Terres Pulverulents et Coherentes.
Gauthier Villars, Paris.

CASAGRANDE,A. (1936)
'Characteristics of cohesionless soils affecting the stability of slopes and earth fills.'
Contributions to Soil Mechanics, 1925 - 1940.
Boston Society of Civil Engineers.

CHEN,L.S. (1948)
'An investigation of stress-strain and strength characteristics of cohesionless soils by triaxial compression tests.'
Proc. 2nd Int. Conf. Soil Mech.& Found. Eng., Vol. 5, pp 35 - 43.

CORNFORTH,D.H. (1961)
'Plane strain failure characteristics of a saturated sand.'
Ph.D. Thesis, University of London.

CORNFORTH,D.H. (1964)
'Some experiments on the influence of strain conditions on the strength of sand.'
Geotechnique, 14, pp 143 - 167.

COX,A.D. (1963)
'The use of non-associated flow rules in soil plasticity.'
R. Armament Res. Dev. Establ. Rep. (B) 2/63.

DANTU,P. (1961)
'Etude mecanique d'un millieu pulverulent forme de spheres egales de compacite maxima.'
Proc. 5th Int. Conf. Soil Mech. & Found. Eng., Vol. 1, pp 61 - 70.

D'APPOLONIA,E. (1968)
'Densification of granular soils by vibrations.'
University of Michigan Engineering Summer Conference,
Vibrations of soils and Foundations.

DAVIS,E.H. (1967)
'A discussion of theories of plasticity and limit analysis in relation to the failure of soil masses.'
Proc. 5th Australia-New Zealand Conf. Soil Mech. & Found. Eng., pp 175 - 182.

DE JONG,G.DE J. (1958)
'The undefiniteness in kinematics for friction materials.'
Proc. Brussels Earth Pressure Conf., Vol. 1, pp 55 - 70.

DERESIEWICZ,H. (1958)
'Mechanics of granular matter.'
Adv. App. Mech., Vol. 5, pp 233 - 306.

DESAI,C.S. (1971)
'Nonlinear analyses using spline functions.'
J. Soil Mech. & Found. Eng. Div., ASCE, 97, SM 10, pp 1461 - 1480.

DRUCKER, D.C., GIBSON, R.E. and HENKEL, D.J. (1957)
'Soil mechanics and work hardening theories of plasticity.'
Trans. ASCE, 122, pp 338 - 346.

DRUCKER, D.C., GREENBERG, H.J. and PRAGER, W. (1952)
'Extended limit design theorems for continuous media.'
Q. Appl. Math., 9, pp 381 - 389.

DUFFY, J. and MINDLIN, R.D. (1957)
'Stress strain relations and vibrations of a granular medium.'
J. App. Mech., Trans. ASME, 24, pp 585 - 593.

DYSON, S. (1970)
'The strength and deformational behaviour of a cohesionless soil under generalised stress conditions.'
Ph.D. Thesis, University of Aston in Birmingham.

ELDIN, A.K.G. (1951)
'Fundamental factors controlling shear properties of sands.'
Ph.D. Thesis, University of London.

EL-SOHBY, M.A. (1964)
'The behaviour of particulate materials under stress.'
Ph.D. Thesis, University of Manchester.

ESCARIO, M.V. and URIEL, S. (1961)
'Optical methods of measuring the cross-section of samples in the triaxial test.'
Proc. 5th Int. Conf. Soil Mech. & Found. Eng., Vol. 1, pp 89 - 93.

FINN, W.D.L. and MITTAL, H.K. (1963)
'Shear strength of soil in a general stress field.'
Symp. Lab. Shear Testing of Soils, Ottawa, ASTM, STP 361, pp 42 - 48.

FINN, W.D.L., WADE, N.H. and LEE, K.L. (1967)
'Volume changes in triaxial and plane strain tests.'
J. Soil Mech. & Found. Eng. Div., ASCE, 93, SM 6, pp 297 - 308.

GIRIJAVALLABHAN, C.V. (1970)
'Stresses in restrained cylinder under axial compression.'
J. Soil Mech. & Found. Eng. Div., ASCE, 96, SM 2, pp 783 - 787.

GRATON, L.C. and FRASER, H.J. (1935)
'Systematic packing of spheres with particular attention to porosity and permeability.'
J. Geology, Vol. 43, pp 785

GREEN, G.E. (1969)
'Strength and compressibility of granular materials under generalised strain conditions.'
Ph.D. Thesis, University of London.

GREEN, G.E. (1971a)
'Strength and deformation of sand measured in an independent stress control cell.'
Proc. Roscoe Mem. Symp., Cambridge, pp 285 - 323.

GREEN, G.E. (1971b)
Discussion on Session 3.
401 - 409

HALL,E.B. and GORDON,B.B. (1963)
'Triaxial testing with large-scale high pressure equipment.'
Symp. Lab. Shear Testing of Soils, Ottawa, ASTM, STP 361, pp 315 - 328.

HARDIN,B.O. and BLACK,W.L. (1966)
'Sand stiffness under various triaxial stresses.'
J. Soil Mech. & Found. Eng. Div., ASCE, 92, SM 2, pp 27 - 42.

HARR,M.E. (1966)
'Foundations of theoretical soil mechanics.'
McGraw-Hill, New York.

HILL,R. (1950)
'The mathematical theory of plasticity.'
Oxford University Press, London.

HIRSCHFELD,R.C. and POULOS,S.J. (1963)
'High-pressure triaxial tests on a compacted sand and an undisturbed silt.'
Symp. Lab. Shear Testing of Soils, Ottawa, ASTM, STP 361, pp 329 - 339.

HOLUBEC,I. (1966)
'The yielding of cohesionless soils.'
Ph.D. Thesis, University of Waterloo, Ontario, Canada.

HORNE,M.R. (1965)
'The behaviour of an assembly of rotund, rigid, cohesionless particles, Parts 1 and 2.'
Proc. Roy. Soc. A, Vol 286, pp 62 - 97.

HORNE,M.R. (1969)
'The behaviour of an assembly of rotund, rigid, cohesionless particles, Part 3.'
Proc. Roy. Soc. A, Vol 310, pp 21 - 34.

ISMAEL,H.A.E. (1969)
'Effect of mean stress and straining conditions on the dilatancy behaviour of sand.'
M.Sc. Thesis, University of Manchester.

JAKY,J. (1944)
'The coefficient of earth pressure at rest,'
Magyar Mernok es Epitesz Egylet Kozlonye.

JAMES,R.G. (1965)
'Stress and strain fields in sand.'
Ph.D. Thesis, University of Cambridge.

JAMES,R.G. and BRANSBY,P.L. (1970)
'Experimental and theoretical investigations of a passive earth pressure problem.'
Geotechnique, 20, No 1, pp 17 - 37.

JANUSKEVICIUS,C.K. and VEY,E. (1965)
'Stresses and strains in triaxial specimens.'
Instruments and apparatus for Rock Mechanics, ASTM, STP 392, pp 37 - 54.

KALLSTENIUS,T. and BERGAU,W. (1961)
'Research on the texture of granular masses.'
J. Soil Mech. & Found. Eng., Vol. 1, pp 165 - 170.

KARST,H., LEGRAND,J. Le TIRANT,P., SARDA,J.P., and WEBER,J. (1965)
'Contribution a l'etude de la mechanique des milieux granularies.'
Proc. 6th Int. Conf. Soil Mech. & Found. Eng., Vol. 1, pp 259 - 263.

KHAYATT,A.J. (1965)
'The influence of stress path on the stress dilatancy behaviour of sand.'
M.Sc. Thesis, University of Manchester.

KHAYATT,A.J. (1967)
Discussion of Lee (1966).
J. Soil Mech. & Found. Eng. Div., ASCE, 93, SM 1, pp 148 - 151.

KING,G.J.W. and DICKIN,E.A. (1970)
'Comparison of stress dilatancy theories.'
J. Soil Mech. & Found. Eng. Div., ASCE, 96, SM 5, pp 1697 - 1714.

KING,G.J.W. and DICKIN,E.A. (1971)
Discussion of King and Dickin (1970).
J. Soil Mech. & Found. Eng. Div., ASCE, 97, SM 11, pp 1598 - 1600.

KIRKPATRICK,W.M. (1965)
'Effect f grain size and grading on the shearing behaviour of granular materials.'
Proc. 6th Int. Conf. Soil Mech. & Found. Eng., Vol. 1, pp 273 - 277.

KIRKPATRICK, W.M. and BELSHAW,D.J. (1968)
'On the interpretation of the triaxial test.'
Geotechnique, 18, pp 336 - 350.

KIRKPATRICK,W.M. and YOUNGER,J.S. (1970)
'Strain conditions in compression cylinder.'
J. Soil Mech. & Found. Eng. Div., ASCE, 96, pp 1683 - 1695.

KO,H.Y. and SCOTT,R.F. (1967)
'A new soil testing apparatus.'
Geotechnique, 17, No 1, pp 40 - 57.

KOERNER,R.M. (1970)
'Effect of particle characteristics on soil strength.'
J. Soil Mech. & Found. Eng. Div.,ASCE, 96, SM 4, pp 1221 - 1234.

KOLBUSZEWSKI,J. (1965)
'Sand particles and their density.'
Lecture delivered at Material Science Club Symp., London.

KONDNER,R.L. (1963)
'Hyperbolic stress-strain response: cohesive soils.'
J. Soil Mech. & Found. Eng. Div., ASCE, 89, SM 1, pp 115 - 143.

KONDNER,R.L. and ZELASKO,J.S. (1963)
'Void ratio effects on the hyperbolic stress-strain response of sand.'
Symp. Lab. Shear Testing of Soils, Ottawa, ASTM, STP 361, pp 250 - 338.

KUMMENEJE,O. (1957)
'To-dimensjonale vakuum-triaxialforsok pa torr sand.'
Norwegian Geotechnical Inst. Internal Report F80. (unpublished)

LADE, P.V. (1972)
'The stress-strain and strength characteristics of cohesionless soils.'
Ph.D. Thesis, University of California, Berkeley.

LEE, I.K. (1966)
'Stress-dilatancy performance of feldspar.'
J. Soil Mech. & Found. Eng. Div., ASCE, 92, SM 2, pp 79 - 103.

LEE, I.K. (1968)
'Soil mechanics, selected topics.'
Butterworth, London.

LEE, I.K. and MORGAN, J.R. (1966)
'Stress and deflection measurements in subgrade materials.'
Proc. 3rd bienn. Conf. Aust. Rd. Res. Bd., Pt. 2, pp 1168

LEE, K.L. (1970)
'Comparison of plane strain and triaxial tests on sand.'
J. Soil Mech. & Found. Eng. Div., ASCE, 96, SM 3, pp 901 - 923.

LEE, K.L. and SEED, H.B. (1967)
'Drained strength characteristics of sands.'
J. Soil Mech. & Found. Eng. Div., ASCE, 93, SM 6, pp 117 - 141.

LEUSSINK, H. and WITTKE, W. (1963)
'Difference in triaxial and plane strain shear strength.'
Symp. Lab. Shear Testing of Soils, Ottawa, ASTM, STP 361, pp 77 - 89.

LEWIN, P.I. (1971)
'A new apparatus for testing a one-dimensionally consolidated clay cube with independent stress control.'
Proc. Roscoe Mem. Symp., Cambridge, pp 324 - 329.

MAKHLOUF, H.M. and STEWART, J.J. (1965)
'Factors influencing the modulus of elasticity of dry sand.'
Proc. 6th Int. Conf. Soil Mech & Founf Eng., Vol. 1, pp 298 - 302.

MANDL, G. and FERNANDEZ LUQUE, R. (1970)
'Fully developed plastic shear flow of granular materials.'
Geotechnique, 20, No 3, pp 277 - 307.

MARACHI, N.D., CHAN, C.K., SEED, H.B. and DUNCAN, J.M. (1969)
'Strength and deformation characteristics of rockfill materials.'
Report No. TE-69-5, Dept. of Civil Eng., University of California.

MENZIES, B.K. (1970)
'Stress-strain anisotropy in sand.'
Ph.D. Thesis, University of London.

MINDLIN, R.E. and DERESIEWICZ, H. (1953)
'Elastic spheres in contact under varying oblique forces.'
J. App. Mech., Vol. 20, pp 327 - 344.

PARIKH, P.V. (1967)
'The shearing behaviour of sand under axisymmetric loading.'
Ph.D. Thesis, University of Manchester.

PARKIN, A.K. (1965)
'On the strength of packed spheres.'
J. Aust. Math. Soc., Vol. 5, part 4, pp 443 - 452.

PARKIN.A.K. (1967)
Correspondence on Barden and Khayatt (1966).
Geotechnique, 17, No 2, pp 171 - 172.

PARKIN, A.K. (1970)
Correspondence on Rowe (1969).
Geotechnique, 20, No 1, pp 113 - 115.

PARRY, R.H.G. (1965)
'Shear strength of saturated remoulded clay.'
Proc. 6th Int. Conf. Soil Mech. & Found. Eng. , Vol. 1, pp 333 - 337.

PARRY, R.H.G. (1971a)
'A study of the influence of intermediate principal stress on ϕ values using a critical state theory.'
Proc. 4th Asian Conf. Soil Mech., Bangkok, pp 159 - 165.

PARRY, R.H.G. (1971b)
Discussion on Session 3.
Proc. Roscoe Mem. Symp., Cambridge, pp 377 - 378.

PERLOFF, W.H. and POMBO, L.E. (1969)
'End restraint effects in the triaxial test.'
Proc. 7th Int. Conf. Soil Mech. & Found. Eng., Vol.1, pp 327 - 333.

POLAKOWSKI, N.H. and RIPLING, E.J. (1966)
'Strength and structure of engineering materials.'
Prentice-Hall, New Jersey, USA.

PONCE, V.M. and BELL, J.M. (1971)
'Shear strength of sand at extremely low pressures.'
J. Soil Mech. & Found. Eng. Div., ASCE, 97, SM 4, pp 625 - 638.

PRAKASH, S and GUPTA, M.K. (1967)
'Compaction of sand under vertical and horizontal vibrations.'
Proc. S.E. Asian Regional Conf. on Soil Mech. & Found. Eng., Bangkok, pp 201 - 210.

PROCTER, D.C. (1967)
'The stress-dilatancy behaviour of dense sand in the hollow cylinder test.'
M.Sc. Thesis, University of Manchester.

PROCTER, D.C. and BARDEN, L. (1971)
'The drained strength of granular material.'
Canadian Geotechnical Jour., Vol. 8, No 8, pp 372 - 383.

RAMAMURTHY, T. (1971)
Discussion on Windisch and Soulie (1970)
J. Soil Mech. & Found Eng. Div., ASCE, 97, SM 4, pp 686 - 690.

READES, D.W. (1972)
'Stress-strain characteristics of a sand under three-dimensional loading.'
Ph.D. Thesis, University of London.

RENNIE,B.C. (1959)
'On the strength of sand.'
J. Australian Math. Soc., 1, pp 71 - 79.

ROSCOE,K.H. (1970)
'The influence of strains in soil mechanics.'
Geotechnique, 20, No 2, pp 129 - 170.

ROSCOE,K.H., ARTHUR,J.R.F. and JAMES,R.G. (1963)
'The determination of strains in soils by an X-ray method.'
Civ. Eng. Publ. Wks. Rev., 58, pp 873 - 876 and 1009 - 1012.

ROSCOE,K.H., SCHOFIELD,A.N. and THURAIRAJAH,A. (1963)
'An evaluation of test data for selecting a yield criterion for soils.'
Symp. Lab. Shear Testing of Soils, Ottawa,ASTM, STP 361, pp 111 - 128.

ROSCOE, K.H., SCHOFIELD,A.N. and WROTH,C.P. (1958)
'On the yielding of soils.'
Geotechnique, 8, pp 22 - 53.

ROWE,P.W. (1962)
'The stress-dilatancy relation for static equilibrium of an assembly of particles in contact.'
Proc. Roy. Soc. A., 269, pp 500 - 527.

ROWE,P.W. (1964a)
Discussion of Rowe (1963).
J. Soil Mech. & Found. Eng. Div., ASCE, 90, SM 4, pp 145 - 180.

ROWE,P.W. (1964b)
Correspondence on Cornforth (1964).
Geotechnique, 14, No 4, pp 361 - 364.

ROWE,P.W. (1969)
'The relation between the shear strength of sands in triaxial compression, plane strain and direct shear.'
Geotechnique, 19, No 1, pp 75 - 86.

ROWE,P.W. (1970)
Correspondence on Rowe (1969).
Geotechnique, 20, No 2, pp 215 - 218.

ROWE,P.W. (1971)
'Theoretical meaning and observed values of deformation parameters for soil.'
Proc. Roscoe Mem. Symp., Cambridge, pp 143 - 194.

ROWE,P.W. (1971)
Discussion of King and Dickin (1970).
J. Soil Mech. & Found. Eng. Div., ASCE, 97, SM 4, pp 704 - 709.

ROWE,P.W. and BARDEN,L. (1964)
'Importance of free ends in triaxial testing.'
J. Soil Mech. & Found. Eng. Div., ASCE, 90, SM 1, pp 1 - 27.

ROWE,P.W., BARDEN,L. and LEE,I.K. (1964)
'Energy components during the triaxial cell and direct shear tests.'
Geotechnique, 14, No 3, pp 247 - 261.

SCHOFIELD,A.N. and WROTH,C.P. (1968)
'Critical state soil mechanics.'
McGraw-Hill, London.

SEED,H.B. and LEE,K.L. (1966)
'Liquefaction of saturated sands during cyclic loading.'
J. Soil Mech. & Found. Eng. Div., ASCE, 92, SM 6, pp 105 - 134.

SELIG,E.T. (1963)
'Effect of vibration on density of sand.'
Proc. 2nd Panamerican Conf. Soil Mech. & Found. Eng.,Sao Paulo, Vol 1, pp 129-144.

SKETCHLEY,C.J. (1971)
Discussion on Session 3.
Proc. Roscoe Mem. Symp., Cambridge, pp 391 - 396.

SMITH,W.O.,FOOTE,P.D. and BUSANG,P.F. (1929)
'Packing of homogeneous apheres.'
Physical Review, 34, pp 1271 - 1274.

SPENCER,A.J.M. (1964)
'A theory of the kinematics of ideal soils under plane strain conditions.'
J. Mech. Phys. Solids, 12, pp 337 - 351.

SULTAN,H.A. and SEED,H.B. (1967)
'Stability of sloping core earth dams.'
J. Soil Mech. & Found. Eng. Div., ASCE, 93, SM 4, pp 45 - 67.

SUTHERLAND,H.B. (1971)
Discussion on Session 3.
Proc. Roscoe Mem. Symp., Cambridge, pp 376 - 377.

TAYLOR,D.W. (1948)
'Fundamentals of soil mechanics.'
Wiley, New York.

THURSTON,C.W. and DERESIEWICZ,H. (1959)
'Analysis of a compression test of model of a granular medium.'
J. App. Mech., Vol. 26, pp 251 - 258.

TIMMERMAN,D.H. and WU, T.H. (1969)
'Behaviour of dry sands under cyclic loading.'
J. Soil Mech. & Found. Eng. Div., ASCE, 95, SM 4, pp 1097 - 1112.

TIMOSHENKO,S. and GOODIER,J.H. (1951)
'Theory of elasticity.'
McGraw-Hill, New York.

TONG,P.Y.L. (1970)
'Plane strain deformation of sands.'
Ph. D. Thesis, University of Manchester.

TROLLOPE,D.H. and PARKIN,A.K. (1963)
Discussion on Rowe (1963)
J. Soil Mech. & Found. Eng. Div., ASCE, 89, SM 6, pp 129 - 133.

TRUESDALE,W.B. and RUSIN,R.W. 91963)
Discussion on 'An evaluation of test data for selecting a yield criterion for soils.'
Symp. Lab. Shear Testing of Soils, Ottawa, ASTM, STP 361, pp 129 - 133.

VESIC,A. and BARKSDALE,R.D. 91963)
Discussion on test methods and new equipment.
Symp. Lab. Shear Testing of Soils, Ottawa, ASTM, STP 361, pp 301 - 305.

WADE,N.H. (1963)
'Plane strain failure characteristics of a saturated clay.'
Ph.D. Thesis, University of London.

WHITMAN,R.V. and ORTIGOSA,P. (1968)
'Densification of sand by vertical vibration.'
Soils Publ. No. 222, M.I.T., Cambridge, Mass., Dept. Civil Engineering.

WIGHTMAN,A. (1967)
'The stress-dilatancy of sands during plane strain compression.'
M.Sc. Thesis, University of Manchester.

WINDISCH,S.J. and SOULIE,M. (1970)
'Technique for study of granular materials.'
J. Soil Mech & Found. Eng. Div., ASCE, 96, SM 4, pp 1113 - 1126.

WOOD,C.C. (1958)
'Shear strength and volume change characteristics of compacted soil under conditions of plane strain.'
Ph.D. Thesis, University of London.

WROTH,C.P. (1972)
'General theories of earth pressures and deformations.'
Proc. 5th European Conf. Soil Mech & Found Eng., Madrid, Vol 2, pp 33 - 52.

WROTH,C.P. and BASSETT,R.H. (1965)
'A stress-strain relationship for the shearing behaviour of sand.'
Geotechnique, 15, No 1, pp 32 - 56.